HAI HUANG

Biophysical Characterization of Three *SCN5A* Mutations Linked to Long QT Syndrome Type 3, Sudden Infant Death Syndrome, and Atrial Fibrillation

Thèse présentée
à la Faculté des études supérieures de l'Université Laval
dans le cadre du programme de doctorat en Médecine Expérimentale
pour l'obtention du grade de Philosophiae doctor (Ph.D)

FACULTE DE MÉDECINE
UNIVERSITÉ LAVAL
QUÉBEC

2010

Résumé

Le gène *SCN5A* encode la sous-unité principale du canal sodique cardiaque ($Na_v1.5$). Ce canal est responsable de l'initiation et de la propagation du potentiel d'action cardiaque. Un dysfonctionnement de ce canal peut causer le syndrome du QT long de type 3 (LQT3) et la fibrillation auriculaire (AF). Les patients atteints du LQT3 sont à risques de développer des arythmies létales, particulièrement des torsades de pointes qui peuvent causer le syndrome de mort subite du nourrisson (SIDS). **Objectifs :** Le but de cette étude est de caractériser les propriétés biophysiques de trois mutations sur le gène *SCN5A* : Y1767C, S1333Y et K1493R. Ces trois mutations ont respectivement été retrouvées chez un patient souffrant du LQT3, chez un patient mort du SIDS et la dernière mutation chez un patient souffrant d'AF. **Méthodes** : Des cellules tsA 201 ont été transfectées avec le gène codant pour le canal sauvage et les gènes codant pour les canaux mutés. Par la suite, leurs caractéristiques biophysiques ont été étudiées par la méthode du patch-clamp en configuration cellule entière. **Résultats** : La mutation Y1767C est située dans le segment 6 du domaine IV (DIVS6). Cette mutation sur le canal produit un courant persistant et un courant de fenêtre augmenté, ces résultats expliquent les phénotypes cliniques des patients affectés de cette mutation. La ranolazine, un nouveau bloqueur des canaux Na^+, peut bloquer efficacement le courant Na^+ persistant et réduire le courant de fenêtre. Ces canaux mutés montrent aussi une augmentation de l'inhibition fréquence-dépendante ainsi qu'une réactivation lente. La mutation S1333Y est situé sur la boucle S4 et S5 du domaine III. L'étude fonctionnelle de ce canal montre un gain de fonction : un courant Na^+ persistant et une augmentation du courant de fenêtre provoquée par un déplacement de -8 mV de l'activation et de +7mV de l'inactivation. La mutation K1493R est située sur la boucle entre les domaines III-IV. Cette mutation provoque un déplacement vers des potentiels plus dépolarisés de l'inactivation est entraîne une augmentation du courant de fenêtre. **Conclusion** : Les manifestations cliniques observées chez les patients sont probablement dues aux changements des propriétés biophysiques provoqués par les trois mutations sur $Na_v1.5$ rapportées dans cette étude. Nous concluons donc que (1) Y1767C est une mutation provoquant le LQT3. L'effet observé par la ranolazine sur cette mutation (la ranolazine agit probablement comme un bloqueur des canaux ouverts) nous donne de nouveaux indices pour le traitement des patients porteurs de cette mutation. (2) La mort subite du nourrisson observé est probablement lié à un syndrome LQT3 associé à la mutation S1333Y. (3) La mutation K1493R provoque de la fibrillation auriculaire causée par une hyperexcitabilité des cardiomyocytes.

Abstract

SCN5A is a major gene known to encode the human cardiac Na^+ channel ($Na_v1.5$) that is responsible for initiation and propagation of cardiac action potentials. Long QT syndrome type 3 (LQT3) and familial atrial fibrillation (AF) could be caused by dysfunctional $Na_v1.5$ channels. Patients with LQT3 are at high risk of developing life-threatening arrhythmias, particularly torsades de pointes, which may lead to sudden infant death syndrome (SIDS). **Objectives**: The goal of the present study is to characterize biophysical properties of three *SCN5A* mutations and to explore the relation of those properties and the clinical effects seen in patients carrying the mutations (Y1767C in LQT3, S1333Y in SIDS, and K1493R in AF patients). **Methods**: Wild-type and mutant channels were transiently expressed in the tsA 201 cell, a branch of the HEK 293 cell. The biophysical properties were studied with the patch clamp technique using the whole cell configuration. **Results:** Y1767C mutation was located in segment 6 of domain IV (DIVS6). The Y1767C mutant channels produced a persistent Na^+ current and an increased window current, which is consistent with clinical data in an affected patient. Ranolazine, a new Na^+ channel blocker, blocked the persistent Na^+ current, reduced the window current, and produced an enhanced frequency-dependent inhibition with a slow recovery process. S1333Y mutation was located in the S4-S5 linker of domain III. A functional study revealed a gain-of-function property of persistent Na^+ current and an enhanced window current generated by a –8 mV shift in activation and a +7 mV shift in inactivation. K1493R mutation was located in the III-IV linker. Its gating properties showed an increased window current caused by a depolarized shift of steady-state inactivation. **Conclusions:** The differences in clinical manifestations associated with these three mutations probably arise from the distinct biophysical abnormalities of the mutant $Na_v1.5$ channels reported in this study. We conclude that (1) Y1767C is an LQT3 mutation. Moreover, ranolazine acted as an open-channel blocker, and ranolazine inhibition of the mutant channel revealed its potential as a pharmacologic target in the affected population; (2) The LQT3-associated mutation S1333Y could be implicated in the sudden death of the SIDS patient, which suggests that neonatal ECG screening may have utility in prevention of SIDS; (3) the K1493R mutation may have caused AF through cardiomyocyte hyperexcitability, in the patient carrying that mutation.

Avant-Propos

I thank the support of all the people whose help made this thesis possible. First and foremost I would like to thank my supervisor, Professor Mohamed Chahine, for giving me the opportunity to complete my project, and for guiding me throughout the critical stages of this work. You have taught me so much more than just science, you showed me what I was capable of achieving and thus you brought the best in me. It was an excellent experience to be under your supervision.

To my other colleagues, Valérie Pouliot, Hugo Poulin, and Olivier Thériault, I would also like to extend my special thanks to you for your helps with valuable suggestions and the necessary technical assistance to fulfill this project.

My parents must be acknowledged for the support that you provided during these past years. My appreciation to you cannot properly be captured in words for your unwavering encouragement and love. You are not only my best friends, but also role models for strength, integrity and perseverance.

Last but no least, I would like to thank Juan Zhao, my dear wife, for your patience, support, and remarkable advice. What all you did for me during this period gave me continuous inspiration. Your support made the completion of this work much easier than if I had to do it alone.

Thank you all!

This work is dedicated to my parents,

to my dear wife, and to my lovely son Kevin

Table des matières

Liste des tableaux

Liste des figures

Liste des abréviations

βAR	β-adrenergic receptor
μ-CTX	μ-conotoxine
A	Alanine
AF	Atrial fibrillation
AKAP	A kinase anchoring protein
AS	Andersen syndrome
ATP	Adenosine triphosphate
BrS	Brugada syndrome
C	Cysteine
CaM	Calmodulin
cAMP	3'-5'-cyclic adenosine monophosphate
cDNA	Complementary DNA
CCD	Cardiac conduction disease
CLC	Chloride voltage-gated channel
CNS	Central nervous system
C-terminus	Carboxyl-terminus
D	Aspartic acid
DAD	Delayed after depolarization
DCM	Dilated cardiomyopathy
DI-DIV	Sodium channel domain 1-4
DRG	Dorsal root ganglion

E	Glutamic acid
EAD	Early after depolarization
ECG	Electrocardiogram
ER	Endoplasmic recticulum
F	Phenylalanine
G	Glycine
GΩ	Giga-ohm
H	Histidine
HBSCI	Sodium voltage-gated channel, protein type I, alpha subunit
HBSCII	Sodium voltage-gated channel, protein type II, alpha subunit
HEK293	Human embryonic kidney cell line
HERG	Human ether a'-go-go related gene/protein
I	Isoleucine
IVF	Idiopathic ventricular fibrillation
I_{Ca-L}	L-type calcium current
I_{Ca-T}	T-type calcium current
I_{KAch}	Acetylcholine-gated potassium current
I_{KATP}	ATP-sensitive potassium current
I_{K1}	Inward potassium current
I_{Kr}	Rapidly activated delayed rectifier potassium current
I_{Ks}	Slowly activated delayed rectifier potassium current
I_{Kur}	Ultra rapid-delayed rectifier potassium current

I_{Na}	Sodium current
I_{to}	Transient outward potassium current
JLNS	Jervell and Lange Nielsen syndrome
K	Lysine
KCNA1	Potassium voltage-gated channel, subfamily A, member 1
KCNE 1 and KCNE2	Potassium voltage-gated channel, subfamily E, member 1 and member 2
KCNJ 2	Potassium inwardly rectifying channel, subfamily J, member 2
KCNQ1 and KCNQ2	Potassium voltage-gated channel, subfamily 1, member 1 and member 2
kDa	Kilodalton
L	Leucine
LQTS	Long QT interval syndrome
M	Methionine
MTS	Methanethiosulfonate
N	Asparagine
$Na_v1.1$ to $Na_v1.9$	Sodium voltage-gated channel, subfamily1, specific sodium channel isoform 1 to 9, alpha subunit
N-terminus	NH_2-terminus
P	Proline
PCCD	Progressive cardiac conduction defect
PKA	Protein kinase A
PKC	Protein Kinase C
PN1	Peripheral nerve sodium channel type 1
PN3	Peripheral nerve sodium channel type 3
PNS	Peripheral nervous system

P-segment	Pore-segment
Q	Glutamine
QTc	QT interval corrected for heart rate
R	Arginine
RBBB	Right bundle branch block
RWS	Romano-Ward syndrome
S	Serine
S1 to S6	Sodium channel transmembrane segment 1-6
SCN1A to SCN10A	Voltage-gated sodium channel, protein type I to X, alpha-subunit
SS1 and SS2	Short segement 1 and short segment 2
SSS	Sick sinus syndrome
STX	Saxitoxin
T	Threonine
TS	Timothy syndrome
tsA201	Embryonic kidney cell line
TTX	Tetrodotoxin
TTX-R	Tetrodoxin resistant
TTX-S	Tetrodoxin sensitive
V	Valine
VT / VF	Ventricular tachycardia / ventricular fibrillation
W	Tryptophane
Y	Tyrosine

Chapter I

General Introduction

1.1 Brief introduction

Voltage-gated Na^+ channels are membrane proteins that are essential to the normal functioning of excitable cells. Their pore-forming principal subunits (α-subunits) can function independently to produce electrical signals in cell membranes. The α-subunits are expressed in combination with one or more auxiliary subunits (β-subunits), which may increase the expression level and modify gating properties of α-subunits such as voltage-dependent activation, inactivation, and recovery from inactivation. Structural elements of α-subunits are required for voltage-dependent activation (S4), selective Na^+ conductance and toxin binding (pore region), and voltage-dependent inactivation (III-IV linker and C-terminus). At least ten distinct isoforms and their encoding genes have been recognized. They have different tissue distributions. $Na_v1.5$, encoded by the *SCN5A* gene, is a major Na^+ channel expressed in the heart, particularly in the intercalated discs. Its mechanisms of action have been explored by mutagenesis, expression in heterologous cells, and functional analysis. The $Na_v1.5$ protein could be modulated to produce changes in expression levels and gating properties by interacting with multiple related proteins. When the *SCN5A* gene is mutated in certain positions, the resulting mutant $Na_v1.5$ channels are particularly dysfunctional, leading to specific cardiac Na^+ channel disorders (also called cardiac Na^+ channelopathies). Both gain- and loss-of-function mutations are suggested to cause cardiac Na^+ channelopathies. Gain-of-function mutations underlie long QT syndrome type 3 (LQT3) and sudden infant death syndrome (SIDS). Loss-of-function mutations underlie Brugada syndrome (BrS), cardiac conduction disease (CCD), and congenital sick sinus syndrome (SSS). Dilated cardiomyopathy (DCM) and atrial fibrillation (AF) have been associated with both gain and loss of functions in $Na_v1.5$ channels, depending on the mutation. These cardiac Na^+ channelopathies may induce cardiac arrhythmias through abnormal impulse and re-entry formation. Life-threatening arrhythmias, particularly torsades de pointes and ventricular tachycardia (VT), may cause syncope or even cardiac sudden death in affected patients. Class I antiarrhythmic drugs have been widely studied in the management of cardiac arrhythmias given their ability to treat abnormal electrical activities and to inhibit cellular activities. These drugs bind preferentially to a particular functional state, usually the open state or inactivated state, depending on the drug. Ranolazine, an unclassified Na^+ channel blocker, was shown to be able to treat LQT patients, and to prevent development of cardiac arrhythemias.

1.2 Voltage-gated Na^+ channel family

The voltage-gated Na^+ channel family comprises ten α-subunit isoforms and six β-subunit subgroups. Expression of the α-subunits alone is sufficient to form the Na^+ channel pore. Therefore, the α-subunits play a specialized functional role in physiology and pharmacology. The physiological functions include Na^+ conduction, Na^+ selectivity, and channel opening and closing. The pharmacological properties arise from their specific drug-binding sites. The β-subunits, in an auxiliary manner, modify the kinetics and voltage-dependent channel gating properties; for example, they modify voltage-dependent activation and inactivation.

1.2.1 Na^+ channel α-subunit isoforms

Ten genes encode distinct Na^+ channels ($Na_v1.1$-$Na_v1.9$ and Na_X) with a common motif, but with differences in amino acid sequences and in physiological characteristics. $Na_v1.1$-$Na_v1.9$ isoforms are voltage-dependent, whereas Na_x is Na^+ concentration-dependent. Table 1.1 lists distribution and properties of these ten isoforms.

The naming convention for Na^+ channel isoforms comprises, in order, the chemical symbol of the principal permeating ion, the principal physiology regulator (in subscript), the gene subfamily, the specific Na^+ channel isoform, and a splice variant identifier (lower-case letter). Thus, $Na_v1.1$ represent sodium channel that regulates voltage, belongs to gene subfamily 1, is an isoform 1, and is a splice variant "a".

The Na^+ channel isoforms are further characterized pharmacologically by their sensitivity to the specific neurotoxin tetrodotoxin, as TTX-sensitive or -resistant (TTX-S or TTX-R) isoforms. The TTX-S isoforms are blocked by nanomolar concentrations of TTX, whereas the TTX-R isoforms are blocked by micromolar concentration of TTX. Although Na^+ channel isoforms are expressed in multiple tissues, they are distributed mainly in the central nervous system (CNS), peripheral nervous system (PNS), and skeletal muscle. The role of neuronal and skeletal muscle Na^+ channels in the heart is discussed in section 1.3.

1.2.1.1 Central nervous system (CNS) α-subunit isoforms

The Na^+ channels found in the CNS include $Na_v1.1$, $Na_v1.2$, $Na_v1.3$, and $Na_v1.6$. These four are highly TTX-sensitive. Phenylalanine residues in the pore-region of domain I (e.g. F385 in

Table 1.1 Properties of Na_v Channels

Channel name	Gene name	Human chromosome location	TTX sensitivity	Tissue localization
$Na_v1.1$	*SCN1A*	2q2a	Sensitive	CNS, PNS, heart
$Na_v1.2$	*SCN2A*	2q23–24	Sensitive	CNS, heart
$Na_v1.3$	*SCN3A*	2q24	Sensitive	CNS, heart
$Na_v1.4$	*SCN4A*	17q23–25	Sensitive	Skeletal muscle
$Na_v1.5$	*SCN5A*	3p21	Resistant	Heart, CNS
$Na_v1.6$	*SCN8A*	12q13	Sensitive	CNS, PNS, heart, glia, nodes of Ranvier
$Na_v1.7$	*SCN9A*	2q24	Sensitive	PNS, Schwann cells
$Na_v1.8$	*SCN10A*	3p22–24	Resistant	PNS
$Na_v1.9$	*SCN11A*	3p21–24	Resistant	PNS
Na_x	*SCN6A/SCN7A*	2q21-23	Resistant	CNS, PNS, heart

Modified from (Chahine *et al.*, 2005).

rNa$_v$1.2 sequence [rat]) are essential for the high-affinity blocking by TTX (Heinemann *et al.*, 1992a). Clinical manifestations arising from mutations in CNS Na^+ channel α-subunits can present as mild ataxia, dystonia, paralysis, and juvenile lethality (Craner *et al.*, 2004; Meisler and Kearney, 2005). The following sections refer to the isoforms of human Na^+ channels and their corresponding genes, except where indicated.

Na$_v$1.1

Na$_v$1.1 is encoded by the *SCN1A* gene, which is clustered on chromosome 2q2a in humans (Noda *et al.*, 1986a). Two splice variants have been identified as Na$_v$1.1a and Na$_v$1.1b. These two variants are distinguished from each other by a 33-nucleotide deletion within exon 11 of Na$_v$1.1a (Noda *et al.*, 1986a; Noda *et al.*, 1986b) and by an 84-nucleotide deletion at the exon 11/12 splice junction in Na$_v$1.1b (Lossin *et al.*, 2002). Na$_v$1.1 was originally identified in the CNS with moderate expression in granule cells and low expression in the pyramidal cell layer, although it is now known to be abundant in the PNS (Klugbauer *et al.*, 1995; Beckh, 1990). For this reason, Na$_v$1.1 is still ranged in the CNS category. Na$_v$1.1 mRNA has been identified in dorsal root ganglia (DRG) neurons with the highest expression detected in large-diameter cells and a lower expression in small nociceptive somata (Black *et al.*, 1996). Functional Na$_v$1.1 current in sensory neurons has not, however, been recorded.

Na$_v$1.2

Na$_v$1.2 is encoded by *SCN2A* gene, located on chromosome 2q23-24 in humans (Beckh, 1990). Na$_v$1.2 is expressed in DRG, but strongly in the hippocampus, especially in granule cells of the dentate gyrus and in the pyramidal cell layer. Na$_v$1.2 has a single splice variant, Na$_v$1.2a, which differs from Na$_v$1.2 in six amino acids at positions 189 (D to N), 209 (D to N), 538 (R to Q), 579 (S to N), 1062 (D to G), and 1356 (L to V) (Auld *et al.*, 1988). Details of its contribution to sensory function are, however, still lacking.

Na$_v$1.3

Na$_v$1.3 is encoded by the *SCN3A* gene located on chromosome 2q24, and is primarily found in human CNS (Malo *et al.*, 1994). The two splice variants identified to date, Na$_v$1.3a and Na$_v$1.3b, contain an additional insertion within exon 12 when compared with the full-length Na$_v$1.3

sequence. $Na_v1.3a$ has a 9-neucleotide insertion, whereas $Na_v1.3b$ has a 96-neucleotide insertion (Schaller *et al.*, 1992). $Na_v1.3$ expression is similar to $Na_v1.1$ but with the exception of channel reexpression of $Na_v1.3$ detected after neuronal damage, such as that caused by axotomy (Hains *et al.*, 2003; Dib-Hajj *et al.*, 1996). $Na_v1.3$ reexpression causes increased neuronal excitability given the rapid recovery of its current from inactivation. This reespression thus contributes to neuropathic pain subsequent to nerve and spinal cord injury (Cummins and Waxman, 1997), and makes $Na_v1.3$ a good candidate target in the development of drugs for neuropathic pain.

$Na_v1.6$

$Na_v1.6$ is encoded by the *SCN8A* gene clustered on chromosome 12q13 in humans (Noda *et al.*, 1986a; Burgess *et al.*, 1995). $Na_v1.6a$ is the only splice variant of $Na_v1.6$ known to date. They differ from each other by 10 amino acids, a result of alternative splice donor sites in exon 10B that encodes the DI-II linker (Dietrich *et al.*, 1998; Plummer *et al.*, 1998). $Na_v1.6$ is expressed abundantly in the CNS (neurons of the hippocampus, cortex, and olfactory bulb), but poorly in the PNS and heart (Trimmer *et al.*, 1989). In neurons, $Na_v1.6$ is a major isoform located at the nodes of Ranvier in myelinated axons (Caldwell *et al.*, 2000). Electrophysiological recordings of this channel in whole-cell experiments have revealed a prominent persistent Na^+ current (persistent I_{Na}) (Burbidge *et al.*, 2002). Under physiological conditions, the persistent I_{Na} may amplify or integrate synaptic potentials and facilitate repetitive firing of action potentials. Mutations in the *SCN8A* gene may link to neuronal dysfunctions: for example, a stop-codon mutation that results in a C-terminal deletion. A patient carrying this loss-of-function mutation was found to have cerebellar atrophy, ataxia, and mental retardation (Trudeau *et al.*, 2006). $Na_v1.6$ was also thought to be important in demyelinating disorders such as multiple sclerosis (MS) given its distribution along unmyelinated axons, which are commonly associated with axonal injury (Black *et al.*, 2002). In MS patients, $Na_v1.6$ was coexpressed with the Ca^{2+}/Na^+ exchanger along the unmyelinated axon. The persistent I_{Na} of $Na_v1.6$ can drive the exchanger to reverse Ca^{2+} flow into the axon with deleterous concequence (Craner *et al.*, 2004).

1.2.1.2 Skeletal and heart muscle α-subunit isoforms

$Na_v1.4$ and $Na_v1.5$ are significantly expressed in denervated muscle and skeletal or cardiac muscle. These two isoforms have opposite TTX-sensitivities. $Na_v1.4$'s sensitivity to TTX is

conferred by a tyrosine residue (Y401 in $rNa_v1.4$ sequence) corresponding to the residue F385 in its counterpart, $rNa_v1.2$ (Backx *et al.*, 1992). In contrast, $Na_v1.5$ is considered relatively resistant to TTX, because it is not blocked until TTX concentration rise to micromolar levels. Homologous residues, C374 in $rNa_v1.5$ and C373 in $hNa_v1.5$, confer this resistance in the rat and human isoforms, respectively (Heinemann *et al.*, 1992a).

$Na_v1.4$

$Na_v1.4$ is encoded by the *SCN4A* gene, mapped on chromosome 17q23-25. It was identified in human adult and neonate muscle at high and low levels, respectively (Kallen *et al.*, 1990; Trimmer *et al.*, 1989). Mutations in the *SCN4A* gene have been recognized to cause three human neuromuscular diseases: hyperkalemic periodic paralysis (Fontaine *et al.*, 1990), paramyotonia congenita (Ebers *et al.*, 1991), and K^+-aggravated myotonias (Mitrovic *et al.*, 1994).

$Na_v1.5$

$Na_v1.5$ is encoded by the *SCN5A* gene, located on chromosome 3q21-24. The gene consists of 28 exons spanning approximately 80 kb (Fig 1.1). $Na_v1.5$ is mainly expressed in the heart, although it is also present in low levels in the piriform cortex (Donahue *et al.*, 2000), subcortical limbic nuclei (Hartmann *et al.*, 1999), jejunal circular smooth muscle (Ou *et al.*, 2002), and neonatal skeletal muscle (Kallen *et al.*, 1990). It is 2016 amino acids in length and has a calculated molecular weight of 227 kDa (Rogart *et al.*, 1989; Gellens *et al.*, 1992). Mutations in the *SCN5A* gene have been shown to cause cardiac diseases (see details in section 1.5). $Na_v1.5$ expression in the piriform cortex and subcortical limbic nuclei, which are involved in epilepsy, may explain the reported correlation between *SCN5A* mutations and epileptic seizures (Aurlien *et al.*, 2009; Nashef *et al.*, 2007). $Na_v1.5$ expression in gastrointestinal tract produce electrical signals that mediate normal gastrointestinal function, so *SCN5A* mutations may underlie the gastrointestinal symptoms experienced by patients with LQT3 (Locke, III *et al.*, 2006). $Na_v1.5$ is expressed in neonatal skeletal muscle, but not expressed in adult human skeletal muscle, suggesting that $Na_v1.5$ is essential for neonatal development of the skeletal muscle system.

$Na_v1.5$ is more sensitive to inhibition by anaesthetic and antiarrhythmic agents such as lidocaine, and has a more negative voltage-dependence of inactivation than PNS channels (Bean *et al.*, 1983; Gellens *et al.*, 1992). There have been four splice variants identified, termed hH_1, hH_{1a},

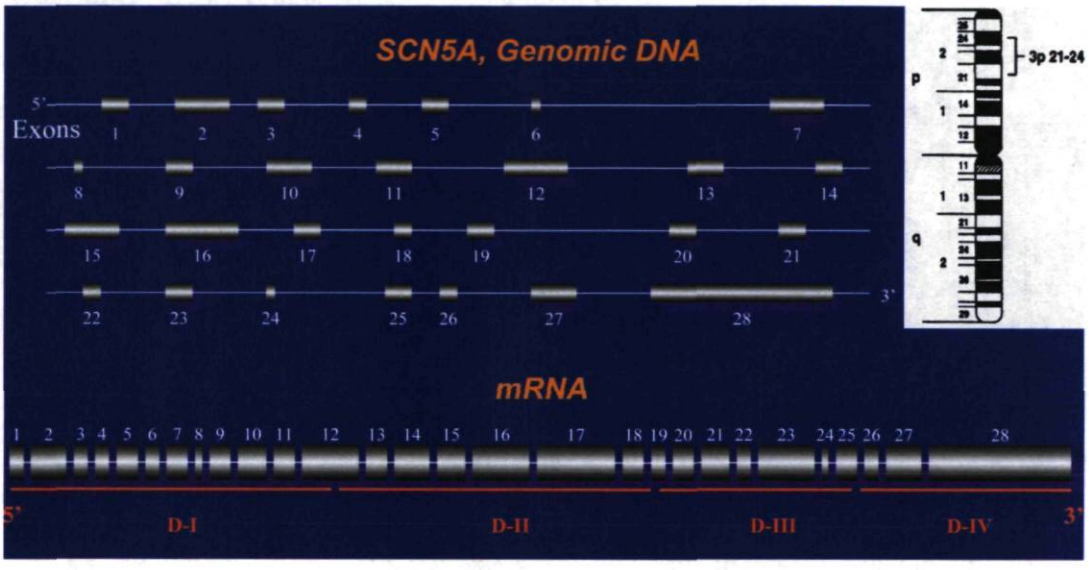

Figure 1.1: Genomic organization of *SCN5A* gene. *SCN5A* is mapped to chromosome 3p21-24. Exons and introns are indicated by boxes (grey) and horizontal lines (white). Domain numbers (orange) are given under corresponding exons.

hH_{1b}, hH_{1c}. The hH_1 consists of 2,016 amino acids containing a glutamine (Q) at position 1077, and therefore it is also called Q1077. The hH_{1a} has only 2,015 amino acids and no glutamine at 1077, thus it is also called Q1077del. Another amino acid difference between hH_1 and hH_{1a} is an alanine (A) for histidine (H) substitution at position 559. Studies of mRNA from the human heart showed presence of both variants, with levels of hH_{1a} being twice those of hH_1, in all heart specimens studied (Makielski *et al.*, 2003; Tan *et al.*, 2005). Therefore, a mutation at any site would be expressed in the settings of both splice variants. The hH_{1b} variant has 2,015 amino acids with a two-amino acid difference compared with hH_{1a}: one with arginine (R) instead of histidine (H) at position 558, the other one with isoleucine (I) instead of leucine (L) at position 618 (Ye *et al.*, 2003). The hH_{1c} construct was obtained from the hH_{1a} by mutating the alanine (A) to threonine (T) at position 559 (Makielski *et al.*, 2003).

1.2.1.3 Peripheral nervous system (PNS) α-subunit isoforms

In the PNS, $Na_v1.7$, $Na_v1.8$, and $Na_v1.9$ are present at high levels, whereas $Na_v1.1$ and $Na_v1.6$ are only present at low levels, so they are not included in this category. $Na_v1.7$ is TTX-S, whereas $Na_v1.8$ and $Na_v1.9$ are TTX-R, that resistance is attributed to the serine residue (e.g. S355 in $rNa_v1.8$ sequence) corresponding to the residue F385 in $rNa_v1.2$ (Tate *et al.*, 1998).

$Na_v1.7$

$Na_v1.7$ is encoded by the *SCN9A* gene, mapped on chromosome 2q24. It is widely distributed in the PNS, and has been detected in Schwann cells, DRG neurons, neuroendocrine cells (Sangameswaran *et al.*, 1997; Belcher *et al.*, 1995; Klugbauer *et al.*, 1995). Aside from the cell body, $Na_v1.7$ is also expressed abundantly in neurites of nociceptive neurons that are usually located at the peripheral end of the neuron (Toledo-Aral *et al.*, 1997). For this reason, $Na_v1.7$ plays a crucial role in the generation of nerve action potentials and in the initial transmission of pain signals to the nervous system (Cummins *et al.*, 2007). Also, $Na_v1.7$ may participate in setting the threshold for cell firing. A lower threshold can increase the response to suprathreshold stimulation for firing action potentials, thus contributing to the pain sensation in nociceptors (Waxman, 2007). Mutations in the *SCN9A* gene may show gain- or loss-of-function properties. The gain-of-function mutations may produce neuronal hyperexcitability, leading to acute or chronic pain in congenital pain syndromes (Dib-Hajj *et al.*, 2005). In contrast, the loss-of-

function mutations may cause congenital insensitivity to pain (Cox *et al.*, 2006; Goldberg *et al.*, 2007).

$Na_v1.8$

$Na_v1.8$ is encoded by the *SCN10A* gene, which is clustered on chromosome 3p22-24. $Na_v1.8$ is of a TTX-R Na^+ channel that has a relatively confined distribution in PNS, and is detected mainly in small diameter sensory nerves of DRG and trigeminal ganglion, which innervate peripheral tissues such as in skin (Akopian *et al.*, 1996; Souslova *et al.*, 1997). These channels are activated at relatively positive voltage levels around +10 mV and have a slow rate of inactivation, which may result in lowered thresholds of depolarization and increased excitability of nociceptive DRG neurons (Zhao *et al.*, 2007). For this reason, $Na_v1.8$ is thought to be closely involved in the mediation of pathologic pain. Up-regulated expression of $Na_v1.8$ contributes to hyperalgesia in inflammation: for example, $Na_v1.8$ may help to maintain the excitability of nociceptor terminals at low temperatures, producing continuous pain sensation in such conditions (Zimmermann *et al.*, 2007). This isoform has been expressed in *Xenopus oocytes*, showing gating properties in good agreement with those of the native Na^+ current in DRG neurons (Vijayaragavan *et al.*, 2001). However, $Na_v1.8$ was poorly expressed in cell lines, probably because of a trafficking defect that reduces the cell surface expression of functional channels by trapping channel proteins in the endoplasmic reticulum (ER). Many attempts have been made to enhance the expression of $Na_v1.8$, including the addition of the annexin II light chain (p11) (Okuse *et al.*, 2002) and β_3-subunit (John *et al.*, 2004). Recently, it was found that co-incubation of lidocaine can significantly increase the expression by releasing channel protein from the ER in tsA 201 cells (Zhao *et al.*, 2007). Additionally, such expression was augmented by the β_1-subunit.

$Na_v1.9$

$Na_v1.9$ is encoded by *SCN11A* gene, localized on chromosome 3p21-24. Like $Na_v1.8$, $Na_v1.9$ is also expressed in small fibres of the DRG and trigeminal ganglion, and participates in the hyperalgesic reaction. Currents carried by $Na_v1.9$ are persistent and are activated at more hyperpolarizing potentials close to resting membrane potentials than those of $Na_v1.8$ (Dib-Hajj *et al.*, 2002). Because of these properties, $Na_v1.9$ may be less likely to contribute to rapid upstroke of action potentials, and more likely to contribute primarily to determine the electrogenic

properties of nociceptive DRG neurons by regulating their resting membrane potentials and by increasing their responses to subthreshold stimulation (Herzog *et al.*, 2001).

1.2.1.4 Atypical Na^+ channels (Na_x)

TTX-R Na_x is encoded by the *SCN6A/SCN7A* gene, mapped on chromosome 2q21-23. It is found in multiple tissues, including uterus, heart, skeletal muscle, brain, kidney and spleen (Fang *et al.*, 2002). Four subgroups have been cloned from rat cortical astrocytes (NaG), rat DRG neurons (SCL11), human heart ($Na_v2.1$), and a mouse atrial tumour cell line ($Na_v2.3$) (Goldin *et al.*, 2000). These clones have similar sequences, and are considered to represent the same Na^+ channel isoform. The subscript letter x represents unknown physiological function. It is considered an atypical Na^+ channel because it has less than 50% of sequence identity to other Na^+ channel isoforms (George, Jr. *et al.*, 1992; Akopian *et al.*, 1997). This difference underlie some structural differences between Na_x and other Na^+ channel isoforms, including fewer positive charges in S4 segments, an IFI motif instead of an IFM motif, and a poorly conserved III-IV linker (Goldin, 2001). Sensing extracellular Na^+ concentration in salt homeostasis regulation is the most important function of Na_x (Watanabe *et al.*, 2000). Its gating activity is Na^+ concentration-dependent, but not voltage-dependent (Akopian *et al.*, 1997). No further biophysiological details have been characterized, however, since Na_x is difficult to express in mammalian cells or *Xenopus* oocytes.

1.2.2 β-subunits

In addition to the major α-subunit, most voltage-gated Na^+ channels have one or more auxiliary β-subunits. So far, at least six types of β-subunits, β_1- β_4, β_{1a}, and β_{1b}, have been cloned and characterized (Isom *et al.*, 1992; Isom *et al.*, 1995; Morgan *et al.*, 2000; Yu *et al.*, 2003; Qin *et al.*, 2003). β_{1a}, and β_{1b} subunits are two splice variants of β_1-subunits. In general, auxiliary β-subunits are 22-36 kDa proteins with a single transmembrane-spanning segment, a long glycosylated extracellular N-terminus, and a short intracellular C-terminus. All types of β-subunits contain extracellular immunoglobulin (Ig) motifs, homologous to the V (variable) -set of Ig superfamily that includes cell adhesion molecules. The role of β-subunits in the heart is discussed in section of 1.3.

β_1-subunit

The β_1-subunit is widely expressed in human skeletal muscle, heart and neuronal tissue, and it is encoded by a single gene *SCN1B* mapped on chromosome 19q13 (Isom *et al.*, 1992). The extracellular Ig domain of the β_1 is thought to be the primary portion interacting with the α-subunit through a site formed by one or more extracellular loops of the α-subunit (Isom, 2001). However, α-β_1 interactions are not strictly confined to the extracellular side. A mutation D1790G in *SCN5A* gene, located in the C-terminal of the α-subunit, has been reported to cause LQT3 by An et al. They speculated that a disruption of α-β_1 interaction occurs from the intracellular side when co-expressed mutant and β_1 proteins into HEK cells (An *et al.*, 1998). However, reports of the gating properties of mutant channels have been inconsistent. For example, persistent I_{Na}, a hallmark mechanism for LQT3, was detected in the study by Baroudi et al (Baroudi and Chahine, 2000), but not seen in the An's study (An *et al.*, 1998).

β_2-subunit

The β_2-subunit is encoded by *SCN2B* gene mapped on chromosome 11q23.3, and is widely present in human CNS, PNS, and the heart (Wollner *et al.*, 1987; Isom *et al.*, 1995). The β_2-subunit participates in the translocation of newly synthesized Na^+ channels from intracellular stores to the plasma membrane of cultured embryonic neurons (Schmidt and Catterall, 1986), suggesting that the β_2-subunit may act as cell adhesion molecules. Moreover, this isoform is homologous to contactin and interacts with extracellular proteins, such as tenascin-C and tenascin-R. Contactin is a glycosyl-phosphatidylinositol cell adhesion protein in neurons. It interacts with membrane glycoproteins, which are present at nodes of Ranvier and are involved in Na^+ channel clustering (Yu *et al.*, 2003).

β_3-subunit

β_3, a subunit most closely related to β_1, is encoded by the *SCN3B* gene, mapped on human chromosome 11q23.3. The β_3-subunit shares 20 to 22% of amino acid homology with β_1 and is widely expressed in the heart, neuronal tissue, adrenal gland, and kidney (Fahmi *et al.*, 2001; Morgan *et al.*, 2000). β_3 expression is complementary to that of the β_1 in many areas in terms of their localization in the adult rat CNS (Morgan *et al.*, 2000). For instance, a high level of β_3 mRNA is present within the olfactory cortex and basal ganglia in the forebrain, where a low level

of the β_1-mRNA is detected. In contrast, a low level of β_3 mRNA is expressed in the thalamic nuclei, where a high level of β_1 mRNA is present.

β_4-subunit

The β_4 subunit is most closely related to the β_2 subunit, with which it shares 35% amino acid homology with β_2. *SCN4B*, localized at chromosome 11q23.3, encodes β_4. It is widely distributed in the brain, spinal cord, some sensory neurons, and heart (Yu *et al.*, 2003). The linkage between α- and β-subunits is important for promoting and stabilizing the channel density in the plasma membrane (Makita *et al.*, 1996).

β_{1a}-subunits

The β_{1a} and β_1 are splice variants of the *SCN1B* gene. Although β_{1a} and β_1 are structurally homologous proteins, they have a little amino acid homology in the region of the C-terminus that produces a novel transmembrane segment and short intracellular domain (Kazen-Gillespie *et al.*, 2000). In immunocytochemical studies, β_{1a} showed to have wide expression similar to β_1-subunit in the heart, dorsal root ganglia, brain, and spinal cord (Kazen-Gillespie *et al.*, 2000). However, the β_{1a} and β_1 have different developmental expression patterns. For example, β_{1a} mRNA is detected early in embryonic brain, but levels drop after birth. In contrast, β_1 expression is not present in the early developmental embryonic brain, and then increases after birth.

β_{1b}-subunits

The β_{1b}-subunit encodes a 268-residue protein that contains novel residues 150-268 in the C-terminal half with identical residues 1-149 in the N-terminal half, compared with β_1-subunits. It has been reported that β_{1b}-subunits are abundantly expressed in the human brain, spinal cord, DRG neuron, and skeletal muscle, but at low levels in the heart (Qin *et al.*, 2003).

1.3 Structure and function of voltage-gated Na^+ channels

1.3.1 Structure of α-subunits

The Na^+ channel consists of a principlal α-subunit (260kDa) and one or more accessory β-subunits (β_1-β_4) (Fig. 1.2). The α-subunit is sufficient to express the channel function and gating properties, which can be modulated by the accessory β-subunits. All Na^+ channel α-subunits

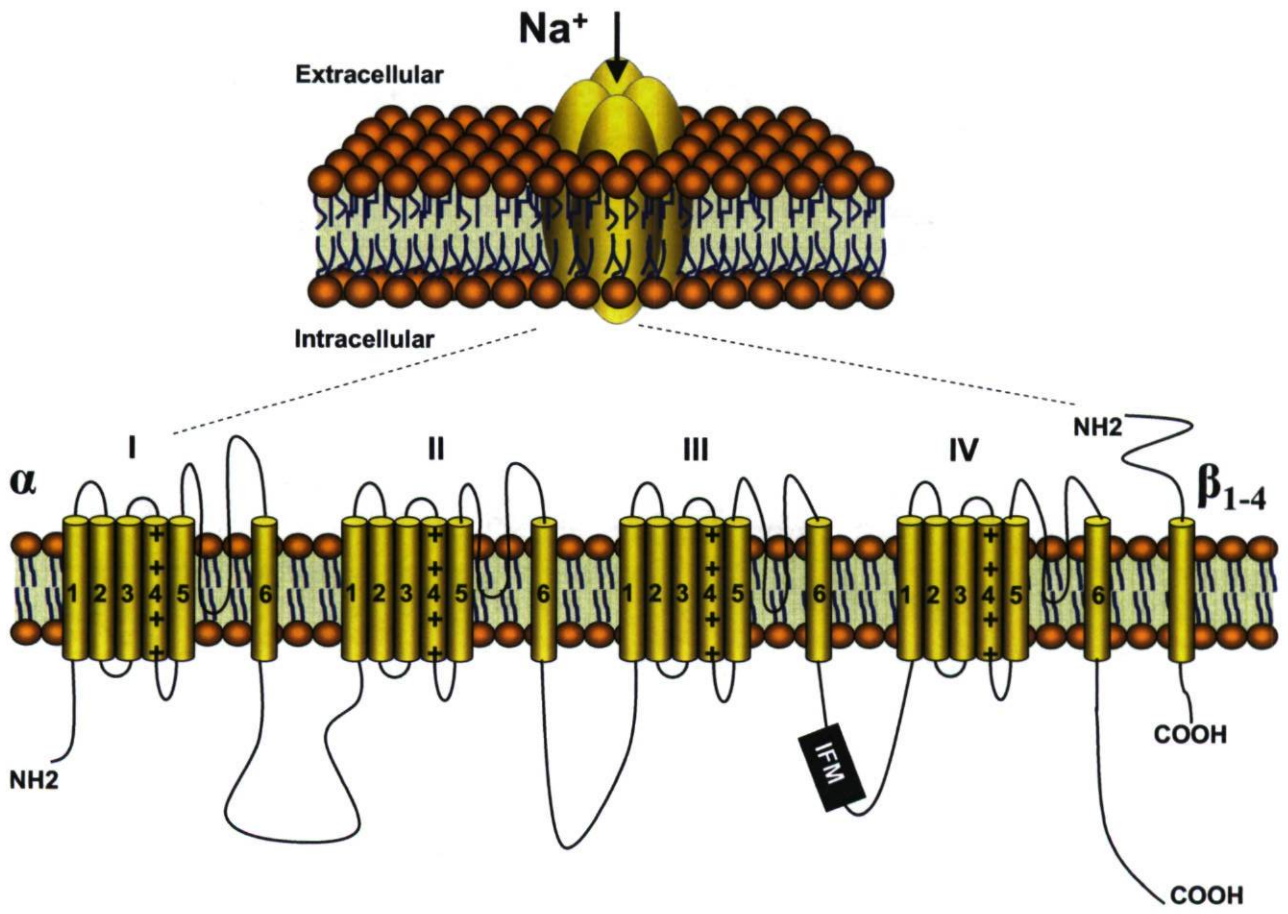

Figure 1.2: A schematic view of the structure of voltage-gated Na^+ channels. The α-subunit is inserted into the lipid bilayer of the cellular membrane and constitutes the channel pore, through which Na^+ ions pass. The subunit consists of four domains (DI-IV). Each domain contains six transmembrane segments. The pore is made up by segements S5-S6, while S4 acts as the voltage sensor. The DIII-IV linker comprises the inactivation motif (IFM). β-subunits have a single transmembrane segment, a long extracellular N-terminus, and a short intracellular C-terminus.

comprise four homologous domains (DI-DIV), each of which contains six transmembrane segments (S1-S6). The DI-DIV domains are connected by cytoplasmic linkers. S5 and S6 in each domain are connected via a hairpin-like P (pore) -loop that lines the outer pore of channels (Gellens *et al.*, 1992; Terlau and Stühmer, 1998). S4 segments in each domain contain positively charged amino acid residues, and are thought to be voltage-gated sensors. These sensors act as gating charges and move across the membrane to trigger channel activation in response to membrane depolarization (Stühmer *et al.*, 1989). The short cytoplasmic intracellular loop connecting domains III and IV acts as the inactivation gate, which bends back into the channel and blocks the pore from the inside during sustained depolarization of the membrane. The inactivation gate is located in the center of a DIII-IV linker with a three-amino-acid stretch, consisting of isoleucine, phenylalanine, and methionine (IFM) (West *et al.*, 1992). Residues of S6 segments in each domain provide the binding site for local anaesthetics, and participate in the formation of the internal vestibule in the P-region (Ragsdale *et al.*, 1994).

1.3.1.1 Model of S4 segments

The S4 segment was first reported as a voltage sensor in mutagenesis studies of the Na^+ channel (Stühmer *et al.*, 1989). The S4 segment is considered as a voltage sensor because of two properties: (1) it is embedded within the lipid bilayer of the membrane because of its hydrophobic property; and (2) it contains four to seven positive charges, usually contributed by arginine, depending on the channel type. This property allows S4 segments to be very sensitive to the change of the membrane voltage. The S4 model was controversial until now. Two models have been proposed, which are conventional (Yang *et al.*, 1996) and paddle models (Jiang *et al.*, 2003). In the conventional model, the voltage sensor was considered as a set of four α-helical structures with positively charged amino acids at every third residue. This proposed structure would transport gating charges outwards to activate Na^+ channels in response to depolarization by moving along a clockwise spiral pathway from one side of the plasma membrane to the other (Yang *et al.*, 1996). This movement is confined within a pore surrounded by hydrophilic and negatively charged amino acid residues to stabilize gating charges in the transmembrane environment. The paddle model was based on x-ray crystallographic studies of a bacterial voltage-gated K^+ channel that revealed an α–helically hairpin-like structure. The N-terminal half of S4 segments and the second part of S3s (S3b-S4 unit) participate in the formation of a loose

protein structure (Jiang *et al.*, 2003). The voltage sensor paddles are thought to be located inside the membrane near the intracellular surface and to extend into cytoplasm from the channel core at resting state (Sigworth, 2003). When the channel opens, positive charges are moved outwards as the paddles swing to the outside surface in a pivoting motion similar to boat oars. The paddle model can better explain why voltage sensors are accessible to small lipid-soluble molecules of local anesthetics. These molecular compounds diffuse up to the paddles from the lipid membrane interior to their binding sites, and work as a gating modifier to alter gating properties by directly interacting with voltage sensors. These two models have a pharmacological difference: At resting state, the paddle model would not be expected to be available for anesthetic binding, whereas the conventional model provides its extracellular end for anesthetic binding.

1.3.1.2 P (pore)-segments

The P-segment is also called P-loop, and is the linker between S5-S6 in each domain of Na^+ channels that separates the pore into the outer and inner pore (Yamagishi *et al.*, 1997; Pérez-garcía *et al.*, 1996). This linker is composed of two parts, short segment 1 (SS1) being on the N-terminal side and short segment 2 (SS2) on the C-terminal side. SS1 segments enter, while SS2 segments exit the membrane to form the channel pore. SS2 is a highly conserved part of the external mouth of the pore and the selectivity filter, thus it has been studied more intensely.

Outer pore and selectivity filter

From the extracellular side of the channel, looking into the pore, outer and inner rings form the narrowest part of the pore. These two rings are situated in SS2 and act on the channel conductance, selectivity, and toxin binding (Backx *et al.*, 1992; Chen *et al.*, 1992; Heinemann *et al.*, 1992b). The outer ring is relatively wide and contains four highly conserved amino acid residues: E403, E758, D1241, and D1532 in I-IV domains (in $rNa_v1.4$ sequence). The inner ring is relatively narrow and also has four highly conserved residues: D400, E755, K1237 and A1529 in domain I-IV (in $rNa_v1.4$ sequence). This DEKA motif is considered to be the Na^+ selectivity filter, in which K1237 in domain III discriminates Na^+ over K^+ and Ca^{2+} (Favre *et al.*, 1996). Additionally, A1529 participates in the selection of conducting monovalent cations. Besides Na^+ selectivity, neurotoxin binding site 1 is also located within the outer pore and provides the receptor site for TTX, STX, and μ-conotoxin to block ion conductance. The model of binding site

1 has been proposed as an antiparallel β-hairpin (Lipkind and Fozzard, 1994) that is predominantly composed of negatively charged amino acids in the outer and inner rings. Neurotoxins containing the positively charged ion guanidinium interact electrostatically with the negatively charged rings to mimic a plug-blocking effect.

Inner pore and local anesthetic receptor site

The inner pore is thought to provide binding sites for local anesthetics (LA), including residues I1760, F1764, V1768, and Y1771 (in $rNa_v1.2$ sequence). Of these, F1764 and Y1771 are the two most important sites for LA binding (Ragsdale *et al.*, 1994; Ragsdale *et al.*, 1996; Yarov-Yarovoy *et al.*, 2001). F1764, which is located closer to the extracellular side, is available for binding to tertiary amino groups of LA. Y1771, located closer to the intracellular side, binds to the aromatic moiety of LA (Kambouris *et al.*, 2000; Viswanathan *et al.*, 2001). Na^+ channels are blocked by either LA or class I antiarrhythmic drugs via these two residues in a voltage-dependent manner (Ragsdale *et al.*, 1994). The blocking effect is augmented at depolarized potentials with or without use-dependent stimulations. Mutations of these two residues, F1764A and Y1771A, reduce the LA binding affinity. The effect of Y1771A is smaller than that of F1764. I1760 and V1768 only affect the efficacy of certain drugs (Liu *et al.*, 2003b; Wang *et al.*, 1998). F1760 and Y1767 residues in $Na_v1.5$ are equivalent to F1764 and Y1771 residues in $rNa_v1.2$ sequence, respectively. They are two important binding sites for class I antiarrhythmic drugs (more details in Chapter II).

1.3.1.3 C-terminus

The C-terminus is a 240-amino-acid cytoplasmic tail of $Na_v1.5$ channels, which is divided into proximal and distal parts, based on their structural and functional considerations. The proximal half consists of six helical structures that are rich in negative charges provided by glutamic and aspartic acids. This part of C-terminus is highly conserved in Na^+ channel isoforms and different species (Cormier *et al.*, 2002). Previous studies show that the proximal part, especially in the first 100-amino-acid stretch of the C-terminus, is involved in the maintenance of inactivation indicating the presence of interactions between the C-terminus and inactivation gate (Deschênes *et al.*, 2001). Further studies show that a deletion starting from the sixth helical segment in the proximal half causes a marked increase in a persistent I_{Na} because of the disruption in such

interactions (Cormier *et al.*, 2002). For this reason, several $Na_v1.5$ mutations in this region can destabilize the inactivation and thereby promote a persistent I_{Na} leading to phenotypes of LQT3 (Clancy and Rudy, 2002; Rivolta *et al.*, 2002; Wei *et al.*, 1999; Baroudi and Chahine, 2000; Veldkamp *et al.*, 2000). The distal half is a positively helical charged region that is not highly conserved. Deletion of the distal half of the C-terminus did not affect activation or inactivation gating, except for a decreased I_{Na} of $Na_v1.5$ (Cormier *et al.*, 2002).

1.3.2 Na^+ channel functional gating: activation, inactivation

Ion gates in channel protiens regulate ion flows into and out of the cell. Two gates are involved in the membrane depolarization, and control the channel's opening and closing in response to changes of the membrane voltage. In general, Na^+ channel kinetic gating is associated with the distinctive opening and closing of these two gates, which control activation and inactivation states. The one gate is called the "m" gate that mediates activation, whereas the other is the "h" gate that mediates inactivation. Inactivation is further divided into closed-steady inactivation, fast inactivation, slow inactivation, and ultra-slow inactivation, depending on their inactivated time constants. These processes can in turn determine channel availability, so they are widely studied for functional analysis of Na^+ channels.

1.3.2.1 Activation

Activation occurs upon membrane depolarization, which opens the ion channels and generates and propagates the action potential. During activation, the rapid outward movement of the S4 segment opens the Na^+ channel pore, which enables a transient inward Na^+ current to traverse the membrane before the channel closes. Note that although the S4 model has variable modes, the inside to outside movement of the S4 segment has been accepted for many years.

1.3.2.2 Closed-state inactivation

After an extremely short delay following activation, depolarization also begins to initiate an inactivation state. The brief delay can drive a small percentage of channels into an inactivated state prior to closing, which suggests that these channels can directly enter into closed state without ever opening. Closed-state inactivation could be used to distinguish $Na_v1.5$ from other Na^+ channel isoforms. $Na_v1.5$ has a small but measurable percentage of channels available for

closed-state inactivation, so it does have a profound role in development of cardiac arrhythmias in inherited cardiac disorders (Sheets and Hanck, 1999; Balser, 2001). Additionally, the effect of closed-sate inactivation may be augmented when $Na_v1.5$ channels are treated by class I antiarrhythmic drugs (Groenewegen *et al.*, 2003a). In contrast, both neuronal and skeletal muscle Na^+ channels exhibit a much smaller number of channels to enter into closed-state inactivation, thus remaining excitable at more depolarized resting membrane potentials (Horn *et al.*, 1981).

1.3.2.3 Fast inactivation

A fast inactivation process (milliseconds) prevents channels from reopening until they have enough time for recovery. This period after fast inactivation is known as the refractory period, which helps to limit the action potential, and to determine the frequency of action potential firing, thereby avoiding a breakdown of ionic gradients and cell death. Fast inactivation is mediated by a "ball-and-chain" mechanism, where inactivation is brought about by the inactivation particle (ball) that is tethered to the intracellular side of the shaker K^+ channel through the N-terminus (chain) (Hoshi *et al.*, 1990). For this reason, fast inactivation is also called N-type inactivation. Similarly, the fast inactivation in Na^+ channels is mediated by a "hinged lid" mechanism (Fig. 1.3). The analogous region in Na^+ channels is the cytoplasmic III-IV linker, which acts as a lid. The inactivation particle in III-IV linker serves as a tethered pore blocker and occludes the inner pore by binding to the docking site like a "latch". The docking site is located in multiple regions, including the S4-S5 linker in the DIII and IV and the cytoplasmic end of the S6 in the DIV (Veldkamp *et al.*, 2000; Shander *et al.*, 1995). Additionally, fast inactivation is also associated with the outward movement of the S4 segment. The relationship between the outward movement of the S4 segment and the inactivation lid during fast inactivation has been studied by investigating the movement of arginine residues (positive charges) through a membrane electric field (negative charges). Depolarization produces conformational changes in the transmenbrane electric field, which release these arginine charges and thus induce gating currents. It was showed that gating currents are slowed or immobilized during fast inactivation when the pore is closing. This finding suggests that the outward movement of the S4 segment may be locked by binding of the III-IV linker (Armstrong and Bezanilla, 1977). Other studies, however, found that DIVS4 gating charges are immobilized by inactivation, independent of whether the III-IV linker lid is bound. This suggests that other parts of Na^+ channels, such as the C-terminus, may immobilize

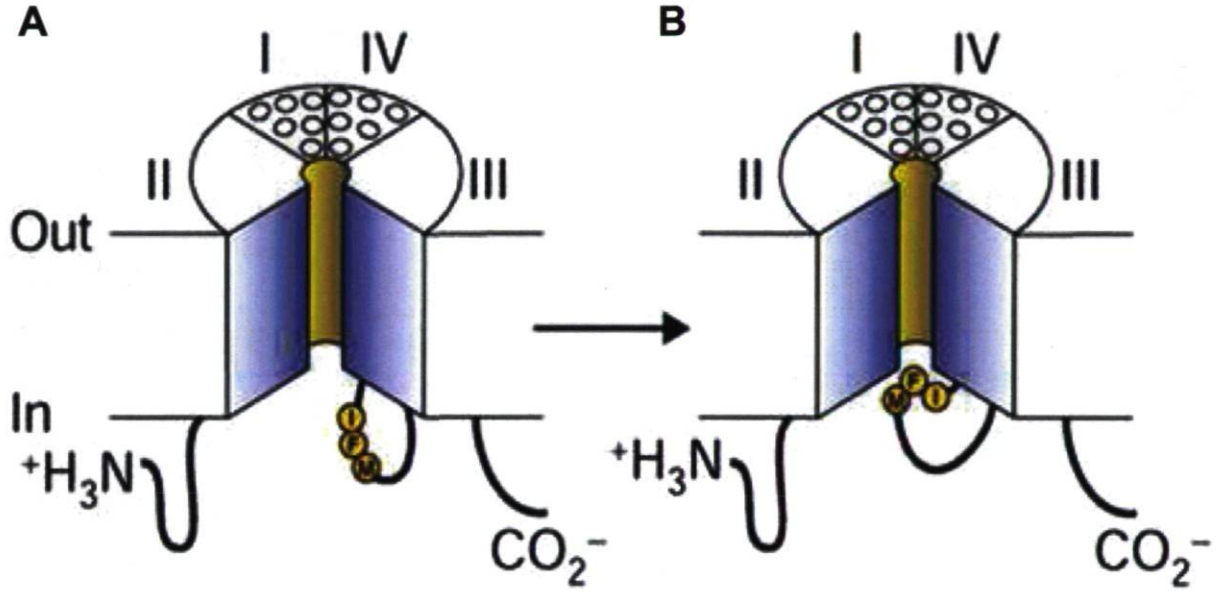

Figure 1.3: The hinged-lid mechanism for the fast inactivation. A. The intracellular loop connecting domains III and IV of the Na^+ channel is depicted as forming a hinged lid with the critical phenylalanine (F1489) within the IFM motif. B. IFM particle occludes the mouth of the pore during the inactivation process. The circles represent the transmembrane helices (Yu and Catterall, 2003).

the gating charges during fast inactivation (Liu *et al.*, 1996; Chahine *et al.*, 1996) (more details about the C-terminus are provided in section 1.3.1.3).

1.3.2.4 Slow inactivation

Na^+ channels enter slow inactivated state with prolonged depolarization. This process is a nonconducting state ranging from hundreds of milliseconds up to several seconds. Slow inactivation was originally found to be associated with mutations in the C-terminus of the shaker K^+ channels (Hoshi *et al.*, 1991; Lopez-Barneo *et al.*, 1993). For this reason, slow inactivation is commonly called C-type inactivation. More recently, a distinct form of slow inactivation was identified in a pore region mutation and called P-type inactivation (Yang *et al.*, 1997). C- and P-type inactivations are distinguished by the fact that the former is voltage-dependent, whereas the latter is not (Olcese *et al.*, 1997). In Na^+ channels, it was found that slow inactivation is present but is only 40% complete in $Na_v1.5$ when compared with 80% observed in $Na_v1.4$ (Richmond *et al.*, 1998). This is caused by a single amino acid difference in the DII S5-S6, the residue V754 in $Na_v1.4$ and equivalent I891 in $Na_v1.5$ (Vilin *et al.*, 2001). Previous studies revealed that the structural basis for slow inactivation involves the P-segment and III-IV linker. The rearrangement of the P-segment is the most common mechanism to mediate slow inactivation. When the glutamic-acid residue in the outer ring of P-segment, particularly E403 (in $rNa_v1.4$ sequence), is mutated, alteration of the ionic permeability is observed, forming slow gating process (Xiong *et al.*, 2003). The inactivation gate (III-IV linker) also contributes to the generation of slow inactivation. When replacing a hydrophobic triplet of residues in the cytoplasmic side (IFM-QQQ), the slow inactivation is enhanced. This result suggests that the inactivation particle (IFM) can mediate fast inactivation and slow inactivation. However, the effect of slow inactivation is limited probably by charge immobilization induced by fast inactivation (Richmond *et al.*, 1998).

1.3.2.5 Ultra-slow inactivation

Ultra-slow inactivation is an even slower process that can take up to 100 seconds. It was initially seen in a *SCN4A* mutation, A1529D in the inner ring of the P-region. A1529D mutation dramatically enhances entry of the channels into an inactivated state from which recovery is very slow. Analogous to C-type inactivation features in K^+ channels, ultra-slow inactivation may be inhibited by μ -conotoxin GIIIA (μ-CTX) R13Q (Dudley, Jr. *et al.*, 2000), a toxin mutant that

may create a pore-blocking effect in the outer pore region. The findings on the A1529 mutation suggest that ultra-slow inactivation may reflect a structural rearrangement of the outer pore, and that such rearrangement will result in destabilization of channels thereby forming the tedious inactivated state (Cormier *et al.*, 2002). Similar to the relationship between fast and slow inactivations, fast inactivation may also limit the extent of ultra-slow inactivation (Hilber *et al.*, 2002).

1.3.3 Gating pore currents

Recently, gating pore currents were recorded when the positively charged residues of S4 in Na^+ (Sokolov *et al.*, 2005; Sokolov *et al.*, 2007) and K^+ channels (Tombola *et al.*, 2005) were mutated. These point mutations allow cation permeation through such a unique gating pore formed by the modified S4 segments, producing a gain-of-function effect (Fig. 1.4). One such example is a hyperpolarization-activated cationic current flowing through mutated S4 in domains II or IV of $Na_v1.4$ channels to cause hypokalemic periodic paralysis (HypoPP) (Sokolov *et al.*, 2007). The leaking cation flow increases resting membrane conductance and Na^+ influx, leading to excessive depolarization. Mutations of the outer two positive charges cause gating pore currents in resting state, whereas mutations of the third gating charge cause gating pore currents in the activated sate (Sokolov *et al.*, 2005).

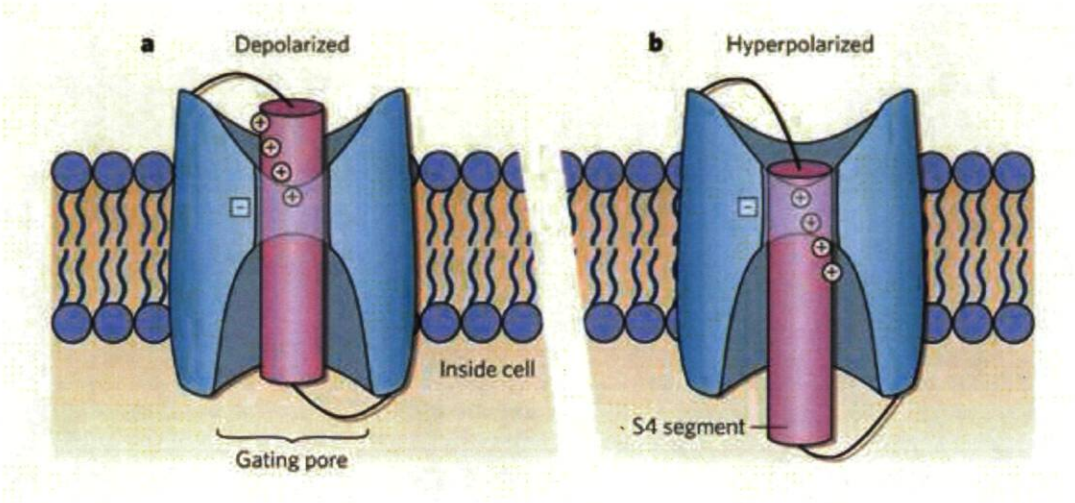

Figure 1.4: Speculative model of the gating pore at two different membrane potentials. The S4 segment (pink), with its four outermost arginine residues (+), is shown within the confines of a gating pore. Water-filled vestibules surround much of this segment. **a,** When a cell is depolarized, the S4 segment moves outwards, opening the activation gate. **b,** The gate shuts when the cell returns to its resting, hyperpolarized state and the S4 segment moves back inwards. Normally, negatively charged residues (-) near the gating pore form electrostatic interactions with positively charged arginines in the S4 segment, preventing ion leakage. However, if one of these arginines is mutated to a neutral residue, current leakage occurs (Horn, 2007).

1.4 Na^+ channels in the heart

Na^+ channels make a major contribution to three phases of the cardiac action potential: phase 0, phase 1, and phase 2. The height of the action potential increases with the increment of extracellular concentration of Na^+. If the Na^+ channel is not completely inactivated or if it reopens, phase 2 will be changed to produce a prolongation of ventricular repolarization because of persistent I_{Na} (Wang *et al.*, 1995b).

The "cardiac Na^+ channels" are referred as to $Na_v1.5$ channels, which are not exclusively identified in the heart as they are also found slightly in the brain and gastrointestinal tract. Previous studies found that left ventricule function was impaied by around 10% after the treatment of low concentration TTX (100 nM). This suggests that some TTX-S Na^+ channel isoforms may be present in the heart (Maier *et al.*, 2002). Actually, besides $Na_v1.5$, other Na^+ channel isoforms ($Na_v1.1$-$Na_v1.4$ and $Na_v1.6$) have been found in adult myocytes of mice with low the expression levels (Haufe *et al.*, 2005a; Maier *et al.*, 2002; Haufe *et al.*, 2005b). $Na_v1.5$ accounts for about 85% of mRNA expression for Na^+ channels, whereas other isoforms ($Na_v1.1$-$Na_v1.4$ and $Na_v1.6$) may contribute to about the remaining 15% in the ventricle. Electrophysiological recordings showed that TTX-S Na^+ currents account for about 10% of peak Na^+ currents. The remaining 90 % was TTX-R currents (Haufe *et al.*, 2005a; Haufe *et al.*, 2005b). These TTX-S currents are, therefore, considered to come from neuronal and skeletal Na^+ channels isofroms, whereas TTX-R currents are known to come from $Na_v1.5$. In addition, $Na_v2.1$ (an isoform of Na_x) mRNA has been identified in human heart tissues (Pereon *et al.*, 2003). No functional data on this isoform in the heart, however, have been reported.

Na^+ channel isoforms in the heart have different subcellular locations. For example, $Na_v1.5$ is localized to the cardiac intercalated discs, which are a kind of undulating double membrane that separates adjacent cells in cardiac muscle fibers, and supports synchronized contraction of cardiac tissue. There are three types of membrane junctions within the intercalated discs, the fascia adherens, macula adherens (aka desmosomes), and gap junctions. Of these, the gap junction enable the spreading of the cardiac action potentials between cardiac myocytes to depolarize the heart. Meanwhile, $Na_v1.1$, $Na_v1.2$, $Na_v1.3$ and $Na_v1.6$ are found primarily in the z-line and t-tubules (Maier *et al.*, 2002; Haufe *et al.*, 2005b), which contribute directly to cardiac contraction. Localization of $Na_v1.4$ and $Na_v2.1$ has not yet been determined. Six groups of β-subunits (β_1-β_4, β_{1A}, β_{1B}) have been identified in the heart with different expression levels. β_1 is

widely localized to the intercalated discs and t-tubules in the heart, β_3 to the t-tubules, and β_2 and β_4 to the intercalated discs (Malhotra *et al.*, 2001; Maier *et al.*, 2004). Although β_1 shares significant homology with β_3, they have different distribution in the heart. The β_1 subunit distributes widely in atria and ventricles, whereas the expression of β_3 subunit is confined to ventricles at a high level and Pukinje cells at a moderate level. That suggests that β_1 has more chance to interact with α-subunits of Na^+ channels in the heart than other β-subunits.

Therefore, a hypothesis has been proposed to explain the mechanisms that regulate cardiac action potentials, as they are transfered among the different subcellular locations. That is: (1) cardiac action potentials are propagated from one myocyte to the next by activating $Na_v1.5$ channels, the most predominant carrier of I_{Na}, at intercalated discs; (2) then, the other isoforms facilitate the propagation of action potentials into the central myocytes through the t-tubular systems (Haufe *et al.*, 2005a); and (3) β-subunits interact with all Na^+ channel isoforms in the specific areas of the heart regulating the properties of Na^+ channels (details in section 1.4.3.3).

1.4.1 Cardiac action potentials

The cardiac action potential is the electrical behavior of the individual cardiac muscle cell, and it differs significantly in different portions of the heart such as ventricle, sinoatrial node, and atrium. The specialized behavior is necessary for normal functions of electrical conduction system in the heart. These cardiac functions have two important properties: automaticity and rhythmicity. Automaticity is the ability of the heart to initiate its own contractions without any external influence, and rhythmicity is the regularity of the pace-making activity. The standard pattern used to describe the cardiac action potential is the ventricular cardiac action potential, which has five phases numbered phase 0 to 4, as shown in Figure 1.5 (Ruan *et al.*, 2009).

Phase 4

Phase 4 is of the resting membrane potential at voltage around –90 mV, which is determined by the sinoatrial node (SAN). The function of the SAN has been correlated with changes of ion channel expression.Cells are ready to be stimulated by adjacent cells to produce a new action potential at this phase. For instance, cells may be excited by the pacemaker current (I_f), which is a nonselective cation current activated in the condition of hyperpolarization primarily in the SAN region (DiFrancesco, 1985; Mangoni and Nargeot, 2008). Recently, "Ca^{2+} clocks" were proposed

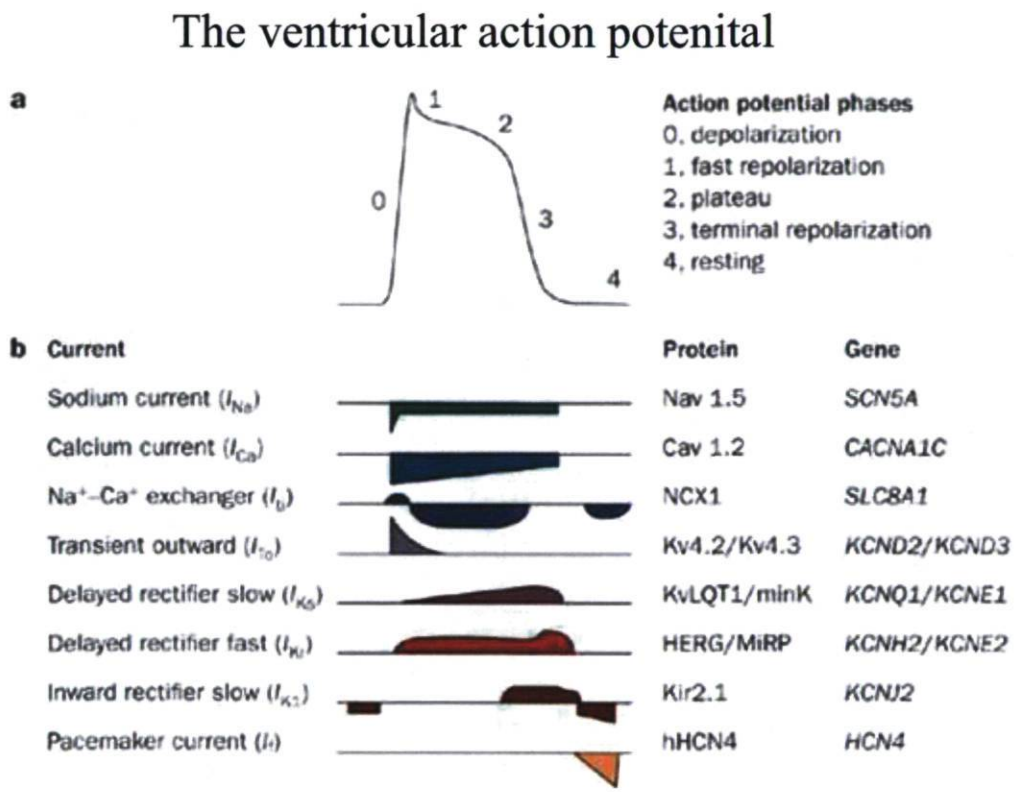

Figure 1.5: The ventricular action potential. a. Schematic of a ventricular action potential comprising phase 0 through phase 4. b. Major sarcolemmal ionic currents (left) underlying the cardiac action potential. Depolarizing currents are described below the line, whereas repolarizing currents are describes above the line. Some channels may conduct in an inward or outward direction, depending on the membrane voltage at any given time point of the electrical cycle. The standard names of proteins and their respective genes are reported on the right (Ruan *et al.*, 2009).

as an alternative mechanism for phase 4, which regulates oscillatory Ca^{2+} releases from the sarcoplasmic reticulum (SR), a major Ca^{2+} store in cells of the SA node. The oscillatory Ca^{2+} releases are activated by phosphorylation of Ca^{2+} cycling proteins, and produces inward membrane currents by activating Na^{+}/Ca^{2+} exchangers (NCE). The inward NCE currents ($I_{Na\text{-}Ca}$) consequently depolarize cellular membrane and initiate the cardiac action potential (Maltsev and Lakatta, 2007).

Phase 0

Phase 0 is the phase of rapid depolarization caused by Na^{+} channel opening if the resting membrane potential suddenly reaches the threshold level at about – 60 to – 70 mV. In this phase, the membrane conductance to Na^{+} ions rises significantly, which generates a rapid upstroke in the action potential. The slope of the upstroke is used to reflect the maximum depolarizing rate calculated with the equation: dV/dt_{max}, where dV is the change of membrane potential in voltage within the maximum duration (dt_{max}) (Grant, 2005).

Phase 1

Phase 1 is a phase of repolarization characterized by the formation of a notch in the action potential. The repolarization is caused by the inactivation of Na^{+} channels and the transient activation of I_{to}, an outward K^{+} current.

Phase 2

Phase 2 is a plateau that reflects a delicate balance between inward and outward currents. The voltage-gated Ca^{2+} inward current (I_{Ca}) is a major component of the inward current. This currents has two types: L type ($I_{Ca\text{-}L}$) and T type ($I_{Ca\text{-}T}$), which are activated by membrane depolarization. $I_{Ca\text{-}L}$ and $I_{Ca\text{-}T}$ plays an important role in cardiac automaticity and the contraction of the myocardial cell, owing to triggering of the excitation-contraction coupling mechanism during phase 2 (Bodi *et al.*, 2005; Ono and Iijima, 2009). In the ventricle, the outward current is also composed of two types of currents: the rapidly activated delayed rectifier potassium current (I_{Kr}) and slowly activated delayed rectifier potassium current (I_{Ks}). Both remain present and continue to repolarize until phase 3. At the plateau phase, three Na^{+} ions are moved into the cell in exchange for each Ca^{2+} ion by the Na^{+}/Ca^{2+} exchanger, generating inward $I_{Na\text{-}Ca}$. Shifts in the

balance of these inward and outward currents can either increase or decrease the action potential duration (APD), respectively, along with QT interval prolongation or shortening (Borchert *et al.*, 2006).

Phase 3

Phase 3 is a rapid repolarization process, caused by I_{Ks} and I_{Kr}, to limit the APD (Sanguinetti and Jurkiewicz, 1990; Matsuura *et al.*, 1987). The Ca^{2+} channels become inactivated during this phase. Finally, the inward K^+ current (I_{K1}) ends the repolarization phase. The net K^+ efflux restores the resting intracellular gradient to –90 mV.

1.4.2 Cardiac action potentials and basic mechanisms of cardiac arrhythmias

In general, two basic mechanisms, including abnormal impulse formation and reentry cause active cardiac arrhythmias. Abnormal impulse formation is induced by triggered activity and spontaneous automaticity. Reentry has three subtypes: reflection, circus movement reentry, and phase-2 reentry (Antzelevitch, 2001a). Triggered activity and reentry are two most important mechanisms for initiation and maintenance of cardiac arrhythmias. Such arrhythmias are usually initiated by triggered activity, and are maintained by the reentrant pathway.

1.4.2.1 Trigger activity

Afterdepolarization is an underlying phenomenon of trigger activity that occurs with abnormal depolarization of cardiomyctes, which probably leads to additional oscillations of membrane potentials. The generation of abnormal impulse is a so-called triggered activity (Volders *et al.*, 2000). The oscillatory events may increase the risk of extrasystoles that can develop into torsades de pointes, tachycardia, and atrial fibrillation, depending on their individual mechanisms. There are two types of afterdepolarization (Fig. 1.6): early afterdepolarization (EAD) and delayed afterdepolariztion (DAD), each of which has specific mechanisms to trigger cardiac arrhythmias. The EAD occurs during the inciting action potential (Fig. 1.6A), and it interrupts phase-2 or -3 of the action potential leading to torsades de pointes and tachycardia. Phase-2 EAD occurs at voltage around –30 mV that is more positive than the voltage levels for phase-3 EAD. The EAD-induced arrhythmias are often based on the setting of action-potential prolongation, and are

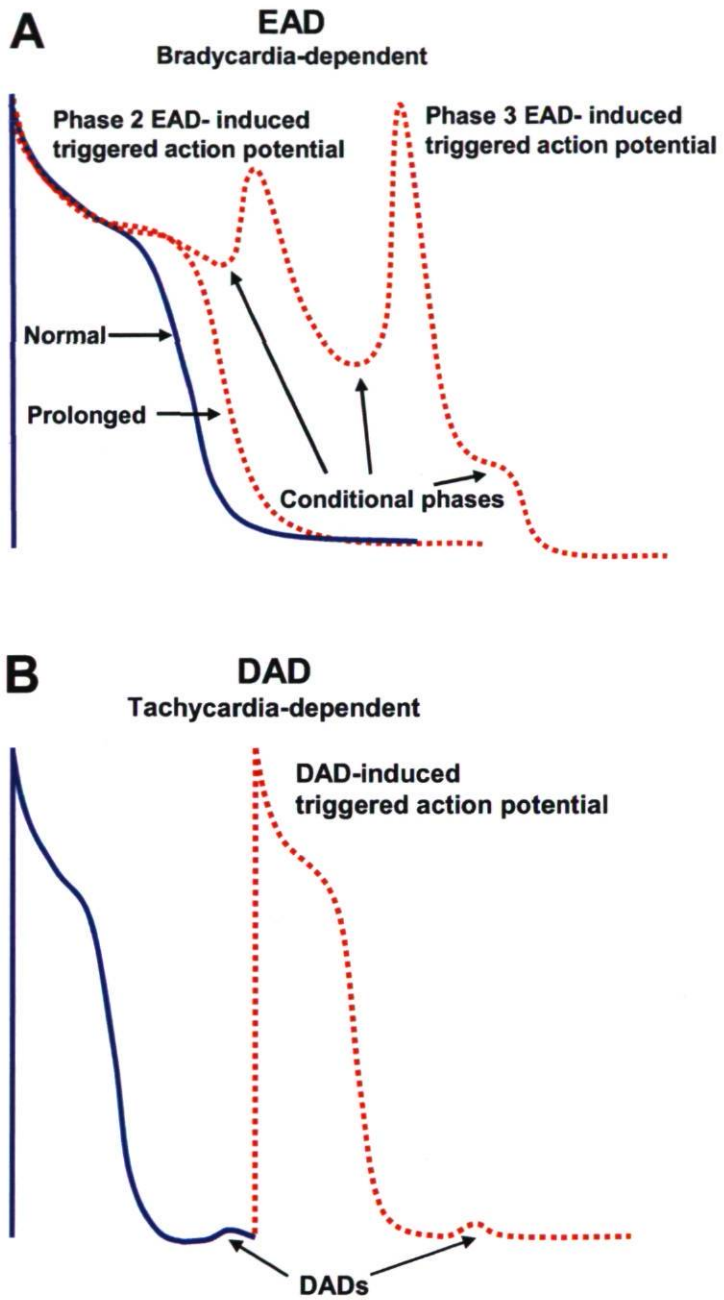

Figure 1.6: Early (EAD) and delayed (DAD) afterdepolarizations and EAD- and DAD-induced triggered action potentials. (A) Phase 2 EAD and phase 3 EAD-induced APs in canine isolated Purkinje fiber preparation treated with d-sotalol (I_{Kr} block). The conditional phase of EAD is defined as the time interval spanning from the moment when membrane potential starts to deviate from normal course to the moment that immediately precedes the EAD upstroke or downstroke. (B) DAD and DAD-induced triggered activity in canine ventricular preparation induced by rapid pacing in the presence of isoproterenol (β-adrenergic agonist, augmenting intracellular calcium activity). Modified from (Burashnikov and Antzelevitch, 2006).

precipitated by the bradycardia or long cardiac pause. The currents involved in the prolongation of the action potential are likely to induce the formation of EAD, primarily including $I_{Ca\text{-}L}$, persistent I_{Na}, $I_{Na\text{-}Ca}$, I_{Kr}, and I_{Ks} (Roden and Spooner, 1999). An increase in $I_{Ca\text{-}L}$ (January and Riddle, 1989) or in a persistent I_{Na} (Fabritz *et al.*, 2003; Tian *et al.*, 2004) may lead to phase-2 EAD. The increased $I_{Na\text{-}Ca}$ (Volders *et al.*, 2000; Burashnikov and Antzelevitch, 1998) and decreased I_{Kr} (Clancy and Rudy, 2001) are thought to be largely responsible for both phase-2 and phase-3 EAD. Interestingly, I_{Ks}-induced EAD was observed in the patient only in the presence of adrenergic stimulation (Shimizu *et al.*, 1998).

DAD is referred to as the abnormal depolarization interrupting phases 2 to 4 of the cardiac action potential (Fig. 1.6B). It occurs after a full repolarization, but before the initiation of the next cardiac action potential (Volders *et al.*, 2000). The underlying mechanisms of DAD are attributed to the elevated cytosolic Ca^{2+} concentration, a condition that triggers spontaneous Ca^{2+} release from the SR during periods of repolarization. Ca^{2+} overload may be accelerated by digitalis toxicity, β-adrenoreceptor stimulation, and low extracellular potassium. DAD events also induce ventricular tachycardia and fibrillation, but they are precipitated in the background of rapid heart rates (Priori *et al.*, 1999).

1.4.2.2 Reentry

Reentry is an important mechanism to initiate and maintain the abnormal impulse formation leading to tachycardiac arrhythmias such as Wolff–Parkinson–White (WPW) syndrome, paroxysmal supraventricular tachycardia (PSVT), atrial fibrillation/flutter (AF/AFL), and ventricular tachycardia/fibrillation (VT/VF).

Reentry occurs when an abnormal impulse, usually a premature activity, continues to propagate and reexcite the heart after expiration of the refractory period under certain required conditions: First, two areas in the myocardium must differ in conductivity or refractoriness and be able to form a closed electrical loop. It has long been known that ventricular myocardium is not homogeneous in electrical conductivity, but is composed of at least three cell types with distinct heterogeneities of electrophysiological and functional properties: epicardial, M, and endocardial cells (Antzelevitch *et al.*, 1999). These three principal ventricular myocardial cell types make a major difference in phase 1 and phase 3 repolarization characteristics that give variable action potential periods and cause transmural repolarization of APD and refractoriness. Normally, M

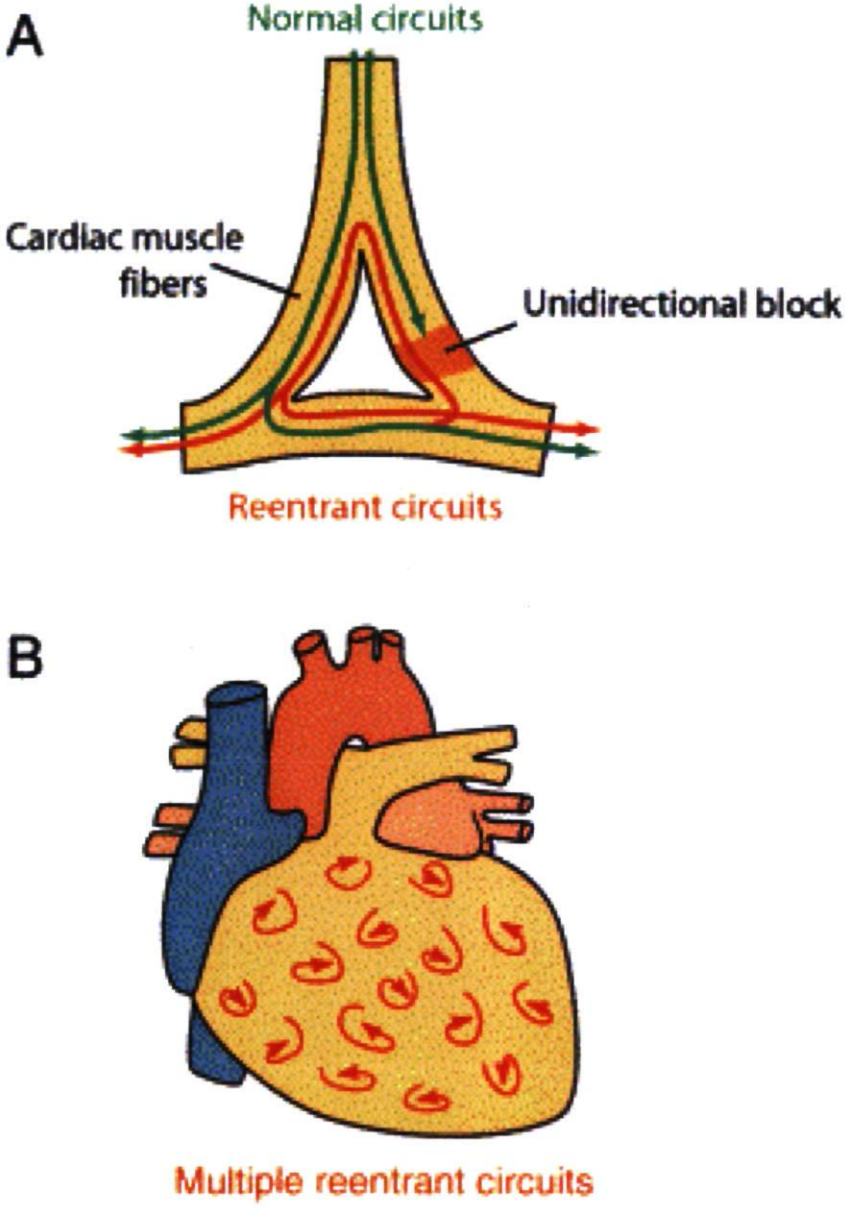

Figure 1.7: Unidirectional Block and Reentry, a Fundamental Mechanism of Arrhythmia. (A) Abnormal cardiac repolarization, conduction, or intracellular calcium homeostasis can lead to episodic unidirectional block, a substrate for arrhythmia. Green arrows represent the normal conduction in a bifurcated pathway. Conduction is blocked in an area of refractory tissue (unidirectional block). If conduction velocity is slowed, then reentry through area of refractory tissue can occur (red arrows). (B) Multiple reentrant circuits (multiple curved arrows) is a mechanism of ventricular fibrillation, the cause of sudden death (Keating and Sanguinetti, 2001).

cells could attenuate the heterogeneities by coupling cell-to-cell inherent differences. Transmural reentry would occur when dysfounction of M cells decouples such heterogeneities between different layers, and generates reentrantable electrical loops in the inact heart (Lesh *et al.*, 1989). The closed electrical loop establishes a reentrant circuit for impulse propagation. Then, a unidirectional block in one pathway, which allows conduction propagate in one direction but blocks propagation in the opposite direction must be established. The conducting period around the loop must be slow or long enough to recover from refractory period and finally, the initially blocked pathway must be excited to enable conduction of a retrograde impulse, and then complete the loop. If all the required conditions are met, reentry will occur as shown in Figure 1.7.

1.4.3 $Na_v1.5$ channel modulations

The proper modulation of $Na_v1.5$ is critical for normal cardiac functions. Although the major properties of cardiac Na^+ channels can be expressed by $Na_v1.5$ itself, they may still behave very differently depending on associated impact factors to transduce various signal cascades. The associated factors include ankyrin proteins, caveolin-3, β-subunits, telethonin, 14-3-3 protein, α-actinin-2, C-terminus interacting proteins, and phosphorylation proteins (Fig. 1.8). C-terminus interacting proteins include Nedd4/Nedd4-like family, fibroblast growth factor homologous factor 1B, Ca^{2+}/calmodulin complex, and syntrophin proteins. Phorsphorylation proteins include protein kinase A, protein kinase C, adenosine monophosphate-activated protein kinase, and tyrosine kinase. These modulatory proteins may influence channel activities, cellular localization, cellular excitability, and expression levels. A large part of these factors are actually various proteins that interact with $Na_v1.5$ to form a macromolecular complex to modulate $Na_v1.5$ properties.

1.4.3.1 Modulation by ankyrin proteins

Ankyrin proteins, encoded by three distinct genes *ANK*1, *ANK*2, and *ANK*3, are a family of membrane adaptor proteins that can anchor membrane proteins to the actin and spectrin cytoskeleton (Cunha and Mohler, 2006), thereby attaching ion channels to specific domains in the plasma membrane (Mohler *et al.*, 2003). Ankyrins typically contain three functional domains,

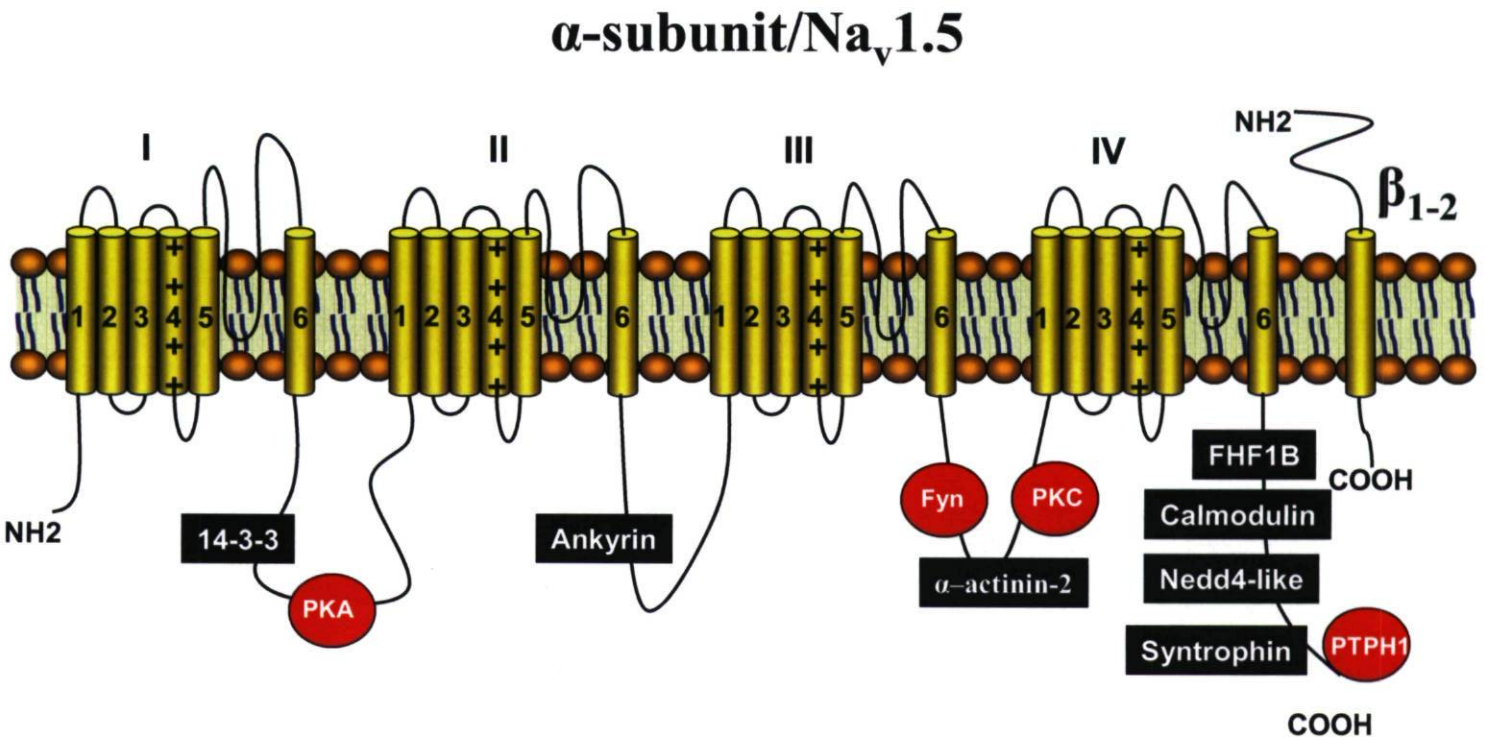

Figure 1.8: Schematic representation of the α-subunit of Na$_v$1.5, two associated β-subunits, and interacting proteins. These proteins include FHF1B, calmodulin, Nedd4-like and syntrophin that interact with the C-terminus of Na$_v$1.5, the 14-3-3 protein interacting with the I-II linker, ankyrin interacting with the II- III linker, and α-actinin-2 interacting with III-IV linker. Four kinases/phosphatases (red), PKA and PTPH1 interact with the the I-II linker and C-terminus respectively, while PKC and Fyn interact with III-IV linker. The extracellular domain of the β1 subunit interacts with the α-subunit loop as shown (dotted lines); the β2 subunit binds covalently to the α subunit via a disulfide bound. Cav-3, telethonin, and AMPK have not been shown here. Modified from (Abriel and Kass, 2005).

including the membrane-binding domain, spectrin-binding domain, and regulatory domain (Moss and Kass, 2005). Both ankyrin-B (encoded by *ANK* 2) and ankyrin-G (encoded by *ANK* 3) are present in the heart. Mutations *ANK* 2 and *ANK* 3 have been associated with different types of cardiac arrhythmias. In cardiomyocytes, ankyrin-B has been detected in the t-tubules, which affects cardiac electrical activity by binding to many cytoplasmic proteins, such as Cl^-/HCO_3^- exchanger, the Na^+-K^+-ATPase, voltage-sensitive Na^+ channels, the Na^+/Ca^{2+}exchanger, and Ca^{2+}-release channels. In general, the loss of function in ankyrin-B mutant channels causes LQTS type 4 (LQT4) and the resulting cardiac arrhythmias in two ways: (1) by combined disruption in the cellular organization of transporters, including the Na^+-K^+ pump, Na^+/Ca^{2+}exchanger, and inositol-1, 4, 5-trisphosphate receptors; and (2) by altering Ca^{2+} signalling in adult cardiomyocytes, thereby triggering arrhythmias (Mohler *et al.*, 2003; Mohler *et al.*, 2004b; Mohler *et al.*, 2003; Mohler *et al.*, 2004b). In addition to LQT4, dysfunction of ankyrin-B can cause drug-induced LQTS and sudden cardiac death, giving rise to the "ankyrin-B cardiac syndrome" (Mohler *et al.*, 2007).

Ankyrin-G is localized to both t-tubules and intercalated discs with a similar staining pattern to that of Na^+ channels (Mohler *et al.*, 2004b). It directly interacts with a specific ankyrin-binding motif containing a conserved 9-amino acid sequence in the linker of the II-III linker. A *SCN5A* mutation E1053K in that binding motif disrupts the interaction between $Na_v1.5$ and ankyrin-G, which reduces expression of channels on the cellular membrane in the affected cardiomyocytes. E1053K channels also slower their gating kinetics, and shift the voltage-dependent activation in the hyperpolarizing direction with an enhanced slow inactivation and closed-sate inactivation. The loss-of-function properties directly result in corresponding BrS (Mohler *et al.*, 2004a).

1.4.3.2 Modulation by caveolin-3 (Cav-3)/ dystrophin/ syntrophin

Recently, the concept of lipid microdomains has been proposed to control protein targeting and protein–protein interactions. Caveolae is a small invaginated membrane structure best characterized by the lipid raft, which is a liquid-ordered phase microdomain (Maguy *et al.*, 2006). Caveolins are the specific structural proteins necessary for the formation of caveolae. Caveolae 1 (Cav-1) and 2 (Cav-2) are coexpressed in most cell types, whereas caveolin -3 (Cav-3) is particularly abundant in skeletal and cardiac myocytes (Williams and Lisanti, 2004). $Na_v1.5$ and Cav-3 proteins are colocalized to plasma membrane (Shibata *et al.*, 2006; Yarbrough *et al.*,

2002b), so Cav-3 may directly play important roles in maintenance of normal function of $Na_v1.5$ channels. Cav-3 mutations have been found in patients with neuromuscular diseases, such as limb-girdle muscular dystrophy and rippling-muscle disease (Williams and Lisanti, 2004), and more recently in patients with LQT9 (Vatta *et al.*, 2006) and sudden cardiac death (Cronk *et al.*, 2007). Cardiac Cav-3 mutations may produce life-threatening events by increasing the persistent I_{Na} that leads to propagation of cardiac action potentials.

Cav-3 participates in the regulation of $Na_v1.5$ function via G-protein pathway, which is a direct pathway of β-adrenergic (βAR) modulation. The stimulatory G-protein subunit (Gαs), may increase the number of functional $Na_v1.5$ channels in the sarcolemma (Matsuda *et al.*, 1992). The resulting I_{Na} of $Na_v1.5$ channels increases by 45% within ten minutes without affecting their single channel characteristics or voltage-dependent inactivation process. In addition, the increased I_{Na} can be completely abolished by anti-cav-3 antibodies (Yarbrough *et al.*, 2002a). This evidence supports the hypothesis that βAR stimulation in Gαs-modulation manner activates the caveolae and thus upregulates $Na_v1.5$ channels at the cellular membrane (Matsuda *et al.*, 1992).

Dystrophin is also a component of caveolae (Doyle *et al.*, 2000), which may indicate another pathway of Cav-3 regulation on $Na_v1.5$ channels through dystrophin multiple-protein complex. Protein syntrophin may provide a direct functional link between $Na_v1.5$ channels and dystrophin complex to the actin cytoskeleton that is also essential for fully functional $Na_v1.5$ channels (Undrovinas *et al.*, 1995). A PDZ [**P**ostsynaptic density protein-95, (PSD95), **D**rosophila disc large tumor suppressor (DlgA), and **Z**onula occludens-1 protein (zo-1)] domain of syntrophin acts as a binding site to the C-terminus of $Na_v1.5$. Nitric oxide synthase, a part of dystrophin complex, is thought to bind directly to syntrophin and to Cav-3, playing a role in myocardial ischemia (Shi *et al.*, 2000; Feron *et al.*, 1996).

1.4.3.3 Modulation by β-subunits

The β-subunits may regulate the properties of α-subunits in the heart by interacting with specific areas of α-subunits with various effects in different expression systems. β_1- and β_3- subunits are noncovalently bound to α-subunits, whereas β_2- and β_4-subunits covalently interact with α-subunits through disulfide bonds. The modulation effects and their mechanisms are subunit-specific. Coexpression of β_1-subunits with $Na_v1.5$ showed variable effects in different expression

systems, and β_1-subunits may increase current densities and shift the steady-state inactivation in a positive direction in HEK 293 cells (Valdivia *et al.*, 2002b), but no effects on steady-state inactivation were observed in *Xenopus* oocytes (Fahmi *et al.*, 2001; Nuss *et al.*, 1995; Qu *et al.*, 1995a). Also, β_1 may modulate the properties of $Na_v1.5$ by interacting with ankyrins B and G, and CaM to fulfill its role as a macromolecular complex (Meadows and Isom, 2005). Modulation of splice variants of β_1 on $Na_v1.5$ has not yet been characterized owing to their low expressed levels in the heart. β_2, is thought to have no function in heart, although this remains controversial (Malhotra *et al.*, 2001). Similar to the effects of β_1, β_3 coexpression with $Na_v1.5$ significantly increases the Na^+ current amplitudes with depolarizing shift in inactivation process and faster recovery from inactivation in *Xenopus* oocytes (Fahmi *et al.*, 2001). Because β_3 is primarily localized to t-tubules whereas $Na_v1.5$ predominantly targets to the intercalated discs, it was hypothesized that β_3 may interact with one of the noncardiac voltage Na^+ channels that are expressed in the cardiac muscle (Maier *et al.*, 2004; Pereon *et al.*, 2003). β_4 plays an important role in the maintenance of cardiac electrical activities. When β_4 was mutated, a persistent I_{Na} of $Na_v1.5$ increased to cause prolongation of cardiac action potentials leading to LQTS type 10 (LQT10) (Medeiros-Domingo *et al.*, 2007).

1.4.3.4 Modulation by telethonin

$Na_v1.5$ has been known to exist in the jejunal circular smooth muscle cells, so $Na_v1.5$ mutations can cause gastrointestinal symptoms in patients with LQT3. Telethonin, a 19-kDa protein encoded by *TCAP* gene, is colocalized with $Na_v1.5$ in the human gastrointestinal smooth muscle. Telethonin has an important function to act as a stretch-sensor protein in muscle (Knoll *et al.*, 2002) through phosphorylation by titin kinase (Mayans *et al.*, 1998) and protein kinase D (Haworth *et al.*, 2004). The *TCAP* mutation (R76C) can cause intestinal pseudo-obstruction by altering the electrical properties of $Na_v1.5$ with changes of a shift in steady-state activation in a hyperpolarizing direction that leads to double-increased window currents (Mazzone *et al.*, 2008).

1.4.3.5 Modulation by 14-3-3 Proteins

The 14-3-3 family has seven members involved in cell signaling, cell growth, division, adhesion, differentiation, apoptosis, and ion-channel regulation. The 14-3-3 family members form a highly conserved cytosolic acidic protein expressed widely in various organisms and tissues, which is

especially colocalized with $Na_v1.5$ in the intercalated discs of cardiomyocytes (Aitken *et al.*, 1992). Thus, 14-3-3 family members may interact with $Na_v1.5$ and modulate $Na_v1.5$ functions in the heart. Particularly, it was found that 14-3-3 η, the last member of 14-3-3 family, can modulate $Na_v1.5$ biophysical properties by binding to the I-II linker (Allouis *et al.*, 2006). Coexpression of 14-3-3 η and $Na_v1.5$ in Cos-7 cells shifts the steady-state curve in a hyperpolarizing direction, and slows recovery from inactivation.

1.4.3.6 Modulation by α-actinin-2

The *ACTN2* gene encodes α-actinin-2, a second isoform of the α-actinin family. These rod-shaped, approximately 100 kDa proteins are composed of an N-terminal actin-binding domain, four central spectrin-like repeat motifs (SRM), and a C-terminal calponin homology domain (CH) that form antiparallel dimers (Beggs *et al.*, 1992). α-actinin-2 has been known to regulate the functional expression of the K^+ channels (Fedida *et al.*, 1999) and help maintain cytoskeleton organization (Djinovic-Carugo *et al.*, 2002). Our group found that α-actinin-2 is also co-localized with $Na_v1.5$ channels along the Z-line of cardiomyocytes and in the plasma membrane, binding to III-IV linkers of $Na_v1.5$ through its SRM. Furthermore, the biophysical data showed that co-expression of α-actinin-2 can increase cellular surface expression of $Na_v1.5$ without affecting gating properties (Ziane *et al.*, 2010).

1.4.3.7 Modulation by the C-terminus interacting proteins

The C-terminus is particularly critical in the $Na_v1.5$ modulation, because it contains several protein–protein interaction motifs that mediate interactions with Nedd4/Nedd4-like family, fibroblast growth factor homologous factor 1B, Ca^{2+}/calmodulin complex, and syntrophin proteins. The modulation effects of syntrophin proteins (more details in 1.4.3.2) will be described in other sections of this thesis.

1.4.3.7.1 Nedd4/Nedd4-like Family

The Nedd4/Nedd4-like family belongs to the members of the ubiquitin-protein ligase enzymes celled E3s. Ubiquitin, a small 76-amino acid protein, covalently binds to its target proteins, which include $Na_v1.5$ channels. This interaction is known as ubiquitination (Hicke and Dunn, 2003). The Nedd4/Nedd4-like family is the key regulatory determinants in the $Na_v1.5$-ubiquitination

reaction, since they are known to bind specifically to the PY motif in the C-terminus of $Na_v1.5$. The PY motif contains the consensus sites in residues proline (P) 1974 and tyrosine (Y) 1977 with a sequence of XPPXY (Rotin *et al.*, 2000). The resulting modulation changes induced by the Nedd4/Nedd4-like family showed a decreased I_{Na} without affecting other gating properties in HEK 293 cells or in *Xenopus* oocytes because of an increase in the internalization rate of $Na_v1.5$ channels expressed in cellular membrane (van Bemmelen *et al.*, 2004; Abriel *et al.*, 2000).

1.4.3.7.2 Fibroblast growth factor homologous factor 1B (FHF1B)

FHF1B belongs to the fibroblast growth factor family which composes to date isoforms FHF 1 through 4. FHF1B was first associated with $Na_v1.9$ (Liu *et al.*, 2001). This protein was recently found to be expressed in the cardiac tissues, where FHF1B probably acts as a scaffold to adapt the protein kinase to channels. The binding site of FHF1B was selectively confined to the proximal part of the C-terminus in $Na_v1.5$, which results in altered gating and a shift in the steady-state inactivation toward hyperpolarizing direction, without affecting other gating processes (Liu *et al.*, 2003a). Interestingly, several LQT3 and BrS mutations are located in the region from amino acid 1,773 through 1,832, and they may interact with FHF1B. For example, the LQT3 mutation D1790G could disrupt the binding of this protein with $Na_v1.5$, normalizing the shift of steady-state inactivation induced by FHF1B (Wehrens *et al.*, 2000).

1.4.3.7.3 Ca^{2+}/calmodulin-dependent protein kinase II (CaMKII)

Intracellular Ca^{2+} is a major second messenger in the translation of electrical signals of cardiac action potentials into the mechanical activities of cardiac contraction by activating a number of Ca^{2+}-dependent proteins through phosphorylation. CaMKII is one of these proteins acting as a serine or threonine kinase in the heart to control Ca^{2+} influx. CaMKII has four isoforms (α, β, γ, and δ), of which δ is most abundant in the heart. In addition, α and β are confined to the nervous tissues, whereas γ is ubiquitously expressed in various tissues (Tobimatsu and Fujisawa, 1989). Each isoform has a catalytic domain, a central regulatory domain, and an association domain responsible for oligomerisation (Maier, 2005). There is an active site in the catalytic domain, which can fulfill phosphrylation on substrates when Ca^{2+}/camodulin (Cam) binds to the regulatory domain. Similar to calcium channels, $Na_v1.5$ also contains a consensus site in the form of IQXXXRXXXXR for Ca^{2+}/Cam-dependent phosphorylation. The IQ motif, the residues of

isoleucine (I) 1908 and glutamine (Q) 1909, is a specific binding site in the C-terminus of $Na_v1.5$ for such phosphorylation (Kim *et al.*, 2004; Tan *et al.*, 2002).

The first indirect evidence for CaMK modulation of $Na_v1.5$ was studied by coexpression of KN-93, a CaMK inhibitor, in HEK 293 cells (Deschênes *et al.*, 2002). Two cardiopathic conditions have recently been reported in the presence of overexpression of CaMKII-δ, such as the cardiomyocyte hypertrophy caused by CaMKII-δ_B (Ramirez *et al.*, 1997) and the heart failure caused by CaMKII-δ_C (Wagner *et al.*, 2006). CaMKII-δ_B is the nuclear isoform of CaMKII-δ, whereas CaMKII-δ_C is cytosolic isoform. CaMKII-δ regulates $Na_v1.5$ functions with some alterations of gating properties: shifting steady-state inactivation in the hyperpolarizing direction, enhancing slow inactivation with a slower recovery process, and significantly increasing persistent I_{Na}. Similar to the effects of $Na_v1.5$ mutation 1795insD, these alterations predominantly present with a loss of function at rapid heart rates characteristic of Na channel function: negative shifts of steady-state inactivation and enhancement of slow inactivation. At slow heart rates, the persistent I_{Na} becomes more predominant, leading to the prolongation of QT intervals with shortened effective refractory periods that easily trigger VT in the setting of heart failure (Wagner *et al.*, 2006).

1.4.3.8 Modulation by protein phosphorylation proteins

Phosphorylation by PKA plays an essential role in the signal transduction pathways that regulate cellular functions in response to extracellular signals, and in the control of intracellular processes. $Na_v1.5$ channels could be modulated traditionally by PKA and PKC phosphorylation. Recently, AMPK and tyrosine were also involved in the regulation of $Na_v1.5$ through the phosphorylation pathway.

1.4.3.8.1 Protein kinase A (PKA)

$Na_v1.5$ contains eight consensus sites for PKA-dependent phosphorylation, which are in the form of KRXXS*, RXXS*, or RXS* in the I-II linker. They are distinct from neuronal channels containing only five consensus sites. PKA recognizes such consensus sites for phosphorylation of a serine (S) or a threonine (T). $Na_v1.5$ is phosphorylated by PKA on two selective residue sites, Ser 526 and Ser 529 residues (Murphy *et al.*, 1996). In contrast, neuronal Na^+ channels have four

phosphorylation sites, such as serine residues at positions: 573, 610, 623, and 687 in rat $Na_v1.2$ sequence (Murphy *et al.*, 1993).

During phosphorylation, PKA is mainly activated in an indirect βAR manner, leading to an increase in intracellular cyclic AMP (cAMP) (Bers, 2002) that might have a maturational role in $Na_v1.5$ development. I_{Na} recorded in cultured neonatal cardiac cell showed a loss-of-function property: a significantly negative shift of steady-state activation and inactivation with shortening gating kinetics of inactivation. This loss-of-function effect was, however, corrected by co-culturing with membrane-permeant cAMP analogues (Lipka *et al.*, 1996). In addition, PKA could also be cross activated upon activation of the α-adrenergic receptors. For example, I_{Na} was unexpectedly increased by PMA, the α-adrenergic receptor stimulatory phorbol ester, in the presence of an inhibitor of conventional PKC. The increased effect was in turn eliminated by inhibition of PKA (Shin and Murray, 2001).

Phosphorylation of Na^+ channels regulates their ability to open or close in response to the changes in membrane potentials. There are two different modulation patterns by PKA in neuronal and cardiac channels: one decreases I_{Na} in neuronal channels and one increases I_{Na} in cardiac channels. I_{Na} of $Na_v1.5$ is increased without changing gating properties (Baba *et al.*, 2004; Hallaq *et al.*, 2006; Zhou *et al.*, 2000). In oocyte experiments, the increased I_{Na} can be abolished with the elimination of three RXR consensus sites in the I–II linker, which are known to mediate retention of proteins in the endoplasmic reticulum (ER) (Zhou *et al.*, 2002). These results suggest that more $Na_v1.5$ channels are exported from endoplasmic reticulum (ER) to cellular membrane by the PKA stimulation. Similar trafficking effects enhanced by PKA stimulation were also observed in HEK 293 cell labeled by green fluorescent protein (GFP) (Hallaq *et al.*, 2006), a tagged protein widely used in heterologous expression systems as a reporter molecule to monitor protein localization. Another study points out that "vesicular trafficking" may be responsible for the PKA-facilitated increase in I_{Na}. This idea is based on the studies showing that the increased I_{Na} could be interrupted by chloroquine (Baba *et al.*, 2004), that is an agent known to disrupt the transportation of membrane vesicles from Golgi complex to plasma membrane.

1.4.3.8.2 Protein kinase C (PKC)

PKC pathway is another phosphorylation pattern to modulate $Na_v1.5$ channels through only one phosphorylation site of S1505 residue in III-IV linkers (Qu *et al.*, 1996), which is equivalent to

the site of S1506 in the neuronal channels. In addition to this common position, three more sites have been found in neuronal Na^+ channels, including S554, S573, and S576 in I-II linkers (Cantrell *et al.*, 2002). PKCs are a family of eleven isozymes, which are divided into three groups based on their structures and activation requirements. They are conventional PKC (cPKC), novel PKC (nPKC), and atypical PKC (aPKC). The cPKC (isozymes: α, β_1, β_2, and γ) is Ca^{2+}-dependent with requirements of phospholipids, diacylglycerol, or phorbol esters for maximal activation. The nPKC (isozymes: δ, ε, η, and θ) is Ca^{2+}-independent, but still requires phospholipids and diacylglycerol for activation. The aPKC (isozymes: ζ and ι/λ) does not interact with Ca^{2+} or diacylglycerol, but is activated by phospholipids or free fatty acids (Battaini, 2001). So far, all isozymes except for γ and θ have been identified in the human heart (Shin *et al.*, 2000). In the rat heart, the isozymes were detected with different levels in certain developing period of the heart (Rybin and Steinberg, 1994).

In contrast to the modulation by PKA, PKC stimulation has been known to reduce I_{Na} of $Na_v1.5$ channels in ventricular cardiomyocytes and in *Xenopus* oocytes expressing $Na_v1.5$ through stimulation of α_1-adrenergic receptors (Weigt *et al.*, 1998; Shin and Murray, 2001). The reduction of I_{Na} may be owing to channel internalization. This hypothesis was tested by applying thymeleatoxin, an agent known to activate cPKC, to successfully inhibit I_{Na} of $Na_v1.5$ (Shin and Murray, 2001). Certain gating alterations may accompany the reduction of I_{Na}, giving a slow time constant and a negative shift in steady-state inactivation that is owed to the change of the inactivation gate III-IV linker (Murray *et al.*, 1997).

1.4.3.8.3 Adenosine monophosphate-activated protein kinase (AMPK)

AMPK, encoded by *PRKAG2* gene, is another type of serine/threonine protein kinase expressed in most mammalian cells, acting as a sensor that monitors the metabolic status of cells. It consists of three subunits, including a catalytic subunit (α) and two regulatory subunits (β and λ) (Arad *et al.*, 2007). Each α subunit contains a highly conserved phosphorylation site at residue T172 crucial for regulating AMPK function. Recently, a mutation T172D in *PRKAG2* gene has been found to modulate gating properties of $Na_v1.5$ channels and thus to induce a persistent I_{Na} accompanied with gating changes such as slowed open-state inactivation and the hyperpolarizing shift of steady-state activation (Light *et al.*, 2003). When mutant channels were expressed in myocytes, The APD was significantly prolonged, leading to potentially arrhythmogenic EADs. In

addition, mutations in the λ2 subunit, second isoform of the λ subunit, lead to several pathological changes in the heart, such as cardiac arrhythmias and cardiac hypertrophy (Gollob, 2003).

1.4.3.8.4 Tyrosine kinase

Tyrosine (Y) phosphorylation is also important for $Na_v1.5$ modulation by binding to III-IV linker. The modulation effects are balanced by the tyrosine kinase and the tyrosine phosphatase activities. The Fyn, a tyrosine kinase, could decrease the $Na_v1.5$ channel availabilities by shifting the steady-state activation in a depolarizing direction (Ahern *et al.*, 2005; Jespersen *et al.*, 2006), whereas PTPH1, a tyrosine phosphatase, showed the opposite effect (Ahern *et al.*, 2005). The phosphorylation site for tyrosine is probably located at the residue T1494 (Ahern *et al.*, 2005).

1.5 Cardiac Na^+ channelopathies

Ion channelopathies are a group of inherited diseases caused by impaired cellular function that results from alterations in control of the ion conductance through ion channels, leading to periodic paralysis in the skeletal muscle, cardiac arrhythmias, renal failure, epilepsy, migraine ataxia, and deafness (Ashcroft, 2006). Normal cardiac excitation and relaxation depend on normal depolarization and repolarization processes. Gene defect and structural abnormality can profoundly influence these two processes, leading to a variety of clinical manifestations ranging from asymptomatic to symptomatic. Many inheritable cardiac diseases are involved in the dysfunction of ion channels, such as K^+, Na^+, and Ca^{2+} channels. Mutations in *SCN5A* gene were initially identified in four families with LQT linked to chromosome 3 (Wang *et al.*, 1995a). Since then, many mutations in *SCN5A* have been associated with Brugada syndrome type 1 (BrS1) (Chen *et al.*, 1998), cardiac conduction disease (CCD) (Tan *et al.*, 2001), sick sinus node syndrome (SSS) (Benson *et al.*, 2003), atrial standstill (AS) (Groenewegen *et al.*, 2003b), atrial fibrillation (AF) (Olson *et al.*, 2005), and dialated cardiomyopathy (DCM) (Olson *et al.*, 2005). Overlapping syndrome can be seen in patients with more than one of these cardiac Na^+ channelopathies (Bezzina *et al.*, 1999). *SCN5A* mutations are also found in the sudden infant death syndrome (SIDS) (Schwartz *et al.*, 2000).

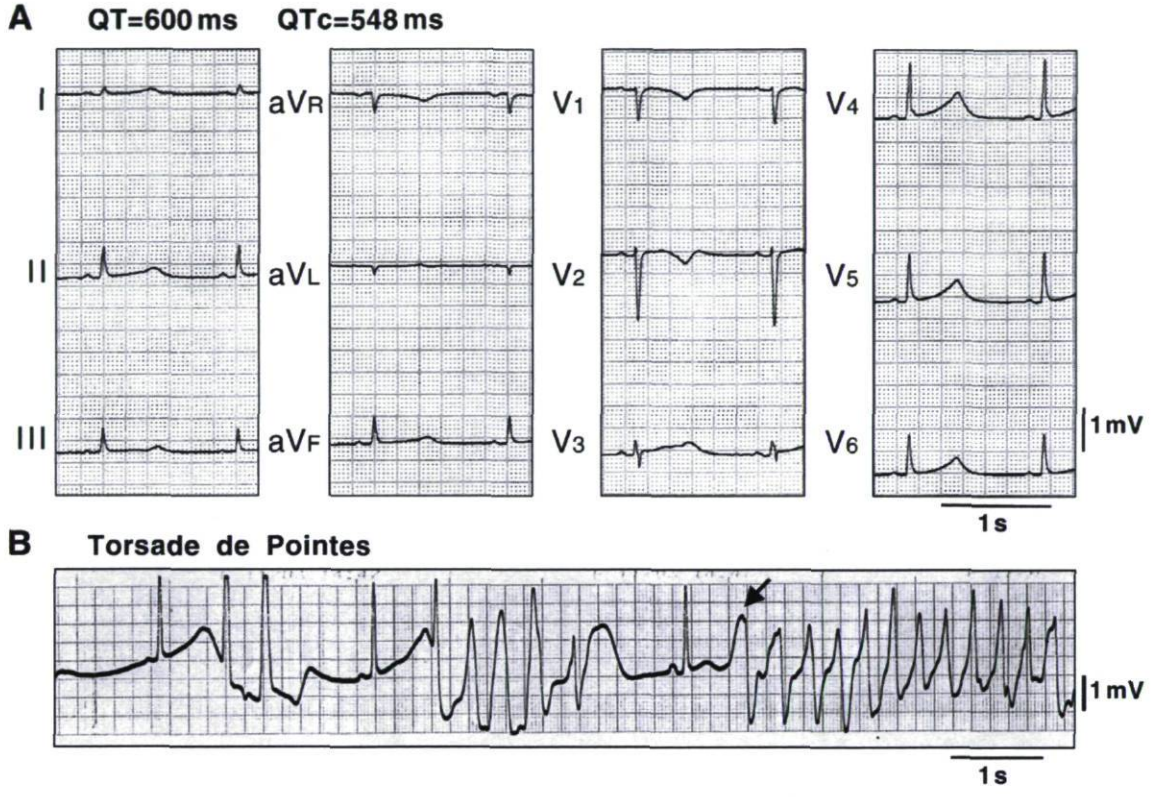

Figure 1.9: Twelve-lead electrocardiogram and torsades de pointes (TdP) in a patient with LQTS syndrome. (A) Remarkable QT prolongation (corrected QT (QTc) interval=548 ms) and a low amplitude T wave with a notched configuration are seen. (B) TdP was induced following the typical short–long–short initiating sequence (Shimizu, 2008).

1.5.1 Long QT syndrome (LQTS)

The LQTS is an inherited cardiac disease which is characterized by a prolonged corrected QT interval (QTc $\geq$ 0.45 seconds) with abnormal T waves in ECG (Fig. 1.9). Patients with LQTS are at a high risk of developing palpitations, syncope, seizures, and sudden cardiac death owing to specific ventricular arrhythmias, especially torsade de pointes (Schwartz *et al.*, 1975). Such clinical events can occur during strong emotional outpouring, sleep or at rest (Keating and Sanguinetti, 2001). There are two clinical types of LQTS, Romano-Ward syndrome (RWS, autosomal dominant) (Romano, 1965) and Jervell-Lange-Nielsen syndrome (JLNS, autosomal recessive) (Jervell and Lange-Nielsen, 1957), depending on genetic transmission patterns. RWS is seen in LQTS patients with normal hearing, whereas JLNS patients are associated with congenital neural deafness. LQTS can be sporadic or acquired. The severity and different prognoses of LQTS depend on the underlying genetic abnormality (Towbin *et al.*, 2001).

1.5.1.1 Genetics of LQTS

To date, ten defective genes have been identified as causing inherited LQTS: *KCNQ1* (LQT1) (Keating *et al.*, 1991), *KCNH2* (LQT2) (Jiang *et al.*, 1994), *SCN5A* (LQT3) (Wang *et al.*, 1995a), *ANK2* (LQT4) (Schott *et al.*, 1995), *KCNE1* (LQT5) (Splawski *et al.*, 1997), *KCNE2* (LQT6) (Abbott *et al.*, 1999), *KCNJ2* (LQT7, Anderson's syndrome) (Tristani-Firouzi *et al.*, 2002; Plaster *et al.*, 2001), *CACN1c* (LQT8, Timothy's syndrome) (Splawski *et al.*, 2004), *CAV3* (LQT9) (Vatta *et al.*, 2006), and *SCN4B* (LQT10) (Medeiros-Domingo *et al.*, 2007). Heterozygous mutations in all these genes cause RWS LQTS, whereas homozygous mutations in *KCNQ1* (Neyroud *et al.*, 1997) and *KCNE1* (Schulze-Bahr *et al.*, 1997) result in JLNS LQTS. Most of the LQTS patients were found to cluster in *KCNQ1* mutations (40 to 45%), *KCNH2* mutations (40 to 45%), and *SCN5A* mutations (5 to 8%). Patients with *SCN5A* mutations, however, have a higher risk of developing fatal cardiac events than those with *KCNQ1* and *KCNH2* mutations (Zareba *et al.*, 1998). Less than 1% of patients were reported to carry other LQTS forms. Most gene mutations of LQTS can markedly alter their specific ion channel properties, leading to a decrease in I_{ks} (*KCNQ1* and *KCNE1*), I_{kr} (*KCNH2* and *KCNE2*) and I_{K1} (*KCNJ2*), and an increase in persistent I_{Na} (*SCN5A*) and $I_{Ca\text{-}L}$ (*CACN1c*). Additionally, *ANK2* was the first non ion channel gene to cause LQTS by complexing with ion channel changes of a loss-of-function effect (details in section 1.4.3.1). *Cav3* and *SCN4B* are two ion channel- associated

proteins, which may be linked to LQTS by an increase in persistent I_{Na} of $Na_v1.5$. All the altered properties can cause prolonged ventricular repolarization, consequently resulting in QT prolongation in ECG. The prolonged action potential can lead to EADs, which may initiate cardiac arrhythmias (Tan *et al.*, 1995).

1.5.1.2 LQT3 Mutations and mouse models

To date, at least 80 LQT3 mutations have been identified. Most of these mutations are missense mutations with few cases of deletion and insertion mutations (Zimmer and Surber, 2008). LQT3 mutations are primarily located in exon 23, 26 and 28, corresponding to the III- IV linker, voltage sensors in domain IV, and the C-terminus of the Na^+ channel, which are important for stablization of the inactivation state in the Na^+ channel. Several LQT3 mutations have been characterized in either knock-in or transgenic over-expression mice. Three most common models for LQT3 have been established in mice using mutations: ΔKPQ (knock-in) (Nuyens *et al.*, 2001), 1795insD (knock-in) (Remme *et al.*, 2006) and N1325S (transgenic over-expression) (Tian *et al.*, 2004). These models are used for examining the consequences of a human LQT3 mutation in a physiological context, allowing the further investigation of arrhythmic mechanisms induced by LQT3 mutations. For example, ΔKPQ (Fabritz *et al.*, 2003) and N1325S (Tian *et al.*, 2004) models can develop EAD events, which are important for the formation of torsade de pointes. This finding provides in turn a chance to further investigate antiarrhythmic effects on such models (Stokoe *et al.*, 2007). Additionally, study results on 1795insD models are consistent with a hypothesis from expression of this mutant channels on heterologous expression systems. That is 1795insD mutant channels may cause overlapping phenotypes of LQT3 predominantly at slow heart rates and BrS1 predominantly at rapid heart rates (Remme *et al.*, 2006). The heart-rate variability is considered as an important environmental modifier. This model thus becomes a useful tool to study the impact of genetic and environmental modifiers on cardiac conduction and repolarization.

1.5.1.3 LQT3 and underlying mechanisms

LQT3 results from the *SCN5A* mutations characterized by a gain-of-Na^+ function that causes the net inward current at phase 2 of cardiac action potentials, leading to prolonged QT interval. Such a gain-of-Na^+ function is achieved by at least three patterns: an increased persistent I_{Na}

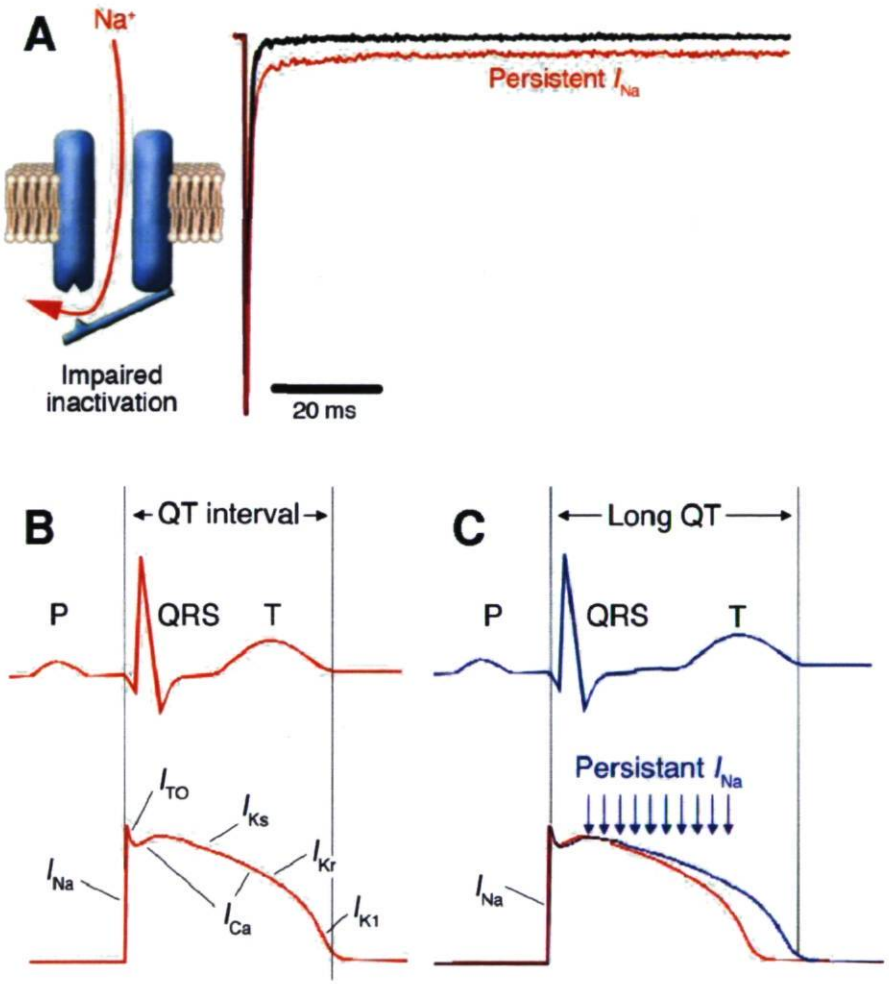

Figure 1.10: Schematic diagrams for a common mechanism for LQT3. (A) The defect is caused by incomplete closure of the inactivation gate (left panel) resulting in an increased level of persistent current (right panel, red trace) as compared with Na_VChs with normal inactivation (black trace). (B) Relationship of surface ECG (top) with a representative cardiac action potential (bottom). The QT interval approximates the action potential duration. Individual ionic currents responsible for different phases of the action potential are labeled. (C) Prolongation of the QT interval and corresponding abnormal cardiac action potential (blue) resulting from persistent Na^+ current. I_{Ca}, calcium current; I_{K1}, inward rectifier current; I_{Kr}, rapid component of delayed rectifier current; I_{Ks}, slow component of delayed rectifier current; I_{Na}, Na^+ current; I_{to}, transient outward current (George, Jr., 2005).

(Chandra *et al.*, 1998; Bennett *et al.*, 1995b), an enlarged window current (Wang *et al.*, 1996a), and an increased current in nonequilibrium condition (Clancy *et al.*, 2003). The most common mechanism for QT interval prolongation in LQT3 is from an increased persistent I_{Na} current that was first found in the mutation ΔKPQ, a three-amino-acid (K1505, P1506 and Q1507 in $hNa_v1.5$ sequence) deletion in the DIII-DIV linker (Chandra *et al.*, 1998). This mutant channel showed a disruption of fast-inactivation kinetics in the whole-cell patch recordings, which destabilizes the fast-inactivation state and causes incomplete closure of the inactivation gate during sustained depolarization (Fig. 1.10). At the single-channel level, the mutant channel shows multiple intermittent reopenings within the first 20 ms. The reopening behavior is thought to induce an increase in persistent I_{Na} over the plateau voltage range. The size of such increased persistent I_{Na} is extremely small, accounting for only 0.5 to 2% of the peak inward Na^+ current. The relationship between the persistent I_{Na} and prolonged action potentials, however, has been confirmed in computational modeling, resulting in a high correlation between Na^+ channel function and cardiac excitability (Bennett *et al.*, 1995b). Our laboratory found that a deletion mutation ΔQKP (Q1507, K1508, and P1509) also similarly increase the persistent I_{Na}. These data suggest that Q1507 residue is important for stabilization of inactivation state (Keller *et al.*, 2003).

A second is owed to steady-state channel reopening called window current. The window current represents the overlapped proportion of steady-state activation and inactivation curves. Shifts of activation and/or inactivation curves can increase the overlapping window so as to be suggested as a potential arrhythmia mechanism in LQT3 (Wang *et al.*, 1996a). A long slow (steady-state) positive ramp protocol was used to explain subtle changes in window current. This ramp protocol is designed to demonstrate noninactivated inward currents from LQT3 mutant channels. This non-inactivated inward current can in turn produce significantly depolarization at action potential plateau, leading to prolongation of QT interval.

A third was recently proposed in the study of mutation I1768V that originally showed a facilitated recovery from fast inactivation with a positive shift of steady-state inactivation. Although persistent I_{Na} was not found in functional studies, this mutant channel can still trigger a reopening behavior under nonequilibrium condition. The nonequilibrium protocol was induced by a negative ramp protocol following a 100-ms depolarization to +20 mV from holding potential -100 mV. This effect is able to prolong phase 2 of cardiac action potentials and trigger ventricular arrhythmias in the computer model easily (Clancy *et al.*, 2003).

1.5.2 Brugada syndrome (BrS)

Brugada syndrome (BrS) is another inherited cardiac disease that increases the risk of sudden cardiac death owing to the development of idiopathic ventricular fibrillation (IVF) in the absence of QT interval prolongation or structural heart disease. It is characterized by right bundle branch block (RBBB) and persistent ST segment elevation in right precordial leads (V1-V3) with normal QT interval. BrS is inherited in an autosomal dominant manner, and is more prevalent among East/Southeast Asians, particularly in Japan (Matsuo *et al.*, 2001) and Thailand (Nademanee *et al.*, 1997). There are three ECG patterns of BrS (Fig. 1.11). Type 1 is characterized by a coved ST segment elevation ≥2 mm (0.2 mV) followed by a negative T wave. This type is required for diagnosis (Wilde *et al.*, 2002a). Type 2 has a saddleback-shaped ST segment elevation for ≥ 2 mm following either a positive or a negative biphasic T wave. This type is an intermediate form of BrS ECG patterns, and thus needs further confirmation by a pharmacological challenge to convert to type 1 pattern or by genetic analysis (Plunkett *et al.*, 2003). Type 3 has either a saddleback or coved-shaped ST segment elevation ≤ 1 mm. The manifestation of the ECG would be more obvious when setting the right precordial leads up to the second intercostal space in some patients (Alings and Wilde, 1999). However, these ECG patterns are variable day-to-day or beat-to-beat, and may not always be present (Veltmann *et al.*, 2006). In patients with normal ECG manifestation, the characteristic BrS ECG pattern could be unmasked by administration of class Ic antiarrhythmic drugs (Brugada *et al.*, 2000a), vagotonic agents (Mizumaki *et al.*, 2004), α-adrenergic agents (Pastor *et al.*, 2001), β-adrenergic blockers (Miyazaki *et al.*, 1996), and cyclic antidepressants (Goldgran-Toledano *et al.*, 2002). Fever (Dumaine *et al.*, 1999; Mok *et al.*, 2003; Keller *et al.*, 2006), alcohol (Pilz and Luft, 2003), and cocaine (Ortega-Carnicer *et al.*, 2001) are also common factors that can unmask the BrS ECG pattern.

1.5.2.1 Genetics of BrS

During the past decades, at least seven BrS genes have been discovered, including *SCN5A* (BrS1) (Chen *et al.*, 1998), *GPD1L* (BrS2) (London *et al.*, 2007), *CACNA1C* (BrS3) (Antzelevitch *et al.*, 2007), *CACNB2* (BrS4) (Antzelevitch *et al.*, 2007), *SCN1B* (BrS5) (Watanabe *et al.*, 2008), *KCNE3* (BrS6) (Delpon *et al.*, 2008), and *SCN3B* (BrS7) (Hu *et al.*, 2009). *SCN5A* mutations directly show a loss-of-function in $Na_v1.5$ channels, which is also present in *SCN1B*, *SCN3B*, and *GPD1L* mutations. The mutation in the *SCN1B* gene failed to interact with $Na_v1.5$ proteins and to

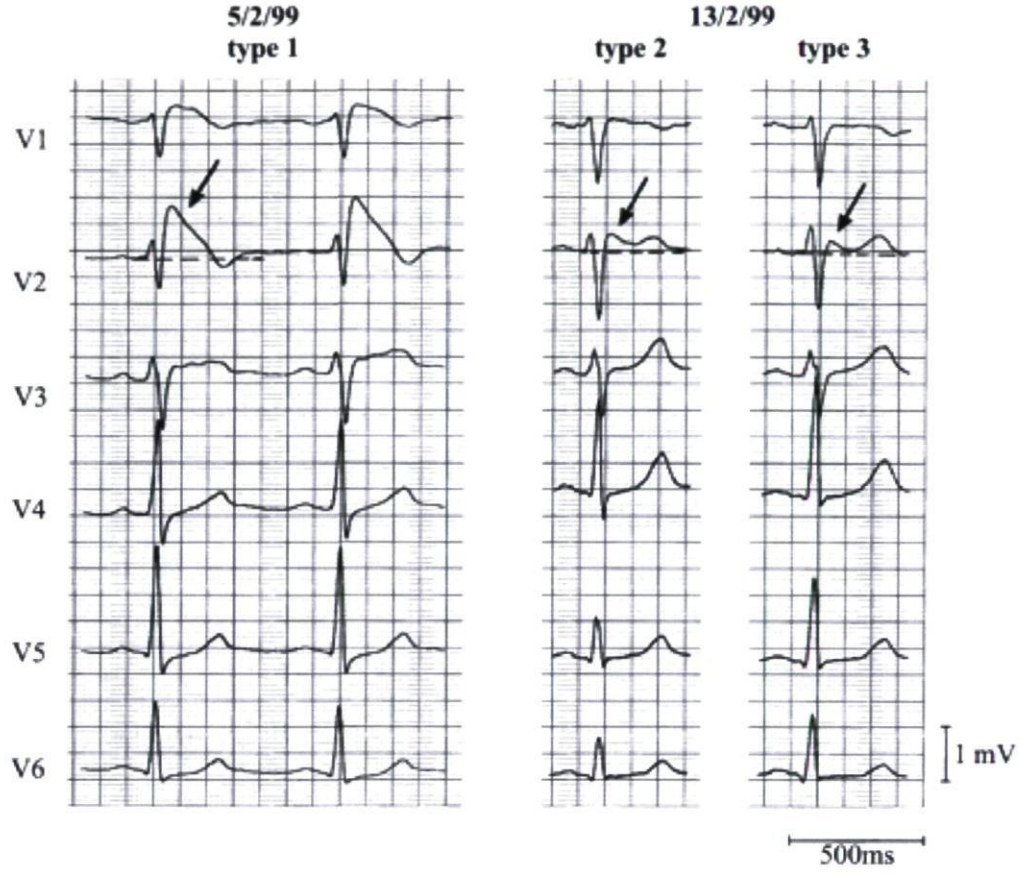

Figure 1.11: Three Types of ST-segment elevation generally observed in patients with the Brugada syndrome. Shown are precordial leads recorded from a patient diagnosed with the Brugada syndrome. Arrows denote the J-wave. Note the dynamic ECG changes occurring over a period of 2 days. The left panel shows a clear Type 1 ECG, which is diagnostic of the Brugada syndrome on February 5, 1999. A saddleback STsegment elevation (Type 2) is observed on February 7, 1999. The ST segment is further normalized on February 13, 1999, showing a Type 3 ECG (Wilde *et al.*, 2002b).

increase I_{Na} densities as normal β_1-subunits did. The *SCN3B* mutation reduced I_{Na} by disrupting the trafficking of $Na_v1.5$ proteins from the endoplasmic recticulum (ER) to sarcolemma. *GPD1L* was recently shown to inhibit the phosphorylation (e.g. PKC effects) of $Na_v1.5$ proteins (Valdivia *et al.*, 2009; Liu *et al.*, 2009). It was hypothized that the *GPD1L* mutation failed to inhibit this regulatory interaction, thus leading to a decreased I_{Na} density (Chahine, 2009). Loss-of-function in Ca^{2+} channels (e.g. $I_{Ca\text{-}L}$) has also been identified in *CACNA1C* and *CACNB2* mutations. Gain-of-function was recently found in *KCNE3* mutations by mediating I_{to} (Delpon *et al.*, 2008). In BrS patients, 15 to 30% carry *SCN5A* mutations (Alings and Wilde, 1999), 11 to12% carry *CACNA1C* and *CACNB2* mutations (Antzelevitch and Nof, 2008). A minor contribution to BrS cases comes from other genes, including *GPD1L*, *SCN1B*, *KCNE3*, and *SCN3B*. All gene mutations are able to directly or indirectly alter cardiac action potentials leading to BrS ECG patterns, depending on which particular ion channel is dysfunctional.

1.5.2.2 BrS1 mutations and BrS1 mouse models

BrS1 links to almost 100 mutations in *SCN5A*, which are widely located in all regions of Na^+ channels. Most of them are missense mutations with a small number of deletion, insertion, and frameshift cases (Zimmer and Surber, 2008). Some mutations in introns affect RNA splicing. These BrS1 mutations are widely located in all regions of Na^+ channels. A mouse model (*SCN5A* knock-out mice) has been established for studying BrS1 (Papadatos *et al.*, 2002). Homozygous knock-out mouse embryos usually die during eight to ten weeks of gestation due to severe cardiac defects such as a decrease in atrial and AV conduction, and an increase in inducibility of ventricular arrhythmias. In contrast, heterozygous mice show normal survival. Because loss-of-function is also the mechanism to cause CCD (details in section 1.5.4), the CCD phenotype can also be seen in this model. For this reason, this *SCN5A* knock-out mice was also used to study the genotype-phenotype relationship in CCD (Benson *et al.*, 2003).

1.5.2.3 BrS1 gating properties

Pathohysiological effects of BrS1 mutations are more complicated than those of LQTS because heterologously expressed Na^+ channel mutants display a broad variety of functional properties.

(1) Expression of a nonfunctional protein owing to premature termination of the polypeptide chain. The premature stop codon may be created when the mutation causes a frameshift (Keller *et*

al., 2005b; Bezzina *et al.*, 2003). The position of stop codons within the transcript results in failure to synthesize the polypeptide chain coded by one allele, and so disables synthesis of the Na^+ channel protein. Therefore, the Na^+ channels fail to express (Antzelevitch *et al.*, 2005; Shin *et al.*, 2007).

(2) Trafficking defects owing to altered processing of the protein. Mutant $Na_v1.5$ channels may not be properly trafficked to the sarcolemma, because they are retained within the ER. The retained proteins in the ER are consequently degraded by the quality control mechanism (Baroudi *et al.*, 2002; Baroudi *et al.*, 2001).

(3) Mutations within the Na^+-conducting pore. Some mutations may introduce an aberrant amino acid in the pore region. The resulting conformational changes within the pore may impede Na^+ permeability (Akai *et al.*, 2000).

(4) Synthesis of a channel protein with altered gating properties, which is also responsible for a decrease in cellular excitability. These changes include: (A) a positive shift in the voltage-dependent activation (Keller *et al.*, 2006); (B) a negative shift in voltage-dependent inactivation (Veldkamp *et al.*, 2000); (C) acceleration of inactivation kinetics of $Na_v1.5$ (Herbert and Chahine, 2006); (D) enhancement of closed-state inactivation (Viswanathan *et al.*, 2001); (E) entry of the Na^+ channel into an intermediate state of inactivation, from which it recovers more slowly (Veldkamp *et al.*, 2000). Interestingly, shifts in the voltage-dependence of activation and inactivation are not always consistent with the loss-of-function characterizations in some BrS1 mutations, depending on different expressing systems. For instance, T1620M mutation showed a positive shift of steady-state inactivation in *Xenopus* oocytes, whereas these was no effect on steady-state inactivation in tsA201 mammalian cells (Baroudi *et al.*, 2000).

1.5.2.4 BrS and underlying mechanisms

There are two hypotheses to explain the ST elevation in BrS ECG manifestations. One is known as the repolarization-disorder hypothesis, and the other is called the depolarization-disorder hypothesis. The repolarization-disorder hypothesis is referred to as nonuniform abbreviation of right ventricular epicardial action potentials (Fig 1.12). The cellular basis of this hypothesis is related to a net efflux of transmembrane current at the end of phase 1 of the ventricular epicardial action potential (Gima and Rudy, 2002). This phase results from the inactivated I_{Na} and the transient I_{to}, a major contributor to determination of the spike-and-dome morphology of the

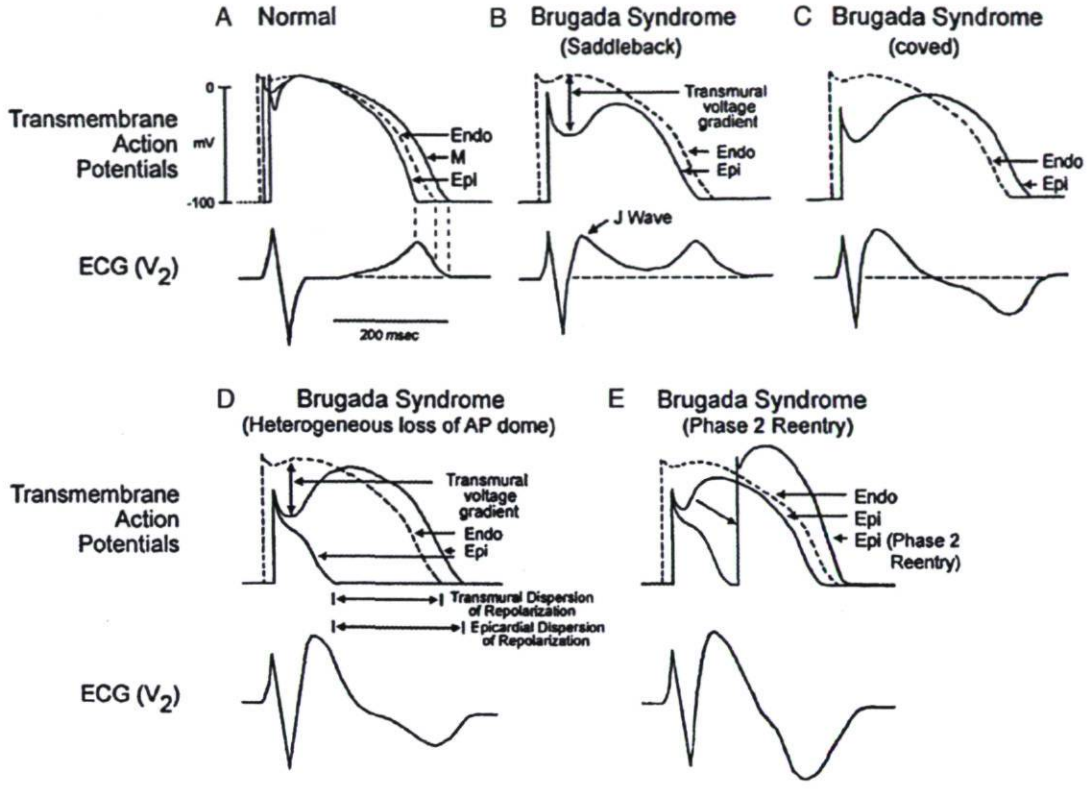

Figure 1.12: Repolarization disorder hypothesis in Brugada syndrome. Epicardial (Epi) myocytes of the right ventricle have larger transient outward current, Ito, than endocardial (Endo) myocytes, resulting in more prominent phase 1 repolarization in Epi than in Endo (A). Also, this causes stronger phase 1 repolarization in Epi than Endo in the presence of the same reduction in Na^+ current, leading either to saddleback ST elevation (B) or, with more phase 1 repolarization, coved-type ST elevation (C), secondary to electrotonic current between Epi and Endo. Furthermore, loss of AP dome ensues when Na^+ current is further reduced (D). If loss of AP dome occurs nonuniformly among Epi myocytes, phase 2 reentry may occur (E) (Antzelevitch, 2001b).

cardiac action potential. I_{to} is normally present in epicardial cells and absent in endocardial cells, particularly in the right ventricular epicardium. The I_{to} consequently produces a prominent "notch" in epicardium that can be more prominent by increasing I_{to} or decreasing I_{Na}, further resulting in an increase in the transmural voltage gradient during phase 1. The increased transmural voltage gradient corresponds to the J wave on surface ECG. Since the transmural voltage gradient is more obvious in the right ventricular epicardium, the ST segment elevation is the most common in right precordial leads V1-V3. Relatively increased I_{to} can also reduce the action potential dome and markedly shorten the APD in epicardium, leading to a relatively longer APD in endocardium. These changes cause the negative T wave in ST elevation. Additionally, the loss of the AP dome can lead to epicardial dispersion of repolarization and refractoriness, and promote reentrant arrhythmias in the form of VT/VF via a phase 2 reentry mechanism (Grant, 2005; Bezzina *et al.*, 2003). This hypothesis is supported by evidence that (1) ST elevation is provoked by the Na^+ channel blocker (Kimura *et al.*, 2004; Brugada *et al.*, 2000b) and the K_{ATP}^+ channel opener (Kimura *et al.*, 2004); (2) BrS phenotype is more prevalent in males owing to the presence of a more prominent I_{to} in males versus females (Di Diego *et al.*, 2002); (3) ST elevation is usually facilitated by slow heart rates (Matsuo *et al.*, 1998); (4) ST elevation is associated with reduced ejection time of right ventricle but not of left ventricle (Tukkie *et al.*, 2004). The transmural voltage gradient in this hypothesis failed to be demonstrated, however, in patients with BrS and transgenic mouse models.

In depolarization-disorder hypothesis, the ST elevation has been ascribed to selective conduction delay in the right ventricle, particularly in the right ventricular outflow tract (RVOT) (Fig 1.13). The delayed depolarization of the RVOT results in a voltage gradient that represents a more negative membrane potential than that of the right ventricle. The resulting driving force causes a current towards the RVOT, thus allowing lead V2, an ECG electrode positioned over the RVOT, to record a positive signal that produces the ST elevation. Then, the voltage gradient is reversed, giving a relatively positive membrane potential in the RVOT. V2 records a negative signal that forms a negative T wave following the elevated ST. Cardiac arrhythmias are the results of regional slow conduction by the reentry mechanism (Meregalli *et al.*, 2005).

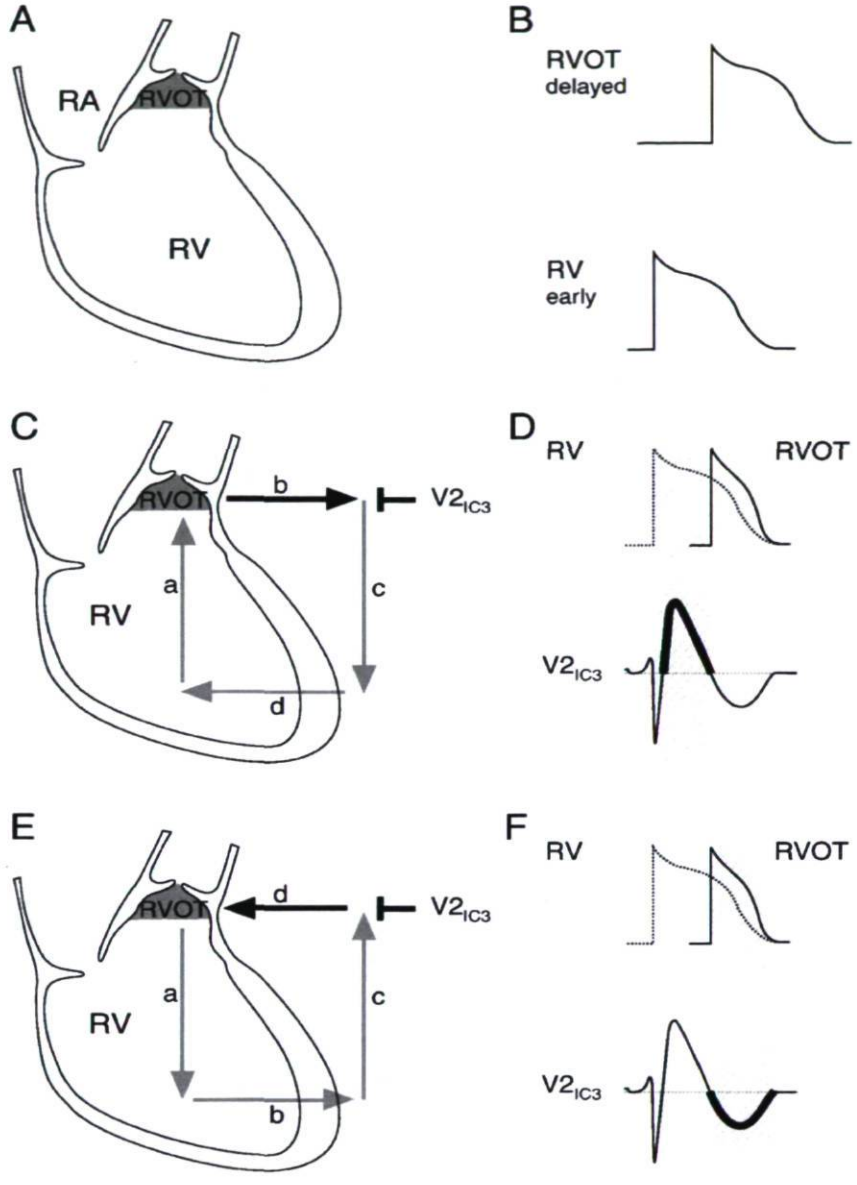

Figure 1.13: Depolarization disorder hypothesis in Brugada syndrome. (A) When conduction is delayed in the RVOT. (B) The action potential in the RVOT (top) is also delayed with respect to the action potential with respect to the action potential in the right ventricle (RV) (bottom). (C) The delayed conduction causes a relative positive membrane potential, thus driving the intercellular current to the RVOT (phase a, the grey arrow). Lead V2 in third intercostal space ($V2_{IC3}$) detects positive signals towards it (phase b, the black arrow). Then, currents pass back from the RVOT to the RV in the extracellular space (phase c, the grey arrow). Finally, currents flow from the exracellular space into the RV (phase d, the grey arrow) to complete a closed-loop circuit. (D) The early and delayed action potentials are detected (top) during phases from a to d, resulting in elevation of the ST segment at the bold-line region (bottom) at phase b and in descent of ST segment at phase d. (E) Following the upstroke of the delayed action potential, the potential gradients between the RV and RVOT are reversed. Lead $V2_{IC3}$ detects negative signals as currents pass away from it (the black arrow). (F) Consequently, the negative T wave (bottom) is observed at the corresponding blod-line region (Meregalli *et al.*, 2005).

1.5.3 Sudden infant death syndrome (SIDS)

SIDS is the leading cause of death during the first year of life among infants with multiple pathogenesis, including abnormalities in respiratory, cardiac, endocrine and potential neurological functions (Makielski, 2006). Higher attack rates of SIDS in some ethnicities indicate that genetic factors may play a role in the development of SIDS. This suggestion was supported by evidence that SIDS was found to have a prolonged cardiac repolarization as seen in LQTS (Schwartz *et al.*, 1998). S941N was first identified as a *SCN5A* mutation directly linked to SIDS in 2000 (Schwartz *et al.*, 2000). Since then, other *SCN5A* mutations (Ackerman *et al.*, 2001; Wedekind *et al.*, 2001; Plant *et al.*, 2006; Huang *et al.*, 2009) and *SCN5A* polymorphisms (Wang *et al.*, 2007a) have been found to be associated with SIDS. Most *SCN5A* mutations in SIDS increase the persistent I_{Na}, frequently in combination with other gating alterations such as early activation and delayed inactivation. The increased window current induced by A1330P mutant channels has also been reported to cause LQT3-related SIDS (Wedekind *et al.*, 2001). Recently, mutations in *Cav3*, the gene originally linked to LQT9 as mentioned earlier, were also found to be a causative genetic factor in the development of SIDS by regulating mutant channels to increase the persistent I_{Na} (Cronk *et al.*, 2007). Interestingly, a loss-of-function property with a hyperpolarizing shift of steady-state inactivation in a *SCN5A* mutation G1084S may be another contributor to the occurrence of SIDS (Otagiri *et al.*, 2008). In addition, a mutation in *GPD1L*, which was originally identified in BrS2, was reported to cause SIDS. Similar to the results of functional studies leading to BrS2, the peak I_{Na} was also decreased when co-expressed mutant channels and $Na_v1.5$ channels in HEK cells (Van Norstrand *et al.*, 2007).

1.5.4 Cardiac conduction disease (CCD)

CCD is characterized by progressive impairment of cardiac conduction system, such as the His-Purkinje system with right or left bundle branch block, and widening the QRS complex. In such conditions, cardiac impulse propagation may be interrupted to form complete atriventricular (AV) block probably along with syncope and even sudden death. Progressive cardiac conduction defect (PCCD), also called Lev-Lenegre disease, is the most common type of CCD (Probst *et al.*, 2003). The severity and the differential phenotypes depend on the underlying genetic abnormality. Interestingly, the severity of symptoms may increase with age in PCCD patients with mutation W1421X (Niu *et al.*, 2006). In general, the generation of CCD in *SCN5A*

mutations is also related to loss-of-Na^+ function, which is incompletely compensated by gain of function. G514C mutation gives such an example in that a positive shift has been observed in the steady-state activation by +10 mV (loss of function) and the steady-state inactivation by +7 mV (gain of function) (Tan *et al.*, 2001). This defect is not sufficient to induce BrS-like ECG patterns, but reduces the action potential upstroke that determines the rates of impulse propagation. In these conditions, cardiac conduction velocity has been confirmed to be reduced significantly by 20% in the computational studies, leading to the phenotypes of CCD (Tan *et al.*, 2001). Another incomplete compensation that causes CCD is achieved by enhancing slow inactivation for some mutations (G298S, D1595N, and T512I) (Wang *et al.*, 2002; Viswanathan *et al.*, 2003). The slight increase in slow inactivation could delay the recovery of Na^+ channels between successive stimulations that may cause a cumulative loss of function, leading to conduction abnormality (Veldkamp *et al.*, 2003).

1.5.5 Sick sinus syndrome (SSS)

Sick sinus syndrome (SSS) is caused by dysfunction of sinus node, which produces a group of sinus arrhythmias, including sinus bradycardia, sinus arrest, atrial standstill, and tachycardia-bradycardia syndrome. Sinus node is a cardiac structure located in the upper right atrium. This structure contains a cluster of cells that are responsible for the initiation of the automatic depolarization in the heart. It was found that I_{Na} is primarily involved in the formation of action potential upstroke in the peripheral sinus-nodal tissue (a latent pacemaker site), whereas $I_{Ca\text{-}L}$ is a major contributor to upstroke in the central sinus node (a normal leading pacemaker site) (Kodama *et al.*, 1997). This finding suggests that $Na_v1.5$ channels maybe essential for action potential propagation from the leading pacemaker site to the surrounding atrial tissue (Lei *et al.*, 2007). Recently, *SCN5A* mutations were found to cause SSS inherited in an autosomal recessive manner by screening pediatric patients with SSS from seven families. Functional studies expressing mutant channels into tsA 201 cells showed a loss-of-function feature characteristic of a reduced I_{Na}, a negative shift of steady-state inactivation and a slow recovery from inactivation (Benson *et al.*, 2003). Reduced expression of I_{Na} may lead to sinus bradycardia and may slow down sinoatrial conduction in heterozygous *SCN5A* knock-out mice, the specific model established to study sinus node dysfunction (Lei *et al.*, 2005). In addition, other loss of functions

in $Na_v1.5$ channels may impair the electrical coupling between pacemaker cells and their surrounding cells, leading to abnormal conduction activities that produce SSS phenotype.

1.5.6 Atrial standstill and atrial fibrillation (AF)

SCN5A mutations have been reported to be involved in atrial dysfunction, including atrial standstill and atrial fibrillation (AF). Atrial standstill is an uncommon arrhythmia that is diagnosed by bradycardia, absence of P waves, and junctional escape rhythm in ECG mainly due to the absence of electrical and mechanical activities in the atria. *SCN5A* mutations contribute to atrial standstill by a loss-of-function property to slow down the cardiac impulse conduction. The loss-of-function property could be either no functional expression of mutant channels (R367H) on membrane surface that generates a overlapping syndrome with BrS1 (Takehara *et al.*, 2004), or depolarizing shift in steay-state activation (D1275N) (Groenewegen *et al.*, 2003b), or a negative shift in steady-state inactivation (L212P) (Makita *et al.*, 2005). Single nucleotide polymorphism (SNP) of connexin 40 (Cx40) is a potential risk factor for the formation of atrial standstill. Cx40 is encoded by *GJA5* gene, and is a gap junction protein specifically expressed in the atrium and the specialized conduction system. These SNPs cause a decreased expression of Cx40, thus augmenting lost-of-function effects in mutations D1275N (Groenewegen *et al.*, 2003b) and L212P (Makita *et al.*, 2005), and consequently leading to atrial standstill.

Atrial fibrillation (AF) is the single most common arrhythmia in clinical practice, and is characterized by rapid and irregular activities in the atrium, leading to a series of rapid irregular P waves (400-600 bpm) and a subsequently irregular ventricular rhythm. The QRS complex is normal during AF. The most important risk factors for AF include age, hypertension, and heart disorders (Krahn *et al.*, 1995). Familial AF may, however, occur in the early years (< age 60). The term lone AF refers to AF patients affected by single genes, but in the absence of aforementioned risk factors (Chugh *et al.*, 2001). Recently, many mutations in six genes have been associated with lone AF patients. These lone AF genes include *KCNQ1* (Chen *et al.*, 2003), *KCNE2* (Yang *et al.*, 2004), *KCNJ2* (Xia *et al.*, 2005), *SCN5A* (Olson *et al.*, 2005), *KCNA5* (Olson *et al.*, 2006), and *GJA5* (Gollob *et al.*, 2006). Mutations in *SCN5A* gene have been reported in approximately 20% of patients with BrS1 (Bigi *et al.*, 2007), and in 2% of patients with LQTS (Johnson *et al.*, 2008). A common polymorphism H558R, present in one-third of the population, is a genetic risk factor for lone AF (Chen *et al.*, 2007). There is a discrepancy in

results of biophysical properties for lone AF, depending on the specific mutations. A loss-of-function property was found in several mutations, giving a decreased I_{Na} (H558R) (Chen *et al.*, 2007) and a negative shift in steady-state inactivation (N1986K) (Ellinor *et al.*, 2008). The decreased I_{Na} can slow down atrial conduction, which is a condition required for the maintenance of arrhythmias in the atrium by reentry mechanism. In contrast, functional study of M1875T showed a gain-of-function property with an increased I_{Na} and a positive shift in steady-state inactivation. The increased I_{Na} might cause failure of cardiomyocytes to repolarize, leading to EADs and triggered activity. In addition, the increase in I_{Na} might also increase conduction velocity and facilitate the maintenance of fibrillation (Makiyama *et al.*, 2008). K1493R is another mutation in *SCN5A* gene to cause AF by increasing window currents of mutant channels. The increased window current can lower the threshold for the action potential firing in atrial tissues (details in Chapter IV).

1.5.7 *SCN5A* mutation-associated dilated cardiomyopathy (DCM)

Dilated cardiomyopathy (DCM) is characterized by dilated cardiac chambers and reduced systolic function, which cause congestive heart failure. Patients with family history of DCM account for about 20 to 25% of idiopathic DCM cases, suggesting that DCM maybe an inherited disease (Michels *et al.*, 1992; Keeling *et al.*, 1995). Various mutations in genes encoding sarcomeric, cytoskeletal, and nuclear proteins have been known to be associated with the disease. Recently several *SCN5A* mutations have been identified as a cause of DCM since it was first linked to the *SCN5A* gene in 1996 (Olson and Keating, 1996). These mutations include two frameshift mutations, such as insertion of TG at position 2550-2551 (Olson *et al.*, 2005) and delQKP 1507-1509 (Shi *et al.*, 2008), and five missense mutations, such as T220I (Benson *et al.*, 2003), D1275N (Olson *et al.*, 2005), R814W (Olson *et al.*, 2005), D1595H (Olson *et al.*, 2005), and A1180V (Ge *et al.*, 2008). With exception of R814W, other mutations were found to be associated with complex clinical phenotypes, including SSS, AV block, atrial or ventricular arrhythmias, and LQT3. For this reason, biophysical properties showed a diverse alteration, including loss-of-function and gain-of-function changes in their gating properties. For loss-of-function mutations, D1275N was previously shown to exhibit a depolarizing shift of steady-state activation in AS patients (Groenewegen *et al.*, 2003b). R814W mutation showed changes of a decrease in I_{Na}, a positive shift in steady-state activation, a negative shift in steady-state

inactivation, enhanced closed-state inactivation, and a slow recovery from inactivation (Nguyen *et al.*, 2008). In contrast, the gain-of-function showed as an increase in window currents in D1595H (Nguyen *et al.*, 2008) and persistent I_{Na} in A1180V (Ge *et al.*, 2008). At this state, it is unclear which major mechanism is involved in the pathogenesis of the DCM.

1.5.8 Overlapping syndrome

The overlapping syndrome refers to multiple phenotypes in a family induced by single *SCN5A* mutations. So far, at least 35 mutations in *SCN5A* gene have been linked to overlapping syndrome since 1999 when mutation 1795*ins*D was first reported to cause LQT3 and BrS1 (Bezzina *et al.*, 1999). Since then, several mutations have been found to have similar overlapping pattern with or without co-expression of SSS (Grant *et al.*, 2002; Makita *et al.*, 2008; Huang *et al.*, 2006; Chen *et al.*, 2005). Most of these mutations were found to cause an overlap between BrS1 and CCD (Remme *et al.*, 2008). A small number of cases are related to SSS and /or atrial standstill in the setting of BrS1 (Rossenbacker *et al.*, 2004; Smits *et al.*, 2002; Makiyama *et al.*, 2005) and to CCD in the setting of LQT3 (Zareba *et al.*, 2001; Lupoglazoff *et al.*, 2001; Chang *et al.*, 2004).

This syndrome focuses on the role of mutants that lead to multiple sets of abnormal biophysical properties except for pure loss-of-function and gain-of-function alterations. E1784K mutation is such an example. It has initially been reported to be associated with LQT3 in two families by our laboratory and another group (Wei *et al.*, 1999; Deschênes *et al.*, 2000). Then, E1784K mutation was also reported in patients with BrS1(Priori *et al.*, 2002). Recently, a cohort of fifteen families with E1784K mutation was reported to be associated with even more clinical phenotypes. 93% of the genetic carriers had LQT3, 22% had BrS1, and 39% had sinus node dysfunction. Whole-cell patch clamp recordings showed multiple gating alterations. The persistent I_{Na} leads to the formation of LQT3, whereas the decreased I_{Na} and negative shift in steady-state inactivation cause BrS1 and sinus node dysfunction (Makita *et al.*, 2008).

Many environmental factors are important in determining the overlapping phenotype, leading to multiple gating changes in overlapping-syndrome mutants. For example, administration of Na^+ channel blockers to a LQT3 patient can unmask the BrS1 ECG pattern (Priori *et al.*, 2000b). Another example is seen in mutation 1795*ins*D, which shows that a gain of function with a

persistent I_{Na} at slow heart rate may cause LQT3, and that a loss of function with enhancement of slow inactivation at rapid heart rate may cause BrS1 (Veldkamp *et al.*, 2000).

1.6 $Na_v1.5$ and its pharmacology

1.6.1 $Na_v1.5$ and class I Antiarrhythmic drugs

Antiarrhythmic drugs are used clinically in the treatment of the various cardiac arrhythmias caused by abnormal electrical activity in the heart. According to the Vaughan Williams classification, antiarrhythmic drugs are divided into four groups termed class I-IV antiarrhythmic drugs (Vaughan Williams, 1992). Of these four groups, class I antiarrhythmic drugs is traditionally the group that mainly acts on $Na_v1.5$ channels by affecting depolarization and repolarization of cardiac action potentials. The depolarization effect is the general mechanism for the antiarrhythmic action, whereas the repolarization effect is variable in different subclasses of class I antiarrhythmic drugs. The depolarization effect is characterized by a slow rate (slope) of V_{max} during phase 0 of the cardiac action potential. This type of action potential is only present in the fast response tissue that is a kind of non-nodal tissue, such as atrial and ventricular myocytes and purkinje tissue, depending upon the opening of $Na_v1.5$ to initiate depolarization (Allessie *et al.*, 1996). Since the slope depends on the activation of $Na_v1.5$ and rapid Na^+ influx, the decreased slope of the phase 0 also reduces the current amplitude of the cardiac action potential. In addition, the slower a cadiomyocytes depolarizes, the more slowly its adjacent cells will be depolarized, thereby leading to reduced action potential propagation. Therefore, the cardiac excitability is consequently suppressed. In contrast, Class I antiarrhythmic drugs have no direct effect on nodal tissue, including SA and AV nodes, since their depolarization depends on L-type Ca^{2+} channels but not $Na_v1.5$ channels (Shorofsky and Balke, 2001).

The inhibitory effect of class I antiarrhythmic drugs is state-dependent. There are three states in the biophysical cycle for $Na_v1.5$: resting, open, and inactivated states (Hodgkin and Huxley, 1952). Class I antiarrhythmic drugs become more affinitive to their binding sites during open or inactivated states. The binding sites for class I antiarrhythmic drugs have been identified as two residues, phenylalanine (F) 1760 and Tyrosine (T) 1767, in the inner mouth of the pore region. Class I antiarrhythmic drugs can access the binding sites through hydrophilic and hydrophobic pathways (Fig 1.14). The neutral form crosses directly over the lipid membrane from outside through the hydrophobic pathway in a manner of "sideway movement", interacting with channels

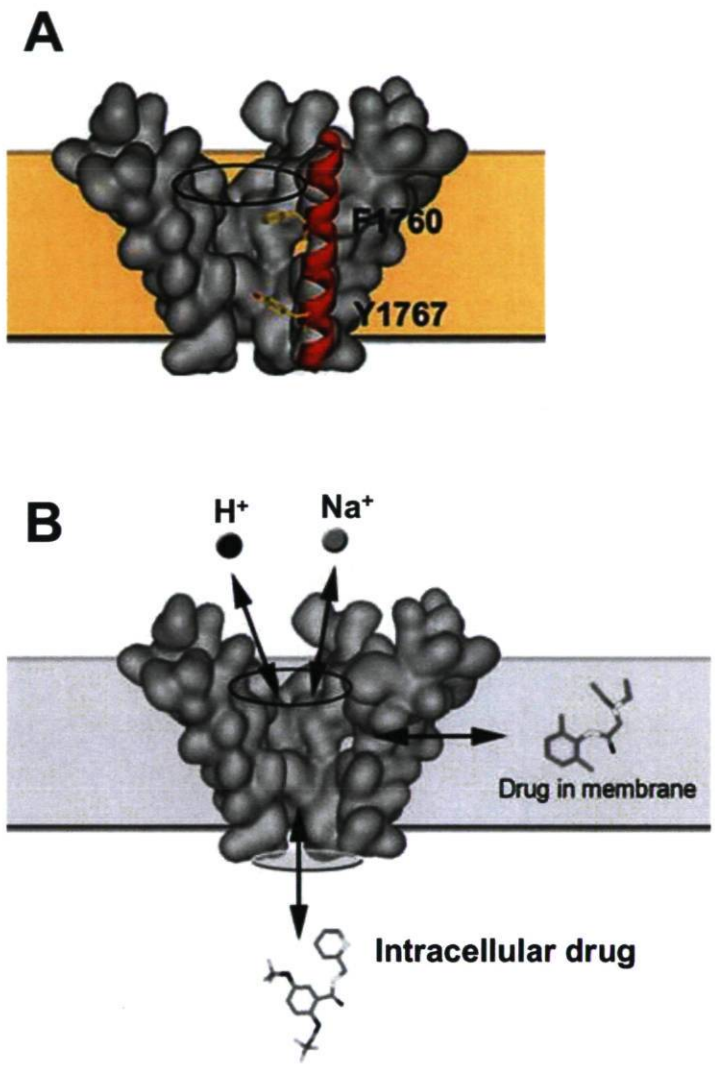

Figure 1.14: The modulated receptor hypothesis. (A) Structural determinants of drug binding. Surface representation of the Na^+ channel with a *helix* representing DIVS6. Shown are the side chains for primary residues implicated in drug binding, F1760 and Y1767. The selectivity filter is indicated by a *black ellipse*. (B) Two distinct pathways exist for drug block. The hydrophilic pathway (*vertical arrows*), is the likely path of a charged flecainide molecule, and requires channel opening for access to the drug receptor. Neutral drug such as lidocaine can reach the receptor through a hydrophobic "sideways movement" membrane pathway (*horizontal arrows*). Extracellular Na^+ ions (*gray circle*) and H^+ (*black circle*) can reach bound drug molecules through the selectivity filter shown as a *black ellipse*. The inactivation gate is shown as a transparent ellipse on the intracellular side of the pore (Glaaser and Clancy, 2006).

at the inactivated state. In contrast, the charged form enters the inner mouth of the pore region from the cytosol through the hydrophilic pathway, binding to the open state. The neutral and charged forms are determined by a concept of pKa, representing the degree of ionization. The greater pKa is, the more strongly the antiarrhythmic drug ionizes. After binding to $Na_v1.5$, the gating properties may show a shift of steady-state inactivation in a hyperpolarizing direction with a slow recovery from inactivation (Hille, 1977).

1.6.2 Subgroups of class I antiarrhythmic drugs

Class I antiarrhythmic drugs are further classified into the three subclasses Ia-c, depending on their differences in kinetics of interaction with Na^+ channels and different effects on the cardiac action potential duration (APD). The interaction kinetics are measured by a value of the binding rate, which is fast for class Ib, intermediate for class Ia, and slow for class Ic. The fast binding class also enables fast dissociation from binding sites. Therapy of class I antiarrhythmic drugs can results in the development of proarrhythmia, either by slowing cardiac conduction to critical levels, or by prolonging the cardiac action potential duration (APD). Proarrhythmic effects can be presented as a new or a more precipitated episode of preexisting arrhythmias. The CAST (cardiac arrhythmia suppression trial) study was designed to assess the therapy impact in a population under high-risk conditions (e.g., ischemia). Resulting data revealed that class Ic is more proarrhythic than other subgroups (The Cardiac Arrhythmia Suppression Trial (CAST) Investigators, 1989; Echt *et al.*, 1991).

1.6.2.1 Class Ia

Class Ia primarily includes quinidine, procainamide, and disopyramide, which provide the effects of increasing the APD and the effective refractory period (ERP) (Carmeliet and Mubagwa, 1998). These effects are associated with not only $Na_v1.5$ blockage, but also potentially blocking K^+ channels (e.g., I_{kr}) that impact phases 2 to 3 of cardiac action potentials (Salata and Wasserstrom, 1988; Yang and Roden, 1996). Tachyarrhythmias caused by the reentry mechanism, on the one hand, could be treated by increasing the effective refractory period. On the other hand, improperly increasing the APD like LQTS in turn increases the risk of developing torsades de pointes. Class Ia has another specific effect on cardiac action potential by inhibiting vagal activities that produce antimuscarinic signs (Nattel, 1993). Although an Ia drug may effectively

depress atrial rates during flutter, it can overcome this depressant effect and lead to an increase in ventricular rates owing to increasing AV conduction.

Quinidine

Because Ia drugs tend to prolong cardiac action potentials, they are often used to treat patients with BrS1, but not LQT3, to prevent life-threatening arrhythmias. In particular, quinidine was successfully used in the treatment of patients with BrS1 to prevent spontaneous VF events (Belhassen *et al.*, 2004; Valdivia *et al.*, 2004; Garg *et al.*, 1998). Further functional studies showed that quinidine may also normalize the trafficking (Valdivia *et al.*, 2004) and electrophysiological (Antzelevitch, 2001b; Imaizumi and Giles, 1987) defects caused by BrS mutations. Interestingly, the normalized electrophysiological defects are relevant effects of quinidine on K^+ channels rather than on $Na_v1.5$ channels. Upon administration of quinidine, I_{to} is significantly suppressed in ventricular epicardial cells, thus abolishing the phase 2 reentrant activity. ECG manifestation, however, is not consistent with the above clinical effects. The elevated ST segment may improve, remain unchanged, or even worsen after quinidine administration (Watanabe *et al.*, 2005; Belhassen *et al.*, 2004). To better understand the relationship between the induction of VT/VF events and quinidine-induced elevation of the ST-segment, a cohort study was performed in 106 patients with BrS1 using hydroquinidine. The results showed no close correlation between them (Hermida *et al.*, 2004). This suggests that the ST-segment manifestations are too weak to fully reflect clinical effects of quinidine in BrS.

1.6.2.2 Class Ib

Lidocaine, mexiletine, and tocainide are examples of class Ib antiarrhythmic drugs. They are nearly pure Na^+ channel blockers which do not block K^+ currents and tend to shorten cardiac APD. However, class Ib drugs do not shorten the ERP, because they slow the recovery of Nav1.5 channels from inactivation. The shortened action potential is probably caused by selectively blocking $Na_v1.5$ in fast response tissues, which normally have long phase 2 periods. The blocked I_{Na} has little effect on conduction velocity in normal fast response tissue, but slows condution in ischemic tissues with less negative resting membrane potentials (Rizzon *et al.*, 1987). The Ib drugs may suppress abnormal automaticity by decreasing the slope of phase 4 that is generated by the pacemaker current (Carmeliet and Saikawa, 1982).

Lidocaine

Although quinidine has been shown to be an effective treatment for patients with BrS1, this therapy is limited in the clinic because pharmacological side-effects that could easily ensue with the doses of up to 1500 mg/day in the study (Belhassen *et al.*, 2004). Other antiarrhythmic drugs, with lower dosages, for treatment of Na^+ channelopathies have also been studied. Recently lidocaine (100 μM) was used in research on BrS1 treatment to correct electrophysiological defects of the mutation. It produced a reduction in use-dependent block and an accelerated recovery from slow inactivation in a patient with BrS1 (Itoh *et al.*, 2007). Lidocaine is characterized by a pKa of 7.6-8.0 with about 50% of the neutral form at physiological pH of 7.4 (Hille, 1977). It can rapidly dissociate from $Na_v1.5$ channels, producing a less accumulating effect in the use-dependent block that causes an increased rate of recovery. Lidocaine was also found to block the persistent I_{Na} of $Na_v1.5$ mutations that caused LQT3 (An *et al.*, 1996) and cardiac sudden death (Huang *et al.*, 2009). Lidocaine may work by driving more channels into closed-state inactivation to shorten the QT interval in treatment of LQT3 with the persistent I_{Na} (Groenewegen *et al.*, 2003a). Peak I_{Na} in these studies was not greatly modified by lidocaine. This phenomenon suggests that pharmacological shortening of APD might not compromise cardiac conduction severely (Bezzina *et al.*, 2001).

Mexiletine

Mexiletine is found to treat both LQT3 and BrS1 effectively. Similar to quinidine, mexiletine is also used in the treatment of patients with BrS1 (Miyazaki *et al.*, 1996). It probably works by rescuing trafficking defect of BrS mutations (Valdivia *et al.*, 2004). Mexiletine rescues the I_{Na} of $Na_v1.5$ by 93-fold, much greater than the 27- fold rescue of quinidine. In addition, mexiletine also suppressed the ST-segment elevation in patients carrying N406S mutation. The suppressed ST-segment elevation becomes noticeable in precordial leads V1 and V2 after discontinuation of mexiletine (Itoh *et al.*, 2007).

In the treatment of LQT3, mexiletine is better than lidocaine for two reasons, first, it has a higher pKa of 9.3 and consequently a larger part of charged form (99%) than that of lidocaine at the physiological pH 7.4, leading to a greater probability to block $Na_v1.5$ at open state (Liu *et al.*, 2003c); secondly an oral formulation is available for mexiletine, but not lidocaine, so patients are more compliant with mexiletine administration. Mexilitine has been clinically observed to correct

the prolonged QT interval in the patient with $Na_v1.5$ mutations (Schwartz *et al.*, 1995; Dumaine *et al.*, 1996). The underlying mechanism is based on the correction of electrophysiological defects caused by blocking the persistent I_{Na} induced by $Na_v1.5$ mutations (Wang *et al.*, 1997). Mexiletine also has the ability to prevent life-threatening arrhythmias (VT/VF) in the LQT3 setting by shortening the cardiac APD dispersion and suppressing EAD in LQT3 knock-in mice (Fabritz *et al.*, 2003).

1.6.2.3 Class Ic

Class Ic, such as flecainide, encainide, and propafenone, acts in a manner similar to the class Ia antiarrhythmic drugs. It also blocks K^+ channels (Duan *et al.*, 1993). The difference between these two groups is that: (1) Ic drugs block $Na_v1.5$ channels more effectively in reducing V_{max} than Ia drugs; (2) Ic drugs cause a smaller increase in the APD in ventricular muscle than do Ia drugs, and they actually decrease the APD in the Purkinje system (Smallwood *et al.*, 1989; Ikeda *et al.*, 1985). In addition, this group has a particular propensity to induce proarrhythmic effects, which restricts their clinical usage (Pratt and Moye, 1990).

Flecainide

Flecainide is the most common agent in the class Ic group. Like mexiletine, flecainide has a pKa of 9.3 and thus may be up to 99% neutral at physiological pH. Despite the proarrhythmic potency associated with its use, flecainide has proved to be effective in the diagnosis of BrS and in treating LQT3. In the case of BrS diagnosis, flecainide and other class Ic drugs can unmask ST-segment elevation in patients with latent BrS (Brugada *et al.*, 2000b; Gasparini *et al.*, 2003). This is attributed to enhancement of closed-state and slow-state inactivations with a slow recovery from slow inactivation, which results in marked tonic and use-dependent I_{Na} blockages (Viswanathan *et al.*, 2001). The marked I_{Na} block thus disrupts the balance between I_{to} and I_{Na} at the end of phase 1 in action potentials, producing marked abbreviation in epicardial layer. In general, the effectiveness of Na^+ channel blockers to unmask BrS ECG pattern is inversely proportional to the rate, at which the drug dissociates from $Na_v1.5$ channels (Shimizu *et al.*, 2000). Class Ic drugs dissociate from $Na_v1.5$ channels more slowly and delay the recovery from the blockage, thus producing the greatest use-dependent block of channels. Therefore, this group is most effective in elevating the ST-segment elevation in patients with latent BrS1.

In the case of LQT3, flecainide has potential therapeutic applications (Benhorin *et al.*, 2000). As with class Ib drugs, previous studies have shown that the blockage of persistent I_{Na} by flecainide can reduce QT prolongation in some LQT3 mutations (Nagatomo *et al.*, 2000; Makita *et al.*, 2008). Some of these mutations were found to overlap with the latent BrS phenotype, so it is critical to investigate the mutant-specific drug interaction to evaluate the risk of developing life-threatening arrhythmias by unmasking BrS phenotype.

1.6.3 $Na_v1.5$ and an unclassified antiarrhythmic drug: ranolazine

Ranolazine is an unclassified Na^+-channel-blocker found to have antiarrhythmic function. Ranolazine is of particular interest in that it may have effects not only on ischemia-related arrhythmias, but also on arrhythmias induced by inherited cardiac disorders (e.g. LQT3). The administration of ranolazine does not adversely modify the patient's hemodynamic parameters such as bradycardia and hypotension (Pepine and Wolff, 1999).

Ranolazine was first clinically used as an antianginal agent in the treatment of angina pectoris given its antiischemic effects. The underlying mechanism may be related to its ability to inhibit the increased persistent I_{Na} that is critical for arrhythmia generation in experimental models of ischemic ventricular tissue (Ju *et al.*, 1996) and heart failure (Undrovinas *et al.*, 2006). The persistent I_{Na} is selectively blocked by ranolazine at clinical concentrations in a ratio of around 38:1 over the peak I_{Na} (Belardinelli *et al.*, 2006). Because of its ability to inhibit persistent I_{Na}, ranolazine was recently included in studies of LQT3. Inhibition of persistent I_{Na} significantly shortens the prolonged APD in the ventricular muscle, particularly in the M cell layer where such persistent I_{Na} is most prominent (Zygmunt *et al.*, 2001). The shortened APD thus limits the increase in transmural dispersion of repolarization, and limits the development of EADs for torsades de pointes. In addition, the persistent I_{Na} can reversely drive the Ca^{2+}/Na^+ exchanger to increase intracellular Ca^{2+} and cause DADs. Therefore, inhibition of persistent I_{Na} can also prevent DAD-triggered arrhythmias by reducing intracellular Ca^{2+} overload (Noble and Noble, 2006; Belardinelli *et al.*, 2006). The binding site of Na^+ channels for ranolazine block has been studied. The resulting data showed that ranolazine shares binding sites with class I antiarrhythmic drugs at DIVS6, particularly at F1760 residue (Fredj *et al.*, 2006), in a use-dependent manner (Mujtaba *et al.*, 2002). However, the role of Y1767 residue in ranolazine blocking effects is still

lacking. Of these experiment data, ranolazine has successfully been used in the treatment of LQT3 patients harboring ΔKPQ mutations (Moss *et al.*, 2008).

In addition to LQT3, ranolazine has also found to be effective in preventing arrhythmogenesis in experimental models of LQT2 and LQT8 by inhibiting I_{Kr} (Schram *et al.*, 2004) and $I_{Ca\text{-}L}$ (Sicouri *et al.*, 2007), respectively. Interestingly, inhibition of I_{Kr} results in minor prolongation of cardiac APD and a small increase in the QT interval on ECG. These alterations could be proarrhythmic. Ranolazine, however, does not trigger EADs and sustained ventricular arrhythmias in the experimental model at high doses (Song *et al.*, 2004; Antzelevitch *et al.*, 2004b), which suggests that ranolazine-induced risk of developing ventricular arrhythmias may depend on the relative magnitudes of changes in I_{Kr}, persistent I_{Na}, and $I_{Ca\text{-}L}$ and on the contributions of these ions to ventricular repolarization.

1.7 Rational and objectives

$Na_v1.5$, encoded by *SCN5A*, is a key Na^+ channel implicated in the generation and propagation of the cardiac action potential. *SCN5A* mutations are located in variable positions of $Na_v1.5$. The present thesis characterizes biophysical properties of three *SCN5A* mutations, Y1767C (DIVS6), S1344Y (DIII S4-S5 linker), and K1493R (III-IV linker), in tsA 201 cells using whole-cell configuration of patch clamp technique to address questions as below:

Y1767C mutation in *SCN5A* gene in chapter II

(1) Y1767C mutation was found in an LQT3 patient with an episode of syncope. The Y1767 residue has been known to contribute to channel gatings (O'Leary and Chahine, 2002), thus Y1767C mutant channels may cause some changes in their gating properties. What are the underlying changes that lead to the Y1767C-induced LQT3 phenotype in the patient?

(2) Y1767 residue is well known to act as a common binding site for class I antiarrhthmiac drugs (Ragsdale *et al.*, 1996). Should any class I antiarrhthmiac drug aiming at resulting gating changes be considered?

(3) Ranolazine has been shown to be effective in the treatment of LQT3 by blocking persistent I_{Na}. The binding site within $Na_v1.5$ channels for ranolazine has been confined to DIVS6, particularly to the residue F1760 (Fredj *et al.*, 2006). The role of Y1767 residue is unclear. What role does Y1767 residue play in ranolazine block?

Hypothesis: We hypothesized that Y1767C mutation may cause LQT3 phenotype in the patient by a gain-of-function property. If persistent I_{Na} is observed from mutant channels, it could be blocked either by class I antiarrhythmic drugs or by other unclassified Na^+ channel blocker such as ranolazine.

S1333Y mutation in *SCN5A* gene in Chapter III

(1) S1333Y mutation was found in a 25-day-old SIDS patient. *SCN5A* mutations have been known to be associated with inherited Na^+ channelopathies leading to various arrhythmias. BrS1 and LQT3 can result in cardiac sudden death by triggering torsades de pointes and idiopathic ventricular tachycardia, respectively. These two disorders are characterized by opposite gating properties: loss-of-function for BrS (Priori *et al.*, 2000a) and gain-of-function for LQT3 (Schwartz *et al.*, 2000). Which one is most likely to cause the sudden death in an infant carrying S1333Y mutation?

(2) The DIII S4-S5 linker in $Na_v1.5$ channels is a docking site for the inactivation particle of the III-IV linker (Smith and Goldin, 1997). What is the role of S1333 residue in this specific region? What gating changes do S1333Y mutant channels produce?

Hypothesis: We hypothesized that S1333Y mutation is the underliyng cause of the sudden death in the patient by gating changes of either gain-of-function or loss-of-function properties. If persistent I_{Na} or increased window currents are observed in mutant channels, LQT3 should be the underlying channelopathy for the sudden death. If peak I_{Na} is decrased or channel availability is decreased in activation or inactivation states, BrS1 should be the underlying channelopathy for the sudden death.

K1493R mutation in *SCN5A* gene in chapter IV

(1) K1493R mutation was found in a patient with idiopathic AF at age 50. Mechanisms for *SCN5A*-related lone AF are controversial primarly with two opposite patterns: loss-of-function (Chen *et al.*, 2007; Ellinor *et al.*, 2008) and gain-of-function (Makiyama *et al.*, 2008) properties. What type of gating property does K1493R produce?

(2) The III-IV linker is known as an inactivation gate in Na^+ channels. The *SCN5A* mutation K1493R localized in III-IV linker was found in an AF patient, so it is hypothesized to give some gating alterations. How do such changes influence the AF patient?

(3) Finally, How does K1493R mutation affect firing activities of action potentials? To better understand effects of K1493R in vivo, firing activities of action potentials would be studied by transiently transfecting mutant channels into atrial cardiomyocytes (HL-1 cells).

Hypothesis: Because K1493R mutation may change conformation of inactivation gate, we hypothesized that K1493R mutant channels could show some changes in fast inactivation state. The changes in gating properties may lead to lone AF in the patient.

1.8 Methods

1.8.1 Patch-clamp technique and heterologous expression system

Patch-clamp technique, which includes the voltage-clamp technique, can be used to investigate the gating properties of mutant Na^+ channels. Wild-type and mutant channels are transfected with β_1 subunits containing a lymphocyte surface antigen (CD8-alpha), respectively. Transfected cells are labelled by beads precoated with antibody to CD8-alpha. A polished glass micropipette is prepared and connected to an amplifier before the experiment. When an isolated transfected cell is selected, the pipette is placed on it. Then, suction is gently applied, which create a gigaseal with the magnitude of several gigaohm (GΩ) and can minimize the leak current between membrane and pipette. After that, various configurations can be applied. Negative pressure is used to break the membrane and generate whole-cell configuration, which is widely used to measure membrane currents from isolated cells. Finally, various protocols can be applied after cellular steady state is attained. An inside-out configuration normally is used for the single channel recording; An outside-out configuration is created through retraction of a whole cell membrane, and is a valuable tool in the investigation of extracellular factors (Fig. 1.15). Biophysical properties of mutant channels are usally characterized by analyzing gating changes and expression levels using patch-clamp studies in heterologous expression systems. The resulting data can provide important information about the genotype-phenotype relationships of Na^+ channelopathies. The most common heterologous expression systems include transiently transfected mammalian cells (HEK 293 and tsA 201) and *Xenopus* oocytes. The HEK293 cell line, derived from human embryonic kidney cells, is the most common mammalian cell line. The tsA 201 cell line is a branch of the HEK 293 cell line by stable transfection SV40 large T antigen (Margolskee *et al.*, 1993). Although these expression systems generally yield consistent results, some inconsistencies coud still be present among them, particularly between *Xenopu* oocytes and mammalian cells (Tan *et al.*, 2003).

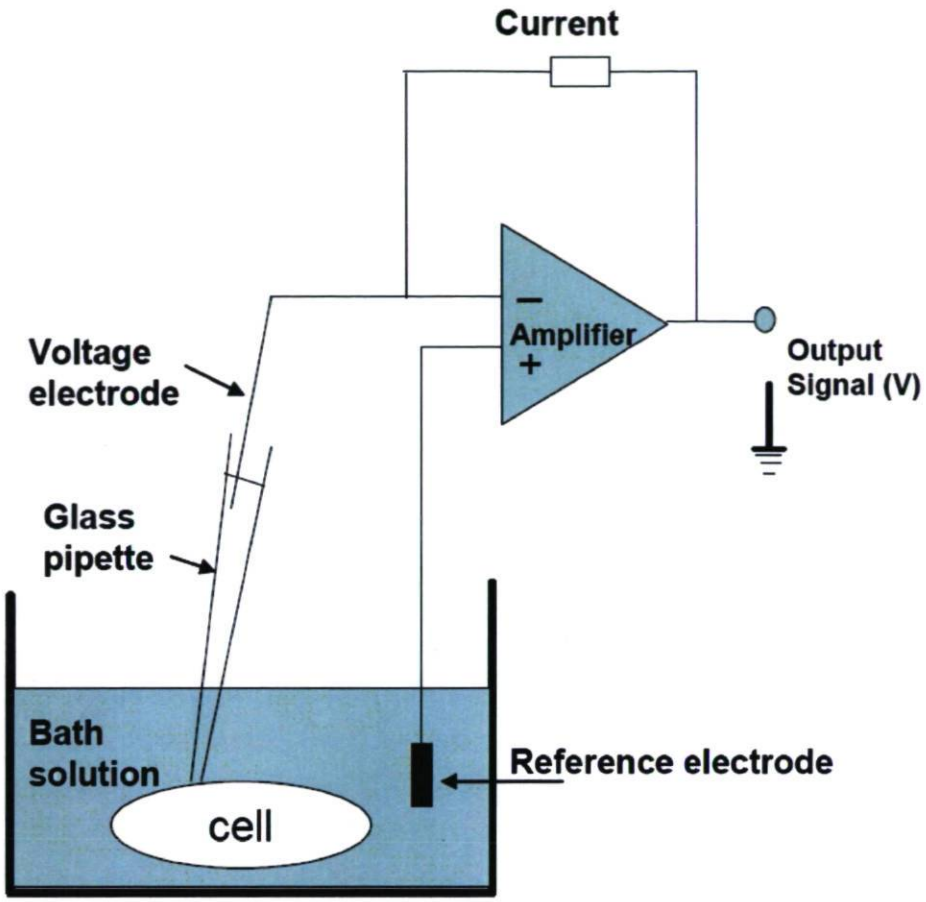

Figure 1.15: Schematic diagram for a typical electrophysiological laboratory set-up. The set-up represents a technique for studying ionic currents at the cellular level. A glass pipette is pressed gently on the cell membrane to form a seal. When suction is applied to the pipette the membrane breaks and the cytoplasm and pipette solution start to equilibrate. Cells are voltage-clamped and currents are recorded with the help of hardware (computer and amplifier) and software (pClamp9.0). (http://etd.ohiolink.edu/send-pdf.cgi/Wu%20Ling.pdf?csu1206732295)

1.8.2 Protocols for recording $Na_v1.5$ currents

Whole-cell current recording

Whole-cell Na^+ currents were recorded by a protocol with depolarizing steps ranging from –100 to +50 mV for 50 ms in 10-mV increments. Current amplitudes (pA) were normalized to cellular membrane capacitance (pF) in the form of current densities (pA/pF), and then were plotted versus voltages to generate current-voltage (*I-V*) curves.

Steady-sate activation

The Na^+ conductance for the various voltages was calculated from the same data and graphically determined reversal potentials as *I-V* curves by the equation $g_{Na} = I/(V–E_{rev})$, where I is the peak Na^+ current at a given voltage V and E_{rev}, the equilibrium potential extrapolated from the graph. The resulting values were normalized to the maximum conductance, and were plotted versus their voltage levels to give steady-state activation curves. Resulting activation curves were fitted to a standard Boltzmann distribution $G\ (V)/G_{max} = 1/\ (1+ \exp\ (–(V–V_{1/2})/k))$, where $G\ (V)$ is the conductance at a given voltage V and G_{max} is the maximum conductance.

Closed-state inactivation

Using a double-pulse protocol, cells were prepulsed to –110 and –100 mV for various durations from 1-500 ms, and then stepped to –30 mV to determine the availability of I_{Na} during the prepulse. Time course was fitted with the following mono-exponential equation: $I = I_{resid} + A \times \exp\ (-t/\tau)$, where I is the current intensity, I_{resid} the asymptotic residual current, and A the current amplitude at time zero.

Steady-state inactivation and recovery from inactivation

Voltage-dependent steady-state inactivation was measured by a 20-ms test pulse to –30 mV after applying 500-ms prepulses ranging from –140 to –10 mV. The test-pulse current amplitude was normalized to the maximum current recorded during the prepulse. The normalized current was plotted versus the prepulse voltage to obtain inactivation curve, which was fitted to a standard Boltzmann distribution function $I(V)/I_{max} = 1/\ (1+ \exp\ ((V–V_{0.5})/k))$, where $I(V)/I_{max}$ is the current ratio and V, the prepulse voltage. The midpoint voltages ($V_{1/2}$) and the slope factor (k) of activation and inactivation were determined from the fit. The probability of window current was

generated by taking the average values at given voltages (V) using parameters of steady-state activation ($V_{1/2\ act}$ and k_{act}) and inactivation ($V_{1/2\ inact}$ and k_{inact}) with the equation: $(1/\ (1+\exp\ ((V_{1/2\ act} - V)/k_{act}))) \times (1/\ (1+\exp\ ((V - V_{1/2\ inact})/\ k_{inact}\ )))$. Recovery from fast inactivation was determined by a two-pulse protocol, where Na^+ channels were inactivated by a conditioning pulse to –30 mV for 40 ms with a recovery interval variable from 0.1 to 200 ms before applying a 20-ms test pulse to –30 mV for the measurement of recovery currents. The peak current in response to the test pulse was normalized to the maximum peak current in response to the conditioning pulse, and was plotted against the recovery time interval. The resulting curve was fitted to a double-exponential function to obtain the fast and slow components of recovery from slow inactivation: $I_{Na} = A_f \times (1-\exp\ [-t/\tau_f]) + A_s \times (1-\exp\ [-t/\tau_s])$, where t is the recovery time interval, τ_f and τ_s, the time constants of the fast and slow components, and A_f and A_s, the fractions of the fast and slow components. Using the similar protocol, the conditioning pulse was held for 500 ms and recovery interval were prolonged up to 9000 ms to give the recovery from slow inactivation.

Slow inactivation

The course of slow activation was assessed using a two-pulse protocol with an initial conditioning prepulse and a final test pulse. A –30 mV prepulse was applied at intervals varying from 1 to 1000 ms, followed by a step returning to –140 mV for 20 ms to allow the channels to recover from fast inactivation. The –30 mV test pulse was applied for 40 ms to estimate the fraction of channels available for activation. The fraction was obtained by dividing the current amplitude in response to the test pulse by the current amplitude in response to the prepulse. Entry into slow inactivation followed a mono-exponential function $I = I_{resid} + A \times \exp\ (-t/\tau)$.

Ramp current

The ramp current was assessed by a depolarizing voltage ramp increased from –140 to +20 mV within 500 ms with a velocity of 0.32 mV/ms. This ramp protocol is used to test the inward Na^+ current when the window current is increased.

Frequency-dependent inhibitions and recovery from frequency-dependent inhibition

Frequency-dependent inhibitions were induced by applying a 50-pulse train for 10 ms at frequencies of 2, 5, 10, 20, and 50 Hz. The inhibition effects were described by the ratio of the

first and the last current amplitudes (P_1/P_{50}), which was then plotted against frequency. The recovery from frequency-dependent inhibition was induced by a 50-pulse train at 50 Hz, and was tested by a 20-ms pulse to –30 mV with a variable recovery interval up to 9000 ms.

Persistent Na^+ current

The persistent Na^+ current was induced by a depolarization to –30 mV directly jumping from –140 mV. The depolarization lasted for 400 ms to mimic a single APD. All protocols mentioned above were held at a holding potential of –140 mV.

Chapter II

Y1767C, a novel *SCN5A* mutation induces a persistent sodium current and potentiates ranolazine inhibition of $Na_v1.5$ channels

Y1767C, a novel *SCN5A* mutation induces a persistent sodium current and potentiates ranolazine inhibition of $Na_v1.5$ channels

Hai Huang[1], Silvia G. Priori[2,3], Carlo Napolitano[3], Michael E. O'Leary[4], Mohamed Chahine[1,5]

[1]Centre de recherche Université Laval Robert-Giffard, Quebec City, QC, Canada, G1J 2G3

[2]Department of Cardiology, Università degli studi di Pavia, Pavia, Italy

[3]Molecular Cardiology, IRCCS Fondazione Salvatore Maugeri, Pavia, Italy

[4]Jefferson Medical College, Jefferson University, Philadelphia, PA, USA

[5]Departement of Medicine, Université Laval, Quebec City, QC, Canada, G1K 7P4

Correspondence to:

Mohamed Chahine, Ph.D.

Centre de recherche Université Laval Robert-Giffard

Local F-6539

2601, chemin de la Canardière

Quebec City, QC, Canada, G1J 2G3

Tel.: (418) 663-5747, ext. 4723

Fax: (418) 663-8756

E-mail: mohamed.chahine@phc.ulaval.ca

2.1 Résumé

Le syndrome du QT long (LQTS) a été lié à des mutations sur le canal sodique cardiaque ($Na_v1.5$) en produisant un courant Na^+ persistant qui provoque une repolarisation ventriculaire retardée et des Torsades de pointes. Nous avons fait l'analyse des mutations de patients souffrant du LQTS et caractérisé les propriétés biophysiques des mutations découvertes. Un patient souffrant du LQT3 était porteur d'une mutation sur le gène *SCN5A* qui substitue par une cystéine une tyrosine hautement conservé (Y1767C) situé près de l'entrée cytoplasmique du pore. Le canal sauvage et le canal mutant ont été exprimés de façon transitoire dans des cellules tsA201, le courant Na^+ à ensuite été enregistré par la méthode du patch-clamp. Cette mutation provoque un courant Na^+ persistant, une activation plus rapide, une réactivation plus rapide et un courant de fenêtre plus grand. Le courant Na^+ persistant produit par le canal Y1767C est bloqué par la ranolazine mais pas par plusieurs anti-arythmiques de classe I. L'inactivation incomplète ainsi que l'activation persistante du canal sodique provoquée par le chevauchement de l'inactivation et de l'activation dépendante du voltage (courant de fenêtre), semble contribuer au phénotype de LQTS chez ce patient. Les résultats montrant que la ranolazine bloque le courant persistant suggère que la ranolazine pourrait s'avéré un traitement efficace pour les patients porteurs de cette mutation. Nos données montrent aussi un rôle unique pour le résidu Y1767 dans l'activation et la formation du pore intracellulaire du canal $Na_v1.5$.

Mots-clés : arythmie ventriculaire, génétique, canaux sodiques, $Na_v1.5$, *SCN5A*, syndrome du QT long, LQT3

2.2 Abstract

Long QT syndrome type 3 (LQT3) has been traced to mutations of the cardiac Na channel ($Na_v1.5$) that produce persistent Na currents leading to delayed ventricular repolarization and Torsades de pointes. We performed mutational analyses of patients suffering from LQTS and characterized the biophysical properties of the mutations that we uncovered. One LQT3 patient carried a mutation in the *SCN5A* gene in which the cysteine was substituted for a highly conserved tyrosine (Y1767C) located near cytoplasmic entrance of the $Na_v1.5$ channel pore. The wild-type and mutant channels were transiently expressed in tsA201 cells, and the Na currents were recorded using the patch-clamp technique. The Y1767C channel produced a persistent Na current, more rapid inactivation, faster recovery from inactivation, and an increased window current. The persistent Na current of the Y1767C channel was blocked by ranolazine but not by many class I antiarrhythmic drugs. The incomplete inactivation, along with the persistent activation of Na channels caused by an overlap of voltage-dependent activation and inactivation, known as window currents, appeared to contribute to the LQTS phenotype in this patient. The blocking effect of ranolazine on the persistent Na current suggested that ranolazine may be an effective therapeutic for treating patients with this mutation. Our data also revealed the unique role for the Y1767 residue in inactivating and forming the intracellular pore of the $Na_v1.5$ Na channel.

Keywords: ventricular arrhythmias, genetics, Na channels, $Na_v1.5$, *SCN5A*, long QT syndrome, LQT3

2.3 Introduction

Long QT syndrome (LQTS) is a congenital cardiac disorder characterized by a prolonged corrected QT interval (QTc >440 ms) on surface electrocardiograms (ECGs) and has been linked to life-threatening arrhythmias and sudden cardiac death (Huang *et al.*, 2009; Mohler *et al.*, 2003). LQTS type 3 (LQT3) mutations cause dysfunctions of the cardiac Na channel ($Na_v1.5$) encoded by the *SCN5A* gene. The $Na_v1.5$ channel is a critical determinant of cardiac excitability and plays a central role in the initiation and propagation of cardiac action potentials. The underlying mechanism of LQT3 has been attributed to persistent Na currents through mutant $Na_v1.5$ channels leading to prolonged repolarization of cardiac action potentials (Keller *et al.*, 2003; Deschênes *et al.*, 2000; Kambouris *et al.*, 1998; Chandra *et al.*, 1998; Wei *et al.*, 1999).

Previous studies revealed that the class I antiarrhythmic agents mexiletine (I B) and flecainide (I C) restore normal QTc intervals in some LQT3 patients by blocking the persistent Na current (Schwartz *et al.*, 1995; Benhorin *et al.*, 2000). Ranolazine, an anti-angina agent, was recently shown to inhibit the persistent Na currents associated with cardiac ischemia and to suppress early after-depolarization (EAD) triggered arrhythmias in an experimental model of LQT3 by blocking the persistent Na current (Wu *et al.*, 2004; Antzelevitch *et al.*, 2004). Ranolazine has recently been successfully used to treat LQTS patients harboring $Na_v1.5$ ΔKPQ mutations (Moss *et al.*, 2008; Fredj *et al.*, 2006). In some instances, ranolazine has been shown to increase the QT interval by suppressing the delayed rectifier current (I_{kr}), but it has not been linked to substantial dispersion of myocardial repolarization, EAD, or Torsades de pointes (Antzelevitch *et al.*, 2004; Hale *et al.*, 2008).

While ranolazine is not classified as an antiarrhythmic drug, its binding site is located near the cytoplasmic entrance of the $Na_v1.5$ channel and overlaps with that of class I antiarrhythmics (Fredj *et al.*, 2006). Ranolazine binding is state dependent and preferentially interacts with open rather than closed or inactivated Na channels (Wang *et al.*, 2008).

A 17-year-old LQTS patient diagnosed with episodic cardiac arrhythmia was found to harbor a Y1767C mutation of the *SCN5A* gene in transmembrane segment 6 of domain IV. Y1767 of $Na_v1.5$ is a highly-conserved tyrosine residue located in the membrane-spanning S6 segment of homologous domain IV that contributes to rapid inactivation and the binding of local anesthetics and antiarrhythmic drugs (Ragsdale *et al.*, 1996; O'Leary and Chahine, 2002). Another LQT3 mutation, V1763M, four amino acids upstream from Y1767, was previously characterized by

persistent Na currents that were insensitive to lidocaine blocking (Chang *et al.*, 2004). This finding suggested that traditional class I antiarrhythmic drugs are not an optimal therapeutic for the treatment of LQT3 patients with mutations in this specific region.

In the present study, we investigated the biophysical properties of the Y1767C mutant of $Na_v1.5$ transiently expressed in tsA201 cells. The Y1767C mutant channels displayed typical LQT3-like biophysical properties, including a increased persistent current, accelerated inactivation kinetics, an increased window current, and faster recovery from fast inactivation. The persistent current of the Y1767C channel was potently blocked by ranolazine but not by other class I antiarrhythmics, suggesting that ranolazine may be a highly selective therapeutic for treating LQTS patients carrying this mutation. Further analysis showed that Y1767 plays a pivotal role in ranolazine blocking.

2.4 Material and Methods

2.4.1 Clinical evaluation

LQTS symptoms were defined as syncope and cardiac arrest. The patient underwent a detailed clinical, particularly cardiovascular, examination, including a standard 12-lead electrocardiogram (ECG), 24-h Holter monitoring, an echocardiogram, and an exercise stress test. The QT interval was measured in lead 2 of the ECG, and the resulting QTc was determined by correcting for the heart rate using Bazett's formula. The patient was diagnosed with LQTS because he (1) exhibited syncope accompanied with a QTc >440 ms; (2) had no obvious abnormal cardiovascular structures, and (3) was not taking any medication that could lengthen the QTc.

2.4.2 Molecular genetics of LQTS patients

The local ethics committee approved the study protocol in accordance with the standards set out in the Declaration of Helsinki. The patient gave written informed consent prior to the clinical and genetic investigations. Genomic DNA was extracted from peripheral lymphocytes. Coding exons of the *KCNQ1*, *KCNH2*, *SCN5A*, *KCNE1*, and *KCNE2* genes were amplified by PCR using flanking intronic primers according to the gene sequence described by Wang et al. (Wang *et al.*, 1996b). PCR products were directly sequenced and analyzed as previously described (Keller *et al.*, 2003).

2.4.3 Sodium channel mutagenesis

Mutant human $Na_v1.5$/Y1767C was generated using a QuickChange TM site-directed mutagenesis kit according to the manufacturer's instructions (Stratagene, La Jolla, CA, USA). The oligonucleotide primers containing the corresponding Y1767C mutation were synthesized using the following sequences:

5′- CTC ATC GTG GTC AAC ATG TGC ATT GCC ATC ATC CTG -3′ (Forward primer) and

5′- CAG GAT GAT GGC AAT GCA CAT GTT GAC CAC GAT- 3′ (Reverse primer).

The mutated site is underlined. Mutant and WT $Na_v1.5$ channels were inserted in the pcDNA1 plasmid, amplified in bacteria (DH5α) and purified using Qiagen columns (Qiagen Inc., Chatsworth, CA, USA).

2.4.4 Heterologous expression of tsA201 cells

TsA201 is a modified human embryonic kidney HEK293 cell line stably transfected by SV40 large T antigen that can promote the replication of viral promoter-containing constructs (Margolskee *et al.*, 1993). The cells were grown in high glucose Dulbecco's modified Eagle's medium (DMEM) supplemented with fetal bovine serum (10%), L-glutamine (2 mM), penicillin G (100 U/ml), and streptomycin (10 mg/ml) (Gibco BRL Life Technologies, Burlington, ON, Canada). The cells were incubated in a 5% CO_2 humidified atmosphere after being transfected with WT or mutant human $Na_v1.5$ cDNA (2 μg) and human β_1-subunit (2 μg) using the calcium-phosphate method as previously described (Deschênes *et al.*, 2000). The human Na channel β_1-subunit and CD8 were inserted in the pIRES bicistronic vector in the form of pCD8-IRES-β_1. Using this strategy, transfected cells that bound beads also expressed the β_1-subunit protein. Transfected cells were incubated in the medium containing anti-CD8-coated beads (Dynabeads CD8, Dynal Biotech A.S.A., Oslo, Norway) for 2 min before performing patch-clamp experiments (Margolskee *et al.*, 1993). Cells expressing CD8 were distinguished from non-transfected cells by visualizing beads fixed on the cell membrane by light microscopy.

2.4.5 Patch clamp electrophysiology

The whole-cell configuration of the patch clamp technique was used to record macroscopic Na currents from transfected tsA201 cells. Patch clamp recordings were obtained using low-resistance, fire-polished electrodes (<1 MΩ) made from 8161 Corning borosilicate glass coated

with Sylgard (Dow-Corning, Midland, MI, USA) to minimize electrode capacitance. Currents were recorded with an Axopatch 200 amplifier (Molecular Devices, Sunnyvale, CA, USA), and series resistance was >80% compensated. Command pulses were generated, and currents were acquired using a Pentium-based computer running pCLAMP software v8.0 equipped with a DigiData 1300 AD converter (Molecular Devices). P/4 leak subtraction was used to compensate for linear leaks and eliminate capacitative transients. Currents were filtered at 5 kHz and digitized at 10 kHz. All recordings were performed at room temperature (22–23°C). Cells were permitted to stabilize for 10 min after establishing the whole-cell configuration before recording currents.

2.4.6 Solutions and reagents

For the whole-cell recordings, the patch pipettes were filled with a solution containing 35 mM NaCl, 105 mM CsF, 10 mM EGTA, and 10 mM Cs-HEPES. The pH was adjusted to 7.4 using 1 N CsOH. The bath solution consisted of 150 mM NaCl, 2 mM KCl, 1.5 mM $CaCl_2$, 1 mM $MgCl_2$, 10 mM glucose, and 10 mM Na-HEPES. The pH was adjusted to pH 7.4 using 1 N NaOH (final Na^+: 152.4 mM). Fluoride did not significantly affect the activation or inactivation states of WT $Na_v1.5$ channels (data not shown). The liquid junction potential between the patch pipette and the bath solution was corrected by –7 mV. Stock 4 mM (ranolazine, quinidine, and flecainide) and 20 mM (mexiletine) solutions were prepared and were diluted in bath solution. Their effects of the drugs were recorded 10 min after application to allow for drug equilibration.

2.4.7 Homology modeling of the D4S6 segment

The DIVS6 segment of $Na_v1.5$ was modeled based on the crystal structure of the S6 segment of the MthK channel (Jiang *et al.*, 2002) using the ZMM software package (Zhorov and Bregestovski, 2000; Blanchet *et al.*, 2007). The alignment of $Na_v1.5$ with MthK S6 segments was performed using ClustalW (Chenna *et al.*, 2003). Model optimization by Monte Carlo energy minimization was performed as previously described, with some variations (Jiang *et al.*, 2002). Briefly, the model was constructed by first assigning the backbone geometry of the template to model residues. Residues that were conserved in both proteins were assigned the same side chain geometry. At non-conserved positions, the side chain torsion angles χ_1 and χ_2 were taken from the template and additional torsion angles of longer side chains were assigned a value of 180°. Bad

contacts in the models were removed using a multi-step relaxation method consisting of four consecutive short MCM trajectories, which were terminated after 50 energy-minimization steps.

2.4.8 Statistical analysis

Recorded data were analyzed using a combination of pCLAMP software v9.0 (Axon Instruments), Microsoft Excel, and SigmaPlot 8.0. Corresponding results were presented as means ± standard errors of the mean. Statistical comparisons were made using the unpaired Student's *t*-test in SigmaStat (Jandel Scientific Software, San Rafael, CA, USA). Differences were considered significant at $p < 0.05$.

2.5 Results

2.5.1 Phenotypic characterization and clinical findings of a unique case of LQTS

A 17-year-old LQTS patient experienced an episodic cardiac arrest during emotional stress. The patient was admitted to the emergency department where normal sinus rhythm was restored by conventional therapies. The electrocardiogram (ECG) revealed a prolonged QTc interval of 510 ms (lead 2) with notched/biphasic T waves (Figure 2.1 A). A prolonged QTc, but no arrhythmia, was also observed by Holter monitoring. The echocardiogram of the patient was unremarkable. An exercise stress test confirmed the QTc prolongation diagnosis, with no signs of reduced coronary reserve or arrhythmia. Beta blocker (propranolol) therapy was initiated (2.5 mg/kg/day) after which the patient remained symptom-free for the following five years. Family screening was limited to the proband's brother (parents were not available for the study), who presented with history of syncope at age 18 and QT prolongation at the baseline ECG (QTC 510 ms). After the LQTS diagnosis, the brother refused any further evaluation, therapy, or ICD implant. He died suddenly at age 26.

2.5.2 Genotyping of the LQTS patient

The genomic DNA of the patient was screened for sequence changes in all 28 exons of the *SCN5A* gene. Sequence analysis revealed a heterozygous A-to-G base change at oligonucleotide position 5300 in exon 28 (Figure 2.1B) that resulted in a tyrosine (Y) to cysteine (C) substitution at position 1767 of the $Na_v1.5$ channel. The same mutation was identified in the proband's

brother. Y1767 is located in the S6 segment of homologous domain IV (DIVS6) and is highly conserved in the Na channels of fish, dogs, rats, mice, and humans.

2.5.3 The Y1767C mutation of $Na_v1.5$ induces a persistent Na current

Whole-cell patch-clamp recordings were used to study the Na currents of the WT and Y1767C channels heterologously expressed in mammalian tsA201 cells. The channels were co-expressed with the β_1 subunit, which is known to modulate the gating and trafficking of cardiac Na channels (Gellens *et al.*, 1992). Representative Na currents of the heterologously expressed WT and Y1767C channels are shown in Figure 2.2A. The peak Na currents at each voltage were normalized to the whole-cell capacitance and plotted *versus* test voltages (Figure 2.2B). The currents activated at voltages more depolarized than –80 mV peaked around –40 mV and had maximal current densities of 657 ± 49 pA/pF (n=9) and 617 ± 34 pA/pF (n=10) for the WT and Y1767C channels, respectively. The time course of the current decay was biexponential with fast (τ_f) and slow (τ_s) time constants at –30 mV of τ_f = 0.7 ± 0.02 ms and τ_s = 8.9 ± 0.3 ms for WT channel (n=9), and τ_f = 0.5 ± 0.01 ms and τ_s = 3.5 ± 0.4 ms for the Y1767C channel (n=10). Over a range of voltages, the time constants of the Y1767C channel were significantly smaller than those of the WT, which is consistent with more rapid inactivation of the mutant channel (Figure 2.2C).

In addition to changes in inactivation kinetics, the Y1767C mutation appeared to increase the fraction of Na current that failed to inactivate during prolonged (>40 ms) depolarization. The residual Na current (Figures 2.3A and 2.3B) measured after 300 ms of depolarization was normalized to the peak currents. The Y1767C mutation significantly increased the amplitude of the persistent current (1.2 ± 0.3 %, n=6) compared to the WT channel (0.2 ± 0.2 %, n=5) (Figure 2.6B). In both cases, the residual currents were completely inhibited by 10 μM of tetrodotoxin (TTX), indicating that the currents were mediated by Na channels. The 5-fold increase in the persistent Na current of the Y1767C channel suggested that this mutation may impair rapid inactivation.

2.5.4 Y1767C has a residual Na current during steady-state inactivation

Figures 2.3C and 3D compare the gating properties of the WT and Y1767C channels. The normalized conductance was calculated from the peak Na currents and was plotted *versus* the test

voltage (Figure 2.3C). The smooth curve was fitted to a Boltzmann function with midpoints ($V_{1/2}$) of –54 ± 1 mV (n=9) and –57 ± 1 mV (n=10) for the WT and Y1767C channels, respectively (Table 2.1). The steady-state inactivation of the WT and Y1767C channels had midpoints of –101 ± 1 mV (n=7) and –101 ± 1 mV (n=6), respectively (Table 2.1). While the midpoints of steady-state inactivation were not significantly different between the WT and Y1767C channels, the mutation produced a 5-fold increase in the residual Na current that failed to inactivate at voltages more depolarized than –40 mV. This finding was consistent with the observed TTX-sensitive persistent Na current at depolarized voltages (Figures 2.3A and 2.3B).

2.5.5 Y1767C increases the $Na_v1.5$ window current

The overlap of the activation and steady-state inactivation of Na channels identifies a hyperpolarized range of voltages (i.e., window) where the channels have a small probability of being partially but not fully inactivated (Attwell *et al.*, 1979). Na channel opening at these voltages is significant because the resulting inward "window" currents tend to depolarize the resting membrane potential and may alter the excitability of cardiomyocytes. Figure 2.4A plots the probability of Na channel opening calculated from the product of the fitted activation and steady-state inactivation parameters (Figure 2.3C). The resulting probability is a biphasic function of voltage with a relatively small component with a peak near –90 mV and a larger component at more depolarized voltages (>–70 mV). These increases in probability result from a combination of the activation, steady-state inactivation, and persistent (i.e., non-inactivating) components of Na channel gating. Figures 2.4B and 2.4C dissect these biphasic functions into their individual window and persistent components. The window component is primarily determined by the overlap of Na channel activation and inactivation. Because of the low probability of Na channel opening within the window, the non-inactivating component of the WT channel did not substantially alter the window amplitude, which was relatively small and reached a peak probability of 0.05% of the maximum at –90 mV (Figure 2.4B). The Y1767C mutation enlarged the window, shifted the peak toward more depolarized voltages (–81 mV), and produced a 3-fold increase in amplitude (0.13%). The increased window predicted that a larger fraction of the Y1767C channels would be activated near the resting membrane potential of cardiomyocytes (≈–90 mV) and at voltages where Na channels activate (>–80 mV).

The second increase in probability occurred over a more depolarized range of voltages (>–70 mV) and was determined by Na channel activation and the persistent (non-inactivating) component of Na channel gating (Figure 2.4C). In the WT channel, the persistent component increased over the range of voltages where $Na_v1.5$ channels activate when they reach a peak of 0.13% of the maximum probability at voltages more depolarized than –40 mV. The Y1767C mutation increased the peak probability 8-fold and caused a hyperpolarizing shift in the range of voltages where the persistent component activates. This apparent shift was not caused by a change in Na channel activation but rather reflected an increased overlap of the persistent and window components of the mutant channel. This overlap, coupled with the substantial increase in the amplitude of the persistent component, may act synergistically to produce sub-threshold activating Na currents in the Y1767C channel.

2.5.6 Y1767C promotes rapid recovery from inactivation

At least two mechanisms could explain the persistent Na current produced by the Y1767C mutation. The mutation could simply decrease the entry of Na channels into the fast-inactivated state. However, this mechanism is inconsistent with measurements of Na current decay indicating that inactivation was more rapid in the mutant channel (Figure 2.2C). Alternatively, the Y1767C mutation could induce persistent Na current by promoting rapid recovery from inactivation. This might be expected if the Y1767C mutation destabilizes fast inactivation similar to what is observed for other LQT3 mutations (Bennett *et al.*, 1995b; Wang *et al.*, 1996a; Wang *et al.*, 2007d). The experiments illustrated in Figure 2.5A employed a double-pulse protocol to directly measure recovery from fast inactivation. The smooth curves are fits to a biexponential equation with fast and slow time constants of 4.3 ± 0.5 ms and 57.3 ± 7.2 ms for the WT channel (n=7) and 2.6 ± 0.1 ms and 38.8 ± 4.4 ms for the Y1767C channel (n=7). The Y1767C mutation significantly reduced both the fast and slow time constants, which is consistent with more rapid recovery from inactivation (Table 2.1). Overall, the data suggested that the Y1767C mutation accelerates the entry into and recovery from the fast inactivated state. The rapid recovery appeared to predominate at depolarized voltages and accounted for the majority of the persistent Na current produced by this mutation.

2.5.7 Y1767C increases the sub-threshold activating Na current

The rapid recovery from inactivation (Figure 2.5A) and the enlarged window current (Figure 2.3D) of the Y1767C channel may enable a small but significant fraction of the Na channels (≤ 1%) to open at unusually hyperpolarized voltages (<–60 mV). These sub-threshold activating Na currents were further investigated using a voltage ramp (–140 to 20 mV) to activate the Na currents (Figure 2.5B). The ramp current of the WT channel began to activate at a relatively hyperpolarized voltage (–100 mV) and reached a maximum of 0.66 ± 0.15% (n=7) of the peak Na current at –80 mV. The ramp current of the Y1767C channel displayed similar activation but peaked at a more depolarized voltage (–70 mV) and was 1.8-fold larger (1.21 ± 0.13%, n=8) than the WT. Varying the duration over which the voltage ramp was applied (0.32-3.2 mV/ms) predictably altered the amplitudes of the ramp currents but did not change the relative differences between the WT and Y1767C currents, indicating that the effects of the mutation did not depend on the rate of the voltage change (data not shown). These sub-threshold-activating Na currents are predicted to depolarize the resting membrane potential and reduce the threshold for initiating action potentials in myocytes carrying the Y1767C mutation.

2.5.8 Ranloazine is a selective inhibitor of the Y1767C mutant persistent Na current

The rapid recovery from inactivation and the resulting persistent Na current caused by the Y1767C mutation appeared to underlie the LQT3 phenotype in this patient. Previous studies have shown that class I antiarrhythmic drugs are effective inhibitors of persistent Na currents linked to LQT3 mutations and have proved to be beneficial in the treatment of patients carrying these mutations (Schwartz *et al.*, 1995; Benhorin *et al.*, 2000). The Y1767C mutation described here is unique because, unlike most LQT3 mutations, it is situated in the DIVS6 segment, a region of Na channels that is known to contribute to local anesthetic binding (Qu *et al.*, 1995b). Previous studies have shown that the Y1767C mutation weakens drug binding to $Na_v1.5$ channels (O'Leary and Chahine, 2002). This raises the possibility that, in addition to inducing persistent Na currents, the Y1767C mutation may also alter the pharmacology of the mutant channel. This was further investigated by examining the effects of several class I antiarrhythmic drugs (quinidine, mexiletine, flecainide, lidocaine) on the Y1767C-induced persistent Na current (Figure 2.6A). At clinically relevant doses (10-150 μM), none of these drugs significantly reduced the persistent Na current of the Y1767C channel. This contrasts with other LQT3 mutations where these drugs are

potent inhibitors of persistent Na currents (Schwartz *et al.*, 1995; Benhorin *et al.*, 2000). Because of its location in the pore and the role of this tyrosine in drug binding, we speculate that the Y1767C mutation weakens Na channel inhibition by disrupting the binding of these antiarrhythmics.

Recent studies have shown that the anti-anginal agent ranolazine is an effective inhibitor of the persistent Na currents resulting from LQT3 mutations (Schwartz *et al.*, 1995; Benhorin *et al.*, 2000; Fredj *et al.*, 2006). Unlike the class I antiarrhythmics, ranolazine (50 μM) significantly reduced the persistent Na current of the Y1767C channel by 74 ± 0.25% (Figures 2.6A and 2.6B). The underlying mechanism was further investigated by applying a series of depolarizing pulses at frequencies between 1 and 50 Hz. In the absence of drug, the pulsing protocols produced only a small reduction in Na current amplitude (Figure 2.7B). Ranolazine (50 μM) significantly reduced the relative peak current amplitude (P_{50}/P_1) of the WT channel by 27 ± 3% (n=8). Surprisingly, the Y1767C mutation potentiated the ranolazine inhibition, reducing the currents by 43 ± 2% (n=8). Figure 2.7A shows that ranolazine was a more effective inhibitor of the Y1767C channel at pulsing frequencies greater than 10 Hz. At lower frequencies (1 to 5 Hz), the ranolazine inhibition of the Y1767C channel was not statistically different from that of the WT channel.

Many class I antiarrhythmic drugs act by preferentially binding to inactivated states of Na channels, resulting in a hyperpolarizing shift in steady-state availability (Chahine *et al.*, 1992). To test this potential mechanism, the effects of ranolazine on the activation and steady-state inactivation of the channels was examined (Supplemental Figure 2.1). Ranolazine reduced the peak current densities of the both the WT (21.2%, n=15) and Y1767C (19.5%, n=16) channels but failed to produce any changes in activation or steady-state inactivation (Table 2.1). These data suggest that while ranolazine inhibited both the WT and mutant channels, it did not alter their gating properties. This is inconsistent with a state-dependent mechanism in which ranolazine preferentially binds to inactivated states. Rather, the strong frequency-dependence of the inhibition suggests the ranolazine may principally act by blocking open channels (Wang *et al.*, 2008a). Ranolazine markedly reduced both the channel opening probability (Supplemental Figure 2.3A) and the window (Supplemental Figure 2.3B) Na current of Y1767C channels, but only caused a slight reduction for WT channels (Supplemental Figures 2.2A and 2.2B). We also tested the effect of ranolazine on another LQT3 mutation (V1763M), which was located at the same region as Y1767C and was characterized by increased persistent Na currents that are

insensitive to lidocaine blocking (Chang *et al.*, 2004). Ranolazine effectively blocked the lidocaine-insensitive persistent Na currents (Supplemental Figure 2.4), but had similar effects on frequency inhibition and recovery from frequency inhibition as WT channels (Supplemental Figure 2.5).

2.5.9 Ranolazine slows the recovery from frequency inhibition of the Y1767C channel

A prominent feature of many class I antiarrhythmics is that they slow the recovery of drug-modified Na channels. A repetitive pulsing protocol was used to induce ranolazine inhibition and assess the recovery time course of the WT and Y1767C channels (Figure 2.7C). In the absence of drug, the recovery from frequency inhibition of the WT and Y1767C channels was similar, indicating that the mutation did not directly alter the recovery from inactivation after repetitive stimulations. Ranolazine significantly increased the fraction of inhibited channels and slowed the recovery time course. The smooth curves are biexponential curve fits with fast (τ_f) and slow (τ_s) time constants of 16 and 2446 ms for the WT channel and 29 and 3987 ms for the Y1767C channel (Table 2.1). The Y1767C channel displayed more pronounced ranolazine frequency-dependent inhibition, and its recovery time course was significantly slower than the WT channel. These data are consistent with the results studies of the persistent Na currents showing that ranolazine is a more potent inhibitor of the Y1767C channel (Figures 2.7A and 2.7B).

2.5.10 Y1767 locates in the pore region as a bulky aromatic residue

Figure 2.8A shows the orientation of the residues predicted by a homology model of the S6 segments based on the M2 helix of the MthK channel (Jiang *et al.*, 2002). Figure 2.8B shows a top view of the model indicating that F1760, V1763, and Y1767 are prominently exposed within the central cavity of the channel.

2.6 Discussion

In the present study, we characterized a novel LQT3 mutation (Y1767C) identified in a 17-year-old male with a classic ECG phenotype and documented episodes of cardiac arrest. Genomic sequencing uncovered an A-to-G base change at position 5300 of the *SCN5A* gene that resulted in a tyrosine-to-cysteine (Y/C) substitution. This mutation (Y1767C) was located in the S6 membrane-spanning region of homologous domain IV (DIVS6) of the cardiac Na channel

($Na_v1.5$). This region of the channel is known to play important roles in fast inactivation and the binding of local anesthetics and antiarrhythmic drugs (Ragsdale *et al.*, 1996; O'Leary and Chahine, 2002). The principal goal of the present study was to investigate the effects of the Y1767C mutation on Na channel gating and to correlate the observed changes with the ECG phenotype and clinical history of the patient.

Electrophysiological analyses of the Y1767C mutant revealed an enhanced persistent Na current at depolarized voltages associated with accelerated inactivation (Figure 2.2C) and rapid recovery from inactivation (Figure 2.5A). The rapid recovery appeared to predominate, allowing an increased fraction of the mutant channels to remain persistently open at depolarized voltages. The lack of an absorbing inactivated state in the Y1767C channel appeared to be the primary cause of the persistent Na current. In addition to rapid recovery, the Y1767C mutation significantly increased the overlap of the activation and steady-state inactivation of the channel (Figure 2.3D). The area between these curves defines a range of voltages (i.e., window) where Na channels may be activated but not inactivated (Attwell *et al.*, 1979). The enlarged window produced by the Y1767C mutation predicted that an increased fraction of the channels may open at hyperpolarized voltages resulting in an inward Na current at sub-threshold membrane potentials, which was consistent with the 1.8-fold increase in ramp current produced by the Y1767C mutation (Figure 2.5B). This current would tend to depolarize the resting membrane potential and reduce the threshold for initiating cardiac action potentials. The increased excitability stemming from sub-threshold activating Na currents, coupled with the prolonged depolarization of the plateau phase of the cardiac action potential resulting from increased persistent Na current, formed the basis of the LQT3 phenotype in this patient.

The Y1767C mutation is situated in DIVS6, a region that has been implicated in both the gating and the antiarrhythmic pharmacology of Na channels (O'Leary and Chahine, 2002). Mutational analyses suggest that residues situated near the C-terminus of the DIVS6 disrupt inactivation by interfering with the binding of the native inactivation gate (McPhee *et al.*, 1994; McPhee *et al.*, 1995). Y1767 is located adjacent to these sites and may contribute to fast inactivation in a similar way. Impaired inactivation provides a plausible explanation for both the rapid inactivation (Figure 2.2C) and recovery from inactivation (Figure 2.5A) produced by the Y1767C mutation. In addition to Na channel gating, DIVS6 is also an important locus for the binding of class I antiarrhythmics and local anesthetics. Two highly conserved aromatic amino acids (F1760,

Y1767) of DIVS6 are known to be critical determinants of local anesthetic binding (Ragsdale *et al.*, 1996). The Y1767C mutation described in the present study is known to weaken drug binding to $Na_v1.5$ channels (O'Leary and Chahine, 2002; O'Leary *et al.*, 2003). This is consistent with the fact that class I antiarrhythmic drugs (quinidine, mexiletine, lidocaine, flecainide) were relatively weak inhibitors of the Y1767C persistent Na current (Figure 2.6A). This finding differs from other LQT3 Na channel mutations where class I antiarrhythmic drugs are potent inhibitors of persistent Na currents (Liu *et al.*, 2003c; Nagatomo *et al.*, 2000; Wang *et al.*, 1997). Unlike the Y1767C mutation described here, these LQT3 mutations are generally located outside the DIVS6 segment and thus removed from sites important for drug binding (Clancy and Kass, 2005). Our data suggested that the Y1767C mutation may weaken the binding of class I antiarrhythmics resulting in persistent Na currents that are insensitive to these drugs.

Ranolazine is an anti-anginal agent that shares a similar structure with class I antiarrhythmics (Fredj *et al.*, 2006) and is an effective inhibitor of the persistent Na currents of both LQT3 mutants and native Na channels of myocardial tissue (Pepine and Wolff, 1999; Undrovinas *et al.*, 2006). In the present study, ranolazine reduced the peak Na currents but did not significantly alter the $V_{1/2}$ values of activation or steady-state inactivation of either the WT or the Y1767C channel (Supplemental Figure 2.1). In response to rapid repetitive depolarization, ranolazine produced a potent use-dependent inhibition of the WT channel (Figures 2.7A and 2.7B). Paradoxically, the Y1767C mutation potentiated the use-dependent inhibition produced by ranolazine. These data suggested that, unlike class I antiarrhythmics, the Y1767C mutation promotes ranolazine binding. The differential effect of the Y1767C mutation on ranolazine and class I antiarrhythmics reflects substantial differences in the mechanisms of binding to and inhibition of Na channels. The strong dependence of ranolazine inhibition on rapid repetitive pulsing and the relative weak inhibition of inactivated channels suggests that the drug may principally inhibit $Na_v1.5$ channels by an open-channel blocking mechanism. This contrasts with most antiarrhythmic drugs that primarily inhibit Na channels by binding with high affinity to inactivated states of the channel (Hille, 1977; Hondeghem and Katzung, 1977). The Y1767C mutation described here is bracketed by two naturally occurring LQT3 mutations (M1766L, I1768V) (Valdivia *et al.*, 2002a; Groenewegen *et al.*, 2003a). Like Y1767, the M1766L mutation induces a persistent Na current at depolarized voltages while I1768V accelerates the recovery from inactivation. Another LQT3 mutation located just upstream from Y1767 (V1763M) induces lidocaine-insensitive persistent Na

currents, suggesting that this mutation may disrupt antiarrhythmic drug binding in a similar way (Chang *et al.*, 2004). These findings support the idea that Y1767C is located within a region of the DIVS6 segment that is important for both the generation of persistent Na currents and antiarrhythmic drug binding.

Recent work demonstrated that mutations near the middle of the DIVS6 segment of the $Na_v1.5$ channel (e.g., F1760A) that weaken antiarrhythmic drug binding also attenuate ranolazine inhibition, suggesting the these drugs share a common binding site (Fredj *et al.*, 2006). Y1767 is situated near the cytoplasmic end of the DIVS6 segment and is an important contributor to the drug binding site of $Na_v1.5$ channels (O'Leary and Chahine, 2002; O'Leary *et al.*, 2003). The aromatic side chain at this position appears to be exposed in the aqueous pore where it is believed to directly interact with bound drugs (Ahern *et al.*, 2008). We speculate that the presence of a bulky aromatic residue in the pore (Figure 2.8) may decrease the accessibility of comparatively large drugs like ranolazine to the cytoplasmic anesthetic binding site. Replacing the tyrosine with the smaller cysteine appears to reduce this steric hindrance and facilitate ranolazine binding. This is substantially different from conventional anesthetics where binding is highly dependent on the presence of an aromatic amino acid at that position for potent use-dependent inhibition (Li *et al.*, 1999). The tyrosine at position 1767 appears to play a dual role in drug binding. Y1767 directly contributes to the local anesthetic binding site of $Na_v1.5$ channels and is critical for the high-affinity binding of many antiarrhythmic drugs. In addition, Y1767 appears to act as an energy barrier that prevents large drugs from gaining access to the cytoplasmic aqueous pore. The V1763 residue is not exposed to the cytoplasmic pore (Figure 2.8). Consequently, ranolazine has a lower accessibility to V1763M mutation because of the barrier effect of Y1767. Indeed, ranolazine has different effects on the frequency and recovery from frequency inhibition of Y1767C (Figure 2.7) and V1763M channels (Supplemental Figure 2.5).

In summary, we characterized the properties of a unique cardiac Na channel mutation identified in a patient suffering from LTQ3. This mutation involved a single base change resulting in a tyrosine (Y) to cysteine (C) substitution at position 1767 (Y1767C). The Y1767C mutation is located in the DIVS6 segment of the Na channel, a region that is known to contribute to both fast inactivation and the binding of antiarrhythmic drugs. Y1767C produced changes in Na channel gating similar to other LQT3 mutations, including persistent Na current at depolarized voltages, an increased window current, accelerated inactivation, and rapid recovery from inactivation. The

changes predicted an increase in the excitability of $Na_v1.5$ channels and enhanced persistent Na current during the plateau phase of the cardiac action potential. These effects appeared to underlie the LQT3 phenotype observed in this patient. Ranolazine was a highly selective inhibitor of the Y1767C-induced persistent Na currents and may be an effective therapeutic for treating LQT3 patients harboring this mutation. This is consistent with the observation that ranolazine reduced both the window and the persistent Na current to control levels. Furthermore, our data revealed that the Y1767 residue plays a unique role in inactivating and in forming the intracellular pore of $Na_v1.5$ Na channels.

2.7 Acknowledgments: This study was supported by grants from the Heart and Stroke Foundation of Québec (HSFQ) and the Canadian Institute of health Research (CIHR, MT-13181).

2.8 Figure legends

Figure 2.1: ECG and the sequencing analysis. (A) ECG features of the patient. The ECG showed a prolonged QTc of 510 ms in lead 2 with notched/diphasic T waves. (B) The sequencing analysis of the mutation Y1767C. Sequencing revealed a single amino acid substitution (A5300G) that led to a single amino acid substitution (Y1767C) in the 6th transmembrane segment of the IVth $Na_v1.5$ domain.

Figure 2.2: Whole-cell currents in tsA201 cells. (A) Representative whole-cell traces of WT (left) and Y167C (right). I_{Na} was elicited with a holding potential of –140 mV, depolarizing from –100 to +50 mV in 10-mV increments lasting 50 ms for each step (see inset protocol). (B) Current-voltage (*I-V*) relationship of WT (•, n=9) and Y1767C (○, n=10). The current amplitude was normalized to the membrane capacitance to obtain a measure of Na current densities. (C) The voltage-dependent time constants of inactivation in WT (• for τ_{slow}, n=9; ○ for τ_{fast}, n=9) and Y1767C (■ for τ_{slow}, n=10; □ for τ_{fast}, n=10). Currents were fitted to a two-exponential function: $I = I_{resid} + A_{fast} \times \exp(-(t-k)/\tau_{fast}) + A_{slow} \times \exp(-(t-k)/\tau_{slow})$. The corresponding time constants τ_{fast} and τ_{slow} were obtained from the equation with significant differences ranging from –60 to +20 mV between WT and Y1767C (* $p<0.05$; ** $p<0.01$).

Figure 2.3: Persistent Na currents and enlarged window currents induced by Y1767C. Persistent Na currents of WT (A) and Y1767C (B). The dashed line represents zero current. The persistent Na currents were induced by a depolarizing step to –30 mV for 400 ms jumping from a holding potential of –140 mV (see protocol in inset). The currents in blue represent the blocking effects of 10 μM TTX. (C) The voltage dependence of steady-state activation and inactivation of WT (• for activation, n=9; ■ for inactivation, n=7), Y1767C (○ for activation, n=10; □ for inactivation, n=6). Activated curves were derived from the same data and their graphically determined reversal potentials as *I-V* curves (Figure 2.2B) and were fitted to a standard Boltzmann equation: $G(V)/G_{max} = 1/(1+\exp((V-V_{1/2})/k))$. The voltage-dependence of inactivation was induced by applying conditioning pre-pulses to membrane potentials ranging from a holding potential of –140 to –10 mV for 500 ms with 10-mV increments and was then measured using a 20-ms test pulse to –30 mV for each step (see protocol in inset). The recorded inactivation data were fitted to a standard Boltzmann equation: $I(V)/I_{max} = 1/(1+\exp((V-$

$V_{1/2})/k)) + C$. (D) Window currents. The window region represents an enlarged portion of overlapping area between activation and inactivation of WT and Y1767C.

Figure 2.4: Effects of Y1767C on the $Na_v1.5$ window current. The overlap of the activation and inactivation of Na channels defines a range of voltages (i.e., window) where the channels are partially activated but not fully inactivated. The probability of being within this window was calculated from the product of the activation and steady-state inactivation parameters (Figure 2.3C) through the equation: $(1/(1+ \exp((V_{1/2act}-V)/k_{act}))) \times ((1-C)/(1+ \exp((V-V_{1/2inact})/k_{inact}))+C)$. (A) This probability is a biphasic function of voltage with a peak at –90 mV and at voltages more depolarized than –40 mV. This pattern resulted from a combination of the window and persistent components of Na channel gating. The individual contributions of the window and persistent components were evaluated and are plotted in Panels B and C. (B) The Y1767C mutation widened the window and increased the peak 3-fold. (C) Y1767C shifted the onset of the persistent component toward more hyperpolarized voltages and increased its amplitude 8-fold.

Figure 2.5: Recovery from fast inactivation and ramp currents. (A) Recovery from fast inactivation of WT (•, n=7) and Y1767C (○, n=7). The currents were induced by a two-pulse protocol with a variable recovery interval ranging from 0.1 to 200 ms. The conditioning pre-pulse lasting 40 ms was depolarized to –30 mV . The currents were measured using a test pulse at –30 mV lasting 20 ms (see protocol in inset). The time constants (values shown in Table 2.1) were obtained using a two-exponential function: $I_{Na} = Y_0+A_f \times (1-\exp [-t/\tau_f]) + A_s \times (1-\exp [-t/\tau_s])$. (B) Representative traces of ramp currents in WT (black) and Y1767C (red). The traces were elicited by 0.32 mV/ms of ramp depolarizations from –140 to +20 mV for 500 ms (see protocol in inset). Ramp currents increased, with a slight shift of their peak voltages to on, for the Y1767C mutation.

Figure 2.6: Effects of class I Na channel blockers and ranolazine on persistent Na currents. (A) Effects on the persistent Na current of channels treated with 150 μM quinidine (top, left), 10 μM mexiletine (top, right), 50 μM flecainide (bottom, left), and 50 μM ranolazine (bottom, right). Using the same protocol as Figure 2.3, 10 μM TTX was used to block the persistent currents after the unsuccessful treatment using class I Na channel blockers. (B) Histogram of the persistent Na currents. The persistent Na current accounted for 0.2 ± 0.2% of the peak current amplitude for WT

(n=5) at –30 mV, and 1.2 ± 0.3% for Y1767C (n=6) (** $p<0.01$). The percentage of the persistent Na currents was reduced to 0.3 ± 0.3% after the ranolazine treatment. The percentages were not statistically reduced by the quinidine (1.8 ± 0.5 %, n=6), mexiletine (1.6 ± 0.4 %, n=5), or flecainide (1.5 ± 0.5 %, n=6) treatments compared to those of the untreated Y1767C channels.

Figure 2.7: Frequency-dependent inhibition and recovery from frequency inhibition. (A) Frequency-dependent inhibition at 20 Hz of WT (•, n=7), Y1767C (○, n=7), WT with ranolazine (■, n=8), and Y1767C with ranolazine (□, n=8). A 50-pulse train was applied at –30 mV for 10 ms, jumping from a holding potential of –140 mV at 20 Hz (see protocol in inset). Each normalized peak current was plotted against the pulse number. (B) Relative amplitudes normalized to the 50th sweep (P_{50}/P_1) with and without ranolazine. Before the ranolazine treatment, there were no differences in normalized currents between WT (•, n= 7) and Y1767C (○, n= 7). After the ranolazine treatment, normalized currents of both WT (■, n= 8) and Y1767C (□, n= 8) were inhibited. There was a further inhibition at high frequency stimuli from 10 to 50 Hz for Y1767C (* $p<0.05$, ** $p<0.01$ vs. WT; $^{\#}$ $p<0.05$, $^{\#\#}$ $p<0.01$ vs. WT with ranolazine). (C) Recovery from frequency-dependent inhibition of WT (•, n=7), Y1767C (○, n=7), WT with ranolazine (■, n=8), and Y1767C with ranolazine (□, n=8). The currents were induced by applying a 50-pulse train of the conditioning pre-pulses to –30 mV for 10 ms at 50 Hz from a holding potential of –140 mV. The test pulses were then applied to –30 mV for 20 ms to measure the peak current amplitudes after a variable duration of 0.1 to 9000 ms. The resulting curves were fitted to a two-exponential function: $I_{Na} = Y_0 + A_f \times (1-\exp[-t/\tau_f]) + A_s \times (1-\exp[-t/\tau_s])$.

Figure 2.8: Homology model of the D4S6 segment. A. Side view of a homology model of the Na channel S6 segments based on the M2 segment of the MthK channel. D1S6 has been removed for clarity. **B.** Top view of the model showing that F1760, V1763, and Y1767 are exposed within the central cavity.

2.9 Reference List

Ahern CA, Eastwood AL, Dougherty DA, and Horn R (2008). Electrostatic contributions of aromatic residues in the local anesthetic receptor of voltage-gated sodium channels. *Circ Res* 102, 86-94.

Antzelevitch C, Belardinelli L, Wu L, Fraser H, Zygmunt AC, Burashnikov A, Di Diego JM, Fish JM, Cordeiro JM, Goodrow RJ, Jr., Scornik F, and Perez G (2004). Electrophysiologic properties and antiarrhythmic actions of a novel antianginal agent. *J Cardiovasc Pharmacol Ther* 9 Suppl 1, S65-S83.

Attwell D, Cohen I, Eisner D, Ohba M, and Ojeda C (1979). The steady state TTX-sensitive ("window") sodium current in cardiac Purkinje fibres. *Pflügers Arch* 379, 137-142.

Benhorin J, Taub R, Goldmit M, Kerem B, Kass RS, Windman I, and Medina A (2000). Effects of flecainide in patients with new *SCN5A* mutation : mutation-specific therapy for long-QT syndrome? *Circulation* 101, 1698-1706.

Bennett PB, Yazawa K, Makita N, and George AL, Jr. (1995). Molecular mechanism for an inherited cardiac arrhythmia. *Nature* 376, 683-685.

Blanchet J, Pilote S, and Chahine M (2007). Acidic residues on the voltage-sensor domain determine the activation of the NaChBac sodium channel. *Biophys J* 92, 3513-3523.

Chahine M, Chen LQ, Barchi RL, Kallen RG, and Horn R (1992). Lidocaine block of human heart sodium channels expressed in *Xenopus* oocytes. *J Mol Cell Cardiol* 24, 1231-1236.

Chandra R, Starmer CF, and Grant AO (1998). Multiple effects of KPQ deletion mutation on gating of human cardiac Na^+ channels expressed in mammalian cells. *Am J Physiol* 274, H1643-H1654.

Chang CC, Acharfi S, Wu MH, Chiang FT, Wang JK, Sung TC, and Chahine M (2004). A novel SCN5A mutation manifests as a malignant form of long QT syndrome with perinatal onset of tachycardia/bradycardia. *Cardiovasc Res* 64, 268-278.

Chenna R, Sugawara H, Koike T, Lopez R, Gibson TJ, Higgins DG, and Thompson JD (2003). Multiple sequence alignment with the Clustal series of programs. *Nucleic Acids Res* 31, 3497-3500.

Clancy CE and Kass RS (2005). Inherited and acquired vulnerability to ventricular arrhythmias: cardiac Na+ and K+ channels. *Physiol Rev* 85, 33-47.

Deschênes I, Baroudi G, Berthet M, Barde I, Chalvidan T, Denjoy I, Guicheney P, and Chahine M (2000). Electrophysiological characterization of SCN5A mutations causing long QT (E1784K) and Brugada (R1512W and R1432G) syndromes. *Cardiovasc Res* 46, 55-65.

Fredj S, Sampson KJ, Liu H, and Kass RS (2006). Molecular basis of ranolazine block of LQT-3 mutant sodium channels: evidence for site of action. *Br J Pharmacol* 148, 16-24.

Gellens ME, George AL, Jr., Chen LQ, Chahine M, Horn R, Barchi RL, and Kallen RG (1992). Primary structure and functional expression of the human cardiac tetrodotoxin-insensitive voltage-dependent sodium channel. *Proc Natl Acad Sci USA* 89, 554-558.

Groenewegen WA, Bezzina CR, van Tintelen JP, Hoorntje TM, Mannens MMAM, Wilde AAM, Jongsma HJ, and Rook MB (2003). A novel LQT3 mutation implicates the human cardiac sodium channel domain IVS6 in inactivation kinetics. *Cardiovasc Res* 57, 1072-1078.

Hale SL, Shryock JC, Belardinelli L, Sweeney M, and Kloner RA (2008). Late sodium current inhibition as a new cardioprotective approach. *J Mol Cell Cardiol* 44, 954-967.

Hille B (1977). Local anesthetics: hydrophilic and hydrophobic pathways for the drug-receptor reaction. *J Gen Physiol* 69, 497-515.

Hondeghem LM and Katzung BG (1977). Time- and voltage-dependent interactions of antiarrhythmic drugs with cardiac sodium channels. *Biochim Biophys Acta* 472, 373-398.

Huang H, Millat G, Rodriguez-Lafrasse C, Rousson R, Kugener B, Chevalier P, and Chahine M (2009). Biophysical characterization of a new SCN5A mutation S1333Y in a SIDS infant linked to long QT syndrome. *FEBS Lett* 583, 890-896.

Jiang Y, Lee A, Chen J, Cadene M, Chait BT, and MacKinnon R (2002). Crystal structure and mechanism of a calcium-gated potassium channel. *Nature* 417, 515-522.

Kambouris NG, Nuss HB, Johns DC, Tomaselli GF, Marban E, and Balser JR (1998). Phenotypic characterization of a novel long-QT syndrome mutation (R1623Q) in the cardiac sodium channel. *Circulation* 97, 640-644.

Keller DI, Acharfi S, Delacrétaz E, Benammar N, Rotter M, Pfammatter JP, Fressart V, Guicheney P, and Chahine M (2003). A novel mutation in *SCN5A*, delQKP 1507-1509, causing long QT syndrome: Role of Q1507 residue in sodium channel inactivation. *J Mol Cell Cardiol* 35, 1513-1521.

Li HL, Galue A, Meadows L, and Ragsdale DS (1999). A molecular basis for the different local anesthetic affinities of resting versus open and inactivated states of the sodium channel. *Mol Pharmacol* 55, 134-141.

Liu H, Atkins J, and Kass RS (2003). Common molecular determinants of flecainide and lidocaine block of heart Na^+ channels: evidence from experiments with neutral and quaternary flecainide analogues. *J Gen Physiol* 121, 199-214.

Margolskee RF, McHendry-Rinde B, and Horn R (1993). Panning transfected cells for electrophysiological studies. *Biotechniques* 15, 906-911.

McPhee JC, Ragsdale DS, Scheuer T, and Catterall WA (1994). A mutation in segment IVS6 disrupts fast inactivation of sodium channels. *Proc Natl Acad Sci USA* 91, 12346-12350.

McPhee JC, Ragsdale DS, Scheuer T, and Catterall WA (1995). A critical role for transmembrane segment IVS6 of the sodium channel alpha subunit in fast inactivation. *J Biol Chem* 270, 12025-12034.

Mohler PJ, Schott JJ, Gramolini AO, Dilly KW, Guatimosim S, DuBell WH, Song LS, Haurogne K, Kyndt F, Ali ME, Rogers TB, Lederer WJ, Escande D, Marec HL, and Bennett V (2003). Ankyrin-B mutation causes type 4 long-QT cardiac arrhythmia and sudden cardiac death. *Nature* 421, 634-639.

Moss AJ, Zareba W, Schwarz KQ, Rosero S, McNitt S, and Robinson JL (2008). Ranolazine shortens repolarization in patients with sustained inward sodium current due to type-3 long-QT syndrome. *J Cardiovasc Electrophysiol* 19, 1289-1293.

Nagatomo T, January CT, and Makielski JC (2000). Preferential block of late sodium current in the LQT3 DeltaKPQ mutant by the class I(C) antiarrhythmic flecainide. *Mol Pharmacol* 57, 101-107.

O'Leary ME and Chahine M (2002). Cocaine binds to a common site on open and inactivated human heart (Nav1.5) sodium channels. *J Physiol* 541, 701-716.

O'Leary ME, Digregorio M, and Chahine M (2003). Closing and inactivation potentiate the cocaethylene inhibition of cardiac sodium channels by distinct mechanisms. *Mol Pharmacol* 64, 1575-1585.

Pepine CJ and Wolff AA (1999). A controlled trial with a novel anti-ischemic agent, ranolazine, in chronic stable angina pectoris that is responsive to conventional antianginal agents. Ranolazine Study Group. *Am J Cardiol* 84, 46-50.

Qu Y, Rogers J, Tanada T, Scheuer T, and Catterall WA (1995). Molecular determinants of drug access to the receptor site for antiarrhythmic drugs in the cardiac Na^+ channel. *Proc Natl Acad Sci USA* 92, 11839-11843.

Ragsdale DS, McPhee JC, Scheuer T, and Catterall WA (1996). Common molecular determinants of local anesthetic, antiarrhythmic, and anticonvulsant block of voltage-gated Na^+ channels. *Proc Natl Acad Sci USA* 93, 9270-9275.

Schwartz PJ, Priori SG, Locati EH, Napolitano C, Cantù F, Towbin JA, Keating MT, Hammoude H, Brown AM, Chen LS, and Colatsky TJ (1995). Long QT syndrome patients with mutations of the *SCN5A* and *HERG* genes have differential responses to Na^+ channel blockade and to increases in heart rate. Implications for gene-specific therapy. *Circulation* 92, 3381-3386.

Undrovinas AI, Belardinelli L, Undrovinas NA, and Sabbah HN (2006). Ranolazine improves abnormal repolarization and contraction in left ventricular myocytes of dogs with heart failure by inhibiting late sodium current. *J Cardiovasc Electrophysiol* 17 Suppl 1, S169-S177.

Valdivia CR, Ackerman MJ, Tester DJ, Wada T, McCormack J, Ye B, and Makielski JC (2002). A novel *SCN5A* arrhythmia mutation, M1766L, with expression defect rescued by mexiletine. *Cardiovasc Res* 55, 279-289.

Wang DW, Desai RR, Crotti L, Arnestad M, Insolia R, Pedrazzini M, Ferrandi C, Vege A, Rognum T, Schwartz PJ, and George AL, Jr. (2007). Cardiac sodium channel dysfunction in sudden infant death syndrome. *Circulation* 115, 368-376.

Wang DW, Yazawa K, George AL, Jr., and Bennett PB (1996a). Characterization of human cardiac Na^+ channel mutations in the congenital long QT syndrome. *Proc Natl Acad Sci USA* 93, 13200-13205.

Wang DW, Yazawa K, Makita N, George AL, Jr., and Bennett PB (1997). Pharmacological targeting of long QT mutant sodium channels. *J Clin Invest* 99, 1714-1720.

Wang GK, Calderon J, and Wang SY (2008). State- and use-dependent block of muscle Nav1.4 and neuronal Nav1.7 voltage-gated Na+ channel isoforms by ranolazine. *Mol Pharmacol* 73, 940-948.

Wang Q, Li Z, Shen J, and Keating MT (1996b). Genomic organization of the human *SCN5A* gene encoding the cardiac sodium channel. *Genomics* 34, 9-16.

Wei J, Wang DW, Alings M, Fish F, Wathen M, Roden DM, and George AL, Jr. (1999). Congenital long-QT syndrome caused by a novel mutation in a conserved acidic domain of the cardiac Na^+ channel. *Circulation* 99, 3165-3171.

Wu L, Shryock JC, Song Y, Li Y, Antzelevitch C, and Belardinelli L (2004). Antiarrhythmic effects of ranolazine in a guinea pig in vitro model of long-QT syndrome. *J Pharmacol Exp Ther* 310, 599-605.

Zhorov BS and Bregestovski PD (2000). Chloride channels of glycine and GABA receptors with blockers: Monte Carlo minimization and structure-activity relationships. *Biophys J* 78, 1786-1803.

A

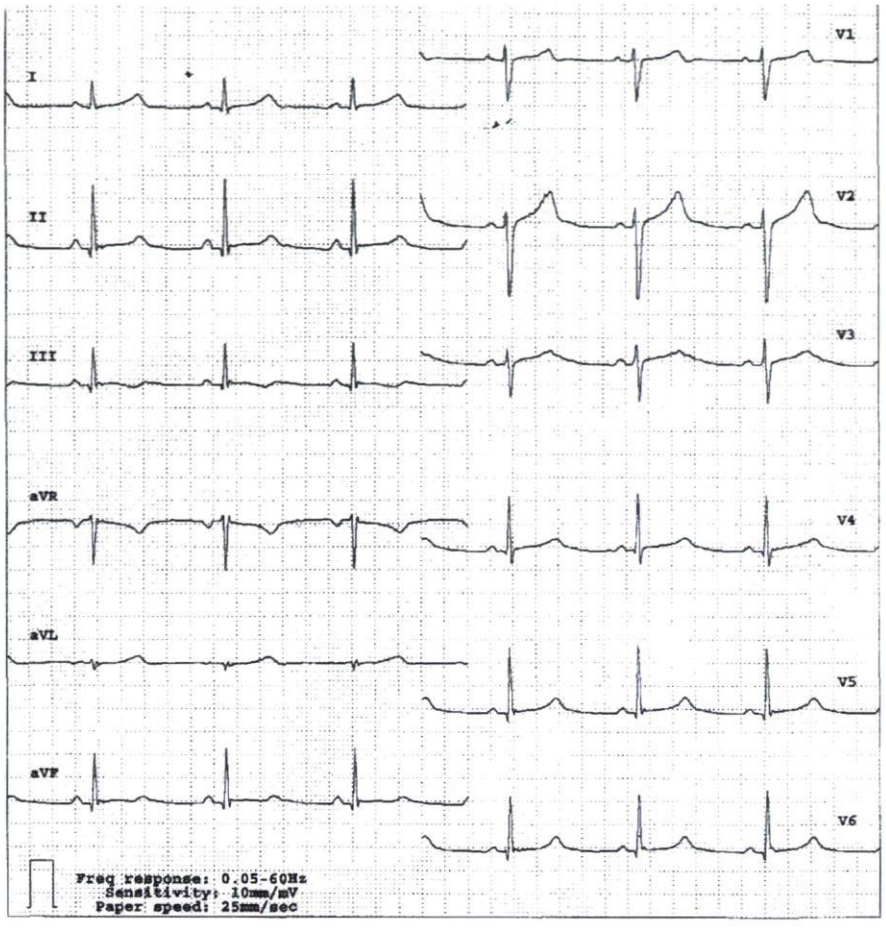
I
II
III
aVR
aVL
aVF
V1
V2
V3
V4
V5
V6
Freq response: 0.05-60Hz
Sensitivity: 10mm/mV
Paper speed: 25mm/sec

B

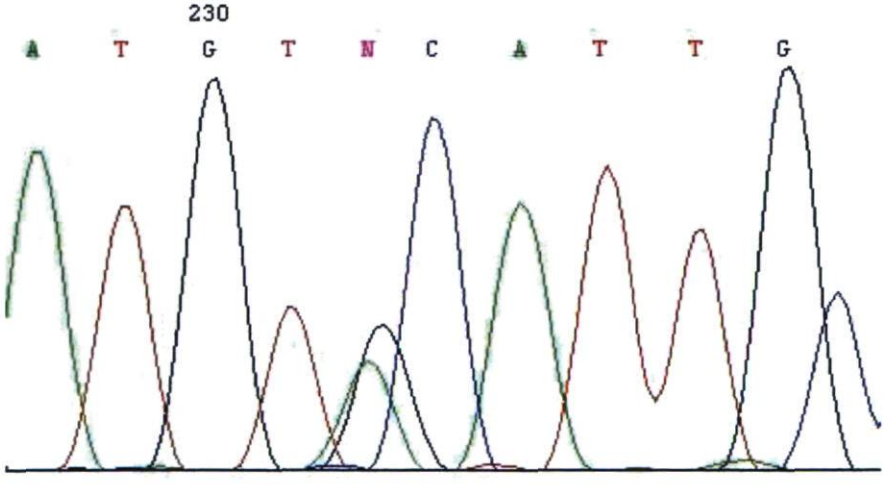
230
A T G T N C A T T G

Figure 2.1

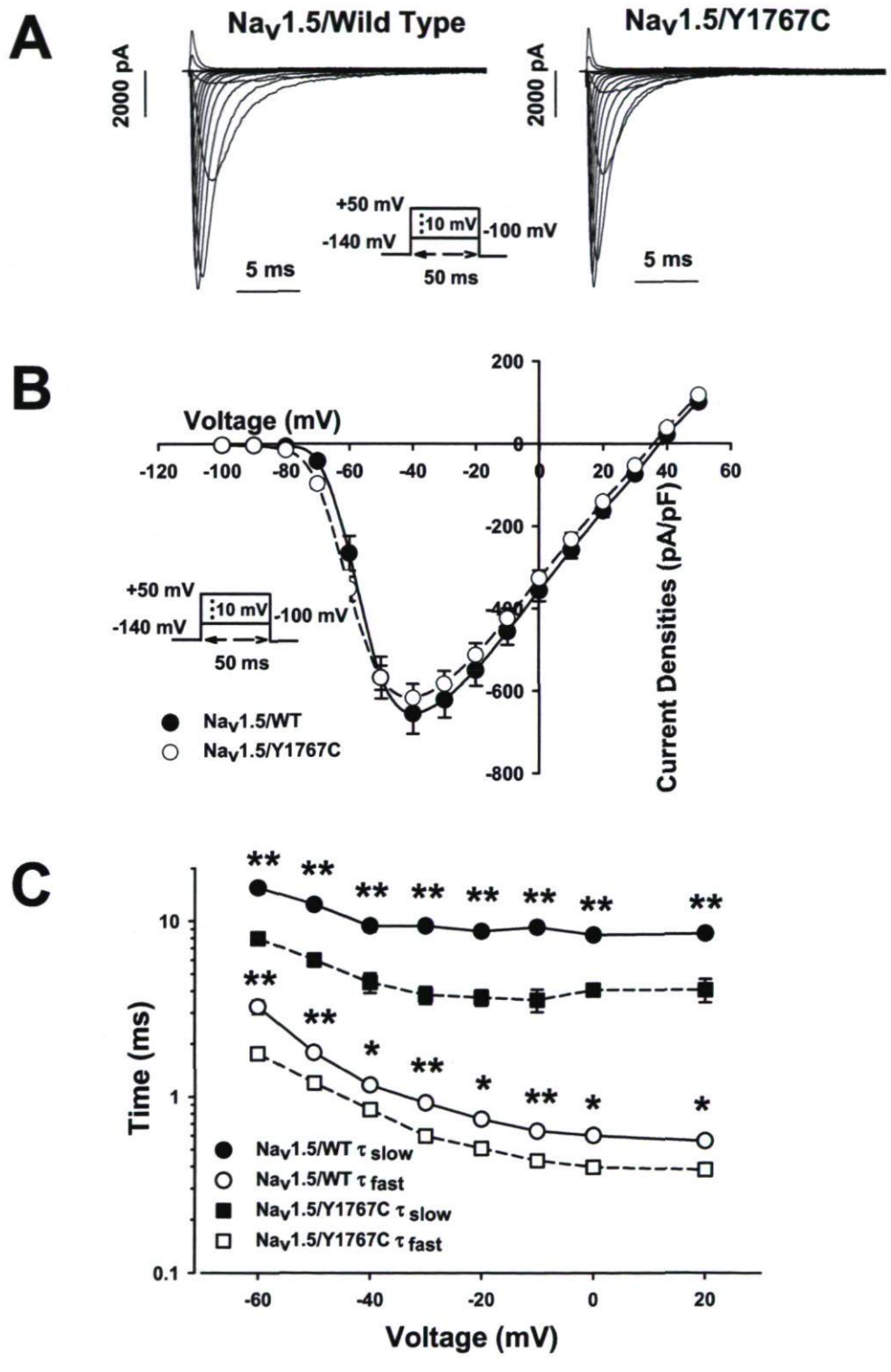
A
Na$_V$1.5/Wild Type
Na$_V$1.5/Y1767C
2000 pA
2000 pA
+50 mV
10 mV
-140 mV
-100 mV
50 ms
5 ms
5 ms
B
Voltage (mV)
200
0
-200
-400
-600
-800
-120
-100
-80
-60
-40
-20
0
20
40
60
Current Densities (pA/pF)
+50 mV
10 mV
-140 mV
-100 mV
50 ms
Na$_V$1.5/WT
Na$_V$1.5/Y1767C
C
Time (ms)
10
1
0.1
Na$_V$1.5/WT τ slow
Na$_V$1.5/WT τ fast
Na$_V$1.5/Y1767C τ slow
Na$_V$1.5/Y1767C τ fast
-60
-40
-20
0
20
Voltage (mV)

Figure 2.2

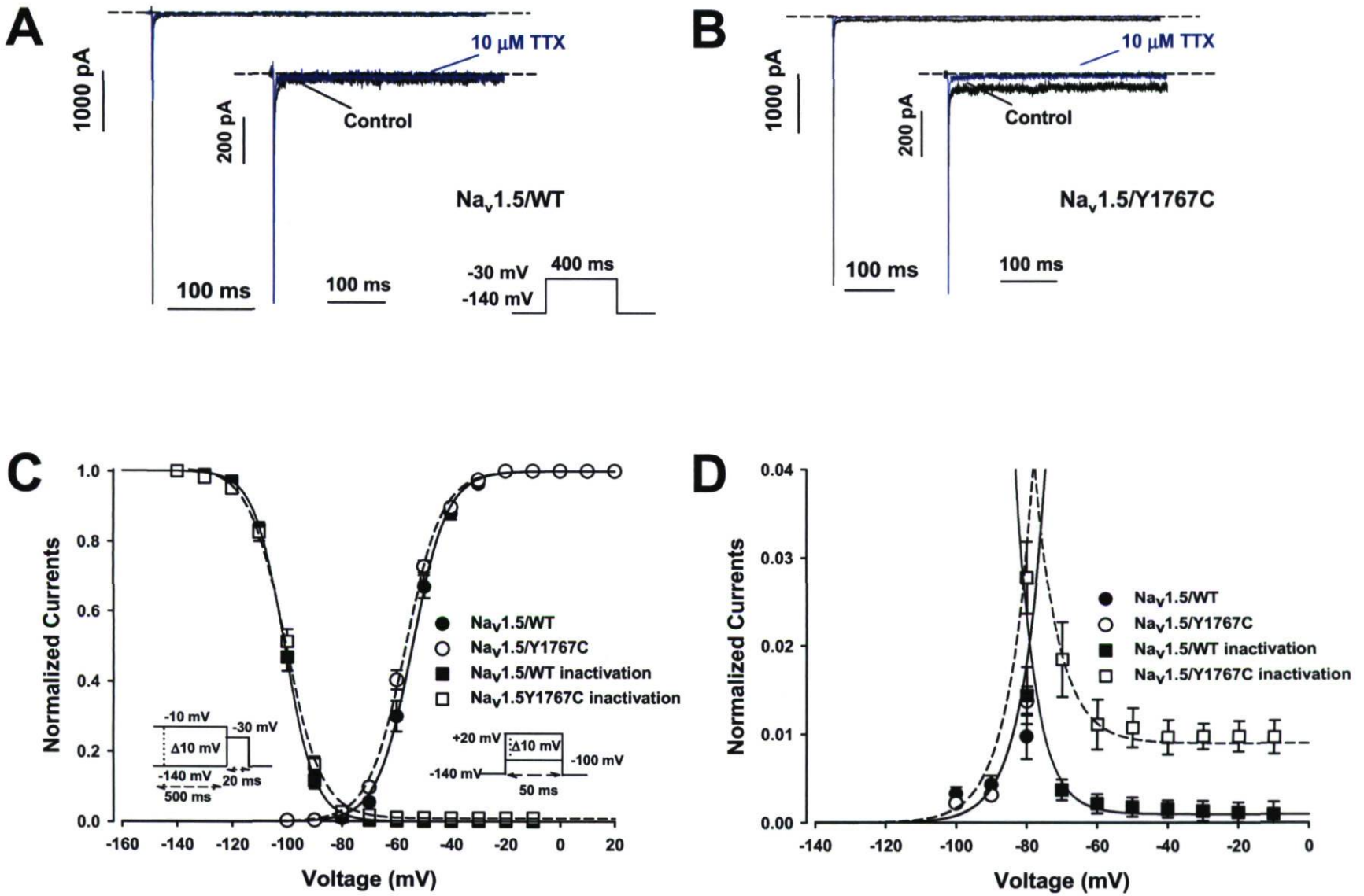
A
1000 pA
200 pA
10 μM TTX
Control
Na$_v$1.5/WT
100 ms
100 ms
-30 mV
-140 mV
400 ms
B
1000 pA
200 pA
10 μM TTX
Control
Na$_v$1.5/Y1767C
100 ms
100 ms
C
Normalized Currents
Voltage (mV)
Na$_v$1.5/WT
Na$_v$1.5/Y1767C
Na$_v$1.5/WT inactivation
Na$_v$1.5Y1767C inactivation
-10 mV
Δ10 mV
-30 mV
-140 mV
20 ms
500 ms
+20 mV
Δ10 mV
-100 mV
-140 mV
50 ms
D
Normalized Currents
Voltage (mV)
Na$_v$1.5/WT
Na$_v$1.5/Y1767C
Na$_v$1.5/WT inactivation
Na$_v$1.5/Y1767C inactivation

Figure 2.3

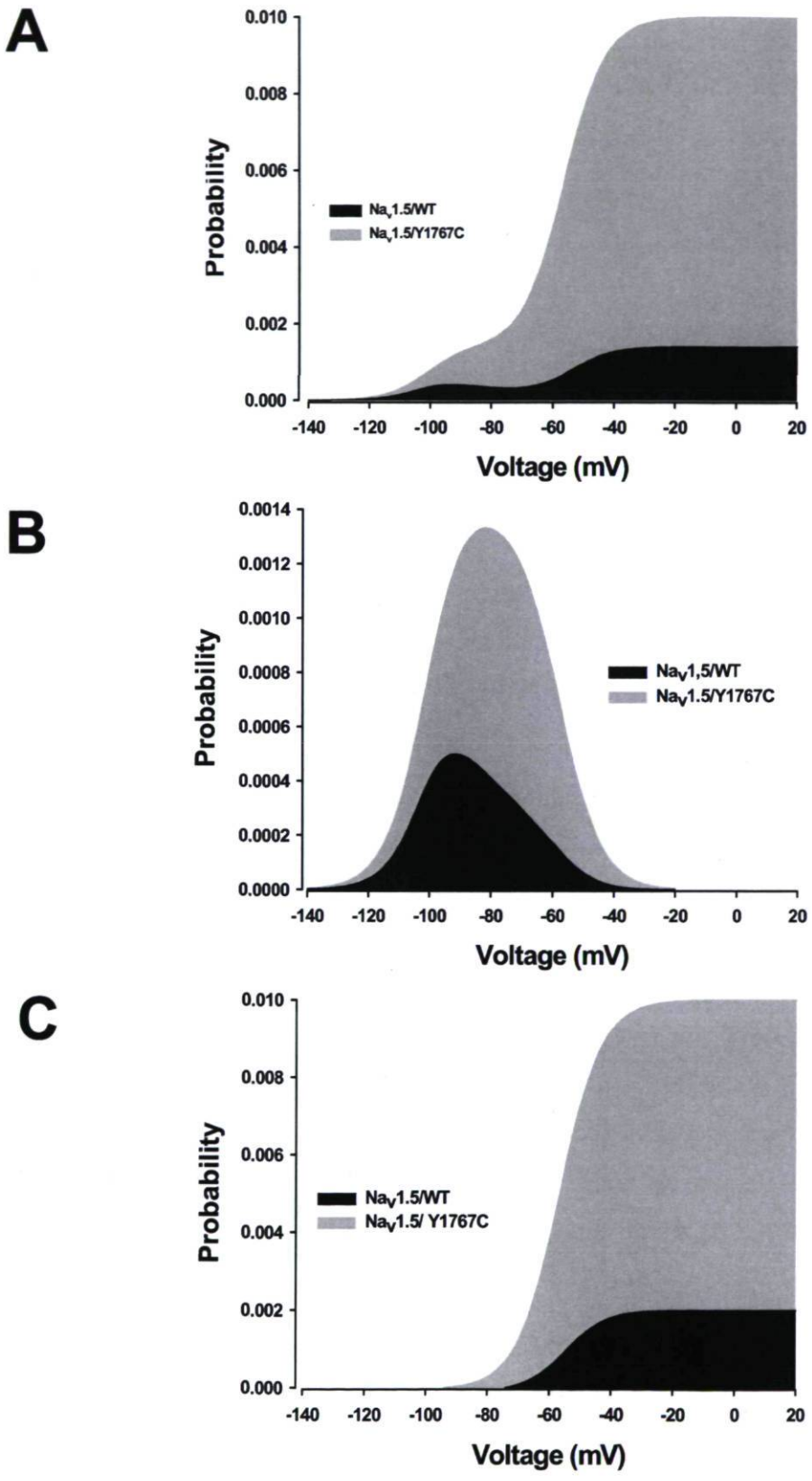
A
0.010
0.008
0.006
0.004
0.002
0.000
Probability
Na$_v$1.5/WT
Na$_v$1.5/Y1767C
-140 -120 -100 -80 -60 -40 -20 0 20
Voltage (mV)
B
0.0014
0.0012
0.0010
0.0008
0.0006
0.0004
0.0002
0.0000
Probability
Na$_V$1,5/WT
Na$_V$1.5/Y1767C
-140 -120 -100 -80 -60 -40 -20 0 20
Voltage (mV)
C
0.010
0.008
0.006
0.004
0.002
0.000
Probability
Na$_V$1.5/WT
Na$_V$1.5/ Y1767C
-140 -120 -100 -80 -60 -40 -20 0 20
Voltage (mV)

Figure 2.4

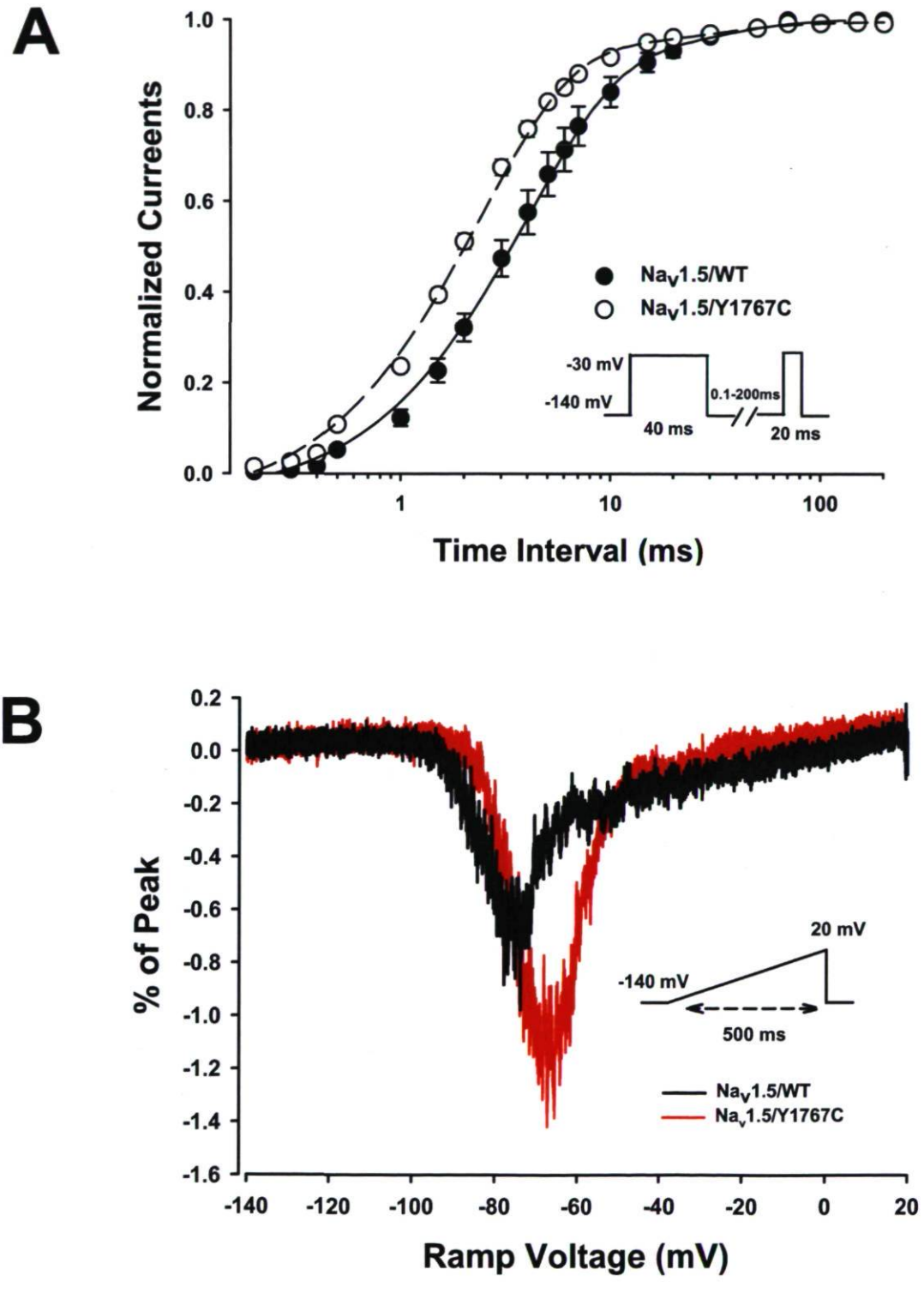
A
Normalized Currents
1.0
0.8
0.6
0.4
0.2
0.0
1
10
100
Time Interval (ms)
Na$_V$1.5/WT
Na$_V$1.5/Y1767C
-30 mV
-140 mV
40 ms
0.1-200ms
20 ms
B
% of Peak
0.2
0.0
-0.2
-0.4
-0.6
-0.8
-1.0
-1.2
-1.4
-1.6
-140
-120
-100
-80
-60
-40
-20
0
20
Ramp Voltage (mV)
20 mV
-140 mV
500 ms
Na$_V$1.5/WT
Na$_v$1.5/Y1767C

Figure 2.5

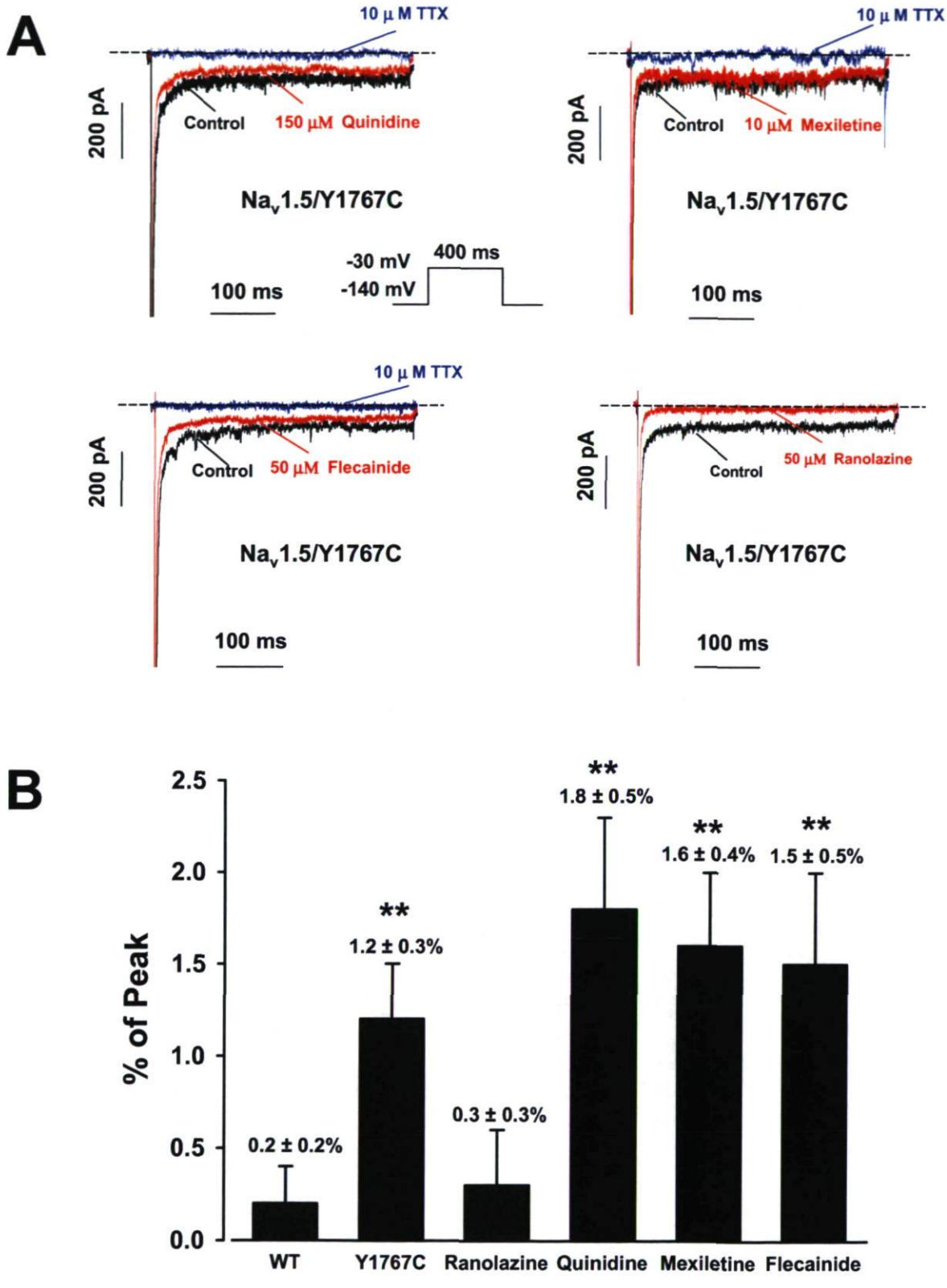
A
10 μ M TTX
200 pA
Control
150 μM Quinidine
Na$_v$1.5/Y1767C
-30 mV
-140 mV
400 ms
100 ms
10 μ M TTX
200 pA
Control
10 μM Mexiletine
Na$_v$1.5/Y1767C
100 ms
10 μ M TTX
200 pA
Control
50 μM Flecainide
Na$_v$1.5/Y1767C
100 ms
200 pA
Control
50 μM Ranolazine
Na$_v$1.5/Y1767C
100 ms
B
% of Peak
2.5
2.0
1.5
1.0
0.5
0.0
0.2 ± 0.2%
**
1.2 ± 0.3%
0.3 ± 0.3%
**
1.8 ± 0.5%
**
1.6 ± 0.4%
**
1.5 ± 0.5%
WT
Y1767C
Ranolazine
Quinidine
Mexiletine
Flecainide

Figure 2.6

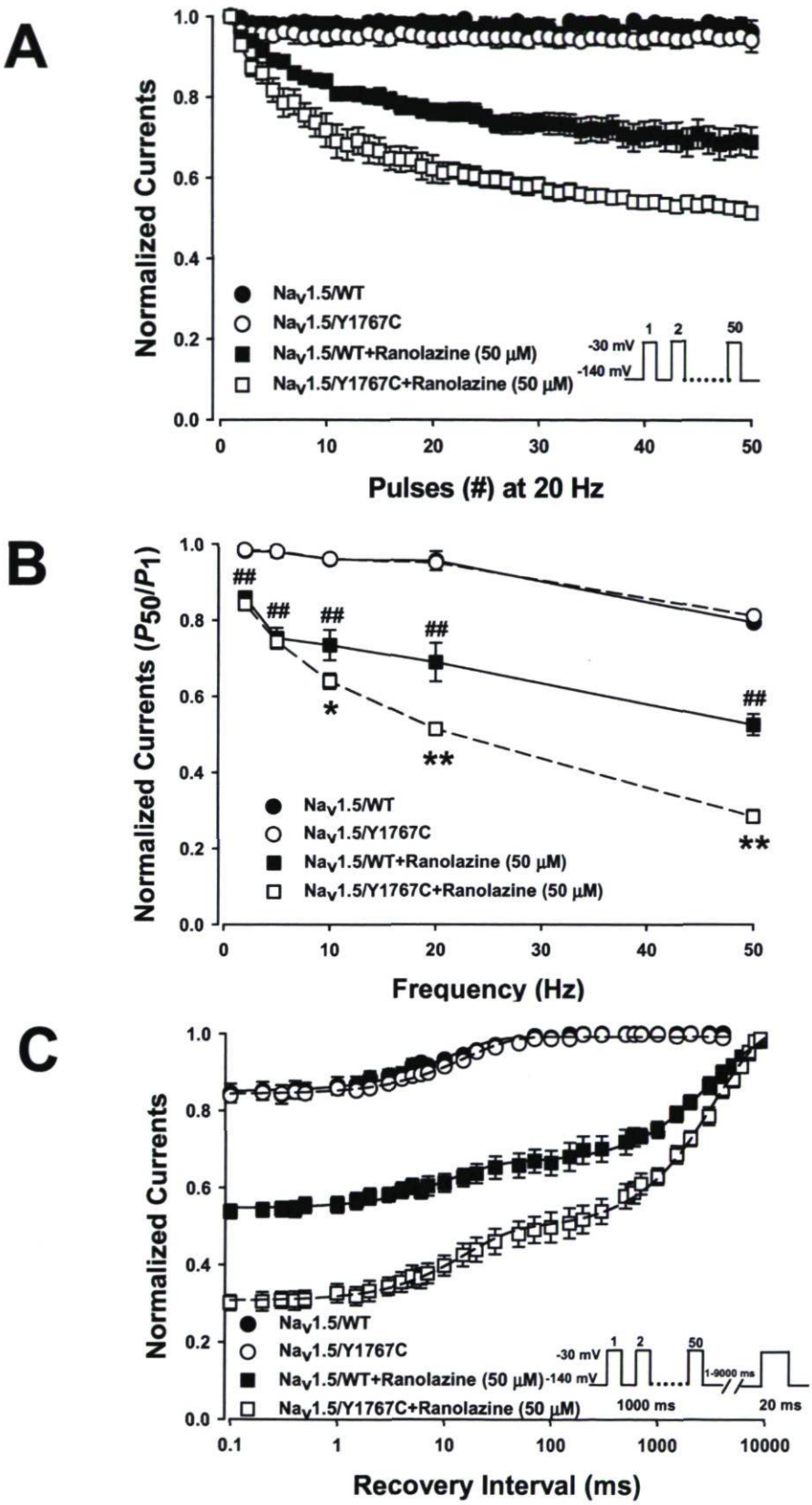
A
Normalized Currents
Pulses (#) at 20 Hz
Na$_V$1.5/WT
Na$_V$1.5/Y1767C
Na$_V$1.5/WT+Ranolazine (50 μM)
Na$_V$1.5/Y1767C+Ranolazine (50 μM)
-30 mV
-140 mV
1
2
50
B
Normalized Currents (P_{50}/P_1)
Frequency (Hz)
##
*
**
C
Normalized Currents
Recovery Interval (ms)
1000 ms
20 ms
1-9000 ms

Figure 2.7

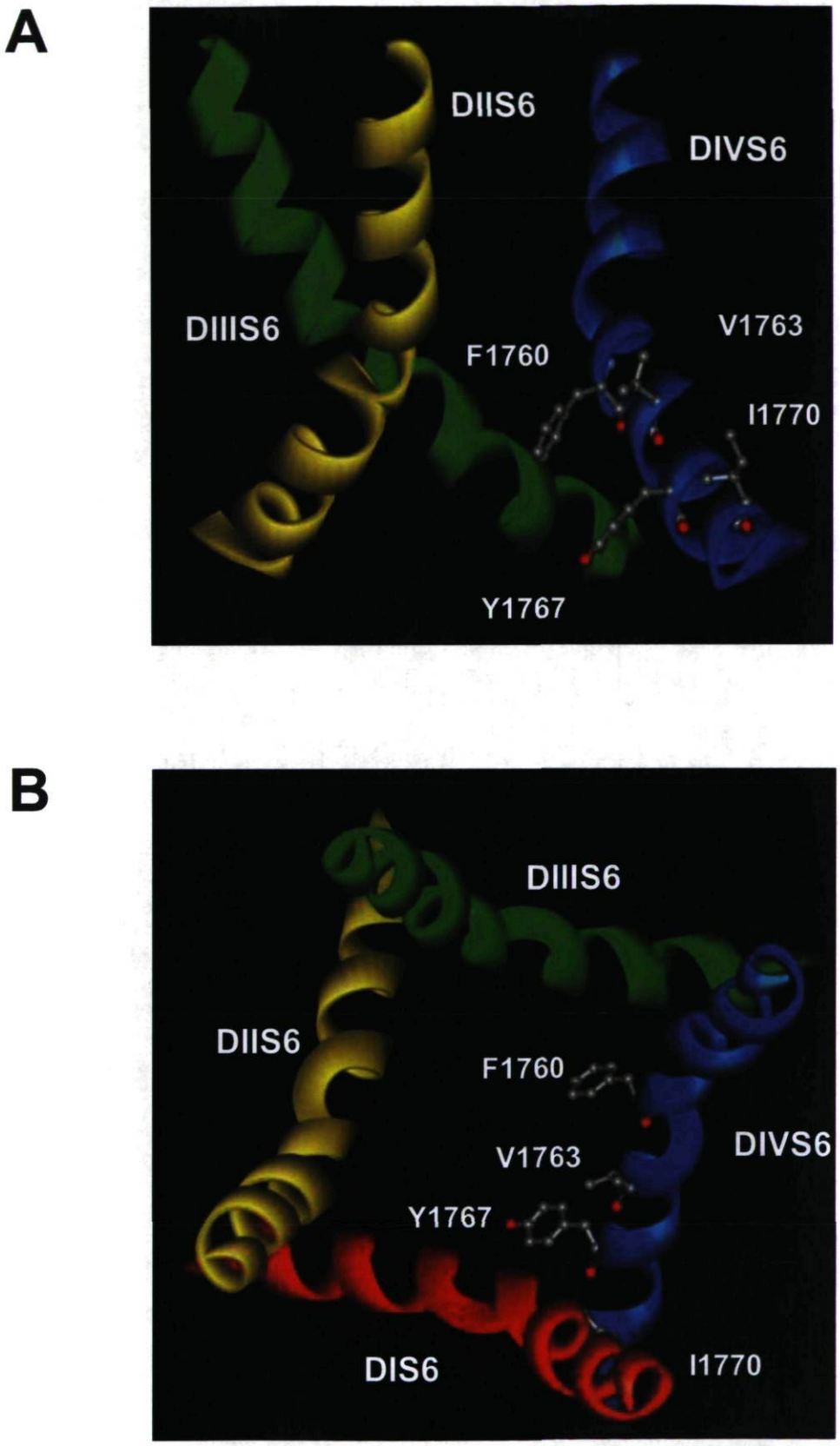
A
DIIS6
DIVS6
DIIIS6
F1760
V1763
I1770
Y1767
B
DIIIS6
DIIS6
F1760
V1763
DIVS6
Y1767
DIS6
I1770

Figure 2.8

Table 2.1 Biophysical properties of $Na_v1.5$/WT and $Na_v1.5$/Y1767C.

	WT	Y1767C	WT + Ranolazine	Y1767C + Ranolazine
Steady-state activation				
$V_{1/2}$ (mV)	–54.3 ± 0.9 (9)	–56.7 ± 0.6 (10)	–55.3 ± 0.9 (15)	–56.3 ± 0.5 (16)
k (mV)	6.5 ± 0.3 (9)	6.8 ± 0.2 (10)	6.2 ± 0.2 (15)	6.2 ± 0.2 (16)
Steady-state inactivation				
$V_{1/2}$ (mV)	–100.9 ± 0.6 (7)	–100.6 ± 0.5 (6)	–103.8 ± 0.8 (15)	–103.1 ± 0.7 (16)
k (mV)	5.5 ± 0.2 (7)	6.6 ± 0.2 ** (6)	5.5 ± 0.1 (15)	6.5 ± 0.1 $^{\#}$ (16)
C (%)	0.2 ± 0.1 (7)	1.0 ± 0.2 ** (6)	0.2 ± 0.1 (8)	0.2 ± 0.2 (8)
Recovery from fast inactivation				
τ_{fast} (ms)	4.3 ± 0.5 (7)	2.6 ± 0.1 ** (7)	4.4 ± 0.6 (12)	2.2 ± 0.3 $^{\#\#}$ (12)
τ_{Slow} (ms)	57.3 ± 7.2 (7)	38.8 ± 4.4 * (7)	53.3 ± 6.6 (12)	35.2 ± 5.0 $^{\#\#}$ (12)
A_{fast} (%)	95.6 ± 5.3 (7)	94.4 ± 3.0 (7)	93.7 ± 3.9 (12)	95.7 ± 2.1 (12)
A_{slow} (%)	4.4 ± 0.6 (7)	5.2 ± 1.3 (7)	6.2 ± 0.8 (12)	4.8 ± 0.8 (12)
Recovery from frequency inhibition				
τ_{fast} (ms)	3.8 ± 0.5 (7)	4.6 ± 0.5 (7)	15.6 ± 3.4 (8)	28.8 ± 3.5 $^{\#\#}$ (8)
τ_{Slow} (ms)	35.1 ± 3.9 (7)	40.8 ± 0.6 (7)	2446.1 ± 415.1 (8)	3986.5 ± 592.2$^{\#\#}$ (8)
A_{fast} (%)	7.8 ± 0.9 (7)	8.1 ± 0.1 (7)	10.2 ± 0.2 (8)	18.4 ± 0.3 $^{\#}$ (8)
A_{slow} (%)	7.9 ± 0.8 (7)	8.9 ± 0.1 (7)	32.8 ± 2.0 (8)	52.5 ± 3.0 $^{\#\#}$ (8)

$V_{1/2}$ = mid point for activation or inactivation; K_v = slow factor for activation or inactivation
C= value of the persistent sodium currents in steady-state inactivation;
τ= time constant;
A = the fractions of recovery component
* = WT versus Y1767C; $^{\#}$ = WT+Ranolazine versus Y1767C+Ranolazine
*, $^{\#}P$ <0.05; **, $^{\#\#}$ P <0.01

2.10 Supplemental figure legends

Supplemental Figure 2.1: Gating properties of steady-state activation and inactivation by ranolazine. (A) Effects of ranolazine on steady-state activation of WT (•, n= 15) and Y1767C mutation (○, n= 16). Channels were studied with the same protocol and fitting equation as Figure 3C with no significant shifts (values shown in Table 2.1). (B) Effects of ranolazine on steady-state inactivation. Using the protocol and fitting equation shown in Figure 3C, ranolazine had no significant effects on Y1767C mutation (values shown in Table 2.1).

Supplemental Figure 2.2: Effects of ranolazine on the WT window current. The window current was studied with the same protocols and fitting equations as Figures 2.4A and 2.4B.

Supplemental Figure 2.3: Effects of ranolazine on the Y1767C window current. The window current of Y1767C mutant channels was studied as shown in Figures 2.4A and 2.4B.

Supplemental Figure 2.4: Effects of ranolazine on persistent Na currents of *SCN5A* mutation V1763M. (A) Effects on the persistent Na currents treated by 50 μM ranolazine with the same protocol as Figures 2.3A and 2.3B. (B) The histogram of the persistent Na currents. The persistent Na currents accounted for 0.2 ± 0.2 % of the peak current amplitude for WT (n=5) at –30 mV, and 1.0 ± 0.3 % for V1763M mutation (n=5) (** $p<0.01$). The percentage of the persistent Na currents was reduced to 0.2 ± 0.1 % after ranolazine treatment.

Supplemental Figure 2.5: Frequency-dependent inhibition and recovery from frequency inhibition of SCN5A mutation V1763M. (A) Frequency-dependent inhibition at 20 Hz of V1763M (▲, n=6) and V1763M with ranolazine (Δ, n=6) using the same protocol as Figure 2.7A. (B) P_{50}/P_1 of V1763M (▲, n=6) and V1763M with ranolazine treatment (Δ, n=6) from 10 to 50 Hz. V1763M mutant channels had similar frequency-inhibition effects to Y1767C channels within the inhibition range. (C) Recovery from frequency-dependent inhibition of V1763M (▲, n=6) and V1763M with ranolazine treatment (Δ, n=6). The protocol was performed and resulting dada were plotted with the same strategies as Figure 2.7C.

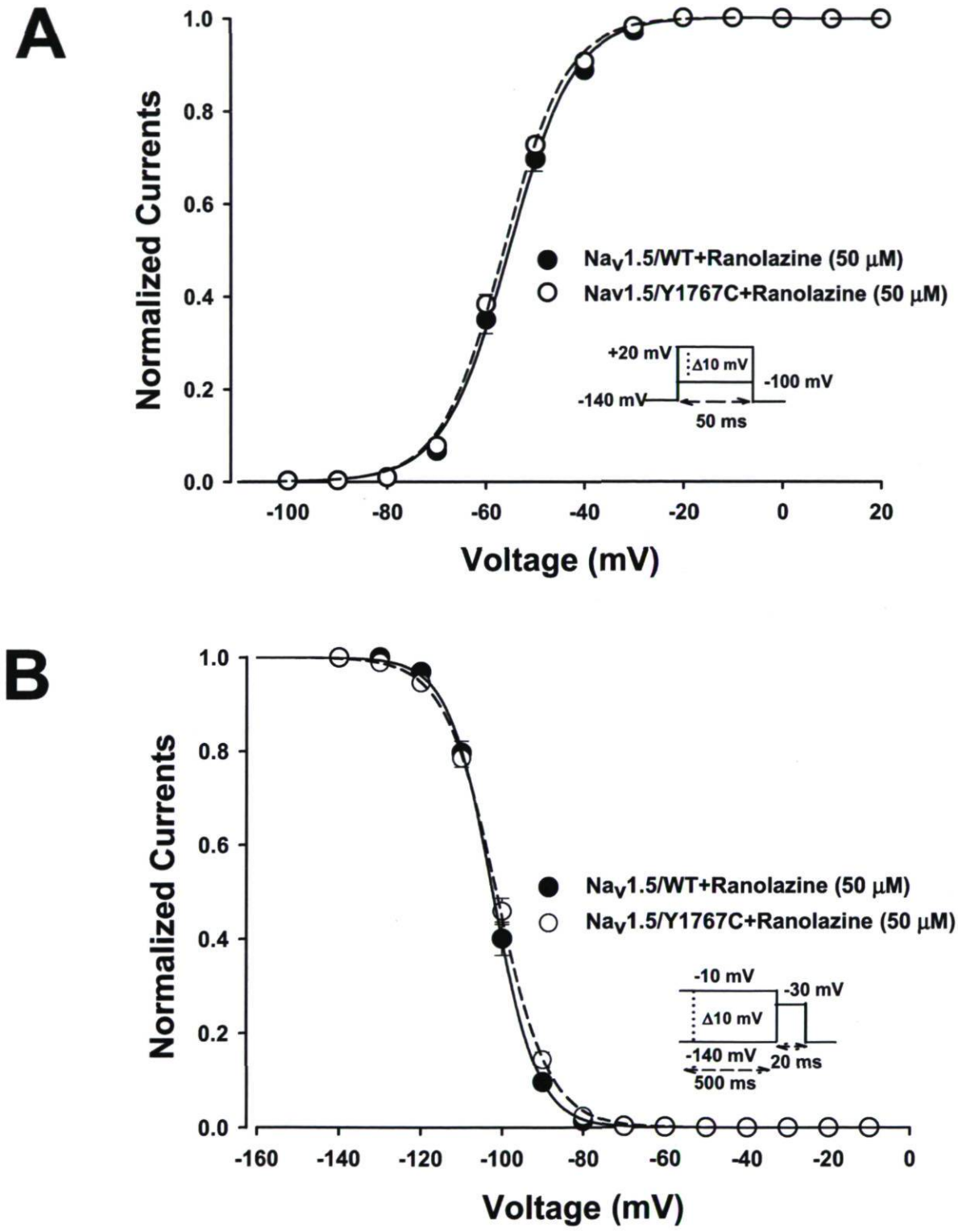

Supplemental Figure 2.1

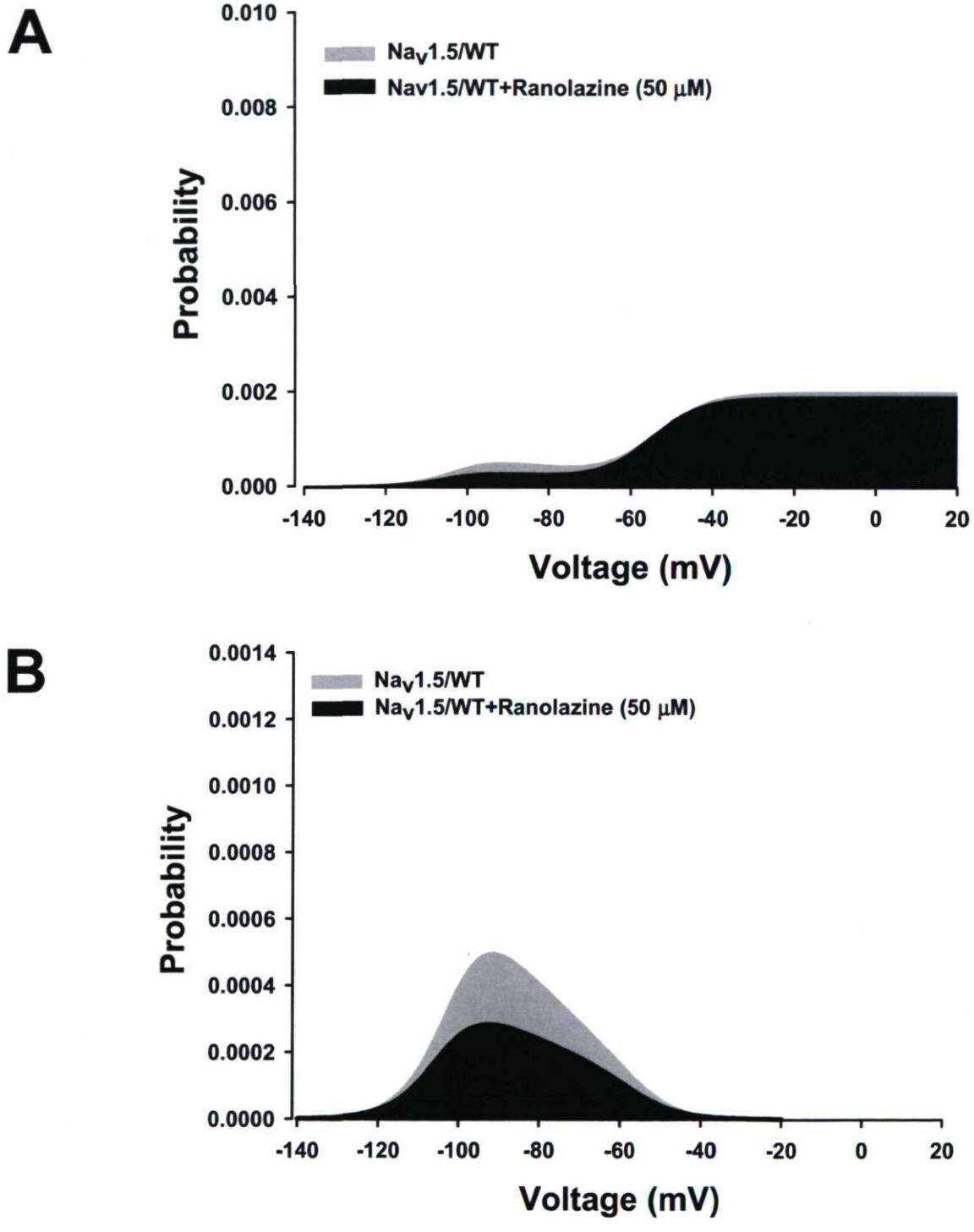

Supplemental Figure 2.2

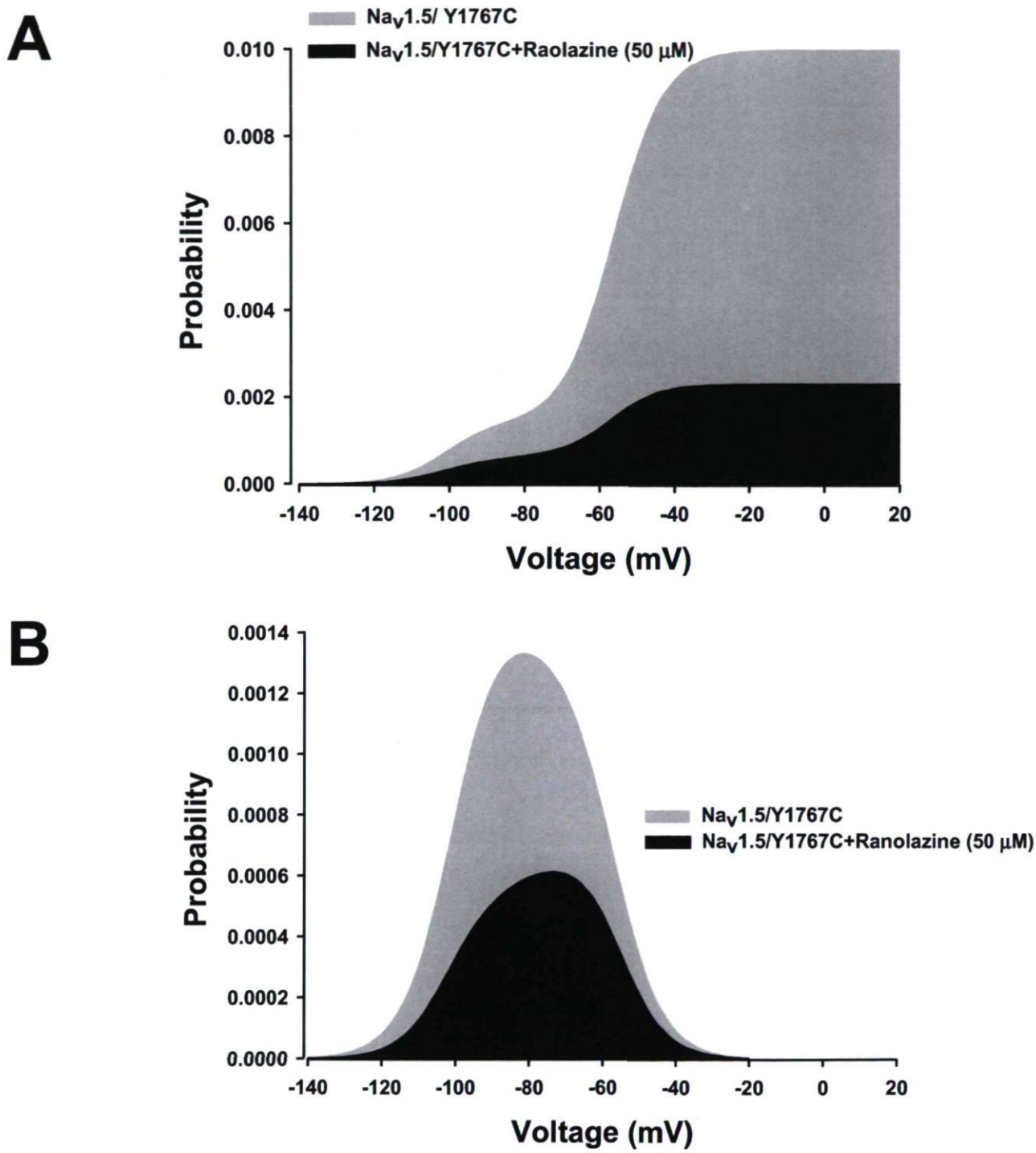

Supplemental Figure 2.3

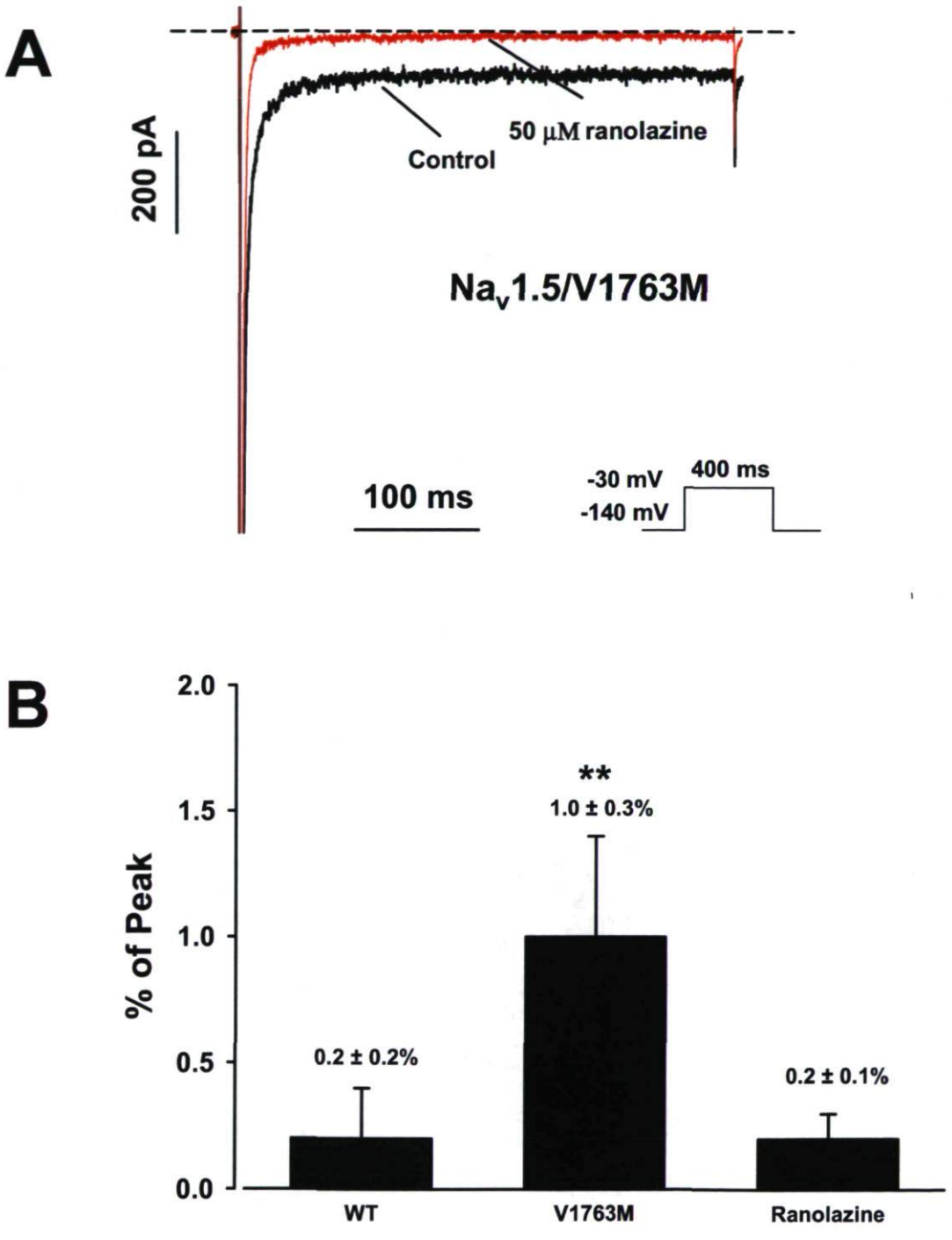

Supplemental Figure 2.4

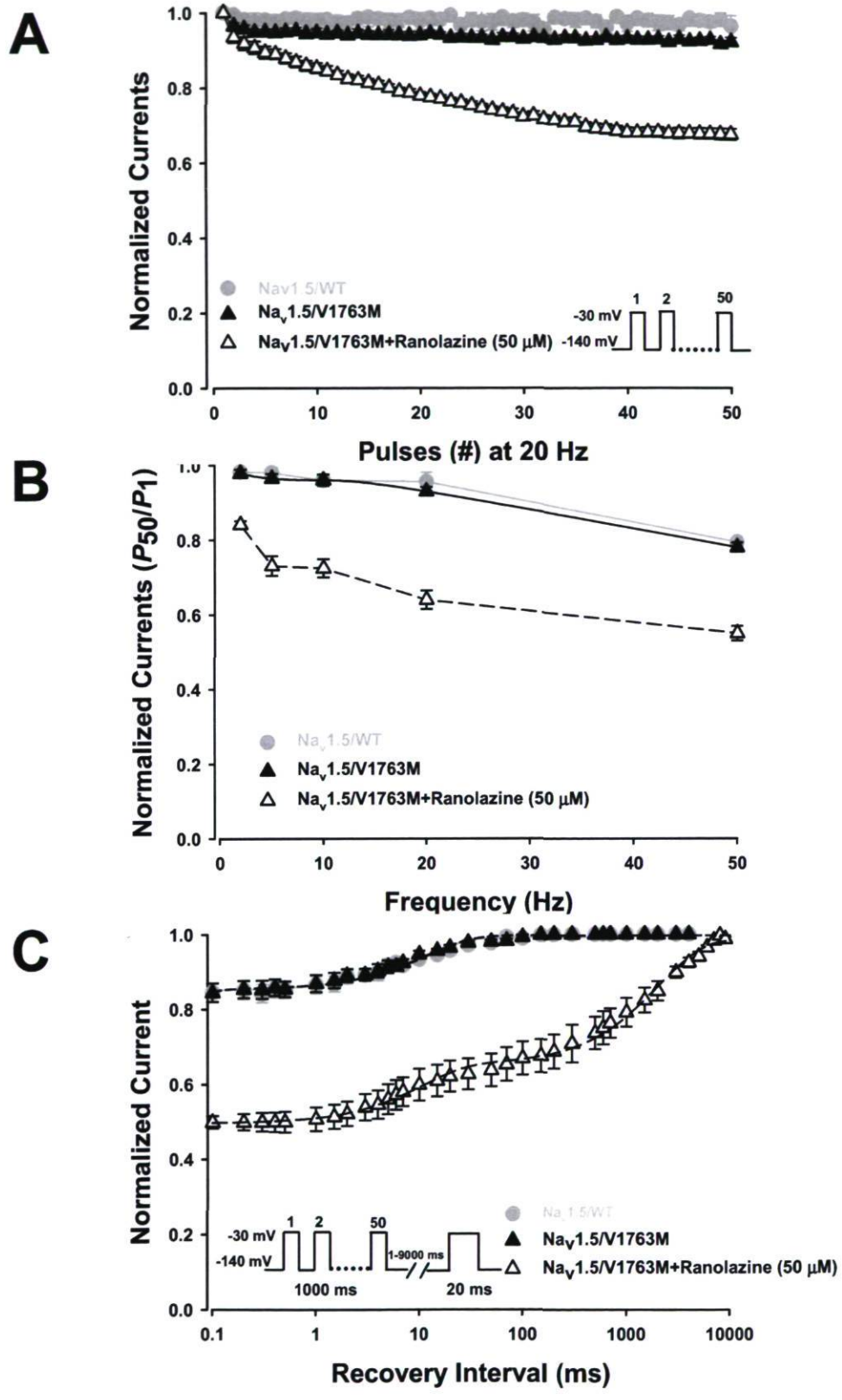

Supplemental Figure 2.5

Chapter III

Biophysical characterization of a new *SCN5A* mutation S1333Y in a SIDS infant linked to long QT syndrome

Article published in *FEBS Lett.*
2009 Mar 4;583(5):890-6. Epub 2009 Feb 10.

Biophysical characterization of a new SCN5A mutation S1333Y in a SIDS infant linked to long QT syndrome.

Hai Huang[a], Gilles Millat[b], Claire Rodriguez-Lafrasse[b], Robert Rousson[b], Béatrice Kugener[c], Philippe Chevalier[d], and Mohamed Chahine[a, e]

[a]Le Centre de recherche Université Laval Robert-Giffard, Quebec City, QC, Canada, G1J 2G3

[b]Laboratoire de Biochimie et Biologie Moléculaire, Hôpital Cardiovasculaire et Pneumologique L Pradel, F-69677 Bron Cedex, France

[c]Unité de Neuro-pédiatrie, Hôpital Debrousse, Lyon, France

[d]Unité de Cardiologie et Soins Intensifs, Hôpital Cardiovasculaire et Pneumologique L Pradel, F-69677 Bron Cedex, France

[e]Departement de Médecine, Université Laval, Quebec City, QC, Canada, G1K 7P4

Running head: A novel *SCN5A* mutation S1333Y in a SIDS patient

Correspondence to:

Mohamed Chahine, Ph.D.

Le Centre de recherche Université Laval Robert-Giffard
Local F-6539
2601, chemin de la Canardière
Quebec City, QC, Canada, G1J 2G3
Tel.: (418) 663-5747, ext. 4723
Fax: (418) 663-8756
E-mail: mohamed.chahine@phc.ulaval.ca

3.1 Résumé

Plusieurs étiologies peuvent contribuer au syndrome de mort subite du nourrisson (SIDS), incluant le syndrome du QT long de type 3 (LQT3). Le but de notre recherche était de caractériser les propriétés biophysiques d'une nouvelle mutation retrouvée sur le gène SCN5A (S1333Y), codant pour le canal Na^+ $Na_v1.5$, chez un enfant mort du SIDS. Les canaux portant cette mutation montre un gain de fonction caractéristique du LQT3, incluant un courant sodique persistant et une augmentation du courant de fenêtre provoqué par un shift de -8 mV de l'activation et de +7mV de l'inactivation. La corrélation entre les propriétés biophysiques et la susceptibilité aux arythmies suggère que le SIDS est lié à un LQT3 associé à la mutation S1333Y.

Mots-clés
Syndrome de mort subite du nourrisson ; génétique ; canaux sodiques ; $Na_v1.5$; SCN5A ; syndrome du QT long

3.2 Abstract

Various entities and genetic etiologies, including inherited long QT syndrome type 3 (LQT3), contribute to sudden infant death syndrome (SIDS). The goal of our research was to biophysically characterize a new SCN5A mutation (S1333Y) in a SIDS infant. S1333Y channels showed the gain of Na^+ channel function characteristic of LQT3, including a persistent inward Na+ current and an enhanced window current that was generated by a –8 mV shift in activation and a +7 mV shift in inactivation. The correlation between the biophysical data and arrhythmia susceptibility suggested that the SIDS was secondary to the LQT3-associated S1333Y mutation.

Keywords: sudden infant death syndrome, genetics, sodium channels, $Na_v1.5$, SCN5A, long QT syndrome

3.3 Introduction

The most common cause of mortality during the first year of life of infants in developed countries is sudden infant death syndrome (SIDS), which is more common in infants placed in a prone position (Dwyer *et al.*, 1991b) or with upper respiratory infections (Vege and Ole, 2004). Other risk factors include bottle feeding, second-hand smoke, overheating, and co-sleeping (Hunt and Hauck, 2006). Previous studies revealed that SIDS is associated with alterations in genes associated with cardiac ion channels, including human cardiac voltage-gated Na^+ channels ($Na_v1.5$) (Opdal and Rognum, 2004b).

Inherited long QT syndrome (LQTS) accounts for about 9.5% of SIDS cases, suggesting that sudden death due to cardiac arrhythmias is an important contributor to SIDS (Arnestad *et al.*, 2007a). LQTS is caused by delayed ventricular repolarization, which leads to fatal ventricular arrhythmias and even sudden death. Inherited LQT3 linked to mutations in *SCN5A* has also been directly linked to SIDS (Ackerman *et al.*, 2001; Wedekind *et al.*, 2001; Schwartz *et al.*, 2000; Plant *et al.*, 2006; Wang *et al.*, 2007c). *SCN5A* is the major gene known to functionally encode the α-subunit of the human cardiac voltage-gated Na^+ channel, which is responsible for the initiation and propagation of the cardiac action potential. The hallmark of the gating change in LQT3 mutations is the presence of persistent inward Na^+ currents due to incomplete inactivation or late re-opening of Na^+ channels, as a result, QT interval prolongation. Most LQT3 mutations are located in the III-IV linker, various domains of the S4-S5 linkers, voltage sensors, and the C-terminus of Na^+ channels, which are associated with the fast inactivation process. The S4-S5 linker of domain III plays a major role in the kinetics and voltage dependence of fast inactivation of Na^+ channels by acting as a docking site for the inactivation particle of the III-IV linker (Smith and Goldin, 1997).

In this work we report a new SIDS mutation (S1333Y) in a 25-day-old infant, which is located in the S4-S5 linker of domain III (Millat *et al.*, 2006), and we characterize its biophysical properties.

3.4 Methods

3.4.1 Clinical evaluation and molecular genetics

The local ethics committee approved the study protocol. The parents provided written informed consent. The death certificate indicated a diagnosis of SIDS, while the autopsy, toxicology, and review of the circumstances of death were negative. Genomic DNA was extracted from whole blood using a WIZARD Genomic DNA Purification kit (Promega, Madison, WI, USA). The coding exons of the *KCNQ1*, *KCNH2*, *SCN5A*, *KCNE1*, and *KCNE2* genes were amplified separately using intronic primers and previously reported PCR conditions (Wang *et al.*, 1996b). Denaturing high performance liquid chromatography (DHPLC) was performed using previously described elution profiles and melting temperatures (Millat *et al.*, 2006). PCR products with divergent chromatographic profiles were directly sequenced on both strands using the BigDye® Terminator v.31 Cycle sequencing kit (Applied Biosystems, Forster City, CA, USA) and were applied to an ABI 3100 automatic sequencer.

3.4.2 Mutagenesis

Mutant hNa_v1.5/S1333Y was generated using a QuickChange TM site-directed mutagenesis kit according to the manufacturer's instructions (Stratagene, La Jolla, CA, USA). The oligo-nucleotide primers containing the corresponding S1333Y mutation were synthesized using the following sequences:

5′- GTG GGC GTC GCC ATC CCG TAC ATC ATG AAC GTC CTC - 3′ (Forward primer) and

5′- GAG GAC GAG GTT CAT GAT GTA CGG GAT GGC GCC CAC- 3′ (Reverse primer)

The mutated site is underlined. Mutant and WT Na_v1.5 channels were inserted in a pcDNA1 construct and were purified using Qiagen columns (Qiagen Inc., Chatsworth, CA, USA).

3.4.3 TsA201 transfection and Patch clamp experiments

Mutant channels were coexpressed with the β subunit in the tsA201 human cell line and characterized using the patch clamp technique in whole cell configuration as already reported (Deschênes *et al.*, 2000).

3.4.4 Solutions and reagents

For the whole-cell recordings, the patch pipettes were filled with 35 mM NaCl, 105 mM CsF, 10 mM EGTA, and 10 mM Cs-HEPES. The pH was adjusted to 7.4 using 1 N CsOH. The bath solution contained 150 mM NaCl, 2 mM KCl, 1.5 mM $CaCl_2$, 1 mM $MgCl_2$, 10 mM glucose, and 10 mM Na-HEPES. The pH was adjusted to pH 7.4 using 1 N NaOH (final Na^+: 152.4 mM). The liquid junction potential between the patch pipette and the bath solution was corrected to –7 mV.

3.4.5 Statistical analysis

Results are presented as means ± standard errors of the mean. Statistical comparisons were made using the unpaired Student's *t*-test in SigmaStat (Jandel Scientific Software, San Rafael, CA, USA). Differences were considered significant at $p < 0.05$.

3.5 Results

3.5.1 Identification of the *SCN5A* mutation S1333Y

The genomic DNA of the SIDS infant was screened for sequence changes in all 28 exons of *SCN5A* by DHPLC analysis. The PCR analysis of the *SCN5A* gene revealed a mutation that was a compound heterozygote with *SCN5A*/S1333Y and *KCNE1*/T20I (Fig. 3.1A and 3.1B). The family members of the infant were screened clinically and genetically. *SCN5A*/S1333Y was a spontaneous mutation and the father was found to be the carrier of the *KCNE1*/T20I mutation with no LQTS-related phenotypes. Other family members were negative in the screen. It was hypothesized that the S1333Y mutation is responsible for the sudden death. The sequencing analysis revealed a heterozygous C-to-A base change at position 3998 in exon 23 that resulted in a serine (S)-to-tyrosine (Y) substitution at residue 1333 (Fig. 3.1C). The mutation was in the S4-S5 linker in domain III, which plays a major role in fast inactivation of the Na^+ channel. This amino acid is highly conserved in the Na^+ channels of many species.

3.5.2 Biophysical characteristics of $Na_v1.5$/S1333Y

Whole-cell Na^+ currents were elicited by depolarizing steps from –100 to +50 mV with a holding potential of –140 mV (Fig. 3.2A). Current amplitudes were normalized to cellular membrane capacitance to generate current-voltage (*I-V*) curves in the form of current densities. Using the same data and graphically determined reversal potentials, the Na^+ conductance for the various

voltages was calculated from the equation G = $I/(V-E_{rev})$, where I is the peak Na^+ current at a given voltage V and E_{rev}, the equilibrium potential extrapolated from the graph. I-V and conductance-voltage (G-V) curves were obtained for S1333Y and WT. The S1333Y mutant and WT channels had similar current densities, suggesting that they were expressed to the same extent on the cell membrane (Fig. 3.2B). The potential of the maximum peak current amplitude of the S1333Y channel was more negative than that of the WT channel (Fig. 3.2B), which may be due to the coupled alteration of steady-state activation and inactivation. To analyze the effect of the S1333Y mutation on fast inactivation kinetics, the time constant τ was measured by fitting the decay of the whole-cell current elicited at each potential with the following double-exponential function: $I = I_{resid} + A_{fast} \times \exp(-(t-k)/\tau_{fast}) + A_{slow} \times \exp(-(t-k)/\tau_{slow})$, where I is the current density, I_{resid} the steady-state asymptotic residue, A_{fast} and A_{slow} are the percentages of channels inactivating with time constants τ_{fast} and τ_{slow}, and k is the time shift. Depolarizing steps from 2 to 50 ms were tested to ensure full current decay and best fit. The S1333Y channel had a significantly longer time constant for the slow component than the WT channel over the entire voltage range from –70 mV to +10 mV (Fig. 3.2C). The most significant difference was at –20 mV, where the time constant τ_{Slow} was 8.56 ± 0.54 ms (n=8) for S1333Y and 4.67 ± 0.36 ms (n=9) for WT. The slower decay of τ_{slow} indicated a decelerated inactivation of open channels. G-V curves were fitted to a standard Boltzmann distribution $G(V)/G_{max} = 1/(1+ \exp(-(V-V_{1/2})/k))$, where $G(V)$ is the conductance at a given voltage V and G_{max} is the maximum conductance. The midpoint of activation voltage ($V_{1/2}$) and the slope factor (k) were determined from the fit. The steady-state activation of the S1333Y mutation was negatively shifted by 8 mV, with no difference in the slope factor (Fig. 3.3A and values in Table 3.1).

Voltage-dependent steady-state inactivation was measured by applying 500 ms pre-pulses ranging from –140 to –30 mV, followed by a 20 ms test pulse at –30 mV. The test pulse current amplitude was normalized to the maximum current recorded during the pre-pulse and plotted versus the pre-pulse voltage to obtain the voltage-dependent inactivation curve, which was fitted to a standard Boltzmann distribution function $I(V)/I_{max} = 1/(1+ \exp((V- V_{1/2})/k))$, where $I(V)/I_{max}$ is the current ratio and V, the pre-pulse voltage. During steady-state inactivation, a +7 mV shift for S1333Y was observed, but the slope factor was not significantly affected (Fig. 3.3A). $V_{1/2}$ and k were generated by fitting each data set with the standard Boltzmann function (see Table 3.1 for values).

Steady-state activation and inactivation shifts appeared to increase the window current for S1333Y, which is generated by the overlap between these two fitting curves (Figs. 3.3B and 3.3C). The window current in LQT3 is associated with steady-state Na^+ channels reopening. S1333Y (Fig. 3.3C) significantly enhanced area of the window current compared to WT (Fig. 3.3B).

During slow inactivation, some voltage-gated Na^+ channels become non-conducting following prolonged membrane depolarization. The course of slow inactivation was assessed using a two-pulse protocol with an initial conditioning pre-pulse and a final test pulse. A –30 mV pre-pulse was applied at intervals varying from 2 to 1000 ms, followed by a step to –140 mV for 20 ms to allow the channels to recover from fast inactivation. The –30 mV test pulse was applied for 40 ms to estimate the fraction of channels available for activation. The fraction was obtained by dividing the current amplitude during the test pulse by the current amplitude during the pre-pulse. Entry into slow inactivation followed a mono-exponential function $I = I_{resid} + A \times \exp(-t/\tau)$, where I is the current intensity, I_{resid} the asymptotic residual current, and A the current amplitude at time zero (see values in Table 3.1). As shown in Figure 3.4A, there was no significant difference in the kinetics of entry into slow inactivation between the S1333Y mutation and WT. Recovery from slow inactivation was measured using a two-pulse protocol, where Na^+ channels were inactivated by a –30 mV conditioning pulse for 500 ms, followed by a –30 mV test pulse after a recovery interval varying from 1 to 2000 ms. The peak current in response to the test pulse was normalized to the maximum peak current in response to the conditioning pulse. The normalized current was plotted against the recovery time interval. The resulting curve was fitted to a double-exponential function to obtain the following fast and slow components of recovery from slow inactivation: $I_{Na} = A_f \times (1-\exp[-t/\tau_f]) + A_s \times (1-\exp[-t/\tau_s])$, where t is the recovery time interval, τ_f and τ_f, the time constants of the fast and slow components, and A_f and A_s, the fractions of the fast and slow components (see values in Table 3.1). The results shown in Figure 3.4B indicate that S1333Y recovered more rapidly from slow inactivation than WT.

The positive shift of the steady-state inactivation may be the result of fewer channels entering into closed-state inactivation (Fig. 3.4C). Closed-state inactivation primarily affects the availability of channels at voltages near the resting membrane potential, thus controlling the Na^+ current amplitude of the action potential. Using a double-pulse protocol, cells were prepulsed to –110 and –100 mV for periods ranging from 1 to 500 ms, and then stepped to –30 mV to

determine the availability of I_{Na} during the pre-pulse. The time course was fitted with the following mono-exponential equation: $I = I_{resid} + A \times \exp(-t/\tau)$ (see values in Table 3.1).

Whole-cell Na^+ currents recorded in tsA201 cells expressing the WT *SCN5A* gene can exhibit a small persistent component whose magnitude depends on the recording conditions. The increased persistent Na^+ current in LQT3 mutants is a major factor in the prolongation of the QT interval. To study the contribution of the persistent current at steady state, we measured the current using a 400 ms depolarization pulse. The persistent current was barely detectable in cells expressing WT channels ($I_{per}/I_{peak} = 0.27 \pm 0.14\%$ n=5), while there was a significant increase in the persistent current in cells expressing the S1333Y mutation ($I_{per}/I_{peak} = 1.16 \pm 0.22\%$, n=6) (Fig. 3.5C). Class I B Na^+ channel blockers (e.g., lidocaine) were reported to normalize prolonged QTc in LQT3 patients (Groenewegen *et al.*, 2003a). We therefore investigated the effect of lidocaine on the persistent inward Na^+ current of the S1333Y mutation. The persistent currents in WT and S1333Y were both blocked by 5 μM tetrodotoxin (TTX) (Figs. 3.5A and 3.5B) and 200 μM lidocaine (Figs. 3.6A and 3.6B), respectively.

3.6 Discussion

In the present study, we biophysically characterized a new *SCN5A* mutation (S1333Y) in an infant who had died of SIDS. The mutation was located in the S4-S5 linker of domain III, which is often associated with inactivation changes in voltage-dependent Na^+ channels. The electrophysiological studies showed persistent Na^+ inward currents accompanied by a –8 mV shift in activation, and a +7 mV shift in inactivation. The window current was enhanced by the shifts of activation and inactivation. The slow component of the fast activation of macroscopic currents of the mutation was slower than that of the WT. The serine at position 1333 is highly conserved, suggesting that this residue may play an important role in the channel gating.

Some inherited arrhythmic disorders (e.g., Brugada syndrome (BrS) and LQTS) appear to be associated with SIDS because they may explain the increased likelihood of sudden death when a trigger event occurs. Since the gating properties of BrS mutations are characterized by a loss of the Na^+ channel function, the present case is unlikely to be related to BrS.

The S1333Y mutation caused a serine-to-tyrosine substitution in the S4-S5 linker of domain III, which is near the proposed docking site of the inactivation particle. This mutation caused similar alterations in activation, fast inactivation, and kinetics of fast inactivation. Many LQT3 mutations

have a persistent Na^+ current along with shortened fast inactivation time constants. However, R1623Q showed a slower rate of current decay that is in agreement with our results (Kambouris *et al.*, 1998). Reduced closed-state inactivation is consistent with the positive shift of inactivation. The rate of recovery from inactivation was also faster, which is in agreement with the findings reported for LQT3 mutations (Δ KPQ, R1644H, and E1784K) (Deschênes *et al.*, 2000; Dumaine *et al.*, 1996; Chandra *et al.*, 1998). Faster recovery may increase the channel availability at the resting membrane potential of the ventricular cells. The shifts of activation and inactivation of the mutant enhanced the window current. This reflects that Na^+ channels may be elicited at more positive membrane potentials. The enhanced window currents can increase the risk of fatal ventricular arrhythmias especially when they coexist with persistent inward Na^+ currents. The A1330P *SCN5A* mutation, which also causes SIDS, is located near the site of the S1333Y mutation. A1330P causes a gain of Na^+ channel function by significantly increasing the window current. Interestingly, this mutation does not induce a persistent Na^+ current (Wedekind *et al.*, 2001).

Mutations in the Na^+ channel associated with LQT3 usually result in a low level of Na^+ current flowing during the plateau phase of the cardiac action potential due to a small persistent current. At least five LQT3 mutations (S941N, A1330P, S1103Y, R1826H, and A997S) have been associated with SIDS (Ackerman *et al.*, 2001; Wedekind *et al.*, 2001; Schwartz *et al.*, 2000; Plant *et al.*, 2006). Of these, two (R1826H and A997S) have a persistent inward Na^+ current. Moreover, in studies on relationships between cardiac polymorphisms and SIDS, a persistent Na^+ current was found in five of eight variants (Wang *et al.*, 2007b). Such a persistent current may cause slower inactivation, resulting in prolonged repolarization and thus a long QT interval. In the present study, the S1333Y mutation caused a persistent current that accounted for $1.16 \pm 0.22\%$ of the current amplitude. While there are no documented clinic findings to support the diagnosis of LQTS, we suspect that fatal ventricular arrhythmia may be triggered by an event such as the prone position during sleep.

We also found that the persistent current induced by S1333Y was sensitive to lidocaine. This suggests that the prolonged QT interval could be normalized by class I B Na^+ channel blockers. The mechanism of blocking the persistent current may be acted by lidocaine stabilizing inactivation, and thereby reducing the probability of dispersed and bursting activities in LQT3 mutant channels (Dumaine and Kirsch, 1998).

In the case presented here, sudden death occurred 25 days after delivery, and resuscitatory efforts were not possible given that SIDS happened too quickly. To prevent the sudden death event, a more effective way would be to diagnose the condition soon after delivery using the ECG that is faster and less expensive to perform. For those with a family history of SIDS and bradycardia, genetic analyses are recommended when the QTc exceeds 440 ms (Schwartz *et al.*, 2000; Schwartz *et al.*, 1998).

3.7 Acknowledgements

We would like to thank Valérie Pouliot for her technical expertise. This study was supported by a funding from the Heart and Stroke Foundation of Québec (HSFQ) and a grant from the Canadian Institutes of Health Research. M. Chahine is a J.C. Edwards Foundation Senior Investigator.

3.8 Figure legends

Figure 3.1: Molecular identification of S1333Y. (A) DHPLC elution profiles of S1333Y identified in exon 23 of *SCN5A* at 62.5°C. (B) DHPLC elution profile of S1333Y identified in exon 23 *SCN5A* 61.1, 61.3, and 62.5°C. (C) Sequencing analysis showing a C-to-A substitution at position 3998 in exon 23, leading to a serine (S)-to-tyrosine (T) substitution at residue 1333.

Figure 3.2: Analysis of whole-cell currents recorded from tsA201 cells expressing WT and S1333Y. (A) I_{Na} from WT (left) and S1333Y (right) were elicited by depolarizing pulses from –100 mV to +50 mV in 10 mV increment for each step. (B) Current-voltage relationship of WT (○, n=9) and S1333Y (•, n=8). The current amplitude was normalized to the membrane capacitance. (C) The voltage-dependent time constants of inactivation in WT (○ for τ_{fast}, n=9; Δ for τ_{slow}, n=9) and S1333Y (• for τ_{fast}, n=8; ▲ for τ_{slow}, n=8). Currents were fitted to a two-exponential function, obtaining the corresponding time constants τ_{fast} and τ_{slow} (* $p<0.05$; ** $p<0.01$).

Figure 3.3: Gating properties of activation, steady-state inactivation, and window currents. (A) Voltage-dependence of steady-state activation and inactivation in WT (Δ for activation, n=9; ○ for inactivation, n=9) and S1333Y (▲for activation, n=8; • for inactivation, n=8). The activated and inactivated currents were generated from the protocols as inset, and their resulting data were fitted to a standard Boltzmann distribution. (B) The enlarged portion of overlap area (light grey) between activation and inactivation for WT. The shaded area represents the window region. (C) The enlarged part of overlap area (dark grey) between activation and inactivation for S1333Y. The shaded area was significantly enhanced than that of WT.

Figure 3.4: Gating properties of slow inactivation, recovery from slow inactivation, and closed-state inactivation. (A) Slow inactivation in WT (○, n=8) and S1333Y (•, n=9). A two-pulse protocol as inset was used to generate the currents. The time constants (shown in Table 3.1) were obtained using a mono-exponential function. (B) Time courses of recovery from slow inactivation in WT (○, n=7) and S1333Y (•, n=7). A 500 ms conditioning pre-pulse was used to monitor recovery by a 20 ms test pulse after a variable recovery interval from 1 ms to 2000 ms (see protocol in inset). The time constants were obtained using a two-exponential function. (C)

Closed-state inactivation in WT (○ for –110 mV, n=9; Δ for –100 mV, n=9) and S1333Y (• for -110 mV, n=9; ▲ for -100 mV, n=10). The protocol in inset elicited the currents, which were fitted to a mono-exponential function.

Figure 3.5: Effect of TTX on the persistent sodium current in WT and S1333Y. The persistent sodium current was generated from a holding potential of +140 mV to –30 mV over 400 ms (see protocol in inset). The dashed line represents zero current. (A) Effect of adding 5 μM TTX to WT for 10 min. (B) Effect of adding 5 μM TTX to S1333Y for 10 min. The persistent sodium current was blocked by TTX. (C) The histogram of the persistent sodium current. The persistent sodium current accounted for 0.27 ± 0.14% of the peak current amplitude for WT (n=5) and 1.16 ± 0.22% for S1333Y (n=6) at –30 mV (** $p<0.01$).

Figure 3.6: Effect of lidocaine on the persistent sodium current in WT and S1333Y. The persistent sodium current was generated from a holding potential of +140 mV to –30 mV for 400 ms (see protocol as inset). The dashed line represents zero current. (A) Effect on WT of an eight-minute treatment with 200 μM lidocaine on WT. (B) Effect on S1333Y of an eight-minute treatment with 200 μM lidocaine. The persistent sodium current was blocked by lidocaine.

3.9 Reference List

Ackerman MJ, Siu BL, Sturner WQ, Tester DJ, Valdivia CR, Makielski JC, and Towbin JA (2001). Postmortem molecular analysis of *SCN5A* defects in sudden infant death syndrome. *J Am Med Assoc* **286**, 2264-2269.

Arnestad M, Crotti L, Rognum TO, Insolia R, Pedrazzini M, Ferrandi C, Vege A, Wang DW, Rhodes TE, George AL, Jr., and Schwartz PJ (2007). Prevalence of long-QT syndrome gene variants in sudden infant death syndrome. *Circulation* **115**, 361-367.

Chandra R, Starmer CF, and Grant AO (1998). Multiple effects of KPQ deletion mutation on gating of human cardiac Na^+ channels expressed in mammalian cells. *Am J Physiol* **274**, H1643-H1654.

Deschênes I, Baroudi G, Berthet M, Barde I, Chalvidan T, Denjoy I, Guicheney P, and Chahine M (2000). Electrophysiological characterization of SCN5A mutations causing long QT (E1784K) and Brugada (R1512W and R1432G) syndromes. *Cardiovasc Res* **46**, 55-65.

Dumaine R and Kirsch GE (1998). Mechanism of lidocaine block of late current in long Q-T mutant Na^+ channels. *Am J Physiol* **274**, H477-H487.

Dumaine R, Wang Q, Keating MT, Hartmann HA, Schwartz PJ, Brown AM, and Kirsch GE (1996). Multiple mechanisms of Na^+ channel-linked long-QT syndrome. *Circ Res* **78**, 916-924.

Dwyer T, Ponsonby AL, Newman NM, and Gibbons LE (1991). Prospective cohort study of prone sleeping position and sudden infant death syndrome. *Lancet* **337**, 1244-1247.

Groenewegen WA, Bezzina CR, van Tintelen JP, Hoorntje TM, Mannens MMAM, Wilde AAM, Jongsma HJ, and Rook MB (2003). A novel LQT3 mutation implicates the human cardiac sodium channel domain IVS6 in inactivation kinetics. *Cardiovasc Res* **57**, 1072-1078.

Hunt CE and Hauck FR (2006). Sudden infant death syndrome. *CMAJ* **174**, 1861-1869.

Kambouris NG, Nuss HB, Johns DC, Tomaselli GF, Marban E, and Balser JR (1998). Phenotypic characterization of a novel long-QT syndrome mutation (R1623Q) in the cardiac sodium channel. *Circulation* **97**, 640-644.

Millat G, Chevalier P, Restier-Miron L., Da Costa A, Bouvagnet P, Kugener B, Fayol L, Gonzàlez Armengod C, Oddou B, Chanavat V, Froidefond E, Perraudin R, Rousson R, and Rodriguez-Lafrasse C (2006). Spectrum of pathogenic mutations and associated polymorphisms in a cohort of 44 unrelated patients with long QT syndrome. *Clin Genet* **70**, 214-227.

Opdal SH and Rognum TO (2004). The sudden infant death syndrome gene: does it exist? *Pediatrics* **114**, e506-e512.

Plant LD, Bowers PN, Liu Q, Morgan T, Zhang T, State MW, Chen W, Kittles RA, and Goldstein SA (2006). A common cardiac sodium channel variant associated with sudden infant death in African Americans, SCN5A S1103Y. *J Clin Invest* **116**, 430-435.

Schwartz PJ, Priori SG, Dumaine R, Napolitano C, Antzelevitch C, Stramba-Badiale M, Richard TA, Berti MR, and Bloise R (2000). A molecular link between the sudden infant death syndrome and the long-QT syndrome. *N Engl J Med* **343**, 262-267.

Schwartz PJ, Stramba-Badiale M, Segantini A, Austoni P, Bosi G, Giorgetti R, Grancini F, Marni ED, Perticone F, Rosti D, and Salice P (1998). Prolongation of the QT interval and the sudden infant death syndrome. *N Engl J Med* **338**, 1709-1714.

Smith MR and Goldin AL (1997). Interaction between the sodium channel inactivation linker and domain III S4-S5. *Biophys J* **73**, 1885-1895.

Vege A and Ole RT (2004). Sudden infant death syndrome, infection and inflammatory responses. *FEMS Immunol Med Microbiol* **42**, 3-10.

Wang DW, Desai RR, Crotti L, Arnestad M, Insolia R, Pedrazzini M, Ferrandi C, Vege A, Rognum T, Schwartz PJ, and George AL, Jr. (2007a). Cardiac sodium channel dysfunction in sudden infant death syndrome. *Circulation* **115**, 368-376.

Wang DW, Desai RR, Crotti L, Arnestad M, Insolia R, Pedrazzini M, Ferrandi C, Vege A, Rognum T, Schwartz PJ, and George AL, Jr. (2007b). Cardiac sodium channel dysfunction in sudden infant death syndrome. *Circulation* **115**, 368-376.

Wang Q, Li Z, Shen J, and Keating MT (1996). Genomic organization of the human *SCN5A* gene encoding the cardiac sodium channel. *Genomics* **34**, 9-16.

Wedekind H, Smits JPP, Schulze-Bahr E, Arnold R, Veldkamp MW, Bajanowski T, Borggrefe M, Brinkmann B, Warnecke I, Funke H, Bhuiyan ZA, Wilde AA, Breithardt G, and Haverkamp

W (2001). De novo mutation in the *SCN5A* gene associated with early onset of sudden infant death. *Circulation* **104**, 1158-1164.

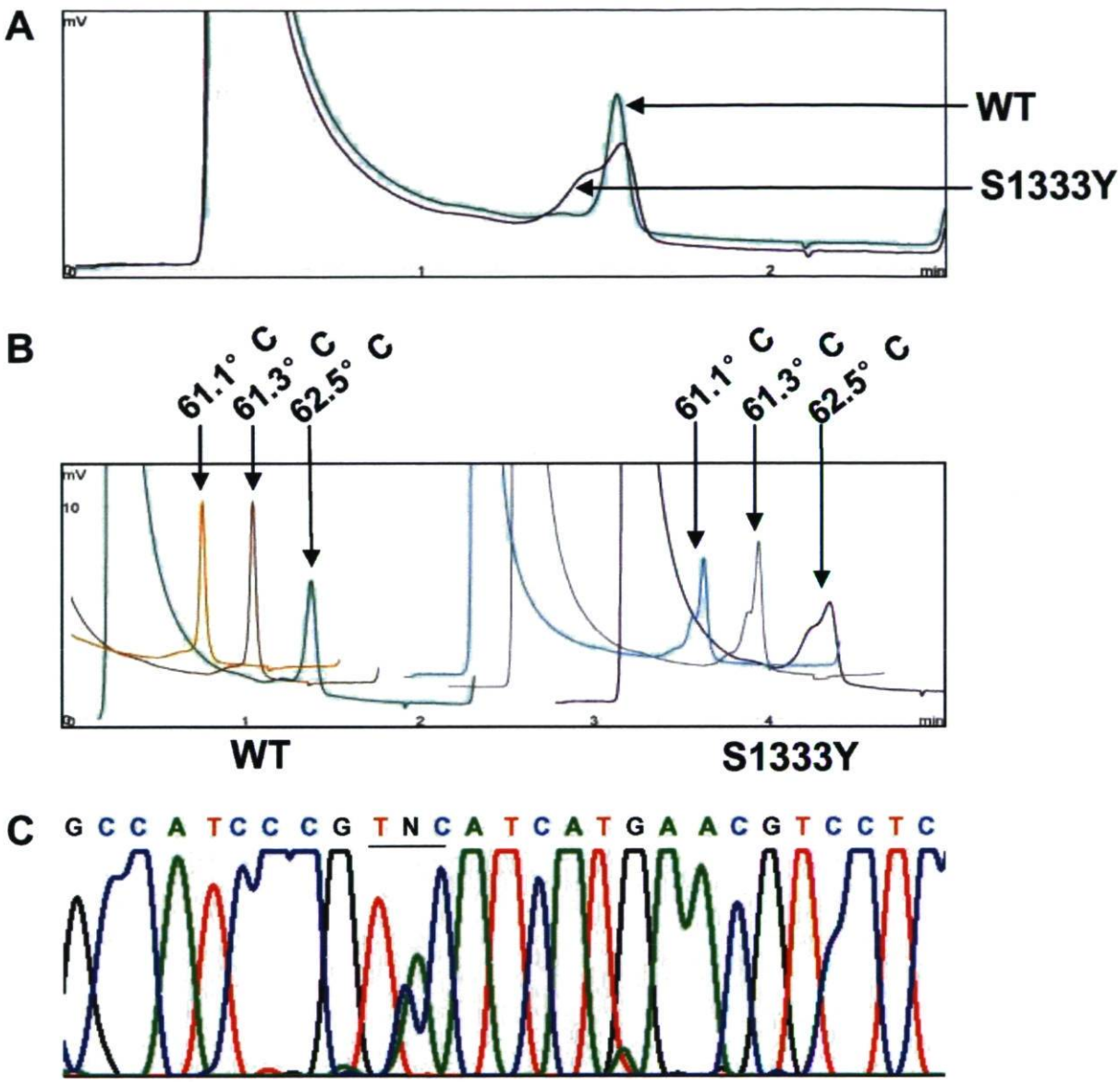
A
mV
WT
S1333Y
min
B
61.1° C
61.3° C
62.5° C
61.1° C
61.3° C
62.5° C
mV
10
min
WT
S1333Y
C
G C C A T C C C G T N C A T C A T G A A C G T C C T C

Figure 3.1

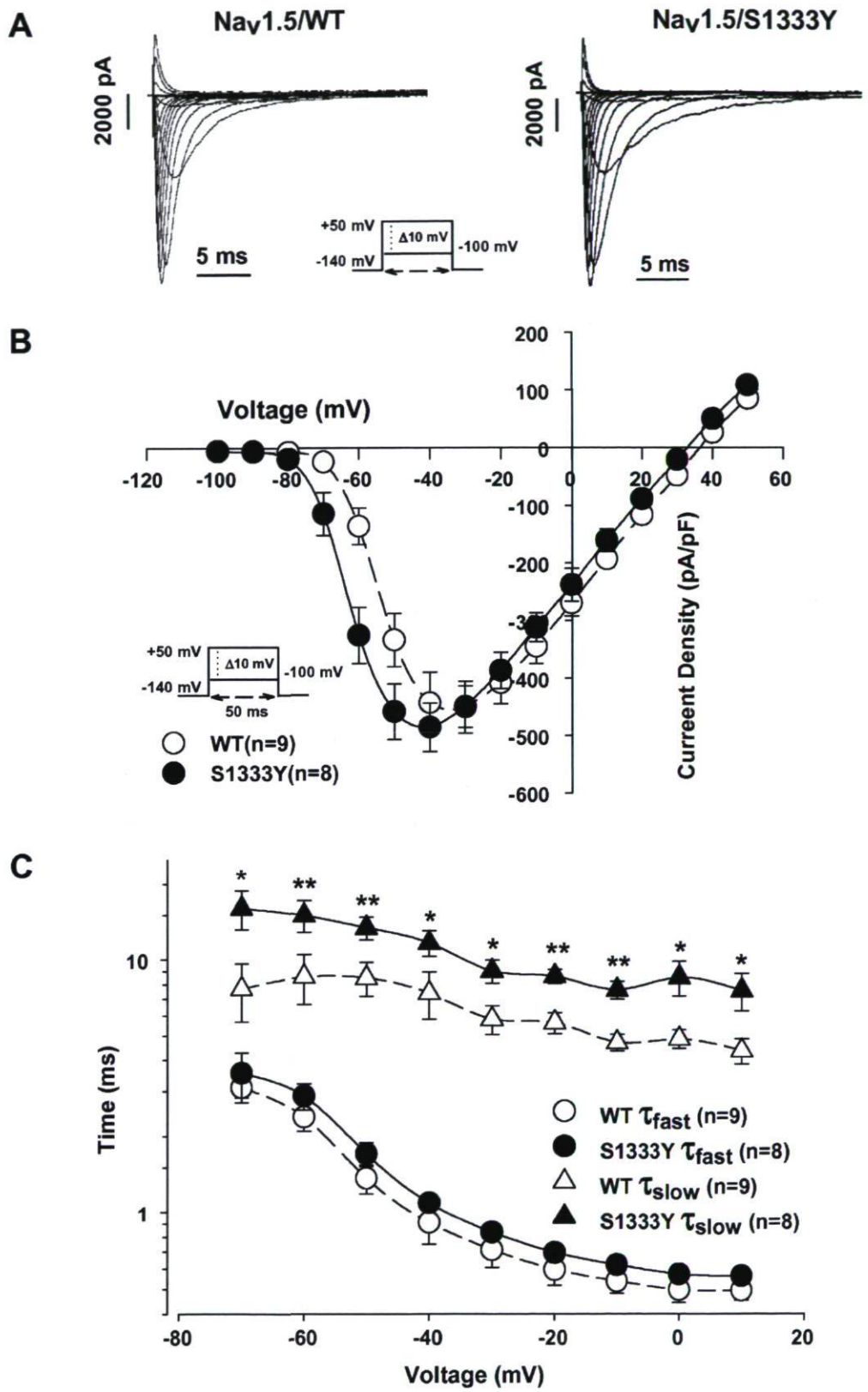
A
Nav1.5/WT
Nav1.5/S1333Y
2000 pA
5 ms
+50 mV
Δ10 mV
-100 mV
-140 mV
B
Voltage (mV)
Current Density (pA/pF)
50 ms
WT(n=9)
S1333Y(n=8)
C
Time (ms)
Voltage (mV)
WT τfast (n=9)
S1333Y τfast (n=8)
WT τslow (n=9)
S1333Y τslow (n=8)

Figure 3.2

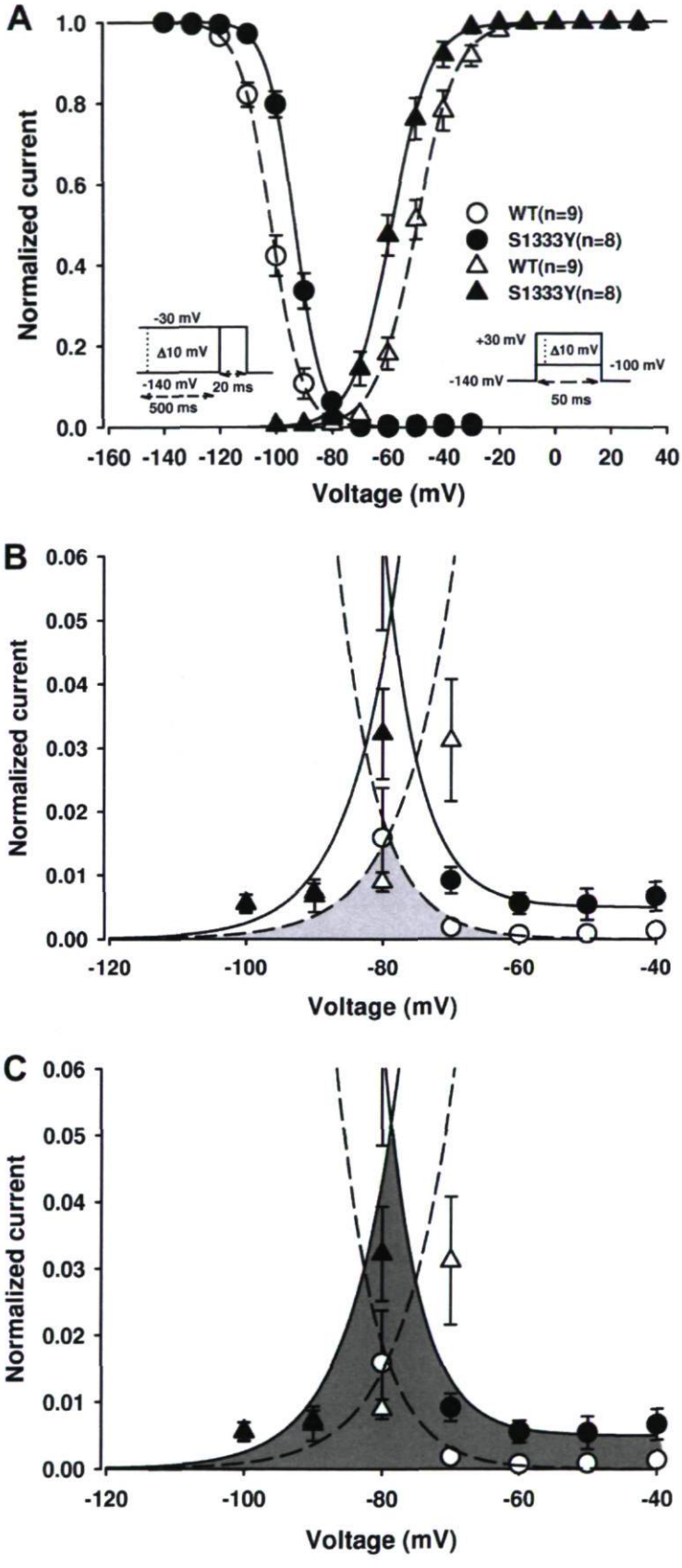
A
Normalized current
1.0
0.8
0.6
0.4
0.2
0.0
-160 -140 -120 -100 -80 -60 -40 -20 0 20 40
Voltage (mV)
WT(n=9)
S1333Y(n=8)
WT(n=9)
S1333Y(n=8)
-30 mV
Δ10 mV
-140 mV
20 ms
500 ms
+30 mV
Δ10 mV
-100 mV
-140 mV
50 ms
B
Normalized current
0.06
0.05
0.04
0.03
0.02
0.01
0.00
-120 -100 -80 -60 -40
Voltage (mV)
C
Normalized current
0.06
0.05
0.04
0.03
0.02
0.01
0.00
-120 -100 -80 -60 -40
Voltage (mV)

Figure 3.3

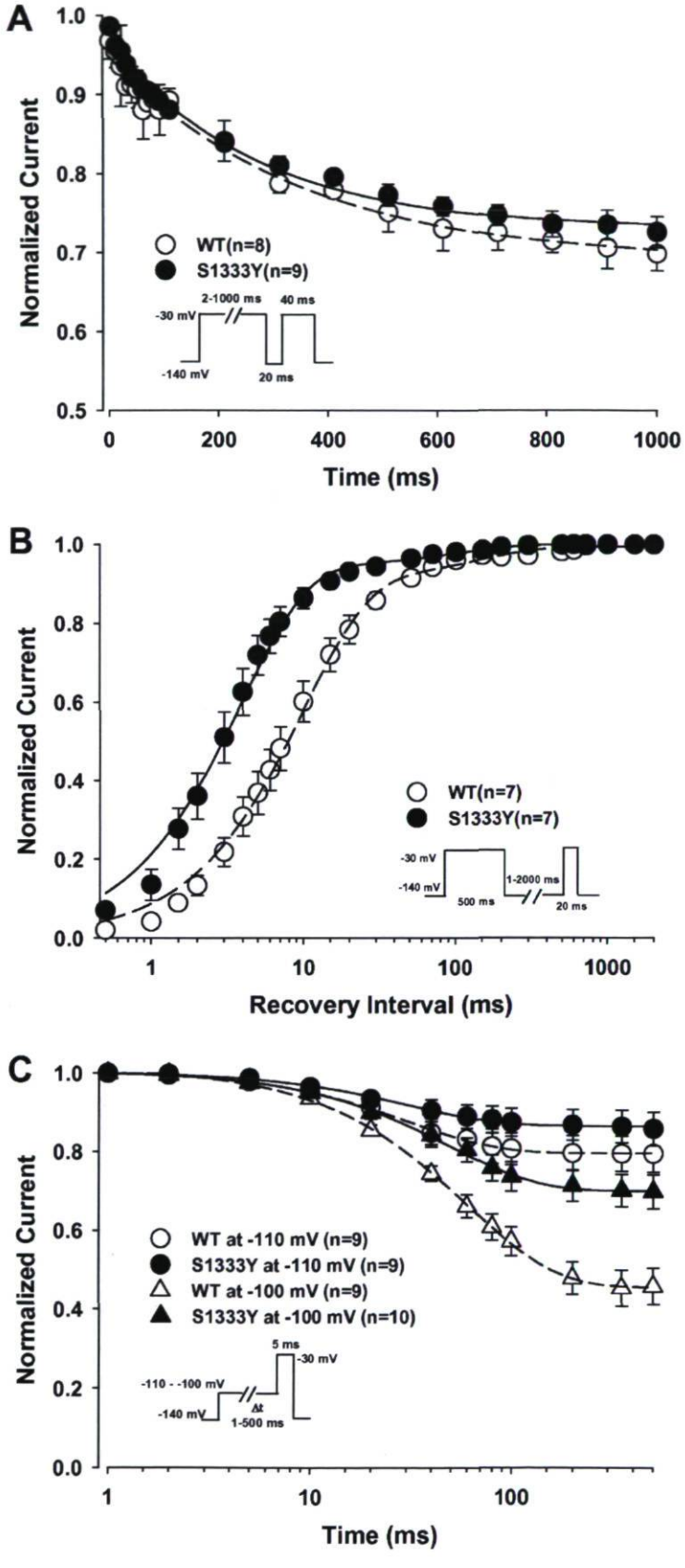
A
Normalized Current
1.0
0.9
0.8
0.7
0.6
0.5
WT(n=8)
S1333Y(n=9)
2-1000 ms
40 ms
-30 mV
-140 mV
20 ms
0
200
400
600
800
1000
Time (ms)
B
Normalized Current
1.0
0.8
0.6
0.4
0.2
0.0
WT(n=7)
S1333Y(n=7)
-30 mV
-140 mV
500 ms
1-2000 ms
20 ms
1
10
100
1000
Recovery Interval (ms)
C
Normalized Current
1.0
0.8
0.6
0.4
0.2
0.0
WT at -110 mV (n=9)
S1333Y at -110 mV (n=9)
WT at -100 mV (n=9)
S1333Y at -100 mV (n=10)
5 ms
-30 mV
-110 - -100 mV
-140 mV
Δt
1-500 ms
1
10
100
Time (ms)

Figure 3.4

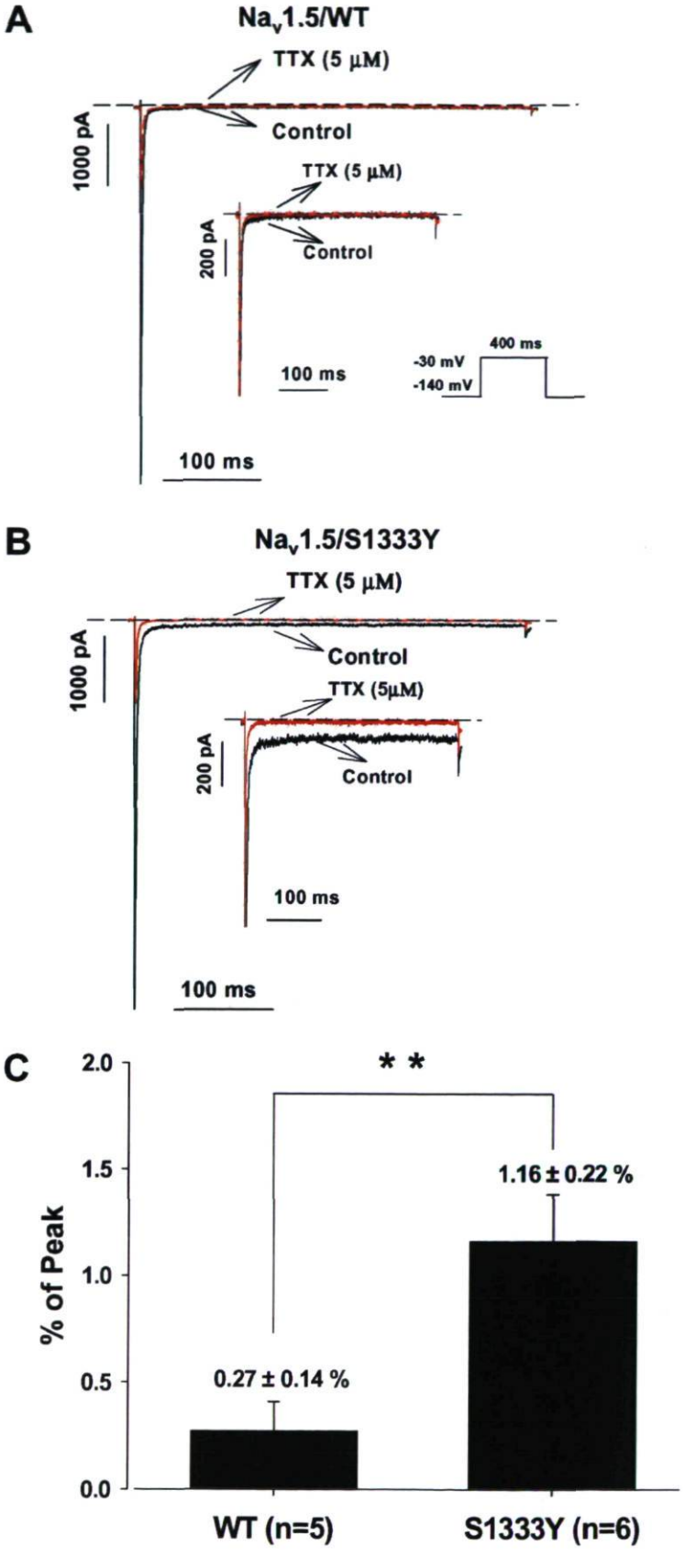
A
Na$_v$1.5/WT
TTX (5 μM)
Control
1000 pA
TTX (5 μM)
200 pA
Control
400 ms
-30 mV
-140 mV
100 ms
100 ms
B
Na$_v$1.5/S1333Y
TTX (5 μM)
Control
1000 pA
TTX (5μM)
200 pA
Control
100 ms
100 ms
C
* *
2.0
1.5
1.0
0.5
0.0
% of Peak
1.16 ± 0.22 %
0.27 ± 0.14 %
WT (n=5)
S1333Y (n=6)

Figure 3.5

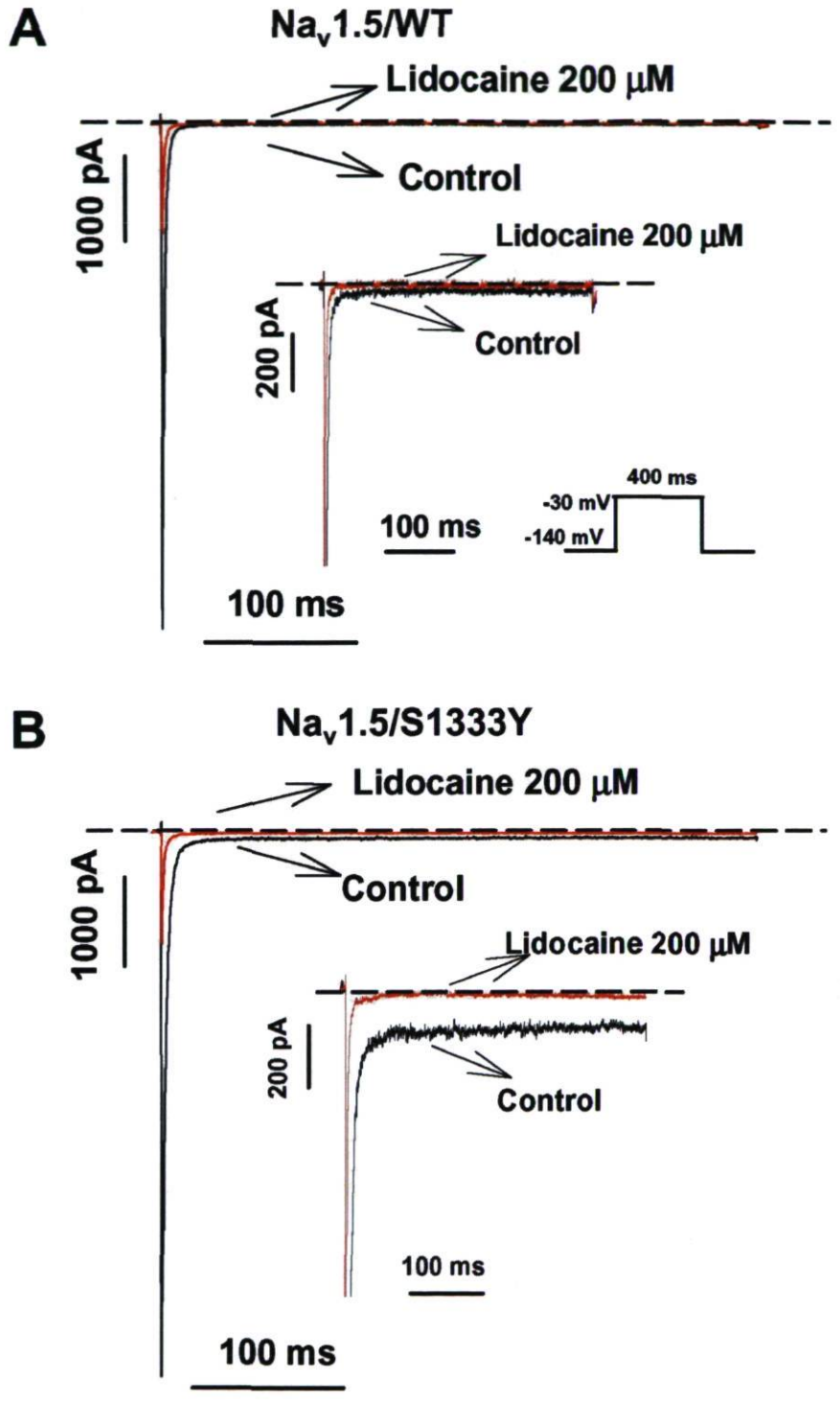
A
Na$_v$1.5/WT
Lidocaine 200 μM
Control
1000 pA
Lidocaine 200 μM
Control
200 pA
400 ms
-30 mV
-140 mV
100 ms
100 ms
B
Na$_v$1.5/S1333Y
Lidocaine 200 μM
Control
1000 pA
Lidocaine 200 μM
200 pA
Control
100 ms
100 ms

Figure 3.6

Table 3.1 Biophysical properties of $Na_v1.5$/WT and $Na_v1.5$/S1333Y.

	$Na_v1.5$/WT	$Na_v1.5$/S1333Y
Steady-state activation		
$V_{1/2}$ (mV)	−50.34 ± 2.06 (n=9)	−58.88 ± 1.25* (n=8)
K (mV)	−6.38 ± 0.27 (n=9)	−6.13 ± 0.34 (n=11)
Steady-state inactivation		
$V_{1/2}$ (mV)	−100.47 ± 1.34 (n=9)	−93.46 ± 0.66 **(n=8)
K (mV)	4.91 ± 0.19 (n=9)	4.91 ± 0.21 (n=8)
Intermediate inactivation		
τ (ms)	327.78 ± 37.10 (n=8)	306.96 ± 22.87 (n=9)
Recovery from intermediate inactivation		
τ_{fast} (ms)	16.49 ± 4.73 (n=7)	4.08 ± 0.60 ** (n=7)
τ_{Slow} (ms)	251.81 ± 60.79 (n=7)	104.41 ± 27.06 * (n=7)
A_{fast} (%)	91.70 ± 0.82 (n=7)	94.33 ± 0.72 (n=7)
A_{slow} (%)	8.30 ± 0.82% (n=7)	5.67 ± 0.72 (n=7)
Closed-state inactivation		
-100 mV		
τ (ms)	89.54 ± 10.76 (n=8)	60.28 ± 4.11 * (n=9)
-90 mV		
τ (ms)	109.51± 14.12 (n=8)	65.82 ± 5.33** (n=10)

$V_{1/2}$ = mid point for activation or inactivation
K_v = slow factor for activation or inactivation
τ = time constant
A = the fractions of recovery component
* $P<0.05$
** $P<0.01$

Chapter IV

Gain-of-function mutation of $Na_v1.5$ in atrial fibrillation enhances cellular excitability and lowers the threshold for action potential firing

Article published in *Biochem Biophys Res Commun.* 2009 Feb 27;380(1):132-7. Epub 2009 Jan 22.

Gain-of-function mutation of $Na_v1.5$ in atrial fibrillation enhances cellular excitability and lowers the threshold for action potential firing

Qiuju Li[c], Hai Huang[a], Gele Liu[c], Khanh Lam[d], Julie Rutberg[c], Martin S. Green[c], David H. Birnie[c], Robert Lemery[c], Mohamed Chahine[a,b] and Michael H. Gollob[c,e] *

[a]Le Centre de Recherche Université Laval Robert-Giffard, Canada

[b]Laval University, Québec, Canada

[c]Division of Cardiology, University of Ottawa Heart Institute, Ottawa, Ont., Canada

[d]Department of Surgery, University of Ottawa Heart Institute, Ottawa, Ont., Canada

[e]Department of Cellular and Molecular Medicine, University of Ottawa, University of Ottawa Heart Institute, 40 Ruskin St., Rm. H350, Ottawa, Ont., Canada K1Y 4W7

Corresponding author.
Address: Department of Cellular and Molecular Medicine
University of Ottawa, University of Ottawa Heart Institute
40 Ruskin St., Rm.
H350, Ottawa, Ont., Canada K1Y 4W7.
Fax: +1 613 761 5060.
E-mail address: mgollob@ottawaheart.ca (M.H. Gollob).

4.1 Contribution role: (1) Testing biophysical characterization of a novel *SCN5A* mutation (K1493R) identified in an AF patient. In the experiments mutant channels were transiently transfected into tsA 201 cells. Then, their biophysical properties were studied by whole-cell configuration of patch clamp technique. (2) Analyzing resulting data. It was found that K1493R mutation caused a gain-of-function property shown as a significant positive shift in voltage-dependent inactivation and a resulting increase in window currents. This property may enhance cellular excitability. (3) Providing Figures 2-3 and their legends. (4) Writing results and discussion related to figures 2 and 3.

4.2 Résumé

Des mutations génétiques sur le gène SCN5A, codant le canal sodique $Na_v1.5$, spécifiques au phénotype de fibrillation auriculaire ont récemment été décrites. Cependant, les données sur les propriétés biophysiques de ces canaux sont rares. Nous avons identifié une nouvelle mutation sur ce gène chez une mère et son fils atteints de fibrillation auriculaire. Cette mutation, K1493R, modifie un acide aminé hautement conservé situé sur la boucle DIII-IV et elle est située 6 acides aminés en aval du motif de l'inactivation rapide des canaux Na^+. L'étude biophysique de cette mutation dans les cellules tsA201 montre un gain de fonction marqué par le déplacement positif l'inactivation dépendante du voltage et un grand courant de rampe près du potentiel de repos de la membrane. Une augmentation de l'excitabilité cellulaire est observée dans les cardiomyocytes auriculaire HL-1 transfectés avec ce canal, incluant des potentiels d'actions spontanés et une diminution du seuil de déclanchement des potentiels d'action. Ces nouvelles données biophysiques fournissent des indices moléculaires montrant que « l'hyperexcitabilité » cellulaire peut provoquer des vulnérabilités pouvant conduire à cette arythmie commune.

Mots-clés

Arythmie ; fibrillation ; génétique ; Nav1.5 ; SCN5A ; hyperexcitabilité ; électrophysiologie ; auriculaire ; cardiomyocyte

4.3 Abstract

Genetic mutations of the cardiac sodium channel (SCN5A) specific only to the phenotype of atrial fibrillation have recently been described. However, data on the biophysical properties of SCN5A variants associated with atrial fibrillation are scarce. In a mother and son with lone atrial fibrillation, we identified a novel SCN5A coding variant, K1493R, which altered a highly conserved residue in the DIII–IV linker and was located six amino acids downstream from the fast inactivation motif of sodium channels. Biophysical studies of K1493R in tsA201 cells demonstrated a significant positive shift in voltage-dependence of inactivation and a large ramp current near resting membrane potential, indicating a gain-of-function. Enhanced cellular excitability was observed in transfected HL-1 atrial cardiomyocytes, including spontaneous action potential depolarizations and a lower threshold for action potential firing. These novel biophysical observations provide molecular evidence linking cellular "hyperexcitability" as a mechanism inducing vulnerability to this common arrhythmia.

Keywords: Arrhythmia; Fibrillation; Genetics; $Na_v1.5$; SCN5A; Hyperexcitability; Electrophysiology; Atria; HL-1; Cardiomyocytes

4.4 Introduction

The cardiac sodium channel ($Na_v1.5$) plays a critical role in the generation of electrical activity in cardiac myocytes. Genetic mutations of the gene encoding the $Na_v1.5$ sodium channel (SCN5A) are associated with a variety of cardiac arrhythmia syndromes, including the Long QT syndrome type 3 (LQT3) (Wang *et al.*, 1995b), Brugada syndrome (Chen *et al.*, 1998), and progressive cardiac conduction disease (Schott *et al.*, 1999). The biophysical abnormalities induced by disease-causing SCN5A mutations are diverse. In LQT3, SCN5Amutations result in a "gain-of-function" effect, invariably leading to a persistent late component of sodium current resulting in action potential prolongation (Bennett *et al.*, 1995b). In contrast, Brugada syndrome and conduction system disease are generally characterized by a primary loss of myocardial sodium current by various mechanisms, including impaired protein trafficking, more rapid inactivation kinetics, or altered voltage-dependence of activation (Baroudi *et al.*, 2001; Rook *et al.*, 1999). A role of SCN5A mutations in the primary pathogenesis of atrial fibrillation (AF) is suggested by the known efficacy of sodium channel blocking agents in diminishing recurrences of AF. Further, genetic screening of SCN5A in a large cohort of patients with lone AF identified rare genetic variants of SCN5A in nearly 6% of AF cases (Darbar *et al.*, 2008). Insight into the biophysical abnormalities of SCN5A mutations associated with lone AF is essential to understanding the molecular mechanisms of this common arrhythmia. In this article, we describe unique electrophysiological characteristics of a novel SCN5A mutation associated with lone AF. The biophysical observations of this mutant $Na_v1.5$ channel are previously undescribed for the cardiac sodium channel, and include the demonstration of enhanced window current occurring near resting membrane potential, spontaneous action potential depolarizations and a lower threshold for action potential firing in transfected atrial cardiomyocytes. This study provides direct evidence of a novel molecular mechanism of cellular "hyperexcitability" inducing vulnerability to AF.

4.5 Methods

4.5.1 Molecular screening

Genomic DNA was extracted from whole blood from probands with "idiopathic" AF. Genetic analysis was performed by direct DNA sequencing of the coding region of the GJA5, KCNQ1, KCNA5, and SCN5A genes. Affected and control patients in this study were of Western

European descent. All study participants provided written informed consent and the research protocol was approved by the Ethics Board of the University of Ottawa Heart Institute.

4.5.2 Expression of $Na_v1.5$ in tsA201 cells and HL-1 atrial myocytes

Mutant $Na_v1.5$ (K1493R) was introduced into a wild-type (wt) $Na_v1.5$ pcDNA1 clone using the QuickChange mutagenesis kit (Stratagene, La Jolla, CA) and sequences confirmed using an ABI 377 DNA sequencer (Perkin-Elmer/Applied Biosytems, Foster City, CA, USA). TsA201 cells were grown in high glucose DMEM supplemented with FBS (10%), l-glutamine (2 mM), penicillin (100 U/ml), and streptomycin (10 mg/ml) (Gibco BRL Life Technologies, Burlington, ON, Canada). The cells were transfected with 5 μg of cDNA coding for wt or mutant channel using the calcium phosphate method.

HL-1 cells, an atrial myocyte derived cell line, were a generous gift from Dr. William Claycomb (Louisiana State University Health Sciences Center, New Orleans, LA). HL-1 cells were grown in 35 mm culture dishes to 50–70% confluency in Claycomb medium containing 10% FBS, 100 U/ml of penicillin, 100 μg/ml streptomycin, and 0.1 mM norepinephrine. Cells were transfected in serum free and antibiotic free Claycomb medium containing 2 μl lipofectamine 2000 and 1 μg $Na_v1.5$/wt or $Na_v1.5$/K1493R mutant expression vectors mixed with 1 μg pECFP expression vector to denote cells that received the wild-type or mutant $Na_v1.5$. Only cells that exhibited cyano fluorescence were selected for further electrophysiological experiments.

4.5.3 Electrophysiological experiments

$Na_v1.5$ currents from tsA201 transfected cells were recorded using the whole-cell configuration of the patch clamp technique. Patch clamp recordings were made using low resistance electrodes (<1 MΩ), and a routine series resistance compensation by an Axopatch 200 amplifier (Axon Instruments, Foster City, CA, USA) was performed to minimize voltage-clamp errors. The patch pipette contained 35 mM NaCl, 105 mM CsF, 10 mM EGTA, and 10 mM Cs-Hepes. The bath solution contained 150 mM NaCl, 2 mM KCl, 1.5 mM $CaCl_2$, 1 mM $MgCl_2$, 10 mM glucose, and 10 mM Na-Hepes. The pH of all solutions was adjusted to 7.4. Voltage-clamp command pulses were generated by microcomputer using pCLAMP software v8.0 (Axon Instruments). Experiments were carried out at room temperature.

In HL-1 atrial cardiomyocytes, recordings were carried out using the current-clamp analysis at room temperature. Cells were perfused with a solution of 140 mM NaCl, 3 mM KCl, 2 mM $MgCl_2$, 2 mM $CaCl_2$, 10 mM Hepes, 10 mM glucose, pH 7.35. The recording pipette had a resistance of 2.5–3.5 MΩ when filled with an internal solution containing (in mM): 140 mM KCl, 5 mM Hepes, 0.5 mM EGTA, 20 mM glucose, 3 mM Na_2ATP, and 0.5 mM GTP, pH 7.35. Action potentials (APs) were induced by injecting a current of 800 pA for a duration of 4 ms. When required, current was applied to set a holding potential of −60 mV. AP traces were acquired and analyzed with pClamp software, filtered at 10 kHz and sampled at 20 kHz. To study the threshold for action potential elicitation, increasing amplitude of current was injected in 50 pA increments ranging from 100 to 800 pA until an AP was induced. The minimum current injected eliciting an AP was considered the threshold.

Data are presented as means ± standard error of the mean (SEM). When indicated, a *t*-test was performed using statistical software in SigmaPlot (Jandel Scientific Software, San Rafael, CA, USA).

4.6 Results

4.6.1 Mutation detection and clinical phenotype

DNA sequencing identified a novel, heterozygous mutation in exon 26 of the SCN5A gene in a single proband and his affected mother. This mutation leads to an amino acid substitution of lysine for arginine (K1493R) in the DIII–IV linker of the $Na_v1.5$ channel (Fig. 4.1A). K1493 is a highly conserved amino acid across species and is six amino acids downstream from the fast inactivation IFM (isoleucine–phenylalanine–methionine) motif of sodium channels (Fig. 4.1B) (West *et al.*, 1992). This genetic variant was absent from 200 alleles of an ethnically matched, healthy control cohort.

The affected proband developed AF at age 50. Coronary angiography documented normal coronary arteries. Echocardiography noted normal left atrial size, and normal left ventricular size and function. Twelve-lead electrocardiograms during normal sinus rhythm and AF consistently demonstrated a normal QTc interval (Fig. 4.1C). The proband's mother was diagnosed with AF at age 63 following many years of symptomatic palpitations. Her previous cardiac investigations documented a normal myocardial perfusion scan and normal parameters on echocardiography,

aside from a mildly enlarged left atrium. The proband's only sibling, a brother, is healthy at age 60, and is not a carrier of the K1493R mutation.

4.6.2 Electrophysiological data

In mammalian tsA201 cells, activation and inactivation kinetics for wt and mutant $Na_v1.5$ showed no differences in peak current or current density (Fig. 4.2A and B). To compare the time course of inactivation for both channels, current decay was fitted with a double exponential function. Fig. 4.2C shows that time constants of both fast and slow inactivation were slower for mutant $Na_v1.5$/K1493R. For example, at +10 mv, $Na_v1.5$/wt: $\tau f = 0.45 \pm 0.02$ ms, $\tau s = 3.72 \pm 0.40$ ms; $Na_v1.5$/K1493R: $\tau f = 0.58 \pm 0.02$ ms, $\tau s = 5.05 \pm 0.54$ ms, $p < 0.01$.

To investigate the gating properties of $Na_v1.5$/K1493R and $Na_v1.5$/wt, we next analyzed the voltage-dependence of steady-state activation and inactivation. The potential for half-maximal activation and slope factor were similar for wt and mutant channels ($Na_v1.5$/wt: $V_{1/2} = -56.59 \pm 1.72$ mV, $k = -5.6$, $n = 6$; $Na_v1.5$/K1493R: $V_{1/2} = -58.17 \pm 0.79$ mV, $k = -5.3$, $n = 6$, $p =$ NS). In contrast, $V_{1/2}$ for inactivation was significantly shifted to more positive potentials for mutant $Na_v1.5$ as compared to $Na_v1.5$/wt channels, without significant change in their respective slope factors ($Na_v1.5$/wt: $V_{1/2} = -104.33 \pm 1.58$ mV, $k = 4.79$, $n = 6$; $Na_v1.5$/K1493R: $V_{1/2} = -99.20 \pm 1.34$ mV, $k = 4.81$, $n = 6$, $p < 0.05$) (Fig. 4.2D). This depolarizing shift in steady-state inactivation produced a greater overlap of activation and inactivation curves resulting in a larger "window current" (Fig. 4.2E), predicting an increase in channel availability in the range of the resting membrane potential of atrial myocytes. To confirm a gain of frequency-dependent current for the mutant channel, currents were elicited by slow ramp depolarizations. Significantly larger ramp currents were elicited for mutant $Na_v1.5$/K1493R channels as compared to wt channels (Fig. 4.2F). The averaged peak ramp current occurred at a voltage of -67.11 ± 1.89 mV for the mutant channel, and was consistently larger than wt channels at all ramp slopes tested (data not shown). In view of the observed gain-of-function properties of the mutant $Na_v1.5$/K1493R, we evaluated whether this mutant imbues a late, persistent inward sodium current. No substantial persistent inward current at the end of a 400 ms depolarization was observed for either wt or mutant channel (Fig. 4.3A and B). Analyses of intermediate inactivation, time course of recovery from slow inactivation, and voltage-dependence of deactivation did not differ between wt and mutant $Na_v1.5$ channels (Fig. 4.3C–E).

Lastly, we assessed the effect of $Na_v1.5$/wt and $Na_v1.5$/K1493R mutant channels on the action potential (AP) duration and cellular excitability in HL-1 atrial cardiomyocytes. Induced AP duration did not differ in cells transiently expressing $Na_v1.5$/wt or $Na_v1.5$/K1493R channels, consistent with the absence of late, persistent sodium current (Fig. 4.4A and B). Next, we measured the threshold of depolarization for elicitation of an all-or-none AP. HL-1 cells expressing mutant $Na_v1.5$/K1493R channels required 25% less depolarizing current for AP elicitation as compared to cells expressing wt channel ($Na_v1.5$/wt 693.3 ± 37.5 pA, $Na_v1.5$/K1493R 525 ± 30 pA, $p < 0.005$) (Fig. 4.4C). In addition, spontaneous cellular depolarizations were observed in 4 of 13 cells (31%) expressing mutant $Na_v1.5$/K1493R as compared to only 2 of 16 cells (12.5%) expressing $Na_v1.5$/wt (Fig. 4.4D), reaffirming a hyperexcitable phenotype induced by mutant $Na_v1.5$/K1493R. Mean amplitude of spontaneous depolarizations was 33.63 ± 17.97 mV in $Na_v1.5$/K1493 expressing cells versus 11.85 ± 1.36 mV in $Na_v1.5$/wt cells ($p < 0.05$). No difference was observed in resting membrane potential of HL-1 cardiomyocytes transfected with wt or mutant $Na_v1.5$ channels (data not shown).

4.7 Discussion

We describe the association of a novel genetic mutation in the voltage-gated cardiac sodium channel gene with lone atrial fibrillation. This missense K1493R mutation was present in a mother and son with early onset atrial fibrillation and no structural heart disease. The highly conserved, charged K1493 residue is located within the cytoplasmic loop domain which joins domains III and IV, and is six amino acids C-terminal to the fast inactivation IFM (isoleucine–phenylalanine–methionine) motif of the sodium channel. The IFM motif is invariable among sodium channels and is crucial to rapid channel inactivation following opening (West *et al.*, 1992; Patton *et al.*, 1992; Miller *et al.*, 2000).

The unique gain-of-function properties exhibited by $Na_v1.5$/K1493R have not been previously described for the voltage-gated cardiac sodium channel. Consistent with the localization of the mutant to the fast inactivating region of the channel, mutant K1493R demonstrated a significant depolarizing shift in fast inactivation These observations correlate with the site-directed mutagenesis studies of Miller et al. showing that deletion of charged lysines within the linker region of domains III and IV hasten the voltage dependence of sodium channel inactivation (Miller *et al.*, 2000). This alteration is expected to increase the fraction of channels available for

activation close to resting potential due to an uncoupling of channel activation and inactivation. The increased overlap between activation and inactivation curves observed in our study resulted in an increased window current for the mutant channel. The window current represents a voltage region in which sodium channels continue to open, and therefore is predicted to lower the excitability threshold for excitable cells (Kearney *et al.*, 2001). Indeed, expression of the wt and $Na_v1.5$/K1493R in HL-1 atrial cardiomyocytes confirmed a significantly lower depolarizing current threshold for single AP firing, and HL-1 cells expressing mutant $Na_v1.5$/K1493R demonstrated spontaneous depolarizations consistent with a hyperexcitable phenotype. AP duration in HL-1 cardiomyocytes were similar between cells expressing wt and mutant $Na_v1.5$ channels, consistent with the absence of late persistent current that is observed in $Na_v1.5$ gain-of-function mutations associated with LQT3.

Although not reported previously in the $Na_v1.5$ channel, non-inactivating sodium channel mutations resulting in larger window currents have been implicated in other inherited disorders of excitability (Kearney *et al.*, 2001; Desaphy *et al.*, 2004; George, Jr., 2005). In multiple animal models of spontaneous seizures, the voltage dependence of sodium current inactivation in neuronal cells was observed to be shifted toward depolarized potentials and resulted in increased window current, similar to our observations for the $Na_v1.5$/K1493R mutant (Vreugdenhil *et al.*, 1998; Gu *et al.*, 2001; Ketelaars *et al.*, 2001; Ellerkmann *et al.*, 2003). The observed biophysical properties of sodium channel mutations responsible for epilepsy are consistent with the known efficacy of anti-epileptic drugs in functioning to shift the voltage dependence of inactivation in the negative direction (Vreugdenhil *et al.*, 1998; Kuo *et al.*, 1997; Reckziegel *et al.*, 1999; Vreugdenhil and Wadman, 1999; Kohling, 2002). Similar findings are seen in myotonic disorders associated with specific SCN4A mutations, whereby therapy with flecainide, a sodium channel blocker, provides clinical benefit (Rosenfeld *et al.*, 1997).

Diverse molecular mechanisms of AF induced by ion channel genetic defects have been described. Gain-of-function mutations of potassium channels KCNQ1, KCNE2, and KCNJ2 are reported to result in a shortening of APD and are predicted to shorten atrial effective refractory period, inducing enhanced vulnerability to re-entry (Chen *et al.*, 2003; Yang *et al.*, 2004; Xia *et al.*, 2005). In contrast, a mutation in KCNA5 resulting in a loss-of-function is reported to increase APD and early-after-depolarizations in atrial myocytes promoting triggered activity (Olson *et al.*, 2006). Connexin40 mutations result in a loss of gap junction conductance and are proposed to

enhance atrial conduction heterogeneity throughout myocardial tissue, facilitating a reentry substrate for AF (Gollob *et al.*, 2006). Functional studies on two previously reported $Na_v1.5$ channel mutations associated with AF have shown contrasting functional differences (Ellinor *et al.*, 2008; Makiyama *et al.*, 2008). Although both mutations were located in the C-terminus of the channel, a hyperpolarizing shift in steady-state inactivation suggesting a loss-of-function was noted in one study (Scornik *et al.*, 2006), while the other reported a depolarizing shift in steady-state inactivation and increased current density (Haissaguerre *et al.*, 1998). The gain-of-function findings of the latter study are similar to ours, although $Na_v1.5$/K1493R did not show an increased current density. The present study elaborates on the functional consequences of a depolarizing shift in steady-state inactivation, demonstrating for the first time that this biophysical abnormality in $Na_v1.5$, in the absence of other kinetic alterations, results in an enhanced window current, a lower threshold for action potential firing, and spontaneous depolarizations when studied in HL-1 atrial cardiomyocytes. These data suggest a distinct mechanism of AF vulnerability due to cellular hyperexcitability that results from a novel gain-of-function in the cardiac sodium channel.

The biophysical observations of $Na_v1.5$/K1493 are similar to those described in other sodium channelopathy diseases associated with hyperexcitability. In the context of atrial fibrillation, rapid focal atrial activity, commonly observed from pulmonary myocardial sleeves, may be the result of repetitive myocyte AP firing. Furthermore, a link between sodium channel activity and autonomic mediated AF has been suggested in a study by Scornik et al., which identified a high expression of $Na_v1.5$ channels in intracardiac ganglia (Scornik *et al.*, 2006). These investigators demonstrated $Na_v1.5$-induced AP activity from these neurons and speculated that a gain-of-function of the $Na_v1.5$ channel might enhance AP activity of intracardiac neurons, augmenting acetylcholine release.

The data from this study provides a potential molecular link to the observations of focal triggers of AF (Haissaguerre *et al.*, 1998), the efficacy of intracardiac ganglia denervation by catheter ablation (Pappone *et al.*, 2004), and the use of sodium channel blockers in reducing AF burden (Burashnikov *et al.*, 2008).

4.8 Acknowledgments

This work was supported in part by grants from the Heart and Stroke Foundations of Ontario (M.H.G.) and Quebec (M.C.), and from the Early Researcher Award program from the Government of Ontario (M.H.G.).

4.9 Figure legends

Figure 4.1 Mutation and clinical data. (A) DNA sequence indicating the mutation in exon 26 of the SCN5A gene. (B) K1493 is in close proximity to the fast inactivation motif (IFM) within the $Na_v1.5$ channel and is highly conserved across species. (C) Representative ECG recording from the proband during atrial fibrillation. A normal QT interval is present.

Figure 4.2 Biophysical properties of $Na_v1.5$/wt and $Na_v1.5$/K1493R expressed in tsA201 cells. (A) Analysis of whole-cell currents recorded from cells expressing wt and mutant channels. Current was elicited by depolarizing pulses from −100 to +50 mV in 10 mV increments. (B) Current–voltage relationship of $Na_v1.5$/wt and $Na_v1.5$/K1493R. The current amplitude was normalized to the membrane capacitance. (C) The voltage-dependence time constants of fast inactivation in wt and K1493R expressing cells. Currents were fitted to a two-exponential function. Asterisks indicate significance ($^{*}p < 0.05$, $^{**}p < 0.01$). (D) Steady-state voltage-dependent properties of activation and inactivation for wt and K1493R sodium channels ($^{*}p < 0.05$, $^{**}p < 0.01$). Voltage-clamp protocols are shown as inset. (E) The view of the overlapping area between activation and steady-state inactivation was expanded from (D). (F) Window currents of wt and K1493R channels. Ramp currents of wt (solid line, $n = 6$) and K1493R (dash line, $n = 6$) sodium channels elicited with 500 ms ramp depolarizations from −140 to 20 mV.

Figure 4.3 Gating properties of the persistent sodium current, slow inactivation, recovery from slow inactivation, and deactivation. The persistent sodium current from wt (A) and K1493R (B) $Na_v1.5$ channels. (C) Slow inactivation, (D) time courses of recovery from slow inactivation, and (E) deactivation from the open state from wt and K1493R $Na_v1.5$ channels. Protocols are indicated in inset.

Figure 4.4 Superimposed AP traces recorded from HL-1 cardiomyocytes. Superimposed AP traces recorded from HL-1 cardiomyocytes transfected with $Na_v1.5$/wt or $Na_v1.5$/K1493R sodium channels (A). (B) The APD_{90} of APs recorded from HL-1 cells expressing wt or K1493 channels. (C) Depolarizing threshold current for elicitation of Aps from HL-1 cells expressing wt ($n = 6$) or K1493R ($n = 8$) sodium channels ($p < 0.005$). (D) Spontaneous all-or-none AP observed from

HL-1 atrial cardiomyocytes expressing $Na_v1.5$/K1493, which was not observed from wt expressing cells.

4.10 Reference list

Baroudi G, Pouliot V, Denjoy I, Guicheney P, Shrier A, and Chahine M (2001). Novel mechanism for Brugada syndrome: defective surface localization of an *SCN5A* mutant (R1432G). *Circ Res* **88**, E78-E83.

Bennett PB, Yazawa K, Makita N, and George AL, Jr. (1995). Molecular mechanism for an inherited cardiac arrhythmia. *Nature* **376**, 683-685.

Burashnikov A, Di Diego JM, Zygmunt AC, Belardinelli L, and Antzelevitch C (2008). Atrial-selective sodium channel block as a strategy for suppression of atrial fibrillation. *Ann N Y Acad Sci* **1123**, 105-112.

Chen Q, Kirsch GE, Zhang D, Brugada R, Brugada J, Brugada P, Potenza D, Moya A, Borggrefe M, Breithardt G, Ortiz-Lopez R, Wang Z, Antzelevitch C, O'Brien RE, Schulze-Bahr E, Keating MT, Towbin JA, and Wang Q (1998). Genetic basis and molecular mechanism for idiopathic ventricular fibrillation. *Nature* **392**, 293-296.

Chen YH, Xu SJ, Bendahhou S, Wang XL, Wang Y, Xu WY, Jin HW, Sun H, Su XY, Zhuang QN, Yang YQ, Li YB, Liu Y, Xu HJ, Li XF, Ma N, Mou CP, Chen Z, Barhanin J, and Huang W (2003). KCNQ1 gain-of-function mutation in familial atrial fibrillation. *Science* **299**, 251-254.

Darbar D, Kannankeril PJ, Donahue BS, Kucera G, Stubblefield T, Haines JL, George AL, Jr., and Roden DM (2008). Cardiac sodium channel (SCN5A) variants associated with atrial fibrillation. *Circulation* **117**, 1927-1935.

Desaphy JF, De LA, Didonna MP, George AL, Jr., and Camerino CD (2004). Different flecainide sensitivity of hNav1.4 channels and myotonic mutants explained by state-dependent block. *J Physiol* **554**, 321-334.

Ellerkmann RK, Remy S, Chen J, Sochivko D, Elger CE, Urban BW, Becker A, and Beck H (2003). Molecular and functional changes in voltage-dependent Na(+) channels following pilocarpine-induced status epilepticus in rat dentate granule cells. *Neuroscience* **119**, 323-333.

Ellinor PT, Nam EG, Shea MA, Milan DJ, Ruskin JN, and MacRae CA (2008). Cardiac sodium channel mutation in atrial fibrillation. *Heart Rhythm* **5**, 99-105.

George AL, Jr. (2005). Inherited disorders of voltage-gated sodium channels. *J Clin Invest* **115**, 1990-1999.

Gollob MH, Jones DL, Krahn AD, Danis L, Gong XQ, Shao Q, Liu X, Veinot JP, Tang AS, Stewart AF, Tesson F, Klein GJ, Yee R, Skanes AC, Guiraudon GM, Ebihara L, and Bai D (2006). Somatic mutations in the connexin 40 gene (GJA5) in atrial fibrillation. *N Engl J Med* **354**, 2677-2688.

Gu XQ, Yao H, and Haddad GG (2001). Increased neuronal excitability and seizures in the Na(+)/H(+) exchanger null mutant mouse. *Am J Physiol Cell Physiol* **281**, C496-C503.

Haissaguerre M, Jais P, Shah DC, Takahashi A, Hocini M, Quiniou G, Garrigue S, Le MA, Le MP, and Clementy J (1998). Spontaneous initiation of atrial fibrillation by ectopic beats originating in the pulmonary veins. *N Engl J Med* **339**, 659-666.

Kearney JA, Plummer NW, Smith MR, Kapur J, Cummins TR, Waxman SG, Goldin AL, and Meisler MH (2001). A gain-of-function mutation in the sodium channel gene Scn2a results in seizures and behavioral abnormalities. *Neuroscience* **102**, 307-317.

Ketelaars SO, Gorter JA, van Vliet EA, Lopes da Silva FH, and Wadman WJ (2001). Sodium currents in isolated rat CA1 pyramidal and dentate granule neurones in the post-status epilepticus model of epilepsy. *Neuroscience* **105**, 109-120.

Kohling R (2002). Voltage-gated sodium channels in epilepsy. *Epilepsia* **43**, 1278-1295.

Kuo CC, Chen RS, Lu L, and Chen RC (1997). Carbamazepine inhibition of neuronal Na+ currents: quantitative distinction from phenytoin and possible therapeutic implications. *Mol Pharmacol* **51**, 1077-1083.

Makiyama T, Akao M, Shizuta S, Doi T, Nishiyama K, Oka Y, Ohno S, Nishio Y, Tsuji K, Itoh H, Kimura T, Kita T, and Horie M (2008). A novel SCN5A gain-of-function mutation M1875T associated with familial atrial fibrillation. *J Am Coll Cardiol* **52**, 1326-1334.

Miller JR, Patel MK, John JE, Mounsey JP, and Moorman JR (2000). Contributions of charged residues in a cytoplasmic linking region to Na channel gating. *Biochim Biophys Acta* **1509**, 275-291.

Olson TM, Alekseev AE, Liu XK, Park S, Zingman LV, Bienengraeber M, Sattiraju S, Ballew JD, Jahangir A, and Terzic A (2006). Kv1.5 channelopathy due to KCNA5 loss-of-function mutation causes human atrial fibrillation. *Hum Mol Genet* **15**, 2185-2191.

Pappone C, Santinelli V, Manguso F, Vicedomini G, Gugliotta F, Augello G, Mazzone P, Tortoriello V, Landoni G, Zangrillo A, Lang C, Tomita T, Mesas C, Mastella E, and Alfieri O (2004). Pulmonary vein denervation enhances long-term benefit after circumferential ablation for paroxysmal atrial fibrillation. *Circulation* **109**, 327-334.

Patton DE, West JW, Catterall WA, and Goldin AL (1992). Amino acid residues required for fast Na^+-channel inactivation: charge neutralizations and deletions in the III-IV linker. *Proc Natl Acad Sci USA* **89**, 10905-10909.

Reckziegel G, Beck H, Schramm J, Urban BW, and Elger CE (1999). Carbamazepine effects on Na+ currents in human dentate granule cells from epileptogenic tissue. *Epilepsia* **40**, 401-407.

Rook MB, Alshinawi CB, Groenewegen WA, van Gelder IC, van Ginneken AC, Jongsma HJ, Mannens MM, and Wilde AA (1999). Human SCN5A gene mutations alter cardiac sodium channel kinetics and are associated with the Brugada syndrome. *Cardiovasc Res* **44**, 507-517.

Rosenfeld J, Sloan-Brown K, and George AL, Jr. (1997). A novel muscle sodium channel mutation causes painful congenital myotonia. *Ann Neurol* **42**, 811-814.

Schott JJ, Alshinawi C, Kyndt F, Probst V, Hoorntje TM, Hulsbeek M, Wilde AAM, Escande D, Mannens MMAM, and Le Marec H (1999). Cardiac conduction defects associate with mutations in *SCN5A*. *Nat Genet* **23**, 20-21.

Scornik FS, Desai M, Brugada R, Guerchicoff A, Pollevick GD, Antzelevitch C, and Perez GJ (2006). Functional expression of "cardiac-type" Nav1.5 sodium channel in canine intracardiac ganglia. *Heart Rhythm* **3**, 842-850.

Vreugdenhil M, Faas GC, and Wadman WJ (1998). Sodium currents in isolated rat CA1 neurons after kindling epileptogenesis. *Neuroscience* **86**, 99-107.

Vreugdenhil M and Wadman WJ (1999). Modulation of sodium currents in rat CA1 neurons by carbamazepine and valproate after kindling epileptogenesis. *Epilepsia* **40**, 1512-1522.

Wang Q, Shen J, Splawski I, Atkinson D, Li Z, Robinson JL, Moss AJ, Towbin JA, and Keating MT (1995). SCN5A mutations associated with an inherited cardiac arrhythmia, long QT syndrome. *Cell* **80**, 805-811.

West JW, Patton DE, Scheuer T, Wang Y, Goldin AL, and Catterall WA (1992). A cluster of hydrophobic amino acid residues required for fast Na^+-channel inactivation. *Proc Natl Acad Sci USA* **89**, 10910-10914.

Xia M, Jin Q, Bendahhou S, He Y, Larroque MM, Chen Y, Zhou Q, Yang Y, Liu Y, Liu B, Zhu Q, Zhou Y, Lin J, Liang B, Li L, Dong X, Pan Z, Wang R, Wan H, Qiu W, Xu W, Eurlings P, Barhanin J, and Chen Y (2005). A Kir2.1 gain-of-function mutation underlies familial atrial fibrillation. *Biochem Biophys Res Commun* **332**, 1012-1019.

Yang Y, Xia M, Jin Q, Bendahhou S, Shi J, Chen Y, Liang B, Lin J, Liu Y, Liu B, Zhou Q, Zhang D, Wang R, Ma N, Su X, Niu K, Pei Y, Xu W, Chen Z, Wan H, Cui J, Barhanin J, and Chen Y (2004). Identification of a KCNE2 gain-of-function mutation in patients with familial atrial fibrillation. *Am J Hum Genet* **75**, 899-905.

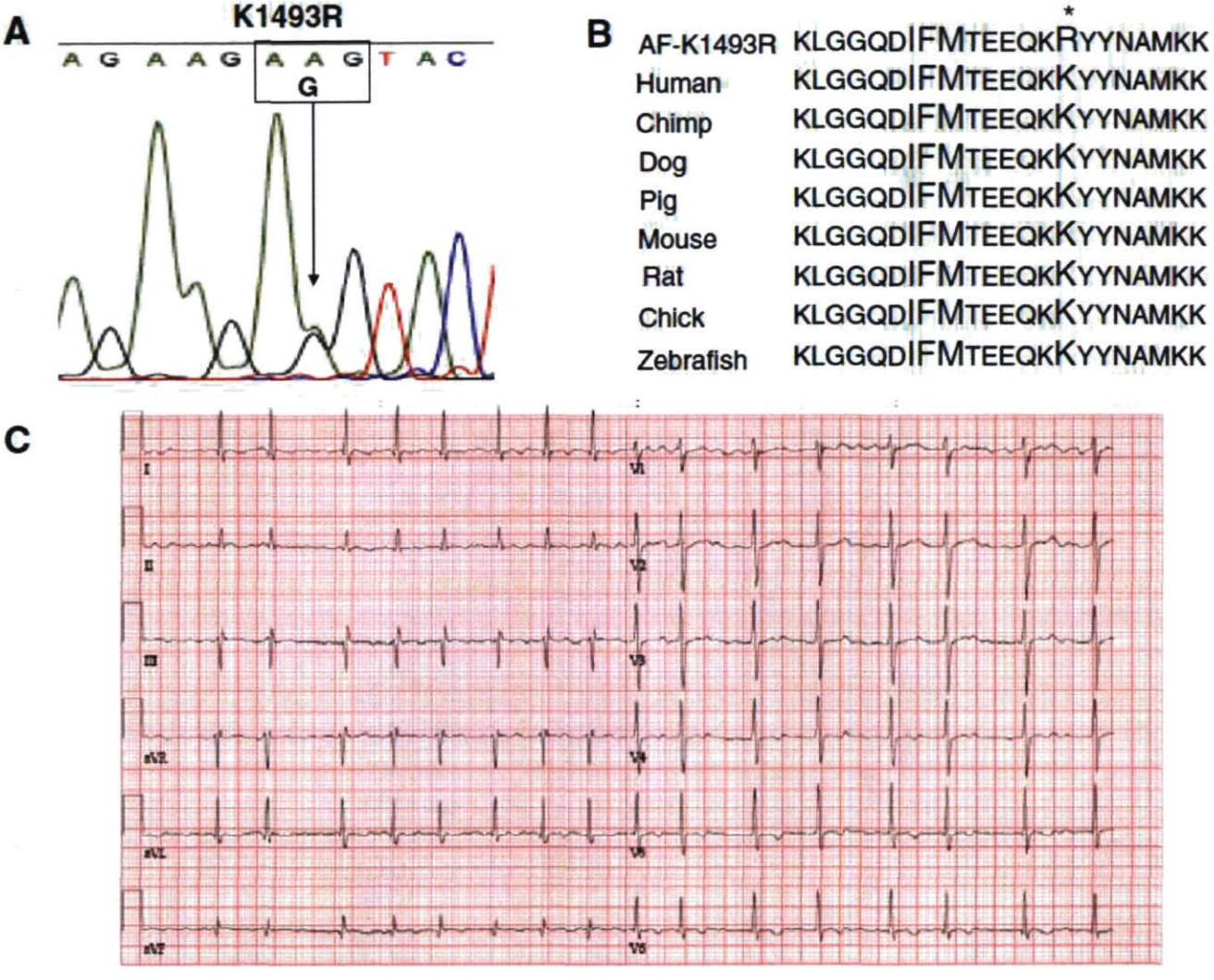
A
K1493R
A G A A G A A G T A C
G
B
AF-K1493R KLGGQDIFMTEEQKRYYNAMKK
Human KLGGQDIFMTEEQKKYYNAMKK
Chimp KLGGQDIFMTEEQKKYYNAMKK
Dog KLGGQDIFMTEEQKKYYNAMKK
Pig KLGGQDIFMTEEQKKYYNAMKK
Mouse KLGGQDIFMTEEQKKYYNAMKK
Rat KLGGQDIFMTEEQKKYYNAMKK
Chick KLGGQDIFMTEEQKKYYNAMKK
Zebrafish KLGGQDIFMTEEQKKYYNAMKK
C

Figure 4.1

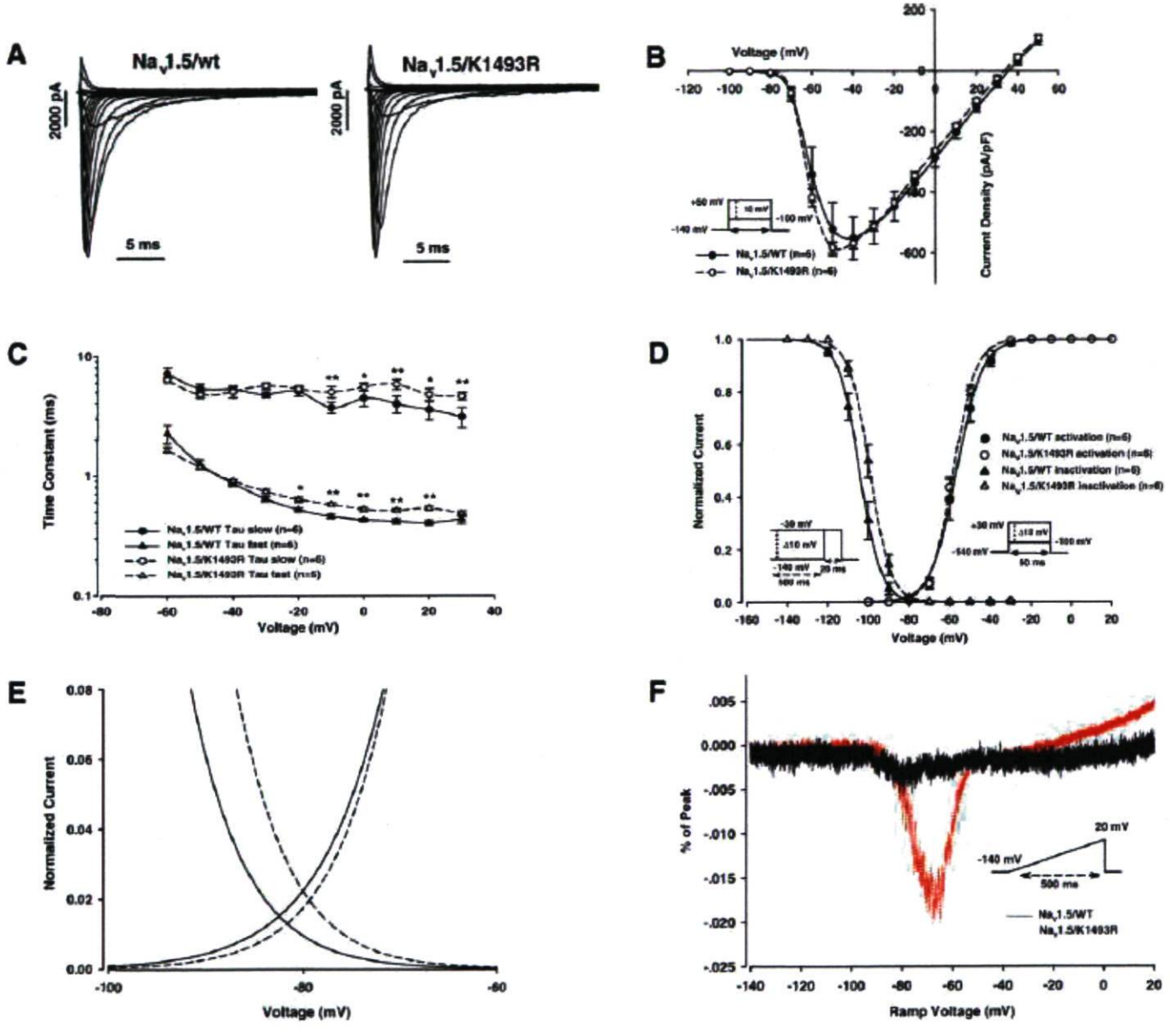
A
Na$_v$1.5/wt
Na$_v$1.5/K1493R
2000 pA
5 ms
B
Voltage (mV)
Current Density (pA/pF)
C
Time Constant (ms)
Voltage (mV)
D
Normalized Current
Voltage (mV)
E
Normalized Current
Voltage (mV)
F
% of Peak
Ramp Voltage (mV)
20 mV
-140 mV
500 ms

Figure 4.2

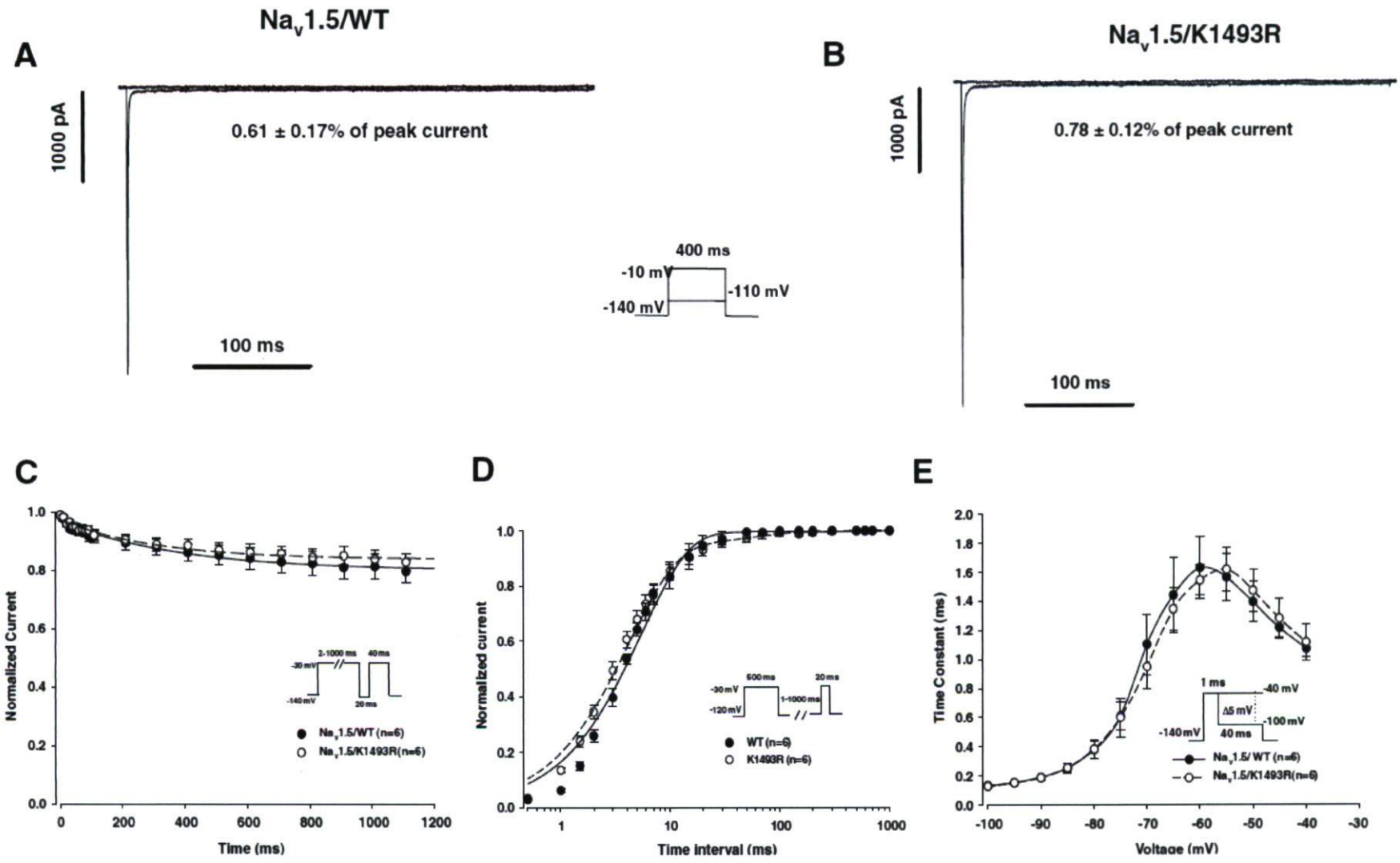
A
Na$_v$1.5/WT
1000 pA
0.61 ± 0.17% of peak current
100 ms
400 ms
-10 mV
-110 mV
-140 mV
B
Na$_v$1.5/K1493R
1000 pA
0.78 ± 0.12% of peak current
100 ms
C
Normalized Current
Time (ms)
Na$_v$1.5/WT (n=6)
Na$_v$1.5/K1493R(n=6)
D
Normalized current
Time interval (ms)
WT (n=6)
K1493R (n=6)
E
Time Constant (ms)
Voltage (mV)
1 ms
-40 mV
Δ5 mV
-100 mV
-140 mV
40 ms
Na$_v$1.5/ WT (n=6)
Na$_v$1.5/K1493R(n=6)

Figure 4.3

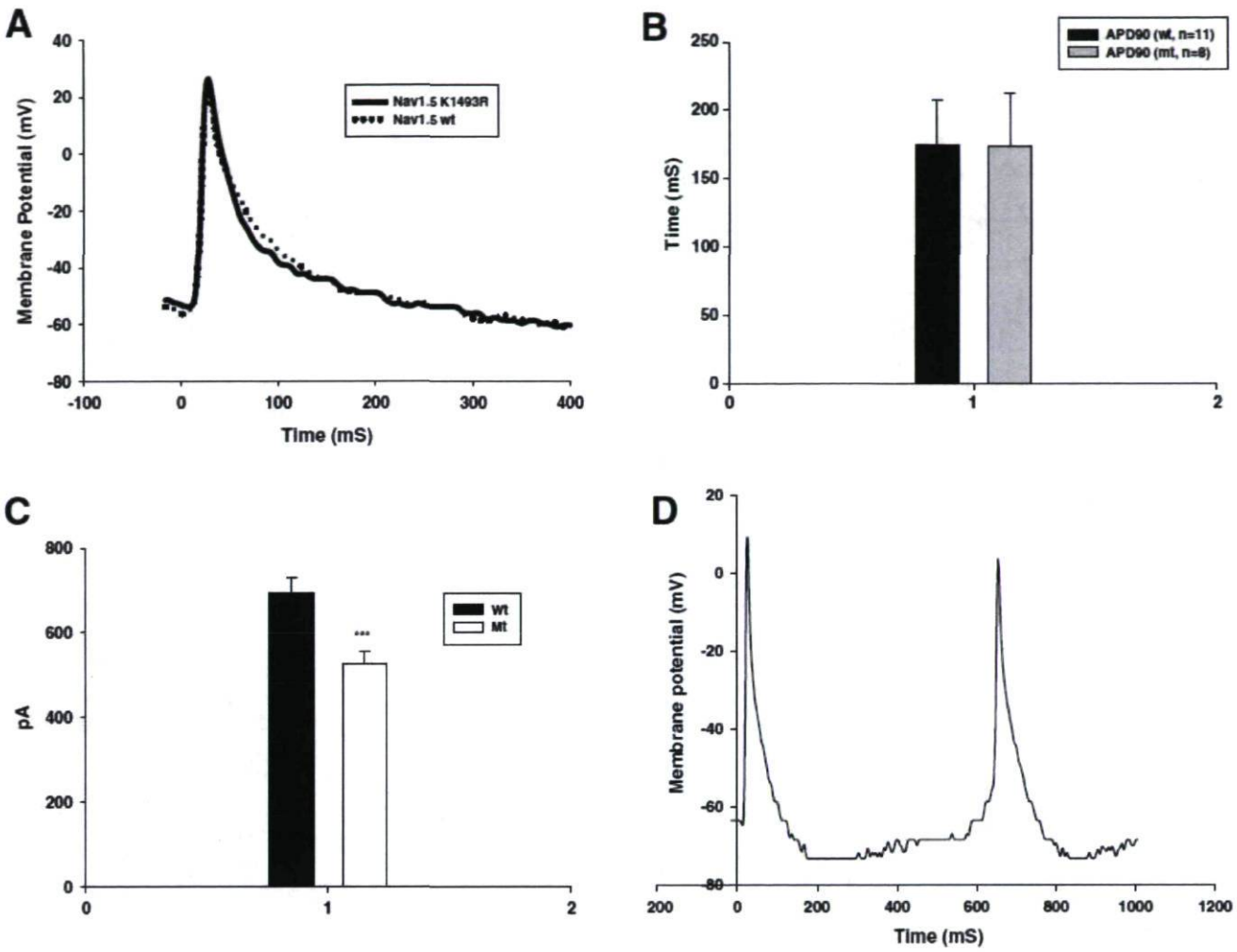
A
Membrane Potential (mV)
Time (mS)
Nav1.5 K1493R
Nav1.5 wt
B
Time (mS)
APD90 (wt, n=11)
APD90 (mt, n=8)
C
pA
Wt
Mt
***
D
Membrane potential (mV)
Time (mS)

Figure 4.4

Chapter V

General Discussion and Prospectives

5.1 General discussion

In the present thesis, three *SCN5A* mutations, Y1767C, S1333Y, and K1493R, were associated with LQT3, SIDS, and lone AF, respectively. Their gating properties of the mutant Na+ channels were characterized in tsA 201 cells by whole-cell configuration of the patch-clamp technique. All three showed a gain-of-function change in their gating properties. Y1767C and S1333Y produced persistent I_{Na} and had increased window currents with different pharmacological effects. The persistent I_{Na} induced by the Y1767C mutant channels was not blocked by the class I antiarrhythmic drugs tested, whereas the persistent I_{Na} induced by S1333Y was indeed sensitive to lidocaine blockage. The K1493R mutant channels showed a gain-of-function in the increased window current, which indicates a new mechanism that could cause AF.

Part I

The *SCN5A* mutation Y1767C was found in a 17-year-old patient with prolonged QT intervals (510 ms) in ECG and a documented episode of cardiac arrest. The patient was prescribed the β-blocker propranolol (2.5 mg/kg/day) after his diagnosis and has remained free of symptoms. His brother had presented with a history of syncope at age 18 and QT prolongation on the baseline ECG (no genomic screening results were done). The brother declined therapy and at age of 26 died a sudden death.

Y1767C mutation was located in the S6 segment of domain IV (DIVS6) of $Na_v1.5$ channels, which is a region associated with both Na^+ channel gating and pharmacology. The biophysical study showed typical LQT3-like biophysical properties with an increased persistent I_{Na}, an accelerated kinetic decay of fast inactivation, an enlarged window current, and a faster recovery from inactivation. The persistent I_{Na} of Y1767C mutation was blocked by ranolazine but not by other class I antiarrhythmic drugs, including quinidine (Ia), lidocaine (Ib), mexelitine (Ib), and flecainide (Ic).The enlarged window current was also markedly diminished by ranolazine. No significant difference in steady-state activation or inactivation was observed after ranolazine treatment, compared with controls.

5.1.1 Y1767C channels and LQT3

Faster decay of inactivation kinetics for Y1767C mutation indicates a destabilization of the inactivation process, which results in the persistent I_{Na} that has long been known as the most common mechanism underlying prolonged QT intervals in LQT3 (Tan *et al.*, 2003; Bennett *et al.*, 1995b). The persistent I_{Na} induced by Y1767C channels can be observed at more positive voltage levels close to the plateau of cardiac action potentials, consequently resulting in its abnormal prolongation. The accelerated recovery from inactivation is probably associated with destabilization of fast inactivation and enables more channels to be available at depolarized voltages in the ventricular cells. The ramp current in this study was increased and shifted in a depolarized direction, which is consistent with the enlarged window current. The peak window current was at voltages close to resting membrane potential (– 80mV), which suggests the risk of developing various arrhythmias increases at subthreshold membrane potentials, especially in the setting of the persistent I_{Na}. The LQT3 phenotype in the patient carrying Y1767C mutation is based on the presence of both the increased persistent I_{Na} and enlarged window current. Ranolazine-related changes in gating properties may provide a new direction for the development of drug therapies for patients carrying Y1767C mutation.

5.1.2 The role of DIVS6 in Na^+ channels

DIVS6 of $Na_v1.5$ channels provide docking sites for the inactivation particle (IMF) and containing binding sites for Na^+ channel blockers (class I antiarrhythmic drugs). Previous studies found that two residues (F1764, V1774 in rat $Na_v1.2$ sequence) act as docking sites in DIVS6 by binding to the IMF particle to block Na^+ conductance and immobilize gating charges. The fast inactivation is consequently interrupted in mutations of these two residues, particularly in V1774 residue. Y1767 residue in the $Na_v1.5$ sequence is equivalent to Y1771 residue in rat $Na_v1.2$ sequence, which is located adjacent to the V1774 residue. Thus, the *SCN5A* mutation Y1767C may have gating effects similar to the V1774 mutation. As a result, gating properties of Y1767C mutation may have changes in kinetics of fast inactivation and recovery from fast inactivation. Three other LQT3-related mutations in the same region with somewhat similar gating changes have been identified. M1766L mutation (Valdivia *et al.*, 2002a) and V1763M mutation, which was characterized in our laboratory (Chang *et al.*, 2004), induced persistent I_{Na} while I1768V accelerated recovery from inactivation (Groenewegen *et al.*, 2003a). In addition to docking sites,

DIVS6 also provides the binding sites for class I antiarrhythmic drugs. F1760 and Y1767 are the two most common binding sites in $Na_v1.5$ channels. Class I antiarrhythmic drugs do not block the persistent I_{Na} induced by Y1767C mutation, suggesting that Y1767C mutation may be less sensitive to the treatment of class I antiarrhythmic drugs, possibly because of impaired binding ability of these drugs to $Na_v1.5$ channels.

5.1.3 The role of ranolazine in blocking Y1767C mutation

Ranolazine is a piperazine derivative that is structurally similar to lidocaine. The molecular weight of ranolazine (427.5) is around 1.8-fold greater than that of lidocaine (234.3). Although ranolazine is structurally similar to class I antiarrhythmic drugs, it affects the persistent I_{Na} induced by Y1767C mutation differently. The persistent I_{Na} is blocked by ranolazine without affecting the steady-state activation and inactivation, which is not the case for several drugs in different subgroups of class I antiarrhythmic drugs. In addition, mutant channels have a further inhibitory effect in use-dependent protocol. All of these data support that: (1) the Y1767 residue is important for high-affinity binding of class I antiarrhythmic drugs. Y1767C mutation may interfere with the blocking effects of these drugs; (2) The persistent I_{Na} induced by Y1767C mutation is potentially blocked by ranolazine, which acts as an open channel blocker. This finding is consistent with the previous results of ranolazine on $Na_v1.4$ and $Na_v1.7$ channels (Wang *et al.*, 2008b). The binding site for ranolazine has been hypothesized at F1760, so Y1767 may hinder the large molecule from accessing its binding site. The blocking effect of ranolazine is prominent when Y1767 is mutated.

Part II

The second *SCN5A* mutation S1333Y studied here was found in a 25-day-old SIDS patient during a gene screen for LQTS (Millat *et al.*, 2006). Besides the S1333Y mutation, forty-five mutations in this study cohort were identified in *KCNQ1, KCNH2, SCN5A, KCNE1* and *KCNE2* genes. Here, we characterize biophysical properties of S1333Y mutation, which is located in the S4-S5 linker of domain III (DIII S4-S5 linker). To study the biophysical properties of the *SCN5A* mutation S1333Y, mutant channels were expressed in tsA 201 cells and were tested by the whole-cell patch clamp technique. The functional studies showed an increased persistent I_{Na}, an enlarged window current produced by the overlapping area between –8 mV shift of steady-state

activation and +7 mV shift of steady-state inactivation. The slow component of inactivation kinetics became longer, but the recovery from inactivation was slow.

5.1.4 SIDS and its risk factors

In elderly people, sudden cardiac death is often attributed to cardiac arrhythmias particularly ventricular fibrillation secondary to coronary artery disease (Spooner *et al.*, 2001). In adolescents and young adults, sudden cardiac death is often related to occult cardiac disease such as arrhythmogenic right ventricular cardiomyopathy (ARVC) and hypertrophic cardiomyopathy (HCM) (Tester and Ackerman, 2006). In neonates and infants, sudden unexplained death is categorized as SIDS, which is the leading cause of death during the first year of life in infants in developed countries. SIDS is further defined as sudden and unexplained death in an infant less than one year old after a thorough investigation including a complete autopsy, a review of clinical history, and an inspection of circumstances of the death. The latest definition of SIDS, including a diagnostic guideline, was adopted at a meeting held in San Diego in 2004 (Krous *et al.*, 2004).

The pathogenesis of SIDS is multifactorial and many risk factors can trigger SIDS events, the two most common being prone sleep position (Dwyer *et al.*, 1991a) and upper respiratory infections (Vege and Ole, 2004). Other risk factors include bottle feeding, exposure to second-hand tobacco smoke, overheating, and co-sleeping (Hunt and Hauck, 2006). Previous studies revealed associated SIDS with alterations in genes associated with medium-chain acyl-coA dehydrogenase (MCAD), cardiac ion channels, thrombosis, and glucose metabolism (Opdal and Rognum, 2004a). Some gene polymorphisms were associated with increased risk of SIDS under certain circumstances, including polymorphisms in genes encoding complement component 4 (C4), HLA-DR, interleukin-6 (IL-6), and interleukin-10 (IL-10) (Bacon, 2008; Vege and Ole, 2004).

Genetic studies in SIDS have shown that mutations in genes associated with LQTS appear to be a major subset, accounting for up to 9.5 % of affected patients (Arnestad *et al.*, 2007b). LQTS can also explain the increased risk of sudden death in patients who develop life-threatening arrhythmias. Recently, a study revealed that 14% of LQTS patients die during their first episode of arrhythmia and that 30% of these events occur during the first year of life (Beinder *et al.*, 2001). In addition, the affected LQTS patients may not respond to the standard medical therapy with β-blockers (Moss *et al.*, 2000). Therefore, early diagnosis and treatment (e.g., ICD) of

LQTS are important to prevent these catastrophic events. In addition to LQTS, a nine-week-old infant with SIDS has been reported in a BrS family (Priori *et al.*, 2000a). A BrS-related gene *GPD1L* may lead mutant channels to give a decreased peak I_{Na} (Van Norstrand *et al.*, 2007). These data support the hypothesis that the SIDS may be a severe form of LQTS or BrS during the infant stage.

5.1.5 SIDS and *SCN5A* mutations

Mutations in *SCN5A* gene have been identified in around 2% of SIDS cases induced by LQTS (Ackerman *et al.*, 2001). In 2000, inherited LQT3 was first linked to SIDS as direct genomic evidence by identifying *SCN5A* mutation S941N in a SIDS infant (Schwartz *et al.*, 2000). A 7-week-old infant was successfully resuscitated from a documented ventricular fibrillation. The post-resuscitational 12-lead ECG showed a corrected QT (QTc) interval of 648 ms, which substantially exceeds the defined value of 440 ms. The functional study of this mutant channel showed an increased persistent I_{Na} that was consistent with the change of prolonged QTc in ECG. Since then, *SCN5A* mutations (A1330P, R1826H, A997S, and S1103Y) have been found to be responsible for the clinical SIDS phenotype. Additionally, another gene screen found that four *SCN5A* mutations (del AL 586-587, R680H, T1304M, F1486L) and five rare *SCN5A* genetic variants (S216L, R1193Q, V1951L, F2004L, P2006A) are linked to SIDS (Arnestad *et al.*, 2007c; Wang *et al.*, 2007a). All of these mutations and rare variants showed defects in voltage-dependent inactivation sometimes with the presence of increased persistent I_{Na} or enlarged window current. This indicates that such a spectrum of biophysical defects may contribute to a pattern, ranging from overt to latent, of pathological SIDS phenotype. In addition to LQT3 mutations, one *SCN5A* mutation G1084S has also been identified in infants with SIDS with a loss-of-function property of a hyperpolarizing shift in steady-state inactivation (Otagiri *et al.*, 2008).

5.1.6 S1333Y channels and SIDS

S1333Y channels produce a gain-of-Na^+ channel function. The increased persistent I_{Na} is the hall-mark mechanism which causes a longer ventricular repolarization, leading to prolonged QT intervals. In addition, the window current is also enlarged owing to shifts of steady-state activation and inactivation. Mutant channels within the voltage range of the window are never

inactivated to zero. The peak window current was at the voltage of –80 mV close to resting membrane potential, resulting in a high risk of patients' developing cardiac arrhythmias by producing sub-threshold activity. In combination of the presence of prolonged repolarization, cardiac myocytes have a propensity to develop EADs that may induce torsades de pointes in the patient (Fabritz *et al.*, 2003; Tian *et al.*, 2004). Since the gating properties of BrS1 mutations are characterized by a loss of the Na^+ channel function, the sudden death event in the present case is unlikely to be related to BrS1, but most probably caused by LQT3.

5.1.7 The role of DIII S4-S5 linker in Na^+ channels

The residue S1333 was highly conserved at the DIII S4-S5 linker in Na^+ channels of many tissues and species. When expressed in tsA 201 cells, mutant channels generated the persistent I_{Na} caused by an impaired inactivation process shown as a depolarizing steady-state inactivation by +7 mV, a slow inactivation kinetics, and a fast recovery from inactivation. Similar changes of impaired inactivation have also been observed in two other highly conserved mutations, for example the *SCN5A* mutation A1330P (Wedekind *et al.*, 2001) and *SCN4A* mutation A1156T (Yang *et al.*, 1994) in the same region. These results support the previous hypothesis that the amino acid sequence of the DIII S4-S5 linker, including the serine, is highly conserved, and forms part of the docking site for the inactivation particle IFM in the inactivation gate in several tissues and species (West *et al.*, 1992).

Part III

K1493R mutation in *SCN5A* gene, found in an AF patient at age 50, is located at the III-IV linker of Na^+ channels. The proband's mother was also diagnosed with AF at age 63, after experiencing many years of symptomatic palpitations. When transiently expressed in tsA 201 cells, mutant channels showed a gain-of-function property in the biophysical study, including slow kinetics of fast inactivation, a hyperpolarizing shift of steady-state inactivation, an enlarged window current, and an increased ramp current. When expressed in atrial cardiomyocytes, mutant channels produced an enhanced cellular excitability with spontaneous action potential depolarisations and a lower threshold for action potential firing.

5.1.8 Candidate genes for lone AF

Recently, many candidate genes for lone AF have been identified, including *KCNQ1* (Chen *et al.*, 2003), *KCNE2* (Yang *et al.*, 2004), *KCNJ2* (Xia *et al.*, 2005), *KCNA5* (Olson *et al.*, 2006), *GJA5* (Gollob *et al.*, 2006), and *SCN5A* (Olson *et al.*, 2005). They display diverse molecular mechanisms with gene-induced ion channel defects to cause AF. For the K^+ channel mutations, mechanisms are divided into two categories, the loss-of-function and gain-of-function gating changes. The loss of function is found in patients with the *KCNA5* mutation, which is reported to cause AF by lengthening APD and promoting EADs that help occurrence of trigger activity. The gain of function is linked to mutations in genes *KCNQ1*, *KCNE2*, and *KCNJ2*. These mutations are reported to cause AF by shortening APDs and effective refractory periods that are thought to help the enhancement of the vulnerability to reentry occurrence that is required for the maintenance of the AF. For the connexin 40 mutations, the loss of function was observed to cause AF by impairing gap-junction assembly or electrical coupling (Gollob *et al.*, 2006). For *SCN5A* mutations (inward ionic flow), underlying mechanisms are opposite to the ones from K^+ channel mutations (outward ionic flow).

5.1.9 K1493R channels in *SCN5A* cause a gain-of-function in lone AF

K1493 is highly conserved at a position of the sixth amino acid downstream from inactivation particle (IFM) of Na^+ channels, which acts as a lid in the "hinged lid" mechanism for the inactivation process. K1493R mutation may lead to some conformational changes in this region, thus producing some gating changes. Biophysical properties of mutant channels were evaluated by patch-clamp technique on tsA 201 cells. The resulting data showed that mutant channels may increase the channel availability by interrupting the inactivation process (slow kinetics of fast inactivation and depolarizing shift of steady-state inactivation). The depolarizing shift of steady-state inactivation directly enlarges the window current that lowers the threshold of action potential firing and consequently facilitates the spontaneous action potential formation in atrial myocytes (HL-1 cells). A previous study showed that *SCN5A* mutations were linked to about 2% of patients with LQT3 that is also characterized by a gain-of-function property (Johnson *et al.*, 2008). Although a gain-of-function property was found in K1493R mutation, a patient's ECG does not manifest the QT interval prolongation owing to the absence of the persistent I_{Na} recorded in the study of K1493R channels. M1875T in *SCN5A* is another AF-associated mutation

to produce similar gating change with the depolarizing shift in steady-state inactivation. Its peak I_{Na} was increased. Increased I_{Na} corresponds with increased atrial excitability owing to failure depolarization that leads to EADs and triggers activity in the affected patient (Makiyama *et al.*, 2008). From a combination of these two cases, it is hypothesized that *SCN5A* gain-of-function mutations may initiate AF by increasing atrial excitability.

5.1.10 Loss-of-function *SCN5A* mutations in lone AF

Two loss-of-function mutations in *SCN5A* have been characterized, since *SCN5A* mutations were first linked to lone AF in patients with DCM (Olson *et al.*, 2005). One is the common polymorphism H558R in *SCN5A*, which was found more often in patients with lone AF than controls. Functional study showed a decreased I_{Na} (Chen *et al.*, 2007). The other is *SCN5A* mutation N1986K, which gave a negative shift of steady-state inactivation in functional study (Ellinor *et al.*, 2008). Therefore, the loss-of-function in $Na_v1.5$ is considered as a mechanism for the maintenance of AF. It is suggested that I_{Na} reduction may increase the atrial vulnerability for AF by slowing the electrical conduction velocity. This may in turn help to shorten the atrial reentry wavelength and to promote re-entry through a single or multiple reentrant circuits (Allessie *et al.*, 1996). Such reentrant circuits are considered as a substrate for the maintenance of AF after an atrial ectopic activity is triggered. This mechanism is supported by evidence that the prolonged atrial conduction intervals, shown as P wave duration in ECG, are often seen in patients with BrS (Morita *et al.*, 2002). Thus, loss-of-function mutations in *SCN5A* predispose patients to AF by facilitating the maintenance of reentrant excitation waves in the atrium.

5.2 Prospectives

Chapters II-IV characterized biophysical properties of three *SCN5A* mutations. Several questions should be figured out in the future. (1) Y1767 residue was shown to decrease the accessibility of ranolazine to its binding site (F1760 residue). However, access of ranolazine may be regulated by the inactivation gate (III-IV linker), so it is necessary to assess the role of Y1767 residue in ranolazine block by removing the regulatory effect of III-IV linkers. (2) some environmental factors (e.g., acidosis) may trigger the sudden death event in SIDS patients. Can acidic condition affect gating properties of S1333Y mutant channels? (3) K1493R mutation was shown to

decrease threshold for firing cardiac action potentials. What is the pharmacological effect on this mutant channel?

5.2.1 The effects of open channel block by ranolazine on Y1767C channels with additional site-directed mutagenesis at DIII–IV linker (IFM/IQM or IFM/QQQ)

The data from chapter II suggest that F1760 and Y1767 residues play different role in ranolazine blocking. Ranolazine blocks Y1767C channels at open state by interacting with F1760 residue. This suggestion is consistent with results of previous studies (Fredj *et al.*, 2006; Mujtaba *et al.*, 2002). Additionally, Y1767 residue is suggested to prevent big-molecule ranolazine from accessing its binding site. The blocking effect of ranolazine is prominent when Y1767 is mutated. The access of ranolazine to its binding sites may be regulated by the inactivation gate, which also prevents charged ranolazine from reaching the binding site under resting conditions and acts to trap ranolazine within the pore as the channels deactivate (Strichartz, 1973). For this reason, more pharmacologic works should be done to further study the role of Y1767 residue by a manner of site-directed mutagenesis known as mutations of IFM/IQM or IFM/QQQ in the inactivation gate. This mutagenesis study has long been used to assess the action of the Na^+ channel blocker by selectively removing the rapid component of fast inactivation (Bennett *et al.*, 1995a; O'Leary and Chahine, 2002; O'Leary *et al.*, 2003). For example, IFM/IQM mutation makes the kinetics of fast inactivation become slower than controls. The slowed kinetics is partially restored by applying lidocaine, which is used for generating another inactivation effect by interacting with its binding sites. The IFM/QQQ mutation is more resistant to the lidocaine block, because the inactivation is much more interrupted by three-site mutagenesis than by single-site mutagenesis (Fan *et al.*, 1996). Based on this idea, blocking effects of ranolazine can be explored in the same manner of site-directed mutagenesis in the future by testing the kinetics of fast inactivation and use-dependent inhibition. A more prominent blocking effect is predicted on Y1767C channels when compared with controls.

5.2.2 Effects of acidosis on S1333Y channels

It has been well known that extracellular acidosis may block peak I_{Na} (Zhang and Siegelbaum, 1991). In contrast, a recent study demonstrated that SIDS-linked *SCN5A* mutation S1103Y displays a persistent I_{Na} up to 5.23% percentage of the peak I_{Na} by applying an acidic (pH 6.7)

intracellular solution (Plant *et al.*, 2006). Under the same acidic conditions, the single channel recordings on mutant channels showed an abnormal late reopening property. These findings support the role of internal acidosis in the development of SIDS (Fig. 5.1). Acidic conditions are widely present in long-standing apnea, respiratory acidosis, and metabolic acidosis in poorly perfused cardiomyocytes. The intracellular pH of cardiac myocytes can decrease to acidic levels even when arterial pH is still around 7.4. Such acidic environmental factor may profoundly impact mutant channels to produce a bigger persistent I_{Na} through a gene-environment interaction. The persistent I_{Na} may in turn trigger acidosis-induced cardiac arrhythmias through the mechanism of EADs. If this hypothesis is true, S1333Y mutation may even have a markedly increased persistent I_{Na}.

5.2.3 Pharmacologic and therapeutic implications on K1493R channels

A previous study showed that flecainide can shorten the QT intervals and restore AF to normal sinus rhythm by inhibiting the persistent I_{Na} in an overlapping mutation for LQT3 and AF (Benito *et al.*, 2008). Similar to this, the present study on the K1493R mutation also provides a potential molecular link to the use of class I antiarrhythmic drugs to reduce the AF burden. Although these drugs can be effective in the management of AF, they may have proarrhythmic effects and paradoxically exacerbate arrhythmias. For example, use of these drugs may cause 1:1 AV conduction during AF owing to conduction delay in the atria. If the fibrillation cycle length prolongs sufficiently to form reentrant circuits, frequent ventricular tachycardia (VT) may occur (Roden, 1998). In addition, a previous study showed that use of Na^+ channel blockers in LQT3 patients may potentially unmask the BrS1 ECG pattern. In that study, a total of 13 patients from 7 LQT3 families received flecainide intravenously at a dose of 2 mg/kg over 10 minutes. As expected, prolonged QT intervals were shortened in 12 of the 13 patients, and concomitant ST segment elevation in leads $V_{1\text{-}3}$ ($\geq$ 2 mm) was observed in 6 of the 13 patients (Priori *et al.*, 2000b). Therefore, further pharmacological studies will be required to determine how Na^+ channel blockers correct gating defects of K1493R mutation, and whether or not these drugs generate other abnormal gating changes to cause other abnormal ECG phenotypes on K1493R channels.

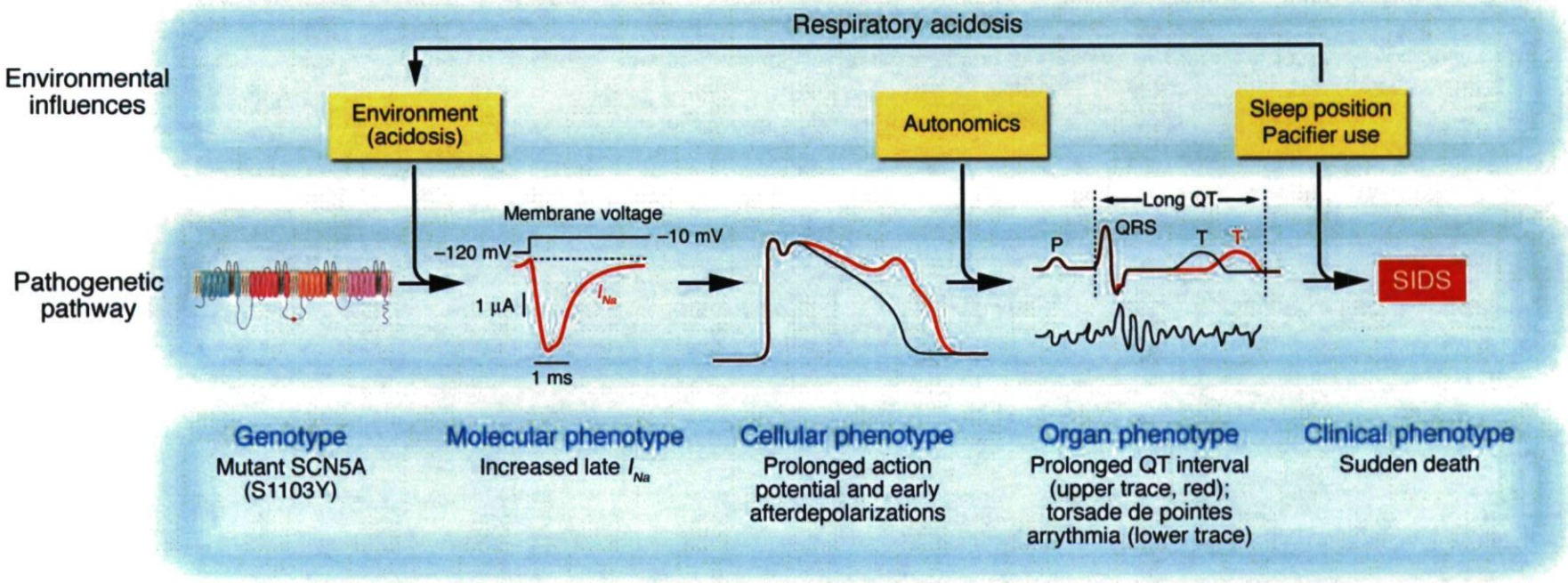

Figure 5.1: An arrhythmogenic pathogenetic pathway for SIDS from patient genotype to clinical phenotype. The figure denotes the pathogenic pathway from genotype to clinical phenotype, with environmental influences noted. The genetic abnormality, in this instance a polymorphism in the cardiac Na^+ channel *SCN5A*, causes a molecular phenotype of increased late Na^+ current (I_{Na}) under the influence of environmental factors such as acidosis. Interacting with other ion currents that may themselves be altered by genetic and environmental factors, the late Na^+ current causes a cellular phenotype of prolonged action potential duration as well as early afterdepolarizations. Prolonged action potential in the cells of the ventricular myocardium and further interaction with environmental factors such as autonomic innervation, which in turn may be affected by genetic factors, produce a tissue/organ phenotype of a prolonged QT interval on the ECG and torsade de pointes arrhythmia in the whole heart. If this is sustained or degenerates to ventricular fibrillation, the clinical phenotype of SIDS results. Environmental and multiple genetic factors may interact at many different levels to produce the characteristic phenotypes at the molecular, cellular, tissue, organ, and clinical levels (Makielski, 2006).

Conclusions

In summary, our studies in tsA 201 cells with whole-cell patch clamp configuration show that (1) Y1767C is an LQT3-ralated mutation. The phenotype induced by Y1767C mutation can be treated by ranolazine given the drug's ability to normalize the gating abnormality through its open-channel-blocking mechanism; (2) S1333Y is a SIDS *SCN5A* mutation, which is characterized by a typical LQT3-like property; (3) K1493R mutation causes lone AF by a hyperexcitability mechanism through a depolarized shift in steady-state inactivation and an enlarged window current.

Bibliographie

Abbott GW, Sesti F, Splawski I, Buck ME, Lehmann MH, Timothy KW, Keating MT, and Goldstein SA (1999). MiRP1 forms I_{Kr} potassium channels with HERG and is associated with cardiac arrhythmia. *Cell* 97, 175-187.

Abriel H, Kamynina E, Horisberger JD, and Staub O (2000). Regulation of the cardiac voltage-gated Na^+ channel (H1) by the ubiquitin-protein ligase Nedd4. *FEBS Lett* 466, 377-380.

Abriel H and Kass RS (2005). Regulation of the voltage-gated cardiac sodium channel Nav1.5 by interacting proteins. *Trends Cardiovasc Med* 15, 35-40.

Ackerman MJ, Siu BL, Sturner WQ, Tester DJ, Valdivia CR, Makielski JC, and Towbin JA (2001). Postmortem molecular analysis of *SCN5A* defects in sudden infant death syndrome. *J Am Med Assoc* 286, 2264-2269.

Ahern CA, Eastwood AL, Dougherty DA, and Horn R (2008). Electrostatic contributions of aromatic residues in the local anesthetic receptor of voltage-gated sodium channels. *Circ Res* 102, 86-94.

Ahern CA, Zhang JF, Wookalis MJ, and Horn R (2005). Modulation of the cardiac sodium channel NaV1.5 by Fyn, a Src family tyrosine kinase. *Circ Res* 96, 991-998.

Aitken A, Collinge DB, van Heusden BP, Isobe T, Roseboom PH, Rosenfeld G, and Soll J (1992). 14-3-3 proteins: a highly conserved, widespread family of eukaryotic proteins. *Trends Biochem Sci* 17, 498-501.

Akai J, Makita N, Sakurada H, Shirai N, Ueda K, Kitabatake A, Nakazawa K, Kimura A, and Hiraoka M (2000). A novel *SCN5A* mutation associated with idiopathic ventricular fibrillation without typical ECG findings of Brugada syndrome . *FEBS Lett* 479, 29-34.

Akopian AN, Sivilotti L, and Wood JN (1996). A tetrodotoxin-resistant voltage-gated sodium channel expressed by sensory neurons. *Nature* 379, 257-262.

Akopian AN, Souslova V, Sivilotti L, and Wood JN (1997). Structure and distribution of a broadly expressed atypical sodium channel. *FEBS Lett* 400, 183-187.

Alings M and Wilde A (1999). "Brugada" syndrome: clinical data and suggested pathophysiological mechanism. *Circulation* 99, 666-673.

Allessie MA, Konings K, Kirchhof CJ, and Wijffels M (1996). Electrophysiologic mechanisms of perpetuation of atrial fibrillation. *Am J Cardiol* 77, 10A-23A.

Allouis M, Le BF, Wilders R, Peroz D, Schott JJ, Noireaud J, Le MH, Merot J, Escande D, and Baro I (2006). 14-3-3 is a regulator of the cardiac voltage-gated sodium channel Nav1.5. *Circ Res* 98, 1538-1546.

An RH, Bangalore R, Rosero SZ, and Kass RS (1996). Lidocaine block of LQT-3 mutant human Na^+ channels. *Circ Res* 79, 103-108.

An RH, Wang XL, Kerem B, Benhorin J, Medina A, Goldmit M, and Kass RS (1998). Novel LQT-3 mutation affects Na^+ channel activity through interactions between α and β 1-subunits. *Circ Res* 83, 141-146.

Antzelevitch C (2001b). The Brugada syndrome: ionic basis and arrhythmia mechanisms. *J Cardiovasc Electrophysiol* 12, 268-272.

Antzelevitch C (2001a). Basic mechanisms of reentrant arrhythmias. *Curr Opin Cardiol* 16, 1-7.

Antzelevitch C, Belardinelli L, Wu L, Fraser H, Zygmunt AC, Burashnikov A, Di Diego JM, Fish JM, Cordeiro JM, Goodrow RJ, Jr., Scornik F, and Perez G (2004a). Electrophysiologic properties and antiarrhythmic actions of a novel antianginal agent. *J Cardiovasc Pharmacol Ther* 9 Suppl 1, S65-S83.

Antzelevitch C, Belardinelli L, Zygmunt AC, Burashnikov A, Di Diego JM, Fish JM, Cordeiro JM, and Thomas G (2004b). Electrophysiological effects of ranolazine, a novel antianginal agent with antiarrhythmic properties. *Circulation* 110, 904-910.

Antzelevitch C, Brugada P, Brugada J, and Brugada R (2005). Brugada syndrome: from cell to bedside. *Curr Probl Cardiol* 30, 9-54.

Antzelevitch C and Nof E (2008). Brugada syndrome: recent advances and controversies. *Curr Cardiol Rep* 10, 376-383.

Antzelevitch C, Pollevick GD, Cordeiro JM, Casis O, Sanguinetti MC, Aizawa Y, Guerchicoff A, Pfeiffer R, Oliva A, Wollnik B, Gelber P, Bonaros EP, Jr., Burashnikov E, Wu Y, Sargent JD, Schickel S, Oberheiden R, Bhatia A, Hsu LF, Haissaguerre M, Schimpf R, Borggrefe M, and Wolpert C (2007). Loss-of-function mutations in the cardiac calcium channel underlie a new clinical entity characterized by ST-segment elevation, short QT intervals, and sudden cardiac death. *Circulation* 115, 442-449.

Antzelevitch C, Shimizu W, Yan GX, Sicouri S, Weissenburger J, Nesterenko VV, Burashnikov A, Di DJ, Saffitz J, and Thomas GP (1999). The M cell: its contribution to the ECG and to normal and abnormal electrical function of the heart. *J Cardiovasc Electrophysiol* 10, 1124-1152.

Arad M, Seidman CE, and Seidman JG (2007). AMP-activated protein kinase in the heart: role during health and disease. *Circ Res* 100, 474-488.

Armstrong CM and Bezanilla F (1977). Inactivation of the sodium channel. II. Gating current experiments. *J Gen Physiol* 70, 567-590.

Arnestad M, Crotti L, Rognum TO, Insolia R, Pedrazzini M, Ferrandi C, Vege A, Wang DW, Rhodes TE, George AL, Jr., and Schwartz PJ (2007c). Prevalence of long-QT syndrome gene variants in sudden infant death syndrome. *Circulation* 115, 361-367.

Arnestad M, Crotti L, Rognum TO, Insolia R, Pedrazzini M, Ferrandi C, Vege A, Wang DW, Rhodes TE, George AL, Jr., and Schwartz PJ (2007b). Prevalence of long-QT syndrome gene variants in sudden infant death syndrome. *Circulation* 115, 361-367.

Arnestad M, Crotti L, Rognum TO, Insolia R, Pedrazzini M, Ferrandi C, Vege A, Wang DW, Rhodes TE, George AL, Jr., and Schwartz PJ (2007a). Prevalence of long-QT syndrome gene variants in sudden infant death syndrome. *Circulation* 115, 361-367.

Ashcroft FM (2006). From molecule to malady. *Nature* 440, 440-447.

Attwell D, Cohen I, Eisner D, Ohba M, and Ojeda C (1979). The steady state TTX-sensitive ("window") sodium current in cardiac Purkinje fibres. *Pflügers Arch* 379, 137-142.

Auld VJ, Goldin AL, Krafte DS, Marshall J, Dunn JM, Catterall WA, Lester HA, Davidson N, and Dunn RJ (1988). A rat brain Na^+ channel α subunit with novel gating properties. *Neuron* 1, 449-461.

Aurlien D, Leren TP, Tauboll E, and Gjerstad L (2009). New SCN5A mutation in a SUDEP victim with idiopathic epilepsy. *Seizure* 18, 158-160.

Baba S, Dun W, and Boyden PA (2004). Can PKA activators rescue Na^+ channel function in epicardial border zone cells that survive in the infarcted canine heart? *Cardiovasc Res* 64, 260-267.

Backx PH, Yue DT, Lawrence JH, Marban E, and Tomaselli GF (1992). Molecular localization of an ion-binding site within the pore of mammalian sodium channels. *Science* 257, 248-251.

Bacon C (2008). Recurrence of sudden infant death syndrome. *Pediatrics* 122, 869-870.

Balser JR (2001). The cardiac sodium channel: gating function and molecular pharmacology. *J Mol Cell Cardiol* 33, 599-613.

Baroudi G, Acharfi S, Larouche C, and Chahine M (2002). Expression and intracellular localization of an SCN5A double mutant R1232W/T1620M implicated in Brugada syndrome. *Circ Res* 90, E11-E16.

Baroudi G, Carbonneau E, Pouliot V, and Chahine M (2000). SCN5A mutation (T1620M) causing brugada syndrome exhibits different phenotypes when expressed in *Xenopus* oocytes and mammalian cells. *FEBS Lett* 467, 12-16.

Baroudi G and Chahine M (2000). Biophysical phenotypes of SCN5A mutations causing long QT and Brugada syndromes. *FEBS Lett* 487, 224-228.

Baroudi G, Pouliot V, Denjoy I, Guicheney P, Shrier A, and Chahine M (2001). Novel mechanism for Brugada syndrome: defective surface localization of an *SCN5A* mutant (R1432G). *Circ Res* 88, E78-E83.

Battaini F (2001). Protein kinase C isoforms as therapeutic targets in nervous system disease states. *Pharmacol Res* 44, 353-361.

Bean BP, Cohen CJ, and Tsien RW (1983). Lidocaine block of cardiac sodium channels. *J Gen Physiol* 81, 613-642.

Beckh S (1990). Differential expression of sodium channel mRNAs in rat peripheral nervous system and innervated tissues. *FEBS Lett* 262, 317-322.

Beggs AH, Byers TJ, Knoll JH, Boyce FM, Bruns GA, and Kunkel LM (1992). Cloning and characterization of two human skeletal muscle alpha-actinin genes located on chromosomes 1 and 11. *J Biol Chem* 267, 9281-9288.

Beinder E, Grancay T, Menendez T, Singer H, and Hofbeck M (2001). Fetal sinus bradycardia and the long QT syndrome. *Am J Obstet Gynecol* 185, 743-747.

Belardinelli L, Shryock JC, and Fraser H (2006). Inhibition of the late sodium current as a potential cardioprotective principle: effects of the late sodium current inhibitor ranolazine. *Heart* 92 Suppl 4, iv6-iv14.

Belcher SM, Zerillo CA, Levenson R, Ritchie JM, and Howe JR (1995). Cloning of a sodium channel α subunit from rabbit Schwann cells. *Proc Natl Acad Sci USA* 92, 11034-11038.

Belhassen B, Glick A, and Viskin S (2004). Efficacy of quinidine in high-risk patients with Brugada syndrome. *Circulation* 110, 1731-1737.

Benhorin J, Taub R, Goldmit M, Kerem B, Kass RS, Windman I, and Medina A (2000). Effects of flecainide in patients with new *SCN5A* mutation : mutation-specific therapy for long-QT syndrome? *Circulation* 101, 1698-1706.

Benito B, Brugada R, Perich RM, Lizotte E, Cinca J, Mont L, Berruezo A, Tolosana JM, Freixa X, Brugada P, and Brugada J (2008). A mutation in the sodium channel is responsible for the association of long QT syndrome and familial atrial fibrillation. *Heart Rhythm* 5, 1434-1440.

Bennett PB, Valenzuela C, Chen LQ, and Kallen RG (1995a). On the molecular nature of the lidocaine receptor of cardiac Na^+ channels. Modification of block by alterations in the α-subunit III-IV interdomain. *Circ Res* 77, 584-592.

Bennett PB, Yazawa K, Makita N, and George AL, Jr. (1995b). Molecular mechanism for an inherited cardiac arrhythmia. *Nature* 376, 683-685.

Benson DW, Wang DW, Dyment M, Knilans TK, Fish FA, Strieper MJ, Rhodes TH, and George AL, Jr. (2003). Congenital sick sinus syndrome caused by recessive mutations in the cardiac sodium channel gene (*SCN5A*). *J Clin Invest* 112, 1019-1028.

Bers DM (2002). Cardiac excitation-contraction coupling. *Nature* 415, 198-205.

Bezzina C, Veldkamp MW, van Den Berg MP, Postma AV, Rook MB, Viersma JW, van Langen IM, Tan-Sindhunata G, Bink-Boelkens MTE, van Der Hout AH, Mannens MMAM, and Wilde AAM (1999). A single Na^+ channel mutation causing both long-QT and Brugada syndromes. *Circ Res* 85, 1206-1213.

Bezzina CR, Rook MB, Groenewegen WA, Herfst LJ, van der Wal AC, Lam J, Jongsma HJ, Wilde AAM, and Mannens MMAM (2003). Compound heterozygosity for mutations (W156X and R225W) in *SCN5A* associated with severe cardiac conduction disturbances and degenerative changes in the conduction system. *Circ Res* 92, 159-168.

Bezzina CR, Rook MB, and Wilde AAM (2001). Cardiac sodium channel and inherited arrhythmia syndromes. *Cardiovasc Res* 49, 257-271.

Bigi MA, Aslani A, and Shahrzad S (2007). Clinical predictors of atrial fibrillation in Brugada syndrome. *Europace* 9, 947-950.

Black JA, Dib-Hajj S, McNabola K, Jeste S, Rizzo MA, Kocsis JD, and Waxman SG (1996). Spinal sensory neurons express multiple sodium channel alpha-subunit mRNAs. *Brain Res Mol Brain Res* 43, 117-131.

Black JA, Renganathan M, and Waxman SG (2002). Sodium channel Na(v)1.6 is expressed along nonmyelinated axons and it contributes to conduction. *Brain Res Mol Brain Res* 105, 19-28.

Blanchet J, Pilote S, and Chahine M (2007). Acidic residues on the voltage-sensor domain determine the activation of the NaChBac sodium channel. *Biophys J* 92, 3513-3523.

Bodi I, Mikala G, Koch SE, Akhter SA, and Schwartz A (2005). The L-type calcium channel in the heart: the beat goes on. *J Clin Invest* 115, 3306-3317.

Borchert B, Lawrenz T, and Stellbrink C (2006). Long and short QT syndrome. *Herzschrittmacherther Elektrophysiol* 17, 205-210.

Brugada J, Brugada R, and Brugada P (2000a). Pharmacological and device approach to therapy of inherited cardiac diseases associated with cardiac arrhythmias and sudden death. *J Electrocardiol* 33 Suppl, 41-47.

Brugada R, Brugada J, Antzelevitch C, Kirsch GE, Potenza D, Towbin JA, and Brugada P (2000b). Sodium channel blockers identify risk for sudden death in patients with ST-segment elevation and right bundle branch block but structurally normal hearts. *Circulation* 101, 510-515.

Burashnikov A and Antzelevitch C (2006). Late-phase 3 EAD. A unique mechanism contributing to initiation of atrial fibrillation. *Pacing Clin Electrophysiol* 29, 290-295.

Burashnikov A and Antzelevitch C (1998). Acceleration-induced action potential prolongation and early afterdepolarizations. *J Cardiovasc Electrophysiol* 9, 934-948.

Burashnikov A, Di Diego JM, Zygmunt AC, Belardinelli L, and Antzelevitch C (2008). Atrial-selective sodium channel block as a strategy for suppression of atrial fibrillation. *Ann N Y Acad Sci* 1123, 105-112.

Burbidge SA, Dale TJ, Powell AJ, Whitaker WRJ, Xie XM, Romanos MA, and Clare JJ (2002). Molecular cloning, distribution and functional analysis of the $NA_{V1.6}$. voltage-gated sodium channel from human brain. *Brain Res Mol Brain Res* 103, 80-90.

Burgess DL, Kohrman DC, Galt J, Plummer NW, Jones JM, Spear B, and Meisler MH (1995). Mutation of a new sodium channel gene, *Scn8a*, in the mouse mutant 'motor endplate disease'. *Nat Genet* 10, 461-465.

Caldwell JH, Schaller KL, Lasher RS, Peles E, and Levinson SR (2000). Sodium channel Na(v)1.6 is localized at nodes of ranvier, dendrites, and synapses. *Proc Natl Acad Sci U S A* 97, 5616-5620.

Cantrell AR, Tibbs VC, Yu FH, Murphy BJ, Sharp EM, Qu Y, Catterall WA, and Scheuer T (2002). Molecular mechanism of convergent regulation of brain Na^+ channels by protein kinase C and protein kinase A anchored to AKAP-15. *Mol Cell Neurosci* 21, 63-80.

Carmeliet E and Mubagwa K (1998). Antiarrhythmic drugs and cardiac ion channels: mechanisms of action. *Prog Biophys Mol Biol* 70, 1-72.

Carmeliet E and Saikawa T (1982). Shortening of the action potential and reduction of pacemaker activity by lidocaine, quinidine, and procainamide in sheep cardiac purkinje fibers. An effect on Na or K currents? *Circ Res* 50, 257-272.

Chahine M (2009). Cardiac metabolic state and Brugada syndrome: a link revealed. *Circ Res* 105, 721-723.

Chahine M, Chen LQ, Barchi RL, Kallen RG, and Horn R (1992). Lidocaine block of human heart sodium channels expressed in *Xenopus* oocytes. *J Mol Cell Cardiol* 24, 1231-1236.

Chahine M, Deschênes I, Chen LQ, and Kallen RG (1996). Electrophysiological characteristics of cloned skeletal and cardiac muscle sodium channels expressed in tsA201 cells. *Am J Physiol* 40, H 498-H 506.

Chahine M, Ziane R, Vijayaragavan K, and Okamura Y (2005). Regulation of Na(v) channels in sensory neurons. *Trends Pharmacol Sci* 26, 496-502.

Chandra R, Starmer CF, and Grant AO (1998). Multiple effects of KPQ deletion mutation on gating of human cardiac Na^+ channels expressed in mammalian cells. *Am J Physiol* 274, H1643-H1654.

Chang CC, Acharfi S, Wu MH, Chiang FT, Wang JK, Sung TC, and Chahine M (2004). A novel SCN5A mutation manifests as a malignant form of long QT syndrome with perinatal onset of tachycardia/bradycardia. *Cardiovasc Res* 64, 268-278.

Chen LQ, Chahine M, Kallen RG, Barchi RL, and Horn R (1992). Chimeric study of sodium channels from rat skeletal and cardiac muscle. *FEBS Lett* 309, 253-257.

Chen LY, Ballew JD, Herron KJ, Rodeheffer RJ, and Olson TM (2007). A common polymorphism in SCN5A is associated with lone atrial fibrillation. *Clin Pharmacol Ther* 81, 35-41.

Chen Q, Kirsch GE, Zhang D, Brugada R, Brugada J, Brugada P, Potenza D, Moya A, Borggrefe M, Breithardt G, Ortiz-Lopez R, Wang Z, Antzelevitch C, O'Brien RE, Schulze-Bahr E, Keating MT, Towbin JA, and Wang Q (1998). Genetic basis and molecular mechanism for idiopathic ventricular fibrillation. *Nature* 392, 293-296.

Chen T, Inoue M, and Sheets MF (2005). Reduced voltage dependence of inactivation in the SCN5A sodium channel mutation delF1617. *Am J Physiol Heart Circ Physiol* 288, H2666-H2676.

Chen YH, Xu SJ, Bendahhou S, Wang XL, Wang Y, Xu WY, Jin HW, Sun H, Su XY, Zhuang QN, Yang YQ, Li YB, Liu Y, Xu HJ, Li XF, Ma N, Mou CP, Chen Z, Barhanin J, and Huang W (2003). KCNQ1 gain-of-function mutation in familial atrial fibrillation. *Science* 299, 251-254.

Chenna R, Sugawara H, Koike T, Lopez R, Gibson TJ, Higgins DG, and Thompson JD (2003). Multiple sequence alignment with the Clustal series of programs. *Nucleic Acids Res* 31, 3497-3500.

Chugh SS, Blackshear JL, Shen WK, Hammill SC, and Gersh BJ (2001). Epidemiology and natural history of atrial fibrillation: clinical implications. *J Am Coll Cardiol* 37, 371-378.

Clancy CE and Kass RS (2005). Inherited and acquired vulnerability to ventricular arrhythmias: cardiac Na+ and K+ channels. *Physiol Rev* 85, 33-47.

Clancy CE and Rudy Y (2001). Cellular consequences of HERG mutations in the long QT syndrome: precursors to sudden cardiac death. *Cardiovasc Res* 50, 301-313.

Clancy CE and Rudy Y (2002). Na^+ channel mutation that causes both Brugada and long-QT syndrome phenotypes: a simulation study of mechanism. *Circulation* 105, 1208-1213.

Clancy CE, Tateyama M, Liu H, Wehrens XH, and Kass RS (2003). Non-equilibrium gating in cardiac Na+ channels: an original mechanism of arrhythmia. *Circulation* 107, 2233-2237.

Cormier JW, Rivolta I, Tateyama M, Yang AS, and Kass RS (2002). Secondary structure of the human cardiac Na^+ channel C terminus: evidence for a role of helical structures in modulation of channel inactivation. *J Biol Chem* 277, 9233-9241.

Cox JJ, Reimann F, Nicholas AK, Thornton G, Roberts E, Springell K, Karbani G, Jafri H, Mannan J, Raashid Y, Al-Gazali L, Hamamy H, Valente EM, Gorman S, Williams R, McHale DP, Wood JN, Gribble FM, and Woods CG (2006). An *SCN9A* channelopathy causes congenital inability to experience pain. *Nature* 444, 894-898.

Craner MJ, Newcombe J, Black JA, Hartle C, Cuzner ML, and Waxman SG (2004). Molecular changes in neurons in multiple sclerosis: altered axonal expression of Nav1.2 and Nav1.6 sodium channels and Na^+/Ca^{2+} exchanger. *Proc Natl Acad Sci U S A* 101, 8168-8173.

Cronk LB, Ye B, Kaku T, Tester DJ, Vatta M, Makielski JC, and Ackerman MJ (2007). Novel mechanism for sudden infant death syndrome: persistent late sodium current secondary to mutations in caveolin-3. *Heart Rhythm* 4, 161-166.

Cummins TR, Sheets PL, and Waxman SG (2007). The roles of sodium channels in nociception: Implications for mechanisms of pain. *Pain* 131, 243-257.

Cummins TR and Waxman SG (1997). Downregulation of tetrodotoxin-resistant sodium currents and upregulation of a rapidly repriming tetrodotoxin-sensitive sodium current in small spinal sensory neurons after nerve injury. *J Neurosci* 17, 3503-3514.

Cunha SR and Mohler PJ (2006). Cardiac ankyrins: Essential components for development and maintenance of excitable membrane domains in heart. *Cardiovasc Res* 71, 22-29.

Darbar D, Kannankeril PJ, Donahue BS, Kucera G, Stubblefield T, Haines JL, George AL, Jr., and Roden DM (2008). Cardiac sodium channel (SCN5A) variants associated with atrial fibrillation. *Circulation* 117, 1927-1935.

Delpon E, Cordeiro JM, Nunez L, Thomsen PE, Guerchicoff A, Pollevick GD, Wu Y, Kanters JK, Larsen CT, Hofman-Bang J, Burashnikov E, Christiansen M, and Antzelevitch C (2008). Functional effects of KCNE3 mutation and its role in the development of Brugada syndrome. *Circ Arrhythm Electrophysiol* 1, 209-218.

Desaphy JF, De LA, Didonna MP, George AL, Jr., and Camerino CD (2004). Different flecainide sensitivity of hNav1.4 channels and myotonic mutants explained by state-dependent block. *J Physiol* 554, 321-334.

Deschênes I, Baroudi G, Berthet M, Barde I, Chalvidan T, Denjoy I, Guicheney P, and Chahine M (2000). Electrophysiological characterization of SCN5A mutations causing long QT (E1784K) and Brugada (R1512W and R1432G) syndromes. *Cardiovasc Res* 46, 55-65.

Deschênes I, Neyroud N, DiSilvestre D, Marbán E, Yue DT, and Tomaselli GF (2002). Isoform-specific modulation of voltage-gated Na^+ channels by calmodulin. *Circ Res* 90, E49-E57.

Deschênes I, Trottier E, and Chahine M (2001). Implication of the C-terminal region of the α-subunit of voltage-gated sodium channels in fast inactivation. *J Membr Biol* 183, 103-114.

Di Diego JM, Cordeiro JM, Goodrow RJ, Fish JM, Zygmunt AC, Perez GJ, Scornik FS, and Antzelevitch C (2002). Ionic and cellular basis for the predominance of the Brugada syndrome phenotype in males. *Circulation* 106, 2004-2011.

Dib-Hajj S, Black JA, Cummins TR, and Waxman SG (2002). NaN/Na_v1.9: a sodium channel with unique properties. *Trends Neurosci* 25, 253-259.

Dib-Hajj S, Black JA, Felts P, and Waxman SG (1996). Down-regulation of transcripts for Na channel α-SNS in spinal sensory neurons following axotomy. *Proc Natl Acad Sci USA* 93, 14950-14954.

Dib-Hajj SD, Rush AM, Cummins TR, Hisama FM, Novella S, Tyrrell L, Marshall L, and Waxman SG (2005). Gain-of-function mutation in Nav1.7 in familial erythromelalgia induces bursting of sensory neurons. *Brain* 128, 1847-1854.

Dietrich PS, McGivern JG, Delgado SG, Koch BD, Eglen RM, Hunter JC, and Sangameswaran L (1998). Functional analysis of a voltage-gated sodium channel and its splice variant from rat dorsal root ganglia. *J Neurochem* 70, 2262-2272.

DiFrancesco D (1985). The cardiac hyperpolarizing-activated current, if. Origins and developments. *Prog Biophys Mol Biol* 46, 163-183.

Djinovic-Carugo K, Gautel M, Ylanne J, and Young P (2002). The spectrin repeat: a structural platform for cytoskeletal protein assemblies. *FEBS Lett* 513, 119-123.

Donahue LM, Coates PW, Lee VH, Ippensen DC, Arze SE, and Poduslo SE (2000). The cardiac sodium channel mRNA is expressed in the developing and adult rat and human brain. *Brain Res* 887, 335-343.

Doyle DD, Goings G, Upshaw-Earley J, Ambler SK, Mondul A, Palfrey HC, and Page E (2000). Dystrophin associates with caveolae of rat cardiac myocytes: relationship to dystroglycan. *Circ Res* 87, 480-488.

Duan D, Fermini B, and Nattel S (1993). Potassium channel blocking properties of propafenone in rabbit atrial myocytes. *J Pharmacol Exp Ther* 264, 1113-1123.

Dudley SC, Jr., Chang N, Hall J, Lipkind G, Fozzard HA, and French RJ (2000). μ-conotoxin GIIIA interactions with the voltage-gated Na^+ channel predict a clockwise arrangement of the domains. *J Gen Physiol* 116, 679-690.

Dumaine R and Kirsch GE (1998). Mechanism of lidocaine block of late current in long Q-T mutant Na^+ channels. *Am J Physiol* 274, H477-H487.

Dumaine R, Towbin JA, Brugada P, Vatta M, Nesterenko DV, Nesterenko VV, Brugada J, Brugada R, and Antzelevitch C (1999). Ionic mechanisms responsible for the electrocardiographic phenotype of the brugada syndrome are temperature dependent. *Circ Res* 85, 803-809.

Dumaine R, Wang Q, Keating MT, Hartmann HA, Schwartz PJ, Brown AM, and Kirsch GE (1996). Multiple mechanisms of Na^+ channel-linked long-QT syndrome. *Circ Res* 78, 916-924.

Dwyer T, Ponsonby AL, Newman NM, and Gibbons LE (1991a). Prospective cohort study of prone sleeping position and sudden infant death syndrome. *Lancet* 337, 1244-1247.

Dwyer T, Ponsonby AL, Newman NM, and Gibbons LE (1991b). Prospective cohort study of prone sleeping position and sudden infant death syndrome. *Lancet* 337, 1244-1247.

Ebers GC, George AL, Jr., Barchi RL, Ting-Passador SS, Kallen RG, Lathrop GM, Beckmann JS, Hahn AF, Brown WF, Campbell RD, and Hudson AJ (1991). Paramyotonia congenita and hyperkalemic periodic paralysis are linked to the adult muscle sodium channel gene. *Ann Neurol* 30, 810-816.

Echt DS, Liebson PR, Mitchell LB, Peters RW, Obias-Manno D, Barker AH, Arensberg D, Baker A, Friedman L, and Greene HL (1991). Mortality and morbidity in patients receiving encainide, flecainide, or placebo. The Cardiac Arrhythmia Suppression Trial. *N Engl J Med* 324, 781-788.

Ellerkmann RK, Remy S, Chen J, Sochivko D, Elger CE, Urban BW, Becker A, and Beck H (2003). Molecular and functional changes in voltage-dependent Na(+) channels following pilocarpine-induced status epilepticus in rat dentate granule cells. *Neuroscience* 119, 323-333.

Ellinor PT, Nam EG, Shea MA, Milan DJ, Ruskin JN, and MacRae CA (2008). Cardiac sodium channel mutation in atrial fibrillation. *Heart Rhythm* 5, 99-105.

Fabritz L, Kirchhof P, Franz MRMR, Nuyens D, Rossenbacker T, Ottenhof A, Haverkamp W, Breithardt G, Carmeliet E, and Carmeliet P (2003). Effect of pacing and mexiletine on dispersion of repolarisation and arrhythmias in ΔKPQ SCN5A (long QT3) mice. *Cardiovasc Res* 57, 1085-1093.

Fahmi AI, Patel M, Stevens EB, Fowden AL, John JE, III, Lee K, Pinnock R, Morgan K, Jackson AP, and Vandenberg JI (2001). The sodium channel β-subunit SCN3b modulates the kinetics of SCN5a and is expressed heterogeneously in sheep heart. *J Physiol* 537, 693-700.

Fan Z, George AL, Jr., Kyle JW, and Makielski JC (1996). Two human paramyotonia congenita mutations have opposite effects on lidocaine block of Na^+ channels expressed in a mammalian cell line. *J Physiol* 496, 275-286.

Fang X, Djouhri L, Black JA, Dib-Hajj SD, Waxman SG, and Lawson SN (2002). The presence and role of the tetrodotoxin-resistant sodium channel $Na_v1.9$ (NaN) in nociceptive primary afferent neurons. *J Neurosci* 22, 7425-7433.

Favre I, Moczydlowski E, and Schild L (1996). On the structural basis for ionic selectivity among Na^+, K^+, and Ca^{2+} in the voltage-gated sodium channel. *Biophys J* 71, 3110-3125.

Fedida D, Maruoka ND, and Lin S (1999). Modulation of slow inactivation in human cardiac Kv1.5 channels by extra- and intracellular permeant cations. *J Physiol* 515, 315-329.

Feron O, Belhassen L, Kobzik L, Smith TW, Kelly RA, and Michel T (1996). Endothelial nitric oxide synthase targeting to caveolae. Specific interactions with caveolin isoforms in cardiac myocytes and endothelial cells. *J Biol Chem* 271, 22810-22814.

Fontaine B, Khurana TS, Hoffman EP, Bruns GA, Haines JL, Trofatter JA, Hanson MP, Rich J, McFarlane H, McKenna Yasek D, Romano D, Gusella JF, and Brown RH, Jr. (1990). Hyperkalemic periodic paralysis and the adult muscle sodium channel α-subunit gene. *Science* 250, 1000-1002.

Fredj S, Sampson KJ, Liu H, and Kass RS (2006). Molecular basis of ranolazine block of LQT-3 mutant sodium channels: evidence for site of action. *Br J Pharmacol* 148, 16-24.

Garg A, Finneran W, and Feld GK (1998). Familial sudden cardiac death associated with a terminal QRS abnormality on surface 12-lead electrocardiogram in the index case. *J Cardiovasc Electrophysiol* 9, 642-647.

Gasparini M, Priori SG, Mantica M, Napolitano C, Galimberti P, Ceriotti C, and Simonini S (2003). Flecainide test in Brugada syndrome: a reproducible but risky tool. *Pacing Clin Electrophysiol* 26, 338-341.

Ge J, Sun A, Paajanen V, Wang S, Su C, Yang Z, Li Y, Wang S, Jia J, Wang K, Zou Y, Gao L, Wang K, and Fan Z (2008). Molecular and clinical characterization of a novel SCN5A mutation associated with atrioventricular block and dilated cardiomyopathy. *Circ Arrhythm Electrophysiol* 1, 83-92.

Gellens ME, George AL, Jr., Chen LQ, Chahine M, Horn R, Barchi RL, and Kallen RG (1992). Primary structure and functional expression of the human cardiac tetrodotoxin-insensitive voltage-dependent sodium channel. *Proc Natl Acad Sci USA* 89, 554-558.

George AL, Jr. (2005). Inherited disorders of voltage-gated sodium channels. *J Clin Invest* 115, 1990-1999.

George AL, Jr., Knittle TJ, and Tamkun MM (1992). Molecular cloning of an atypical voltage-gated sodium channel expressed in human heart and uterus: evidence for a distinct gene family. *Proc Natl Acad Sci USA* 89, 4893-4897.

Gima K and Rudy Y (2002). Ionic current basis of electrocardiographic waveforms: a model study. *Circ Res* 90, 889-896.

Glaaser IW and Clancy CE (2006). Cardiac Na+ channels as therapeutic targets for antiarrhythmic agents. *Handb Exp Pharmacol* 99-121.

Goldberg YP, MacFarlane J, MacDonald ML, Thompson J, Dube MP, Mattice M, Fraser R, Young C, Hossain S, Pape T, Payne B, Radomski C, Donaldson G, Ives E, Cox J, Younghusband HB, Green R, Duff A, Boltshauser E, Grinspan GA, Dimon JH, Sibley BG, Andria G, Toscano E, Kerdraon J, Bowsher D, Pimstone SN, Samuels ME, Sherrington R, and Hayden MR (2007). Loss-of-function mutations in the Nav1.7 gene underlie congenital indifference to pain in multiple human populations. *Clin Genet* 71, 311-319.

Goldgran-Toledano D, Sideris G, and Kevorkian JP (2002). Overdose of cyclic antidepressants and the Brugada syndrome. *N Engl J Med* 346, 1591-1592.

Goldin AL (2001). Resurgence of sodium channel research. *Annu Rev Physiol* 63, 871-894.

Goldin AL, Barchi RL, Caldwell JH, Hofmann F, Howe JR, Hunter JC, Kallen RG, Mandel G, Meisler MH, Berwald-Netter Y, Noda M, Tamkun MM, Waxman SG, Wood JN, and Catterall WA (2000). Nomenclature of voltage-gated sodium channels. *Neuron* 28, 365-368.

Gollob MH (2003). Glycogen storage disease as a unifying mechanism of disease in the PRKAG2 cardiac syndrome. *Biochem Soc Trans* 31, 228-231.

Gollob MH, Jones DL, Krahn AD, Danis L, Gong XQ, Shao Q, Liu X, Veinot JP, Tang AS, Stewart AF, Tesson F, Klein GJ, Yee R, Skanes AC, Guiraudon GM, Ebihara L, and Bai D (2006). Somatic mutations in the connexin 40 gene (GJA5) in atrial fibrillation. *N Engl J Med* 354, 2677-2688.

Grant AO (2005). Electrophysiological basis and genetics of Brugada syndrome. *J Cardiovasc Electrophysiol* 16, S3-S7.

Grant AO, Carboni MP, Neplioueva V, Starmer CF, Memmi M, Napolitano C, and Priori S (2002). Long QT syndrome, Brugada syndrome, and conduction system disease are linked to a single sodium channel mutation. *J Clin Invest* 110, 1201-1209.

Groenewegen WA, Bezzina CR, van Tintelen JP, Hoorntje TM, Mannens MMAM, Wilde AAM, Jongsma HJ, and Rook MB (2003a). A novel LQT3 mutation implicates the human cardiac sodium channel domain IVS6 in inactivation kinetics. *Cardiovasc Res* 57, 1072-1078.

Groenewegen WA, Firouzi M, Bezzina CR, Vliex S, van Langen IM, Sandkuijl L, Smits JPP, Hulsbeek M, Rook MB, Jongsma HJ, and Wilde AAM (2003b). A cardiac sodium channel mutation cosegregates with a rare connexin40 genotype in familial atrial standstill. *Circ Res* 92, 14-22.

Gu XQ, Yao H, and Haddad GG (2001). Increased neuronal excitability and seizures in the Na(+)/H(+) exchanger null mutant mouse. *Am J Physiol Cell Physiol* 281, C496-C503.

Hains BC, Klein JP, Saab CY, Craner MJ, Black JA, and Waxman SG (2003). Upregulation of sodium channel Nav1.3 and functional involvement in neuronal hyperexcitability associated with central neuropathic pain after spinal cord injury. *J Neurosci* 23, 8881-8892.

Haissaguerre M, Jais P, Shah DC, Takahashi A, Hocini M, Quiniou G, Garrigue S, Le MA, Le MP, and Clementy J (1998). Spontaneous initiation of atrial fibrillation by ectopic beats originating in the pulmonary veins. *N Engl J Med* 339, 659-666.

Hale SL, Shryock JC, Belardinelli L, Sweeney M, and Kloner RA (2008). Late sodium current inhibition as a new cardioprotective approach. *J Mol Cell Cardiol* 44, 954-967.

Hallaq H, Yang Z, Viswanathan PC, Fukuda K, Shen W, Wang DW, Wells KS, Zhou J, Yi J, and Murray KT (2006). Quantitation of protein kinase A-mediated trafficking of cardiac sodium channels in living cells. *Cardiovasc Res* 72, 250-261.

Hartmann HA, Colom LV, Sutherland ML, and Noebels JL (1999). Selective localization of cardiac SCN5A sodium channels in limbic regions of rat brain. *Nat Neurosci* 2, 593-595.

Haufe V, Camacho JA, Dumaine R, Gunther B, Bollensdorff C, von Banchet GS, Benndorf K, and Zimmer T (2005a). Expression pattern of neuronal and skeletal muscle voltage-gated Na+ channels in the developing mouse heart. *J Physiol* 564, 683-696.

Haufe V, Cordeiro JM, Zimmer T, Wu YS, Schiccitano S, Benndorf K, and Dumaine R (2005b). Contribution of neuronal sodium channels to the cardiac fast sodium current INa is greater in dog heart Purkinje fibers than in ventricles. *Cardiovasc Res* 65, 117-127.

Haworth RS, Cuello F, Herron TJ, Franzen G, Kentish JC, Gautel M, and Avkiran M (2004). Protein kinase D is a novel mediator of cardiac troponin I phosphorylation and regulates myofilament function. *Circ Res* 95, 1091-1099.

Heinemann SH, Terlau H, and Imoto K (1992a). Molecular basis for pharmacological differences between brain and cardiac sodium channels. *Pflügers Arch* 422, 90-92.

Heinemann SH, Terlau H, Stühmer W, Imoto K, and Numa S (1992b). Calcium channel characteristics conferred on the sodium channel by single mutations. *Nature* 356, 441-443.

Herbert E and Chahine M (2006). Clinical aspects and physiopathology of Brugada syndrome: review of current concepts. *Can J Physiol Pharmacol* 84, 795-802.

Hermida JS, Denjoy I, Clerc J, Extramiana F, Jarry G, Milliez P, Guicheney P, Di FS, Rey JL, Cauchemez B, and Leenhardt A (2004). Hydroquinidine therapy in Brugada syndrome. *J Am Coll Cardiol* 43, 1853-1860.

Herzog RI, Cummins TR, and Waxman SG (2001). Persistent TTX-resistant Na^+ current affects resting potential and response to depolarization in simulated spinal sensory neurons. *J Neurophysiol* 86, 1351-1364.

Hicke L and Dunn R (2003). Regulation of membrane protein transport by ubiquitin and ubiquitin-binding proteins. *Annu Rev Cell Dev Biol* 19, 141-172.

Hilber K, Sandtner W, Kudlacek O, Schreiner B, Glaaser I, Schutz W, Fozzard HA, Dudley SC, and Todt H (2002). Interaction between fast and ultra-slow inactivation in the voltage-gated sodium channel. Does the inactivation gate stabilize the channel structure? *J Biol Chem* 277, 37105-37115.

Hille B (1977). Local anesthetics: hydrophilic and hydrophobic pathways for the drug-receptor reaction. *J Gen Physiol* 69, 497-515.

Hodgkin AL and Huxley AF (1952). A quantitative description of membrane current and its application to conduction and excitation in nerve. *J Physiol* 117, 500-544.

Hondeghem LM and Katzung BG (1977). Time- and voltage-dependent interactions of antiarrhythmic drugs with cardiac sodium channels. *Biochim Biophys Acta* 472, 373-398.

Horn R (2007). Physiology: legacy of leaky channels. *Nature* 446, 32-34.

Horn R, Patlak J, and Stevens CF (1981). Sodium channels need not open before they inactivate. *Nature* 291, 426-427.

Hoshi T, Zagotta WN, and Aldrich RW (1990). Biophysical and molecular mechanisms of Shaker potassium channel inactivation . *Science* 250, 533-538.

Hoshi T, Zagotta WN, and Aldrich RW (1991). Two types of inactivation in *Shaker* K^+ channels: effects of alterations in the carboxy-terminal region. *Neuron* 7, 547-556.

Hu D, Barajas-Martinez H, Burashnikov E, Springer M, Wu Y, Varro A, Pfeiffer R, Koopmann TT, Cordeiro JM, Guerchicoff A, Pollevick GD, and Antzelevitch C (2009). A Mutation in the {beta}3 Subunit of the Cardiac Sodium Channel Associated With Brugada ECG Phenotype. *Circulation: Cardiovascular Genetics* 2, 270-278.

Huang H, Millat G, Rodriguez-Lafrasse C, Rousson R, Kugener B, Chevalier P, and Chahine M (2009). Biophysical characterization of a new SCN5A mutation S1333Y in a SIDS infant linked to long QT syndrome. *FEBS Lett* 583, 890-896.

Huang H, Zhao J, Barrane FZ, Champagne J, and Chahine M (2006). Nav1.5/R1193Q polymorphism is associated with both long QT and Brugada syndromes. *Can J Cardiol* 22, 309-313.

Hunt CE and Hauck FR (2006). Sudden infant death syndrome. *CMAJ* 174, 1861-1869.

Ikeda N, Singh BN, Davis LD, and Hauswirth O (1985). Effects of flecainide on the electrophysiologic properties of isolated canine and rabbit myocardial fibers. *J Am Coll Cardiol* 5, 303-310.

Imaizumi Y and Giles WR (1987). Quinidine-induced inhibition of transient outward current in cardiac muscle. *Am J Physiol* 253, H704-H708.

Isom LL (2001). Sodium channel beta subunits: anything but auxiliary. *Neuroscientist* 7, 42-54.

Isom LL, De Jongh KS, Patton DE, Reber BF, Offord J, Charbonneau H, Walsh K, Goldin AL, and Catterall WA (1992). Primary structure and functional expression of the β_1 subunit of the rat brain sodium channel. *Science* 256, 839-842.

Isom LL, Ragsdale DS, De Jongh KS, Westenbroek RE, Reber BFX, Scheuer T, and Catterall WA (1995). Structure and function of the β2 subunit of brain sodium channels, a transmembrane glycoprotein with a CAM motif. *Cell* 83, 433-442.

Itoh H, Tsuji K, Sakaguchi T, Nagaoka I, Oka Y, Nakazawa Y, Yao T, Jo H, Ashihara T, Ito M, Horie M, and Imoto K (2007). A paradoxical effect of lidocaine for the N406S mutation of SCN5A associated with Brugada syndrome. *Int J Cardiol* 121, 239-248.

January CT and Riddle JM (1989). Early afterdepolarizations: mechanism of induction and block. A role for L-type Ca2+ current. *Circ Res* 64, 977-990.

Jervell A and Lange-Nielsen F (1957). Congenital deaf-mutism, functional heart disease with prolongation of the Q-T interval and sudden death. *Am Heart J* 54, 59-68.

Jespersen T, Gavillet B, van Bemmelen MX, Cordonier S, Thomas MA, Staub O, and Abriel H (2006). Cardiac sodium channel Nav1.5 interacts with and is regulated by the protein tyrosine phosphatase PTPH1. *Biochem Biophys Res Commun* 348, 1455-1462.

Jiang C, Atkinson D, Towbin JA, Splawski I, Lehmann MH, Li H, Timothy K, Taggart RT, Schwartz PJ, Vincent GM, Moss AJ, and Keating MT (1994). Two long QT syndrome loci map to chromosomes 3 and 7 with evidence for further heterogeneity. *Nat Genet* 8, 141-147.

Jiang Y, Lee A, Chen J, Cadene M, Chait BT, and MacKinnon R (2002). Crystal structure and mechanism of a calcium-gated potassium channel. *Nature* 417, 515-522.

Jiang Y, Ruta V, Chen J, Lee A, and MacKinnon R (2003). The principle of gating charge movement in a voltage-dependent K^+ channel. *Nature* 423, 42-48.

John VH, Main MJ, Powell AJ, Gladwell ZM, Hick C, Sidhu HS, Clare JJ, Tate S, and Trezise DJ (2004). Heterologous expression and functional analysis of rat NaV1.8 (SNS) voltage-gated sodium channels in the dorsal root ganglion neuroblastoma cell line ND7-23. *Neuropharmacol* 46, 425-438.

Johnson JN, Tester DJ, Perry J, Salisbury BA, Reed CR, and Ackerman MJ (2008). Prevalence of early-onset atrial fibrillation in congenital long QT syndrome. *Heart Rhythm* 5, 704-709.

Ju YK, Saint DA, and Gage PW (1996). Hypoxia increases persistent sodium current in rat ventricular myocytes. *J Physiol* 497, 337-347.

Kallen RG, Sheng ZH, Yang J, Chen LQ, Rogart RB, and Barchi RL (1990). Primary structure and expression of a sodium channel characteristic of denervated and immature rat skeletal muscle. *Neuron* 4, 233-242.

Kambouris NG, Nuss HB, Johns DC, Marbán E, Tomaselli GF, and Balser JR (2000). A revised view of cardiac sodium channel "blockade" in the long-QT syndrome. *J Clin Invest* 105, 1133-1140.

Kambouris NG, Nuss HB, Johns DC, Tomaselli GF, Marban E, and Balser JR (1998). Phenotypic characterization of a novel long-QT syndrome mutation (R1623Q) in the cardiac sodium channel. *Circulation* 97, 640-644.

Kazen-Gillespie KA, Ragsdale DS, D'Andrea MR, Mattei LN, Rogers KE, and Isom LL (2000). Cloning, localization, and functional expression of sodium channel β1A subunits. *J Biol Chem* 275, 1079-1088.

Kearney JA, Plummer NW, Smith MR, Kapur J, Cummins TR, Waxman SG, Goldin AL, and Meisler MH (2001). A gain-of-function mutation in the sodium channel gene Scn2a results in seizures and behavioral abnormalities. *Neuroscience* 102, 307-317.

Keating M, Atkinson D, Dunn C, Timothy K, Vincent GM, and Leppert M (1991). Linkage of a cardiac arrhythmia, the long QT syndrome, and the Harvey *ras*-1 gene . *Science* 252, 704-706.

Keating MT and Sanguinetti MC (2001). Molecular and cellular mechanisms of cardiac arrhythmias. *Cell* 104, 569-580.

Keeling PJ, Gang Y, Smith G, Seo H, Bent SE, Murday V, Caforio AL, and McKenna WJ (1995). Familial dilated cardiomyopathy in the United Kingdom. *Br Heart J* 73, 417-421.

Keller DI, Acharfi S, Delacrétaz E, Benammar N, Rotter M, Pfammatter JP, Fressart V, Guicheney P, and Chahine M (2003). A novel mutation in *SCN5A*, delQKP 1507-1509, causing long QT syndrome: Role of Q1507 residue in sodium channel inactivation. *J Mol Cell Cardiol* 35, 1513-1521.

Keller DI, Barrane FZ, Gouas L, Martin J, Pilote S, Suarez V, Osswald S, Brink M, Guicheney P, Schwick N, and Chahine M (2005b). A novel nonsense mutation in the SCN5A gene leads to Brugada syndrome and a silent gene mutation carrier state. *Can J Cardiol* 21, 925-931.

Keller DI, Barrane FZ, Gouas L, Martin J, Pilote S, Suarez V, Osswald S, Brink M, Guicheney P, Schwick N, and Chahine M (2005a). A novel nonsense mutation in the SCN5A gene leads to Brugada syndrome and a silent gene mutation carrier state. *Can J Cardiol* 21, 925-931.

Keller DI, Huang H, Zhao J, Frank R, Suarez V, Delacretaz E, Brink M, Osswald S, Schwick N, and Chahine M (2006). A novel SCN5A mutation, F1344S, identified in a patient with Brugada syndrome and fever-induced ventricular fibrillation. *Cardiovasc Res* 70, 521-529.

Ketelaars SO, Gorter JA, van Vliet EA, Lopes da Silva FH, and Wadman WJ (2001). Sodium currents in isolated rat CA1 pyramidal and dentate granule neurones in the post-status epilepticus model of epilepsy. *Neuroscience* 105, 109-120.

Kim J, Ghosh S, Liu H, Tateyama M, Kass RS, and Pitt GS (2004). Calmodulin mediates Ca^{2+} sensitivity of sodium channels. *J Biol Chem* 279, 45004-45012.

Kimura M, Kobayashi T, Owada S, Ashikaga K, Higuma T, Sasaki S, Iwasa A, Motomura S, and Okumura K (2004). Mechanism of ST elevation and ventricular arrhythmias in an experimental Brugada syndrome model. *Circulation* 109, 125-131.

Klugbauer N, Lacinova L, Flockerzi V, and Hofmann F (1995). Structure and functional expression of a new member of the tetrodotoxin- sensitive voltage-activated sodium channel family from human neuroendocrine cells. *EMBO J* 14, 1084-1090.

Knoll R, Hoshijima M, Hoffman HM, Person V, Lorenzen-Schmidt I, Bang ML, Hayashi T, Shiga N, Yasukawa H, Schaper W, McKenna W, Yokoyama M, Schork NJ, Omens JH, McCulloch AD, Kimura A, Gregorio CC, Poller W, Schaper J, Schultheiss HP, and Chien KR (2002). The cardiac mechanical stretch sensor machinery involves a Z disc complex that is defective in a subset of human dilated cardiomyopathy. *Cell* 111, 943-955.

Kodama I, Nikmaram MR, Boyett MR, Suzuki R, Honjo H, and Owen JM (1997). Regional differences in the role of the Ca2+ and Na+ currents in pacemaker activity in the sinoatrial node. *Am J Physiol* 272, H2793-H2806.

Kohling R (2002). Voltage-gated sodium channels in epilepsy. *Epilepsia* 43, 1278-1295.

Krahn AD, Manfreda J, Tate RB, Mathewson FA, and Cuddy TE (1995). The natural history of atrial fibrillation: incidence, risk factors, and prognosis in the Manitoba Follow-Up Study. *Am J Med* 98, 476-484.

Krous HF, Beckwith JB, Byard RW, Rognum TO, Bajanowski T, Corey T, Cutz E, Hanzlick R, Keens TG, and Mitchell EA (2004). Sudden infant death syndrome and unclassified sudden infant deaths: a definitional and diagnostic approach. *Pediatrics* 114, 234-238.

Kuo CC, Chen RS, Lu L, and Chen RC (1997). Carbamazepine inhibition of neuronal Na+ currents: quantitative distinction from phenytoin and possible therapeutic implications. *Mol Pharmacol* 51, 1077-1083.

Lei M, Goddard C, Liu J, Leoni AL, Royer A, Fung SS, Xiao G, Ma A, Zhang H, Charpentier F, Vandenberg JI, Colledge WH, Grace AA, and Huang CL (2005). Sinus node dysfunction following targeted disruption of the murine cardiac sodium channel gene Scn5a. *J Physiol* 567, 387-400.

Lei M, Zhang H, Grace AA, and Huang CL (2007). SCN5A and sinoatrial node pacemaker function. *Cardiovasc Res* 74, 356-365.

Lesh MD, Pring M, and Spear JF (1989). Cellular uncoupling can unmask dispersion of action potential duration in ventricular myocardium. A computer modeling study. *Circ Res* 65, 1426-1440.

Li HL, Galue A, Meadows L, and Ragsdale DS (1999). A molecular basis for the different local anesthetic affinities of resting versus open and inactivated states of the sodium channel. *Mol Pharmacol* 55, 134-141.

Li Q, Huang H, Liu G, Lam K, Rutberg J, Green MS, Birnie DH, Lemery R, Chahine M, and Gollob MH (2009). Gain-of-function mutation of Nav1.5 in atrial fibrillation enhances cellular excitability and lowers the threshold for action potential firing. *Biochem Biophys Res Commun* 380, 132-137.

Light PE, Wallace CHR, and Dyck JRB (2003). Constitutively active adenosine monophosphate-activated protein kinase regulates voltage-gated sodium channels in ventricular myocytes. *Circulation* 107, 1962-1965.

Lin MT, Wu MH, Chang CC, Chiu SN, Theriault O, Huang H, Christe G, Ficker E, and Chahine M (2008). In utero onset of long QT syndrome with atrioventricular block and spontaneous or lidocaine-induced ventricular tachycardia: compound effects of hERG pore region mutation and SCN5A N-terminus variant. *Heart Rhythm* 5, 1567-1574.

Lipka LJ, Siegelbaum SA, Robinson RB, and Berman MF (1996). An analogue of cAMP mimics developmental change in neonatal rat ventricular myocyte sodium current kinetics. *Am J Physiol* 270, H194-H199.

Lipkind GM and Fozzard HA (1994). A structural model of the tetrodotoxin and saxitoxin binding site of the Na^+ channel. *Biophys J* 66, 1-13.

Liu CJ, Dib-Hajj SD, Renganathan M, Cummins TR, and Waxman SG (2003a). Modulation of the cardiac sodium channel Nav1.5 by fibroblast growth factor homologous factor 1B. *J Biol Chem* 278, 1029-1036.

Liu C, Dib-Hajj SD, and Waxman SG (2001). Fibroblast growth factor homologous factor 1B binds to the C terminus of the tetrodotoxin-resistant sodium channel rNav1.9a (NaN). *J Biol Chem* 276, 18925-18933.

Liu G, Yarov-Yarovoy V, Nobbs M, Clare JJ, Scheuer T, and Catterall WA (2003b). Differential interactions of lamotrigine and related drugs with transmembrane segment IVS6 of voltage-gated sodium channels. *Neuropharmacol* 44, 413-422.

Liu H, Atkins J, and Kass RS (2003c). Common molecular determinants of flecainide and lidocaine block of heart Na^+ channels: evidence from experiments with neutral and quaternary flecainide analogues. *J Gen Physiol* 121, 199-214.

Liu M, Sanyal S, Gao G, Gurung IS, Zhu X, Gaconnet G, Kerchner LJ, Shang LL, Huang CL, Grace A, London B, and Dudley SC, Jr. (2009). Cardiac Na+ current regulation by pyridine nucleotides. *Circ Res* 105, 737-745.

Liu Y, Jurman ME, and Yellen G (1996). Dynamic rearrangement of the outer mouth of a K^+ channel during gating. *Neuron* 16, 859-867.

Locke GR, III, Ackerman MJ, Zinsmeister AR, Thapa P, and Farrugia G (2006). Gastrointestinal symptoms in families of patients with an SCN5A-encoded cardiac channelopathy: evidence of an intestinal channelopathy. *Am J Gastroenterol* 101, 1299-1304.

London B, Michalec M, Mehdi H, Zhu X, Kerchner L, Sanyal S, Viswanathan PC, Pfahnl AE, Shang LL, Madhusudanan M, Baty CJ, Lagana S, Aleong R, Gutmann R, Ackerman MJ, McNamara DM, Weiss R, and Dudley SC, Jr. (2007). Mutation in glycerol-3-phosphate dehydrogenase 1 like gene (GPD1-L) decreases cardiac Na+ current and causes inherited arrhythmias. *Circulation* 116, 2260-2268.

Lopez-Barneo J, Hoshi T, Heinemann SH, and Aldrich RW (1993). Effects of external cations and mutations in the pore region on C-type inactivation of *Shaker* potassium channels. *Receptors Channels* 1, 61-71.

Lossin C, Wang DW, Rhodes TH, Vanoye CG, and George AL, Jr. (2002). Molecular basis of an inherited epilepsy. *Neuron* 34, 877-884.

Lupoglazoff JM, Cheav T, Baroudi G, Berthet M, Denjoy I, Cauchemez B, Extramiana F, Chahine M, and Guicheney P (2001). Homozygous *SCN5A* mutation in long-QT syndrome with functional two-to-one atrioventricular block. *Circ Res* 89, E16-E21.

Maguy A, Hebert TE, and Nattel S (2006). Involvement of lipid rafts and caveolae in cardiac ion channel function. *Cardiovasc Res* 69, 798-807.

Maier LS (2005). CaMKIIdelta overexpression in hypertrophy and heart failure: cellular consequences for excitation-contraction coupling. *Braz J Med Biol Res* 38, 1293-1302.

Maier SKG, Westenbroek RE, McCormick KA, Curtis R, Scheuer T, and Catterall WA (2004). Distinct subcellular localization of different sodium channel α and β subunits in single ventricular myocytes from mouse heart. *Circulation* 109, 1421-1427.

Maier SKG, Westenbroek RE, Schenkman KA, Feigl EO, Scheuer T, and Catterall WA (2002). An unexpected role for brain-type sodium channels in coupling of cell surface depolarization to contraction in the heart. *Proc Natl Acad Sci USA* 99, 4073-4078.

Makielski JC (2006). SIDS: genetic and environmental influences may cause arrhythmia in this silent killer. *J Clin Invest* 116, 297-299.

Makielski JC, Ye B, Valdivia CR, Pagel MD, Pu J, Tester DJ, and Ackerman MJ (2003). A ubiquitous splice variant and a common polymorphism affect heterologous expression of recombinant human SCN5A heart sodium channels. *Circ Res* 93, 821-828.

Makita N, Behr E, Shimizu W, Horie M, Sunami A, Crotti L, Schulze-Bahr E, Fukuhara S, Mochizuki N, Makiyama T, Itoh H, Christiansen M, McKeown P, Miyamoto K, Kamakura S, Tsutsui H, Schwartz PJ, George AL, Jr., and Roden DM (2008). The E1784K mutation in SCN5A is associated with mixed clinical phenotype of type 3 long QT syndrome. *J Clin Invest* 118, 2219-2229.

Makita N, Bennett PB, and George AL, Jr. (1996). Molecular determinants of β_1 subunit-induced gating modulation in voltage-dependent Na^+ channels. *J Neurosci* 16, 7117-7127.

Makita N, Sasaki K, Groenewegen WA, Yokota T, Yokoshiki H, Murakami T, and Tsutsui H (2005). Congenital atrial standstill associated with coinheritance of a novel SCN5A mutation and connexin 40 polymorphisms. *Heart Rhythm* 2, 1128-1134.

Makiyama T, Akao M, Shizuta S, Doi T, Nishiyama K, Oka Y, Ohno S, Nishio Y, Tsuji K, Itoh H, Kimura T, Kita T, and Horie M (2008). A novel SCN5A gain-of-function mutation M1875T associated with familial atrial fibrillation. *J Am Coll Cardiol* 52, 1326-1334.

Makiyama T, Akao M, Tsuji K, Doi T, Ohno S, Takenaka K, Kobori A, Ninomiya T, Yoshida H, Takano M, Makita N, Yanagisawa F, Higashi Y, Takeyama Y, Kita T, and Horie M (2005). High risk for bradyarrhythmic complications in patients with Brugada syndrome caused by SCN5A gene mutations. *J Am Coll Cardiol* 46, 2100-2106.

Malhotra JD, Chen C, Rivolta I, Abriel H, Malhotra R, Mattei LN, Brosius FC, Kass RS, and Isom LL (2001). Characterization of sodium channel α- and β-Subunits in rat and mouse cardiac myocytes. *Circulation* 103, 1303-1310.

Malo MS, Srivastava K, Andresen JM, Chen XN, Korenberg JR, and Ingram VM (1994). Targeted gene walking by low stringency polymerase chain reaction: assignment of a putative human brain sodium channel gene (*SCN3A*) to chromosome 2q24-31. *Proc Natl Acad Sci U S A* 91, 2975-2979.

Maltsev VA and Lakatta EG (2007). Normal heart rhythm is initiated and regulated by an intracellular calcium clock within pacemaker cells. *Heart Lung Circ* 16, 335-348.

Mangoni ME and Nargeot J (2008). Genesis and regulation of the heart automaticity. *Physiol Rev* 88, 919-982.

Margolskee RF, McHendry-Rinde B, and Horn R (1993). Panning transfected cells for electrophysiological studies. *Biotechniques* 15, 906-911.

Matsuda JJ, Lee H, and Shibata EF (1992). Enhancement of rabbit cardiac sodium channels by beta-adrenergic stimulation. *Circ Res* 70, 199-207.

Matsuo K, Akahoshi M, Nakashima E, Suyama A, Seto S, Hayano M, and Yano K (2001). The prevalence, incidence and prognostic value of the Brugada-type electrocardiogram: a population-based study of four decades. *J Am Coll Cardiol* 38, 765-770.

Matsuo K, Shimizu W, Kurita T, Inagaki M, Aihara N, and Kamakura S (1998). Dynamic changes of 12-lead electrocardiograms in a patient with Brugada syndrome. *J Cardiovasc Electrophysiol* 9, 508-512.

Matsuura H, Ehara T, and Imoto Y (1987). An analysis of the delayed outward current in single ventricular cells of the guinea-pig. *Pflugers Arch* 410, 596-603.

Mayans O, van d, V, Wilm M, Mues A, Young P, Furst DO, Wilmanns M, and Gautel M (1998). Structural basis for activation of the titin kinase domain during myofibrillogenesis. *Nature* 395, 863-869.

Mazzone A, Strege PR, Tester DJ, Bernard CE, Faulkner G, De GR, Makielski JC, Stanghellini V, Gibbons SJ, Ackerman MJ, and Farrugia G (2008). A mutation in telethonin alters Nav1.5 function. *J Biol Chem* 283, 16537-16544.

McPhee JC, Ragsdale DS, Scheuer T, and Catterall WA (1994). A mutation in segment IVS6 disrupts fast inactivation of sodium channels. *Proc Natl Acad Sci USA* 91, 12346-12350.

McPhee JC, Ragsdale DS, Scheuer T, and Catterall WA (1995). A critical role for transmembrane segment IVS6 of the sodium channel alpha subunit in fast inactivation. *J Biol Chem* 270, 12025-12034.

Meadows LS and Isom LL (2005). Sodium channels as macromolecular complexes: implications for inherited arrhythmia syndromes. *Cardiovasc Res* 67, 448-458.

Medeiros-Domingo A, Kaku T, Tester DJ, Iturralde-Torres P, Itty A, Ye B, Valdivia C, Ueda K, Canizales-Quinteros S, Tusie-Luna MT, Makielski JC, and Ackerman MJ (2007). SCN4B-encoded sodium channel beta4 subunit in congenital long-QT syndrome. *Circulation* 116, 134-142.

Meisler MH and Kearney JA (2005). Sodium channel mutations in epilepsy and other neurological disorders. *J Clin Invest* 115, 2010-2017.

Meregalli PG, Wilde AA, and Tan HL (2005). Pathophysiological mechanisms of Brugada syndrome: depolarization disorder, repolarization disorder, or more? *Cardiovasc Res* 67, 367-378.

Michels VV, Moll PP, Miller FA, Tajik AJ, Chu JS, Driscoll DJ, Burnett JC, Rodeheffer RJ, Chesebro JH, and Tazelaar HD (1992). The frequency of familial dilated cardiomyopathy in a series of patients with idiopathic dilated cardiomyopathy. *N Engl J Med* 326, 77-82.

Millat G, Chevalier P, Restier-Miron L., Da Costa A, Bouvagnet P, Kugener B, Fayol L, Gonzàlez Armengod C, Oddou B, Chanavat V, Froidefond E, Perraudin R, Rousson R, and Rodriguez-Lafrasse C (2006). Spectrum of pathogenic mutations and associated polymorphisms in a cohort of 44 unrelated patients with long QT syndrome. *Clin Genet* 70, 214-227.

Miller JR, Patel MK, John JE, Mounsey JP, and Moorman JR (2000). Contributions of charged residues in a cytoplasmic linking region to Na channel gating. *Biochim Biophys Acta* 1509, 275-291.

Mitrovic N, George AL, Jr., Heine R, Wagner S, pika U, Hartlaub U, Zhou M, Lerche H, Fahlke C, and Lehmann-Horn F (1994). K^+-aggravated myotonia: destabilization of the inactivated state of the human muscle Na^+ channel by the V1589M mutation. *J Physiol* 478, 395-402.

Miyazaki T, Mitamura H, Miyoshi S, Soejima K, Aizawa Y, and Ogawa S (1996). Autonomic and antiarrhythmic drug modulation of ST segment elevation in patients with Brugada syndrome. *J Am Coll Cardiol* 27, 1061-1070.

Mizumaki K, Fujiki A, Tsuneda T, Sakabe M, Nishida K, Sugao M, and Inoue H (2004). Vagal activity modulates spontaneous augmentation of ST elevation in the daily life of patients with Brugada syndrome. *J Cardiovasc Electrophysiol* 15, 667-673.

Mohler PJ, Le SS, Denjoy I, Lowe JS, Guicheney P, Caron L, Driskell IM, Schott JJ, Norris K, Leenhardt A, Kim RB, Escande D, and Roden DM (2007). Defining the cellular phenotype of "ankyrin-B syndrome" variants: human ANK2 variants associated with clinical phenotypes display a spectrum of activities in cardiomyocytes. *Circulation* 115, 432-441.

Mohler PJ, Rivolta I, Napolitano C, Lemaillet G, Lambert S, Priori SG, and Bennett V (2004a). Nav1.5 E1053K mutation causing Brugada syndrome blocks binding to ankyrin-G and expression of Nav1.5 on the surface of cardiomyocytes. *Proc Natl Acad Sci U S A* 101, 17533-17538.

Mohler PJ, Schott JJ, Gramolini AO, Dilly KW, Guatimosim S, DuBell WH, Song LS, Haurogne K, Kyndt F, Ali ME, Rogers TB, Lederer WJ, Escande D, Marec HL, and Bennett V (2003). Ankyrin-B mutation causes type 4 long-QT cardiac arrhythmia and sudden cardiac death. *Nature* 421, 634-639.

Mohler PJ, Splawski I, Napolitano C, Bottelli G, Sharpe L, Timothy K, Priori SG, Keating MT, and Bennett V (2004b). A cardiac arrhythmia syndrome caused by loss of ankyrin-B function. *Proc Natl Acad Sci U S A* 101, 9137-9142.

Mok NS, Priori SG, Napolitano C, Chan NY, Chahine M, and Baroudi G (2003). A newly characterized SCN5A mutation underlying Brugada syndrome unmasked by hyperthermia. *J Cardiovasc Electrophysiol* 14, 407-411.

Morgan K, Stevens EB, Shah B, Cox PJ, Dixon AK, Lee K, Pinnock RD, Hughes J, Richardson PJ, Mizuguchi K, and Jackson AP (2000). β3: an additional auxiliary subunit of the voltage-sensitive sodium channel that modulates channel gating with distinct kinetics. *Proc Natl Acad Sci USA* 97, 2308-2313.

Morita H, Kusano-Fukushima K, Nagase S, Fujimoto Y, Hisamatsu K, Fujio H, Haraoka K, Kobayashi M, Morita ST, Nakamura K, Emori T, Matsubara H, Hina K, Kita T, Fukatani M, and Ohe T (2002). Atrial fibrillation and atrial vulnerability in patients with Brugada syndrome. *J Am Coll Cardiol* 40, 1437-1444.

Moss AJ and Kass RS (2005). Long QT syndrome: from channels to cardiac arrhythmias. *J Clin Invest* 115, 2018-2024.

Moss AJ, Zareba W, Hall WJ, Schwartz PJ, Crampton RS, Benhorin J, Vincent GM, Locati EH, Priori SG, Napolitano C, Medina A, Zhang L, Robinson JL, Timothy K, Towbin JA, and Andrews ML (2000). Effectiveness and limitations of beta-blocker therapy in congenital long-QT syndrome. *Circulation* 101, 616-623.

Moss AJ, Zareba W, Schwarz KQ, Rosero S, McNitt S, and Robinson JL (2008). Ranolazine shortens repolarization in patients with sustained inward sodium current due to type-3 long-QT syndrome. *J Cardiovasc Electrophysiol* 19, 1289-1293.

Mujtaba MG, Wang SY, and Wang GK (2002). Prenylamine block of Nav1.5 channel is mediated via a receptor distinct from that of local anesthetics. *Mol Pharmacol* 62, 415-422.

Murphy BJ, Rogers J, Perdichizzi AP, Colvin AA, and Catterall WA (1996). cAMP-dependent phosphorylation of two sites in the a subunit of the cardiac sodium channel. *J Biol Chem* 271, 28837-28843.

Murphy BJ, Rossie S, De Jongh KS, and Catterall WA (1993). Identification of the sites of selective phosphorylation and dephosphorylation of the rat brain Na^+ channel α subunit by cAMP-dependent protein kinase and phosphoprotein phosphatases. *J Biol Chem* 268, 27355-27362.

Murray KT, Hu NN, Daw JR, Shin HG, Watson MT, Mashburn AB, and George AL, Jr. (1997). Functional effects of protein kinase C activation on the human cardiac Na^+ channel. *Circ Res* 80, 370-376.

Nademanee K, Veerakul G, Nimmannit S, Chaowakul V, Bhuripanyo K, Likittanasombat K, Tunsanga K, Kuasirikul S, Malasit P, Tansupasawadikul S, and Tatsanavivat P (1997). Arrhythmogenic marker for the sudden unexplained death syndrome in Thai men. *Circulation* 96, 2595-2600.

Nagatomo T, January CT, and Makielski JC (2000). Preferential block of late sodium current in the LQT3 DeltaKPQ mutant by the class I(C) antiarrhythmic flecainide. *Mol Pharmacol* 57, 101-107.

Nashef L, Hindocha N, and Makoff A (2007). Risk factors in sudden death in epilepsy (SUDEP): the quest for mechanisms. *Epilepsia* 48, 859-871.

Nattel S (1993). Comparative mechanisms of action of antiarrhythmic drugs. *Am J Cardiol* 72, 13F-17F.

Neyroud N, Tesson F, Denjoy I, Leibovici M, Donger C, Barhanin J, Fauré S, Gary F, Coumel P, Petit C, Schwartz K, and Guicheney P (1997). A novel mutation in the potassium channel gene *KVLQT1* causes the Jervell and Lange-Nielsen cardioauditory syndrome . *Nat Genet* 15, 186-189.

Nguyen TP, Wang DW, Rhodes TH, and George AL, Jr. (2008). Divergent biophysical defects caused by mutant sodium channels in dilated cardiomyopathy with arrhythmia. *Circ Res* 102, 364-371.

Niu DM, Hwang B, Hwang HW, Wang NH, Wu JY, Lee PC, Chien JC, Shieh RC, and Chen YT (2006). A common SCN5A polymorphism attenuates a severe cardiac phenotype caused by a nonsense SCN5A mutation in a Chinese family with an inherited cardiac conduction defect. *J Med Genet* 43, 817-821.

Noble D and Noble PJ (2006). Late sodium current in the pathophysiology of cardiovascular disease: consequences of sodium-calcium overload. *Heart* 92 Suppl 4, iv1-iv5.

Noda M, Ikeda T, Kayano T, Suzuki H, Takeshima H, Kurasaki M, Takahashi H, and Numa S (1986a). Existence of distinct sodium channel messenger RNAs in rat brain. *Nature* 320, 188-192.

Noda M, Ikeda T, Suzuki H, Takeshima H, Takahashi T, Kuno M, and Numa S (1986b). Expression of functional sodium channels from cloned cDNA. *Nature* 322, 826-828.

Nuss HB, Chiamvimonvat N, Pérez-garcía MT, Tomaselli GF, and Marbán E (1995). Functional association of the β1 subunit with human cardiac (hH1) and rat skeletal muscle (μ1) sodium channel α subunits expressed in *Xenopus* oocytes. *J Gen Physiol* 106, 1171-1191.

Nuyens D, Stengl M, Dugarmaa S, Rossenbacker T, Compernolle V, Rudy Y, Smits JF, Flameng W, Clancy CE, Moons L, Vos MA, Dewerchin M, Benndorf K, Collen D, Carmeliet E, and Carmeliet P (2001). Abrupt rate accelerations or premature beats cause life-threatening arrhythmias in mice with long-QT3 syndrome. *Nat Med* 7, 1021-1027.

O'Leary ME and Chahine M (2002). Cocaine binds to a common site on open and inactivated human heart (Nav1.5) sodium channels. *J Physiol* 541, 701-716.

O'Leary ME, Digregorio M, and Chahine M (2003). Closing and inactivation potentiate the cocaethylene inhibition of cardiac sodium channels by distinct mechanisms. *Mol Pharmacol* 64, 1575-1585.

Okuse K, Malik-Hall M, Baker MD, Poon WYL, Kong H, Chao MV, and Wood JN (2002). Annexin II light chain regulates sensory neuron-specific sodium channel expression. *Nature* 417, 653-656.

Olcese R, Latorre R, Toro L, Bezanilla F, and Stefani E (1997). Correlation between charge movement and ionic current during slow inactivation in Shaker K+ channels. *J Gen Physiol* 110, 579-589.

Olson TM, Alekseev AE, Liu XK, Park S, Zingman LV, Bienengraeber M, Sattiraju S, Ballew JD, Jahangir A, and Terzic A (2006). Kv1.5 channelopathy due to KCNA5 loss-of-function mutation causes human atrial fibrillation. *Hum Mol Genet* 15, 2185-2191.

Olson TM and Keating MT (1996). Mapping a cardiomyopathy locus to chromosome 3p22-p25. *J Clin Invest* 97, 528-532.

Olson TM, Michels VV, Ballew JD, Reyna SP, Karst ML, Herron KJ, Horton SC, Rodeheffer RJ, and Anderson JL (2005). Sodium channel mutations and susceptibility to heart failure and atrial fibrillation. *J Am Med Assoc* 293, 447-454.

Ono K and Iijima T (2009). Cardiac T-type Ca(2+) channels in the heart. *J Mol Cell Cardiol.*

Opdal SH and Rognum TO (2004a). The sudden infant death syndrome gene: does it exist? *Pediatrics* 114, e506-e512.

Opdal SH and Rognum TO (2004b). The sudden infant death syndrome gene: does it exist? *Pediatrics* 114, e506-e512.

Ortega-Carnicer J, Bertos-Polo J, and Gutierrez-Tirado C (2001). Aborted sudden death, transient Brugada pattern, and wide QRS dysrrhythmias after massive cocaine ingestion. *J Electrocardiol* 34, 345-349.

Otagiri T, Kijima K, Osawa M, Ishii K, Makita N, Matoba R, Umetsu K, and Hayasaka K (2008). Cardiac ion channel gene mutations in sudden infant death syndrome. *Pediatr Res* 64, 482-487.

Ou Y, Gibbons SJ, Miller SM, Strege PR, Rich A, Distad MA, Ackerman MJ, Rae JL, Szurszewski JH, and Farrugia G (2002). SCN5A is expressed in human jejunal circular smooth muscle cells. *Neurogastroenterol Motil* 14, 477-486.

Papadatos GA, Wallerstein PMR, Head CEG, Ratcliff R, Brady PA, Benndorf K, Saumarez RC, Trezise AEO, Huang CLH, Vandenberg JI, Colledge WH, and Grace AA (2002). Slowed conduction and ventricular tachycardia after targeted disruption of the cardiac sodium channel gene *Scn5a*. *Proc Natl Acad Sci USA* 99, 6210-6215.

Pappone C, Santinelli V, Manguso F, Vicedomini G, Gugliotta F, Augello G, Mazzone P, Tortoriello V, Landoni G, Zangrillo A, Lang C, Tomita T, Mesas C, Mastella E, and Alfieri O (2004). Pulmonary vein denervation enhances long-term benefit after circumferential ablation for paroxysmal atrial fibrillation. *Circulation* 109, 327-334.

Pastor A, Nunez A, Cantale C, and Cosio FG (2001). Asymptomatic Brugada syndrome case unmasked during dimenhydrinate infusion. *J Cardiovasc Electrophysiol* 12, 1192-1194.

Patton DE, West JW, Catterall WA, and Goldin AL (1992). Amino acid residues required for fast Na^+-channel inactivation: charge neutralizations and deletions in the III-IV linker. *Proc Natl Acad Sci USA* 89, 10905-10909.

Pepine CJ and Wolff AA (1999). A controlled trial with a novel anti-ischemic agent, ranolazine, in chronic stable angina pectoris that is responsive to conventional antianginal agents. Ranolazine Study Group. *Am J Cardiol* 84, 46-50.

Pereon Y, Lande G, Demolombe S, Nguyen The Tich, Sternberg D, Le MH, and David A (2003). Paramyotonia congenita with an SCN4A mutation affecting cardiac repolarization. *Neurology* 60, 340-342.

Pérez-garcía MT, Chiamvimonvat N, Marban E, and Tomaselli GF (1996). Structure of the sodium channel pore revealed by serial cysteine mutagenesis. *Proc Natl Acad Sci USA* 93, 300-304.

Pilz B and Luft FC (2003). Acquired Brugada syndrome. *Am J Cardiol* 92, 771.

Plant LD, Bowers PN, Liu Q, Morgan T, Zhang T, State MW, Chen W, Kittles RA, and Goldstein SA (2006). A common cardiac sodium channel variant associated with sudden infant death in African Americans, SCN5A S1103Y. *J Clin Invest* 116, 430-435.

Plaster NM, Tawil R, Tristani-Firouzi M, Canun S, Bendahhou S, Tsunoda A, Donaldson MR, Iannaccone ST, Brunt E, Barohn R, Clark J, Deymeer F, George AL, Jr., Fish FA, Hahn A, Nitu A, Ozdemir C, Serdaroglu P, Subramony SH, Wolfe G, Fu YH, and Ptacek LJ (2001). Mutations in Kir2.1 cause the developmental and episodic electrical phenotypes of Andersen's syndrome. *Cell* 105, 511-519.

Plummer NW, Galt J, Jones JM, Burgess DL, Sprunger LK, Kohrman DC, and Meisler MH (1998). Exon organization, coding sequence, physical mapping, and polymorphic intragenic markers for the human neuronal sodium channel gene *SCN8A*. *Genomics* 54, 287-296.

Plunkett A, Hulse JA, Mishra B, and Gill J (2003). Variable presentation of Brugada syndrome: lessons from three generations with syncope. *BMJ* 326, 1078-1079.

Pratt CM and Moye LA (1990). The Cardiac Arrhythmia Suppression Trial: background, interim results and implications. *Am J Cardiol* 65, 20B-29B.

Priori SG, Barhanin J, Hauer RN, Haverkamp W, Jongsma HJ, Kleber AG, McKenna WJ, Roden DM, Rudy Y, Schwartz K, Schwartz PJ, Towbin JA, and Wilde A (1999). Genetic and molecular basis of cardiac arrhythmias; impact on clinical management. Study group on molecular basis of arrhythmias of the working group on arrhythmias of the european society of cardiology. *Eur Heart J* 20, 174-195.

Priori SG, Napolitano C, Gasparini M, Pappone C, Della Bella P, Giordano U, Bloise R, Giustetto C, De Nardis R, Grillo M, Ronchetti E, Faggiano G, and Nastoli J (2002). Natural history of Brugada syndrome: insights for risk stratification and management. *Circulation* 105, 1342-1347.

Priori SG, Napolitano C, Giordano U, Collisani G, and Memmi M (2000a). Brugada syndrome and sudden cardiac death in children. *Lancet* 355, 808-809.

Priori SG, Napolitano C, Schwartz PJ, Bloise R, Crotti L, and Ronchetti E (2000b). The elusive link between LQT3 and Brugada syndrome: the role of flecainide challenge. *Circulation* 102, 945-947.

Probst V, Kyndt F, Potet F, Trochu JN, Mialet G, Demolombe S, Schott JJ, Baro I, Escande D, and Le MH (2003). Haploinsufficiency in combination with aging causes SCN5A-linked hereditary Lenegre disease. *J Am Coll Cardiol* 41, 643-652.

Qin N, D'Andrea MR, Lubin ML, Shafaee N, Codd EE, and Correa AM (2003). Molecular cloning and functional expression of the human sodium channel β_{1B} subunit, a novel splicing variant of the $\beta 1$ subunit. *Eur J Biochem* 270, 4762-4770.

Qu Y, Isom LL, Westenbroek RE, Rogers JC, Tanada TN, McCormick KA, Scheuer T, and Catterall WA (1995a). Modulation of cardiac Na^+ channel expression in *Xenopus* oocytes by $\beta 1$ subunits. *J Biol Chem* 270, 25696-25701.

Qu Y, Rogers J, Tanada T, Scheuer T, and Catterall WA (1995b). Molecular determinants of drug access to the receptor site for antiarrhythmic drugs in the cardiac Na^+ channel. *Proc Natl Acad Sci USA* 92, 11839-11843.

Qu Y, Rogers JC, Tanada TN, Catterall WA, and Scheuer T (1996). Phosphorylation of S1505 in the cardiac Na^+ channel inactivation gate is required for modulation by protein kinase C. *J Gen Physiol* 108, 375-379.

Ragsdale DS, McPhee JC, Scheuer T, and Catterall WA (1994). Molecular determinants of state-dependent block of Na^+ channels by local anesthetics. *Science* 265, 1724-1728.

Ragsdale DS, McPhee JC, Scheuer T, and Catterall WA (1996). Common molecular determinants of local anesthetic, antiarrhythmic, and anticonvulsant block of voltage-gated Na^+ channels. *Proc Natl Acad Sci USA* 93, 9270-9275.

Ramirez MT, Zhao XL, Schulman H, and Brown JH (1997). The nuclear deltaB isoform of Ca2+/calmodulin-dependent protein kinase II regulates atrial natriuretic factor gene expression in ventricular myocytes. *J Biol Chem* 272, 31203-31208.

Reckziegel G, Beck H, Schramm J, Urban BW, and Elger CE (1999). Carbamazepine effects on Na+ currents in human dentate granule cells from epileptogenic tissue. *Epilepsia* 40, 401-407.

Remme CA, Verkerk AO, Nuyens D, van Ginneken AC, van BS, Belterman CN, Wilders R, van Roon MA, Tan HL, Wilde AA, Carmeliet P, de Bakker JM, Veldkamp MW, and Bezzina CR (2006). Overlap syndrome of cardiac sodium channel disease in mice carrying the equivalent mutation of human SCN5A-1795insD. *Circulation* 114, 2584-2594.

Remme CA, Wilde AA, and Bezzina CR (2008). Cardiac sodium channel overlap syndromes: different faces of SCN5A mutations. *Trends Cardiovasc Med* 18, 78-87.

Richmond JE, Featherstone DE, Hartmann HA, and Ruben PC (1998). Slow inactivation in human cardiac sodium channels. *Biophys J* 74, 2945-2952.

Rivolta I, Clancy CE, Tateyama M, Liu H, Priori SG, and Kass RS (2002). A novel *SCN5A* mutation associated with long QT-3: altered inactivation kinetics and channel dysfunction. *Physiol Genomics* 10, 191-197.

Rizzon P, Di BM, Favale S, and Visani L (1987). Class 1B agents lidocaine, mexiletine, tocainide, phenytoin. *Eur Heart J* 8 Suppl A, 21-25.

Roden DM (1998). Mechanisms and management of proarrhythmia. *Am J Cardiol* 82, 49I-57I.

Roden DM and Spooner PM (1999). Inherited long QT syndromes: a paradigm for understanding arrhythmogenesis. *J Cardiovasc Electrophysiol* 10, 1664-1683.

Rogart RB, Cribbs LL, Muglia LK, Kephart DD, and Kaiser MW (1989). Molecular cloning of a putative tetrodotoxin-resistant rat heart Na^+ channel isoform. *Proc Natl Acad Sci USA* 86, 8170-8174.

Romano C (1965). Congenital cardiac arrhythmia. *Lancet* 17, 658-659.

Rook MB, Alshinawi CB, Groenewegen WA, van Gelder IC, van Ginneken AC, Jongsma HJ, Mannens MM, and Wilde AA (1999). Human SCN5A gene mutations alter cardiac sodium channel kinetics and are associated with the Brugada syndrome. *Cardiovasc Res* 44, 507-517.

Rosenfeld J, Sloan-Brown K, and George AL, Jr. (1997). A novel muscle sodium channel mutation causes painful congenital myotonia. *Ann Neurol* 42, 811-814.

Rossenbacker T, Carroll SJ, Liu H, Kuiperi C, de Ravel TJ, Devriendt K, Carmeliet P, Kass RS, and Heidbuchel H (2004). Novel pore mutation in SCN5A manifests as a spectrum of phenotypes ranging from atrial flutter, conduction disease, and Brugada syndrome to sudden cardiac death. *Heart Rhythm* 1, 610-615.

Rotin D, Staub O, and Haguenauer-Tsapis R (2000). Ubiquitination and endocytosis of plasma membrane proteins: role of Nedd4/Rsp5p family of ubiquitin-protein ligases. *J Membr Biol* 176, 1-17.

Ruan Y, Liu N, and Priori SG (2009). Sodium channel mutations and arrhythmias. *Nat Rev Cardiol* 6, 337-348.

Rybin VO and Steinberg SF (1994). Protein kinase C isoform expression and regulation in the developing rat heart. *Circ Res* 74, 299-309.

Salata JJ and Wasserstrom JA (1988). Effects of quinidine on action potentials and ionic currents in isolated canine ventricular myocytes. *Circ Res* 62, 324-337.

Sangameswaran L, Fish LM, Koch BD, Rabert DK, Delgado SG, Ilnicka M, Jakeman LB, Novakovic S, Wong K, Sze P, Tzoumaka E, Stewart GR, Herman RC, Chan H, Eglen RM, and Hunter JC (1997). A novel tetrodotoxin-sensitive, voltage-gated sodium channel expressed in rat and human dorsal root ganglia. *J Biol Chem* 272, 14805-14809.

Sanguinetti MC and Jurkiewicz NK (1990). Two components of cardiac delayed rectifier K+ current. Differential sensitivity to block by class III antiarrhythmic agents. *J Gen Physiol* 96, 195-215.

Schaller KL, Krzemien DM, McKenna NM, and Caldwell JH (1992). Alternatively spliced sodium channel transcripts in brain and muscle. *J Neurosci* 12, 1370-1381.

Schmidt JW and Catterall WA (1986). Biosynthesis and processing of the α subunit of the voltage-sensitive sodium channel in rat brain neurons. *Cell* 46, 437-444.

Schott JJ, Alshinawi C, Kyndt F, Probst V, Hoorntje TM, Hulsbeek M, Wilde AAM, Escande D, Mannens MMAM, and Le Marec H (1999). Cardiac conduction defects associate with mutations in *SCN5A*. *Nat Genet* 23, 20-21.

Schott JJ, Charpentier F, Peltier S, Foley P, Drouin E, Bouhour JB, Donnelly P, Vergnaud G, Bachner L, Moisan JP, Le Marec H, and Pascal O (1995). Mapping of a gene for long QT syndrome to chromosome 4q25-27. *Am J Hum Genet* 57, 1114-1122.

Schram G, Zhang L, Derakhchan K, Ehrlich JR, Belardinelli L, and Nattel S (2004). Ranolazine: ion-channel-blocking actions and in vivo electrophysiological effects. *Br J Pharmacol* 142, 1300-1308.

Schulze-Bahr E, Wang Q, Wedekind H, Haverkamp W, Chen Q, Sun Y, Rubie C, Hördt M, Towbin JA, Borggrefe M, Assmann G, Qu X, Somberg JC, Breithardt G, Oberti C, and Funke H (1997). KCNE1 mutations cause jervell and Lange-Nielsen syndrome. *Nat Genet* 17, 267-268.

Schwartz PJ, Periti M, and Malliani A (1975). The long Q-T syndrome. *Am Heart J* 89, 378-390.

Schwartz PJ, Priori SG, Dumaine R, Napolitano C, Antzelevitch C, Stramba-Badiale M, Richard TA, Berti MR, and Bloise R (2000). A molecular link between the sudden infant death syndrome and the long-QT syndrome. *N Engl J Med* 343, 262-267.

Schwartz PJ, Priori SG, Locati EH, Napolitano C, Cantù F, Towbin JA, Keating MT, Hammoude H, Brown AM, Chen LS, and Colatsky TJ (1995). Long QT syndrome patients with mutations of the *SCN5A* and *HERG* genes have differential responses to Na^+ channel blockade and to increases in heart rate. Implications for gene-specific therapy. *Circulation* 92, 3381-3386.

Schwartz PJ, Stramba-Badiale M, Segantini A, Austoni P, Bosi G, Giorgetti R, Grancini F, Marni ED, Perticone F, Rosti D, and Salice P (1998). Prolongation of the QT interval and the sudden infant death syndrome. *N Engl J Med* 338, 1709-1714.

Scornik FS, Desai M, Brugada R, Guerchicoff A, Pollevick GD, Antzelevitch C, and Perez GJ (2006). Functional expression of "cardiac-type" Nav1.5 sodium channel in canine intracardiac ganglia. *Heart Rhythm* 3, 842-850.

Shander GS, Fan Z, and Makielski JC (1995). Slowly recovering cardiac sodium current in rat ventricular myocytes: effects of conditioning duration and recovery potential. *J Cardiovasc Electrophysiol* 6, 786-795.

Sheets MF and Hanck DA (1999). Gating of skeletal and cardiac muscle sodium channels in mammalian cells. *J Physiol* 514, 425-436.

Shi R, Zhang Y, Yang C, Huang C, Zhou X, Qiang H, Grace AA, Huang CL, and Ma A (2008). The cardiac sodium channel mutation delQKP 1507-1509 is associated with the expanding phenotypic spectrum of LQT3, conduction disorder, dilated cardiomyopathy, and high incidence of youth sudden death. *Europace* 10, 1329-1335.

Shi Y, Pritchard KA, Jr., Holman P, Rafiee P, Griffith OW, Kalyanaraman B, and Baker JE (2000). Chronic myocardial hypoxia increases nitric oxide synthase and decreases caveolin-3. *Free Radic Biol Med* 29, 695-703.

Shibata EF, Brown TL, Washburn ZW, Bai J, Revak TJ, and Butters CA (2006). Autonomic regulation of voltage-gated cardiac ion channels. *J Cardiovasc Electrophysiol* 17 Suppl 1, S34-S42.

Shimizu W (2008). Clinical impact of genetic studies in lethal inherited cardiac arrhythmias. *Circ J* 72, 1926-1936.

Shimizu W, Antzelevitch C, Suyama K, Kurita T, Taguchi A, Aihara N, Takaki H, Sunagawa K, and Kamakura S (2000). Effect of sodium channel blockers on ST segment, QRS duration, and corrected QT interval in patients with Brugada syndrome. *J Cardiovasc Electrophysiol* 11, 1320-1329.

Shimizu W, Kurita T, Matsuo K, Suyama K, Aihara N, Kamakura S, Towbin JA, and Shimomura K (1998). Improvement of repolarization abnormalities by a K+ channel opener in the LQT1 form of congenital long-QT syndrome. *Circulation* 97, 1581-1588.

Shin DJ, Jang Y, Park HY, Lee JE, Yang K, Kim E, Bae Y, Kim J, Kim J, Kim SS, Lee MH, Chahine M, and Yoon SK (2004). Genetic analysis of the cardiac sodium channel gene SCN5A in Koreans with Brugada syndrome. *J Hum Genet* 49, 573-578.

Shin DJ, Kim E, Park SB, Jang WC, Bae Y, Han J, Jang Y, Joung B, Lee MH, Kim SS, Huang H, Chahine M, and Yoon SK (2007). A novel mutation in the SCN5A gene is associated with Brugada syndrome. *Life Sci* 80, 716-724.

Shin HG, Barnett JV, Chang P, Reddy S, Drinkwater DC, Pierson RN, Wiley RG, and Murray KT (2000). Molecular heterogeneity of protein kinase C expression in human ventricle. *Cardiovasc Res* 48, 285-299.

Shin HG and Murray KT (2001). Conventional protein kinase C isoforms and cross-activation of protein kinase A regulate cardiac Na+ current. *FEBS Lett* 495, 154-158.

Shorofsky SR and Balke CW (2001). Calcium currents and arrhythmias: insights from molecular biology. *Am J Med* 110, 127-140.

Sicouri S, Timothy KW, Zygmunt AC, Glass A, Goodrow RJ, Belardinelli L, and Antzelevitch C (2007). Cellular basis for the electrocardiographic and arrhythmic manifestations of Timothy syndrome: effects of ranolazine. *Heart Rhythm* 4, 638-647.

Sigworth FJ (2003). Structural biology: Life's transistors. *Nature* 423, 21-22.

Smallwood JK, Robertson DW, and Steinberg MI (1989). Electrophysiological effects of flecainide enantiomers in canine Purkinje fibres. *Naunyn Schmiedebergs Arch Pharmacol* 339, 625-629.

Smith MR and Goldin AL (1997). Interaction between the sodium channel inactivation linker and domain III S4-S5. *Biophys J* 73, 1885-1895.

Smits JPP, Eckardt L, Probst V, Bezzina CR, Schott JJ, Remme CA, Haverkamp W, Breithardt G, Escande D, Schulze-Bahr E, LeMarec H, and Wilde AAM (2002). Genotype-phenotype relationship in Brugada syndrome: electrocardiographic features differentiate *SCN5A*-related patients from non-*SCN5A*-related patients. *J Am Coll Cardiol* 40, 350-356.

Sokolov S, Scheuer T, and Catterall WA (2005). Ion permeation through a voltage-sensitive gating pore in brain sodium channels having voltage sensor mutations. *Neuron* 47, 183-189.

Sokolov S, Scheuer T, and Catterall WA (2007). Gating pore current in an inherited ion channelopathy. *Nature* 446, 76-78.

Song Y, Shryock JC, Wu L, and Belardinelli L (2004). Antagonism by ranolazine of the pro-arrhythmic effects of increasing late INa in guinea pig ventricular myocytes. *J Cardiovasc Pharmacol* 44, 192-199.

Souslova VA, Fox M, Wood JN, and Akopian AN (1997). Cloning and characterization of a mouse sensory neuron tetrodotoxin- resistant voltage-gated sodium channel gene, Scn10a. *Genomics* 41, 201-209.

Splawski I, Timothy KW, Sharpe LM, Decher N, Kumar P, Bloise R, Napolitano C, Schwartz PJ, Joseph RM, Condouris K, Tager-Flusberg H, Priori SG, Sanguinetti MC, and Keating MT (2004). Ca(V)1.2 calcium channel dysfunction causes a multisystem disorder including arrhythmia and autism. *Cell* 119, 19-31.

Splawski I, Tristani-Firouzi M, Lehmann MH, Sanguinetti MC, and Keating MT (1997). Mutations in the hminK gene cause long QT syndrome and suppress I_{Ks} function. *Nat Genet* 17, 338-340.

Spooner PM, Albert C, Benjamin EJ, Boineau R, Elston RC, George AL, Jr., Jouven X, Kuller LH, MacCluer JW, Marban E, Muller JE, Schwartz PJ, Siscovick DS, Tracy RP, Zareba W, and Zipes DP (2001). Sudden cardiac death, genes, and arrhythmogenesis : consideration of new population and mechanistic approaches from a national heart, lung, and blood institute workshop, part I. *Circulation* 103, 2361-2364.

Stokoe KS, Thomas G, Goddard CA, Colledge WH, Grace AA, and Huang CL (2007). Effects of flecainide and quinidine on arrhythmogenic properties of Scn5a+/Delta murine hearts modelling long QT syndrome 3. *J Physiol* 578, 69-84.

Strichartz GR (1973). The inhibition of sodium currents in myelinated nerve by quaternary derivatives of lidocaine. *J Gen Physiol* 62, 37-57.

Stühmer W, Conti F, Suzuki H, Wang XD, Noda M, Yahagi N, Kubo H, and Numa S (1989). Structural parts involved in activation and inactivation of the sodium channel. *Nature* 339, 597-603.

Takehara N, Makita N, Kawabe J, Sato N, Kawamura Y, Kitabatake A, and Kikuchi K (2004). A cardiac sodium channel mutation identified in Brugada syndrome associated with atrial standstill. *J Intern Med* 255, 137-142.

Tan BH, Valdivia CR, Rok BA, Ye B, Ruwaldt KM, Tester DJ, Ackerman MJ, and Makielski JC (2005). Common human SCN5A polymorphisms have altered electrophysiology when expressed in Q1077 splice variants. *Heart Rhythm* 2, 741-747.

Tan HL, Bezzina CR, Smits JPP, Verkerk AO, and Wilde AAM (2003). Genetic control of sodium channel function. *Cardiovasc Res* 57, 961-973.

Tan HL, Bink-Boelkens MT, Bezzina CR, Viswanathan PC, Beaufort-Krol GC, van Tintelen PJ, van Den Berg MP, Wilde AA, and Balser JR (2001). A sodium-channel mutation causes isolated cardiac conduction disease. *Nature* 409, 1043-1047.

Tan HL, Hou CJY, Lauer MR, and Sung RJ (1995). Electrophysiologic mechanisms of the long QT interval syndromes and torsade de pointes. *Ann Intern Med* 122, 701-714.

Tan HL, Kupershmidt S, Zhang R, Stepanovic S, Roden DM, Wilde AAM, Anderson ME, and Balser JR (2002). A calcium sensor in the sodium channel modulates cardiac excitability. *Nature* 415, 442-447.

Tate S, Benn S, Hick C, Trezise D, John V, Mannion RJ, Costigan M, Plumpton C, Grose D, Gladwell Z, Kendall G, Dale K, Bountra C, and Woolf CJ (1998). Two sodium channels contribute to the TTX-R sodium current in primary sensory neurons. *Nat Neurosci* 1, 653-655.

Terlau H and Stuhmer W (1998). Structure and function of voltage-gated ion channels. *Naturwissenschaften* 85, 437-444.

Tester DJ and Ackerman MJ (2006). The role of molecular autopsy in unexplained sudden cardiac death. *Curr Opin Cardiol* 21, 166-172.

The Cardiac Arrhythmia Suppression Trial (CAST) Investigators (1989). Preliminary report: effect of encainide and flecainide on mortality in a randomized trial of arrhythmia suppression after myocardial infarction. The Cardiac Arrhythmia Suppression Trial (CAST) Investigators [see comments]. *N Engl J Med* 321, 406-412.

Tian XL, Yong SL, Wan X, Wu L, Chung MK, Tchou PJ, Rosenbaum DS, Van Wagoner DR, Kirsch GE, and Wang Q (2004). Mechanisms by which *SCN5A* mutation N1325S causes cardiac arrhythmias and sudden death in vivo. *Cardiovasc Res* 61, 256-267.

Tobimatsu T and Fujisawa H (1989). Tissue-specific expression of four types of rat calmodulin-dependent protein kinase II mRNAs. *J Biol Chem* 264, 17907-17912.

Toledo-Aral JJ, Moss BL, He ZJ, Koszowski AG, Whisenand T, Levinson SR, Wolf JJ, Silos-Santiago I, Halegoua S, and Mandel G (1997). Identification of PN1, a predominant voltage-dependent sodium channel expressed principally in peripheral neurons. *Proc Natl Acad Sci USA* 94, 1527-1532.

Tombola F, Pathak MM, and Isacoff EY (2005). Voltage-sensing arginines in a potassium channel permeate and occlude cation-selective pores. *Neuron* 45, 379-388.

Towbin JA, Wang Z, and Li H (2001). Genotype and severity of long QT syndrome. *Drug Metab Dispos* 29, 574-579.

Trimmer JS, Cooperman SS, Tomiko SA, Zhou J, Crean SM, Boyle MB, Kallen RG, Sheng Z, Barchi RL, Sigworth FJ, Goodman RH, Agnew WS, and Mandel G (1989). Primary structure and functional expression of a mammalian skeletal muscle sodium channel. *Neuron* 3, 33-49.

Tristani-Firouzi M, Jensen JL, Donaldson MR, Sansone V, Meola G, Hahn A, Bendahhou S, Kwiecinski H, Fidzianska A, Plaster N, Fu YH, Ptacek LJ, and Tawil R (2002). Functional and clinical characterization of KCNJ2 mutations associated with LQT7 (Andersen syndrome). *J Clin Invest* 110, 381-388.

Trudeau MM, Dalton JC, Day JW, Ranum LP, and Meisler MH (2006). Heterozygosity for a protein truncation mutation of sodium channel SCN8A in a patient with cerebellar atrophy, ataxia, and mental retardation. *J Med Genet* 43, 527-530.

Tukkie R, Sogaard P, Vleugels J, de G, I, Wilde AA, and Tan HL (2004). Delay in right ventricular activation contributes to Brugada syndrome. *Circulation* 109, 1272-1277.

Undrovinas AI, Belardinelli L, Undrovinas NA, and Sabbah HN (2006). Ranolazine improves abnormal repolarization and contraction in left ventricular myocytes of dogs with heart failure by inhibiting late sodium current. *J Cardiovasc Electrophysiol* 17 Suppl 1, S169-S177.

Undrovinas AI, Shander GS, and Makielski JC (1995). Cytoskeleton modulates gating of voltage-dependent sodium channel in heart. *Am J Physiol* 269, H203-H214.

Valdivia CR, Ackerman MJ, Tester DJ, Wada T, McCormack J, Ye B, and Makielski JC (2002a). A novel *SCN5A* arrhythmia mutation, M1766L, with expression defect rescued by mexiletine. *Cardiovasc Res* 55, 279-289.

Valdivia CR, Nagatomo T, and Makielski JC (2002b). Late Na currents affected by alpha subunit isoform and beta1 subunit co-expression in HEK293 cells. *J Mol Cell Cardiol* 34, 1029-1039.

Valdivia CR, Tester DJ, Rok BA, Porter CBJ, Munger TM, Jahangir A, Makielski JC, and Ackerman MJ (2004). A trafficking defective, Brugada syndrome-causing SCN5A mutation rescued by drugs. *Cardiovasc Res* 62, 53-62.

Valdivia CR, Ueda K, Ackerman MJ, and Makielski JC (2009). GPD1L links redox state to cardiac excitability by PKC-dependent phosphorylation of the sodium channel SCN5A. *Am J Physiol Heart Circ Physiol* 297, H1446-H1452.

van Bemmelen MX, Rougier JS, Gavillet B, Apotheloz F, Daidie D, Tateyama M, Rivolta I, Thomas MA, Kass RS, Staub O, and Abriel H (2004). Cardiac voltage-gated sodium channel Nav1.5 is regulated by Nedd4-2 mediated ubiquitination. *Circ Res* 95, 284-291.

Van Norstrand DW, Valdivia CR, Tester DJ, Ueda K, London B, Makielski JC, and Ackerman MJ (2007). Molecular and functional characterization of novel glycerol-3-phosphate dehydrogenase 1 like gene (GPD1-L) mutations in sudden infant death syndrome. *Circulation* 116, 2253-2259.

Vatta M, Ackerman MJ, Ye B, Makielski JC, Ughanze EE, Taylor EW, Tester DJ, Balijepalli RC, Foell JD, Li Z, Kamp TJ, and Towbin JA (2006). Mutant caveolin-3 induces persistent late sodium current and is associated with long-QT syndrome. *Circulation* 114, 2104-2112.

Vaughan Williams EM (1992). Classifying antiarrhythmic actions: by facts or speculation. *J Clin Pharmacol* 32, 964-977.

Vege A and Ole RT (2004). Sudden infant death syndrome, infection and inflammatory responses. *FEMS Immunol Med Microbiol* 42, 3-10.

Veldkamp MW, Viswanathan PC, Bezzina C, Baartscheer A, Wilde AAM, and Balser JR (2000). Two distinct congenital arrhythmias evoked by a multidysfunctional Na^+ channel. *Circ Res* 86, E91-E97.

Veldkamp MW, Wilders R, Baartscheer A, Zegers JG, Bezzina CR, and Wilde AAM (2003). Contribution of sodium channel mutations to bradycardia and sinus node dysfunction in LQT3 families. *Circ Res* 92, 976-983.

Veltmann C, Schimpf R, Echternach C, Eckardt L, Kuschyk J, Streitner F, Spehl S, Borggrefe M, and Wolpert C (2006). A prospective study on spontaneous fluctuations between diagnostic and non-diagnostic ECGs in Brugada syndrome: implications for correct phenotyping and risk stratification. *Eur Heart J* 27, 2544-2552.

Vijayaragavan K, O'Leary ME, and Chahine M (2001). Gating properties of $Na_v1.7$ and $Na_v1.8$ peripheral nerve sodium channels. *J Neurosci* 21, 7909-7918.

Vilin YY, Fujimoto E, and Ruben PC (2001). A single residue differentiates between human cardiac and skeletal muscle Na^+ channel slow inactivation. *Biophys J* 80, 2221-2230.

Viswanathan PC, Benson DW, and Balser JR (2003). A common SCN5A polymorphism modulates the biophysical effects of an SCN5A mutation. *J Clin Invest* 111, 341-346.

Viswanathan PC, Bezzina CR, George AL, Jr., Roden DM, Wilde AAM, and Balser JR (2001). Gating-dependent mechanisms for flecainide action in *SCN5A*-linked arrhythmia syndromes. *Circulation* 104, 1200-1205.

Volders PG, Vos MA, Szabo B, Sipido KR, de Groot SH, Gorgels AP, Wellens HJ, and Lazzara R (2000). Progress in the understanding of cardiac early afterdepolarizations and torsades de pointes: time to revise current concepts. *Cardiovasc Res* 46, 376-392.

Vreugdenhil M, Faas GC, and Wadman WJ (1998). Sodium currents in isolated rat CA1 neurons after kindling epileptogenesis. *Neuroscience* 86, 99-107.

Vreugdenhil M and Wadman WJ (1999). Modulation of sodium currents in rat CA1 neurons by carbamazepine and valproate after kindling epileptogenesis. *Epilepsia* 40, 1512-1522.

Wagner S, Dybkova N, Rasenack EC, Jacobshagen C, Fabritz L, Kirchhof P, Maier SK, Zhang T, Hasenfuss G, Brown JH, Bers DM, and Maier LS (2006). Ca2+/calmodulin-dependent protein kinase II regulates cardiac Na+ channels. *J Clin Invest* 116, 3127-3138.

Wang DW, Desai RR, Crotti L, Arnestad M, Insolia R, Pedrazzini M, Ferrandi C, Vege A, Rognum T, Schwartz PJ, and George AL, Jr. (2007d). Cardiac sodium channel dysfunction in sudden infant death syndrome. *Circulation* 115, 368-376.

Wang DW, Desai RR, Crotti L, Arnestad M, Insolia R, Pedrazzini M, Ferrandi C, Vege A, Rognum T, Schwartz PJ, and George AL, Jr. (2007a). Cardiac sodium channel dysfunction in sudden infant death syndrome. *Circulation* 115, 368-376.

Wang DW, Desai RR, Crotti L, Arnestad M, Insolia R, Pedrazzini M, Ferrandi C, Vege A, Rognum T, Schwartz PJ, and George AL, Jr. (2007c). Cardiac sodium channel dysfunction in sudden infant death syndrome. *Circulation* 115, 368-376.

Wang DW, Desai RR, Crotti L, Arnestad M, Insolia R, Pedrazzini M, Ferrandi C, Vege A, Rognum T, Schwartz PJ, and George AL, Jr. (2007b). Cardiac sodium channel dysfunction in sudden infant death syndrome. *Circulation* 115, 368-376.

Wang DW, Viswanathan PC, Balser JR, George AL, Jr., and Benson DW (2002). Clinical, genetic, and biophysical characterization of *SCN5A* mutations associated with atrioventricular conduction block. *Circulation* 105, 341-346.

Wang DW, Yazawa K, George AL, Jr., and Bennett PB (1996a). Characterization of human cardiac Na^+ channel mutations in the congenital long QT syndrome. *Proc Natl Acad Sci USA* 93, 13200-13205.

Wang DW, Yazawa K, Makita N, George AL, Jr., and Bennett PB (1997). Pharmacological targeting of long QT mutant sodium channels. *J Clin Invest* 99, 1714-1720.

Wang GK, Calderon J, and Wang SY (2008b). the most important risk factor for maternal death? State- and use-dependent block of muscle Nav1.4 and neuronal Nav1.7 voltage-gated Na+ channel isoforms by ranolazine. *Mol Pharmacol* 73, 940-948.

Wang GK, Calderon J, and Wang SY (2008a). State- and use-dependent block of muscle Nav1.4 and neuronal Nav1.7 voltage-gated Na+ channel isoforms by ranolazine. *Mol Pharmacol* 73, 940-948.

Wang GK, Quan C, and Wang S (1998). A common local anesthetic receptor for benzocaine and etidocaine in voltage-gated mu1 Na+ channels. *Pflugers Arch* 435, 293-302.

Wang Q, Li Z, Shen J, and Keating MT (1996b). Genomic organization of the human *SCN5A* gene encoding the cardiac sodium channel. *Genomics* 34, 9-16.

Wang Q, Shen J, Li Z, Timothy K, Vincent GM, Priori SG, Schwartz PJ, and Keating MT (1995a). Cardiac sodium channel mutations in patients with long QT syndrome, an inherited cardiac arrhythmia. *Hum Mol Genet* 4, 1603-1607.

Wang Q, Shen J, Splawski I, Atkinson D, Li Z, Robinson JL, Moss AJ, Towbin JA, and Keating MT (1995b). SCN5A mutations associated with an inherited cardiac arrhythmia, long QT syndrome. *Cell* 80, 805-811.

Watanabe E, Fujikawa A, Matsunaga H, Yasoshima Y, Sako N, Yamamoto T, Saegusa C, and Noda M (2000). Na_v2/NaG channel is involved in control of salt-intake behavior in the CNS. *J Neurosci* 20, 7743-7751.

Watanabe H, Chinushi M, Washizuka T, Sugiura H, Hirono T, Komura S, Hosaka Y, Yamaura M, Tanabe Y, furushima H, Fujita S, and Aizawa Y (2005). Variable electrocardiographic effects of short-term quinidine sulfate administration in Brugada syndrome. *Pacing Clin Electrophysiol* 28, 372-377.

Watanabe H, Koopmann TT, Le SS, Yang T, Ingram CR, Schott JJ, Demolombe S, Probst V, Anselme F, Escande D, Wiesfeld AC, Pfeufer A, Kaab S, Wichmann HE, Hasdemir C, Aizawa Y, Wilde AA, Roden DM, and Bezzina CR (2008). Sodium channel beta1 subunit mutations associated with Brugada syndrome and cardiac conduction disease in humans. *J Clin Invest* 118, 2260-2268.

Waxman SG (2007). Nav1.7, its mutations, and the syndromes that they cause. *Neurology* 69, 505-507.

Wedekind H, Smits JPP, Schulze-Bahr E, Arnold R, Veldkamp MW, Bajanowski T, Borggrefe M, Brinkmann B, Warnecke I, Funke H, Bhuiyan ZA, Wilde AA, Breithardt G, and Haverkamp W (2001). De novo mutation in the *SCN5A* gene associated with early onset of sudden infant death. *Circulation* 104, 1158-1164.

Wehrens XHT, Abriel H, Cabo C, Benhorin J, and Kass RS (2000). Arrhythmogenic mechanism of an LQT-3 mutation of the human heart Na^+ channel α-subunit: A computational analysis. *Circulation* 102, 584-590.

Wei J, Wang DW, Alings M, Fish F, Wathen M, Roden DM, and George AL, Jr. (1999). Congenital long-QT syndrome caused by a novel mutation in a conserved acidic domain of the cardiac Na^+ channel. *Circulation* 99, 3165-3171.

Weigt HU, Kwok WM, Rehmert GC, and Bosnjak ZJ (1998). Modulation of the cardiac sodium current by inhalational anesthetics in the absence and presence of beta-stimulation. *Anesthesiology* 88, 114-124.

West JW, Patton DE, Scheuer T, Wang Y, Goldin AL, and Catterall WA (1992). A cluster of hydrophobic amino acid residues required for fast Na^+-channel inactivation. *Proc Natl Acad Sci USA* 89, 10910-10914.

Wilde AAM, Antzelevitch C, Borggrefe M, Brugada J, Brugada R, Brugada P, Corrado D, Hauer RNW, Kass RS, Nademanee K, Priori SG, and Towbin JA (2002b). Proposed diagnostic criteria for the Brugada syndrome. *Eur Heart J* 23, 1648-1654.

Wilde AAM, Antzelevitch C, Borggrefe M, Brugada J, Brugada R, Brugada P, Corrado D, Hauer RNW, Kass RS, Nademanee K, Priori SG, and Towbin JA (2002a). Proposed diagnostic criteria for the Brugada syndrome: consensus report. *Circulation* 106, 2514-2519.

Williams TM and Lisanti MP (2004). The Caveolin genes: from cell biology to medicine. *Ann Med* 36, 584-595.

Wollner DA, Messner DJ, and Catterall WA (1987). β 2 subunits of sodium channels from vertebrate brain. Studies with subunit-specific antibodies. *J Biol Chem* 262, 14709-14715.

Wu L, Shryock JC, Song Y, Li Y, Antzelevitch C, and Belardinelli L (2004). Antiarrhythmic effects of ranolazine in a guinea pig in vitro model of long-QT syndrome. *J Pharmacol Exp Ther* 310, 599-605.

Xia M, Jin Q, Bendahhou S, He Y, Larroque MM, Chen Y, Zhou Q, Yang Y, Liu Y, Liu B, Zhu Q, Zhou Y, Lin J, Liang B, Li L, Dong X, Pan Z, Wang R, Wan H, Qiu W, Xu W, Eurlings P, Barhanin J, and Chen Y (2005). A Kir2.1 gain-of-function mutation underlies familial atrial fibrillation. *Biochem Biophys Res Commun* 332, 1012-1019.

Xiong W, Li RA, Tian Y, and Tomaselli GF (2003). Molecular motions of the outer ring of charge of the sodium channel: do they couple to slow inactivation? *J Gen Physiol* 122, 323-332.

Yamagishi T, Janecki M, Marban E, and Tomaselli GF (1997). Topology of the P segments in the sodium channel pore revealed by cysteine mutagenesis. *Biophys J* 73, 195-204.

Yang N, George AL, Jr., and Horn R (1996). Molecular basis of charge movement in voltage-gated sodium channels. *Neuron* 16, 113-122.

Yang N, Ji S, Zhou M, Ptácek LJ, Barchi RL, Horn R, and George AL, Jr. (1994). Sodium channel mutations in paramyotonia congenita exhibit similar biophysical phenotypes *in vitro*. *Proc Natl Acad Sci USA* 91, 12785-12789.

Yang T and Roden DM (1996). Extracellular potassium modulation of drug block of I_{Kr}. Implications for torsade de pointes and reverse use-dependence. *Circulation* 93, 407-411.

Yang Y, Xia M, Jin Q, Bendahhou S, Shi J, Chen Y, Liang B, Lin J, Liu Y, Liu B, Zhou Q, Zhang D, Wang R, Ma N, Su X, Niu K, Pei Y, Xu W, Chen Z, Wan H, Cui J, Barhanin J, and

Chen Y (2004). Identification of a KCNE2 gain-of-function mutation in patients with familial atrial fibrillation. *Am J Hum Genet* 75, 899-905.

Yang Y, Yan Y, and Sigworth FJ (1997). How does the W434F mutation block current in Shaker potassium channels? *J Gen Physiol* 109, 779-789.

Yarbrough TL, Lu T, Lee HC, and Shibata EF (2002b). Localization of cardiac sodium channels in caveolin-rich membrane domains: regulation of sodium current amplitude. *Circ Res* 90, 443-449.

Yarbrough TL, Lu T, Lee HC, and Shibata EF (2002a). Localization of cardiac sodium channels in caveolin-rich membrane domains: regulation of sodium current amplitude. *Circ Res* 90, 443-449.

Yarov-Yarovoy V, Brown J, Sharp EM, Clare JJ, Scheuer T, and Catterall WA (2001). Molecular determinants of voltage-dependent gating and binding of pore-blocking drugs in transmembrane segment IIIS6 of the Na^+ channel α subunit. *J Biol Chem* 276, 20-27.

Ye B, Valdivia CR, Ackerman MJ, and Makielski JC (2003). A common human *SCN5A* polymorphism modifies expression of an arrhythmia causing mutation. *Physiol Genomics* 12, 187-193.

Yu FH and Catterall WA (2003). Overview of the voltage-gated sodium channel family. *Genome Biol* 4, 207.

Yu FH, Westenbroek RE, Silos-Santiago I, McCormick KA, Lawson D, Ge P, Ferriera H, Lilly J, Distefano PS, Catterall WA, Scheuer T, and Curtis R (2003). Sodium channel β4, a new disulfide-linked auxiliary subunit with similarity to β2. *J Neurosci* 23, 7577-7585.

Zareba W, Moss AJ, Schwartz PJ, Vincent GM, Robinson JL, Priori SG, Benhorin J, Locati EH, Towbin JA, Keating MT, Lehmann MH, and Hall WJ (1998). Influence of genotype on the clinical course of the long-QT syndrome. International Long-QT Syndrome Registry Research Group. *N Engl J Med* 339, 960-965.

Zareba W, Sattari MN, Rosero S, Couderc JP, and Moss AJ (2001). Altered atrial, atrioventricular, and ventricular conduction in patients with the long QT syndrome caused by the DeltaKPQ SCN5A sodium channel gene mutation. *Am J Cardiol* 88, 1311-1314.

Zhang JF and Siegelbaum SA (1991). Effects of external protons on single cardiac sodium channels from guinea pig ventricular myocytes. *J Gen Physiol* 98, 1065-1083.

Zhao J, Ziane R, Chatelier A, O'Leary ME, and Chahine M (2007). Lidocaine promotes the trafficking and functional expression of Na(v)1.8 sodium channels in mammalian cells. *J Neurophysiol* 98, 467-477.

Zhorov BS and Bregestovski PD (2000). Chloride channels of glycine and GABA receptors with blockers: Monte Carlo minimization and structure-activity relationships. *Biophys J* 78, 1786-1803.

Zhou J, Shin HG, Yi J, Shen W, Williams CP, and Murray KT (2002). Phosphorylation and putative ER retention signals are required for protein kinase A-mediated potentiation of cardiac sodium current. *Circ Res* 91, 540-546.

Zhou J, Yi J, Hu NN, George AL, Jr., and Murray KT (2000). Activation of protein kinase A modulates trafficking of the human cardiac sodium channel in *Xenopus* oocytes. *Circ Res* 87, 33-38.

Ziane R, Huang H, Moghadaszadeh B, Beggs AH, Levesque G, and Chahine M (2010). Cell membrane expression of cardiac sodium channel Na(v)1.5 is modulated by alpha-actinin-2 interaction. *Biochemistry* 49, 166-178.

Zimmer T and Surber R (2008). SCN5A channelopathies--an update on mutations and mechanisms. *Prog Biophys Mol Biol* 98, 120-136.

Zimmermann K, Leffler A, Babes A, Cendan CM, Carr RW, Kobayashi J, Nau C, Wood JN, and Reeh PW (2007). Sensory neuron sodium channel Nav1.8 is essential for pain at low temperatures. *Nature* 447, 855-858.

Zygmunt AC, Eddlestone GT, Thomas GP, Nesterenko VV, and Antzelevitch C (2001). Larger late sodium conductance in M cells contributes to electrical heterogeneity in canine ventricle. *Am J Physiol* 281, H689-H697.

Appendix I

Summary of *SCN5A* mutations associated with cardic Na^+ channelopathies in our laboratory

Summary of *SCN5A* mutations associated with Na^+ channelopathies in our laboratory

Mutation	Region	Disease	Gating property	Reference
S1333Y	DIII S4-S5 linker	SIDS		(Huang *et al.*, 2009)
K1493R	DIII-IV linker	AF	Increased window current	(Li *et al.*, 2009)
R43Q	N-terminus	Combination with hERG mutation to cause LQT2	Hyperpolarizing shift in steady-state activation after lidocaine treatment	(Lin *et al.*, 2008)
W1191X	DII-III linker	BrS1	No current	(Shin *et al.*, 2007)
R1193Q	DII-III linker	LQT3/BrS1	Persistent I_{Na} and hyperpolarizing and shift in steady-state inactivation	(Huang *et al.*, 2006)
F1344S	DIIIS5	BrS1	Depolarizing shift in steady-state activation	(Keller *et al.*, 2006)
W822X	DIIS4	BrS1	No current	(Keller *et al.*, 2005a)
G1262S	DIIIS2	BrS1	No biophysical characterization results	(Shin *et al.*, 2004)
V1763M	DIVS6	LQT3/ 2:1 AV block	Persistent I_{Na}	(Chang *et al.*, 2004)
delQKP 1507-1509	DIII-IV linker	LQT3	Persistent I_{Na}	(Keller *et al.*, 2003)
H681P	DII-III linker	BrS1	Hyperpolarizing shift of steady-state inactivation and decrease window current	(Mok *et al.*, 2003)
R1232W+ T1620M	DIVS3-S4 linker DIIIS1-S2 linker	BrS1	No current	(Baroudi *et al.*, 2002)
E1784K	DIVS6	LQT3	Persistent I_{Na}	(Deschênes *et al.*, 2000)
R1512W	DIII-IV linker	BrS1	A slowing of both inactivation and recovery from inactivation.	(Deschênes *et al.*, 2000)
R1432G	DIIIS5–S6	BrS1	No current	(Deschênes *et al.*, 2000)
D1790G	DIVS6	LQT3/BrS1	Persistent I_{Na} and decreased peak I_{Na}	(Baroudi and Chahine, 2000)
T1620M	DIIIS1-S2 linker	BrS1	A faster recovery from inactivation and a depolarizing shift of steady-state inactivation in *Xenopus oocytes.* a slower recovery from inactivation in tsA 201 cells	(Baroudi *et al.*, 2000)
Y1767C	DIVS6	LQT3	Persistent I_{Na} and increased window current	Chapter II (Unpublished)
R219H	DIS4	DCM	No gating changes	Unpublished
A204V	DIS3	BrS1	No gating changes	Unpublished
L1988R	C-terminus	BrS1	No gating changes	Unpublished
P1089L	DII-III linker	BrS1	No gating changes	Unpublished

Appendix II

Reprints of all published articles

FEBS Letters 583 (2009) 890–896

FEBS Letters

journal homepage: www.FEBSLetters.org

Biophysical characterization of a new *SCN5A* mutation S1333Y in a SIDS infant linked to long QT syndrome

Hai Huang [a], Gilles Millat [b], Claire Rodriguez-Lafrasse [b], Robert Rousson [b], Béatrice Kugener [c], Philippe Chevalier [d], Mohamed Chahine [a,e,*]

[a] Le Centre de Recherche Université Laval Robert-Giffard, Local F-6539, 2601 Chemin de la Canardière, Québec City, QC, Canada G1J 2G3
[b] Laboratoire de Biochimie et Biologie Moléculaire, Hôpital Cardiovasculaire et Pneumologique L Pradel, F-69677 Bron Cedex, France
[c] Unité de Neuro-pédiatrie, Hôpital Debrousse, Lyon, France
[d] Unité de Cardiologie et Soins Intensifs, Hôpital Cardiovasculaire et Pneumologique L Pradel, F-69677 Bron Cedex, France
[e] Departement de Médecine, Université Laval, Québec City, QC, Canada G1K 7P4

ARTICLE INFO

Article history:
Received 12 January 2009
Revised 3 February 2009
Accepted 4 February 2009
Available online 10 February 2009

Edited by Maurice Montal

Keywords:
Sudden infant death syndrome
Genetics
Na^+ channel
$Na_v1.5$
Long QT syndrome
SCN5A

ABSTRACT

Various entities and genetic etiologies, including inherited long QT syndrome type 3 (LQT3), contribute to sudden infant death syndrome (SIDS). The goal of our research was to biophysically characterize a new *SCN5A* mutation (S1333Y) in a SIDS infant. S1333Y channels showed the gain of Na^+ channel function characteristic of LQT3, including a persistent inward Na^+ current and an enhanced window current that was generated by a −8 mV shift in activation and a +7 mV shift in inactivation. The correlation between the biophysical data and arrhythmia susceptibility suggested that the SIDS was secondary to the LQT3-associated S1333Y mutation.

1. Introduction

The most common cause of mortality during the first year of life of infants in developed countries is sudden infant death syndrome (SIDS), which is more common in infants placed in a prone position [1] or with upper respiratory infections [2]. Other risk factors include bottle feeding, second-hand smoke, overheating, and co-sleeping [3]. Previous studies revealed that SIDS is associated with alterations in genes associated with cardiac ion channels, including human cardiac voltage-gated Na^+ channels ($Na_v1.5$) [4].

Inherited long QT syndrome (LQTS) accounts for about 9.5% of SIDS cases, suggesting that sudden death due to cardiac arrhythmias is an important contributor to SIDS [5]. LQTS is caused by delayed ventricular repolarization, which leads to fatal ventricular arrhythmias and even sudden death. Inherited LQT3 linked to mutations in *SCN5A* has also been directly linked to SIDS [6–10]. *SCN5A* is the major gene known to functionally encode the α-subunit of the human cardiac voltage-gated Na^+ channel, which is responsible for the initiation and propagation of the cardiac action potential. The hallmark of the gating change in LQT3 mutations is the presence of persistent inward Na^+ currents due to incomplete inactivation or late re-opening of Na^+ channels, as a result, QT interval prolongation. Most LQT3 mutations are located in the III–IV linker, various domains of the S4–S5 linkers, voltage sensors, and the C-terminus of Na^+ channels, which are associated with the fast inactivation process. The S4–S5 linker of domain III plays a major role in the kinetics and voltage dependence of fast inactivation of Na^+ channels by acting as a docking site for the inactivation particle of the III–IV linker [11].

In this work we report a new SIDS mutation (S1333Y) in a 25-day-old infant, which is located in the S4–S5 linker of domain III [12], and we characterize its biophysical properties.

2. Methods

2.1. Clinical evaluation and molecular genetics

The local ethics committee approved the study protocol. The parents provided written informed consent. The death certificate indicated a diagnosis of SIDS, while the autopsy, toxicology, and review of the circumstances of death were negative. Genomic DNA

* Corresponding author. Address: Le Centre de Recherche Université Laval Robert-Giffard, Local F-6539, 2601 Chemin de la Canardière, Québec City, QC, Canada G1J 2G3. Fax: +1 418 663 8756.
E-mail address: mohamed.chahine@phc.ulaval.ca (M. Chahine).

0014-5793/$36.00
doi:10.1016/j.febslet.2009.02.007

was extracted from whole blood using a WIZARD Genomic DNA Purification kit (Promega, Madison, WI, USA). The coding exons of the *KCNQ1*, *KCNH2*, *SCN5A*, *KCNE1*, and *KCNE2* genes were amplified separately using intronic primers and previously reported PCR conditions [13]. Denaturing high performance liquid chromatography (DHPLC) was performed using previously described elution profiles and melting temperatures [12]. PCR products with divergent chromatographic profiles were directly sequenced on both strands using the BigDye® Terminator v.31 Cycle sequencing kit (Applied Biosystems, Forster City, CA, USA) and were applied to an ABI 3100 automatic sequencer.

2.2. Mutagenesis

Mutant hNa$_v$1.5/S1333Y was generated using a QuickChange TM site-directed mutagenesis kit according to the manufacturer's instructions (Stratagene, La Jolla, CA, USA). The oligo-nucleotide primers containing the corresponding S1333Y mutation were synthesized using the following sequences:

5′-GTG GCC GTC GCC ATC CCG TAC ATC ATG AAC GTC CTC-3′ (forward primer) and 5′-GAG GAC GAG GTT CAT GAT GTA CGG GAT GGC GCC CAC-3′ (reverse primer).

The mutated site is underlined. Mutant and WT Na$_v$1.5 channels were inserted in a pcDNA1 construct and were purified using Qiagen columns (Qiagen Inc., Chatsworth, CA, USA).

2.3. TsA201 transfection and patch clamp experiments

Mutant channels were coexpressed with the β subunit in the tsA201 human cell line and characterized using the patch clamp technique in whole-cell configuration as already reported [14].

2.4. Solutions and reagents

For the whole-cell recordings, the patch pipettes were filled with 35 mM NaCl, 105 mM CsF, 10 mM EGTA, and 10 mM Cs-HEPES. The pH was adjusted to 7.4 using 1 N CsOH. The bath solution contained 150 mM NaCl, 2 mM KCl, 1.5 mM $CaCl_2$, 1 mM $MgCl_2$, 10 mM glucose, and 10 mM Na-HEPES. The pH was adjusted to pH 7.4 using 1 N NaOH (final Na^+: 152.4 mM). The liquid junction potential between the patch pipette and the bath solution was corrected to −7 mV.

2.5. Statistical analysis

Results are presented as means ± standard errors of the mean. Statistical comparisons were made using the unpaired Student's *t*-test in SigmaStat (Jandel Scientific Software, San Rafael, CA, USA). Differences were considered significant at $P < 0.05$.

3. Results

3.1. Identification of the SCN5A mutation S1333Y

The genomic DNA of the SIDS infant was screened for sequence changes in all 28 exons of *SCN5A* by DHPLC analysis. The PCR analysis of the *SCN5A* gene revealed a mutation that was a compound heterozygote with *SCN5A*/S1333Y and *KCNE1*/T20I (Fig. 1A and B). The family members of the infant were screened clinically and genetically. *SCN5A*/S1333Y was a spontaneous mutation and the father was found to be the carrier of the *KCNE1*/T20I mutation with no LQTS-related phenotypes. Other family members were negative in the screen. It was hypothesized that the S1333Y mutation is

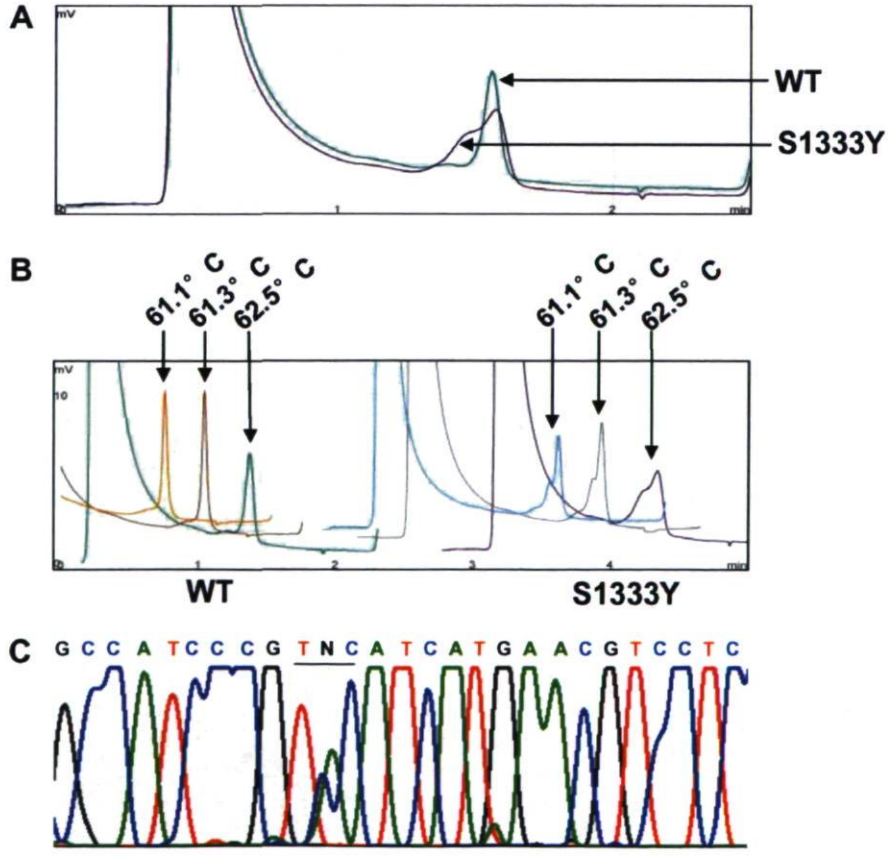

Fig. 1. Molecular identification of S1333Y. (A) DHPLC elution profiles of S1333Y identified in exon 23 of *SCN5A* at 62.5 °C. (B) DHPLC elution profile of S1333Y identified in exon 23 of *SCN5A* at 61.1, 61.3, and 62.5 °C. (C) Sequencing analysis showing a C-to-A substitution at position 3998 in exon 23, leading to a serine (S)-to-tyrosine (T) substitution at residue 1333.

responsible for the sudden death event in the patient. The sequencing analysis revealed a heterozygous C-to-A base change at position 3998 in exon 23 that resulted in a serine (S)-to-tyrosine (Y) substitution at residue 1333 (Fig. 1C). The mutation was in the S4–S5 linker in domain III, which plays a major role in fast inactivation of the Na^+ channel. This amino acid is highly conserved in the Na^+ channels of many species.

3.2. Biophysical characteristics of $Na_v1.5$/S1333Y

Whole-cell Na^+ currents were elicited by depolarizing steps from −100 to +50 mV with a holding potential of −140 mV (Fig. 2A). Current amplitudes were normalized to cellular membrane capacitance to generate current–voltage (I–V) curves in the form of current densities. Using the same data and graphically determined reversal potentials, the Na^+ conductance for the various voltages was calculated from the equation $G = I/(V - E_{rev})$, where I is the peak Na^+ current at a given voltage V and E_{rev}, the equilibrium potential extrapolated from the graph. I–V and conductance–voltage (G–V) curves were obtained for S1333Y and WT. The S1333Y mutant and WT channels had similar current densities, suggesting that they were expressed to the same extent on the cell membrane (Fig. 2B). The potential of the maximum peak current amplitude of the S1333Y channel was more negative than

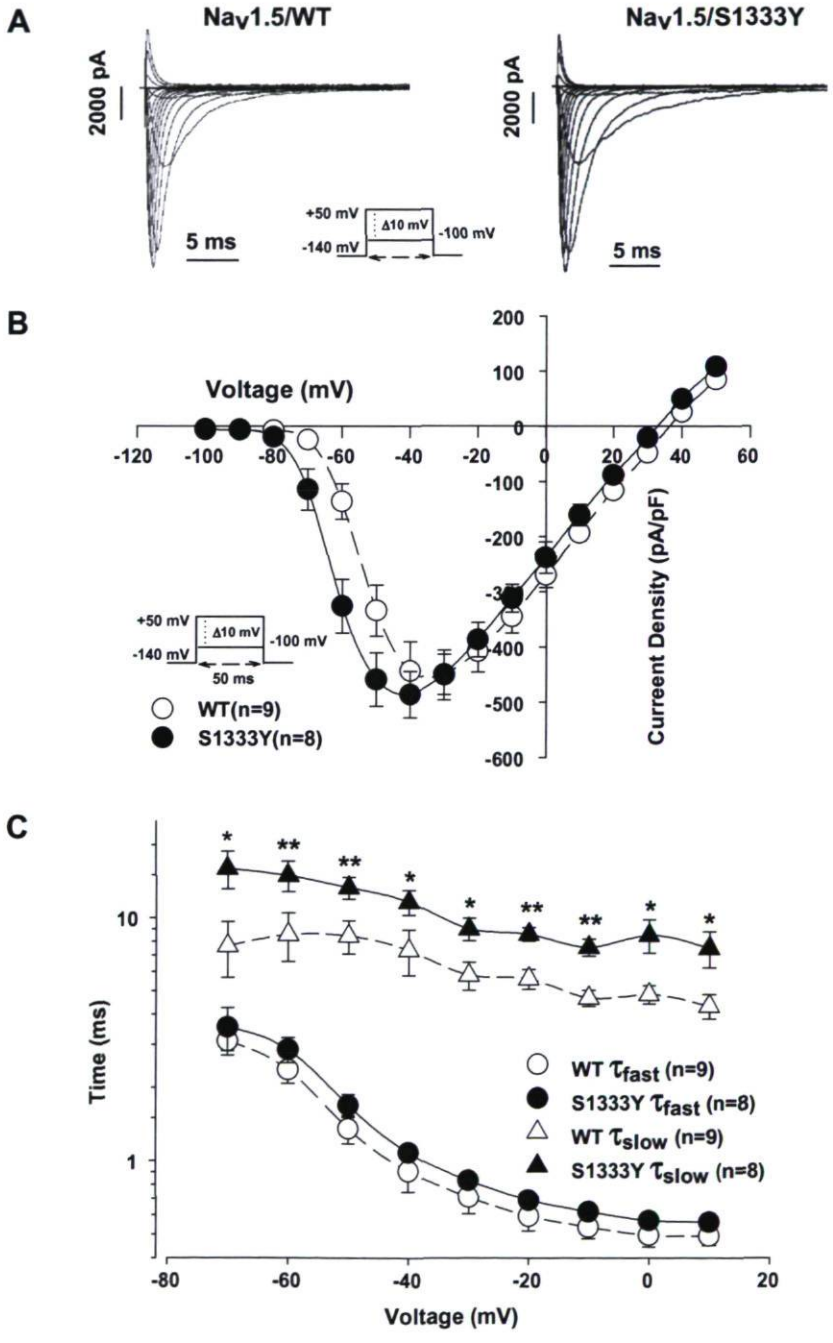

Fig. 2. Analysis of whole-cell currents recorded from tsA201 cells expressing WT and S1333Y. (A) I_{Na} from WT (left) and S1333Y (right) were elicited by depolarizing pulses from −100 mV to +50 mV in 10 mV increment for each step. (B) Current–voltage relationship of WT (○, $n = 9$) and S1333Y (●, $n = 8$). The current amplitude was normalized to the membrane capacitance. (C) The voltage-dependent time constants of inactivation in WT (○ for τ_{fast}, $n = 9$ and △ for τ_{slow}, $n = 9$) and S1333Y (● for τ_{fast}, $n = 8$ and ▲ for τ_{slow}, $n = 8$). Currents were fitted to a two-exponential function, obtaining the corresponding time constants τ_{fast} and τ_{slow} ($^*P < 0.05$ and $^{**}P < 0.01$).

that of the WT channel (Fig. 2B), which may be due to the coupled alteration of steady-state activation and inactivation. To analyze the effect of the S1333Y mutation on fast inactivation kinetics, the time constant τ was measured by fitting the decay of the whole-cell current elicited at each potential with the following double-exponential function: $I = I_{resid} + A_{fast} \times \exp(-(t-k)/\tau_{fast}) + A_{slow} \times \exp(-(t-k)/\tau_{slow})$, where I is the current density, I_{resid} the steady-state asymptotic residue, A_{fast} and A_{slow} are the percentages of channels inactivating with time constants τ_{fast} and τ_{slow}, and k is the time shift. Depolarizing steps from 2 to 50 ms were tested to ensure full current decay and the best fit. The S1333Y channel had a significantly longer time constant for the slow component than the WT channel over the entire voltage range from −70 mV to +10 mV (Fig. 2C). The most significant difference was at −20 mV, where the time constant τ_{slow} was 8.56 ± 0.54 ms ($n = 8$) for S1333Y and 4.67 ± 0.36 ms ($n = 9$) for WT. The slower decay of τ_{slow} indicated a decelerated inactivation of open channels. G–V curves were fitted to a standard Boltzmann distribution $G(V)/G_{max} = 1/(1 + \exp(-(V - V_{1/2})/k))$, where $G(V)$ is the conductance at a given voltage V and G_{max} is the maximum conductance. The midpoint of activation voltage ($V_{1/2}$) and the slope factor (k) were determined from the fit. The steady-state activation of the S1333Y mutation was negatively shifted by 8 mV, with no difference in the slope factor (Fig. 3A, and values in Table 1).

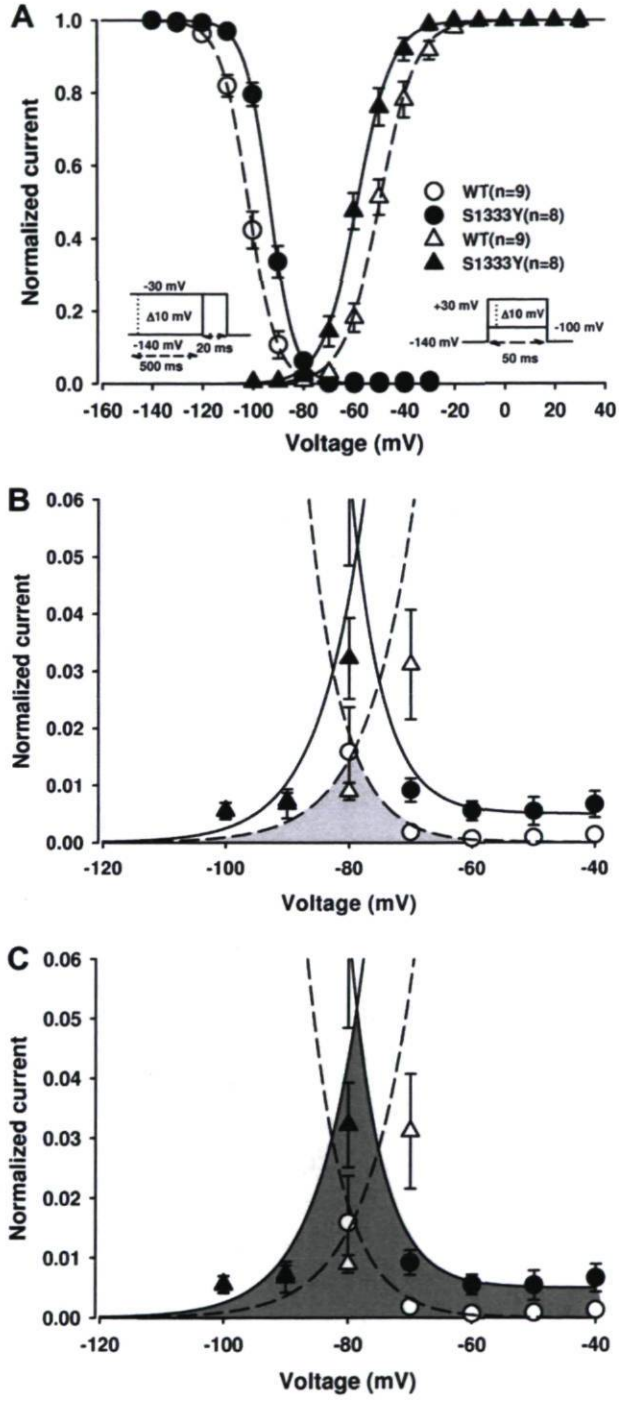

Fig. 3. The gating properties of steady-state activation and inactivation, and window currents. (A) Voltage-dependence of steady-state activation and inactivation in WT (△ for activation, $n = 9$ and ○ for inactivation, $n = 9$) and S1333Y (▲ for activation, $n = 8$ and ● for inactivation, $n = 8$). The activated and inactivated currents were generated from the protocols as inset, and their resulting data were fitted to a standard Boltzmann distribution. (B) The enlarged portion of overlap area (light grey) between activation and inactivation for WT. The shaded area represents the window region. (C) The enlarged part of overlap area (dark grey) between activation and inactivation for S1333Y. The shaded area was significantly enhanced than that of WT.

Voltage-dependent steady-state inactivation was measured by applying 500 ms pre-pulses ranging from −140 to −30 mV, followed by a 20 ms test pulse at −30 mV. The test pulse current amplitude was normalized to the maximum current recorded during the pre-pulse and plotted versus the pre-pulse voltage to obtain the voltage-dependent inactivation curve, which was fitted to a standard Boltzmann distribution function $I(V)/I_{max} = 1/(1 + \exp((V - V_{1/2})/k))$, where $I(V)/I_{max}$ is the current ratio and V, the pre-pulse voltage. During steady-state inactivation, $a + 7$ mV shift for S1333Y was observed, but the slope factor was not significantly affected (Fig. 3A). $V_{1/2}$ and k were generated by fitting each data set with the standard Boltzmann function (see Table 1 for values).

Steady-state activation and inactivation shifts appeared to increase the window current for S1333Y, which is generated by the overlap between these two fitting curves (Fig. 3B and C). The window current in LQT3 is associated with steady-state Na^+ channels reopening. S1333Y (Fig. 3C) significantly enhanced area of the window current compared to WT (Fig. 3B).

During slow inactivation, some voltage-gated Na^+ channels become non-conducting following prolonged membrane depolarization. The course of slow inactivation was assessed using a two-pulse protocol with an initial conditioning pre-pulse and a final

Table 1
Biophysical properties of $Na_v1.5$/WT and $Na_v1.5$/S1333Y.

	$Na_v1.5$/WT	$Na_v1.5$/S1333Y
Steady-state activation		
$V_{1/2}$ (mV)	−50.34 ± 2.06 ($n = 9$)	−58.88 ± 1.25* ($n = 8$)
K (mV)	−6.38 ± 0.27 ($n = 9$)	−6.13 ± 0.34 ($n = 8$)
Steady-state inactivation		
$V_{1/2}$ (mV)	−100.47 ± 1.34 ($n = 9$)	−93.46 ± 0.66** ($n = 8$)
K (mV)	4.91 ± 0.19 ($n = 9$)	4.91 ± 0.21 ($n = 8$)
Slow inactivation		
τ (ms)	327.78 ± 37.10 ($n = 8$)	306.96 ± 22.87 ($n = 9$)
Recovery from slow inactivation		
τ_{fast} (ms)	16.49 ± 4.73 ($n = 7$)	4.08 ± 0.60** ($n = 7$)
τ_{slow} (ms)	251.81 ± 60.79 ($n = 7$)	104.41 ± 27.06* ($n = 7$)
A_{fast}	91.7 ± 0.82% ($n = 7$)	94.33 ± 0.72% ($n = 7$)
A_{slow}	8.3 ± 0.82% ($n = 7$)	5.67 ± 0.72% ($n = 7$)
Closed-state inactivation		
−110 mV		
τ (ms)	89.54 ± 10.76 ($n = 9$)	60.28 ± 4.11* ($n = 9$)
−100 mV		
τ (ms)	109.51 ± 14.12 ($n = 9$)	65.82 ± 5.33** ($n = 10$)

$V_{1/2}$ = midpoint for activation or inactivation; K_v = slow factor for activation or inactivation; τ = time constant; and A = fraction of recovery component.
* $P < 0.05$.
** $P < 0.01$.

test pulse. A −30 mV pre-pulse was applied at intervals varying from 2 to 1000 ms, followed by a step to −140 mV for 20 ms to allow the channels to recover from fast inactivation. The −30 mV test pulse was applied for 40 ms to estimate the fraction of channels available for activation. The fraction was obtained by dividing the current amplitude during the test pulse by the current amplitude during the pre-pulse. Entry into slow inactivation followed a mono-exponential function $I = I_{resid} + A \times \exp(-t/\tau)$, where I is the current intensity, I_{resid} the asymptotic residual current, and A the current amplitude at time zero (see values in Table 1). As shown in Fig. 4A, there was no significant difference in the kinetics of entry into slow inactivation between the S1333Y mutation and WT. Recovery from slow inactivation was measured using a two-pulse protocol, where Na^+ channels were inactivated by a

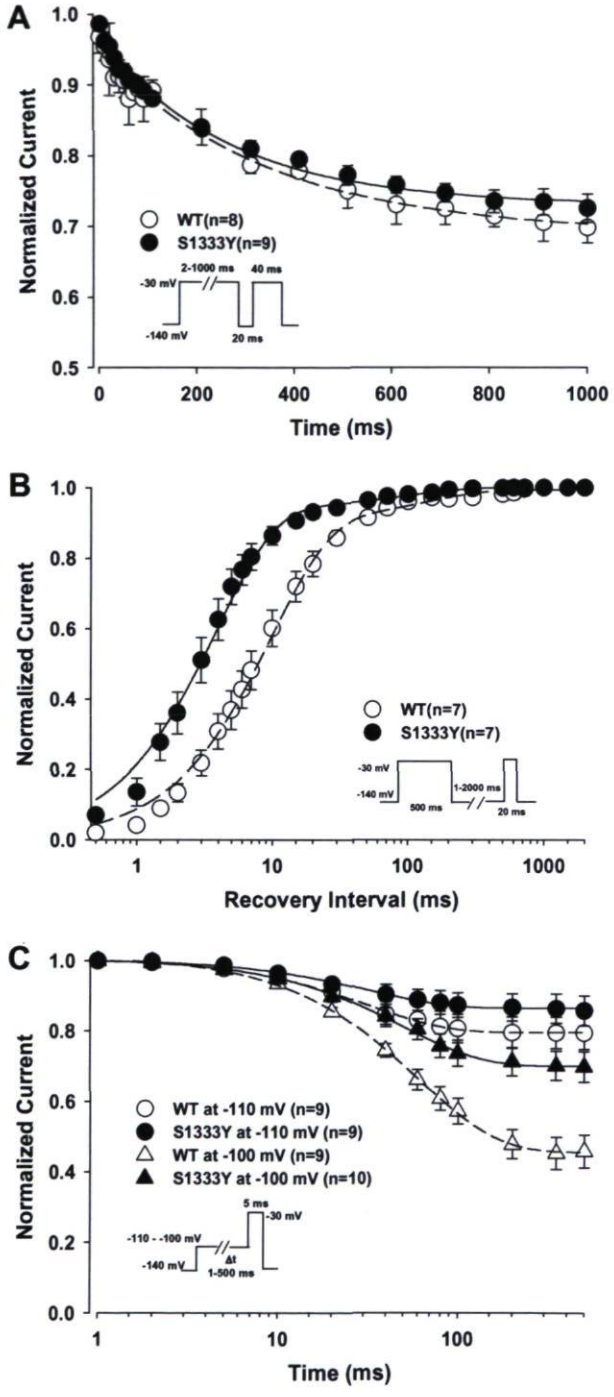

Fig. 4. The gating properties of slow inactivation, recovery from slow inactivation, and closed-state inactivation. (A) Slow inactivation in WT (○, $n = 8$) and S1333Y (●, $n = 9$). A two-pulse protocol as inset was used to generate the currents. The time constants (shown in Table 1) were obtained using a mono-exponential function. (B) Time courses of recovery from slow inactivation in WT (○, $n = 7$) and S1333Y (●, $n = 7$). A 500 ms conditioning pre-pulse was used to monitor recovery by a 20 ms test pulse after a variable recovery interval from 1 to 2000 ms (see protocol in inset). The time constants were obtained using a two-exponential function. (C) Closed-state inactivation in WT (○ for −110 mV, $n = 9$ and △ for −100 mV, $n = 9$) and S1333Y (● for −110 mV, $n = 9$ and ▲ for −100 mV, $n = 10$). The protocol in inset elicited the currents, which were fitted to a mono-exponential function.

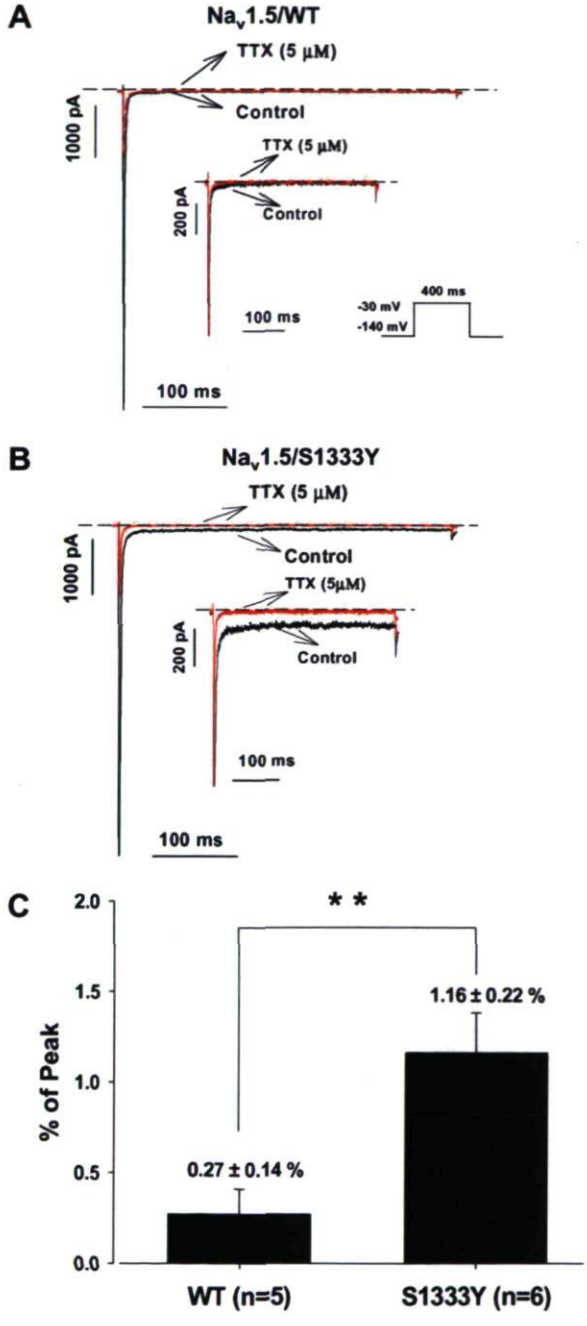

Fig. 5. Effect of TTX on the persistent sodium current in WT and S1333Y. The persistent sodium current was generated from a holding potential of +140 mV to −30 mV over 400 ms (see protocol in inset). The dashed line represents zero current. (A) Effect of adding 5 μM TTX to WT for 10 min. (B) Effect of adding 5 μM TTX to S1333Y for 10 min. The persistent sodium current was blocked by TTX. (C) The histogram of the persistent sodium current. The persistent sodium current accounted for 0.27 ± 0.14% of the peak current amplitude for WT ($n = 5$) and 1.16 ± 0.22% for S1333Y ($n = 6$) at −30 mV ($^{**}P < 0.01$).

−30 mV conditioning pulse for 500 ms, followed by a −30 mV test pulse after a recovery interval varying from 1 to 2000 ms. The peak current in response to the test pulse was normalized to the maximum peak current in response to the conditioning pulse. The normalized current was plotted against the recovery time interval. The resulting curve was fitted to a double-exponential function to obtain the following fast and slow components of recovery from slow inactivation: $I_{Na} = A_f \times (1 - \exp[-t/\tau_f]) + A_s \times (1 - \exp[-t/\tau_s])$, where t is the recovery time interval, τ_f and τ_f, the time constants of the fast and slow components, and A_f and A_s, the fractions of the fast and slow components (see values in Table 1). The results shown in Fig. 4B indicate that S1333Y recovered more rapidly from slow inactivation than WT.

The positive shift of the steady-state inactivation may be the result of fewer channels entering into closed-state inactivation (Fig. 4C). Closed-state inactivation primarily affects the availability of channels at voltages near the resting membrane potential, thus controlling the Na^+ current amplitude of the action potential. Using a double-pulse protocol, cells were pre-pulsed to −110 and −100 mV for periods ranging from 1 to 500 ms, and then stepped to −30 mV to determine the availability of I_{Na} during the pre-pulse. The time course was fitted with the following mono-exponential equation: $I = I_{resid} + A \times \exp(-t/\tau)$ (see values in Table 1).

Whole-cell Na^+ currents recorded in tsA201 cells expressing the WT *SCN5A* gene can exhibit a small persistent component whose magnitude depends on the recording conditions. The increased persistent Na^+ current in LQT3 mutants is a major factor in the prolongation of the QT interval. To study the contribution of the persistent current at steady-state, we measured the current using a 400 ms depolarization pulse. The persistent current was barely detectable in cells expressing WT channels ($I_{per}/I_{peak} = 0.27 \pm 0.14\%$, $n = 5$), while there was a significant increase in the persistent current in cells expressing the S1333Y mutation ($I_{per}/I_{peak} = 1.16 \pm 0.22\%$, $n = 6$) (Fig. 5C). Class I B Na^+ channel blockers (e.g., lidocaine) were reported to normalize prolonged QTc in LQT3 patients [15]. We therefore investigated the effect of lidocaine on the persistent inward Na^+ current of the S1333Y mutation. The persistent currents in WT and S1333Y were both blocked by 5 μM tetrodotoxin (TTX) (Fig. 5A and B) and 200 μM lidocaine (Fig. 6A and B), respectively.

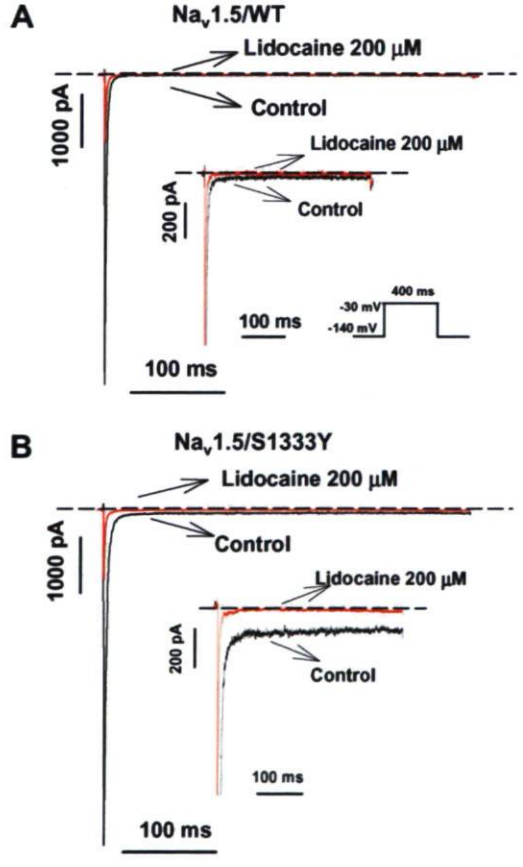

Fig. 6. Effect of lidocaine on the persistent sodium current in WT and S1333Y. The persistent sodium current was generated from a holding potential of +140 mV to −30 mV for 400 ms (see protocol as inset). The dashed line represents zero current. (A) Effect on WT of an 8-min treatment with 200 μM lidocaine on WT. (B) Effect on S1333Y of an 8-min treatment with 200 μM lidocaine. The persistent sodium current was blocked by lidocaine.

4. Discussion

In the present study, we biophysically characterized a new *SCN5A* mutation (S1333Y) in an infant who had died of SIDS. The mutation was located in the S4–S5 linker of domain III, which is often associated with inactivation changes in voltage-dependent Na^+ channels. The electrophysiological studies showed persistent Na^+ inward currents accompanied by a −8 mV shift in activation, and a +7 mV shift in inactivation. The window current was therefore enhanced by the shifts of activation and inactivation. The slow component of the fast activation of macroscopic currents of the mutation was slower than that of the WT. The serine at position 1333 is highly conserved, suggesting that this residue may play an important role in the channel gating.

Some inherited arrhythmic disorders (e.g., Brugada syndrome (BrS) and LQTS) appear to be associated with SIDS because they may explain the increased likelihood of sudden death when a trigger event occurs. Since the gating properties of BrS mutations are characterized by a loss of the Na^+ channel function, the present case is unlikely to be related to BrS.

The S1333Y mutation caused a serine-to-tyrosine substitution in the S4–S5 linker of domain III, which is near the proposed docking site of the inactivation particle. This mutation caused similar alterations in activation, fast inactivation, and kinetics of fast inactivation. Many LQT3 mutations have a persistent Na^+ current along with shortened fast inactivation time constants. However, R1623Q showed a slower rate of current decay that is in agreement with our results [16]. Reduced closed-state inactivation is consistent with the positive shift of inactivation. The rate of recovery from inactivation was also faster, which is in agreement with the findings reported for LQT3 mutations (ΔKPQ, R1644H, and E1784K) [14,17,18]. Faster recovery may increase the channel availability at the resting membrane potential of the ventricular cells. The shifts of activation and inactivation of the mutant enhanced the window current and an action potential could be triggered in this narrow region, The enhanced window currents can increase the risk of fatal ventricular arrhythmias especially when they coexist with persistent inward Na^+ currents. The A1330P *SCN5A* mutation, which also causes SIDS, is located near the site of the S1333Y mutation. A1330P causes a gain of Na^+ channel function by significantly increasing the window current. Interestingly, this mutation does not induce a persistent Na^+ current [7].

Mutations in the Na^+ channel associated with LQT3 usually result in a persistent Na^+ current flowing during the plateau phase of the cardiac action potential. At least five LQT3 mutations (S941N, A1330P, S1103Y, R1826H, and A997S) have been associated with SIDS [6–9]. Of these, two (R1826H and A997S) have a persistent inward Na^+ current. Moreover, in studies on relationships between cardiac polymorphisms and SIDS, a persistent Na^+ current was found in five of eight variants [19]. Such a persistent current may cause slower inactivation, resulting in prolonged

repolarization and thus a long QT interval. In the present study, the S1333Y mutation caused a persistent current that accounted for 1.16 ± 0.22% of the current amplitude. While there are no documented clinic findings to support the diagnosis of LQTS, we suspect that fatal ventricular arrhythmia may be triggered by an event such as the prone position during sleep.

We also found that the persistent current induced by S1333Y was sensitive to lidocaine. This suggests that the prolonged QT interval could be normalized by class I B Na^+ channel blockers. The mechanism of blocking the persistent current may be acted by lidocaine stabilizing inactivation, and thereby reducing the probability of dispersed and bursting activities in LQT3 mutant channels [20].

In the case presented here, sudden death occurred 25 days after delivery, and resuscitatory efforts were not possible given that SIDS happened too quickly. To prevent the sudden death event, a more effective way would be to diagnose the condition soon after delivery using the ECG that is faster and less expensive to perform. For those with a family history of SIDS and bradycardia, genetic analyses are recommended when the QTc exceeds 440 ms [8,21].

Acknowledgements

We would like to thank Valérie Pouliot for her technical assistance. This study was supported by a funding from the Heart and Stroke Foundation of Québec (HSFQ) and a grant from the Canadian Institutes of Health Research. M. Chahine is a J.C. Edwards Foundation Senior Investigator.

References

[1] Dwyer, T., Ponsonby, A.L., Newman, N.M. and Gibbons, L.E. (1991) Prospective cohort study of prone sleeping position and sudden infant death syndrome. Lancet 337, 1244–1247.
[2] Vege, A. and Ole, R.T. (2004) Sudden infant death syndrome, infection and inflammatory responses. FEMS Immunol. Med. Microbiol. 42, 3–10.
[3] Hunt, C.E. and Hauck, F.R. (2006) Sudden infant death syndrome. CMAJ 174, 1861–1869.
[4] Opdal, S.H. and Rognum, T.O. (2004) The sudden infant death syndrome gene: does it exist? Pediatrics 114, e506–e512.
[5] Arnestad, M., Crotti, L., Rognum, T.O., Insolia, R., Pedrazzini, M., Ferrandi, C., et al. (2007) Prevalence of long-QT syndrome gene variants in sudden infant death syndrome. Circulation 115, 361–367.
[6] Ackerman, M.J., Siu, B.L., Sturner, W.Q., Tester, D.J., Valdivia, C.R., Makielski, J.C., et al. (2001) Postmortem molecular analysis of *SCN5A* defects in sudden infant death syndrome. J. Am. Med. Assoc. 286, 2264–2269.
[7] Wedekind, H., Smits, J.P.P., Schulze-Bahr, E., Arnold, R., Veldkamp, M.W., Bajanowski, T., et al. (2001) De novo mutation in the *SCN5A* gene associated with early onset of sudden infant death. Circulation 104, 1158–1164.
[8] Schwartz, P.J., Priori, S.G., Dumaine, R., Napolitano, C., Antzelevitch, C., Stramba-Badiale, M., et al. (2000) A molecular link between the sudden infant death syndrome and the long-QT syndrome. New Engl. J. Med. 343, 262–267.
[9] Plant, L.D., Bowers, P.N., Liu, Q., Morgan, T., Zhang, T., State, M.W., et al. (2006) A common cardiac sodium channel variant associated with sudden infant death in African Americans, SCN5A S1103Y. J. Clin. Invest. 116, 430–435.
[10] Wang, D.W., Desai, R.R., Crotti, L., Arnestad, M., Insolia, R., Pedrazzini, M., et al. (2007) Cardiac sodium channel dysfunction in sudden infant death syndrome. Circulation 115, 368–376.
[11] Smith, M.R. and Goldin, A.L. (1997) Interaction between the sodium channel inactivation linker and domain III S4–S5. Biophys J. 73, 1885–1895.
[12] Millat, G., Chevalier, P., Restier-Miron, L., Da Costa, A., Bouvagnet, P., Kugener, B., et al. (2006) Spectrum of pathogenic mutations and associated polymorphisms in a cohort of 44 unrelated patients with long QT syndrome. Clin. Genet. 70, 214–227.
[13] Wang, Q., Li, Z., Shen, J. and Keating, M.T. (1996) Genomic organization of the human *SCN5A* gene encoding the cardiac sodium channel. Genomics 34, 9–16.
[14] Deschênes, I., Baroudi, G., Berthet, M., Barde, I., Chalvidan, T., Denjoy, I., et al. (2000) Electrophysiological characterization of SCN5A mutations causing long QT (E1784K) and Brugada (R1512W and R1432G) syndromes. Cardiovasc. Res. 46, 55–65.
[15] Groenewegen, W.A., Bezzina, C.R., van Tintelen, J.P., Hoorntje, T.M., Mannens, M.M.A.M., Wilde, A.A.M., et al. (2003) A novel LQT3 mutation implicates the human cardiac sodium channel domain IVS6 in inactivation kinetics. Cardiovasc. Res. 57, 1072–1078.
[16] Kambouris, N.G., Nuss, H.B., Johns, D.C., Tomaselli, G.F., Marban, E. and Balser, J.R. (1998) Phenotypic characterization of a novel long-QT syndrome mutation (R1623Q) in the cardiac sodium channel. Circulation 97, 640–644.
[17] Dumaine, R., Wang, Q., Keating, M.T., Hartmann, H.A., Schwartz, P.J., Brown, A.M., et al. (1996) Multiple mechanisms of Na^+ channel-linked long-QT syndrome. Circ. Res. 78, 916–924.
[18] Chandra, R., Starmer, C.F. and Grant, A.O. (1998) Multiple effects of KPQ deletion mutation on gating of human cardiac Na^+ channels expressed in mammalian cells. Am. J. Physiol. 274, H1643–H1654.
[19] Wang, D.W., Desai, R.R., Crotti, L., Arnestad, M., Insolia, R., Pedrazzini, M., et al. (2007) Cardiac sodium channel dysfunction in sudden infant death syndrome. Circulation 115, 368–376.
[20] Dumaine, R. and Kirsch, G.E. (1998) Mechanism of lidocaine block of late current in long Q-T mutant Na^+ channels. Am. J. Physiol. 274, H477–H487.
[21] Schwartz, P.J., Stramba-Badiale, M., Segantini, A., Austoni, P., Bosi, G., Giorgetti, R., et al. (1998) Prolongation of the QT interval and the sudden infant death syndrome. New Engl. J. Med. 338, 1709–1714.

Biochemical and Biophysical Research Communications 380 (2009) 132–137

Contents lists available at ScienceDirect

Biochemical and Biophysical Research Communications

journal homepage: www.elsevier.com/locate/ybbrc

Gain-of-function mutation of $Na_v1.5$ in atrial fibrillation enhances cellular excitability and lowers the threshold for action potential firing

Qiuju Li [c], Hai Huang [a], Gele Liu [c], Khanh Lam [d], Julie Rutberg [c], Martin S. Green [c], David H. Birnie [c], Robert Lemery [c], Mohamed Chahine [a,b], Michael H. Gollob [c,e,*]

[a] Le Centre de Recherche Université Laval Robert-Giffard, Canada
[b] Laval University, Québec, Canada
[c] Division of Cardiology, University of Ottawa Heart Institute, Ottawa, Ont., Canada
[d] Department of Surgery, University of Ottawa Heart Institute, Ottawa, Ont., Canada
[e] Department of Cellular and Molecular Medicine, University of Ottawa, University of Ottawa Heart Institute, 40 Ruskin St., Rm. H350, Ottawa, Ont., Canada K1Y 4W7

ARTICLE INFO

Article history:
Received 17 December 2008
Available online 22 January 2009

Keywords:
Arrhythmia
Fibrillation
Genetics
$Na_v1.5$
SCN5A
Hyperexcitability
Electrophysiology
Atria
HL-1
Cardiomyocytes

ABSTRACT

Genetic mutations of the cardiac sodium channel (SCN5A) specific only to the phenotype of atrial fibrillation have recently been described. However, data on the biophysical properties of SCN5A variants associated with atrial fibrillation are scarce. In a mother and son with lone atrial fibrillation, we identified a novel SCN5A coding variant, K1493R, which altered a highly conserved residue in the DIII–IV linker and was located six amino acids downstream from the fast inactivation motif of sodium channels. Biophysical studies of K1493R in tsA201 cells demonstrated a significant positive shift in voltage-dependence of inactivation and a large ramp current near resting membrane potential, indicating a gain-of-function. Enhanced cellular excitability was observed in transfected HL-1 atrial cardiomyocytes, including spontaneous action potential depolarizations and a lower threshold for action potential firing. These novel biophysical observations provide molecular evidence linking cellular "hyperexcitability" as a mechanism inducing vulnerability to this common arrhythmia.

The cardiac sodium channel ($Na_v1.5$) plays a critical role in the generation of electrical activity in cardiac myocytes. Genetic mutations of the gene encoding the $Na_v1.5$ sodium channel (SCN5A) are associated with a variety of cardiac arrhythmia syndromes, including the Long QT syndrome type 3 (LQT3) [1], Brugada syndrome [2], and progressive cardiac conduction disease [3]. The biophysical abnormalities induced by disease-causing SCN5A mutations are diverse. In LQT3, SCN5A mutations result in a "gain-of-function" effect, invariably leading to a persistent late component of sodium current resulting in action potential prolongation [4]. In contrast, Brugada syndrome and conduction system disease are generally characterized by a primary loss of myocardial sodium current by various mechanisms, including impaired protein trafficking, more rapid inactivation kinetics, or altered voltage-dependence of activation [5,6].

A role of SCN5A mutations in the primary pathogenesis of atrial fibrillation (AF) is suggested by the known efficacy of sodium channel blocking agents in diminishing recurrences of AF. Further, genetic screening of SCN5A in a large cohort of patients with lone AF identified rare genetic variants of SCN5A in nearly 6% of AF cases [7]. Insight into the biophysical abnormalities of SCN5A mutations associated with lone AF is essential to understanding the molecular mechanisms of this common arrhythmia.

In this article, we describe unique electrophysiological characteristics of a novel SCN5A mutation associated with lone AF. The biophysical observations of this mutant $Na_v1.5$ channel are previously undescribed for the cardiac sodium channel, and include the demonstration of enhanced window current occurring near resting membrane potential, spontaneous action potential depolarizations and a lower threshold for action potential firing in transfected atrial cardiomyocytes. This study provides direct evidence of a novel molecular mechanism of cellular "hyperexcitability" inducing vulnerability to AF.

Methods

Molecular screening. Genomic DNA was extracted from whole blood from probands with "idiopathic" AF. Genetic analysis was

* Corresponding author. Address: Department of Cellular and Molecular Medicine, University of Ottawa, University of Ottawa Heart Institute, 40 Ruskin St., Rm. H350, Ottawa, Ont., Canada K1Y 4W7. Fax: +1 613 761 5060.
E-mail address: mgollob@ottawaheart.ca (M.H. Gollob).

0006-291X/$ - see front matter © 2009 Elsevier Inc. All rights reserved.
doi:10.1016/j.bbrc.2009.01.052

performed by direct DNA sequencing of the coding region of the GJA5, KCNQ1, KCNA5, and SCN5A genes. Affected and control patients in this study were of Western European descent. All study participants provided written informed consent and the research protocol was approved by the Ethics Board of the University of Ottawa Heart Institute.

Expression of $Na_v1.5$ in tsA201 cells and HL-1 atrial myocytes. Mutant $Na_v1.5$ (K1493R) was introduced into a wild-type (wt) $Na_v1.5$ pcDNA1 clone using the QuickChange mutagenesis kit (Stratagene, La Jolla, CA) and sequences confirmed using an ABI 377 DNA sequencer (Perkin-Elmer/Applied Biosytems, Foster City, CA, USA). TsA201 cells were grown in high glucose DMEM supplemented with FBS (10%), L-glutamine (2 mM), penicillin (100 U/ml), and streptomycin (10 mg/ml) (Gibco BRL Life Technologies, Burlington, ON, Canada). The cells were transfected with 5 μg of cDNA coding for wt or mutant channel using the calcium phosphate method.

HL-1 cells, an atrial myocyte derived cell line, were a generous gift from Dr. William Claycomb (Louisiana State University Health Sciences Center, New Orleans, LA). HL-1 cells were grown in 35 mm culture dishes to 50–70% confluency in Claycomb medium containing 10% FBS, 100 U/ml of penicillin, 100 μg/ml streptomycin, and 0.1 mM norepinephrine. Cells were transfected in serum free and antibiotic free Claycomb medium containing 2 μl lipofectamine 2000 and 1 μg $Na_v1.5$/wt or $Na_v1.5$/K1493R mutant expression vectors mixed with 1 μg pECFP expression vector to denote cells that received the wild-type or mutant $Na_v1.5$. Only cells that exhibited cyano fluorescence were selected for further electrophysiological experiments.

Electrophysiological experiments. $Na_v1.5$ currents from tsA201 transfected cells were recorded using the whole-cell configuration of the patch clamp technique. Patch clamp recordings were made using low resistance electrodes (<1 MΩ), and a routine series resistance compensation by an Axopatch 200 amplifier (Axon Instruments, Foster City, CA, USA) was performed to minimize voltage-clamp errors. The patch pipette contained 35 mM NaCl, 105 mM CsF, 10 mM EGTA, and 10 mM Cs-Hepes. The bath solution contained 150 mM NaCl, 2 mM KCl, 1.5 mM $CaCl_2$, 1 mM $MgCl_2$, 10 mM glucose, and 10 mM Na-Hepes. The pH of all solutions was adjusted to 7.4. Voltage-clamp command pulses were generated by microcomputer using pCLAMP software v8.0 (Axon Instruments). Experiments were carried out at room temperature.

In HL-1 atrial cardiomyocytes, recordings were carried out using the current-clamp analysis at room temperature. Cells were perfused with a solution of 140 mM NaCl, 3 mM KCl, 2 mM $MgCl_2$, 2 mM $CaCl_2$, 10 mM Hepes, 10 mM glucose, pH 7.35. The recording pipette had a resistance of 2.5–3.5 MΩ when filled with an internal solution containing (in mM): 140 mM KCl, 5 mM Hepes, 0.5 mM EGTA, 20 mM glucose, 3 mM Na_2ATP, and 0.5 mM GTP, pH 7.35. Action potentials (APs) were induced by injecting a current of 800 pA for a duration of 4 ms. When required, current was applied to set a holding potential of −60 mV. AP traces were acquired and analyzed with pClamp software, filtered at 10 kHz and sampled at 20 kHz. To study the threshold for action potential elicitation, increasing amplitude of current was injected in 50 pA increments ranging from 100 to 800 pA until an AP was induced. The minimum current injected eliciting an AP was considered the threshold.

Data are presented as means ± standard error of the mean (SEM). When indicated, a *t*-test was performed using statistical software in SigmaPlot (Jandel Scientific Software, San Rafael, CA, USA).

Results

Mutation detection and clinical phenotype

DNA sequencing identified a novel, heterozygous mutation in exon 26 of the SCN5A gene in a single proband and his affected mother. This mutation leads to an amino acid substitution of lysine for arginine (K1493R) in the DIII–IV linker of the $Na_v1.5$ channel (Fig. 1A). K1493 is a highly conserved amino acid across species and is six amino acids downstream from the fast inactivation IFM (isoleucine–phenylalanine–methionine) motif of sodium channels (Fig. 1B) [8]. This genetic variant was absent from 200 alleles of an ethnically matched, healthy control cohort.

The affected proband developed AF at age 50. Coronary angiography documented normal coronary arteries. Echocardiography noted normal left atrial size, and normal left ventricular size and function. Twelve-lead electrocardiograms during normal sinus rhythm and AF consistently demonstrated a normal QTc interval (Fig. 1C). The proband's mother was diagnosed with AF at age 63 following many years of symptomatic palpitations. Her previous cardiac investigations documented a normal myocardial perfusion scan and normal parameters on echocardiography, aside from a mildly enlarged left atrium. The proband's only sibling, a brother, is healthy at age 60, and is not a carrier of the K1493R mutation.

Electrophysiological data

In mammalian tsA201 cells, activation and inactivation kinetics for wt and mutant $Na_v1.5$ showed no differences in peak current or current density (Fig. 2A and B). To compare the time course of inactivation for both channels, current decay was fitted with a double exponential function. Fig. 2C shows that time constants of both fast and slow inactivation were slower for mutant $Na_v1.5$/K1493R. For example, at +10 mv, $Na_v1.5$/wt: $\tau f = 0.45 \pm 0.02$ ms, $\tau s = 3.72 \pm 0.40$ ms; $Na_v1.5$/K1493R: $\tau f = 0.58 \pm 0.02$ ms, $\tau s = 5.05 \pm 0.54$ ms, $p < 0.01$.

To investigate the gating properties of $Na_v1.5$/K1493R and $Na_v1.5$/wt, we next analyzed the voltage-dependence of steady-state activation and inactivation. The potential for half-maximal activation and slope factor were similar for wt and mutant channels ($Na_v1.5$/wt: $V_{1/2} = -56.59 \pm 1.72$ mV, $k = -5.6$, $n = 6$; $Na_v1.5$/K1493R: $V_{1/2} = -58.17 \pm 0.79$ mV, $k = -5.3$, $n = 6$, p = NS). In contrast, $V_{1/2}$ for inactivation was significantly shifted to more positive potentials for mutant $Na_v1.5$ as compared to $Na_v1.5$/wt channels, without significant change in their respective slope factors ($Na_v1.5$/wt: $V_{1/2} = -104.33 \pm 1.58$ mV, $k = 4.79$, $n = 6$; $Na_v1.5$/K1493R: $V_{1/2} = -99.20 \pm 1.34$ mV, $k = 4.81$, $n = 6$, $p < 0.05$) (Fig. 2D). This depolarizing shift in steady-state inactivation produced a greater overlap of activation and inactivation curves resulting in a larger "window current" (Fig. 2E), predicting an increase in channel availability in the range of the resting membrane potential of atrial myocytes. To confirm a gain of frequency-dependent current for the mutant channel, currents were elicited by slow ramp depolarizations. Significantly larger ramp currents were elicited for mutant $Na_v1.5$/K1493R channels as compared to wt channels (Fig. 2F). The averaged peak ramp current occurred at a voltage of -67.11 ± 1.89 mV for the mutant channel, and was consistently larger than wt channels at all ramp slopes tested (data not shown). In view of the observed gain-of-function properties of the mutant $Na_v1.5$/K1493R, we evaluated whether this mutant imbues a late, persistent inward sodium current. No substantial persistent inward current at the end of a 400 ms depolarization was observed for either wt or mutant channel (Fig. 3A and B). Analyses of intermediate inactivation, time course of recovery from slow inactivation, and voltage-dependence of deactivation did not differ between wt and mutant $Na_v1.5$ channels (Fig. 3C–E).

Lastly, we assessed the effect of $Na_v1.5$/wt and $Na_v1.5$/K1493R mutant channels on the action potential (AP) duration and cellular excitability in HL-1 atrial cardiomyocytes. Induced AP duration did not differ in cells transiently expressing $Na_v1.5$/wt or $Na_v1.5$/K1493R channels, consistent with the absence of late, persistent sodium current (Fig. 4A and B). Next, we measured the threshold

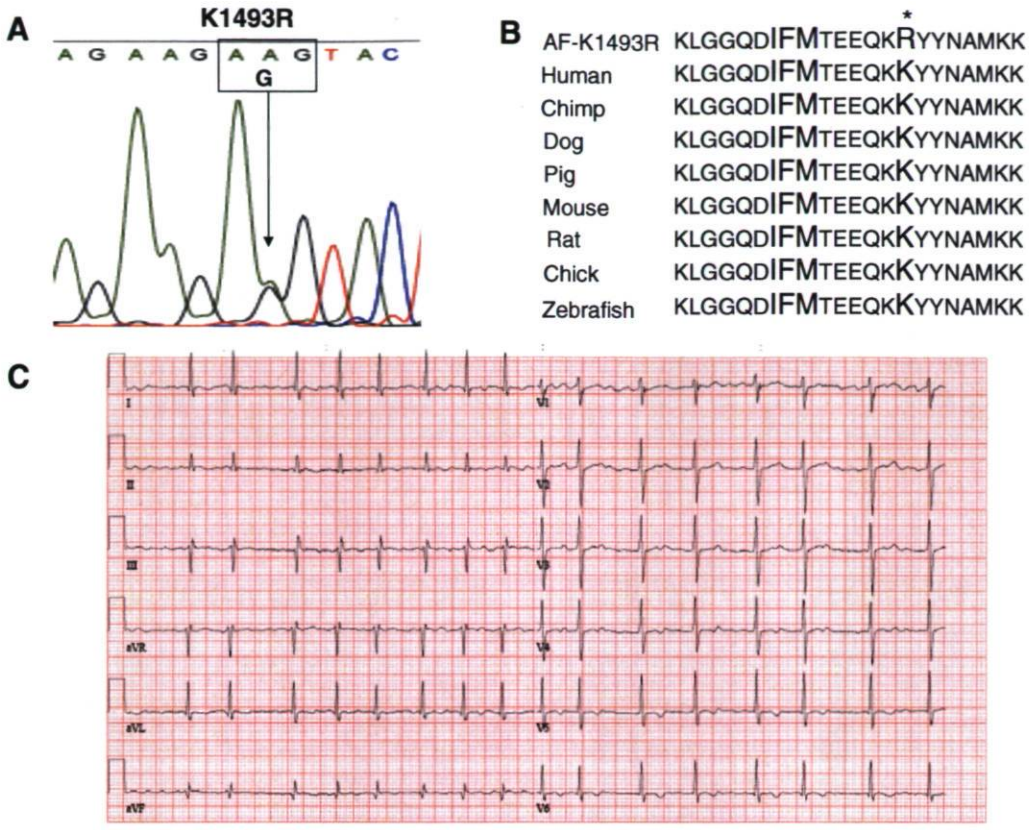

Fig. 1. Mutation and clinical data. (A) DNA sequence indicating the mutation in exon 26 of the SCN5A gene. (B) K1493 is in close proximity to the fast inactivation motif (IFM) within the $Na_v1.5$ channel and is highly conserved across species. (C) Representative ECG recording from the proband during atrial fibrillation. A normal QT interval is present.

of depolarization for elicitation of an all-or-none AP. HL-1 cells expressing mutant $Na_v1.5$/K1493R channels required 25% less depolarizing current for AP elicitation as compared to cells expressing wt channel ($Na_v1.5$/wt 693.3 ± 37.5 pA, $Na_v1.5$/K1493R 525 ± 30 pA, $p < 0.005$) (Fig. 4C). In addition, spontaneous cellular depolarizations were observed in 4 of 13 cells (31%) expressing mutant $Na_v1.5$/K1493R as compared to only 2 of 16 cells (12.5%) expressing $Na_v1.5$/wt (Fig. 4D), reaffirming a hyperexcitable phenotype induced by mutant $Na_v1.5$/K1493R. Mean amplitude of spontaneous depolarizations was 33.63 ± 17.97 mV in $Na_v1.5$/K1493 expressing cells versus 11.85 ± 1.36 mV in $Na_v1.5$/wt cells ($p < 0.05$). No difference was observed in resting membrane potential of HL-1 cardiomyocytes transfected with wt or mutant $Na_v1.5$ channels (data not shown).

Discussion

We describe the association of a novel genetic mutation in the voltage-gated cardiac sodium channel gene with lone atrial fibrillation. This missense K1493R mutation was present in a mother and son with early onset atrial fibrillation and no structural heart disease. The highly conserved, charged K1493 residue is located within the cytoplasmic loop domain which joins domains III and IV, and is six amino acids C-terminal to the fast inactivation IFM (isoleucine–phenylalanine–methionine) motif of the sodium channel. The IFM motif is invariable among sodium channels and is crucial to rapid channel inactivation following opening [8–10].

The unique gain-of-function properties exhibited by $Na_v1.5$/K1493R have not been previously described for the voltage-gated cardiac sodium channel. Consistent with the localization of the mutant to the fast inactivating region of the channel, mutant K1493R demonstrated a significant depolarizing shift in fast inactivation. These observations correlate with the site-directed mutagenesis studies of Miller et al. showing that deletion of charged lysines within the linker region of domains III and IV hasten the voltage dependence of sodium channel inactivation [10]. This alteration is expected to increase the fraction of channels available for activation close to resting potential due to an uncoupling of channel activation and inactivation. The increased overlap between activation and inactivation curves observed in our study resulted in an increased window current for the mutant channel. The window current represents a voltage region in which sodium channels continue to open, and therefore is predicted to lower the excitability threshold for excitable cells [11]. Indeed, expression of the wt and $Na_v1.5$/K1493R in HL-1 atrial cardiomyocytes confirmed a significantly lower depolarizing current threshold for single AP firing, and HL-1 cells expressing mutant $Na_v1.5$/K1493R demonstrated spontaneous depolarizations consistent with a hyperexcitable phenotype. AP duration in HL-1 cardiomyocytes were similar between cells expressing wt and mutant $Na_v1.5$ channels, consistent with the absence of late persistent current that is observed in $Na_v1.5$ gain-of-function mutations associated with LQT3.

Although not reported previously in the $Na_v1.5$ channel, non-inactivating sodium channel mutations resulting in larger window currents have been implicated in other inherited disorders of excitability [11–13]. In multiple animal models of spontaneous seizures, the voltage dependence of sodium current inactivation in neuronal cells was observed to be shifted toward depolarized potentials and resulted in increased window current, similar to our observations for the $Na_v1.5$/K1493R mutant [14–17]. The observed biophysical properties of sodium channel mutations responsible for epilepsy are consistent with the known efficacy of anti-epileptic drugs in functioning to shift the voltage dependence of inactivation in the

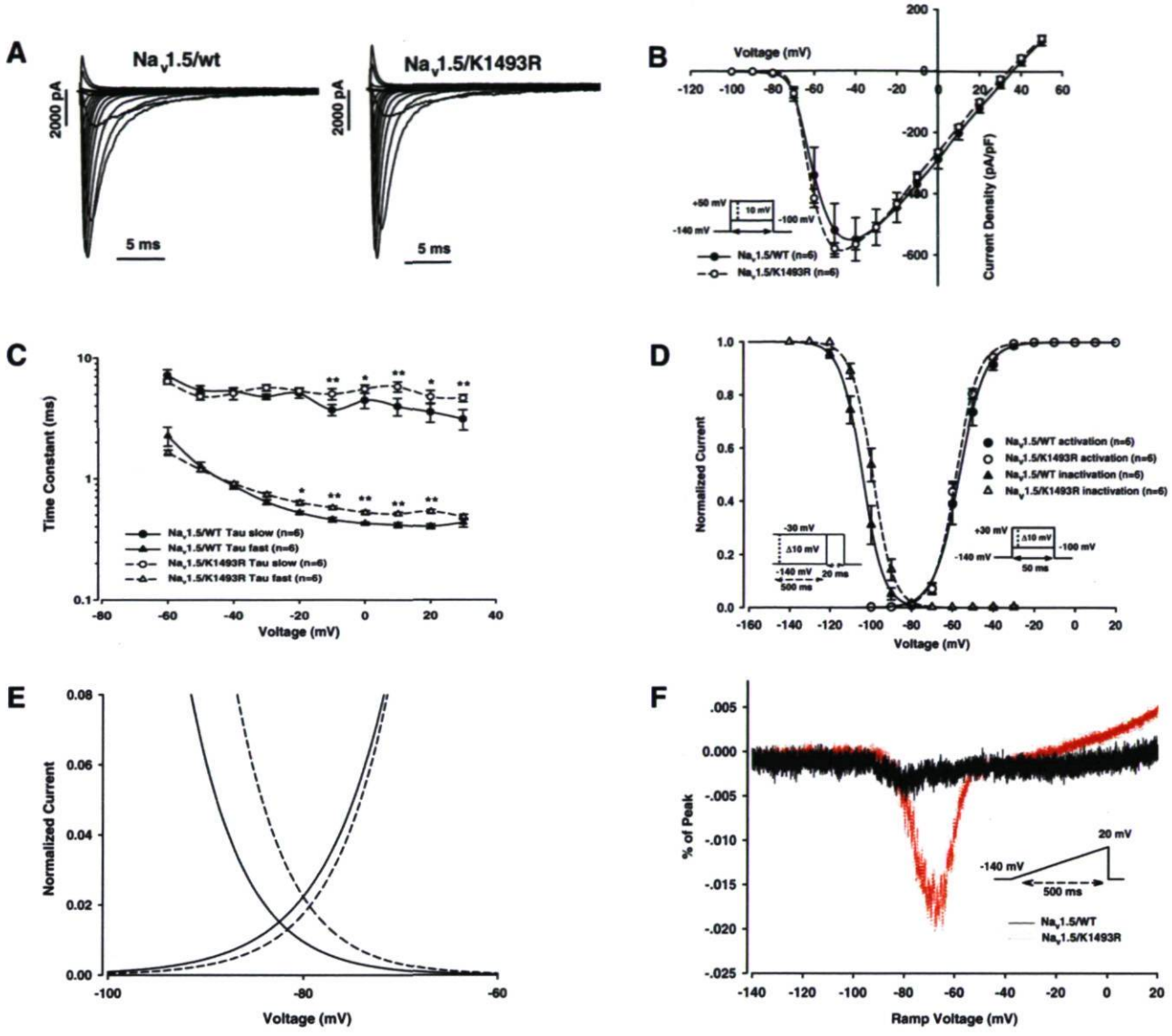

Fig. 2. Biophysical properties of Na$_v$1.5/wt and Na$_v$1.5/K1493R expressed in tsA201 cells. (A) Analysis of whole-cell currents recorded from cells expressing wt and mutant channels. Current was elicited by depolarizing pulses from −100 to +50 mV in 10 mV increments. (B) Current–voltage relationship of Na$_v$1.5/wt and Na$_v$1.5/K1493R. The current amplitude was normalized to the membrane capacitance. (C) The voltage-dependence time constants of fast inactivation in wt and K1493R expressing cells. Currents were fitted to a two-exponential function. Asterisks indicate significance ($^*p < 0.05$, $^{**}p < 0.01$). (D) Steady-state voltage-dependent properties of activation and inactivation for wt and K1493R sodium channels ($^*p < 0.05$, $^{**}p < 0.01$). Voltage-clamp protocols are shown as inset. (E) The view of the overlapping area between activation and steady-state inactivation was expanded from (D). (F) Window currents of wt and K1493R channels. Ramp currents of wt (solid line, $n = 6$) and K1493R (dash line, $n = 6$) sodium channels elicited with 500 ms ramp depolarizations from −140 to 20 mV.

negative direction [14,18–21]. Similar findings are seen in myotonic disorders associated with specific SCN4A mutations, whereby therapy with flecainide, a sodium channel blocker, provides clinical benefit [22].

Diverse molecular mechanisms of AF induced by ion channel genetic defects have been described. Gain-of-function mutations of potassium channels KCNQ1, KCNE2, and KCNJ2 are reported to result in a shortening of APD and are predicted to shorten atrial effective refractory period, inducing enhanced vulnerability to re-entry [23–25]. In contrast, a mutation in KCNA5 resulting in a loss-of-function is reported to increase APD and early-after-depolarizations in atrial myocytes promoting triggered activity [26]. Connexin40 mutations result in a loss of gap junction conductance and are proposed to enhance atrial conduction heterogeneity throughout myocardial tissue, facilitating a reentry substrate for AF [27]. Functional studies on two previously reported Na$_v$1.5 channel mutations associated with AF have shown contrasting functional differences [28,29]. Although both mutations were located in the C-terminus of the channel, a hyperpolarizing shift in steady-state inactivation suggesting a loss-of-function was noted in one study [30], while the other reported a depolarizing shift in steady-state inactivation and increased current density [31]. The gain-of-function findings of the latter study are similar to ours, although Na$_v$1.5/K1493R did not show an increased current density. The present study elaborates on the functional consequences of a depolarizing shift in steady-state inactivation, demonstrating for the first time that this biophysical abnormality in Na$_v$1.5, in the absence of other kinetic alterations, results in an enhanced window current, a lower threshold for action potential firing, and spontaneous depolarizations when studied in HL-1 atrial cardiomyocytes. These data suggest a distinct mechanism of AF vulnerability due to cellular hyperexcitability that results from a novel gain-of-function in the cardiac sodium channel.

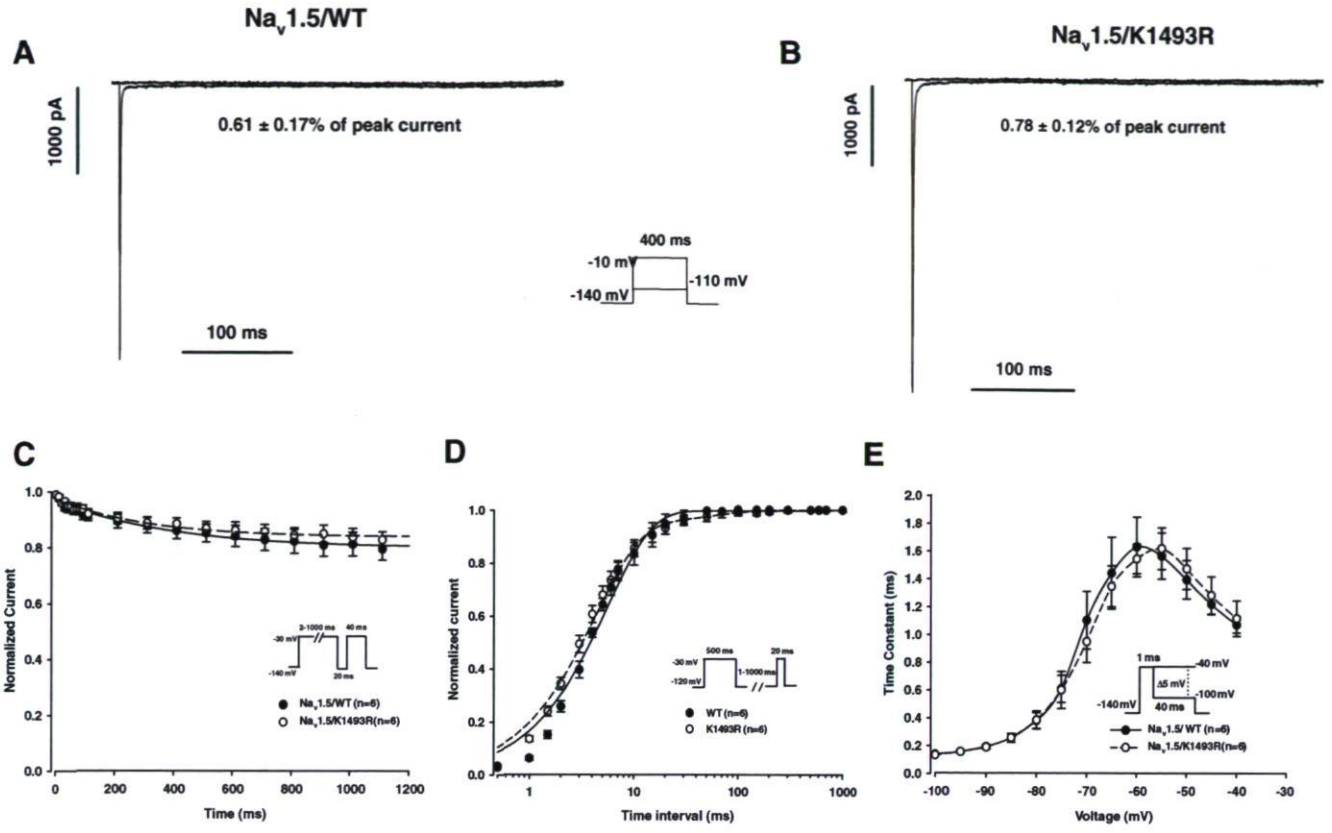

Fig. 3. The persistent sodium current from wt (A) and K1493R (B) $Na_v1.5$ channels. (C) Slow inactivation, (D) time courses of recovery from slow inactivation, and (E) deactivation from the open state from wt and K1493R $Na_v1.5$ channels. Protocols are indicated in inset.

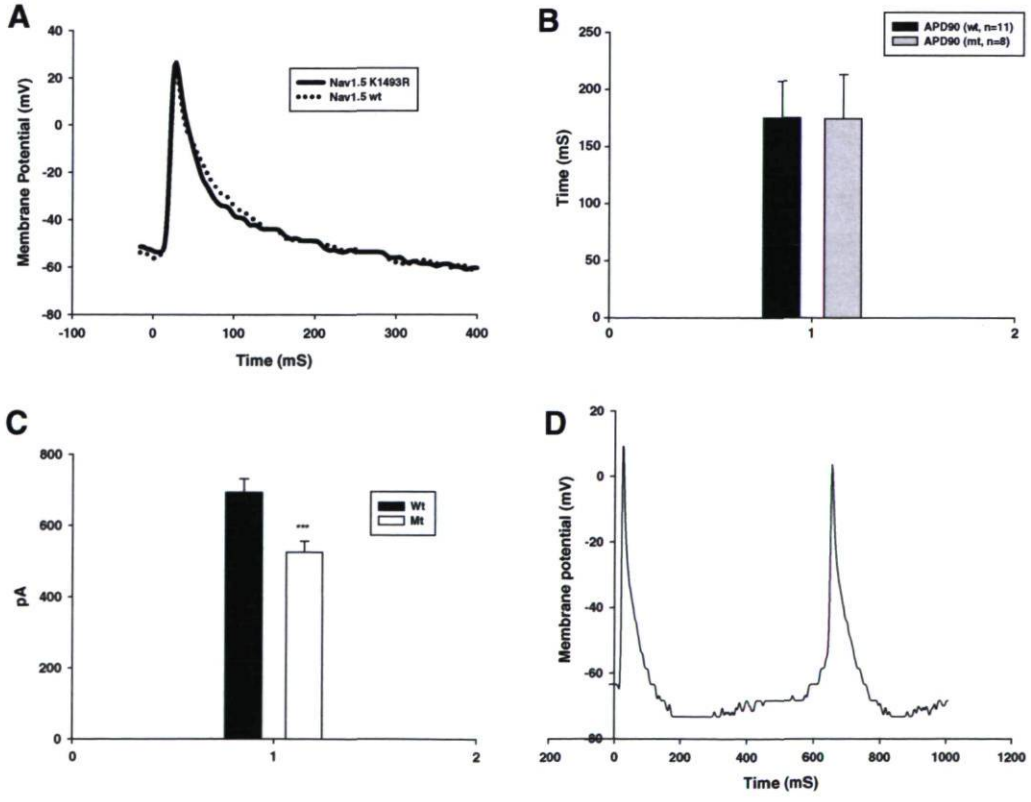

Fig. 4. Superimposed AP traces recorded from HL-1 cardiomyocytes transfected with $Na_v1.5$/wt or $Na_v1.5$/K1493R sodium channels (A). (B) The APD_{90} of APs recorded from HL-1 cells expressing wt or K1493 channels. (C) Depolarizing threshold current for elicitation of Aps from HL-1 cells expressing wt ($n = 6$) or K1493R ($n = 8$) sodium channels ($p < 0.005$). (D) Spontaneous all-or-none AP observed from HL-1 atrial cardiomyocytes expressing $Na_v1.5$/K1493, which was not observed from wt expressing cells.

The biophysical observations of $Na_v1.5$/K1493 are similar to those described in other sodium channelopathy diseases associated with hyperexcitability. In the context of atrial fibrillation, rapid focal atrial activity, commonly observed from pulmonary myocardial sleeves, may be the result of repetitive myocyte AP firing. Furthermore, a link between sodium channel activity and autonomic mediated AF has been suggested in a study by Scornik et al., which identified a high expression of $Na_v1.5$ channels in intracardiac ganglia [30]. These investigators demonstrated $Na_v1.5$-induced AP activity from these neurons and speculated that a gain-of-function of the $Na_v1.5$ channel might enhance AP activity of intracardiac neurons, augmenting acetylcholine release.

The data from this study provides a potential molecular link to the observations of focal triggers of AF [31], the efficacy of intracardiac ganglia denervation by catheter ablation [32], and the use of sodium channel blockers in reducing AF burden [33].

Acknowledgments

This work was supported in part by grants from the Heart and Stroke Foundations of Ontario (M.H.G.) and Quebec (M.C.), and from the Early Researcher Award program from the Government of Ontario (M.H.G.).

References

[1] Q. Wang, J. Shen, I. Splawski, D. Atkinson, Z. Li, J.L. Robinson, A.J. Moss, J.A. Towbin, M.T. Keating, SCN5A mutations associated with an inherited cardiac arrhythmia, long QT syndrome, Cell 80 (1995) 805–811.
[2] Q. Chen, G.E. Kirsch, D. Zhang, R. Brugada, J. Brugada, P. Brugada, D. Potenza, A. Moya, M. Borggrefe, G. Breithardt, R. Ortiz-Lopez, Z. Wang, C. Antzelevitch, R.E. O'Brien, E. Shulze-Bahr, M.T. Keating, J.A. Towbin, Q. Wang, Genetic basis and molecular mechanism for idiopathic ventricular fibrillation, Nature 392 (1998) 293–296.
[3] J.J. Schott, C. Alshinawi, F. Kyndt, V. Probst, T.M. Hoorntje, M. Hulsbeek, A.A. Wilde, D. Escande, M.M. Mannens, H. Le Marec, Cardiac conduction defects associate with mutations in SCN5A, Nat. Genet. 23 (1999) 20–21.
[4] P.B. Bennett, K. Yazawa, N. Makita, A.L. George Jr., Molecular mechanism for an inherited cardiac arrhythmia, Nature 376 (1995) 683–685.
[5] G. Baroudi, V. Pouliot, I. Denjoy, P. Guicheney, A. Shrier, M. Chahine, Novel mechanism for Brugada syndrome: defective surface localization of an SCN5A mutant (R1432G), Circ. Res. 88 (2001) E78–E83.
[6] M.B. Rook, A.C. Bezzina, W.A. Groenewegen, I.C. van Gelder, A.C. van Ginneken, H.J. Jongsma, M.M. Mannens, A.A. Wilde, Human SCN5A gene mutations alter cardiac sodium channel kinetics and are associated with the Brugada syndrome, Cardiovasc. Res. 44 (1999) 507–517.
[7] D. Darbar, P.J. Kannankeril, B.S. Donahue, G. Kucera, T. Stubblefield, J.L. Haines, A.L. George Jr., D.M. Roden, Cardiac sodium channel (SCN5A) variants associated with atrial fibrillation, Circulation 117 (2008) 1927–1935.
[8] J.W. West, D.E. Patton, T. Scheuer, Y. Wang, A.L. Goldin, W.A. Catterall, A cluster of hydrophobic amino acid residues required for fast Na(+)-channel inactivation, Proc. Natl. Acad. Sci. USA 89 (1992) 10910–10914.
[9] D.E. Patton, J.W. West, W.A. Catterall, A.L. Goldin, Amino acid residues required for fast Na(+)-channel inactivation: charge neutralizations and deletions in the III–IV linker, Proc. Natl. Acad. Sci. USA 89 (1992) 10905–10909.
[10] J.R. Miller, M.K. Patel, J.E. John, P. Mounsey, J.R. Moorman, Contributions of charged residues in a cytoplasmic linking region to Na channel gating, Biochim. Biophys. Acta 1509 (2000) 275–291.
[11] J.A. Kearney, N.W. Plummer, M.R. Smith, J. Kapur, T.R. Cummins, S.G. Waxman, A.L. Goldin, M.H. Meisler, A gain-of-function mutation in the sodium channel gene *Scn2a* results in seizures and behavioural abnormalities, Neuroscience 102 (2001) 307–317.
[12] J.F. Desaphy, A. De Luca, M.P. Didonna, A.L. George, C.D. Conte, Different flecainide sensitivity of hNav1.4 channels and myotonic mutants explained by state-dependent block, J. Physiol. 554 (2003) 321–334.
[13] A.L. George Jr., Inherited disorders of voltage-gated sodium channels, J. Clin. Invest. 115 (2005) 1990–1999.
[14] M. Vreugdenhil, G.C. Faas, W.J. Wadman, Sodium currents in isolated rat CA1 neurons after kindling epileptogenesis, Neuroscience 86 (1998) 99–107.
[15] X.Q. Gu, H. Yao, G.G. Haddad, Increased neuronal excitability and seizures in the Na^+/H^+ exchanger null mutant mouse, Am. J. Physiol. Cell Physiol. 281 (2001) C496–C503.
[16] S.O.M. Ketelaars, J.A. Gorter, E.A. van Vliet, F.H. Lopes da Silva, W.J. Wadman, Sodium currents in isolated rat CA1 pyramidal and dentate granule neurons in the post-status epilepticus model of epilepsy, Neuroscience 105 (2001) 109–120.
[17] R.K. Ellerkmann, S. Remy, J. Chen, D. Sochivko, C.E. Elger, B.W. Urgan, A. Becker, H. Beck, Molecular and functional changes in voltage-dependent Na^+ channels following pilocarpine-induced status epilepticus in rat dentate granule cells, Neuroscience 119 (2003) 323–333.
[18] C.C. Kuo, R.S. Chen, L. Lu, R.C. Chen, Carbamazepine inhibition of neuronal Na^+ currents: quantitative distinction from phenytoin and possible therapeutic implications, Mol. Pharmacol. 51 (1997) 1077–1083.
[19] G. Reckziegel, H. Beck, J. Schramm, B.W. Urgan, C.E. Elger, Carbamazepine effects on Na^+ currents in human dentate granule cells from epileptogenic tissue, Epilepsia 40 (1999) 401–407.
[20] M. Vreugdenhil, W.J. Wadman, Modulation of sodium currents in rat CA1 neurons by carbamazepine and valproate after kindling epileptogenesis, Epilepsia 40 (1999) 1512–1522.
[21] R. Kohling, Voltage-gated sodium channels in epilepsy, Epilepsia 43 (2002) 1278–1295.
[22] J. Rosenfeld, K. Sloan-Brown, A.L. George Jr., A novel muscle sodium channel mutation causes painful congenital myotonia, Ann. Neurol. 42 (1997) 811–814.
[23] Y.H. Chen, S.J. Xu, S. Bendahhou, X.L. Wang, Y. Wang, W.Y. Xu, H.W. Jin, H. Sun, X.Y. Su, Q.N. Zhuang, Y.Q. Yang, Y.B. Li, Y. Liu, H.J. Xu, X.F. Li, N. Ma, C.P. Mou, Z. Chen, J. Barhanin, W. Huang, KCNQ1 gain-of-function mutation in familial atrial fibrillation, Science 299 (2003) 251–254.
[24] Y. Yang, M. Xia, Q. Jin, S. Bendahhou, J. Shi, Y. Chen, B. Liang, J. Lin, Y. Liu, B. Liu, Q. Zhou, D. Zhang, R. Wang, N. Ma, X. Su, K. Niu, Y. Pei, W. Xu, Z. Chen, H. Wan, J. Cui, J. Barhanin, Y. Chen, Identification of a KCNE2 gain-of-function mutation in patients with familial atrial fibrillation, Am. J. Hum. Genet. 75 (2004) 899–905.
[25] M. Xia, Q. Jin, S. Bendahhou, Y. He, M.M. Larroque, Y. Chen, Q. Zhou, Y. Yang, Y. Liu, B. Liu, Q. Zhu, Y. Zhou, J. Lin, B. Liang, L. Li, X. Dong, Z. Pan, R. Wang, H. Wan, W. Qiu, W. Xu, P. Eurlings, J. Barhanin, Y. Chen, A Kir2.1 gain-of-function mutation underlies familial atrial fibrillation, Biochem. Biophys. Res. Commun. 332 (2005) 1012–1019.
[26] T.M. Olson, A.E. Alekseev, X.K. Liu, S. Park, L.V. Zingman, M. Bienengraeber, S. Sattiraju, J.D. Ballew, A. Jahangir, A. Terzic, Kv1.5 channelopathy due to KCNA5 loss-of-function mutation causes human atrial fibrillation, Hum. Mol. Genet. 15 (2006) 2185–2191.
[27] M.H. Gollob, D.L. Jones, A.D. Krahn, L. Danis, X.Q. Gong, Q. Shao, X. Liu, J.P. Veinot, A.S. Tang, F. Tesson, G.J. Klein, R. Yee, A.C. Skanes, G.M. Guiraudon, D. Bai, Somatic mutations in the connexin 40 gene (GJA5) in atrial fibrillation, N. Engl. J. Med. 354 (2006) 2677–2688.
[28] P.T. Ellinor, E.G. Nam, M.A. Shea, D.J. Milan, J.N. Ruskin, C.A. MacRae, Cardiac sodium channel mutation in atrial fibrillation, Heart Rhythm 5 (2008) 99–105.
[29] T. Makiyama, M. Akao, S. Shizuta, T. Doi, K. Nishiyama, Y. Oka, S. Ohno, Y. Nishio, K. Tsuji, H. Itoh, T. Kimura, T. Kita, M. Horie, A novel SCN5A gain-of-function mutation M1875T associated with familial atrial fibrillation, J. Am. Coll. Cardiol. 52 (2008) 1326–1334.
[30] F.S. Scornik, M. Desai, R. Brugada, A. Guerchicoff, G.D. Pollevick, C. Antzelevitch, G.J. Perez, Functional expression of "cardiac-type" $Na_v1.5$ sodium channels in canine intracardiac ganglia, Heart Rhythm 3 (2006) 842–850.
[31] M. Haissaguerre, P. Jais, D.C. Shah, A. Takahashi, M. Hocini, G. Quinuou, A. Le Mouroux, P. Le Metayer, J. Clementy, Spontaneous initiation of atrial fibrillation by ectopic beats originating in the pulmonary veins, N. Engl. J. Med. 339 (1998) 659–666.
[32] C. Pappone, V. Santinelli, F. Manquso, G. Vicedomini, F. Gugliotta, G. Augello, P. Mazzone, V. Tortoriello, G. Landoni, A. Zangrillo, C. Lang, T. Tomita, C. Mesas, E. Mastella, O. Alfieri, Pulmonary vein denervation enhances long-term benefit after circumferential ablation for paroxysmal atrial fibrillation, Circulation 109 (2004) 327–334.
[33] A. Burashnikov, J.M. Di Diego, A.C. Zygmunt, L. Belardinelli, C. Antzelevitch, Atrial-selective sodium channel block as a strategy for suppression of atrial fibrillation, Ann. NY Acad. Sci. 1123 (2008) 105–112.

Cell Membrane Expression of Cardiac Sodium Channel $Na_v1.5$ Is Modulated by α-Actinin-2 Interaction

Ziane R, **Huang H**, Moghadaszadeh B, Beggs AH, Levesque G, & Chahine M.
Biochemistry (2010) **49**, 166-178.

Contribution role: (1) Doing experiments regarding modulation effects of α-actinin-2 on $Na_v1.5$ channels by whole-cell configuration of patch-clamp technique. (2) Analyzing resulting data. It was found that co-expression of α-actinin-2 in tsA 201 cells can increase peak INa of Nav1.5 channels without affecting gating properties. (2) Providing Figures 9 and 10, and their legends. (3) Writing results and discussion related to figures 9 and 10.

166 *Biochemistry* **2010,** *49,* 166–178
DOI: 10.1021/bi901086v

BIOCHEMISTRY
including biophysical chemistry & molecular biology
Article

Cell Membrane Expression of Cardiac Sodium Channel $Na_v1.5$ Is Modulated by α-Actinin-2 Interaction†

Rahima Ziane,‡ Hai Huang,‡ Behzad Moghadaszadeh,∥ Alan H. Beggs,∥ Georges Levesque,§ and Mohamed Chahine*,‡

‡*Centre de Recherche Université Laval Robert-Giffard, and* §*Centre de Recherche du CHUL (CHUQ), Unité de Neurosciences, Université Laval, Quebec City, QC, Canada, and* ∥*Division of Genetics and Program in Genomics, Children's Hospital Boston, Harvard Medical School, 320 Longwood Avenue, Boston, Massachusetts 02115*

Received June 26, 2009; Revised Manuscript Received November 25, 2009

ABSTRACT: Cardiac sodium channel $Na_v1.5$ plays a critical role in heart excitability and conduction. The molecular mechanism that underlies the expression of $Na_v1.5$ at the cell membrane is poorly understood. Previous studies demonstrated that cytoskeleton proteins can be involved in the regulation of cell surface expression and localization of several ion channels. We performed a yeast two-hybrid screen to identify $Na_v1.5$-associated proteins that may be involved in channel function and expression. We identified α-actinin-2 as an interacting partner of the cytoplasmic loop connecting domains III and IV of $Na_v1.5$ ($Na_v1.5$/LIII−IV). Co-immunoprecipitation and His_6 pull-down assays confirmed the physical association between $Na_v1.5$ and α-actinin-2 and showed that the spectrin-like repeat domain is essential for binding of α-actinin-2 to $Na_v1.5$. Patch-clamp studies revealed that the interaction with α-actinin-2 increases sodium channel density without changing their gating properties. Consistent with these findings, coexpression of α-actinin-2 and $Na_v1.5$ in tsA201 cells led to an increase in the level of expression of $Na_v1.5$ at the cell membrane as determined by cell surface biotinylation. Lastly, immunostaining experiments showed that α-actinin-2 was colocalized with $Na_v1.5$ along the Z-lines and in the plasma membrane. Our data suggest that α-actinin-2, which is known to regulate the functional expression of the potassium channels, may play a role in anchoring $Na_v1.5$ to the membrane by connecting the channel to the actin cytoskeleton network.

Muscular contraction and neuronal firing are physiological responses to voltage-gated sodium channel activation in excitable tissues. $Na_v1.5$[1] is the major voltage-sensitive sodium channel in the heart and is responsible for the normal electrical excitability and conduction of the cardiomyocytes. Mutations in the *SCN5A* gene encoding the $Na_v1.5$ protein are associated with several arrhythmogenic syndromes, including long QT syndrome, Brugada syndrome, conduction disorders, sudden infant death syndrome, and dilated cardiomyopathy (*1*, *2*).

$Na_v1.5$ is a transmembrane protein consisting of a single pore-forming α-subunit and several auxiliary β-subunits. Recent studies showed that $Na_v1.5$-associated proteins modulate not only $Na_v1.5$ activity but also its biosynthesis, localization, and/or degradation (*3*). For example, the β_1 and β_2 subunits interact with other proteins and stabilize channel density within the plasma membrane (*4*). In addition, the β_1 and β_3 subunits may enhance the trafficking efficiency of sodium channels in the endoplasmic reticulum (*5*, *6*). Besides the β-subunits, adapter proteins such as syntrophin, dystrophin, and ankyrin have also been shown to participate in the targeting and stabilization of skeletal and cardiac sodium channels at the cell membrane (*7*−*9*), while the ubiquitine-protein ligase (Nedd4-2) acts on $Na_v1.5$ by decreasing channel density at the cell membrane (*3*). Despite this variety of accessory proteins, the precise composition and role of the cardiac sodium channel complex remain poorly understood. It is logical to predict that many more proteins are involved in the dynamic networks of protein−protein interactions with $Na_v1.5$. Here, we describe a novel binding partner of the cardiac sodium channel, α-actinin-2.

α-Actinins belong to a superfamily of F-actin cross-linking proteins that includes spectrin and dystrophin. The four known α-actinin isoforms are encoded by four separate genes (*10*). All four isoforms are 100 kDa, rod-shaped molecules that form antiparallel dimers composed of an N-terminal actin-binding domain, four central spectrin-like repeat motifs (SRM), and a C-terminal calponin homology domain (CH) (*11*). α-Actinins perform a number of important physiological functions, many of which involve binding interactions with other proteins. They link various transmembrane proteins to the actin filament network (*12*−*14*), regulate K^+ channel activity (*15*), and help to maintain cytoskeleton organization (*16*). We performed a yeast two-hybrid screen using LIII−IV as bait to screen a human

†This study was supported by grants from the Heart and Stroke Foundation of Quebec (HSFQ) and the Canadian Institute of Health Research (CIHR, MT-13181). M.C. is an Edwards Senior Investigator (Joseph C. Edwards Foundation). B.M. and A.H.B. were supported by Grant R01-AR44345 from the National Institute of Arthritis and Musculoskeletal and Skin Diseases of the National Institutes of Health (NIH) and by Grant 3971 from the Muscular Dystrophy Association. Confocal microscopy was performed at the Children's Hospital Mental Retardation and Developmental Disabilities Research Center Imaging Core with funding from NIH Grant P30 HD18655.

*To whom correspondence should be addressed: Centre de Recherche Université Laval Robert-Giffard, local F-6539, 2601 chemin de la Canardière, Quebec City, QC, Canada G1J 2G3. Telephone: (418) 663-5747, ext. 4723. Fax: (418) 663-8756. E-mail: mohamed.chahine@phc.ulaval.ca.

[1]Abbreviations: $Na_v1.5$, cardiac voltage-gated sodium channel; *SCN5A*, cardiac voltage-gated sodium channel gene; CH, calponin homology domain; SRM, spectrin-like repeat motifs; EF, EF-hand domain; LIII−IV, $Na_v1.5$/LIII−IV.

Published on Web 11/27/2009

heart cDNA library. Among the partners that we identified, we specifically investigated α-actinin-2. We provide evidence that $Na_v1.5$ binds to the central spectrin rod domain of α-actinin-2. Moreover, we explored the physiological role of α-actinin-2 by the coexpression of α-actinin-2 and $Na_v1.5$ in tsA201 cells, a mammalian cell line. Our results show that α-actinin-2 is a partner for $Na_v1.5$, which may directly or indirectly modulate channel expression and function.

MATERIALS AND METHODS

Yeast Two-Hybrid Plasmid Constructs. The yeast two-hybrid bait vector was obtained using Gateway recombination cloning technology (Invitrogen). The full-length LIII−IV (amino acids 1471−1523) was amplified by PCR from the pcDNA1-$Na_v1.5$ vector. The PCR product was recombined into the pDEST32 vector (Invitrogen) by an LR reaction, resulting in translational fusions between the open reading frame and the GAL4 DNA binding domain. Full-length LIII−IV and full-length α-actinin-2 (amino acids 1−894) constructs were also recombined in the pGBKT7 and pGADT7 vectors and expressed as fusion proteins with a GAL4 DNA binding domain and a GAL4 activation domain, respectively (Matchmaker, Clontech). All the constructs were verified by sequencing.

Mammalian Expression Constructs. The coding segment of human $Na_v1.5$ was cloned into the HindIII and XbaI sites of pcDNA1 (Invitrogen) (*17*). The His_6-LIII−IV fusion protein construct and the pcDNA3-V5-tagged $Na_v1.5$ vector were kindly provided by C. Ahern (Jefferson Medical College, Philadelphia, PA). The human sodium channel β_1 subunit and $Na_v1.8$ channel were constructed in the piRES vector (Invitrogen). The cDNA encoding the calponin hand domain (amino acids 1−86) of human α-actinin-2 was generated by PCR from a pcDNA3-α-actinin-2 vector (kindly provided by D. Fedida, University of British Columbia, Vancouver, BC) and subcloned into the EcoRI and EcoRV sites of pcDNA3.1 (Invitrogen) in frame with the NH_2-terminal Xpress epitope. Five cDNA fragments encoding C-terminally truncated α-actinin-2 [pcDNA3-α-actinin-2/SPEC1 (amino acids 1−390), pcDNA3-α-actinin-2/SPEC2 (amino acids 1−505), pcDNA3-α-actinin-2/SPEC3 (amino acids 1−626), and pcDNA3-α-actinin-2/SPEC4 (amino acids 1−739)] and pcDNA3-Xpress tagged-2 CH domain were generated by introducing stop codons into specific regions of the α-actinin-2 gene. Full-length human α-actinin-1, -3, and -4 cDNAs were used as previously described (*11*). All constructs were sequenced prior to use.

Yeast Two-Hybrid Screen. The two-hybrid screen was performed in yeast strain MaV203 (MATα; *leu*2−3,112; *trp*1−901; *his*3Δ200; *ade*2−101; *cyh*2R; *can*1R; *gal*4Δ; *gal*80Δ; *GAL*1::*lacZ*; $HIS3_{UAS\text{-}GAL1}$::*HIS*3@*LYS*2; *SPAL*10::*URA*3) containing HIS3, LacZ, and URA reporter genes under the control of the GAL4-activating sequences. Briefly, after assessing self-activation and determining the basal expression of the HIS3 reporter gene, we transformed the bait plasmid pDEST32/LIII−IV into yeast strain MaV203 together with a cDNA library prepared from human heart in prey vector pPC86 (Invitrogen) using the lithium acetate method. Candidate clones were selected by plating cotransformants on selective medium lacking tryptophan, leucine, and histidine (−TLH) and supplemented with 10 mM 3-amino-1,2,4-triazole. The clones were confirmed by induction of the URA reporter gene, which allowed growth on synthetic dropout media lacking leucine, tryptophan, and uracil. Plasmids were isolated from candidate clones, and retransformation assays were conducted to verify the interactions using the Matchmaker yeast two-hybrid protocol (Clontech). The selected plasmids were sequenced, and the insert sequences obtained were subjected to BLAST searches.

Cell Culture and DNA Transfection. tsA201 cells, a mammalian cell line derived from human embryonic kidney HEK293 cells by stable transfection with SV40 large T antigen, were grown in high-glucose DMEM supplemented with fetal bovine serum (10%), L-glutamine (2 mM), penicillin G (100 units/mL), and streptomycin (10 mg/mL) (Gibco BRL Life Technologies) in a 5% CO_2 humid atmosphere incubator. In the cotransfection experiments, the DNA ratios of the two plasmids were adjusted to yield approximately equal amounts of expressed proteins. For the patch-clamp experiments, the transfections were performed according to the method of Margolskee et al. (*18*), with a few modifications.

Co-Immunoprecipitation (Co-IP) Assay. Because neither α-actinin-2 nor $Na_v1.5$ is endogenously expressed in tsA201 cells, the cells were transfected with both α-actinin-2 and $Na_v1.5$ cDNA using the calcium phosphate method. The transfections were conducted using 80% confluent cells in a 10 cm plate. The cells were harvested and lysed in STEN buffer [50 mM Tris (pH 7.5), 150 mM NaCl, and 1% (v/v) Triton X-100] supplemented with complete mini EDTA-free protease inhibitors (Roche Diagnostics). The cell lysates were clarified by centrifugation at 15000*g* for 30 min. Equal volumes (500 μL) of cell lysates were incubated with a polyclonal rabbit anti-III−IV loop (2 μg) (Upstate) overnight at 4 °C. Protein G cross-linked to agarose beads (40 μL) (Calbiochem) was added, and the incubation was continued for an additional 4 h. After a quick centrifugation at 5000*g*, the pellet was rinsed five times with STEN buffer to eliminate nonspecific binding. We eluted the immune complexes by boiling the samples for 5 min in reducing sample buffer [0.5 M Tris-HCl (pH 6.8), 20% glycerol, 10% SDS, 0.1% bromophenol blue, and 5% β-mercaptoethanol], separated them via SDS−PAGE, and transferred them onto a polyvinylidene fluoride (PVDF) membrane (Millipore). The membrane was probed with an anti-α-actinin-2 "4B" antibody, and the protein signal was visualized by enhanced chemiluminescence according to the manufacturer's instructions (Amersham Biosciences). For reciprocal co-IP, a rabbit polyclonal anti-α-actinin-2 antibody was used for the immunoprecipitation and the anti-LIII−IV antibody was used for the Western blot analysis. A similar procedure was followed to study the interaction between the α-actinin isoforms and $Na_v1.5$ by coexpressing V5-tagged $Na_v1.5$ with either α-actinin-1, α-actinin-3, or α-actinin-4 in tsA201 cells. The α-actinin isoforms were immunoprecipitated with an anti-V5 antibody (Invitrogen), and the blots were probed with the respective primary antibody (anti-α-actinin-1 "3A3", anti-α-actinin-3 "5A3", or anti-α-actinin-4 "6A3"). For the immunoprecipitation analysis of α-actinin and sodium channel isoforms in native tissue, frozen stripped mouse brain, heart, and skeletal muscle were ground to a fine powder in liquid nitrogen. The powders were further homogenized in STEN lysis buffer using five strokes of a glass homogenizer. The lysates were incubated on ice for 30 min and then microcentrifuged for 15 min at 4 °C. The cell lysates were precleared on protein G beads for 30 min at 4 °C prior to the IP analysis. Equal volumes of supernatants were incubated with 2 μg of anti-LIII−IV antibody and 40 μL of protein G beads for 4 h at 4 °C. After being extensively

washed, the immunoprecipitates were resolved by SDS−PAGE and transferred to PVDF membranes. The membranes were immunoblotted with either the anti-α-actinin-2 antibody, the anti-α-actinin-3 antibody, or the anti-LIII−IV antibody. Lysates were also immunoprecipitated with rabbit preimmune IgG (negative control).

Immunoblots. Cell lysates and immunoprecipitated proteins were separated via 10% SDS−PAGE and transferred to PVDF membranes in transfer buffer (150 mM glycine, 20 mM Tris base, and 20% methanol) for 2 h at 4 °C. The blots were blocked with 5% nonfat skim milk in TBST (50 mM Tris-HCl, 150 mM NaCl, and 0.1% Tween 20) and then incubated with the appropriate primary antibodies [anti-III−IV loop (1:500), anti-V5 (1:5000), anti-α-actinin-1 (1:1000), anti-α-actinin-2 (1:20000), anti-α-actinin-3 (1:1000), anti-α-actinin-4 (1:1000) (*19*), and anti-Xpress (1:5000, Invitrogen)] in blocking buffer for 1 h at room temperature (RT). After three washes with TBST, the blots were incubated with HRP-conjugated goat anti-rabbit antibody or HRP-conjugated goat anti-mouse antibody (1:10000) (Jackson ImmunoResearch Laboratories) for 1 h at RT. The proteins were visualized using an enhanced chemiluminescence detection system (Amersham Bioscience).

Expression and Purification of the His_6 Fusion Protein. Recombinant His_6-LIII−IV fusion protein (amino acids 1471−1523) was transformed into XL1-Blue competent cells (Stratagene). An overnight culture was diluted (1:50) in fresh Luria-Bertani broth, grown to an A_{600} of 0.5, and induced with 1 mM isopropyl β-D-thiogalactopyranoside (Sigma) for 7 h at 37 °C. An XL1-Blue pellet of cells harboring the His_6-LIII−IV fusion protein was resuspended in 200 mM Tris (pH 8), 300 mM NaCl, and 10 mM imidazole supplemented with an EDTA-free complete protease inhibitor mixture (Roche Applied Science) and sonicated six times for 2 s. The bacterial lysate was then centrifuged at 10000*g* for 30 min, and the supernatant was applied to Ni^{2+}-NTA columns (Qiagen) according to the manufacturer's instructions.

Blot Overlay Assay. The interaction between the His_6-LIII−IV fusion protein and α-actinin-2 was assayed using blot overlay assays. tsA201 cells were transiently transfected with increasing amounts (15−45 μg) of cDNA encoding α-actinin-2. Twenty-four hours post-transfection, the cells were washed twice with PBS and lysed in STEN buffer. The cell homogenates were clarified by centrifugation at 15000*g* for 30 min at 4 °C. Equal volumes of whole cell lysates were subjected to SDS−PAGE and blotted onto PVDF membranes. The blots were blocked in 4% nonfat dry milk in Tris-buffered saline supplemented with 0.1% Tween 20 (TBST) overnight at 4 °C, incubated with either 5 mL of 1 μg/mL purified His_6-LIII−IV fusion protein or 5 mL of 1 μg/mL bovine serum albumin (Sigma) in TBST containing 5% skim milk for 90 min at RT, washed three times with TBST, incubated at RT with the polyclonal anti-LIII−IV antibody, washed three times with TBST, and then incubated with HRP-conjugated anti-rabbit antibody. After six washes with TBST, the bands were visualized by ECL. Untransfected tsA201 cells (Unt) and bovine serum albumin protein (BSA) were used as negative controls.

His Pull-Down Assay. The His pull-down assay was performed using the purified His_6-LIII−IV fusion protein to pull down full-length α-actinin-2 or C-terminally truncated α-actinin-2 fragments, which were then detected by specific antibodies. Briefly, the His_6-LIII−IV fusion protein was purified on a Ni^{2+}-NTA column, and 2 μg of purified His_6-LIII−IV fusion protein was bound to Ni^{2+}-NTA beads in PBS for 4 h with rotation. The beads were washed twice for 10 min in PBS containing 0.1% Triton X-100 and once in STEN buffer. The washed beads were incubated with equal volumes (500 μL) of tsA201 cell lysates expressing full-length α-actinin-2 or C-terminally truncated α-actinin-2 proteins in STEN buffer for 1 h at RT. The complexes were centrifuged and extensively washed with 200 mM Tris (pH 8), 300 mM NaCl, and 20 mM imidazole to prevent nonspecific binding. Bound proteins were eluted with the same buffer containing 250 mM imidazole. The samples were then boiled for 5 min in reducing sample buffer and analyzed by Western blotting using the corresponding antibodies. tsA201 cell lysates expressing α-actinin-2 or its C-terminally truncated fragments were also incubated with Ni^{2+}-NTA beads alone as a negative control.

Biotinylation of Cell Surface Proteins. Cell surface proteins were isolated using Pinpoint Cell Surface Protein Isolation kits based on the manufacturer's protocol (Pierce). The $Na_v1.5$ channel was transfected into tsA201 cells together with an empty vector (mock) or increasing amounts (1.5−5 μg) of cDNA encoding α-actinin-2. Forty-eight hours post-transfection, the cells were washed three times with PBS and then incubated with 10 mL of a freshly prepared EZ-Link Sulfo-NHS-SS-Biotin solution in PBS for 30 min at 4 °C with intermittent mixing. This reagent is cell membrane-impermeable and does not label an overexpressed intracell protein (β-tubilin), which was used as a negative control for this assay. The reaction was ended by the addition of 500 μL of quenching solution, and the cells were washed twice with TBS [25 mM Tris-HCl (pH 7.2) and 150 mM NaCl]. The cells were lysed in 500 μL of lysis buffer containing protease inhibitors, sonicated, and incubated on ice for 30 min, to isolate the biotinylated proteins. The clarified cell lysates were incubated with an immobilized NeutrAvidin gel for 1 h at RT by end-over-end mixing. Unbound proteins were removed by three washes with TBS containing protease inhibitors. The biotinylated proteins prebound to the NeutrAvidin gel were eluted using SDS−PAGE sample buffer containing 50 mM DTT for 1 h at RT. $Na_v1.5$ channels in total cell lysates and streptavidin precipitates were analyzed by Western blotting using an anti-LIII−IV antibody. Total cell lysates were also probed for the Na^+/K^+-ATPase α1 subunit, a plasma membrane marker (positive control). To confirm that the biotinylation reagent did not leak into the cell and label intracell proteins, we stripped and reprobed the same blot using an anti-β-tubulin antibody (1:10000; E7, DSHB).

Sodium Current Recordings. The macroscopic sodium currents of transfected tsA201 cells were recorded using the whole-cell configuration of the patch-clamp technique as previously described (*20*). Briefly, patch electrodes were made from 8161 Corning borosilicate glass and coated with Sylgard (Dow-Corning) to minimize their capacitance. Patch-clamp recordings were taken using low-resistance electrodes (< 1 MΩ). Routine series resistance compensation using an Axopatch 200 amplifier (Molecular Devices) was performed to values of $> 80\%$ to minimize voltage-clamp errors. Voltage-clamp command pulses were generated by a microcomputer using pCLAMP version 8.0 (Molecular Devices). Sodium currents were filtered at 5 kHz, digitized at 10 kHz, and stored on a microcomputer equipped with an AD converter (Digidata 1300, Molecular Devices). The data were analyzed using a combination of pCLAMP version 9.0 (Molecular Devices), Microsoft Excel, and SigmaPlot for Windows version 8.0 (SPSS Inc., Chicago, IL).

Immunohistochemistry. The primary antibodies used were rabbit anti-$Na_v1.5$ (Sigma-Aldrich) raised against a purified peptide (DRLPKSDSEDGPRALNQLSC) and monoclonal anti-sarcomeric α-actinin (clone EA53) (Sigma-Aldrich). The secondary antibodies used were Alexa Fluor 488 goat anti-rabbit IgG and Alexa Fluor 594 goat anti-mouse IgG (Invitrogen). A human adult cardiac ventricle autopsy specimen was snap-frozen and cut into 10 μm sections, which were fixed in methanol. The slides were blocked in 10% fetal bovine serum for 30 min and then incubated with primary antibodies [anti-$Na_v1.5$ and anti-α-actinin (1:70)] for 2 h at RT. After three 5 min washes in PBS, the slides were incubated with secondary antibodies (1:200) for 30 min at RT, washed again in PBS, and mounted using Vectashield hardset mounting medium with DAPI (to counterstain nuclei) (Vector Laboratories). The immunolabeled cryosections were examined using an LSM 510 META two-photon confocal microscope (Carl Zeiss AG). Argon and helium/neon lasers were used to detect Alexa Fluor 488 and 594, respectively. DAPI was detected using a two-photon chameleon laser. Twenty-two 0.45 μm serial optical sections were produced with a 2048 × 2048 pixel resolution. For colocalization quatification, two slides labeled with both primary antibodies and only one secondary antibody each were used to threshold confocal images for green ($Na_v1.5$) and red (sarcomeric α-actinin-2) fluorescence. Then the same conditions for staining and imaging were applied to doubly labeled slides stained with both primary and both secondary antibodies. Colocalization coefficients were calculated by deviding the number of colocalized pixels by the total number of either red or green pixels that were above the background threshold. In all images, the measurements were based on regions of interest drawn around individual myocytes that did not contain autofluorescent lipofuscin deposits. Images were analyzed and processed using LSM image (Carl Zeiss AG) and Adobe Photoshop CS version 2.0 (Adobe Systems).

RESULTS

α-Actinin-2 Was Identified as a Candidate Protein That Interacts with $Na_v1.5$ Using a Yeast Two-Hybrid Screen. LIII−IV (amino acids 1471−1523) was used as bait to screen a human heart cDNA library for candidate proteins involved in the regulation of $Na_v1.5$ function using the yeast two-hybrid method (Figure 1A). After screening 10^6−10^7 clones, we isolated four positive clones, which are listed in Table I of the Supporting Information. Most clones were excluded as false positives as they were derived from mitochondrial DNA or because the encoded peptides were out of frame with the GAL4 activation domain. One of the positive clones encoded a 2 kb cDNA fragment of human cardiac α-actinin-2 (GenBank accession number NM-001103). The α-actinin-2 clone comprised amino acids 388−887, including part of the SRM and the Ca^{2+} binding domain. To determine the specificity of the protein interaction, LIII−IV and full-length α-actinin-2 were subcloned as fusion constructs with either the Gal-4 DNA binding domain (BD) in the pGBKT7 vector or the Gal-4 DNA activating domain (AD) in the pGADT7 vector. AH109 yeast cells were then cotransformed with both constructs. The empty DNA binding domain (pGBKT7-empty) and the activation domain (pGADT7-empty) vectors were used as negative controls. All the transformants grew on synthetic complete medium lacking leucine and tryptophan (−TL), indicating that they carried the bait and prey plasmids (Figure 1B, top panel). In contrast, yeast cotransformed

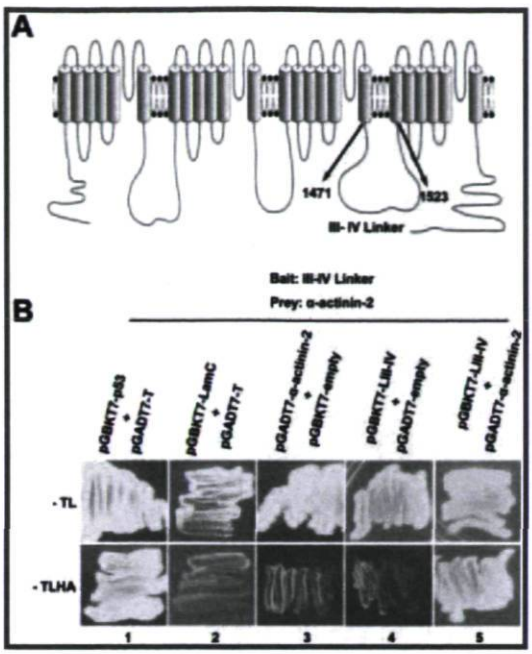

FIGURE 1: Yeast two-hybrid screens of a human heart cDNA library identified α-actinin-2 as a binding partner of the $Na_v1.5$/LIII−IV region. (A) Transmembrane topology of the $Na_v1.5$ α-subunit showing the four homologous domains, each of which is composed of six membrane-spanning segments. The location of the III−IV linker (LIII−IV), which was used as bait, is indicated by the arrows. The numbers correspond to the amino acid positions. (B) α-Actinin-2 was isolated from a yeast two-hybrid screen and subcloned into the pGADT7 vector (pGADT7-α-actinin-2). To confirm the interaction between LIII−IV/BD and α-actinin-2/AD, the AH109 yeast strain was cotransformed with pGBKT7-LIII−IV and -bait constructs with pGADT7-α-actinin-2 and -prey or pGADT7-empty vector as negative controls. p53 (pGBKT7-p53) and SV40 large T-antigen (pGADT7-T) cotransformants were used as positive controls, whereas lamin C (pGBKT7-LamC) and pGADT7-T cotransformants were used as negative controls. The viability of the isolated clones and controls was assessed on medium that lacked tryptophan and leucine (−TL) (cotransformed cells survive) and on counter-selective medium that lacked tryptophan, leucine, histidine, and adenine (−TLHA) (only yeast cells with an interaction between bait and prey proteins survived). The interaction was monitored by histidine and adenine prototrophy. Yeasts cotransformed with either the positive control (pGBKT7-p53 and pGADT7-T) or pGBKT7-LIII−IV and pGADT7-α-actinin-2 grew on the −TLHA plate (bottom panel, lanes 1 and 5). This experiment was repeated four times with similar results.

with either the positive control (Figure 1B, bottom panel, lane 1) or the $Na_v1.5$/LIII−IV and an α-actinin-2 plasmid (Figure 1B, bottom panel, lane 5) grew more efficiently on synthetic complete medium lacking tryptophan, leucine, histidine, and adenine (−TLHA) than yeast cotransformed with either the negative or empty vector controls (Figure 1B, bottom panel, lanes 2−4, respectively). These results demonstrated that the α-actinin-2 prey and the $Na_v1.5$/LIII−IV bait are not self-activating (Figure 1B, bottom panel, lanes 3 and 4, respectively) and that α-actinin-2 and the $Na_v1.5$/LIII−IV bait physically interact in yeast, leading to the activation of a reporter gene (Figure 1B, bottom panel, lane 5). In contrast, the N-terminal region and the cytoplasmic I−II loop of $Na_v1.5$ did not interact with α-actinin-2 (Figure I of the Supporting Information).

α-Actinin-2 Associates with $Na_v1.5$ in Cotransfected tsA201 Cells. To determine whether $Na_v1.5$ and α-actinin-2 associate with one another, co-immunoprecipitations (Co-IP) were employed to determine whether an antibody against one

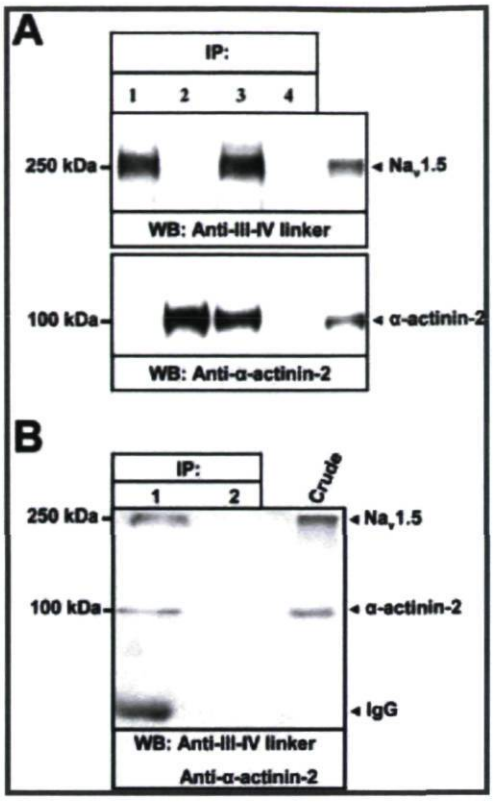

FIGURE 2: α-Actinin-2 and $Na_v1.5$ interacted in mammalian cells. (A) tsA201 cells were transiently transfected with $Na_v1.5$ alone (positive control, lane 1), α-actinin-2 alone (positive control, lane 2), or both (lane 3). The cells were solubilized, and the lysates were immunoprecipitated (IP) with anti-LIII−IV (IP, 1 and 3) or anti-α-actinin-2 antibody (IP, 2) and immunoblotted (IB) with either anti-LIII−IV (top panel) or anti-α-actinin-2 antibody (bottom panel). The anti-LIII−IV antibody immunoprecipitated α-actinin-2 in tsA201 cells coexpressing both proteins (lane 3) but not in tsA201 cells transfected with α-actinin-2 alone (negative control, lane 4). (B) Reciprocal co-immunoprecipitation with the α-actinin-2 antibody for immunoprecipitation and anti-LIII−IV and anti-α-actinin-2 antibodies for Western blotting. tsA201 cells expressing α-actinin-2 and $Na_v1.5$ (lane 1) or $Na_v1.5$ alone (lane 2) were immunoprecipitated with anti-α-actinin-2 antibody (IP, 1 and 2), and the blots were probed with anti-LIII−IV and anti-α-actinin-2 antibodies. The α-actinin-2 antibody (lane 1), but not an irrelevant control antibody (lane 2), specifically co-immunoprecipitated $Na_v1.5$, indicating a bona fide interaction between α-actinin-2 and $Na_v1.5$. The crude extracts represent the cell lysates probed with anti-LIII−IV and anti-α-actinin-2 antibodies and show $Na_v1.5$ and α-actinin-2 levels comparable to those in the sample used for the IP experiment. The arrows indicate the main immunoprecipitation bands. This experiment was repeated three times with similar results.

component, either anti-LIII−IV or anti-α-actinin-2, would co-precipitate the other component. tsA201 cells were cotransfected with constructs for both components. Lysates of transfected cells were co-immunoprecipitated and analyzed for $Na_v1.5$ and α-actinin-2 by immunoblotting (Figure 2A). tsA201 cells were also transfected with the $Na_v1.5$ (lane 1) or α-actinin-2 (lane 2) constructs alone (positive controls). When protein extracts of these cells were immunoprecipitated with either anti-LIII−IV (IP, 1) or anti-α-actinin-2 (IP, 2) antibodies and analyzed by Western blotting with the anti-LIII−IV (top panel) or anti-α-actinin-2 (bottom panel) antibody, the only detectable band, in both cases, was the component that had been transfected. However, when the lysates of the tsA201 cells cotransfected with $Na_v1.5$ and α-actinin-2 were immunoprecipitated with the anti-LIII−IV antibody (IP, 3), there were both $Na_v1.5$ (top panel, lane 3) and α-actinin-2 (bottom panel, lane 3) bands on the blots. Cells transfected with α-actinin-2 alone were used as a negative control. No bands were detected when the negative control lysate was immunoprecipitated with the anti-LIII−IV antibody (lane 4). Reciprocal immunoprecipitation experiments confirmed that $Na_v1.5$ bound to α-actinin-2. As shown in Figure 2B, the α-actinin-2 antibody efficiently immunoprecipitated $Na_v1.5$ in lysates from tsA201 cells cotransfected with $Na_v1.5$ and α-actinin-2 (lane 1) but not in lysates from tsA201 cells transfected with $Na_v1.5$ alone (lane 2). These results demonstrated that full-length $Na_v1.5$ is capable of interacting with full-length α-actinin-2 in mammalian cells.

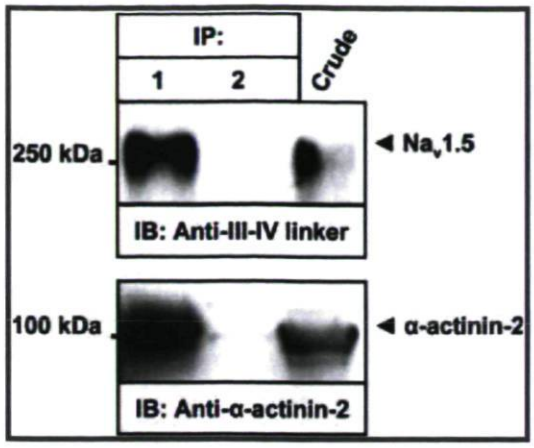

FIGURE 3: Co-immunoprecipitation of α-actinin-2 and $Na_v1.5$ in mouse heart tissue. (A) Proteins were extracted from adult mouse heart in STEN buffer and subjected to immunoprecipitation analysis using either rabbit anti-III−IV loop antibody (LIII−IV) (lane 1) or nonspecific rabbit IgG (lane 2) as described in Materials and Methods. Extracts (Crude) and/or immunoprecipitates (IP) were analyzed by SDS−PAGE and immunoblotted (IB) using either anti-LIII−IV antibody (top panel) or anti-α-actinin-2 antibody (bottom panel). Lysate from heart homogenate (Crude) was used as the positive control. The IgG negative control in lane 2 excluded binding of nonspecific α-actinin-2 to the $Na_v1.5$ channel.

α-Actinin-2 Associates with $Na_v1.5$ in Cardiac Tissue. To assess the physiological relevance of the α-actinin-2 and $Na_v1.5$ interaction further, a co-immunoprecipitation experiment on mouse cardiac homogenate and double immunolabeling on human cardiac muscle tissue were performed. Using soluble extracts from mouse heart, which had been shown by Western blotting to contain both α-actinin-2 and $Na_v1.5$ proteins (Figure 3), the anti-III−IV linker antibody could co-immunoprecipitate a band at ~100 kDa, which was detected using an anti-α-actinin-2 antibody (Figure 3, bottom panel, lane 1). This band did not appear when an irrelevant rabbit IgG was used for immunoprecipitation (Figure 3, bottom panel, lane 2), showing that the reaction was specific and that α-actinin-2 interacts with $Na_v1.5$ *in vivo*.

α-Actinin-2 Isoforms Bind $Na_v1.5$ in Mammalian Cells. Because of the high degree of identity between α-actinin isoforms (*21*), we investigated the interaction between α-actinin isoforms and $Na_v1.5$ using an experimental setup similar to the one described above. Figure 4 shows that α-actinin-1, α-actinin-3, and α-actinin-4 were able to bind to $Na_v1.5$ (Figure 4A−C, lane 1). Mouse preimmune IgG (Figure 4A−C, lane 2) did not immunoprecipitate α-actinin isoforms from tsA201 cells cotransfected with $Na_v1.5$ and the α-actinin isoforms (α-actinin-1, α-actinin-3, or α-actinin-4) (negative control).

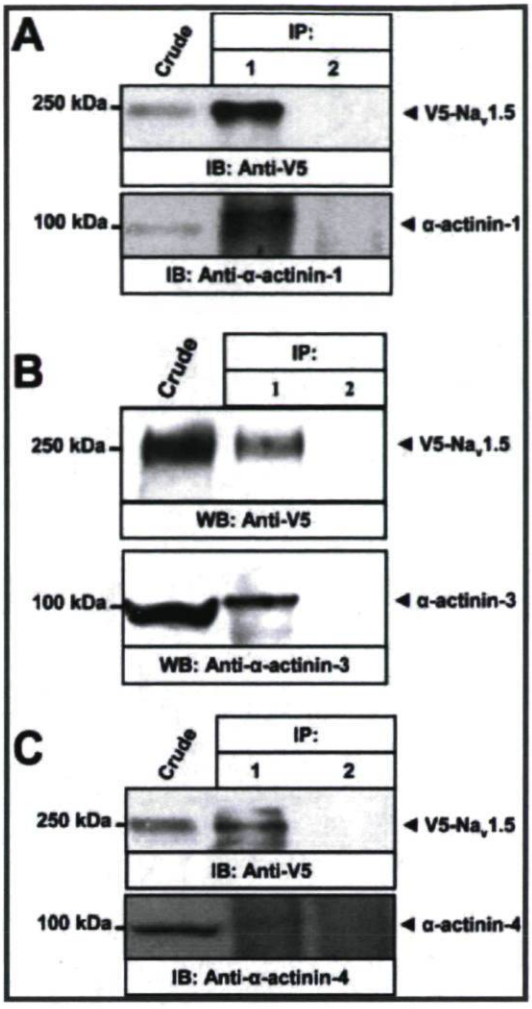

FIGURE 4: α-Actinin isoforms and $Na_v1.5$ interacted in a heterologous expression system. (A) tsA201 cells were transfected with V5-tagged $Na_v1.5$ (V5−$Na_v1.5$) and α-actinin-1 and homogenized in lysis buffer. The cell lysates were immunoprecipitated with anti-V5 antibody (IP, 1) or mouse preimmune serum (negative control) (IP, 2). The blots were probed with anti-V5 antibody (top panel) or anti-α-actinin-1 antibody (bottom panel). The V5 antibody precipitated α-actinin-1 from tsA201 cells cotransfected with V5−$Na_v1.5$ and α-actinin-1 (lane 1) but not the preimmune serum (lane 2). (B) The V5 antibody, but not the preimmune serum (bottom panel, lane 2), immunoprecipitated α-actinin-3 from tsA201 cells cotransfected with V5−$Na_v1.5$ and α-actinin-3 (bottom panel, lane 1). (C) The V5 antibody, but not the preimmune serum (bottom panel, lane 2), immunoprecipitated α-actinin-4 from tsA201 cells transiently expressing $Na_v1.5$ and α-actinin-4 (bottom panel, lane 1). These experiments were repeated three times with similar results.

α-Actinin-2 Binds Directly to the LIII−IV Region of $Na_v1.5$ in Vitro. Recombinant proteins were used in blot overlay and histidine pull-down (His pull-down) assays to verify the interaction between α-actinin-2 and $Na_v1.5$ *in vitro* (Figure 5). tsA201 cells were transiently transfected with increasing amounts (15−45 μg) of cDNA encoding α-actinin-2. Twenty-four hours later, the transfected cells were lysed and the cell extracts were separated by SDS−PAGE and blotted onto PVDF membranes. The blots were incubated with either purified His_6-LIII−IV fusion protein or BSA (negative control). Binding of His_6-LIII−IV fusion protein to α-actinin-2 was revealed by immunoblotting using the anti-LIII−IV antibody. As shown in Figure 5A, His_6-LIII−IV fusion protein bound to α-actinin-2 (top panel, lanes 1−3), while no binding was detected in untransfected tsA201 cells (top panel, lane 4) or blot overlays

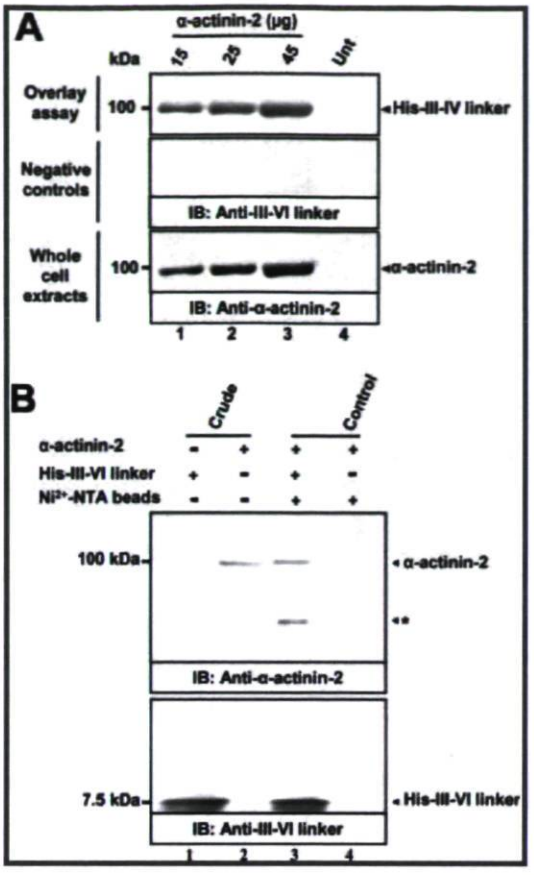

FIGURE 5: α-Actinin-2 and $Na_v1.5$/LIII−IV interacted *in vitro*. (A) Blot overlay assay showing the *in vitro* interaction of α-actinin-2 with the His_6-LIII−IV fusion protein. Increasing amounts (15, 25, and 45 μg) of cDNA encoding α-actinin-2 transiently expressed in tsA201 cells were separated by SDS−PAGE and transferred to PVDF membranes. The blots were used to detect the expression of α-actinin-2 proteins (whole cell extracts, bottom panel) or were incubated with either 1 μg/mL purified LIII−IV fusion protein (overlay assay, top panel) or 1 μg/mL BSA (negative control, middle panel) followed by anti-LIII−IV (top and middle panels) or anti-α-actinin-2 antibody (bottom panel). The LIII−IV fusion protein bound specifically to α-actinin-2 in a dose-dependent manner (top panel, lanes 1−3). No binding was detected in the control lane containing extracts from untransfected tsA201 cells (top panel, lane 4) or in the blot incubated with BSA (middle panel). (B) A His pull-down experiment was performed as described in Materials and Methods. tsA201 cell extracts transiently expressing α-actinin-2 were incubated with either His_6-LIII−IV fusion protein prebound to Ni^{2+}-NTA beads or Ni^{2+}-NTA beads alone (negative control). After being extensively washed, bound proteins were eluted and separated via 10% SDS−PAGE which were then blotted with anti-α-actinin-2 antibody (top panel) or anti-LIII−IV antibody (bottom panel): lanes 1 and 2, extract starting material; lane 3, His_6-LIII−IV fusion protein retained from extract; and lane 4, Ni^{2+}-NTA beads alone (negative control). The asterisk indicates that the band detected in lane 3 may be a degradation product of the His_6-LIII−IV fusion protein. These experiments were repeated four times with similar results.

incubated with BSA (middle panel, lanes 1−4). These results suggest that the His_6-LIII−IV protein binds specifically to α-actinin-2 in a dose-dependent manner. To further confirm this interaction, His pull-down experiments were conducted (Figure 5B). In the first attempt, His_6-LIII−IV protein was expressed in *Escherichia coli*, purified, and immobilized on nickel (Ni^{2+}-NTA) beads (lane 1). The tsA201 cell extracts transiently expressing α-actinin-2 (lane 2) were incubated with either His_6-LIII−IV protein prebound to Ni^{2+}-NTA beads (lane 3) or Ni^{2+}-NTA beads alone (lane 4). The extracts were separated by

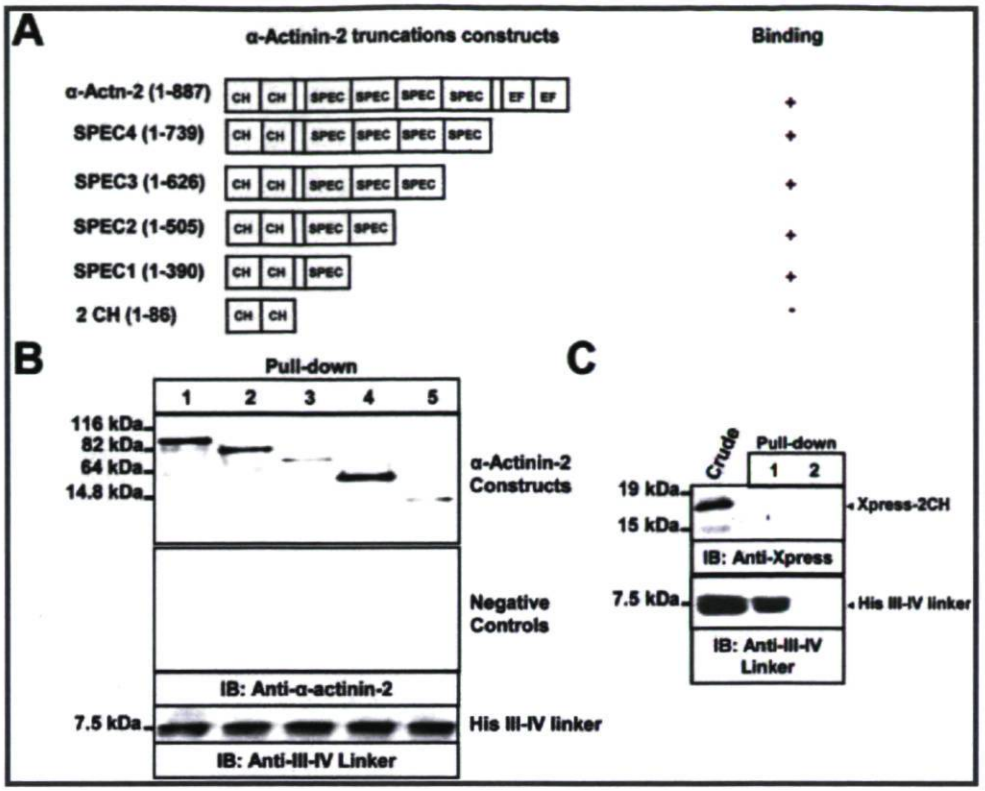

FIGURE 6: Spectrin-like repeat motifs of α-actinin-2 were required for the interaction with the $Na_v1.5$/LIII−IV protein. (A) Schematic representation of full-length α-actinin-2 and the C-terminally truncated α-actinin-2 specific fragments used to map the α-actinin-2 binding sites for LIII−IV. α-Actinin-2 domains are abbreviated as follows: 2 CH, calponin homology domain; SPEC1−SPEC4, SRM; EF, EF-hand domain. The numbers refer to the amino acid residues in the α-actinin-2 constructs. The binding or lack of binding of the various α-actinin-2 segments to LIII−IV, as shown in panel B, is indicated by a plus or minus sign, respectively. (B and C) His pull-down assays. tsA201 cells transiently expressing full-length α-actinin-2 (positive control, lane 1) or C-terminally truncated α-actinin-2 fragments [the SPEC4 domain (lane 2), the SPEC3 domain (lane 3), the SPEC2 domain (lane 4), the SPEC1 domain (lane 5), and the Xpress-tagged 2 CH domain (C, lane 1)] were incubated with either His_6-LIII−IV fusion protein prebound to Ni^{2+}-NTA beads or Ni^{2+}-NTA beads alone (negative control). Proteins bound to the His_6 fusion proteins or nickel beads were eluted and analyzed by Western blotting using an anti-α-actinin-2 (B, first panel) or anti-Xpress tag (C, first panel) antibody. These experiments were repeated three times with similar results.

SDS−PAGE and transferred to PDVF membranes. The blots were then incubated with anti-α-actinin-2 or anti-LIII−IV antibodies. As expected, the His_6-LIII−IV fusion protein successfully pulled down α-actinin-2 (lane 3), whereas no binding was observed with nickel beads alone (negative control, lane 4). The results of the His pull-down assays were in agreement with the overlay results and also showed that there was a direct interaction between α-actinin-2 and LIII−IV *in vitro*.

The Spectrin-like Repeat Motifs Are Required for the Interaction with the $Na_v1.5$/LIII−IV Protein. α-Actinin-2 contains two actin-binding domains (2 CH), four SRM (SPEC1−SPEC4), and an EF. To gain a more precise picture of the LIII−IV binding region of α-actinin-2, we generated five α-actinin-2 C-terminal truncation constructs (Figure 6A) and examined their ability to interact with the His_6-LIII−IV fusion protein using His pull-down assays. As shown in Figure 6B, the four SRM constructs (SPEC1−SPEC4), but not the two CH constructs (Figure 6C, top panel, lane 1), efficiently interacted with the His_6-LIII−IV fusion protein prebound to nickel beads (Figure 6C, top panel, lanes 2−5). Moreover, there was no significant association between the α-actinin-2 truncated contruct derivatives and the nickel beads alone (negative control) (Figure 6B, bottom panel, and Figure 6C, top panel, lane 2). These findings suggested that the central rod domain (amino acids 87−739), or at least one SRM (amino acids 87−390), of α-actinin-2 is essential for binding to LIII−IV. Interestingly, the central rod domain is also important for binding of α-actinin-2 to other ions channels such as NMDA receptors (*22*).

α-Actinin-2 and $Na_v1.5$ Colocalize in Human Cardiac Muscle Tissue. We used indirect double-label immunofluorescence and confocal microscopy to determine whether these two proteins colocalize (Figure 7). A series of 0.45 μm confocal optical serial sections showed that $Na_v1.5$ has a similar striated expression pattern in myocytes (Figure 7A,D), some diffuse intracell and surface labeling, and, occasionally, a dotted pattern outlining the striations, whereas the α-actinin-2 staining revealed, as expected, a striated pattern corresponding to sarcomeric Z-lines (Figure 7B,E). In the merged images, the striations and dots corresponding to $Na_v1.5$ [Figure 7C,F (yellow)] demonstrate that $Na_v1.5$ colocalized with α-actinin-2 along certain portions of the Z-lines. This is a further confirmation by the quatification of immunostaining of colocalization. A portion of 22 myocytes from 12 confocal images were used to quatify the colocalization of $Na_v1.5$ and α-actinin-2. The average colocalization coefficients were 0.45 ± 0.12 and 0.65 ± 0.14 for the green ($Na_v1.5$) and red channels (α-actinin-2), respectively. This suggests that 45% of $Na_v1.5$ staining colocalizes with α-actinin-2, while 65% of the α-actinin-2 signal colocalizes with $Na_v1.5$. To determine the degree of nonspecific binding, cardiomyocytes were incubated with a secondary antibody alone. Interestingly, no signal above background was detected, suggesting that the co-immunodetection is indeed specific (Figure 7G−I).

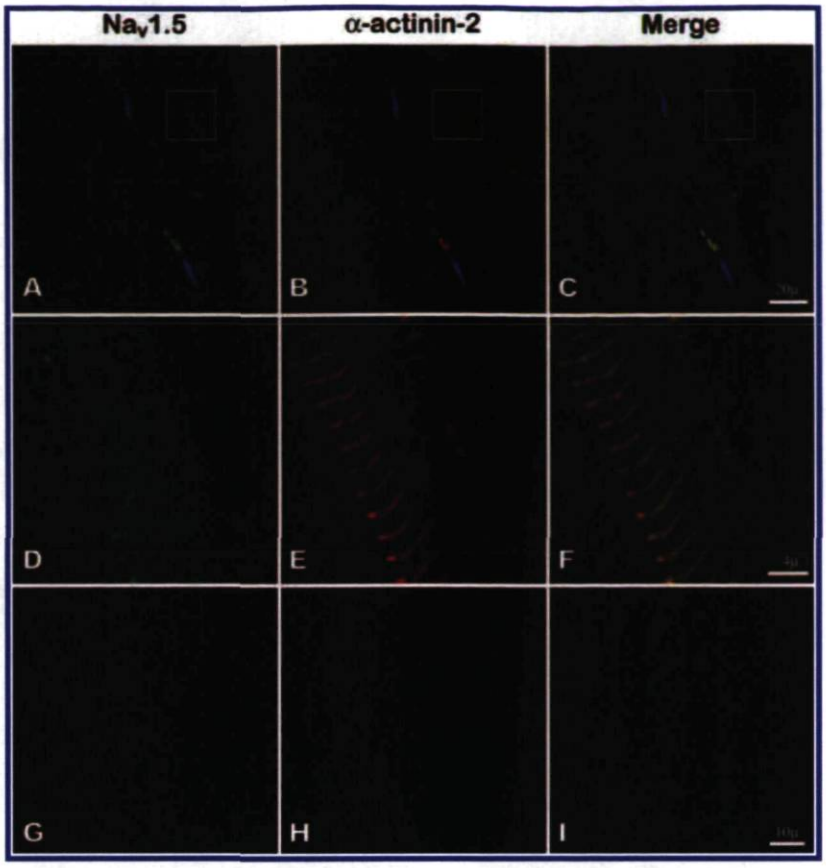

FIGURE 7: Na$_v$1.5 and α-actinin-2 colocalized in human cardiac tissue. Confocal microscopic examination of 0.45 μm sections of a human cardiac ventricle autopsy section stained with anti-Na$_v$1.5 (green in panels A, C, D, and F) and anti-α-actinin-2 4B antibodies (red in panels B, C, E, and F). Nuclei are stained with DAPI (blue) in all images. Merged images (C and F) show yellow striations, confirming the colocalization of α-actinin-2 and Na$_v$1.5 at Z-lines. Panels D−F are higher magnifications of the boxed regions. The rod-shaped structures in panels A−C fluoresced at all wavelengths and were also seen in unstained sections. They represent lipofuscin deposits in this autopsy specimen from an aged individual. Panels G−I show cardiomyocytes that were incubated with the secondary antibody alone. This experiment was performed three times with similar results.

α-Actinin-2 Interacts with Other Sodium Channel Isoforms in Cyto and in Vivo. The high degree of conservation of the LIII−IV polypeptide sequence among different tissues (*23*) and the presence of α-actinin-2 in skeletal muscle and the brain (*24*) suggest that α-actinin-2 may also interact with sodium channels expressed in these tissues. To verify this hypothesis, we performed immunoprecipitation experiments *in vivo* and *in cyto*. Mouse skeletal muscle protein extracts were immunoprecipitated with either an anti-LIII−IV polyclonal antibody [Figure 8A (IP, 1)] or with control preimmune IgG [Figure 8A (IP, 2)]. Bound proteins were detected by Western blotting using an anti-α-actinin-2 or anti-LIII−IV antibody. α-Actinin-2 protein was efficiently precipitated by the anti-LIII−IV antibody (Figure 8A, middle panel, lane 1) but not by the negative control serum (Figure 8A, middle panel, lane 2). Since the Na$_v$1.4 channel is strongly expressed in adult skeletal muscle (*25*), the endogenous adult skeletal muscle sodium channel immunoprecipitated with α-actinin-2 is most likely Na$_v$1.4. Interestingly, like α-actinin-2, α-actinin-3 is also expressed in skeletal muscle, where it forms heterodimers with α-actinin-2 (*19*). Because of this, we decided to explore a putative interaction between α-actinin-3 and skeletal sodium channels. Skeletal muscle samples were immunoprecipitated with an anti-LIII−IV antibody, and the blot was probed with anti-α-actinin-3 antibody. α-Actinin-3 was immunoprecipitated by the anti-LIII−IV antibody (Figure 8A, bottom panel, lane 1). These results demonstrated that α-actinin-2 and α-actinin-3 interact with endogenous skeletal sodium channels and suggested that both may be involved in the same channel complex in skeletal muscle. The anti-LIII−IV antibody also precipitated α-actinin-2 from mouse brain tissue extract (Figure 8B, lane 1). However, more experiments with specific antibodies will be needed to determine which brain sodium channel isoform is involved in this interaction. Lastly, we also observed an interaction between Na$_v$1.8, a sensory neuron-specific sodium channel, and α-actinin-2 in a heterologous expression system (Figure II of the Supporting Information). Our findings thus demonstrate that α-actinin-2 interacts with other sodium channel isoforms in skeletal muscle and brain tissue.

α-Actinin-2 Increases Sodium Current Density in a Mammalian Expression System. To investigate the functional consequences of α-actinin-2 expression on Na$_v$1.5 channel gating, we used the patch-clamp technique in the whole-cell configuration (Figure 9). We measured whole-cell sodium currents in tsA201 cells transiently transfected with either Na$_v$1.5 and the β_1 subunit (control) or Na$_v$1.5 and the β_1 subunit coexpressed with α-actinin-2. As shown in Figure 9A, the maximum sodium current density measured at −30 mV (estimated by dividing the peak current value by the membrane capacitance, p*A*/p*F*) of the control was, on average, 68% higher ($p < 0.01$) than when it was coexpressed with α-actinin-2 (Figure 9B), despite the fact that coexpressing Na$_v$1.5 and the β_1 subunit with α-actinin-2 did not alter cell capacitance [12.94 ± 1.43 pF ($n = 6$) vs 16.69 ± 1.7 pF ($n = 6$); p = ns]. Steady-state activation and inactivation gating

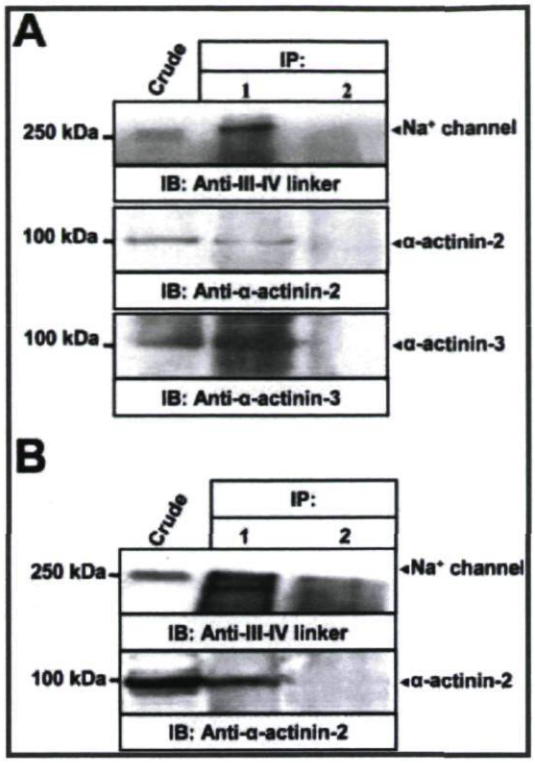

FIGURE 8: α-Actinin-2 interacted with endogenous sodium channels in mouse skeletal muscle and brain tissue. (A) Protein lysates extracted from adult mouse skeletal muscle cells were immunoprecipitated with anti-LIII−IV antibody (IP, 1) or preimmune IgG (negative control) (IP, 2). Signals were detected using anti-LIII−IV (top panel), anti-α-actinin-2 (middle panel), or anti-α-actinin-3 (bottom panel) antibody. The anti-LIII−IV antibody, but not the preimmune serum (middle and bottom panels, lane 2), immunoprecipitated α-actinin-2 and α-actinin-3 (middle and bottom panels, lane 1). α-Actinin-2 and α-actinin-3 specifically associated with skeletal muscle sodium channels *in vivo*. (B) Similarly, soluble sodium channel proteins extracted from adult mouse brain were immunoprecipitated with the anti-LIII−IV antibody (IP, 1) or rabbit preimmune IgG negative control (IP, 2), and the blots were probed with the anti-LIII−IV antibody (top panel) or the anti-α-actinin-2 antibody (bottom panel). α-Actinin-2 bound to endogenous sodium channels in mouse brain tissue. Aliquots of total cell extracts (Crude) were also loaded on the gel to serve as a positive control for the Western blotting. This experiment was performed three times with similar results.

properties were evaluated using the pulse protocols shown in the insets of Figure 10A,B. Neither the activation kinetics (Figure 10A; $V_{1/2act} = -49.60 \pm 2.13$ mV ($n = 6$) versus -51.40 ± 2.08 mV ($n = 6$), p = ns) nor the inactivation kinetics (Figure 10B; $V_{1/2act} = -101.85 \pm 2.32$ mV ($n = 6$) versus -102.47 ± 2.78 mV ($n = 6$), p = ns) of $Na_v1.5$ were altered by the coexpression with α-actinin-2. In conclusion, these results clearly showed that α-actinin-2 increases whole-cell $Na_v1.5$ currents.

α-Actinin-2 Increases the Level of Cell Surface Expression of $Na_v1.5$. The electrophysiological data presented so far argue for an α-actinin-2-mediated increase in the number of functional $Na_v1.5$ channels on the cell surface. To determine whether α-actinin-2 overexpression increases the number of $Na_v1.5$ channels in the plasma membrane, we isolated cell surface proteins by protein biotinylation using a membrane-impermeant biotin ester (Figure 11). Proteins isolated by neutravidin resin affinity precipitation were separated by SDS−PAGE, transferred to PVDF membranes, and immunoblotted with anti-LIII−IV, anti-Na^+/K^+-ATPase α1 subunit, and anti-β-tubulin antibodies.

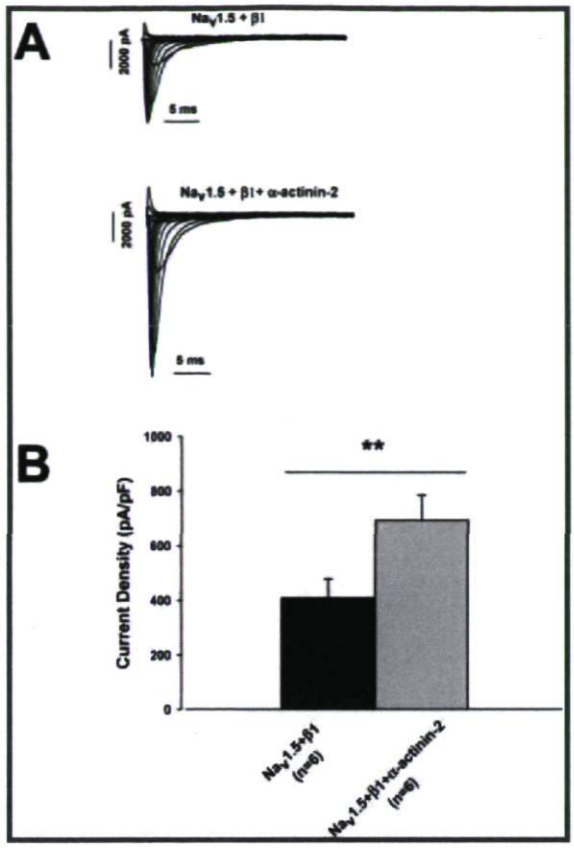

FIGURE 9: Overexpression of α-actinin-2 in tsA201 cells expressing $Na_v1.5$ increased sodium current densities. (A) Representative traces of currents recorded from control and cotransfected tsA201 cells transiently expressing $Na_v1.5+\beta_1$ (top) and $Na_v1.5+\beta_1+$α-actinin-2 (bottom). (B) Bar graph showing current densities at −30 mV in control cells ($Na_v1.5+\beta_1$) with current amplitudes of 409 ± 69.56 pA/pF ($n = 6$) and in cotransfected cells ($Na_v1.5+\beta_1+$ α-actinin-2) with current amplitudes of 693.80 ± 81.80 pA/pF ($n = 6$) (** $P < 0.01$).

The Na^+/K^+-ATPase α1 subunit was analyzed to ensure that equal amounts of protein extract (with and without α-actinin-2) were used (Figure 11, third panel). The absence of β-tubulin in the biotin-labeled samples indicated that the biotin reagent selectively labeled proteins in the plasma membrane (panel 4). As shown in Figure 11, overexpression of α-actinin-2 increased the amount of $Na_v1.5$ channel at the cell surface (panel 2, lanes 3 and 4, respectively) compared with an empty vector control (second panel, lane 1) or the $Na_v1.5$ channel expressed alone (panel 2, lane 2). These results also showed that the expression of the biotinylated $Na_v1.5$ channel depends on the amount of transfected α-actinin-2 cDNA. The total amount of $Na_v1.5$ was similar in the extracts (first panel 1). The quatification of the data shows a significant 4-fold increase in the level of $Na_v.5$ cell surface expression when contransfected with 5 μg of DNA encoding α-actinin-2 (Figure 11B). In contrast, the absence of β-tubulin in the streptavidin isolates indicated that biotin cannot penetrate the cell. These findings showed that α-actinin-2 mediates $Na_v1.5$ channel plasma membrane expression, which is consistent with the observation that coexpression of α-actinin-2 increases sodium channel densities.

DISCUSSION

We used a yeast two-hybrid screen to identify protein partners of the human cardiac sodium channel. We present evidence that

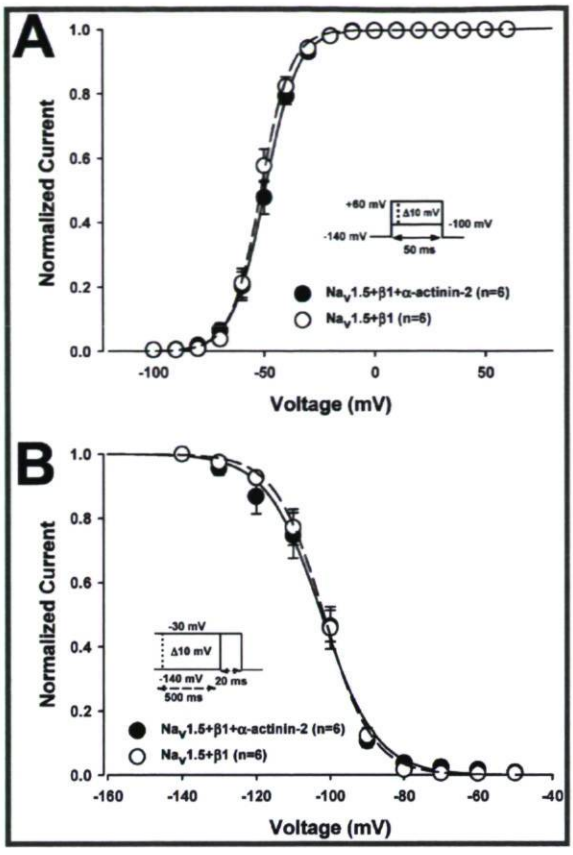

FIGURE 10: Overexpression of α-actinin-2 did not affect the steady-state activation and inactivation of $Na_v1.5$ channels. Steady-state activation (A) and inactivation (B) curves in tsA201 cells transiently cotransfected with $Na_v1.5$ and the β_1 subunit with or without α-actinin-2. Currents were elicited using 50 ms depolarization steps from −100 to 60 mV in 10 mV increments. The cells were held at a holding potential of −140 mV (see the inset for the protocol). The activation curves were constructed using the following Boltzmann equation: $G/G_{max} = 1/[1 + \exp(V_{1/2} - V)/k_v]$, where G is the measured conductance, G_{max} is the maximal conductance, $V_{1/2}$ is the voltage at which the channels are half-activated, and k_v is the slope factor. The fitting generated a $V_{1/2}$ of -49.60 ± 2.13 mV with a k_v of -6.45 ± 1.31 mV for $Na_v1.5$, β_1 subunit, and α-actinin-2 ($n = 6$) and a $V_{1/2}$ of -51.40 ± 2.08 mV with a k_v of -6.10 ± 1.45 mV for $Na_v1.5$ and β_1 subunit ($n = 6$). For the inactivation curves, the peak current (I) was normalized relative to the maximal value (I_{max}). The peak current amplitude was elicited by 20 ms test pulses to −30 mV after 500 ms prepulses at potentials ranging from −140 to −30 mV (see the inset for the protocol). The inactivation curves were fitted to the following Boltzmann equation: $I/I_{max} = a(1/\{1 + \exp[(V - V_{1/2})/k_v]\})$, where V is the membrane potential during the prepulse, $V_{1/2}$ is the voltage at which the channels are half-inactivated, and k_v is the slope factor. The fitting generated a $V_{1/2}$ of -102.47 ± 2.78 mV with a k_v of 6.42 ± 2.02 mV for $Na_v1.5$, β_1 subunit, and α-actinin-2 ($n = 6$) and a $V_{1/2}$ of -101.85 ± 2.32 mV with a k_v of 6.04 ± 2.11 mV for $Na_v1.5$ and β_1 subunit ($n = 6$).

α-actinin-2 specifically binds to the LIII−IV polypeptide *in vitro* and *in cyto*. Colocalization of $Na_v1.5$ and α-actinin-2 in the regions where T-tubules contact Z-lines in human cardiac ventricles and the ability of α-actinin-2 to modulate sodium current densities and cell surface expression of the channel in tsA201 cells suggest that the interaction is physiologically relevant.

Given the high degree of sequence identity (50%) among sodium channels (*26*), we were not surprised that α-actinin-2 also bound to other sodium channels such as $Na_v1.8$ and endogenous sodium channels from skeletal muscle and brain tissue. There are two sodium channel isoforms ($Na_v1.4$ and $Na_v1.5$) in skeletal

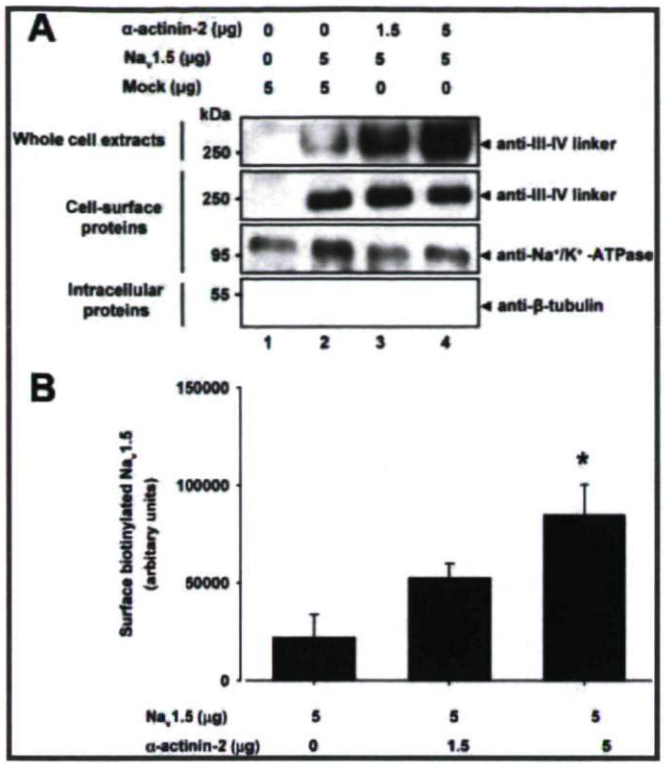

FIGURE 11: Coexpression of α-actinin-2 and $Na_v1.5$ increased the level of cell surface expression of $Na_v1.5$. (A) $Na_v1.5$ channels were transfected into tsA201 cells with empty vector (mock) or increasing amounts (1.5−5 g) of cDNA encoding α-actinin-2. Forty-eight hours later, the total membrane proteins were labeled with a membrane-impermeable biotinylation reagent and isolated membrane proteins were labeled with streptavidin beads. Channel immunoreactivity in the whole cell lysates (positive control, first panel) and in the streptavidin precipitates (second panel) was detected using an anti-LIII−IV antibody. Cell surface expression of $Na_v1.5$ in the presence of α-actinin-2 (second panel, lanes 3 and 4) and in the absence of α-actinin-2 (second panel, lane 1). The blots were also probed with anti-Na^+/K^+-ATPase α1 antibody as a cell surface protein marker (third panel) and with anti-β-tubilin antibody as a negative control (fourth panel). This experiment was repeated at least four times, and similar results were obtained. (B) Quantification of the data.

muscle. The $Na_v1.4$ channel is more strongly expressed in adult than in neonatal rat skeletal muscle, whereas the $Na_v1.5$ channel can be detected in neonatal skeletal muscle and after denervation of adult muscle (*27*, *28*). The endogenous skeletal sodium channel involved in the interaction with α-actinin-2 is thus most likely $Na_v1.4$. However, the functional significance of the α-actinin-2−sodium channel isoform interaction has yet to be determined in native tissue, where both are well expressed.

α-Actinin-2 belongs to the large family of spectrin-like proteins (*29*). There are four α-actinin genes, two nonskeletal muscle isoforms, α-actinin-1 and -4, and two skeletal muscle isoforms, α-actinin-2 and -3 (*10*), all of which share a general structure than can be divided into three functionally distinct domains [two highly conserved CH domains in the N-terminus that are necessary for actin binding, followed by four SRM that make up a central rod domain that is required for the antiparallel dimerization of α-actinin-2, and two carboxy-terminal EF-hand CaM domains (*11*)]. The SRM of α-actinin-2, which is the region that interacts with $Na_v1.5$, has been mapped. The structure of the central rod domain of actinin is a twisted antiparallel homodimer. The four SRM in this domain form tight dimer contacts and a rigid connection between two actin-binding domains positioned at the two ends of the actinin dimer. The SRM are

also important interaction sites for a number of structural and signaling proteins such as NMDA receptors, potassium channels ($K_v1.4$ and $K_v1.5$), the polycystin-2 channel, and the transient receptor potential polycystin 3 (TRPP3) (*13*, *16*, *22*, *30*).

Because of the high level of sequence identity between α-actinin isoforms, we looked at whether $Na_v1.5$ interacted with all the α-actinin isoforms. Interestingly, we found that α-actinin-1, α-actinin-3, and α-actinin-4 interacted with $Na_v1.5$ in a heterologous expression system. We also showed that skeletal muscle sodium channels interact with two skeletal muscle isoforms of α-actinin (α-actinin-2 and α-actinin-3) *in vivo*. The nonmuscle α-actinin isoforms (α-actinin-1 and -4), like α-actinin-2, have been implicated in the anchoring of other ion channels to the cytoskeleton. The interaction of α-actinin-1 with the $mGlu_{5b}$ receptor modulates the cell surface expression of the receptor. This is dependent on the binding of α-actinin-1 to the actin cytoskeleton (*31*). It has been suggested that α-actinin-4 may link acid-sensing ion channel 1a (ASIC1a) to a macromolecular complex in the postsynaptic membrane where it regulates ASIC1a activity (*32*). It thus appears that α-actinin isoforms play a dual role as a component of the actin cytoskeleton and as a molecule that targets and anchors receptors to the plasma membrane.

α-Actinin-2 and the $Na_v1.5$ Channel Colocalize in Human Cardiac Tissue. Our immunocytochemical experiments revealed a striated, occasionally dotted, staining pattern, which is consistent with localization at T-tubules, with additional diffuse staining within the sarcoplasm and at cell membranes similar to the distribution reported by others (*33*−*35*). The $Na_v1.5$-positive striations colocalized with α-actinin-2 positive Z-lines, indicating that the interaction between $Na_v1.5$ channels and α-actinin-2 likely occurs in regions where T-tubules contact Z-lines. In cardiomyocytes, α-actinin-2 is essentially localized at the Z-line (*24*). However, the precise localization of $Na_v1.5$ in cardiomyocytes is somewhat controversial. It is known that a pool of $Na_v1.5$ is localized at specialized cell−cell junctions or intercalated disks (*36*, *37*). The presence of $Na_v1.5$ in lateral membranes and T-tubules, however, is still a matter of discussion (*34*, *37*). It is interesting to note that $Na_v1.5$ interacts with dystrophin, which is predominantly localized in the transverse tubule/Z-line (*38*) but is not present in intercalated disks (*39*). The loss of dystrophin affected the expression levels of $Na_v1.5$, leading to a reduced sodium current density. Hence, the hypothesis that at least two pools of $Na_v1.5$ channels exist in the plasma membrane of cardiomyocytes cannot be excluded (*9*). The first pool would be localized in lateral membranes and would consist of dystrophin-associated proteins, whereas the second pool would be localized in the intercalated disks. Our results support this hypothesis and suggest that the localization of $Na_v1.5$ in the T-tubules appears to be dependent on its interaction with proteins such as α-actinin-2, dystrophin, syntrophin, and other PDZ domain proteins. Furthermore, the differential localization of $Na_v1.5$ channels in intercalated disks versus T-tubules is likely related to age. Kucera et al. (*40*) showed that $Na_v1.5$ is localized in nascent intercalated disks in neonatal cardiac myocytes, whereas Haufe et al. (*41*) reported that $Na_v1.5$ is expressed in the intercalated disks as well as at the Z-lines in cardiomyocytes isolated from 38-day-old mice (*42*). Interestingly, Haufe et al. (*41*) also observed that tetrodotoxin-sensitive $Na_v1.1$ in canine cells is mainly expressed in intercalated disks with only a faint Z-line distribution. Consequently, there may be additional species-specific roles for tetrodotoxin-sensitive sodium channel isoforms. As such, species differences must be taken into account when studying the cardiac distribution of $Na_v1.5$. With all this together, the precise localization of $Na_v1.5$ in cardiomyocytes is somewhat controversial. The use of distinct sources of antibodies, different species, and technical procedures might underlie such differences, although such controversies are still a matter of further discussion (*34*, *37*). Differentially localized sodium channels may have different physiological roles (*36*, *37*).

What Is the Functional Significance of the Interaction of α-Actinin-2 with the $Na_v1.5$ Channel? Patch-clamp experiments showed that the expression of α-actinin-2 in tsA201 cells transiently transfected with $Na_v1.5$ resulted in an average 68% increase in the whole-cell sodium current density. However, the biophysical properties of the channel were not altered, and only the channel density was increased. Cell surface biotinylation experiments clearly supported this finding and demonstrated that there is much more $Na_v1.5$ protein on the surface of tsA201 cells coexpressing α-actinin-2. Our findings are in agreement with the proposed mode of α-actinin-2 action on voltage-gated K^+ channels (*43*) and point to a model in which α-actinin-2 increases the number of $Na_v1.5$ channels and/or availability on the cell surface, which in turn causes an increase in sodium current densities. However, indirect effects mediated through other cell targets of α-actinin-2 cannot be excluded. α-Actinin-2-associated proteins such as dystrophin also interact with the C-terminus of $Na_v1.5$ and play an important role in the appropriate expression and function of the channel in T-tubule membranes (*9*, *44*). Interestingly, the C-terminus of $Na_v1.5$ has been reported to interact with the LIII−IV fusion protein and form a complex that stabilizes the inactivated gate-occluded channel (*45*). Through these multiple interactions, α-actinin-2 may act together with dystrophin to ensure the proper localization and stabilization of $Na_v1.5$ channels in these regions. The absence of dystrophin in mdx^{5cv} cardiomyocytes significantly decreases sodium current densities and $Na_v1.5$ protein levels, whereas $Na_v1.5$ mRNA levels remain unchanged (*9*). We also observed a reduced level of expression of $Na_v1.5$ protein in mdx^{5cv} cardiomyocytes (data not shown). Conversely, the absence of dystrophin had no apparent effect on the cell expression of α-actinin-2. Likewise, the loss of dystrophin has been reported to modify the expression of sodium channels in skeletal muscle (*46*), while the tissue distribution of α-actinin-2 is unaffected (*47*). Most importantly, the expression in mdx mice of a chimeric microdystrophin transgene containing the four SRM of α-actinin-2 has been shown to ensure the correct assembly and localization of the dystrophin−glycoprotein complex in the sacrolemma at levels approximately equal to those associated with full-length dystrophin and to provide some protection from contraction-induced injury (*48*). One interpretation of these results is that α-actinin-2 may replace dystrophin when it is missing. Lastly, our findings support the notion that α-actinin-2 may be involved in the proper expression of $Na_v1.5$ by anchoring the channel at the cell membrane, making it less likely to be internalized and subsequently degraded. However, we cannot rule out the possibility of another indirect mechanism involving an α-actinin-2-associated protein complex containing dystrophin.

Do Changes in the Expression Level of $Na_v1.5$ Alter Cardiac Function? Changes in the sodium current densities and cell surface expression of $Na_v1.5$ are important determinants of the clinical phenotype of some cardiac disorders such as in Brugada syndrome (*49*, *50*). A significant increase in sodium current densities has been observed in cardiomyocytes from

guinea pigs with cardiac hypertrophy and failure (*51*), while a decrease in the level of membrane expression of $Na_v1.5$ has been observed in a dog model of atrial fibrillation (*49*, *50*). Similarly, Baba et al. (*52*) showed that dog cardiomyocytes isolated from infarcted zones have reduced sodium current densities associated with a marked loss of $Na_v1.5$ staining in T-tubules. In contrast, $Na_v1.5$ staining was unaffected in the intercalated disks. It is tempting to speculate that α-actinin-2 is involved in this phenomenon. Recently, two studies showed that a loss of function mutation in the $Na_v1.5$ gene leads to dilated cardiomyopathy and atrial fibrillation in humans (*2*, *53*). Interestingly, α-actinin-2 mutations have also been associated with dilated cardiomyopathy (*54*). It would thus be interesting to analyze α-actinin-2 expression levels in pathological states and determine how α-actinin-2 mutations affect the expression and function of $Na_v1.5$ and lead to similar cardiac diseases. Further experiments exploring the physiological role of α-actinin-2 *in vivo* in mammalian myocardia are warranted. Resolving these issues will likely provide more insights into its role and its relevance in myocardial function and may provide interesting targets for new therapeutic strategies for treating lethal arrhythmias associated with $Na_v1.5$.

In conclusion, this study suggests that α-actinin-2 can promote or stabilize the targeting of the $Na_v1.5$ channel at specific subcellular membrane domains by interacting with the channel directly and/or indirectly through α-actinin-2-associated proteins or a yet to be discovered adaptor protein.

SUPPORTING INFORMATION AVAILABLE

Table I and Figures I and II. This material is available free of charge via the Internet at http://pubs.acs.org.

REFERENCES

1. George, A. L., Jr. (2005) Inherited disorders of voltage-gated sodium channels. *J. Clin. Invest. 115*, 1990–1999.
2. McNair, W. P., Ku, L., Taylor, M. R., Fain, P. R., Dao, D., Wolfel, E., and Mestroni, L. (2004) SCN5A mutation associated with dilated cardiomyopathy, conduction disorder, and arrhythmia. *Circulation 110*, 2163–2167.
3. Rougier, J. S., van Bemmelen, M. X., Bruce, M. C., Jespersen, T., Gavillet, B., Apothéloz, F., Cordonier, S., Staub, O., Rotin, D., and Abriel, H. (2005) Molecular Determinants of Voltage-Gated Sodium Channel Regulation by the Nedd4/Nedd4-like Proteins. *Am. J. Physiol. 288*, C692–C701.
4. McEwen, D. P., Meadows, L. S., Chen, C., Thyagarajan, V., and Isom, L. L. (2004) Sodium channel β1 subunit-mediated modulation of Nav1.2 currents and cell surface density is dependent on interactions with contactin and ankyrin. *J. Biol. Chem. 279*, 16044–16049.
5. Fahmi, A. I., Patel, M., Stevens, E. B., Fowden, A. L., John, J. E., III, Lee, K., Pinnock, R., Morgan, K., Jackson, A. P., and Vandenberg, J. I. (2001) The sodium channel β-subunit SCN3b modulates the kinetics of SCN5a and is expressed heterogeneously in sheep heart. *J. Physiol. 537*, 693–700.
6. Zimmer, T., Biskup, C., Bollensdorff, C., and Benndorf, K. (2002) The β1 subunit but not the β2 subunit colocalizes with the human heart Na^+ channel (hH1) already within the endoplasmic reticulum. *J. Membr. Biol. 186*, 13–21.
7. Lemaillet, G., Walker, B., and Lambert, S. (2003) Identification of a conserved ankyrin-binding motif in the family of sodium channel α subunits. *J. Biol. Chem. 278*, 27333–27339.
8. Mohler, P. J., Rivolta, I., Napolitano, C., Lemaillet, G., Lambert, S., Priori, S. G., and Bennett, V. (2004) Nav1.5 E1053K mutation causing Brugada syndrome blocks binding to ankyrin-G and expression of Nav1.5 on the surface of cardiomyocytes. *Proc. Natl. Acad. Sci. U.S.A. 101*, 17533–17538.
9. Gavillet, B., Rougier, J. S., Domenighetti, A. A., Behar, R., Boixel, C., Ruchat, P., Lehr, H. A., Pedrazzini, T., and Abriel, H. (2006) Cardiac sodium channel Nav1.5 is regulated by a multiprotein complex composed of syntrophins and dystrophin. *Circ. Res. 99*, 407–414.
10. Takada, F., and Beggs, A. H. (2002) α-Actinins. In Encyclopedia of Molecular Medicine (Creighton, T. E., Ed.) pp 122−127, John Wiley & Sons, Inc., New York.
11. Beggs, A. H., Byers, T. J., Knoll, J. H., Boyce, F. M., Bruns, G. A., and Kunkel, L. M. (1992) Cloning and characterization of two human skeletal muscle α-actinin genes located on chromosomes 1 and 11. *J. Biol. Chem. 267*, 9281–9288.
12. Otey, C. A., and Carpen, O. (2004) α-Actinin revisited: A fresh look at an old player. *Cell Motil. Cytoskeleton 58*, 104–111.
13. Li, Q., Montalbetti, N., Shen, P. Y., Dai, X. Q., Cheeseman, C. I., Karpinski, E., Wu, G., Cantiello, H. F., and Chen, X. Z. (2005) α-Actinin associates with polycystin-2 and regulates its channel activity. *Hum. Mol. Genet. 14*, 1587–1603.
14. Schulz, T. W., Nakagawa, T., Licznerski, P., Pawlak, V., Kolleker, A., Rozov, A., Kim, J., Dittgen, T., Kohr, G., Sheng, M., Seeburg, P. H., and Osten, P. (2004) Actin/αactinin-dependent transport of AMPA receptors in dendritic spines: Role of the PDZ-LIM protein RIL. *J. Neurosci. 24*, 8584–8594.
15. Fedida, D., Maruoka, N. D., and Lin, S. (1999) Modulation of slow inactivation in human cardiac Kv1.5 channels by extra- and intracellular permeant cations. *J. Physiol. 515*, 315–329.
16. Djinovic-Carugo, K., Gautel, M., Ylanne, J., and Young, P. (2002) The spectrin repeat: A structural platform for cytoskeletal protein assemblies. *FEBS Lett. 513*, 119–123.
17. Gellens, M. E., George, A. L., Jr., Chen, L. Q., Chahine, M., Horn, R., Barchi, R. L., and Kallen, R. G. (1992) Primary structure and functional expression of the human cardiac tetrodotoxin-insensitive voltage-dependent sodium channel. *Proc. Natl. Acad. Sci. U.S.A. 89*, 554–558.
18. Margolskee, R. F., McHendry-Rinde, B., and Horn, R. (1993) Panning transfected cells for electrophysiological studies. *BioTechniques 15*, 906–911.
19. Chan, Y. M., Tong, H. Q., Beggs, A. H., and Kunkel, L. M. (1998) Human skeletal muscle-specific α-actinin-2 and -3 isoforms form homodimers and heterodimers *in vitro* and *in vivo*. *Biochem. Biophys. Res. Commun. 248*, 134–139.
20. Chahine, M., Pilote, S., Pouliot, V., Takami, H., and Sato, C. (2004) Role of arginine residues on the S4 segment of the *Bacillus halodurans* Na^+ channel in voltage-sensing. *J. Membr. Biol. 201*, 9–24.
21. Virel, A., and Backman, L. (2004) Molecular evolution and structure of α-actinin. *Mol. Biol. Evol. 21*, 1024–1031.
22. Wyszynski, M., Kharazia, V., Shanghvi, R., Rao, A., Beggs, A. H., Craig, A. M., Weinberg, R., and Sheng, M. (1998) Differential regional expression and ultrastructural localization of α-actinin-2, a putative NMDA receptor-anchoring protein, in rat brain. *J. Neurosci. 18*, 1383–1392.
23. Hartmann, H. A., Tiedeman, A. A., Chen, S. F., Brown, A. M., and Kirsch, G. E. (1994) Effects of III-IV linker mutations on human heart Na^+ channel inactivation gating. *Circ. Res. 75*, 114–122.
24. Mills, M., Yang, N., Weinberger, R., Vander Woude, D. L., Beggs, A. H., Easteal, S., and North, K. (2001) Differential expression of the actin-binding proteins, α-actinin-2 and -3, in different species: Implications for the evolution of functional redundancy. *Hum. Mol. Genet. 10*, 1335–1346.
25. Trimmer, J. S., Cooperman, S. S., Agnew, W. S., and Mandel, G. (1990) Regulation of muscle sodium channel transcripts during development and in response to denervation. *Dev. Biol. 142*, 360–367.
26. Goldin, A. L., Barchi, R. L., Caldwell, J. H., Hofmann, F., Howe, J. R., Hunter, J. C., Kallen, R. G., Mandel, G., Meisler, M. H., Berwald-Netter, Y., Noda, M., Tamkun, M. M., Waxman, S. G., Wood, J. N., and Catterall, W. A. (2000) Nomenclature of voltage-gated sodium channels. *Neuron 28*, 365–368.
27. Goldin, A. L. (1999) Diversity of mammalian voltage-gated sodium channels. *Ann. N.Y. Acad. Sci. 868*, 38–50.
28. Kallen, R. G., Sheng, Z. H., Yang, J., Chen, L. Q., Rogart, R. B., and Barchi, R. L. (1990) Primary structure and expression of a sodium channel characteristic of denervated and immature rat skeletal muscle. *Neuron 4*, 233–242.
29. Sjoblom, B., Salmazo, A., and Djinovic-Carugo, K. (2008) α-Actinin structure and regulation. *Cell. Mol. Life Sci. 65*, 2688–2701.
30. Cukovic, D., Lu, G. W. K., Wible, B., Steele, D. F., and Fedida, D. (2001) A discrete amino terminal domain of Kv1.5 and Kv1.4 potassium channels interacts with the spectrin repeats of α-actinin-2. *FEBS Lett. 498*, 87–92.
31. Cabello, N., Remelli, R., Canela, L., Soriguera, A., Mallol, J., Canela, E. I., Robbins, M. J., Lluis, C., Franco, R., McIlhinney, J., and

Ciruela, F. (2007) Actin-binding protein α-actinin-1 interacts with the metabotropic glutamate receptor type 5b and modulates the cell surface expression and function of the receptor. *J. Biol. Chem. 282*, 12143–12153.
32. Schnizler, M. K., Schnizler, K., Zha, X. M., Hall, D. D., Wemmie, J. A., Hell, J. W., and Welsh, M. J. (2009) The cytoskeletal protein α-actinin regulates acid-sensing ion channel 1a through a C-terminal interaction. *J. Biol. Chem. 284*, 2697–2705.
33. Wagner, S., Dybkova, N., Rasenack, E. C. L., Jacobshagen, C., Fabritz, L., Kirchhof, P., Maier, S. K. G., Zhang, T., Hasenfuss, G., Brown, J. H., Bers, D. M., and Maier, L. S. (2006) Ca^{2+}/calmodulin-dependent protein kinase II regulates cardiac Na^+ channels. *J. Clin. Invest. 116*, 3127–3138.
34. Dominguez, J. N., de la Rosa, A., Navarro, F., Franco, D., and Aranega, A. E. (2008) Tissue distribution and subcellular localization of the cardiac sodium channel during mouse heart development. *Cardiovasc. Res. 78*, 45–52.
35. Qu, Y., Karnabi, E., Chahine, M., Vassalle, M., and Boutjdir, M. (2007) Expression of skeletal muscle $Na_V1.4$ Na channel isoform in canine cardiac Purkinje myocytes. *Biochem. Biophys. Res. Commun. 355*, 28–33.
36. Cohen, S. A. (1996) Immunocytochemical localization of rH1 sodium channel in adult rat heart atria and ventricle. Presence in terminal intercalated disks. *Circulation 94*, 3083–3086.
37. Maier, S. K. G., Westenbroek, R. E., McCormick, K. A., Curtis, R., Scheuer, T., and Catterall, W. A. (2004) Distinct subcellular localization of different sodium channel α and β subunits in single ventricular myocytes from mouse heart. *Circulation 109*, 1421–1427.
38. Peri, V., Ajdukovic, B., Holland, P., and Tuana, B. S. (1994) Dystrophin predominantly localizes to the transverse tubule/Z-line regions of single ventricular myocytes and exhibits distinct associations with the membrane. *Mol. Cell. Biochem. 130*, 57–65.
39. Kaprielian, R. R., Stevenson, S., Rothery, S. M., Cullen, M. J., and Severs, N. J. (2000) Distinct patterns of dystrophin organization in myocyte sarcolemma and transverse tubules of normal and diseased human myocardium. *Circulation 101*, 2586–2594.
40. Kucera, J. P., Rohr, S., and Rudy, Y. (2002) Localization of sodium channels in intercalated disks modulates cardiac conduction. *Circ. Res. 91*, 1176–1182.
41. Haufe, V., Camacho, J. A., Dumaine, R., Gunther, B., Bollensdorff, C., von Banchet, G. S., Benndorf, K., and Zimmer, T. (2005) Expression pattern of neuronal and skeletal muscle voltage-gated Na^+ channels in the developing mouse heart. *J. Physiol. 564*, 683–696.
42. Haufe, V., Cordeiro, J. M., Zimmer, T., Wu, Y. S., Schiccitano, S., Benndorf, K., and Dumaine, R. (2005) Contribution of neuronal sodium channels to the cardiac fast sodium current INa is greater in dog heart Purkinje fibers than in ventricles. *Cardiovasc. Res. 65*, 117–127.
43. Maruoka, N. D., Steele, D. F., Au, B. P. Y., Dan, P., Zhang, X., Moore, E. D. W., and Fedida, D. (2000) α-Actinin-2 couples to cardiac Kv1.5 channels, regulating current density and channel localization in HEK cells. *FEBS Lett. 473*, 188–194.
44. Hance, J. E., Fu, S. Y., Watkins, S. C., Beggs, A. H., and Michalak, M. (1999) α-Actinin-2 is a new component of the dystrophin-glycoprotein complex. *Arch. Biochem. Biophys. 365*, 216–222.
45. Motoike, H. K., Liu, H., Glaaser, I. W., Yang, A. S. Y., Tateyama, M., and Kass, R. S. (2004) The Na^+ channel inactivation gate is a molecular complex: A novel role of the COOH-terminal domain. *J. Gen. Physiol. 123*, 155–165.
46. Ribaux, P., Bleicher, F., Couble, M. L., Amsellem, J., Cohen, S. A., Berthier, C., and Blaineau, S. (2001) Voltage-gated sodium channel (SkM1) content in dystrophin-deficient muscle. *Pfluegers Arch. 441*, 746–755.
47. Williams, M. W., and Bloch, R. J. (1999) Extensive but coordinated reorganization of the membrane skeleton in myofibers of dystrophic (mdx) mice. *J. Cell Biol. 144*, 1259–1270.
48. Harper, S. Q., Hauser, M. A., DelloRusso, C., Duan, D., Crawford, R. W., Phelps, S. F., Harper, H. A., Robinson, A. S., Engelhardt, J. F., Brooks, S. V., and Chamberlain, J. S. (2002) Modular flexibility of dystrophin: Implications for gene therapy of Duchenne muscular dystrophy. *Nat. Med. 8*, 253–261.
49. Baroudi, G., Pouliot, V., Denjoy, I., Guicheney, P., Shrier, A., and Chahine, M. (2001) Novel mechanism for Brugada syndrome: Defective surface localization of an *SCN5A* mutant (R1432G). *Circ. Res. 88*, E78–E83.
50. Brugada, J., Brugada, R., and Brugada, P. (1998) Right bundle-branch block and ST-segment elevation in leads V_1 through V_3: A marker for sudden death in patients without demonstrable structural heart disease. *Circulation 97*, 457–460.
51. Ahmmed, G. U., Dong, P. H., Song, G., Ball, N. A., Xu, Y., Walsh, R. A., and Chiamvimonvat, N. (2000) Changes in Ca^{2+} cycling proteins underlie cardiac action potential prolongation in a pressure-overloaded guinea pig model with cardiac hypertrophy and failure. *Circ. Res. 86*, 558–570.
52. Baba, S., Dun, W., Cabo, C., and Boyden, P. A. (2005) Remodeling in cells from different regions of the reentrant circuit during ventricular tachycardia. *Circulation 112*, 2386–2396.
53. Olson, T. M., Michels, V. V., Ballew, J. D., Reyna, S. P., Karst, M. L., Herron, K. J., Horton, S. C., Rodeheffer, R. J., and Anderson, J. L. (2005) Sodium channel mutations and susceptibility to heart failure and atrial fibrillation. *J. Am. Med. Assoc. 293*, 447–454.
54. Mohapatra, B., Jimenez, S., Lin, J. H., Bowles, K. R., Coveler, K. J., Marx, J. G., Chrisco, M. A., Murphy, R. T., Lurie, P. R., Schwartz, R. J., Elliott, P. M., Vatta, M., McKenna, W., Towbin, J. A., and Bowles, N. E. (2003) Mutations in the muscle LIM protein and α-actinin-2 genes in dilated cardiomyopathy and endocardial fibroelastosis. *Mol. Genet. Metab. 80*, 207–215.

In utero onset of long QT syndrome with atrioventricular block and spontaneous or lidocaine-induced ventricular tachycardia: compound effects of hERG pore region mutation and SCN5A N-terminus variant.

Lin, M.T., Wu, M.H., Chang, C.C., Chiu, S.N., Theriault, O., **Huang, H.**, Christe, G., Ficker, E., Chahine, M.

Heart Rhythm. (2008) **5**, 1567-1574.

Contribution role: (1) Doing experiments regarding biophysical characterization of *SCN5A* mutation R43Q and its changes in gating properties with the treatment of lidocaine by whole-cell configuration of patch-clamp technique. (2) Analyzing resulting data. In tsA201 cells transfected with R43Q mutant and WT channels, there were no significant differences for Na+ currents between these two groups. However, lidocaine caused a hyperpolarizing shift of the activation for mutant channels, which resulted in enhanced widow currents. This finding suggested that R43Q mutation may be responsible for the development of ventricular tachycardia in the background of AV block caused by *hERG* mutation F627L in the patient. All resulting data were listed in Table 1. (3) Providing Figures 5-8, and their legends. (4) Writing sections of results and discussion related to figures 5-8.

In utero onset of long QT syndrome with atrioventricular block and spontaneous or lidocaine-induced ventricular tachycardia: Compound effects of hERG pore region mutation and SCN5A N-terminus variant

Ming-Tai Lin, MD,* Mei-Hwan Wu, MD,* Chien-Chih Chang, MD,*,† Shuenn-Nan Chiu, MD,* Olivier Thériault, Msc,‡ Hai Huang, MD,‡ Georges Christé, PhD,§ Eckhard Ficker, PhD,¶ Mohamed Chahine, PhD‡‖

*From the *Department of Pediatrics, National Taiwan University Hospital and College of Medicine, National Taiwan University, Taipei, Taiwan, †Department of Pediatrics, Ming-Shen General Hospital, Taoyuan, Taiwan, ‡Le Centre de Recherche, Université Laval Robert-Giffard, Québec, Canada, §INSERM, Lyon, France, ¶Case Western Reservation University, Cleveland, Ohio, and ‖Department of Medicine, Laval University, Quebec, Canada.*

BACKGROUND Mexiletine may protect patients with long QT syndrome (LQTS) type 3 from arrhythmias. However, we found an unusual in utero presentation of intermittent atrioventricular block and ventricular tachycardia (spontaneous or lidocaine-induced) in a fetus and his sibling with LQTS.

OBJECTIVE The purpose of this study was to investigate the underlying channelopathy and functional alteration.

METHODS Mutations were searched in KCNQ1, HERG, KCNE1, KCNE2, and SCN5A genes. In expressed mutants, whole-cell voltage clamp defined the electrophysiologic properties.

RESULTS Novel missense mutations involving hERG (F627L) at the pore region and SCN5A (R43Q) at the N-terminus were found in the proband and in family members with prolonged QT interval. In oocytes injected with mRNA encoding hERG/ F627L, almost zero K^+ currents were elicited. In coinjected oocytes, the currents were decreased to half. In tsA201 cells transfected with SCN5A/R43Q, although the baseline kinetics of the Na current were similar to wild type, lidocaine caused a unique hyperpolarizing shift of the activation and increased the availability of Na currents at resting voltages. Window currents were enhanced due to a right shift of steady-state inactivation. These electrophysiologic alterations after lidocaine may lead to the development of ventricular tachycardia.

CONCLUSION We identified a novel hERG/F627L mutation that results in LQTS with fetal onset of atrioventricular block and ventricular tachycardia. A coexisting SCN5A/R43Q variant, although it per se does not prolong repolarization, contributes to the development of ventricular tachyarrhythmias after lidocaine. Patients with such latent lidocaine-induced phenotype who are given lidocaine or mexiletine may be at risk.

KEYWORDS Congenital long QT syndrome; Atrioventricular block; Ventricular tachycardia; SCN5A; hERG; Mutation; Variant; Lidocaine

(Heart Rhythm 2008;5:1567–1574)

Introduction

Congenital long QT syndrome (LQTS) is an inherited cardiac channelopathy. Patients are at high risk for potentially fatal ventricular tachyarrhythmias, especially torsade de pointes, due to abnormally prolonged repolarization.[1,2] Ventricular tachyarrhythmias during the fetal or perinatal stages may be associated with functional atrioventricular (AV) block and carry a worse prognosis.[3,4] Mutations have been identified in 10 genes encoding cardiac ion channels and their auxiliary subunits, which are involved in shaping the cardiac action potential (KCNQ1 [LQTS1], hERG [LQTS2], SCN5A [LQTS3], ANK2 [LQTS4], KCNE1 [LQTS5], KCNE2 [LQTS6], KCNJ2 [LQTS7], CACNA1C [LQTS8], CAV3 [LQTS9], SCN4B [LQTS10]). The majority of mutations are in the KCNQ1 (30%–35%), hERG (25%–30%) and SCN5A (5%–10%) genes.[1–5] KCNQ1/ KCNE1 and hERG code for voltage-gated potassium chan-

This study was supported in part by a grant from the Cardiac Children Foundation ROC (CCF0602). This study also was supported by grants from the Heart and Stroke Foundation of Québec (HSFQ) and the Canadian Institutes of Health Research MT-13181. Dr. Chahine is a J.C. Edwards Foundation Senior Investigator. **Address reprint requests and correspondence:** Dr. Mei-Hwan Wu, Department of Pediatrics, National Taiwan University Hospital, No. 7, Chung-Shen South Road, Taipei, Taiwan 100. E-mail address: wumh@ntu.edu.tw. (Received June 16, 2008; accepted August 8, 2008.)

1547-5271/$ -see front matter doi:10.1016/j.hrthm.2008.08.010

nels (I_{Ks} and I_{Kr}, respectively), and SCN5A encodes a sodium channel α subunit.[6,7] Further diversity appears with an increasing number of compound heterozygote mutations, within one or even two different LQTS genes reported.[8–12] Such compound mutations may increase the risk of arrhythmia and are associated with more severe forms of LQTS. However, to date only limited studies have reported functional alterations.

Mexiletine has been proposed as a gene-specific therapy for patients with LQTS type 3 caused by Na channelopathy. Mexiletine may shorten the QT interval and protect patients from arrhythmias in a mutation-specific fashion.[13,14] However, we had found an unusual *in utero* presentation of intermittent AV block and ventricular tachycardia (spontaneous or lidocaine induced) in a fetus and his sibling with LQTS. The purpose of this study was to investigate the mutations and the resultant electrophysiologic properties of the channels.

Methods

The study was approved by the Institutional Committee on Human Research at National Taiwan University Hospital. The investigation conforms to the principles outlined in the Declaration of Helsinki.

Clinical evaluation

The referred proband and eight family members underwent clinical evaluation and 12-lead ECG. QT interval was measured on lead II and corrected for heart rate using the Bazett formula.

Mutational analysis

Previously reported primer pairs were used to amplify all exons of KCNQ1, HERG, KCNE1, KCNE2, and SCN5A from genomic DNA. All of these exons were screened for the presence of nucleotide sequence polymorphisms by single-strand conformational polymorphism (SSCP). Amplification reactions were carried out using 40 ng template DNA, 8 pmol primers, 2 μL dNTPs (2.5 mM), 0.8 μL Mg^{2+} (25 mM), and Taq polymerase. Polymerase chain reaction (PCR) products were analyzed by SSCP according to the manufacturer's protocol (GeneGel Excel, Amersham Pharmacia Biotech, Uppsala, Sweden). When abnormal migration patterns were observed, PCR products were reamplified and sequenced by the dideoxynucleotide chain termination method (DNA Sequencing Kit–BigDye Terminator Cycle Sequencing v 2.0, PE Biosystems Foster City, CA) with fluorescent dideoxynucleotides on an ABI-Prism 373 DNA sequencer (Applied Biosystems Foster City, CA). Results were analyzed using the Genotyper program (PE Biosystems).

Mutagenesis

For the hERG/F627L mutation, site-directed mutagenesis was performed on the hERG-pGH19 (6.9 kb) construct provided by Dr. Gail A. Robertson (University of Wisconsin-Madison Medical School) with the following sense and antisense oligonucleotides, respectively (mutated nucleotides are underlined):

5′-CTC ACC AGT GTG GGC **CTC** GGC AAC GTC TCT CCC-**3′**

5′-GGG AGA GAC GTT GCC GAG GCC CAC ACT GGT GAG-3′

For $NA_V1.5$/R43Q, we used $Na_V1.5$ (hH1) and the following sense and antisense oligonucleotides, respectively (mutated nucleotides are underlined):

5′-C ACC TTG CAG GAG AGC CAA GAG GGG CTG CCC GAG-3′

5′-CTC GGG CAG CCC CTC TTG GCT CTC CTG CAA GGA C-3′

Mutagenesis was performed according to the Quick Change kit from Stratagene (La Jolla, CA, USA). The mutated sites were confirmed by automatic sequencing. Capped mRNAs of wild type (WT) and mutated hERG were produced using the SP6 mMESSAGE mMACHINE from Ambion (Austin, TX, USA).

Preparation of *Xenopus* oocytes

Detailed preparation of *Xenopus* oocytes has been described previously.[15] In brief, oocytes were subjected to 2 mg/mL collagenase, then stage V or VI oocytes were microinjected with 5 ng capped mRNA encoding either WT hERG, mutant hERG, or both. The oocytes were maintained at 18°C in a twofold diluted solution of Leibovitz L-15 medium (Gibco, Grand Island, NY, USA) enriched with 15 mM 4-(2-hydroxyethyl)-1-piperazine-methanesulfonic acid (HEPES, pH 7.6, adjusted with NaOH), 1 mM glutamine, and 50 μg/μL gentamicin. Oocytes were used for experimentation 1 to 3 days after injection.

Macroscopic K currents from mRNA-microinjected oocytes were recorded using voltage-clamp technique with two 3M KCl-filled microelectrodes. Membrane potential was controlled by a Warner oocyte clamp (Warner Instrument Corp., Hamden, CT, USA). Voltage commands were generated using pCLAMP software version 5.5 (Axon Instruments, Foster City, CA, USA). Currents were filtered at 2 kHz (–3 dB; four-pole Bessel filter). The Ringer bathing solution contained the following (in mM): 116 NaCl, 2 KCl, 1.8 $CaCl_2$, 2.9 $MgCl_2$, and 5 HEPES (pH 7.6). All experiments were carried out at room temperature (22°C).

Transfection of tsA201 cell line

TsA201 is a mammalian cell line derived from human embryonic kidney HEK293 cells by stable transfection with SV40 large T antigen.[16] Macroscopic Na currents from tsA201-transfected cells were recorded using the whole-cell configuration of the patch-clamp technique.[17,18] Lidocaine (Sigma, St. Louis, MO, USA) was used at 10 μM concentration.

Western blot analysis

The polyclonal anti-hERG antibody (rabbit hERGbasic) was raised in rabbits against a C-terminal peptide corre-

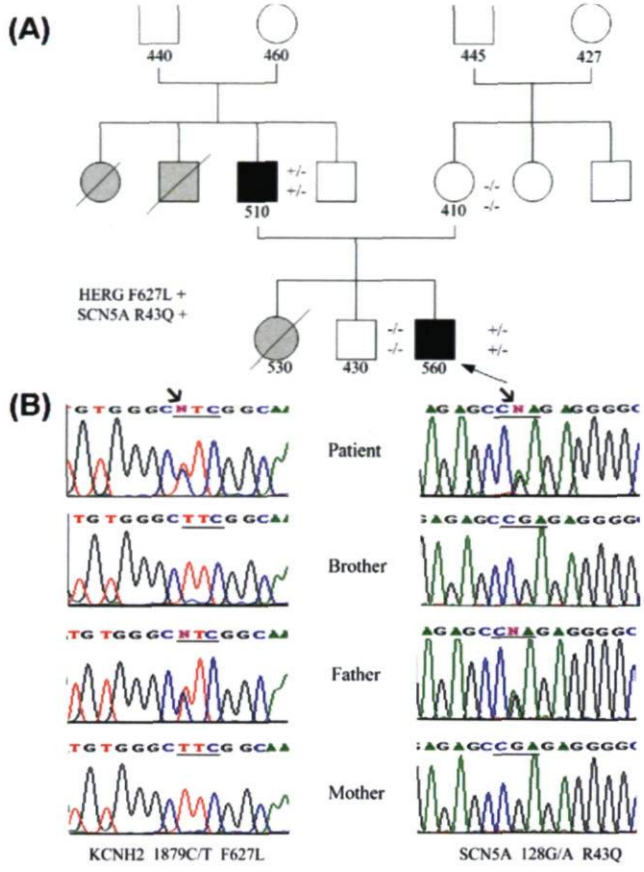

Figure 1 **A:** Pedigree of the study family. *Arrow* indicates the proband. Individuals are assigned as affected *(black)*, unaffected *(white)*, or uncertain *(gray)* phenotype. Genotypes are shown beside each symbol. **B:** DNA sequence chromatograms showing the HERG heterozygous mutation with a C to T transition *(arrow)* resulting in a phenylalanine to leucine substitution at codon 627 and the SCN5A heterozygous mutation with a G to A transition *(arrow)* resulting in an arginine to glutamine substitution at codon 43 in the proband and his father. The results from his mother and brother were normal.

sponding to hERG aa residues 883–901.[19] Antiserum, hERGbasic, was purified on an affinity column consisting of the C-terminal peptide used for immunization (aa 883–901: RQRKRKLSFRRRTDKDTEQ). In briefly, HEK/hERG cells were solubilized for 1 hour at 4°C in lysis buffer containing 150 mM NaCl, 1 mM EDTA, 50 mM Tris, pH 8.0, 1% Triton X-100, and protease inhibitors (Complete, Roche Diagnostics, Indianapolis, IN, USA). Protein concentrations were determined by the bicinchoninic acid (BCA) method (Pierce, Rockford, IL, USA). Proteins were separated on sodium dodecyl sulfate (SDS) polyacrylamide gels, transferred to polyvinylidene difluoride membranes, and developed using the hERGbasic antibody followed by ECL Plus (GE Healthcare, Piscataway, NJ, USA).

Statistical analysis

Data are expressed as mean ± SEM. When indicated, a t-test was performed using statistical software in SigmaStat (Jandel Scientific Software, San Rafael, CA, USA). $P < .05$ was considered significant.

Results

Phenotypic characterization

The clinical history has been described elsewhere.[20] In brief, the fetus was referred at gestational week 25 due to intermittent AV block. Fetal echocardiography showed normal growth and cardiac structure. The atrial rate was 110 to 120/min and associated with a 3:2 AV block. The family history revealed that an uncle and an aunt had died of sudden death, as did a sibling with LQTS (Figure 1A). This sibling had intermittent ventricular tachycardia and functional AV block during fetal life and died 3 days after birth. At gestational week 26, frequent 2:1 AV block and nonsustained ventricular tachycardia were noted. At that time, we adopted a treatment strategy for perinatal onset LQTS, starting with lidocaine infusion to assess the potential benefit from mexiletine. The mother received lidocaine intravenous infusion (10 μg/kg/min) under fetal echocardiographic monitoring. The fetus developed sustained ventricular tachycardia approximately 30 minutes after lidocaine infusion (Figure 2A). The tachycardia converted to 2:1 AV block only after lidocaine was discontinued (Figure 2B). At gestational week 27, incessant ventricular tachycardia (210–230/min) was noted. Subsequent maternal administration of propranolol controlled the tachycardia. The proband grew steadily and was delivered at nearly full term. ECG recorded after birth revealed sinus bradycardia (108/min) with a corrected QT interval of 0.60 second (Figure 2C) and intermittent 3:2 to 2:1 functional AV block (Figure 2D). The functional AV block was related to an extremely prolonged QT interval that was not properly shortened with increasing heart rate. He subsequently received oral propranolol and nicorandil and experienced no ventricular tachycardia. Evaluation at age 5 years revealed a well-developed child.

Genetic characterization

SSCP analyses of KCNQ1, KCNE1, and KCNE2 revealed no abnormal conformers. Abnormal migration pattern was found in one fragment encompassing exon 7 of the HERG gene and one fragment encompassing exon 2 of the SCN5A gene. Sequence analyses of the hERG gene revealed a heterozygous mutation leading to a single base substitution ($C^{1879} \rightarrow T$), resulting in a Phe→Leu (F627L) substitution in the pore of the hERG channel. The F627L mutation was also found in the proband's father (Figure 1B). Sequence analyses of SCN5A gene showed another heterozygous mutation, $G^{128} \rightarrow A$, resulting in an Arg→Gln (R43Q) substitution in the N-terminus (Figure 1B). Only the father had this second mutation. Both mutations were not identified in 100 unrelated, unaffected control individuals.

We also found three silent DNA changes that would not alter the amino acid sequence. One was located at SCN5A and two were located at hERG: (1) C to T at position 5457 of SCN5A (distribution of genotypes in controls: CC: CT: TT = 0.18: 0.44: 0.38); (2) C to T at nucleotide position 1467 of hERG (distribution of genotypes in controls: CC: CT: TT = 0.14: 0.36: 0.50); and (3) C to T at position 1539

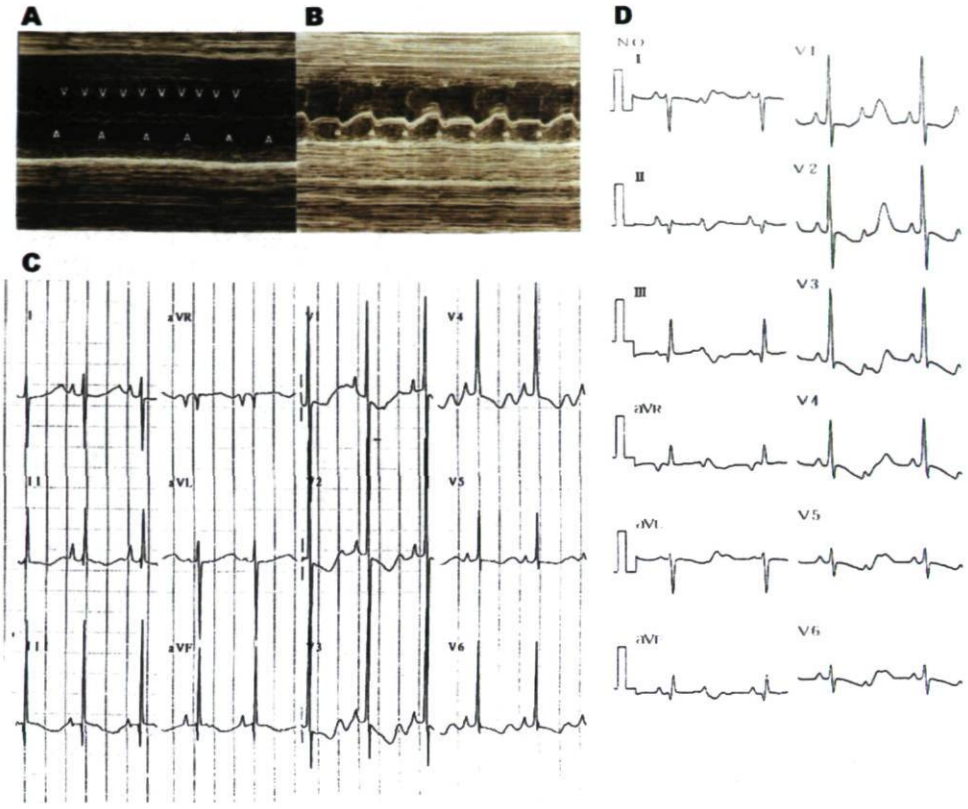

Figure 2 **A:** M-mode fetal echocardiogram with simultaneous recording of the left ventricle (V) and left atrium (A). Ventricular tachycardia was impressed due to the rapid ventricular rate with dissociated ventriculoatrial conduction. **B:** Tachycardia stopped after lidocaine was discontinued, and the rhythm showed an atrial rate of 130/min that conducted to the ventricle in a 2:1 fashion. **C:** Standard ECG recorded soon after birth. Paper speed 25 mm/s; 1 mV = 10 mm. The corrected QT interval at a sinus rate of 104/min was 0.60 second, and the T wave was broad. **D:** On the same day, when the sinus rate accelerated to 140/min, 2:1 pseudo-AV block developed due to an extremely prolonged QT interval.

of hERG (distribution of genotypes in controls: CC: CT: TT = 0.21: 0.41: 0.38). These changes were benign single nucleotide polymorphisms, seen in both the LQTS patient and the normal control population.

Biochemical and biophysical characterization of mutants

Western blot comparing hERG WT and hERG/F627L transiently expressed in HEK293 cells using FuGENE (Roche Applied Science, Indianapolis, IN, USA) revealed that hERG/F627L expressed considerably less hERG protein, either in the fully glycosylated (fg) or core glycosylated (cg) form, compared with the WT hERG protein (Figure 3). The blot also showed that fg was less pronounced. demonstrating some trafficking deficiency of mutant HERG protein as well. These experiments were carried out in triplicate; therefore, the figure is representative of the data.

Capped mRNA encoding wild-type (hERG/WT) or mutant (hERG/F627L) potassium channels were injected separately or coinjected into *Xenopus laevis* oocytes. The resulting currents are shown in Figure 4. Injection of hERG/WT mRNA was followed 2 days later by strong expression of the hERG/WT channel (Figure 4A). However, oocytes injected with mRNA encoding the hERG/ F627L mutant channels exhibited K^+ currents of lower amplitude (Figure 4C), with an altered current–voltage (I/V) relationship in response to the conditioning pulse and almost no current in the second pulse (Figures 4E and 4F). Coinjection of the same amount of both mRNAs resulted in a 50% decrease in K^+ current amplitude (Figure 4B). Furthermore, the currents exhibited similar voltage dependence upon activation (Figures 4E and 4F).

$Na_V1.5$/WT and $Na_V1.5$/R43Q mutant channels were transfected with the auxiliary β_1 subunit in tsA201 cells. The biophysical properties of $Na_V1.5$/WT and $Na_V1.5$/R43Q with and without lidocaine are summarized in Table 1. The resulting Na currents showed similar fast activation and inactivation kinetics. However, the mutant exhibited a unique left shift toward more hyperpolarized voltages of the activation curve and a pronounced block after lidocaine. There were no persistent late Na currents in either $Na_V1.5$/WT or $Na_V1.5$/R43Q (Figure 5). Illustrative whole-cell currents obtained in response to depolarizing steps between −100 and +50 mV are shown in Figure 6A. The I/V relationship was not significantly affected by this mutation, but lidocaine resulted in a left shift of I/V relations (Figure 6B).

Steady-state activation and inactivation were not significantly different between WT and mutant (Figure 7A). Lidocaine 10 μM caused a left shift of inactivation in both, but the degree of shift was less in the mutant. In addition, an unusual left shift to hyperpolarizing voltages of the activation was observed only in the mutant (Figure 7A). Thus, the window currents would be more in the mutant. Lidocaine slowed the recovery of Na channels from inactivation, and the extent of suppression was greater in the mutant than in the WT form (Figure 7B and Table 1). Similarly, use-

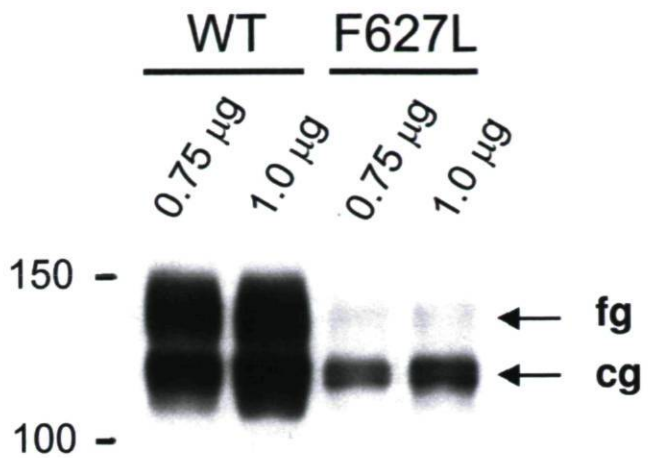

Figure 3 Western blot comparing hERG WT and hERG/F627L transiently expressed in HEK293 cells using FuGENE. HEK293 cells were transfected with different amounts of cDNA (0.75 and 1 μg). The hERG WT was expressed as a fully glycosylated, mature 160-kDa form (fg) and a core-glycosylated, ER resident 135-kDa form (cg). The hERG/F627L expressed considerably less hERG protein in the fully glycosylated (fg) or core glycosylated (cg) forms than in the WT hERG protein.

dependent block by lidocaine was more pronounced in the mutant than in the WT form (Figure 8).

Discussion

In this study, we identified a novel compound hERG mutation and SCN5A variant in a family with LQTS. The SCN5A/R43Q variant was located at the N-terminus region and to date is the only SCN5A variant that can result in latent lidocaine-induced phenotype of arrhythmia. Whereas the hERG/F627L mutation results in the phenotype of LQTS by decreased I_{Kr}, the SCN5A/R43Q variant, though it *per se* does not prolong repolarization, causes unusual hyperpolarizing shift of the activation kinetics and may contribute to the development of ventricular tachyarrhythmia after lidocaine.

Previously recognized SCN5A mutations causing LQTS mostly result in a persistent inward sodium current that can be ameliorated by sodium channel blockers, including lidocaine.[21] Clinical observations also advocate that lidocaine can effectively rescue patients with LQT3 from ventricular tachycardia.[4,22] None of these SCN5A mutations have been associated with lidocaine-induced arrhythmia. Based on these observations, we set a treatment strategy, starting with lidocaine infusion to assess the potential benefits from lidocaine and mexiletine, which had also been applied in this fetus through maternal administration. However, an unusual lidocaine-induced ventricular tachycardia was observed. We did not repeat the lidocaine test in the proband after birth because of medical ethics consideration. Nonetheless, the SCN5A/R43Q variant, identified in this family, exhibits an unusual kinetics of Na channels after lidocaine and is the first genetic variant responsible for latent lidocaine-induced phenotype of ventricular arrhythmia. The SCN5A/R43Q variant *per se* behaves like WT; however, after lidocaine, the I/V curve shifts to the left, thereby increasing the availability of Na current at resting voltages and eliciting Na current at a membrane potential approximately −60 mV. In fetuses, the membrane potential is less negative than in the adult and can approach this vulnerable voltage range.[23] In addition, the window current after lidocaine is enhanced due to a hyperpolarizing (left) shift of the activation curve along with a lesser degree of leftward shift of steady-state inactivation in the mutant. Although lidocaine-induced use-dependent block was greater in the mutants, the difference was small at the heart rate of 230 bpm (3.9 Hz), which was the rate of clinical ventricular tachycardia in our patient. Thus, we may deduce that most of the lidocaine-induced increase in window current should remain under tachycardia despite this use-dependent block. The increased availability of Na current at resting voltages after lidocaine in this variant will lower the threshold for regenerative depolarization of the membrane. As a consequence, a lower minimal fraction of recovery from inactivation shall be required for membrane excitability to be restored, which may shorten the refractory period. Due to the hERG mutation-induced decrease in I_{Kr} current, a prolonged action potential plateau is maintained,

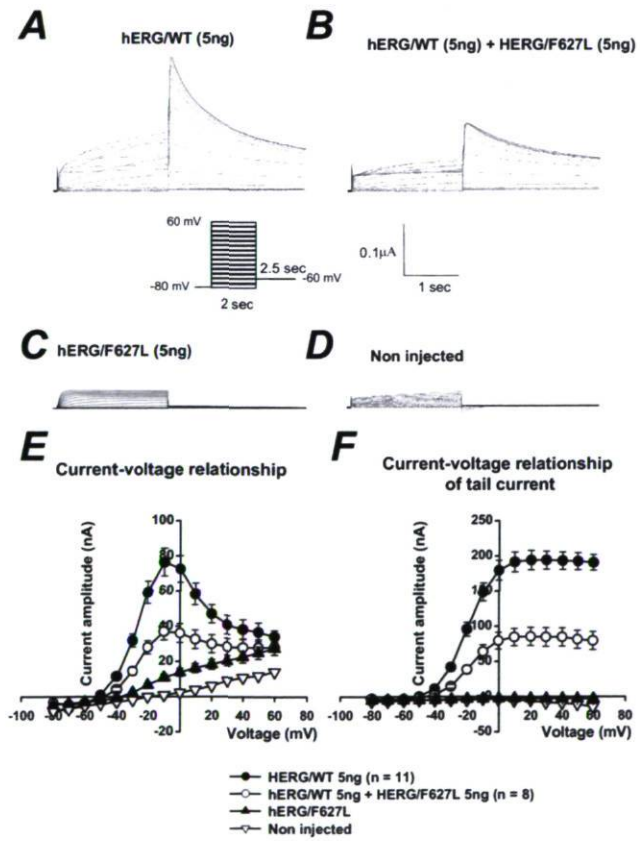

Figure 4 hERG potassium currents recorded from *Xenopus* oocytes injected with cRNA encoding for either hERG/WT (**A**) or hERG/F627L (**C**) or coinjected with hERG/WT and hERG/F627L (**B**) or noninjected (**D**). Potassium currents were elicited from a holding potential of −80 mV with a 2-second test pulse duration, beginning at −80 mV to +60 mV in 10-mV increments followed by a step potential of 2 seconds to evoke tail currents. In panel C, no current was recorded from oocytes injected with mRNA encoding hERG/F627L only. The I/V relations in response to the conditioning pulse (**E**) and in the second pulse (**F**) are summarized.

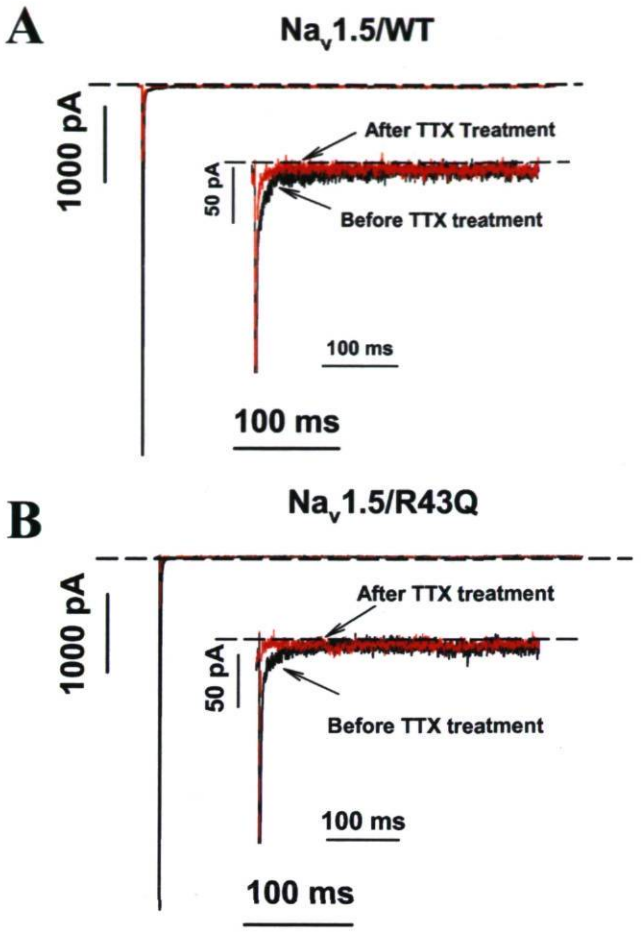

Figure 5 Persistent sodium currents from $NA_V1.5$/WT (**A**) and $Na_V1.5$/R43Q. (**B**) Currents were generated from a holding potential of −140 mV to −10 mV for 400 ms. *Dashed line* represents zero currents. After 5 μM TTX treatment, both currents from $Na_V1.5$/WT and $Na_V1.5$/R43Q were blocked. TTX = Tetrodotoxin.

with the known propensity to develop an extrasystole from early afterdepolarizations. In this patient, with increased window currents and a shorter refractory period from SCN5A/R43Q variant after lidocaine, such an extrasystole from early afterdepolarizations due to prolonged action potential plateau from hERG/F627L mutant may lead to sustained ventricular reentry. Previously recognized mutations in the N-terminus region of SCN5A were identified in several patients with Brugada syndrome (R27H, G35S, and R104Q) and in one elderly patient with LQTS (G9V).[24–27] However, the structure-function studies of these mutations have not been carried out.

Compound mutations account for 4% to 8 % of the mutations identified in patients with LQTS, but few functional studies have been performed.[10–12] Compound mutations may involve the same or different LQTS genes (e.g., two independent KCNQ1 mutations, KCNQ1 + KCNH mutations, KCNQ1 + SCN5A mutations, or rarely hERG + SCN5A mutations).[9–12] Functional hERG channels develop from coassembly of four subunits into a tetrameric protein on the cell membrane. Each subunit contains six membrane-spanning domains (S1–S6) flanked by amino (N)-terminus and carboxyl (C)-terminus regions, with the pore region extending from S5 to S6. Mutations over the pore regions account for approximately one third of hERG mutations, commonly resulting in defective I_{Kr} channels and thereby loss of function in I_{Kr}.[28,29] The phenotypes of pore region mutations were associated with longer QT intervals and a higher risk of cardiac events compared with the nonpore region.[29] Compound mutations involving hERG genes have been identified in pore and nonpore regions, with most of them associated with mutations on the KCNQ1 gene.[10,12] Our patient may be the first reported case with a hERG pore region mutation and a SCN5A variant with complex electrophysiologic interaction other than additive prolongation of the repolarization.

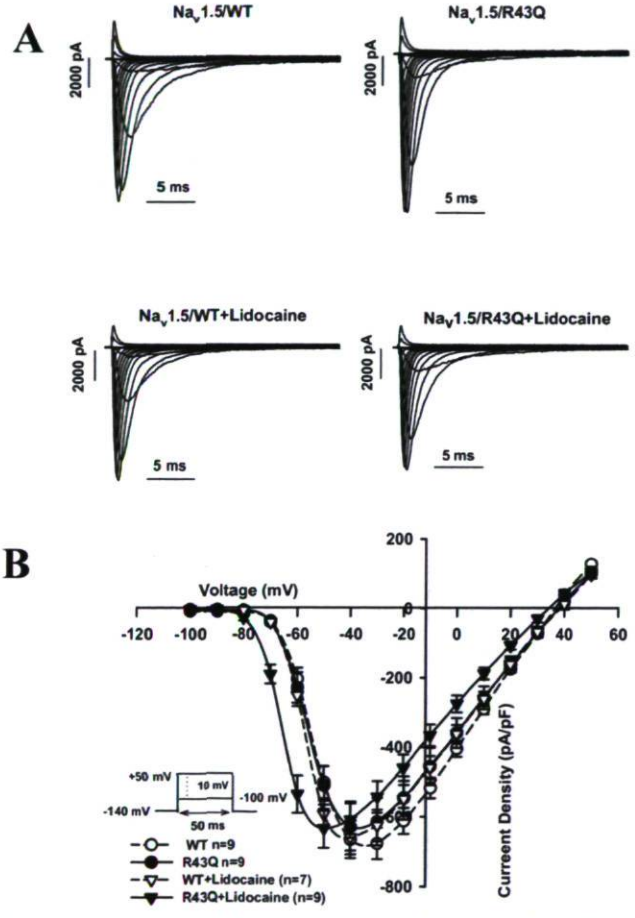

Figure 6 Analysis of whole-cell currents recorded from tsA201 cell line expressing $Na_V1.5$/WT and $Na_V1.5$/R43Q with and without lidocaine. **A:** Families of whole-cell currents from $Na_V1.5$/WT, $Na_V1.5$/R43Q, $Na_V1.5$/WT with lidocaine, and $Na_V1.5$/R43Q with lidocaine. I_{Na} was elicited by depolarizing pulses from −100 mV to +50 mV in 10-mV increments. The holding potential was −140 mV. **B:** Protocol used shown in the *inset*. Current-voltage relationships of $Na_V1.5$/WT (○, n = 9), $Na_V1.5$/R43Q (●, n = 9), $Na_V1.5$/WT with lidocaine (Δ, n = 7), and $Na_V1.5$/R43Q with lidocaine (▲, n = 9). The current amplitude was normalized to the cellular membrane capacitance. The curve for $Na_V1.5$/R43Q with lidocaine was significantly shifted to negative potentials. There was no significant difference for current densities among the currents of $Na_V1.5$/WT and $Na_V1.5$/R43Q with and without lidocaine.

Table 1 Biophysical properties of $Na_V1.5$/WT and $Na_V1.5$/R43Q with and without lidocaine treatment

	$Na_V1.5$/WT	$Na_V1.5$/R43Q	$Na_V1.5$/WT + lidocaine	$Na_V1.5$/R43Q + lidocaine
Steady-state activation				
$V_{1/2}$ (mV)	−54.64 ± 0.74 (n = 7)	−54.93 ± 1.27 (n = 8)	−54.29 ± 0.36 (n = 9)	−65.84 ± 0.62## (n = 8)
Kv (mV)	−6.50 ± 0.68 (n = 7)	−6.47 ± 0.23 (n = 8)	−5.83 ± 0.53 (n = 9)	−5.96 ± 0.48 (n = 8)
Steady-state inactivation				
$V_{1/2}$ (mV)	−99.04 ± 0.87 (n = 8)	−100.81 ± 1.02 (n = 7)	−108.65 ± 0.92** (n = 7)	−107.66 ± 0.70## (n = 8)
Kv (mV)	4.83 ± 0.15 (n = 8)	4.81 ± 0.16 (n = 7)	5.13 ± 0.15 (n = 7)	5.07 ± 1.41 (n = 8)
Recovery from intermediate inactivation				
τ_{fast} (ms)	7.02 ± 0.50 (n = 7)	8.58 ± 1.52 (n = 7)	8.11 ± 0.66 (n = 8)	8.83 ± 0.46 (n = 9)
τ_{slow} (ms)	93.89 ± 5.02 (n = 7)	108.28 ± 13.08 (n = 7)	245.05 ± 22.55** (n = 8)	254.24 ± 19.14## (n = 9)
A_{fast} (%)	71.68 ± 1.35 (n = 7)	69.39 ± 1.91 (n = 7)	62.63 ± 0.74** (n = 8)	60.03 ± 1.50# (n = 9)
A_{slow} (%)	27.81 ± 1.25 (n = 7)	30.32 ± 2.12 (n = 7)	34.73 ± 0.70* (n = 8)	38.00 ± 1.5# (n = 9)

$V_{1/2}$ = midpoint for activation or inactivation; K_V = slow factor for activation or inactivation; τ = time constant; A_{fast} = fractions of the fast recovery component; A_{slow} = fractions of the slow recovery component.

*$P < .05$ vs $Na_V1.5$/WT; #$P < .05$ vs $Na_V1.5$/WT with lidocaine treatment.

**$P < .01$ vs $Na_V1.5$/WT; ##$P < .01$ vs $Na_V1.5$/WT with lidocaine treatment.

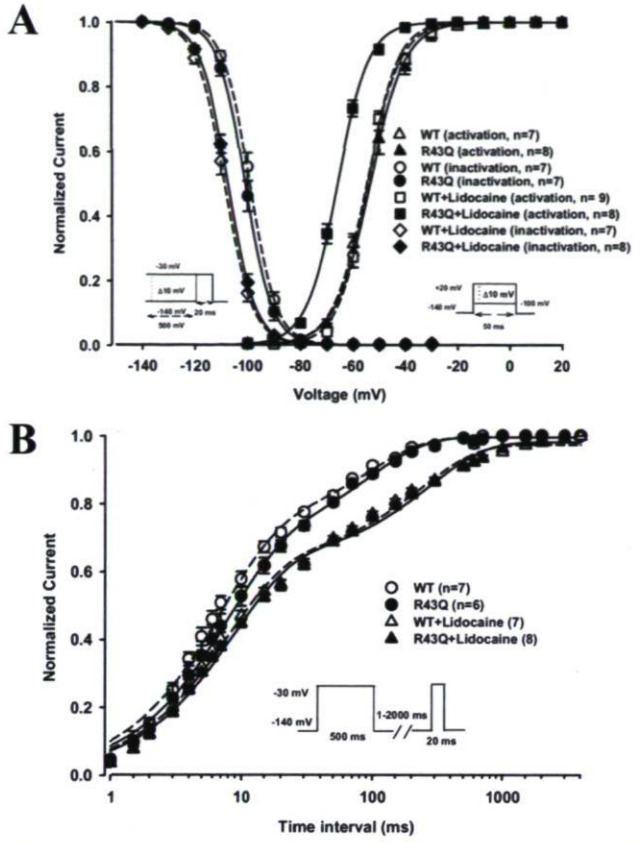

Figure 7 Gating properties of steady-state activation, inactivation, and recovery from inactivation. **A:** Effects of lidocaine 10 μM on steady-state activation: Δ = $Na_V1.5$/WT (n = 7), ▲ = $Na_V1.5$/R43Q (n = 8), □ = $Na_V1.5$/WT with lidocaine (n = 9), and ■ = $Na_V1.5$/R43Q with lidocaine (n = 8); and inactivation: ○ = $Na_V1.5$/WT (n = 8), ● for $Na_V1.5$/R43Q, n = 7, ◇ = $Na_V1.5$/WT with lidocaine (n = 7); and ◆ = $Na_V1.5$/R43Q with lidocaine (n = 8). Activated currents were generated from a holding potential of –140 mV, following 50-ms voltage steps from –100 to +20 mV in 10-mV increments (see protocol in *inset*). There was an 11-mV shift for $Na_V1.5$/R43Q to negative potentials after lidocaine. Voltage dependence of inactivation was obtained by measuring the peak Na^+ current during a 20-ms test pulse of –30 mV, which followed a 500-ms prepulse to membrane potentials between –140 and –30 mV from a holding potential of –140 mV (see protocol in *inset*). After treatment with 10 μM lidocaine, the curves of both $Na_V1.5$/WT and $Na_V1.5$/R43Q were shifted to negative potentials, but there was no significant difference between them. Data are fitted to a Boltzmann equation (parameters given in Table 1). **B:** Effects of lidocaine 10 μM on recovery from intermediate inactivation: ○ = $Na_V1.5$/WT (n = 7), ● = $Na_V1.5$/R43Q (n = 7), Δ = $Na_V1.5$/WT with lidocaine (n = 8), ▲ = $Na_V1.5$/R43Q with lidocaine (n = 9). A 500-ms conditioning prepulse was used to monitor recovery by a 20-ms test pulse after a variable recovery interval from 1 to 2,000 ms (see protocol in *inset*). Time constants (Table 1) were yielded by a two-exponential function: $y = A_1 \times (1-\exp[-t/\tau_1]) + A_2 \times (1-\exp[-t/\tau_2])$. Time constants for both $Na_V1.5$/WT and $Na_V1.5$/R43Q after lidocaine were slower than those for $Na_V1.5$/WT and $Na_V1.5$/R43Q before lidocaine, but there was no significant difference between them (Table 1).

Conclusion

We identified a novel hERG/F627L mutation that results in LQTS with fetal onset of AV block and ventricular tachycardia. A coexisting SCN5A/R43Q variant, although it *per se* does not prolong repolarization, contributes to the development of ventricular tachyarrhythmia after lidocaine. Pa-

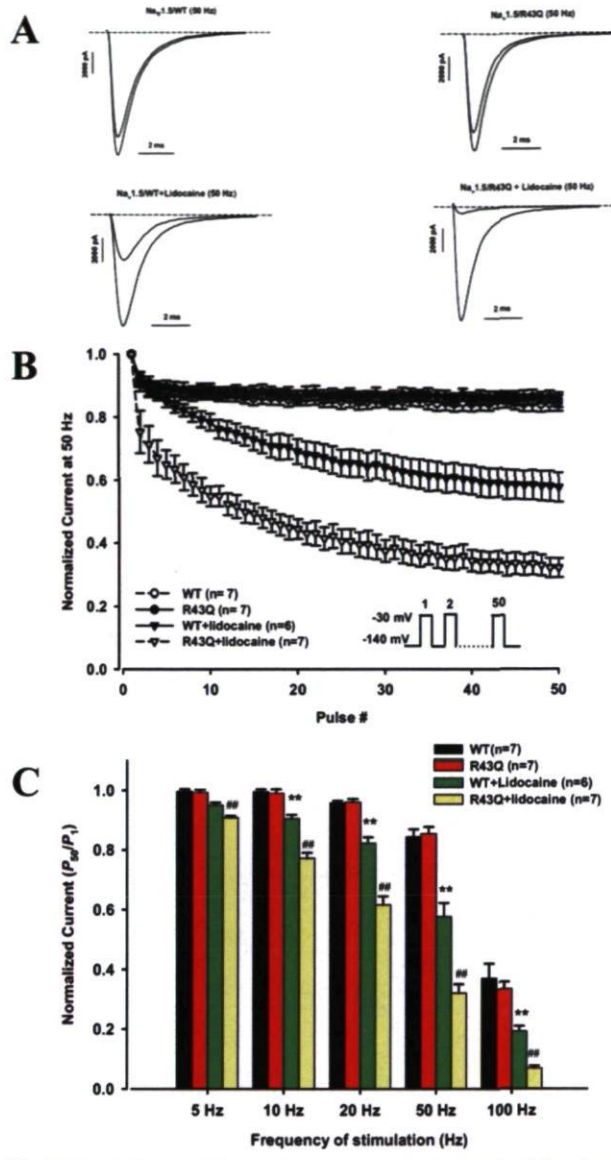

Figure 8 Effects of frequency-dependent inhibition by lidocaine. **A:** Frequency-dependent inhibition of $Na_V1.5$/WT and $Na_V1.5$/R43Q sodium currents with and without lidocaine 10 μM. A train of 50 pulses was applied at 40 and –30 mV at frequencies between 10 and 100 Hz. Peak currents elicited by each test pulse were normalized to the current of the first pulse P_n/P_1 (where n = 1–50) and plotted against the pulse number. Pulse duration was 8 ms. Holding and interpulse potentials were –140 mV. **B:** Ratio of currents elicited by the 50th and first pulses (P_{50}/P_1) versus the pulsing frequency. The current of $Na_V1.5$/WT was inhibited by lidocaine. There was a further reduction of $Na_V1.5$/R43Q after lidocaine. **C:** Representative raw current traces of $Na_V1.5$/WT and $Na_V1.5$/R43Q stimulated at 50 Hz with and without lidocaine 10 μM. $^{**}P < .01$ vs $Na_V1.5$/WT; $^{\#\#}P < .01$ vs $Na_V1.5$/WT with lidocaine.

tients with such latent lidocaine-induced phenotype who are given lidocaine or mexiletine may be at risk.

References

1. Roberts R. Genomics and cardiac arrhythmias. J Am Coll Cardiol 2006;47:9–21.
2. Schwartz PJ. The congenital long QT syndromes from genotype to phenotype: clinical implications. J Intern Med 2006;259:39–47.
3. Lupoglazoff JM, Denjoy I, Villain E, et al. Long QT syndrome in neonates: conduction disorders associated with HERG mutations and sinus bradycardia with KCNQ1 mutations. J Am Coll Cardiol 2004;43:826–830.
4. Chang CC, Acharfi S, Wu MH, et al. A novel SCN5A mutation manifests as a malignant form of long QT syndrome with perinatal onset of tachycardia/bradycardia. Cardiovasc Res 2004;64:268–278.
5. Lehnart SE, Ackerman MJ, Benson DW Jr, et al. Inherited arrhythmias. A National Heart, Lung, and Blood Institute and Office of Rare Diseases workshop consensus report about the diagnosis, phenotyping, molecular mechanisms, and therapeutic approaches for primary cardiomyopathies of gene mutations affecting ion channel function. Circulation 2007;116:2325–2345.
6. Wang Q, Shen J, Splawski I, et al. SCN5A mutations associated with an inherited cardiac arrhythmia, long QT syndrome. Cell 1995;80:1–20.
7. Curran ME, Splawski I, Timothy KW, et al. A molecular basis for cardiac arrhythmia: HERG mutations cause long QT syndrome. Cell 1995;80:795–803.
8. Schwartz PJ, Priori SG, Napolitano C. How really rare are rare disease. J Cardiovase Electrophysiol 2003;14:1120–1121.
9. Westenskow P, Splawski I, Timothy KW, et al. Compound mutations: a common cause of severe long-QT syndrome. Circulation 2004;109:1834–1841.
10. Wang Z, Li H, Moss AJ, et al. Compound heterozygous mutations in KVLQT1 cause Jervell and Lange-Nielson syndrome. Mol Gen Metab 2002;75:308–316.
11. Lasen LA, Fosdal I, Anderson PS, et al. Recessive Romano-Ward syndrome associated with compound heterozygosity for two mutations in the KVLQT1 gene. Eur J Hum Genet 1999;7:724–728.
12. Yamaguchi M, Shimizu M, Ino H, et al. Compound heterozygosity for mutations Asp(611)Tyr in KCNQ1 and Asp(609)Gly in KCNH2 associated with severe long QT syndrome. Clin Sci (Lond) 2005;108;143–150.
13. Shimizu W, Aiba T, Antzelevitch C. Specific therapy based on the genotype and cellular mechanism in inherited cardiac arrhythmias. Long QT syndrome and Brugada syndrome. Curr Pharm Des 2005;11:1561–1572.
14. Ruan Y, Liu N, Bloise R, et al. Gating properties of SCN5A mutations and the response to mexiletine in long-QT syndrome type 3 patients. Circulation 2007;116;1137–1144.
15. Chahine M, Chen LQ, Barchi RL, et al. Lidocaine block of human heart sodium channels expressed in Xenopus oocytes. J Mol Cell Cardiol 1992;24:1231–1236.
16. Margolskee RF, McHendry-Rinde B, Horn R. Panning transfected cells for electrophysiological studies. Biotechniques 1993;15:906–911.
17. Keller DI, Acharfi S, Delacretaz E, et al. A novel mutation in SCN5A, delQKP 1507-1509, causing long QT syndrome: role of Q1507 residue in sodium channel inactivation. J Mol Cell Cardiol 2003;35:1513–1521.
18. Hamill OP, Marty A, Neher E, et al. Improved patch-clamp techniques for high-resolution current recording from cells and cell-free membrane patches. Pflugers Arch 1981:391:85–100.
19. Roti EC, Myers CD, Ayers RA, et al. Interaction with GM130 during HERG ion channel trafficking. Disruption by type 2 congenital long QT syndrome mutations. Human ether-à-go-go-related Gene. J Biol Chem 2002;277:47779–47785.
20. Chang IK, Shyu MK, Lee CN, et al. Prenatal diagnosis and treatment of fetal long QT syndrome: a case report. Prenatal Diag 2002;22:1209–1212.
21. Tan HL. Sodium channel variants in heart disease: expanding horizons. J Cardiovasc Electrophysiol 2006;17:S151–S157.
22. Betrian Blasco P, Antunez Jimenez MI, Falcon Gonzalez LH, et al. Neonatal life-threatening arrhythmia responding to lidocaine, a probable LQTS3. Int J Cardiol 2007;117:e61–e63.
23. Wu MH, Su MJ, Lue HC. Age-related quinidine effects on ionic currents of rabbit cardiac myocytes. J Mol Cell Cardiol 1994;26:1167–1177.
24. Levy-Nissenbaum E, Eldar M, Wang Q, et al. Genetic analysis of Brugada syndrome in Israel: two novel mutations and possible genetic heterogeneity. Genet Test 2001;5:331–334.
25. Millat G, Chevalier P, Restier-Miron L, et al. Spectrum of pathogenic mutations and associated polymorphisms in a cohort of 44 unrelated patients with long QT syndrome. Clin Genet 2006;70:214–227.
26. Priori SG, Napolitano C, Gasparini M, et al. Natural history of Brugada syndrome: insights for risk stratification and management. Circulation 2002;105:1342–1347.
27. Vatta M, Dumaine R, Antzelevitch C, et al. Novel mutations in domain I of SCN5A cause Brugada syndrome. Mol Genet Metab 2002;75:317–324.
28. Splawski I, Shen J, Timothy KW, et al. Spectrum of mutations in long-QT syndrome genes. KVLQT1, HERG, SCN5A, KCNE1, and KCNE2, Circulation 2000;102:1178–1185.
29. Moss AJ, Zareba W, Kaufman ES, et al. Increased risk of arrhythmic events in long-QT syndrome with mutations in pore region of the human ether-a-go-go-related gene potassium channel. Circulation 2002;105:794–799.

A novel mutation in the SCN5A gene is associated with Brugada syndrome

Shin DJ, Kim E, Park SB, Jang WC, Bae Y, Han J, Jang Y, Joung B, Lee MH, Kim SS, **Huang H**, Chahine M, & Yoon SK (2007).

Life Sci (2007) **80**, 716-724

Contribution role: (1) Testing biophysical characterization of a novel *SCN5A* mutation (W1191X) identified in a family with Brugada syndrome. Currents were recorded from tsA 201 cells transiently transfected with mutant and WT channels by whole-cell configuration of patch-clamp technique. (2) Analyzing resulting data. It was found that W1191X mutant channels failed to generate Na^+ current, which may lead to ST-segment elevations in patient's ECG. (3) Providing Figures 6 -7, and their legends. (4) Writing sections of results and discussion related to figures 6 and 7.

Available online at www.sciencedirect.com
ScienceDirect
Life Sciences 80 (2007) 716–724
Life Sciences
www.elsevier.com/locate/lifescie

A novel mutation in the *SCN5A* gene is associated with Brugada syndrome

Dong-Jik Shin [a], Eunmin Kim [b,c], Sang-Bum Park [d], Won-Cheoul Jang [d], Yoonsun Bae [b,1], Jihye Han [b,1], Yangsoo Jang [a,e], Boyoung Joung [e], Moon Hyoung Lee [e], Sung Soon Kim [e], Hai Huang [f], Mohamed Chahine [f,*], Sungjoo Kim Yoon [b,c,*]

[a] *Cardiovascular Genome Center, Yonsei University Medical Center, Seoul 120-752, Republic of Korea*
[b] *Research Institute of Molecular Genetics, The Catholic University of Korea, Seoul 137–701, Republic of Korea*
[c] *Department of Biomedical Sciences, The Catholic University of Korea, Seoul 137–701, Republic of Korea*
[d] *Department of Chemistry, School of Advanced Science, Dankook University, Cheonan, 330–714, Republic of Korea*
[e] *Department of Cardiology, Yonsei Cardiovascular Center, Seoul 120–752, Republic of Korea*
[f] *Laval Hospital Research Centre and Department of Medicine, Université Laval, Quebec, Quebec, Canada*

Received 19 May 2006; accepted 28 October 2006

Abstract

Brugada syndrome (BS) is an inherited cardiac disorder associated with a high risk of sudden cardiac death and is caused by mutations in the *SCN5A* gene encoding the cardiac sodium channel α-subunit ($Na_v1.5$). The aim of this study was to identify the genetic cause of familial BS and characterize the electrophysiological properties of a novel *SCN5A* mutation (W1191X). Four families and one patient with BS were screened for *SCN5A* mutations by PCR and direct sequencing. Wild-type (WT) and mutant $Na_v1.5$ channels were expressed in tsA201 cells, and the sodium currents (I_{Na}) were analyzed using the whole-cell patch-clamp technique. A novel mutation, W1191X, was identified in a family with BS. Expression of the WT or the mutant channel ($Na_v1.5$/W1191X) co-transfected with the β_1-subunit in tsA201 cells resulted in a loss of function of $Na_v1.5$ channels. While voltage-clamp recordings of the WT channel showed a distinct acceleration of $Na_v1.5$ activation and fast inactivation kinetics, the $Na_v1.5$/W1191X mutant failed to generate any currents. Co-expression of the WT channel and the mutant channel resulted in a 50% reduction in I_{Na}. No effect on activation and inactivation were observed with this heterozygous expression. The W1191X mutation is associated with BS and resulted in the loss of function of the cardiac sodium channel.

Keywords: Brugada syndrome; Sodium channel; Electrophysiology; Mutation; *SCN5A*

Introduction

Brugada syndrome (BS) is an inherited electrical cardiac disorder characterized by an incomplete right bundle branch block (RBBB), a typical electrocardiogram (ECG) pattern of ST-segment elevation in the right precordial leads V_1 to V_3, a structurally normal heart, and a highly increased risk of sudden cardiac death as a result of polymorphic ventricular tachycardia (VT) or ventricular fibrillation (VF) (Brugada and Brugada, 1992; Antzelevitch et al., 2002). This disorder is not related to acute ischemia, electrolyte abnormalities or structural heart diseases (Wilde et al., 2002). BS is a familial disease with autosomal dominant transmission. While BS has been observed worldwide, it is more common in Southeast Asian and Japanese populations (Nademanee et al., 1997) and, interestingly, manifests much more frequently in men than women (Priori et al., 2002). The mean age at onset of clinical events (syncope or cardiac arrest) is 30–40 years, although severe forms with earlier onset and even neonatal expression have been reported (Priori et al., 2000).

The cardiac sodium channel is responsible for the generation of the rapid upstroke of the cardiac action potential and plays a key role in cardiac impulse propagation (Balser, 1999). Sodium

* Corresponding authors. Yoon is to be contacted at Research Institute of Molecular Genetics, The Catholic University of Korea, Seoul 137–701, Republic of Korea. Tel./fax: +82 2 590 2603. Chahine, Laval Hospital Research Centre and Department of Medicine, Université Laval, Quebec, Quebec, Canada. Tel.: +1 418 656 8711x5447; fax: +1 418 656 4509.
E-mail addresses: mohamed.chahine@phc.ulaval.ca (M. Chahine), sjkyoon@catholic.ac.kr (S.K. Yoon).
[1] The current address of these authors is the Cardiovascular Genome Center, Yonsei University Medical Center, Seuol 120-752, Republic of Korea.

0024-3205/$ - see front matter © 2006 Elsevier Inc. All rights reserved.
doi:10.1016/j.lfs.2006.10.025

channels are heterodimeric assemblies composed of a pore forming α-subunit and several regulatory β-subunits. The α-subunit consists of four homologous domains (DI–DIV). Each domain contains six transmembrane segments (S1–S6) connected by short linking intracellular segments (Cohen and Barchi, 1992). The *SCN5A* gene that encodes the α-subunit of the human cardiac voltage-gated sodium channel ($Na_v1.5$) (Antzelevitch et al., 2002) is located on chromosome 3p21 and consists of 28 exons spanning approximately 80 kb (Wang et al., 1996). While several candidate genes are considered plausible, thus far BS has been linked only to mutations in *SCN5A*. Understanding the molecular and cellular mechanisms leading to BS remains limited, and, to date, a minority (approximately 20%) of patients with BS have been found to carry a mutation in this gene (Priori et al., 2000). Several reports have estimated the prevalence of Brugada-type ECG changes at approximately 0.1–0.7% in the general population worldwide (Hermida et al., 2000; Matsuo et al., 2001). Genetic studies have demonstrated that some cases of BS and chromosome 3-linked long-QT syndrome (LQT3) are allelic variations of *SCN5A*.

To date, several dozen *SCN5A* mutations in patients with BS have been identified. Three categories of *SCN5A* mutations have been reported in BS: missense, splice-donor, and frameshift (Chen et al., 1998; Deschênes et al., 2000; Naccarelli and Antzelevitch, 2001). Functional analyses have revealed that most *SCN5A* mutations lead to a loss of function of cardiac sodium channels by reducing the sodium current (I_{Na}) available during the early phase of the cardiac action potential (Balser, 1999; Baroudi et al., 2000). Because I_{Na} plays an important role in human heart excitation and contraction, functional variations in these sodium channels can cause variable cardiac biophysical abnormalities (Wang et al., 2000). Studies conducted over the past decade have shown that rebalancing the currents active at the end of phase 1, which leads to an accentuation of the action potential notch in the right ventricular epicardium, is responsible for the accentuated J-wave or ST segment elevation linked with BS (Antzelevitch, 2001). Yan and Antzelevitch (1999) have suggested that a decrease in the depolarizing inward sodium current leads to early repolarization in the right ventricular epicardium where the transient outward K^+ current (I_{to}) is large. This causes a voltage gradient from endocardium to epicardium, ST elevation on the ECG, and susceptibility to arrhythmias caused by phase 2 re-entry.

In the present study, we report two mutations in *SCN5A*. One is novel (W1191X) and the other is a previously reported (S1710L) mutation. We also conducted a functional analysis of the novel mutation and propose a mechanism for its contribution to the BS phenotype in the patients.

Materials and methods

Subjects and clinical data

Our study population consisted of 34 individuals including 33 members arising from four unrelated families and one patient. Of these, five individuals, one from each family and the one patient, were initially diagnosed with BS. All were recruited from the Yonsei Cardiovascular Genome Center (Republic of Korea). The protocol for this study was approved by the Ethics Committee of Yonsei University and the study was carried out under its guidelines. Informed consent was obtained from all participants.

The diagnosis of BS was based on a 12-lead electrocardiogram (ECG) with the following ECG parameters: (1) at least a 2 mm ST-segment elevation in more than one right precordial lead (V_1 to V_3) with an RBBB morphology and (2) a J-wave elevation >0.2 mV at baseline. In addition, the absence of a structural abnormality was noted by echocardiography. Three types of ST-segment elevation patterns are recognized. Type 1 is characterized by a prominent coved ST-segment elevation displaying J-wave amplitude or a ST-segment elevation ≥2 mm or 0.2 mV at its peak followed by a negative T-wave, with little or no isoelectric separation. Type 2 also has a high take-off ST-segment >elevation, but in this case, J-wave amplitude (≥2 mm) gives rise to a gradually descending ST-segment elevation (remaining ≥1 mm above the baseline), followed by a positive or biphasic T-wave that results in a saddleback configuration. Type 3 is characterized by a right precordial ST-segment saddleback and/or coved elevation of <1 mm (Wilde et al., 2002). A challenge test was performed in a subset of family members by infusing 2 mg/kg of flecainide for 10 min. Two hundred individuals with no a history of structural heart disorder, heart failure, syncope, VF, or ventricular tachycardia (VT) were recruited as unrelated healthy control subjects.

Genetic analysis of SCN5A

The mutation analysis was carried out by polymerase chain reaction (PCR) followed by direct sequencing. Genomic DNAs from the probands as well as a normal subject from each family were sequenced for the all coding regions and the flanking introns of *SCN5A*. Genomic DNA was extracted from peripheral blood leukocytes using QIAamp® DNA blood kits (Qiagen, Valencia, CA). The PCR was performed using modified primers located in the intronic sequences and amplification conditions as previously described (Wang et al., 1996). The amplified

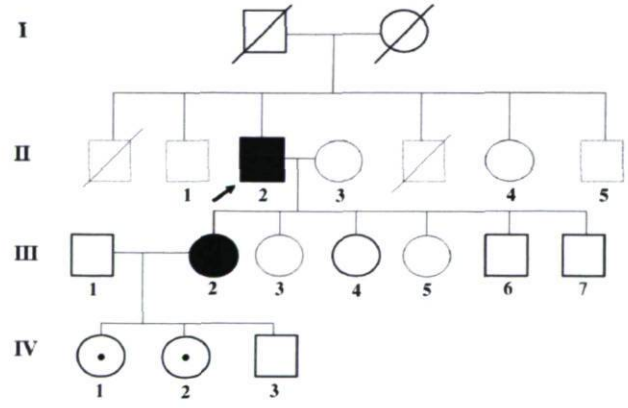

Fig. 1. Pedigree structure of a family (KBSF3) with BS. Circles indicate females; squares indicate males. Filled symbols indicate affected individuals; symbols with a central point indicate asymptomatic W1191X mutation carriers. The proband with BS is marked by an arrow.

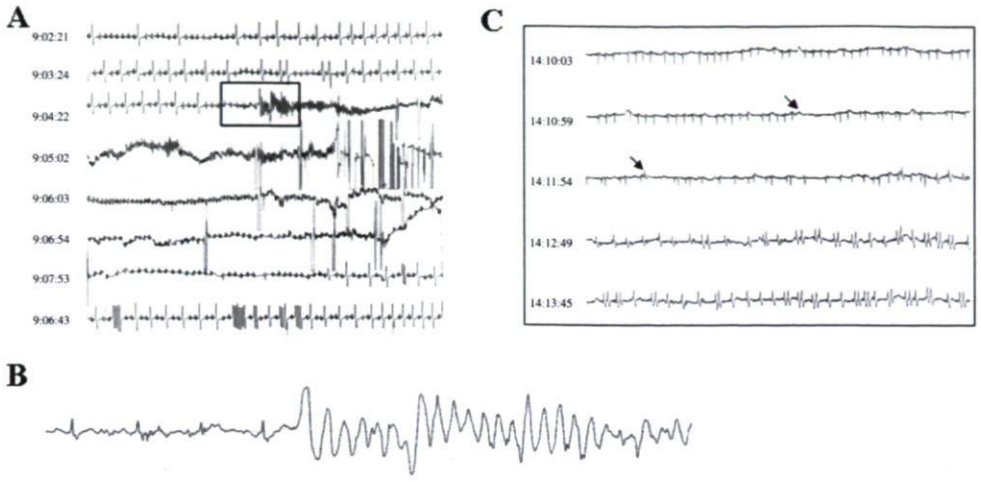

Fig. 2. Telemetry monitoring on the second day of hospitalization. (A) Polymorphic ventricular tachycardia (PMVT) was documented, and the proband had a syncope. PMVT was terminated spontaneously. (B) Magnified view of box in (A). Polymorphic ventricular tachycardia was induced by PVC without previous a pause. (C) Telemetry monitoring of the proband's daughter (III-2) during a flecainide challenge test. A four-second sinus pause (upper arrow) and RBBB pattern (lower arrow) were observed after the infusion of 40 mg of flecainide.

products were purified using QIAquick® PCR purification kits (Qiagen) and directly sequenced using ABI PRISM Big Dye Terminator Cycle Sequencing Ready Reaction kits and an ABI PRISM 3100 DNA analyzer (Applied Biosystems, Foster City, CA). Sequences were compared with the reference genomic and cDNA sequences of *SCN5A* (GenBank accession numbers NT 022517.17 and AY148488.1, respectively) using BLASTN. Once the mutation was identified, the PCR product was used to determine denaturing high-performance liquid chromatography (DHPLC) conditions. A DHPLC analysis with a WAVE™ System Model 3500 (Transgenomic, Omaha, NE) was used to detect for sequence variations in a control group of 200 individuals from the same ethnicity (Korean) as previously reported (Underhill et al., 1997; Ackerman et al., 2001). DHPLC

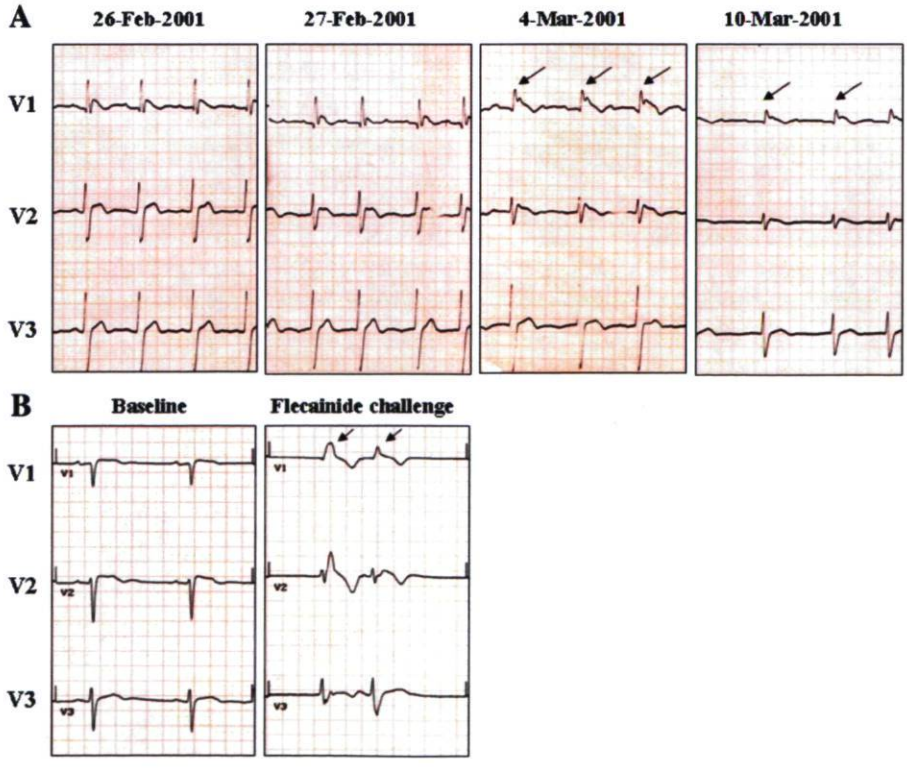

Fig. 3. ECG recordings of the two patients in a Korean family (KBSF3) with BS with different patterns in precordial leads V_1 to V_3. (A) ECG patterns of the proband (II-2). Dynamic ECG changes without a drug challenge test for 1 month are shown. (B) ECG recordings of the proband's daughter (III-2). The ECG pattern in the left panel shows the baseline condition, which converts to the coved-type and severe sinus dysfunction after the infusion of 40 mg of flecainide as shown in the right panel and in Fig. 2C. The arrows in the two panels indicate the J-wave.

was performed on DNA amplification products using optimal temperature conditions (at 60 °C). Sequences underlying abnormal DHPLC profiles were validated by reamplification of the same genomic DNA and were analyzed by direct DNA sequencing as described above.

Site-directed mutagenesis

Mutant $Na_v1.5$/W1191X was generated using QuickChange™ site-directed mutagenesis kits according to the manufacturer's instructions (Stratagene, La Jolla, CA). The $Na_v1.5$/mutants were constructed using the following 33-nucleotide mutagenic sense and antisense primers:

5′-GCC CCA GGG AAG GTC TGA TGG CGG TTG CGC AAG-3′

5′-CTT GCG CAA CCG CCA TCA GAC CTT CCC TGG GGC-3′

Mutated sites are underlined. Mutant and WT $Na_v1.5$ in a pcDNA1 construct were purified using Qiagen columns (Qiagen).

Transfection of the tsA201 cell line

The tsA201 cells were grown in high glucose DMEM supplemented with FBS (10%), L-glutamine (2 mM), penicillin (100 U/ml) and streptomycin (10 mg/ml) (Gibco BRL Life Technologies, Burlington, ON, Canada) and were incubated in a 5% CO_2 humidified atmosphere. The cells were transfected using the calcium phosphate method (Margolskee et al., 1993) with the following modification to facilitate the identification of individual transfected cells: cells were co-transfected with the expression vector piERS/CD8/β_1 which conferred expression of the β_1-subunit as well as a lymphocyte surface antigen (CD8-a) (Jurman et al., 1994). Using this strategy, we were able to select for transfected cells using anti-CD8-a coated beads. Five micrograms of plasmid DNA coding for WT or mutant Na^+ channels, and 5 μg of piERS/CD8/β_1 were used. For patch-clamp experiments, 2 to 3-day-post-transfection cells were incubated for 5 min in a medium containing anti-CD8-a coated beads (Dynabeads M-450 CD8-a) (Jurman et al., 1994). Unattached beads were removed by washing. The beads were prepared according to the manufacturer's instructions (Dynal, Oslo, Norway). Cells expressing CD8-a on their surface fixed the beads and were visually distinguishable from non-transfected cells by light microscopy.

Patch-clamp method

Macroscopic Na^+ currents from tsA201-transfected cells were recorded using the whole-cell configuration of the patch-

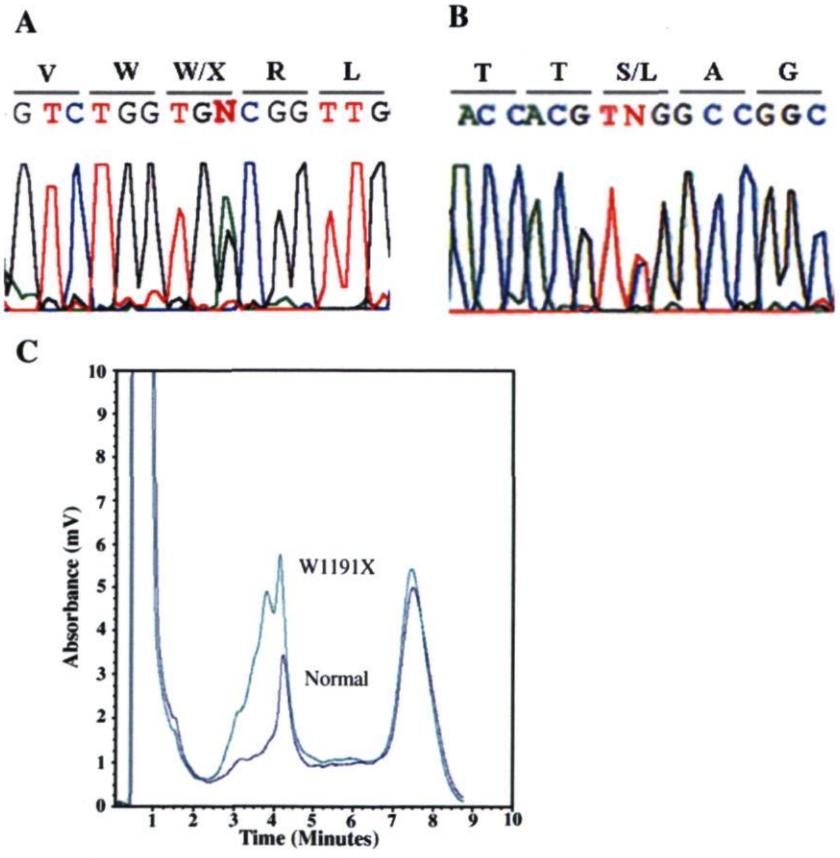

Fig. 4. Genetic analysis of the two individuals with *SCN5A* mutations. (A) Direct DNA sequencing analysis of *SCN5A* exon 20 from a proband (II-2). The DNA sequence indicates a non-sense mutation (G-to-A base substitution), which results in a tryptophan-to-stop codon substitution at amino acid position 1191. (B) DNA sequence electropherogram shows a missense mutation (S1710L) in *SCN5A* exon 28 in a patient with BS (SV525). (C) DHPLC confirms an abnormal elution profile in affected cases (II-2 and III-2), two asymptomatic carriers (IV-1 and IV-2) in a family, and 200 unrelated control subjects.

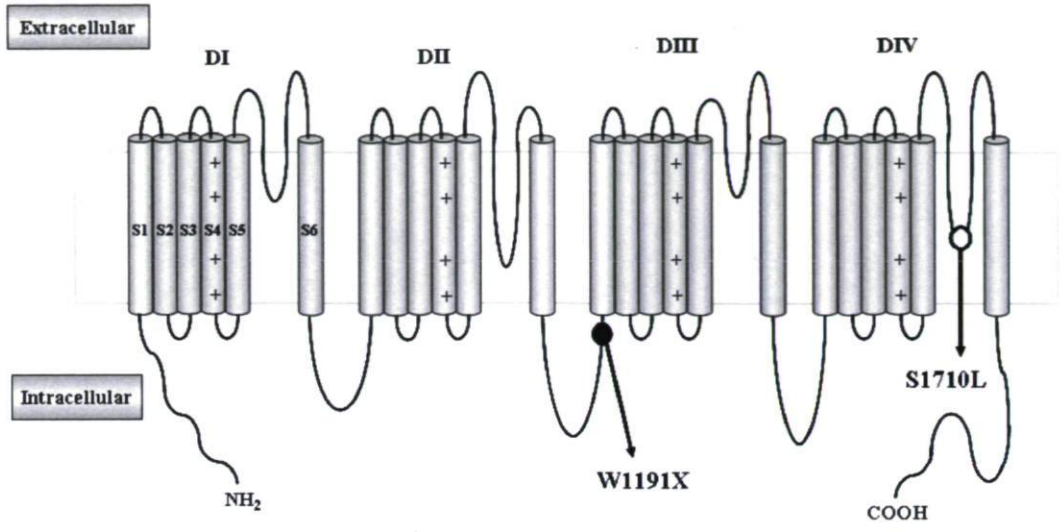

Fig. 5. Schematic membrane topology of the human cardiac sodium channel. The locations of the W1191X and S1710L mutations are indicated by circles and arrows.

clamp technique (Hamill et al., 1981). Patch electrodes were made from 8161 Corning borosilicate glass and coated with Sylgard (Dow-Corning, Midland, MI) to minimize their capacitance. Patch-clamp recordings were made using low resistance electrodes (<1 MΩ), and a routine series resistance compensation by an Axopatch 200 amplifier (Axon Instruments, Foster City, CA) was performed to values >80% to minimize voltage-clamp errors. Voltage-clamp command pulses were generated by microcomputer using pCLAMP software v8.0 (Axon Instruments). Na^+ currents were filtered at 5 kHz, digitized at 10 kHz, and stored on a microcomputer equipped with an AD converter (Digidata 1300, Axon Instruments). Data analysis was performed using a combination of pCLAMP software v9.0 (Axon Instruments), Microsoft Excel and SigmaPlot 2001 for Windows v7.0 (SPSS Chicago, IL).

Solutions and reagents

For whole-cell recordings, the patch pipette contained 35 mM NaCl, 105 mM CsF, 10 mM EGTA, and 10 mM Cs-HEPES. The pH was adjusted to 7.4 using 1 N CsOH. The bath solution contained 150 mM NaCl, 2 mM KCl, 1.5 mM $CaCl_2$, 1 mM $MgCl_2$, 10 mM glucose, and 10 mM Na-HEPES. The pH was adjusted to 7.4 with 1 N NaOH. A −7 mV correction of the liquid junction potential between the patch pipette and the bath solutions was performed. The recordings were made 10 min after obtaining the whole-cell configuration in order to allow the current to stabilize and achieve adequate diffusion of the contents of the patch electrode. Experiments were carried out at room temperature (22–23 °C).

Results

Clinical characteristics

Four probands and one patient with a type 1 BS-type ECG (all males; 22–74 years of age) were enrolled in our study. One proband, a 74-year-old man (II-2, Fig. 1) from the KBSF3 family, had been initially referred with two episodes of syncope that had occurred on February 23 and 26, 2001. An ECG of atrial flutter 1:1 conduction with aberrant conduction was documented on February 27, 2001. He had undergone bidirectional isthmic conduction block in May 2001. At that time, VF was induced by a triple ventricular extrastimulation of

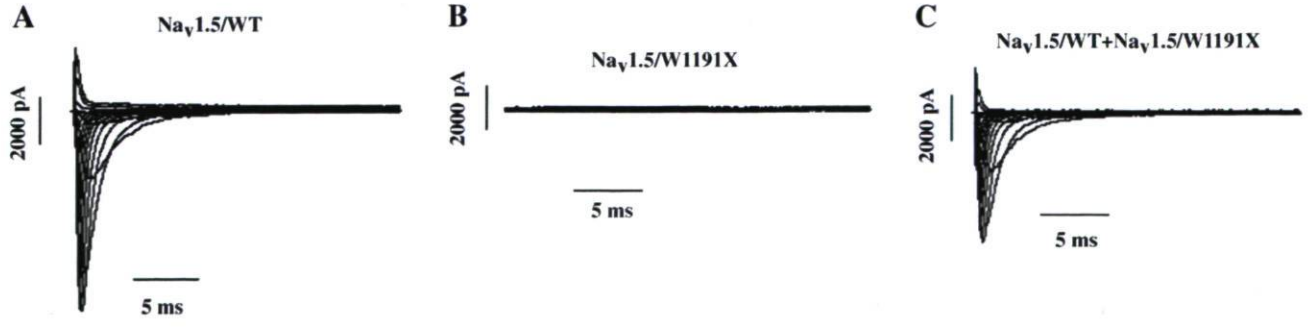

Fig. 6. Representative traces of a family of whole-cell sodium currents from (A) $Na_v1.5$/WT, (B) $Na_v1.5$/W1191X expressed, and (C) $Na_v1.5$/WT+$Na_v1.5$/W1191X co-expressed in the tsA201 cell line. Currents were generated from a holding potential of −140 mV from −80 to +50 mV for 30 ms in 10 mV increments.

500/270/230/240 ms at apex. Because VF can be induced by triple extrastimulation with an idiosyncratic response, further management for VF was not performed. However, he was hospitalized with a recurrent syncope on December 18, 2003. He had a syncope again on the second day of hospitalization, and polymorphic ventricular tachycardia (PMVT) was documented by telemetry monitoring (Fig. 2A–C). The ECG recordings from the proband showed the dynamic ECG changes (Fig. 3A). He had an abnormal prolonged QT interval (467 ms), PR interval (216 ms), and QRS duration (140 ms). Coved ST-segment elevation (type 1) was evident in leads V_1 and V_{1-2}. He had 14 episodes of VF, which were successfully terminated with shock delivery by implantable cardioverter defibrillator (ICD). His familial history revealed that his daughter (III-2) had had a syncope and several episodes of dizziness with sinus dysfunction. She had showed RBBB and coved-type ST-segment elevation with a 40 mg dose of flecainide as well as severe sinus dysfunction (Fig. 3B). With the exception of III-2, all five offspring of the proband turned out to be clinically normal.

Individual case SV525 had a family history of sudden cardiac death. The initial 12-lead baseline ECG had an asymptomatic pattern but flecainide unmasked a type 1 ECG phenotype (data not shown). An ICD was implanted to prevent sudden cardiac death in all patients with BS.

Genetic analysis

All the probands and a normal family member from each family were screened for all the exons and flanking introns of *SCN5A* by PCR-direct DNA sequencing. Once the mutation had been identified in a family, other family members were screened for the mutation by PCR-DHPLC-direct sequencing. PCR-DHPLC was used to determine the absence of the mutation in control subjects. *SCN5A* mutations were identified in one family (KBSF3) and one patient (SV525), while four polymorphisms were found in the study subjects.

A novel heterozygous nonsense mutation was identified in one family (KBSF3). DNA sequencing analysis of *SCN5A* in the proband revealed a G-to-A base substitution at position 3973 in exon 20 (Fig. 4A), which presumably causes a change from a tryptophan (W) to a stop codon at position 1191 in the protein (W1191X). Among the family members tested for the mutation (II-2, III-1, III-2, III-4, III-6, III-7, IV-1, IV-2, and IV-3), we confirmed by DHPLC the abnormal conformer in four (II-2, III-2, IV-1, and IV-2), including the proband (Fig. 4C). Sequencing analysis confirmed that W1191X was heterozygous that these individuals had no other *SCN5A* mutations. Two granddaughters of the proband (IV-1 and IV-2) had the W1191X mutation. However, their ECGs exhibited normal patterns after administration of flecainide.

We also identified a previously reported BS *SCN5A* mutation (S1710L) (Fig. 4B) in a patient with BS (SV525) (Akai et al., 2000). While this mutation was found in an idiopathic ventricular fibrillation (IVF) patient who did not have a typical Brugada ECG pattern, the heterologously expressed S1710L mutant sodium channel is known to present severe alterations in channel inactivation and activation that result in decreased

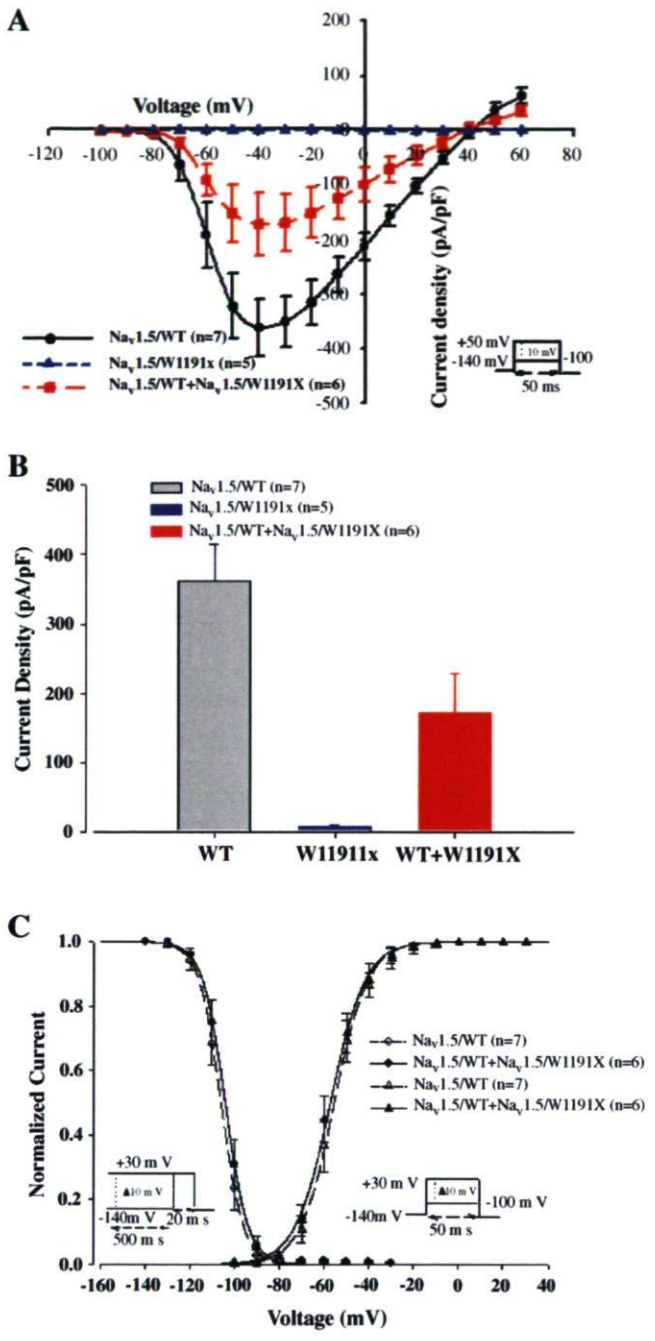

Fig. 7. (A) Current–voltage (*I*/*V*) relationships of $Na_v1.5$/WT, $Na_v1.5$/W1191X and $Na_v1.5$/WT+$Na_v1.5$/W1191X, where peak current amplitude was plotted against voltage. (B) Current densities of $Na_v1.5$/WT, $Na_v1.5$/W1191X and $Na_v1.5$/WT+$Na_v1.5$/W1191X. A 50% reduction in sodium channel density for $Na_v1.5$/WT+$Na_v1.5$/W1191X and no expression for $Na_v1.5$/W1191X. (C) Steady-state activation and inactivation of $Na_v1.5$/WT (Δ for activation, $n=7$; ○ for inactivation, $n=7$) and $Na_v1.5$/WT co-expressed with $Na_v1.5$/W1191X (▲ for activation, $n=6$; ● for inactivation, $n=6$). For activation, $V_{1/2}=-55.52\pm2.48$ mV and $k_v=-6.75\pm0.35$ mV for $Na_v1.5$/WT, and $V_{1/2}=-56.51\pm4.24$ mV and $k_v=-5.97\pm0.35$ mV for $Na_v1.5$/WT co-expressed with $Na_v1.5$/W1191X. For inactivation, $V_{1/2}=-105.82\pm1.58$ and $k_v=4.65\pm0.22$ for $Na_v1.5$/WT, and $V_{1/2}=-104.18\pm2.09$ and $k_v=4.73\pm0.06$ for $Na_v1.5$/WT co-expressed with $Na_v1.5$/W1191X. Activated currents were generated from a holding potential of −140 mV following 50 ms voltage steps from −100 mV to +20 mV in 10 mV increments. The voltage-dependence of inactivation was obtained by measuring the peak Na^+ current during a 20 ms test pulse to −30 mV, which followed a 500 ms pre-pulse to membrane potentials between −140 and −30 mV from a holding potential of −140 mV.

sodium current amplitude (Akai et al., 2000). This mutation is located in the S5–S6 linker that forms part of the channel pore (Fig. 5). The W1191X and S1710L mutations were not found in unrelated normal control individuals or any other study subjects. In addition, four single nucleotide polymorphisms (SNPs) [A29A (G87A; exon 2), H558R (A1673G; exon 12), D1818D (T5454C; exon 28) and IVS24+53T>C (intron 24)] were found in both control subjects and BS patients. These variants have been previously reported in several ethnic populations (Iwasa et al., 2000; Viswanathan et al., 2003; Chen et al., 2004; Maekawa et al., 2005). The allelic frequencies of these SNPs (29A, 558R, 1818D and IVS24+53C) in 150 normal Korean controls were 0.263, 0.167, 0.333, and 0.687, respectively.

Biophysical analysis of SCN5A W1191X

Macroscopic sodium currents were recorded from tsA201 cells expressing either WT ($Na_v1.5$/WT) or mutant channels ($Na_v1.5$/W1191X) co-transfected with the β_1-subunit (see Materials and methods for more details on identifying cells expressing the β_1-subunit) (Fig. 6). Mutant $Na_v1.5$/W1191X, did not exhibit any currents (Figs. 6B and 7A). The resulting sodium currents from WT, and WT co-expressed with W1191X, had fast activation and inactivation kinetics (Fig. 6C). Furthermore, co-expression of the WT channel and the mutant channel resulted in a 50% reduction in sodium currents (Fig. 7B), suggesting that there is no dominant negative effect of the mutation. No significant effect on steady-state activation and inactivation was observed (Fig. 7C).

Discussion

In this report, we investigated the genetic and biophysical characteristics of the *SCN5A* gene in Korean BS patients and control subjects. The BS patients had typical ECGs with RBBB and ST-segment elevation in leads V_1 through V_3 both before and after the administration of a sodium channel blocker. They had no structural heart abnormalities. The clinical and ECG criteria were based on those previously reported (Brugada and Brugada, 1997; Wilde et al., 2002).

To date, a number of *SCN5A* mutations associated with BS have been reported (Chen et al., 1998; Deschênes et al., 2000; Makiyama et al., 2005). We identified two mutations in the *SCN5A* gene in Korean BS patients. One of these mutations was a novel heterozygous nonsense mutation (W1191X), which to our knowledge, has not been previously reported in any ethnic group. This mutation occurred in the linker between domains II and III of *SCN5A*, a few residues upstream from the boundary of the S1 transmembrane segment in domain III. This residue is highly conserved in various mammalian sodium channel isoforms. The functional significance of the linker is not yet clear. However, a recent study of a mutation in this linker region has shown that the voltage-dependence of steady-state activation remains unchanged while inactivation displays a negative shift (Wang et al., 2004). The W1191X mutation was inherited as an autosomal dominant trait in this family. The same *SCN5A* mutation was found in four individuals in the family of the proband. Other mutations of this gene were not detected in this family. In addition, the mutation was absent in 200 unrelated normal subjects. The proband (II-2), a 74-year-old man, and his 52-year-old daughter (III-2) had typical Brugada-type ECG patterns and carried the same heterozygous mutant allele. Of interest is the fact that this proband had atrial arrhythmia (AA), a prolonged QTc interval, and first degree A–V block. QTc prolongation and first degree A–V block in the index patients were not related to cardioversion, radiofrequency ablation of atrial flutter, myocardial ischemia or medication. This suggests that *SCN5A* mutations may lead to both type 3 LQT syndrome and BS. In addition, since his daughter also had AA, the AA in the proband might be related to the *SCN5A* mutation. However, we could not confirm that the AA in this BS patient was related to a genetic defect, since it is not uncommon in the patient's age group.

Two granddaughters of the proband, a 27-year-old woman (IV-1) and her 25-year-old sister (IV-2), both had the W1191X mutation. However, their ECGs did not show Brugada-type patterns, and flecainide challenges did not unmask the type 1 BS ECG pattern. Priori et al. (2000) reported false negative results when flecainide and procainamide are used to unmask the syndrome.

One possible explanation for the negative response in the presence of an *SCN5A* mutation is the incomplete penetrance of BS that appears to be dependent on age and sex. Indeed, Schulze-Bahr et al. (2003) reported complete penetrance in adult patients but incomplete penetrance in young subjects. In addition, there is a greater correlation between the phenotypic expression of BS and sex than for other autosomally dominant transmitted arrhythmic diseases. Although mutant alleles responsible for BS are transmitted equally to both sexes, the clinical phenotype is more predominant in males than in females (Priori et al., 2002; Wilde et al., 2002). The basis for this discrepancy between the sexes is unclear. However, a recent study showed a more prominent I_{to}-mediated action potential notch in the right ventricular (RV) epicardium of males than of females (Di Diego et al., 2002). This could explain why BS is eight to ten times more prevalent in men than in women. A similar penetrance mode was observed in our family. As such, the concept of age- and sex-dependent ECG findings in BS might be applicable to this family.

Another possible explanation for the variable Brugada-type ECG patterns in this family is that unidentified factors may modulate the BS phenotype expressed by an *SCN5A* mutation. To test this possibility, we looked for the H558R polymorphism that is known to modulate the biophysical effects of *SCN5A* mutations (T512I and M1166L) on sodium channel function (Viswanathan et al., 2003; Ye et al., 2003). We found that all the family members including unaffected individuals, were H558 homozygotes, indicating that H558R polymorphism could not be a factor influencing the BS phenotype.

$Na_v1.5$/W1191X resulted in a loss of cardiac sodium channel function. This mutation was predicted to prematurely truncate the sodium channel protein, removing domains III and IV and might have led to a loss of channel function via haploinsufficiency. This concept is supported by other surveys reporting that

the haploinsufficiency of the $Na_v1.5$ protein is a plausible explanation for the reduced sodium current (Benson et al., 2003; Keller et al., 2005a,b). In our *in vitro* experiments, the tsA201 cells transfected with $Na_v1.5$/W1191X did not express a sodium current whereas the co-expression of this mutant with WT channels resulted in a 50% reduction in sodium currents. This suggests that $Na_v1.5$/W1191X did not exert a dominant negative effect that could lead to a serious BS phenotype. This finding is consistent with recent reports demonstrating that some truncated sodium channel proteins can cause BS (Baroudi et al., 2004; Keller et al., 2005a,b; Todd et al., 2005).

We identified a known heterozygous missense *SCN5A* mutation (S1710L) in a patient with BS (SV525). Akai et al. (2000) reported the S1710L mutation in a symptomatic IVF patient who had no history of a typical BS ECG phenotype. This mutant sodium channel features an acceleration in current decay together with a large hyperpolarizing shift of steady-state inactivation and a depolarizing shift of activation. Our result suggests that the S1710L mutation in *SCN5A* is related to clinical phenotypes of IVF and BS with variable clinical features. The occurrence of the S1710L mutation in both IVF and BS patients indicates that the BS and IVF subgroups are at least genetically overlap and may be allelic disorders that result from defects in the *SCN5A* gene such as congenital LQT syndrome (LQT3) and hereditary A–V block (Schott et al., 1999).

Two of the five BS patients in our study had *SCN5A* mutations, while none were identified in the other three BS patients. Several recent studies have described BS patients with no *SCN5A* mutations (Smits et al., 2002; Takahata et al., 2003; Shin et al., 2004). These results are consistent with our findings, which provide support for the possibility of genetic heterogeneity in BS (Priori et al., 2000).

Conclusion

In summary, we describe a novel heterozygous non-sense mutation (W1191X) of the *SCN5A* gene in a Korean family with BS. The biophysical data confirmed that the loss of function caused by the $Na_v1.5$/W1191X mutation led to BS in our patients. This is consistent with the findings of other studies indicating that the loss of function of *SCN5A* is responsible for the clinical features of BS. We will continue our search for genes responsible for BS in subjects in whom no *SCN5A* mutations have been identified.

Acknowledgements

We would like to thank all the participants in this study. We are grateful to Ms. H.S. Kim for arranging the clinical data and Dr. H.J. Jin for the technical assistance. This work was supported by a grant from Korean Research Foundation Grant (KRF-2002-075-C00020) for Dr. D.J. Shin, a grant from Ministry of Health and Welfare, Republic of Korea (A000385) for Dr. S.J.K. Yoon, and grants from the Heart and Stroke Foundation of Québec and the Canadian Institutes of Health Research (MT-13181) for Dr. M. Chahine. Dr. M. Chahine is an Edwards Senior Investigator (Joseph C. Edwards Foundation).

References

Ackerman, M.J., Siu, B.L., Sturner, W.Q., Tester, D.J., Valdivia, C.R., Makielski, J.C., Towbin, J.A., 2001. Postmortem molecular analysis of *SCN5A* defects in sudden infant death syndrome. The Journal of the American Medical Association 286, 2264–2269.

Akai, J., Makita, N., Sakurada, H., Shirai, N., Ueda, K., Kitabatake, A., Nakazawa, K., Kimura, A., Hiraoka, M., 2000. A novel *SCN5A* mutation associated with idiopathic ventricular fibrillation without typical ECG findings of Brugada syndrome. FEBS Letters 479, 29–34.

Antzelevitch, C., 2001. Electrical heterogeneity, cardiac arrhythmias, and sodium channel. Circulation Research 87, 964–965.

Antzelevitch, C., Brugada, P., Brugada, J., Brugada, R., Shimizu, W., Gussak, I., Perez Riera, A.R., 2002. Brugada syndrome: a decade of progress. Circulation Research 91, 1114–1118.

Balser, J.R., 1999. Structure and function of the cardiac sodium channels. Cardiovascular Research 42, 327–338.

Baroudi, G., Carbonneau, E., Pouliot, V., Chahine, M., 2000. *SCN5A* mutation (T1620M) causing Brugada syndrome exhibits different phenotypes when expressed in Xenopus oocytes and mammalian cells. FEBS Letters 467, 12–16.

Baroudi, G., Napolitano, C., Priori, S.G., Bufalo, A.D., Chahine, M., 2004. Loss of function associated with novel mutations of the *SCN5A* gene in patients with Brugada syndrome. Canadian Journal of Cardiology 20, 425–430.

Benson, D.W., Wang, D.W., Dyment, M., Knilans, T.K., Fish, F.A., Strieper, M.J., Rhodes, T.H., George Jr., A.L., 2003. Congenital sick sinus syndrome caused by recessive mutations in the cardiac sodium channel gene (*SCN5A*). The Journal of Clinical Investigation 112, 1019–1028.

Brugada, P., Brugada, J., 1992. Right bundle branch block, persistent ST segment elevation and sudden cardiac death: a distinct clinical and electrocardiographic syndrome. A multicenter report. Journal of the American College of Cardiology 20, 1391–1396.

Brugada, J., Brugada, P., 1997. Further characterization of the syndrome of right bundle branch block, ST segment elevation, and sudden cardiac death. Journal of Cardiovascular Electrophysiology 8, 325–331.

Chen, Q., Kirsch, G.E., Zhang, D., Brugada, R., Brugada, J., Brugada, P., Potenza, D., Moya, A., Borggrefe, M., Breithardt, G., Ortiz-Lopez, R., Wang, Z., Antzelevitch, C., O'Brien, R.E., Schulze-Bahr, E., Keating, M.T., Towbin, J.A., Wang, Q., 1998. Genetic basis and molecular mechanism for idiopathic ventricular fibrillation. Nature 392, 293–296.

Chen, J.Z., Xie, X.D., Wang, X.X., Tao, M., Shang, Y.P., Guo, X.G., 2004. Single nucleotide polymorphisms of the *SCN5A* gene in Han Chinese and their relation with Brugada syndrome. Chinese Medical Journal 117, 652–656.

Cohen, S.A., Barchi, R.L., 1992. Cardiac sodium channel structure and function. Trends in Cardiovascular Medicine 2, 133–140.

Deschênes, I., Baroudi, G., Berthet, M., Barde, I., Chalvidan, T., Denjoy, I., Guicheney, P., Chahine, M., 2000. Electrophysiological characterization of *SCN5A* mutations causing long QT (E1784K) and Brugada (R1512W and R1432G) syndromes. Cardiovascular Research 46, 55–65.

Di Diego, J.M., Cordeiro, J.M., Goodrow, R.J., Fish, J.M., Zygmunt, A.C., Perez, G.J., Scornik, F.S., Antzelevitch, C., 2002. Ionic and cellular basis for the predominance of the Brugada syndrome phenotype in males. Circulation 106, 2004–2011.

Hamill, O.P., Marty, A., Neher, E., Sakmann, B., Sigworth, F.J., 1981. Improved patch-clamp techniques for high-resolution current recording from cells and cell-free membrane patches. Pflügers Archiv: European Journal of Physiology 391, 85–100.

Hermida, J.S., Lemoine, J.L., Aoun, F.B., Jarry, G., Rey, J.L., Quiret, J.C., 2000. Prevalence of the Brugada syndrome in an apparently healthy population. American Journal of Cardiology 86, 91–94.

Iwasa, H., Itoh, T., Nagai, R., Nakamura, Y., Tanaka, T., 2000. Twenty single nucleotide polymorphisms (SNPs) and their allelic frequencies in four genes that are responsible for familial long QT syndrome in the Japanese population. Journal of Human Genetics 45, 182–183.

Jurman, M.E., Boland, L.M., Liu, Y., Yellen, G., 1994. Visual identification of individual transfected cells for electrophysiology using antibody-coated beads. Biotechniques 17, 876–881.

Keller, D.I., Barrane, F.Z., Gouas, L., Martin, J., Pilote, S., Suarez, V., Osswald, S., Brink, M., Guicheney, P., Schwick, N., Chahine, M., 2005a. A novel nonsense mutation in the *SCN5A* gene leads to Brugada syndrome and a silent gene mutation carrier state. Canadian Journal of Cardiology 21, 925–931.

Keller, D.I., Rougier, J.S., Kucera, J.P., Benammar, N., Fressart, V., Guicheney, P., Madle, A., Fromer, M., Schlapfer, J., Abriel, H., 2005b. Brugada syndrome and fever: genetic and molecular characterization of patients carrying *SCN5A* mutations. Cardiovascular Research 67, 510–519.

Maekawa, K., Saito, Y., Ozawa, S., Adachi-Akahane, S., Kawamoto, M., Komamura, K., Shimizu, W., Ueno, K., Kamakura, S., Kamatani, N., Kitakaze, M., Sawada, J., 2005. Genetic polymorphisms and haplotypes of the human cardiac sodium channel alpha subunit gene (*SCN5A*) in Japanese and their association with arrhythmia. Annals of Human Genetics 69, 413–428.

Makiyama, T., Akao, M., Tsuji, K., Doi, T., Ohno, S., Takenaka, K., Kobori, A., Ninomiya, T., Yoshida, H., Takano, M., Makita, N., Yanagisawa, F., Higashi, Y., Takeyama, Y., Kita, T., Horie, M., 2005. High risk for bradyarrhythmic complications in patients with Brugada syndrome caused by *SCN5A* gene mutations. Journal of the American College of Cardiology 46, 2100–2106.

Margolskee, R.F., McHendry-Rinde, B., Horn, R., 1993. Panning transfected cells for electrophysiological studies. Biotechniques 15, 906–911.

Matsuo, K., Akahoshi, M., Nakashima, E., Suyama, A., Seto, S., Hayano, M., Yano, K., 2001. The prevalence, incidence and prognostic value of the Brugada-type electrocardiogram: a population-based study of four decades. Journal of the American College of Cardiology 38, 765–770.

Naccarelli, G.V., Antzelevitch, C., 2001. The Brugada syndrome: clinical, genetic, cellular, and molecular abnormalities. The American Journal of Medicine 110, 573–581.

Nademanee, K., Veerakul, G., Nimmannit, S., Chaowakul, V., Bhuripanyo, K., Likittanasombat, K., Tunsanga, K., Kuasirikul, S., Malasit, P., Tansupasawadikul, S., Tatsanavivat, P., 1997. Arrhythmogenic marker for the sudden unexplained death syndrome in Thai men. Circulation 96, 2595–2600.

Priori, S.G., Napolitano, C., Giordano, U., Collisani, G., Memmi, M., 2000. Brugada syndrome and sudden cardiac death in children. Lancet 355, 808–809.

Priori, S.G., Napolitano, C., Gasparini, M., Pappone, C., Della Bella, P., Giordano, U., Bloise, R., Giustetto, C., De Nardis, R., Grillo, M., Ronchetti, E., Faggiano, G., Nastoli, J., 2002. Natural history of Brugada syndrome: insights for risk stratification and management. Circulation 105, 1342–1347.

Schott, J.J., Alshinawi, C., Kyndt, F., Probst, V., Hoorntje, T.M., Hulsbeek, M., Wilde, A.A., Escande, D., Mannens, M.M., Le Marec, H., 1999. Cardiac conduction defects associated with mutations in *SCN5A*. Nature Genetics 23, 20–21.

Schulze-Bahr, E., Eckardt, L., Breithardt, G., Seidl, K., Wichter, T., Wolpert, C., Borggrefe, M., Haverkamp, W., 2003. Sodium channel gene (*SCN5A*) mutations in 44 index patients with Brugada syndrome: different incidences in familial and sporadic disease. Human Mutation 21, 651–652.

Shin, D.J., Jang, Y.S., Park, H.Y., Lee, J.E., Yang, K.J., Kim, E.M., Bae, Y.J., Kim, J.M., Kim, J.K., Kim, S.S., Lee, M.H., Chahine, M., Yoon, S.J.K., 2004. Genetic analysis of the cardiac sodium channel gene *SCN5A* in Koreans with Brugada syndrome. Journal of Human Genetics 49, 573–578.

Smits, J.P., Eckardt, L., Probst, V., Bezzina, C.R., Schott, J.J., Remme, C.A., Haverkamp, W., Breithardt, G., Escande, D., Schulze-Bahr, E., Le Marec, H., Wilde, A.A., 2002. Genotype–phenotype relationship in Brugada syndrome: electrocardiographic features differentiate *SCN5A*-related patients from non-*SCN5A*-related patients. Journal of the American College of Cardiology 40, 350–356.

Takahata, T., Yasui-Furukori, N., Sasaki, S., Igarashi, T., Okumura, K., Munakata, A., Tateishi, T., 2003. Nucleotide changes in the translated region of *SCN5A* from Japanese patients with Brugada syndrome and control subjects. Life Sciences 72, 2391–2399.

Todd, S.J., Campbell, M.J., Roden, D.M., Kannankeril, P.J., 2005. Novel Brugada *SCN5A* mutation causing sudden death in children. Heart Rhythm 2, 540–543.

Underhill, P.A., Jin, L., Lin, A.A., Mehdi, S.Q., Jenkins, T., Vollrath, D., Davis, R.W., Cavalli-Sforza, L.L., Oefner, P.J., 1997. Detection of numerous Y chromosome biallelic polymorphisms by denaturing high-performance liquid chromatography. Genome Research 7, 996–1005.

Viswanathan, P.C., Benson, D.W., Balser, J.R., 2003. A common *SCN5A* polymorphism modulates the biophysical effects of an *SCN5A* mutation. The Journal of Clinical Investigation 111, 341–346.

Wang, Q., Li, Z., Shen, J., Keating, M.T., 1996. Genomic organization of the human *SCN5A* gene encoding the cardiac sodium channel. Genomics 34, 9–16.

Wang, D.W., Makita, N., Kitabatake, A., Balser, J.R., George Jr., A.L., 2000. Enhanced Na^+ channel intermediate inactivation in Brugada syndrome. Circulation Research 87, E37–E43.

Wang, Q., Chen, S., Chen, Q., Wan, X., Shen, J., Hoeltge, G.A., Timur, A.A., Keating, M.T., Kirsch, G.E., 2004. The common *SCN5A* mutation R1193Q causes LQTS-type electrophysiological alterations of the cardiac sodium channel. Journal of Medical Genetics 41, e66.

Wilde, A.A., Antzelevitch, C., Borggrefe, M., Brugada, J., Brugada, R., Brugada, P., Corrado, D., Hauer, R.N., Kass, R.S., Nademanee, K., Priori, S.G., Towbin, J.A., Study Group on the Molecular Basis of Arrhythmias of the European Society of Cardiology, 2002. Proposed diagnostic criteria for the Brugada syndrome: consensus report. Circulation 106, 2514–2519.

Yan, G.X., Antzelevitch, C., 1999. Cellular basis for the Brugada syndrome and other mechanisms of arrhythmogenesis associated with ST-segment elevation. Circulation 100, 1660–1666.

Ye, B., Valdivia, C.R., Ackerman, M.J., Makielski, J.C., 2003. A common human *SCN5A* polymorphism modifies expression of an arrhythmia causing mutation. Physiological Genomics 12, 187–193.